

**Design of advanced materials and nano delivery
approaches for enhancing activity against Methicillin
resistant *Staphylococcus aureus***

by

Calvin A. Omolo

(MPharm – University of KwaZulu-Natal)

Submitted as fulfilment of the requirements for the degree of Doctor of
Philosophy in Pharmaceutics at the Discipline of Pharmaceutical Sciences of the
School of Health Sciences at the University of KwaZulu-Natal



UNIVERSITY OF TM
KWAZULU-NATAL

INYUVESI
YAKWAZULU-NATALI

Supervisor:

Professor Thirumala Govender
(PhD, University of Nottingham, United Kingdom)

Co-supervisor:

Dr. Chunderika Mocktar
(PhD, University of KwaZulu-Natal, South Africa)

Date submitted: December 6th 2018

“You are always a student, never a master. You have to keep moving forward”

- Conrad Hall -

“This thesis is dedicated to the child who listens to that inner voice telling him/her to go the extra mile even when odds are stacked against them.... keep pushing because the sky is the limit”

Declaration 1 – Plagiarism

I, Mr. Calvin A. Omolo, declare that

1. The research data reported in this thesis, except where otherwise indicated is my own original work.
2. This thesis has not been submitted for any degree or examination at any other university.
3. This thesis does not contain data, pictures, graphs, or other information belonging to other people, unless specifically acknowledged as being sourced from other people.
4. This thesis does not contain any other persons' writing, unless specifically acknowledged as being sources from other researchers. Where other written sources have been quoted, then:
 - a. Their words have been rephrased but the general information attributed to them has been referenced;
 - b. Where their exact words have been used, their writing has been placed inside quotation marks, and referenced.
5. Where I have reproduced a publication of which I am an author, co-author, or editor, I have indicated in detail which part of the publication was written by myself alone and have fully referenced such publications.
6. This dissertation does not contain any graphics, text or tables copied from the internet, unless specifically acknowledged, and the source being detailed in the reference sections of the dissertation.

Signed:



Date:

25th November 2018

I, Professor Thirumala Govender as supervisor of the Ph.D. studies hereby consent to the submission of this Ph.D. thesis.

Signed:



Date:

5th December 2018

I, Dr. Chunderika Mocktar as co-supervisor of the Ph.D. studies hereby consent to the submission of this Ph.D. thesis.

Signed:



Date:

28th November 2018

Declaration 2 –Publications

Details of contribution to publications that form part and/or include research presented in this thesis:

Amphiphilic Dendrimers for Drug Delivery

Torchillin, V., Handbook of Materials for Nanomedicine, 2nd ed, Omolo, C. A, Sikwal, R. D., Kalhapure, R. S, & Govender, T (2018). Amphiphilic Dendrimers for Drug Delivery, Pan Stanford Publishing Pte, Singapore 2018. (under press production).

A Hybrid of mPEG-b-PCL and G1-PEA Dendrimer for Enhancing Nano Delivery of Antibiotics

Omolo, C. A., Kalhapure, R. S., Agrawal, N., Jadhav, M, Rambharose, S., Mocktar, C., & Govender, T. (2018). A Hybrid of mPEG-b-PCL and G1-PEA Dendrimer for Enhancing Nano Delivery of Antibiotics. *Journal of Controlled Release*, 290, 112–128. (Impact factor 7.877). DOI: 10.1016/j.jconrel.2018.10.005

Formulation and Molecular Dynamics Simulations of a Fusidic Acid Nanosuspension for Simultaneously Enhancing Solubility and Antibacterial Activity.

Omolo, C. A., Kalhapure, R. S., Agrawal, N., Rambharose, S., Mocktar, C., & Govender, T. (2018). Formulation and Molecular Dynamics Simulations of a Fusidic Acid Nanosuspension for Simultaneously Enhancing Solubility and Antibacterial Activity. *Molecular Pharmaceutics*, 15(8), 3512-3526. (Impact factor 4.556). DOI: 10.1021/acs.molpharmaceut.8b00505.

Liposomes with pH Responsive “On and Off” Switches for Targeted and Intracellular Delivery of Antibiotics.

Omolo, C. A, Megrab, N. A., Kalhapure, R. S., Agrawal, N, Jadhav, M, Mocktar, C, Rambharose.S, Maduray, K, Nkambule. B, Govender. T. (2018). Liposomes with pH Responsive “On and Off” Switches for Targeted and Intracellular Delivery of Antibiotics. *European Journal of Pharmaceutical Sciences*. (Communicated manuscript, Manuscript ID EJPS-S-18-02306). (Impact Factor 3.466.)

The published first author manuscripts can be found in Chapters three to five of this thesis.

Mr. Omolo C.A. performed the literature search, contributed to the design of the general flow, writing of the first draft of the book chapter and undertook all revisions. He also contributed to the inception, conceptualization, design of the projects, modification, optimization of methods, preparation, characterization in terms of synthesis and structural elucidation techniques such as Fourier-transform infrared (FT-IR) spectroscopy, Proton and ¹³Carbon nuclear magnetic resonance spectroscopy (¹H NMR and C¹³ NMR), gel permeation chromatography, MALDI TOF analysis and the bio-safety of all the materials synthesized for the studies in this thesis. He also contributed to the formulation and characterization of the nano based drug delivery system that were formulated from the synthesized materials in terms of ; particle size, polydispersity index, zeta potential, surface morphology, entrapment efficiency, *in vitro* drug release, differential scanning calorimetry (DSC), *in vitro* and *in vivo* antimicrobial activity, the mathematical modelling in terms of the *in vitro* release kinetics data and stability studies and Molecular dynamics (MD) simulations studies. Mr. C.A Omolo also wrote the first drafts of all the first authored papers and undertook all revisions. Dr. R.S. Kalhapure assisted with the inception, overall design of the project, solving of any technical problems and supervision of the studies. Dr. S. Rambharose assisted in performing the cytotoxicity studies of the synthesized materials and in the *in vivo* antibacterial activity studies. Dr. C. Mocktar supervised the *in vitro* and *in vivo* antibacterial activity studies. Dr. M. Jadhav assisted in synthesis and characterization of the synthesized materials and proof reading of manuscripts. Dr. N. Agrawal, assisted in MD simulation studies, Dr. N.A Megrab, helped in the liposome formulation and *in vitro* drug release, Dr. K. Maduray, assisted in advanced cell culturing for intracellular studies, Dr. B. Nkambule. supervised the flow cytometry studies while Dr. D. Sikwal, wrote first draft of some sections of the book chapter. Prof. T. Govender served as supervisor and was responsible for project conceptualization, problem solving, editing of papers and abstracts as well as general supervision of all studies.

Research output from the dissertation

1. First authored Publications

The following research papers were published as results generated from specific objectives from this study and they include: -

- Torchillin, V., Handbook of Materials for Nanomedicine, 2nd ed, Omolo, C. A, Sikwal, R. D., Kalhapure, R. S, & Govender, T. (2018). Amphiphilic Dendrimers for Drug Delivery, Pan Stanford Publishing Pte, Singapore 2018. (under press production).
- Omolo, C. A., Kalhapure, R. S., Agrawal, N., Jadhav, M, Rambharose, S., Mocktar, C., & Govender, T. (2018). A Hybrid of mPEG-b-PCL and G1-PEA Dendrimer for Enhancing Nano Delivery of Antibiotics. Journal of Controlled Release, 290, 112–128. (Impact factor 7.877). DOI: 10.1016/j.jconrel.2018.10.005.
- Omolo, C. A., Kalhapure, R. S., Agrawal, N., Rambharose, S., Mocktar, C., & Govender, T. (2018). Formulation and Molecular Dynamics Simulations of a Fusidic Acid Nanosuspension for Simultaneously Enhancing Solubility and Antibacterial Activity. Molecular Pharmaceutics, 15(8), 3512-3526. (Impact factor 4.556). DOI: 10.1021/acs.molpharmaceut.8b00505.
- Omolo, C. A, Megrab, N. A., Kalhapure, R. S., Agrawal, N, Jadhav, M, Mocktar, C, Rambharose.S, Maduray, K, Nkambule. B, Govender. T. (2018). Liposomes with pH Responsive “On and Off” Switches for Targeted and Intracellular Delivery of Antibiotics. European Journal of Pharmaceutical Sciences. (Communicated manuscript, Manuscript ID EJPS-S-18-02306). (Impact Factor 3.466.)

2. Conference Presentations

The following conference presentations were produced from data generated from this study:

- Calvin A. Omolo, Rahul S. Kalhapure, Sanjeev Rambharose, Chunderika Mocktar, Thirumala Govender, A novel six-armed PEG-b-PCL copolymer (6m-PEPEA) based on G1-PETIM dendrimer for nano delivery of vancomycin. The AAPS Annual Meeting and Exposition Nov 12 - 15, 2017, San Diego, USA. (Poster presentation)
- Calvin A. Omolo, Rahul S. Kalhapure, Mahantesh Jadhav, Sanjeev Rambharose, Chunderika Mocktar, Thirumala Govender, A novel six-armed PEG-b-PCL copolymer based on G1 PETIM dendrimer for nano delivery of vancomycin. International Conference on Nanomedicine and Nanobiotechnology, September 25 - 27, 2017 Barcelona, Spain. (Poster presentation)
- Omolo, C. A., Kalhapure, R. S., Agrawal, N., Rambharose, S., Mocktar, C., & Govender, T. (2018). Formulation and Molecular Dynamics Simulations of a Fusidic Acid Nanosuspension for Simultaneously Enhancing Solubility and Antibacterial activity. Applied Nanotechnology and Nanoscience International Conference. October 22-24 Berlin Germany. (Oral presentation).
- Omolo, C. A., Kalhapure, R. S., Agrawal, N., Rambharose, S., Mocktar, C., & Govender, T. (2018). Formulation and Molecular Dynamics Simulations of a Fusidic Acid Nanosuspension for Simultaneously Enhancing Solubility and Antibacterial activity. 38th Annual Conference of the Academy of Pharmaceutical Sciences, July 06-08, 2017 Johannesburg, South Africa (Poster presentation).
- Calvin A. Omolo, Rahul S. Kalhapure, Mahantesh Jadhav, Sanjeev Rambharose, Chunderika Mocktar, Thirumala Govender, A novel six-armed PEG-b-PCL copolymer based on G1 PETIM dendrimer for nano delivery of vancomycin. College of Health Sciences Annual Research Symposium, University of KwaZulu Natal, October 05-06 2017 Durban, South Africa. (Oral presentation).

The posters can be found in Appendix IV, V and VIII.

3. Co-authored publications

The following are co-authored publications related to the studies on synthesis of advanced materials for combating antimicrobial resistance.

- Mhule D., Kalhapure, R. S., Jadhav, M., Omolo, C. A., Rambharose, S., Waddad, A. Y., Mocktar, C., & Govender, T. (2018). Synthesis of an oleic acid-based pH-responsive lipid and its application in nano delivery of vancomycin, *International Journal of Pharmaceutics*, 550(1-2), 149-159. DOI: 10.1016/j.ijpharm.2018.08.025 (Impact factor 2.297) (appendix X).
- Mbuso F., Kalhapure, R. S., Dhumal D., Agrawal, N., Omolo C.A., Akamanchi K.G., and Govender T. (2018). Antimicrobial cell penetrating peptides with bacterial cell specificity: pharmacophore modelling, quantitative structure activity relationship and molecular dynamics simulation, *Journal of Biomolecular Structure & Dynamics*, 1-31 in Press, DOI:10.1080/07391102.2018.1484814 (Impact factor 3.107). (Impact factor 3.862) (appendix XI)
- Faya, M., Kalhapure, R. S., Kumalo, H. M., Waddad, A. Y., Omolo, C., & Govender, T. (2017). Conjugates and nano-delivery of antimicrobial peptides for enhancing therapeutic activity, *Journal of Drug Delivery Science and Technology*, 44, 153-171. DOI: 10.1016/j.jddst.2017.12.010 (Impact factor 2.297) (appendix XII)

Abstract

Infectious diseases, including bacterial infections, continue to be a significant cause of morbidity and mortality globally, antimicrobial resistance has further made them fatal. Limitations of conventional dosage forms have been found to be one of the contributing factors to antimicrobial resistance. Novel nano delivery systems are showing potential to combat antimicrobial resistance. The search for novel materials for efficient delivery of antibiotics is an active research area. The aim of the study was to design and synthesize advanced materials and explore nano-based strategies for preparations of novel drug delivery systems to treat SA and MRSA infections. In this study two novel materials; a linear polymer dendrimer hybrid star polymer (3-mPEA) comprising of a generation one poly (ester-amine) dendrimer (G1-PEA) and copolymer of methoxy poly (ethylene glycol)-b-poly(ϵ -caprolactone) (mPEG-b-PCL) and oleic acid based quaternary lipid (QL) were synthesized and characterized and Poloxamer 188 (P188) material available in the market were employed to formulate three nano drug delivery systems for efficient and targeted delivery of antibiotics. The synthesized materials and the drug delivery system were found to be biosafe after exhibiting cell viability above 75% in all the cell lines tested on using MTT assay. The formulated nano based systems were evaluated for sizes, polydispersity indices (PDI), zeta potential (ZP), surface morphology, drug release, *in vitro* and *in vivo* antibacterial activity. Nanovesicles were formulated from 3-mPEA and they had sizes, PDI, ZP and entrapment efficiency of 52.48 ± 2.6 nm, 0.103 ± 0.047 , -7.3 ± 1.3 mV and $76.49 \pm 2.4\%$. respectively. QL lipid was employed to formulate vancomycin (VCM) loaded liposomes with Oleic acid based ‘On’ and ‘Off’ pH responsive switches for infection site and intracellular bacteria targeting. They were found to have the size of 98.88 ± 01.92 at pH 7.4. and exhibited surface charge switching from negative at pH 7.4 to positive charge accompanied by faster drug release at pH 6.0. Fusidic acid nanosuspension (FA-NS) with size, PDI and ZP of 265 ± 2.25 nm, 0.158 ± 0.026 and -16.9 ± 0.794 mV respectively was formulated from P188. The drug release profile from both the nanovesicles and liposomes was found to have sustained release. *In vitro* antibacterial activity for the nanovesicles, FA-NS and liposomes showed 8, 6 and 4-fold better activity at pH 7.4, while the liposome being a pH responsive antibacterial system at pH 6 showed 8- and 16- fold better activity against both Methicillin susceptible (MSSA) and resistant *Staphylococcus aureus* (MRSA) respectively when compared with the bare drugs. An *in vivo* BALB/c mice, skin infection model revealed that treatment with VCM-loaded nanovesicles, liposomes and FA-Ns significantly reduced the MRSA burden compared to bare drugs and untreated groups. There was a 20, 6.33 and 76-fold reduction in the MRSA load in mice skin treated with nanovesicles, liposomes and FA-NS respectively compared to those treated with bare VCM and fusidic acid. In summary, synthesized material showed to be biosafe and potential for the development of nano-based drug delivery systems of antibiotics against bacterial infections. The data from this study has resulted in one book chapter and 3 first authored and 3 co-authored research publications.

Acknowledgements

I extend my gratitude to those, who so generously contributed to the work presented in this thesis, without them the completion of this project would not have been possible. I sincerely would like to thank the following people:

First of all, I would like to show my sincere appreciation to my supervisor, Professor Thirumala Govender, who accepted me as her student with open arms and without any hesitation. You have been a pillar of strength, guidance, motivation, compassion. Your insistence for me to strive for excellence and always steering me in the right direction will always be remembered. I've learnt invaluable life skills and knowledge from you; without your insight and expertise I would not have finished my thesis successfully.

Thank you to my co-supervisor Dr. Chunderika Mocktar for encouraging me to pursue further studies and not rest on my laurels after graduating with my master's degree. I also convey my heartfelt thanks for your supervision, caring support, advice, creative criticism, and approachable nature that has allowed me to learn valuable lab techniques and skills in general from you. Your motivation, assistance, support, and guidance throughout the project has been of great importance and I'm grateful for it.

Special thanks go to my post-doctoral mentor Dr. Rahul Kalhapure for your assistance in the design of those projects as well as your continued guidance and motivation. I will forever be indebted to you, for being with me every step of the way, helping me tackle any problem encountered along the way, instilling invaluable skills that will be crucial in my career ahead.

Special mention goes to my colleagues, Dr. Ayman Waddad, Dr. Ramesh Ganimani, Dr. Sanjeev Rambharose, Dr. Manthesh Jadhav, Dr. Dhiraj Sikwal, Dr. Ruma Maji, Andile Mbuso Faya, Ms., Nawras Abdelmoniem, Ms., Victoria Fasiku, Danford Mhule, Sifiso Makhatini, Pavan Walvekar, Abdeen Mohamed, Daniel Hassan, Melissa Ramtahal and Leslie Murugan for all the support, technical assistance in the lab and life-long friendship.

My sincere thanks go to all the organizations, which gave me their indispensable generous resources, including the National Research Foundation, UKZN Nanotechnology Platform and the College of Health Sciences at UKZN. Without their support and financial help, it would not have been possible for me to pursue and to complete this thesis project successfully. My appreciation goes to Ms. Carrin Martin for your editorial assistance, the Electron Microscope Unit, and Biomedical Resource Unit at UKZN for your technical support.

Thank you to my family and my wife, for your complete support and motivation throughout my studies. You have molded me into the person that I am today, and I will continue to pursue my dreams and I hope to make you proud. Thank you for always believing in me and pushing me for greatness. Lastly but not the least I give my thanks to the Almighty God for the gift of life, wisdom, grit, perseverance, health, and humility as I travelled this journey.

Table of Contents

Declaration 1 – Plagiarism	iii
Declaration 2 –Publications	iv
Research output from the dissertation	v
Abstract.....	viii
Acknowledgements	ix
CHAPTER 1, INTRODUCTION	1
1.1 Introduction.....	1
1.2 Background.....	1
1.3 Problem statement.....	7
1.4 Aims and objectives of this study	7
1.5 Novelty of the study.....	9
1.6 Rationale of the study	11
1.7 Overview of dissertation.....	12
CHAPTER 2, BOOK CHAPTER.....	19
2.1 Introduction.....	19
2.2 Graphical abstract	20
2.3 Book Chapter	21
2.1 INTRODUCTION	22
2.2 CLASSIFICATION OF AMPHIPHILIC DENDRIMERS	24
2.2.1 Amphiphilic layered dendrimers.....	24
2.2.2 Amphiphilic diblock or Janus dendrimers	25
2.2.3 Facially amphiphilic dendrimers.....	26
2.3.0 APPLICATIONS IN DRUG DELIVERY.....	26
2.3.1 Non-stimuli-responsive (NSR) self-assembling dendrimers	27
2.3.1.1 Amphiphilic layered dendrimers based NSR delivery systems	27
2.3.1.2 Janus dendrimers based NSR delivery systems	32
2.3.1.3 Facially amphiphilic dendrimer based NSR delivery systems.....	40
2.3.2 Stimuli-responsive (SR) self-assembling dendrimers.....	43
2.3.2.1 Amphiphilic layered dendrimer based SR delivery systems.....	44
2.3.2.2 Janus dendrimer based SR delivery systems.....	46
2.3.2.3 Facially amphiphilic dendrimer based SR delivery systems.....	48
2.3.3. Low molecular weight dendritic amphiphiles in drug delivery	53
2.4 CONCLUSION AND FUTURE PERSPECTIVE.....	58
2.5 REFERENCES	59
CHAPTER 3, EXPERIMENTAL PAPER 1	63
3.1 Introduction.....	63
3.2 Graphical abstract	64

3.4 Published manuscript.....	65
3.5 Abstract.....	66
3.6 Introduction.....	67
3.7 Materials, instrumentation and methods.....	69
3.9.0 Results and discussion.....	82
3.10 Conclusions.....	99
CHAPTER 4, EXPERIMENTAL PAPER 2.....	106
4.1 Introduction.....	106
4.2 Graphical abstract.....	108
4.3 Published manuscript.....	109
4.4 Abstract.....	110
4.6. Materials and Methods.....	114
4.7. Results and Discussion.....	126
4.8 Conclusion.....	146
4.9 References.....	147
CHAPTER 5, EXPERIMENTAL PAPER 3.....	152
5.1 Introduction.....	152
5.2 Graphical abstract.....	153
5.3 Published manuscript.....	154
5.4 Abstract.....	155
5.6. Materials and methods.....	159
5.7. Results.....	168
5.7. Discussion.....	182
5.8 Conclusion.....	189
5.9 References.....	190
CHAPTER 6, CO-AUTHORED PAPERS.....	198
6.1 Introduction.....	198
6.2 Published co-authored paper 1.....	199
6.2.1 Abstract.....	199
6.3 Published co-authored paper 2.....	200
6.3.1 Abstract.....	200
6.4 Published co-authored paper 3.....	201
6.4.1 Abstract.....	201
CHAPTER 7, CONCLUSION.....	202
7.1 General conclusions.....	202
7.2 Significance of the findings in the study.....	205
7.3 Recommendations for future studies.....	207
7.4 Conclusion.....	208

List of Abbreviations

3-Mpea	Linear Block Copolymer Dendrimer Hybrid Star Polymer	MIC	Minimum Inhibitory Concentration
A549	Adenocarcinoma Human Alveolar Epithelial	Mpeg	Monomethoxy Polyethylene Glycol
AMR	Antimicrobial Resistance	MRSA	Methicillin Resistant <i>Staphylococcus Aureus</i>
BCS	Biopharmaceutical Classification System	MSSA	Methicillin Susceptible <i>Staphylococcus Aureus</i>
CFU	Colony Finding Unit	MST	Microscale Thermophoresis
DCM	Dichloromethane	MTT	3-(4, 5-Dimethylthiazolyl-2)-2,5-Diphenyltetrazolium Bromide
DLS	Dynamic Light Scattering	NCE	New Chemical Entity
DMSO	Dimethyl Sulfoxide	NMR	Nuclear Magnetic Resonance Spectroscopy
DSC	Differential Scanning Calorimetry	OA	Oleic Acid
EE	Encapsulation Efficiency	OA-QL LIPO	Ph Responsive Liposome
FA	Fusidic Acid	P188	Ploxamer 188
FACS	Fluorescence-Activated Cell Sorting	PI	Propidium Iodide
FA-NS	Fusidic Acid Nanosuspension	PDI	Polydispersity Index
FBS	Fetal Bovine Serum	PVP	Polyvinylpyrrolidone
FT-IR	Fourier-Transform Infrared	QL	Quaternary Lipid
GDP	Gross Domestic Product	RMSE	Root Mean Square Error
H&E	Hematoxylin and Eosin	SA	<i>Staphylococcus Aureus</i>
HEK 293	Human Embryonic Kidney 293 Cells	Scvs	Small Colony Variants in Persistent Infections
HIV	Human Immunodeficiency Virus	SDS	Sodium Dodecyl Sulfate
HSA	Human Serum Albumin	TEM	Transmission Electron Microscopy
LPDH	Linear Polymers-Dendrimer Hybrids	THF	Tetrahydrofuran
MALDI-TOF	Matrix-Assisted Laser Desorption/Ionization Time of Flight	UKZN	University of Kwazulu-Natal
MD	Molecular Dynamics	V-3-Mpea	Vancomycin Loaded Nanovesicles
MDT	Mean Dissolution Time	VCM	Vancomycin
MHA	Mueller Hinton Agar	VDW	Van Der Waals
MHB	Mueller Hinton Broth	WHO	World Health Organization
VRSA	VCM Resistant <i>S.Aureus</i>	XRD	X-Ray Diffraction

List of Figures and Tables

NUMBER	TITLE	PAGE
CHAPTER 1 – INTRODUCTION (FIGURES)		
Figure 1	Death Attributable to AMR Compared to Major Causes of Death	3
Figure 2	New Antibiotics Approvals 2000-2015 With Highlights of New Classes	5
CHAPTER 2 – Book Chapter (FIGURES)		
Figure	Graphical Abstract	40
Figure 1	Classification of Amphiphilic Dendrimers Depending on the Structural Arrangement of The Hydrophilic and Hydrophobic	45
Figure 2	Facially Amphiphilic Dendrimer Prepared Consisting of Amphiphilic Benzylic Monomer with Hydrophilic Carboxylic Group and Hydrophobic Dodecyl Chains	47
Figure 3	Structure of G4-PGLSA dendrimers and hydrophobic guest molecules	50
Figure 4	Cytotoxicity Assay with human Breast Cancer, MCF-7, Cells	51
Figure 5	Release Profile Of [G4.5]-PGLSA-Coona Encapsulated 10HCPT	52
Figure 6	Structural representation of two janus dendrimers	54
Figure 7	Scanning electron microscopy analysis of the dendritic derivatives	55
Figure 8	SEM images of vitrified cold dried 1.0% amphiphilic dendritic hydrogel	56
Figure 9	Synthesis of amphiphilic janus dendrimers through click chemistry.	57
Figure 10	Structure of biphenyl monomer and orthogonal placement of the monomers in the dendrimers	61
Scheme 1	Synthesis of facially amphiphilic dendrimers	62
Figure 11	Pictorial representation of self-assembly of facially amphiphilic dendrimers	64
Figure 12	Multi stimuli responsive amphiphilic layered dendrimer	66
Figure 13	Schematic representation of enzyme triggered disassembly of nano micelles releasing payloads	68
Figure 14	Synthetic strategy of rupturing amphiphilic dendrimers	70

Figure 15	Structure of dendritic amphiphiles for SiRNA delivery	75
Scheme 1	Synthesis of G2 octamine dendritic amphiphile	75
Figure 15	Determination of CMC of glycine amphiphiles	76
CHAPTER 2 – Book Chapter (TABLES)		
Table 1	Non-stimuli responsive self-assembling amphiphilic dendrimers as drug carriers	59
Table 2	Stimuli-responsive self-assembling dendrimers for drug delivery	71
Table 3	Summary of low molecular weight dendritic amphiphiles based drug delivery systems	78
Table 4	Percentage cell viability and percentage decrease in bacterial cells growth after exposure to Mpeg-OA-VM polymersomes and bare vancomycin	64
CHAPTER 3 – Experimental Paper (FIGURES)		
Figure	Graphical abstract	86
Scheme 1	Synthesis and characterization of the hybrid dendrimer	92 - 93
Figure 1	Mass peaks distribution as determined by MALDI TOF	96
Figure 2	Cytotoxicity evaluation of various concentrations of 3-Mpea	106
Figure 3	Schematic of drug encapsulation into nanovesicles	108
Figure 4	TEM of V-3-Mpea nanovesicles, size distribution of nanovesicles determined by DLS and thermograms	109
Figure 5	Self-assembly of 3-mPEA snapshots	110
Figure 6	MST binding affinity study	112
Figure 7	In vitro drug release profile of v-3-mPEA nanovesicles and bare VCM	114
Figure 8	HRTEM images of MRSA after incubation with V-3-Mpea	116
Figure 9	Fluorescence microscopy micrographs of the untreated, VCM treated and V-3-mPEA treated MRSA biofilms	118
Figure 10	<i>In vivo</i> and <i>in vitro</i> antimicrobial activity	120

Figure 11	Histo-morphological evaluation post 48 h treatment	122
CHAPTER 3 – Experimental Paper (Tables)		
Table 1	Different ratio of drug polymer with their respective EE	107
Table 2	Average binding energy and its components obtained from the MM-PBSA calculation for 3-mPEA dimer	111
Table 3	The effect of HSA on 3-mPEA nanovesicles after incubation	113
Table 4	Release kinetics data from different models	114
Table 5	MICs of bare VCM, blank and VCM loaded 3-mPEA, against <i>S. Aureus</i> and MRSA	115
CHAPTER 4 – Experimental Paper (Figures)		
Figure	Graphical abstract	131
Scheme 1	QL synthesis scheme	138
Figure 1	Cell viability of A 549, MCF 7 And Hep G2 Cells against various concentrations of QL lipid	150
Figure 2	Opening and closing of the gates in the liposome at pH 7.4 and acidic pH	151
Figure 3	Increase in the size of liposomes with a decrease in pH and TEM images of the liposomes	152
Figure 4	DSC thermograms	153
Figure 5	<i>In vitro</i> VCM release from bare VCM solution, liposomal formulations and PC liposomes	154
Figure 6	Four representative images of QL interaction with deprotonated OA at four different time points	158
Figure 7	Time evolution of COM distance between QL-OAD	158
Figure 8	Flow cytometry, intracellular and <i>in vivo</i> antibacterial activity	162
Figure 9	Proposed mechanism of intracellular delivery of VCM and enhancement of antibacterial activity by the pH responsive liposome	164

Figure 10	H&E stained micrographs photographs of the skin samples for the controls and different treatment groups	165
Figure 11	Time evolution of COM distance of QL and upper leaflet PO ₄ atoms	167
CHAPTER 4 – Experimental Paper (Tables)		
Table 1	Curve fitting of the <i>in vitro</i> VCM release data from the liposome formulation at pH 6 and pH 7.4	155
Table 2	Average distance between QL-OAD and QL-OAP during interaction time	156
Table 3	Average binding energy and its components obtained from the MM-PBSA calculation for the QL-OAD and QL-OAP complexes.	159
Table 4	MIC of QL lipids and controls at pH 7.4	160
Table 5	MIC of QL lipids and controls at pH 7.4	161
Table 6	Average binding energy and its components obtained from the MM-PBSA calculation for the QL and POPC bilayer.	168
Table 7	Effect of storage on liposomal formulation over three months	169
CHAPTER 5 – Experimental Paper (Figures)		
Figure	Graphical abstract	177
Figure 1	Chemical structure of FA	180
Figure 2	Structure of monomer units of P188 and FA	186
Figure 3	TEM image of smaller particles showing coalescence to form larger thermodynamically stable larger particles	192
Figure 4	Effect of surfactant concentration on particle size	194
Figure 5	The effect of increasing drug concentration on particle sizes and homogeneity of the formed particles	195
Figure 6	Structures of FA and P188 at four different time points of simulations	197
Figure 7	Time evolution of COM distance between P188 and FA	198

Figure 8	Morphology of the optimized FA-NS particles	199
Figure 9	FT-IR, DSC thermogram and diffractograms	200
Figure 10	Solubility of FA-NS and FA and water	202
Figure 11	Cytotoxicity evaluation of FA-NS against various concentrations of P188	202
Figure 12	Flow cytometry dot plots and histograms	204
Figure 13	MRSA burden after 48 h of treatment	205
Figure 14	Photomicrographs of the control and the treated skin selections for light microscopy (LM) stained with H&E	206
CHAPTER 5 – Experimental Paper (Tables)		
Table 1	Effect of surfactant type on stabilizing the nanosuspension	193
Table 2	Effect of organic solvents on nanosuspension formation	194
Table 3	Average binding energy and its components obtained from the MM-PBSA calculation for the P188-FA complex.	198
Table 4	Stability studies of FA-NS	201
Table 5	MIC of FA and FA-NS	203

CHAPTER 1

INTRODUCTION

CHAPTER 1, INTRODUCTION

1.1 Introduction

This chapter includes a brief background to the study, indicating the status of infectious diseases and the various challenges with antibiotic therapy. It further provides details on strategic solutions to improve antibiotic therapy, the resulting aims and objectives of the study, as well as novelty of the study and the structure of the following chapters.

1.2 Background

The discovery of penicillin in 1928, its resulting production and introduction as the main option for treating infectious diseases resulted in the antibiotic boom and control of bacterial related infections. In 1962, Sir McFarland Burnett stated ‘By the end of the Second World War it was possible to say that almost all of the major practical problems of dealing with infectious diseases had been solved’ [1]. At that time, his statement was logical, as control and prevention measures had decreased the incidence of many infectious diseases, and with the ability to continue to identify new antibiotics came the opportunity to address new problems. However, over time, emerging, and re-emerging infectious diseases constituted to be major public-health problem globally. According to the World Health Organisation (WHO), diarrhoeal diseases are the second leading cause of death in children under five years old, and are responsible for approximately 525 000 deaths every year [2]. Although infectious diseases, especially from bacteria, are major contributors of causes of mortality, they also have been associated with the occurrence of non-communicable diseases, such as cancers, cardiovascular disease, asthma and gastrointestinal problems [3, 4]. Overall, infectious diseases have shown to impact negatively on the quality of life and economic burden of the global population [5, 6]. Thus, there is a call for ‘reinventing the wheel’ and finding new methods to treat and control infectious diseases.

In his Nobel prize acceptance speech, Alexander Fleming warned about and predicted the emergence of resistance strains due to misuse of antibiotics [7]. True to his prediction, resistance began to emerge within 10 years of the wide-scale introduction of penicillin [8]. Globally, the ability to treat common infectious diseases is still threatened by antimicrobial resistance (AMR). As of 2013, according to the Centre for Disease Control (CDC) annual statistics in the USA, more than two million people acquire infections that are resistant to

antibiotics, and at least 23,000 people die as a result. The same report shows that the cost implications due to AMR translates to US\$20 billion in excess direct health care costs, with additional costs to society for lost productivity as high as US\$35 billion a year [9]. A review of Antimicrobial Resistance chaired by Jim O’Neill paints a grim picture regarding AMR [10]. The review indicates that by the year 2050, mortality due to AMR will be 10 million annually, which will surpass other major causes of death, such as cancer, diabetes and road accidents globally, with a cost of US\$100 trillion impact on the world GDP, 80% of which will occur in low income countries in Africa and Asia (Figure 1.1). The WHO has echoed the earlier Alexander Fleming concerns and warns of the return to pre-antibiotic era if a proper response to the current trend in antibiotic resistance is not provided [11].

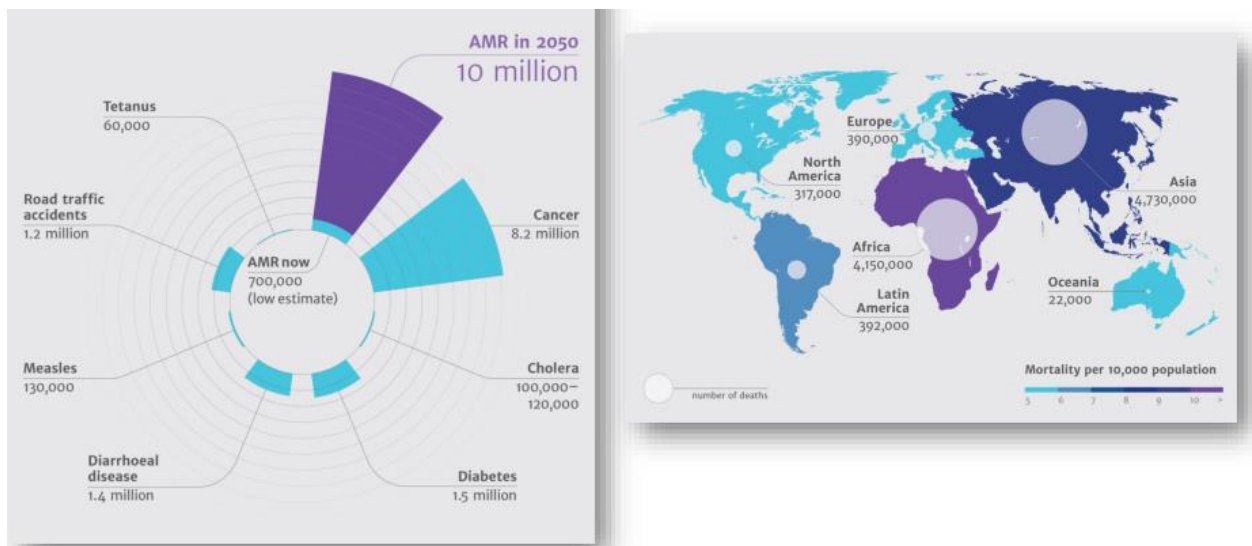


Figure 1. Death attributable to AMR compared to major causes of death [10]

One of the serious resistant strain of bacteria that has risen to be of global concern is methicillin-resistant *Staphylococcus aureus* (MRSA). Since its discovery in a London hospital in 1960, it has become a superbug of global concern [12]. Recent research findings estimate the incidence of MRSA to be 2.4% in Europe, 4.8% in North America, 5.4% in South America, 2.5% in Asia and 3.1% in Africa[13]. MRSA causes serious morbidity and mortality globally, for example, in Australia, Cameron *et al.* reported that annually, this amounted to 147,000 bed-days, including 1600 bed-days in intensive care due to MRSA infections. They also reported MRSA comorbidity as a serious problem with a cost of \$3.5b, and the cost to the health care system being \$1.9b annually [14].The debilitating effects of MRSA have further been aggravated by community based infections that are increasing its distribution. MRSA is

reported to be resistant to various drugs, including vancomycin, which is considered to be one of the last resort for treating bacteria, with the emergence of strains that are vancomycin resistant [11-13], it's the bacteria being listed by the WHO as a superbug, needing high priority for research to develop new treatment alternatives [15]. The bacterial resistance to currently used antibiotic, and the chances of developing resistance to new antimicrobial drugs, suggest that there is an urgent need to develop novel approaches for treating microbial infections.

Antibiotics have been delivered via conventional dosage forms since their market introduction in 1945. The limitations of conventional dosage forms are well documented, and include, inadequate concentrations of the antibiotics at the infection site, exposure of healthy cells to antibiotics, fast degradation and quick elimination in the bloodstream, enhanced frequency of administration and poor patient compliance due side effects [16, 17]. These limitations are recognised as a major contributing factor to the development of resistance and have led to the short window period between the introduction of antibiotics and development of resistance, which has resulted in the antibiotic pipeline drying up as the replacement of obsolete formulations is slower than new ones being introduced. Moreover, due to low return on investments, short product life circle and complicated regulatory approval procedures, pharmaceutical companies are abandoning research and development into new antibiotics [18-21]. As a result, only 30 antibiotics and two β -lactam/ β -lactamase inhibitor combinations have been launched since 2000, and seven new antibiotics and two new β -lactam/ β -lactamase inhibitor combinations have been introduced since 2013 [22-27]. From the list, very few antibiotics with new modes of action have been introduced, as shown in Figure 2 [28].

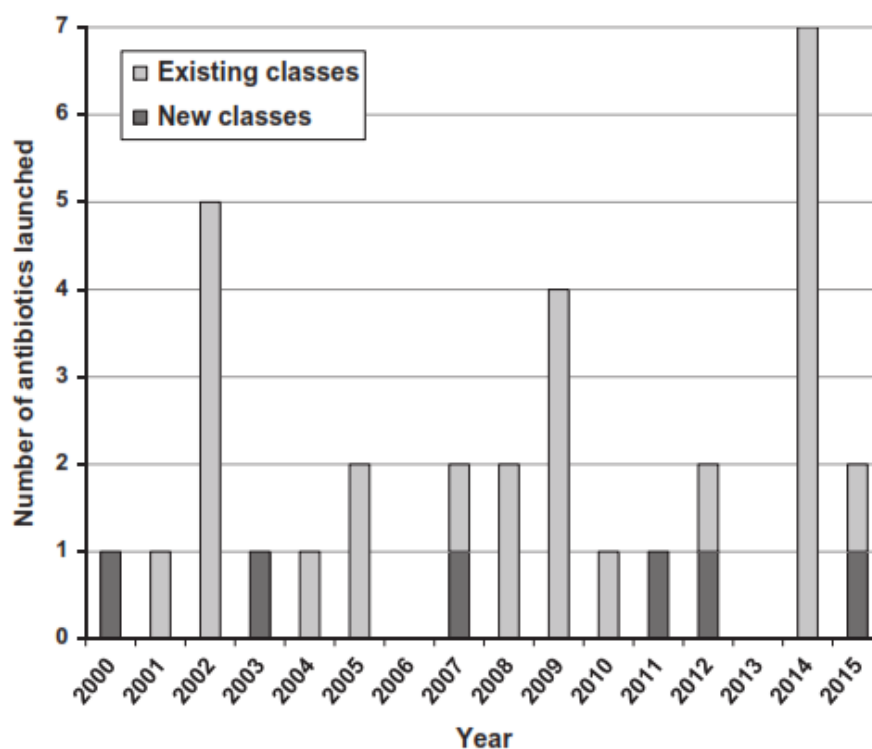


Figure 2. New antibiotics approvals 2000-2015 with highlights of new classes [29].

Nanotechnology involves the fine tuning of materials on an atomic, molecular and supramolecular scale, the goal being to create materials, devices and systems with essentially new properties and functions [30]. In the past three decades, the growth of nanotechnology has been considerable, and promises to bring another leap in medical and medical devices application. Nanotechnology is proving to be an effective strategy in enhancing activity, protecting the antibiotics in the market and addressing the problems of bacterial resistance, with some nano drug delivery systems already in the market [31-34]. These various nanoantibiotics offer several advantages, such as i) targeting the site of infection, ii) preventing exposure of the drug to healthy cells, iii) enhanced solubility, iv) sustainable and well controlled drug release, v) uniform distribution in the target tissue, vi) better patient-compliance, vi) improved cellular internalization, and vii) less side effects [35]. However, the application of nanotechnology for antibiotic therapy is still in its infancy compared to other medical conditions, such as cardiovascular disease and cancer. Therefore, in order to address the limitations associated with conventional dosage forms of antibiotics and the growing bacterial resistance to antibiotics, novel nanoantibiotic approaches are warranted.

In order to formulate nanodrug delivery systems that have desirable properties, such as disease targeting and long circulation, there is a need for the design and synthesis of advanced materials to prepare superior novel nano drug delivery systems with enhanced antibacterial activity. Of the various nanoparticulate drug delivery systems reported to effectively deliver antibiotics, we explored three novel approaches in this study, namely: i) nanovesicles devised from linear polymers-dendrimer hybrids (LPDH) (V-3-mPEA), ii) pH responsive Liposome (OA-QL lipo) with On and Off pH responsive switches and iii) Fusidic acid nanosuspension (FA-NS) to effectively target and treat methicillin susceptible and resistant *Staphylococcus aureus* infections. LPDH's are known to self-assemble to form core-shell aggregates, such as unimolecular and conventional micelles, vesicles and polymeric nanoparticles [36-40]. Hybrids of linear polymers and dendrimers embody some positive traits from both the dendrimers and the attached linear polymers for efficient drug delivery [41, 42]. Moreover, the ability to functionalize their end groups fine-tunes dendrimers for targeted delivery, long circulation [43], biodegradability [44], and covalent attachment of the drugs for sustained release [45]. There are several reports on LPDHs to deliver drugs [46, 47], although most involved the PEGylation of the dendrimers to make LPDH [46, 47], and the only reports for antibiotics have been through PEGylation of PAMAM dendrimers [48, 49]. This highlights the feasibility and importance of developing LPDH for delivery of antibiotics.

Nano-systems are being designed to respond to specific site of a disease condition for the targeted delivery of drugs. Liposomes are such drug delivery systems due to the versatility in their formulation of stimuli responsive biomaterials, which can be incorporated for site specific delivery of drugs [50]. Studies report that they have been engineered to possess distinctive properties, such as: long systemic circulation to target specific cells and receptors, respond to various stimuli, such as redox environment, and a change in temperature and pH, with most of the reports being for cancer delivery [51, 52]. Current pH responsive liposomal systems for antibiotics delivery includes: gentamycin [53], which employed phospholipid-cholesterol hemisuccinate as pH responsive material, and for vancomycin, where intramolecular protonation and deprotonation of Zwitterionic lipids was responsible for pH response, as reported by our and other research groups [54]. The treatment of *S. aureus* infections is often problematic, due to the slow response to therapy and the high frequency of infection recurrence. This is as a result of the ability of the bacteria to localize the endosomes and phagolysosomes of the cells that are acidic, thereby making them their reservoirs [55] to form small colony variants in persistent infections (SCVs). These SCVs are shielded from the drugs, as they find

it difficult to penetrate inside the cells [56]. Due to their membrane fusogenic ability, liposomes can effectively be employed in the intracellular delivery of antibiotics, and with the addition of pH responsive properties, they can also target the acidic phagolysosomes, which acts as reservoir of intracellular MRSA [57]. Therefore, designing liposomal systems that are pH responsive and have cell wall penetration could prove to be useful in eliminating the SCVs.

Nanosuspensions are solid dispersions of drugs in the sub-micron scale that are suspended in liquid vehicles, with the particles being stabilized with surfactants, polymers or both [58]. Nano-suspensions offer increased dissolution rates, enhanced bioavailability and activity, and complete entrapment of insoluble drugs by forming stable solid dispersions in their amorphous state [59]. More than 40% of NCEs (new chemical entities) developed in the pharmaceutical industry are practically insoluble in water, this being a major challenge for formulation scientists [59]. As described by the Noyes–Whitney, and Kelvin and Ostwald-Freundlich equations, particle size reduction can lead to increased dissolution rate and absorption due to greater surface area, amplified dissolution pressure and increased adhesiveness to surfaces/cell membranes [60-62]. Nanosuspensions have been successfully used to improve the activity of a wide range of anti-infectives, such as triclosan, ciprofloxacin, itraconazole and miconazole [63-65]. Despite fusidic acid (FA) being an effective agent against gram positive bacteria, there has been only one report for enhancing its solubility and activity using nano-micelles, moreover, it involved the use of a newly synthesized material i.e. polyester dendrimers [66]. A Nano-precipitation antisolvent technique used to formulate nanosuspensions has shown to have advantages, such as little energy input, readily available machinery and easy scale-up. It also allows for the preparation of nano-suspensions without the use of additional specialized materials, such as the reported study. Thus, delivery via nanosuspensions could be an alternative method for delivering drugs with water solubility and enhanced activity.

An improved delivery of antibiotics can be achieved via the proposed novel drug delivery systems, especially for vancomycin (VCM) and FA. Vancomycin is a glycopeptide antibiotic that acts by inhibiting the biosynthesis of peptidoglycan and the assembly of N-acetyl muramic acid – N-acetyl glucosamine (NAM-NAG)-polypeptide, resulting in a less rigid and more permeable peptidoglycan layer in the bacteria [67]. It is currently used in the treatment and prophylaxis of serious and fatal infections caused by Gram-positive bacteria, such as *S. aureus* and other *Staphylococcus* species that remain unresponsive to other antibiotics therapy [68]. The increasing occurrence of MRSA, with a simultaneous decrease in the susceptibility of *S.*

aureus to vancomycin, increases the chances of develop VCM resistant *S. aureus* (VRSA), which is just as life-threatening as MRSA, but harder to treat [69, 70]. FA is a fusidane antibiotic that is derived from *Fusidium coccineum* and is a tetracyclic triterpenoid, active against a wide range of bacteria, has low toxicity and a unique mechanism of action that lacks significant cross resistance to other antibacterial classes [71, 72]. An increase in the rate of global antimicrobial resistance has promogulated research interest in FA, even in markets where it lacked registration, for example, the USA, and it is in clinical trials for approval as a potentially valuable therapeutic option [73, 74]. Therefore, the purpose of this study was to improve the antibacterial performance of VCM and FA using LPDHs derived nanovesicles, advanced liposomes with “On and Off” pH responsive switches, and nano-suspension systems against *S. aureus* and MRSA. Therefore, Chapters 3, 4 and 5 represents the first efforts undertaken on the development of new nanosystem to efficiently deliver antibiotics against methicillin susceptible and resistant *S. aureus*.

1.3 Problem statement

Infectious diseases, including bacterial infections, continue to be a significant cause of morbidity and mortality globally. Conventional dosage forms have several limitations, including inadequate drug concentration at infection/target sites, exposure to normal flora, fast degradation and quick elimination in the bloodstream, high frequency of administration, severe side effects and poor patient compliance. These factors contribute to suboptimal therapeutic outcomes and the current global antimicrobial resistance crisis. Nano-drug delivery systems are showing significant potential for overcoming the limitations associated with conventional dosage forms. The identification of novel nano-based strategies to enhance antibacterial activity and therapy, and to target infection sites, can therefore contribute to enhancing patient therapy and disease treatments. The design and synthesis of advanced materials and nanobased strategies for developing nanoformulations is necessary to improve antibacterial activity of currently available antibiotics.

1.4 Aims and objectives of this study

The broad aim of this study was to design advanced materials and explore nano-based strategies for preparations of nano drug delivery systems to treat *S. aureus* and MRSA infections. The specific research aims of the three novel nano-formulations developed in this study for enhancing antibacterial activity are highlighted with their respective Objectives.

Aim 1

This study aimed was to synthesize a novel linear block copolymer dendrimer hybrid star polymer by modifying the generation one poly ester amine dendrimer (G1-PEA) with a diblock copolymer of methoxy poly (ethylene glycol)-b-poly(ϵ -caprolactone) (mPEG-b-PCL) to yield (3-mPEA) and explore its potential for delivering antimicrobials via nanovesicles

In order to achieve this aim, the objectives of the study were to:

1. Use a five-step synthetic scheme to synthesize linear block copolymer dendrimer hybrid 3 arm star polymer (3-mPEA).
2. Characterise 3-mPEA using structural elucidation techniques such as FT-IR, ^1H NMR and ^{13}C NMR, gel permeation chromatography and MALDI-TOF.
3. Determine the *in vitro* toxicity of the synthesized 3-mPEA safety to confirm its use in biological systems.
4. Formulate VCM loaded nanovesicles from 3-mPEA and evaluate the formulated nanovesicles in terms of size, PDI, zeta potential, morphology, entrapment efficiency, *in vitro* drug release, flow cytometry *in vitro* and *in vivo* antibacterial activity.
5. Perform molecular dynamics simulation to understand the mechanism of the vesicle's formation.
6. Determine the binding affinity of 3-mPEA and nanovesicles to human serum albumin (HSA) to indicate its potential for long circulation.

Aim 2

This study aimed to synthesize a novel Oleic acid based quaternary lipid (QL) and employ it in formulating liposomes having “On and Off” pH responsive switches for infection site-specific delivery of antibiotics.

In order to achieve this aim, the objectives of the study were to:

1. Synthesize the quaternary lipid (QL) and characterise it using structural elucidation techniques such as FT-IR, ^1H NMR and C^{13} NMR.
2. Determine the *in vitro* toxicity of the synthesized QL lipid safety to confirm its use in biological systems.
3. Formulate VCM loaded liposomes with On and Off pH responsive switches and evaluate them in terms of size, PDI, zeta potential, morphology, entrapment efficiency, *in vitro* drug release, *in vitro* and *in vivo* antibacterial activity.

4. Perform molecular dynamics simulation to understand the mechanism of “On and Off” pH responsive switches of the liposome.
5. Determine the efficacy of the liposome in clearing intracellular MRSA in macrophages and HEK 293 cells.
6. Perform molecular dynamics simulation of the QL lipid with a model bacterial membrane to determine the binding affinity of the lipids towards gram positive bacteria.

Aim 3

This study aimed to prepare a nanosuspension (FA-NS) of FA to simultaneously enhance its aqueous solubility and antibacterial activity against *S. aureus* and MRSA.

In order to achieve this aim, the objectives of the study were to:

1. Screen different surfactants available in the market to identify a potential surfactant to provide a stable nanosuspension.
2. Optimise formulating parameters for preparing a stable fusidic acid nanosuspension (FA-NS) and characterise it in terms of particle size, polydispersity index, zeta potential, surface morphology, differential scanning calorimetry (DSC), X-ray diffraction (XRD), Fourier-transform infrared (FT-IR) spectroscopy, flow cytometry, *in vitro* and *in vivo* antimicrobial activity, aqueous solubility and stability.
3. Perform molecular dynamics simulations to identify the possible interactions of the surfactant with drug and the energy components that contribute to the stability of the nanosuspension.

1.5 Novelty of the study

The novelty of the work is presented in the three experimental studies.

Aim 1

The research work performed in this study is novel for the following reasons:

There are several reports of drug delivery using linear dendrimer hybrid star polymers, with most reports having been via PEGylation of PAMAM dendrimers. This research was the first report of drug delivery of any class of drug using linear copolymer dendrimer hybrid star polymer comprising of generation one Poly ester amine dendrimer (G1-PEA) with a diblock copolymer of methoxy poly (ethylene glycol)-b-poly(ϵ -caprolactone) (mPEG-b-PCL)

Although there are several reports on the synthesis of linear polymers and dendrimers, a 3-mPEA linear dendrimer hybrid star polymer is a novel material and has not been reported in the literature for any medical application.

The use of linear dendrimers hybrids is widely reported in the literature for cancer drugs and gene delivery. This research was the first report of the delivery of an antibiotic using a linear dendrimer hybrid star polymer.

There are several methods in the literature for evaluating the binding affinity of materials to human serum albumin. Microscale Thermophoresis is a state of the art technique that is very sensitive and precise and is being used in the pharmaceutical and biomedical industry to assess interactions and binding affinities. This research is the first report to evaluate the binding affinity of materials to human serum albumin using Microscale Thermophoresis.

Aim 2

The research work performed in this study is novel for the following reasons:

This paper reports the synthesis of a novel oleic acid quaternary lipid QL lipid that has not been reported in the literature for application in delivering any class of drug.

For delivery of drugs using liposomes with pH responsive lipids, all reports have involved intramolecular protonation and deprotonation of the lipids due to changes in pH. There are no reports of employing a supramolecular electrostatic complex that forms acid sensitive switches that results in a pH responsive liposome for targeted delivery of antibiotics. This research is the first report of drug delivery of any class of drug via liposomes with “On and Off” pH response switches for the targeted delivery of antibiotics.

Intracellular bacterial infections are troublesome to treat, as bare drugs have low penetration inside the cells. Intracellular bacteria use acidic phagolysosomes and endosomes as reservoirs. There have been several reports to address this problem with liposomes, as they are fusogenic and have good membrane penetrability. This paper reports for the first time the targeting of intracellular bacterial infections using a pH responsive liposome with “On and Off” switches, which has never been reported before. The acidic pH of phagolysosomes and endosomes will switch-On the pH depended release of the drug of the liposomes, resulting in a clearance of intracellular bacteria.

Aim 3

The research work conducted in this study is novel for the following reasons:

Despite FA being an effective antibiotic, there is only one report for enhancing its solubility using the synthesis of polyester dendrimers. This is the first report using surfactants available in the market (Poloxamer 188) to enhance aqueous solubility of FA.

Although various nanosuspensions have been reported for antibiotic drugs of BCS class II drugs for enhancing aqueous solubility, this study reports for the first time a novel nanosuspension of FA stabilized by Poloxamer 188 (P188) for simultaneously enhancing aqueous solubility and antibacterial activity.

1.6 Rationale of the study

The nano drug delivery approaches developed in this study are novel and can contribute to overcoming the problems of bacterial resistance to antibiotics and limitations associated with their conventional dosage forms. The significance of this study is highlighted below:

New pharmaceutical products: The proposed 3-mPEA, VCM-OA-QL lipo and FA-NS are new pharmaceutical products not yet reported that can stimulate the local pharmaceutical industries to manufacture cost-effective superior medicines.

Improved patient therapy and disease treatment: Both the proposed formulations can improve patient therapy and treatment of various diseases associated with bacterial infections by enhancing antibacterial performance, minimizing doses, lowering side effects and improving patient compliance. It can therefore contribute to enhancing the quality of lives of patients and saving lives.

Creation of new knowledge to the scientific community: The studies proposed can lead to new knowledge being generated in pharmaceutical sciences. It can include the following:

- Synthesis schemes for new materials, preparation procedures for the novel drug delivery systems and their properties *in vitro*, *in silico* and *in vivo* can contribute to creation of new scientific knowledge.
- The extensive *in vivo* testing of these novel systems can provide knowledge for *in vitro in vivo* correlations.

Stimulation of new research: The proposed V-3-mPEA, FA-NS and OA-QL-lipo systems holds great promise as nano-delivery systems and therefore can generate new potential research areas including the following:

- The newly proposed 3-mPEA can be utilized for delivery of other classes of drugs for treatment of various disease conditions such as cardiovascular diseases, HIV/AIDS, pain treatments (central nervous system related conditions), gene therapy related diseases, metabolic diseases etc.
- The newly designed FA-NS could stimulate research in the development of nanosuspensions for other BCS class II drugs as more than 40% of NCEs developed in the pharmaceutical industry are practically insoluble in water making it a major challenge for developing dosage forms.
- The elimination of intracellular MRSA with novel OA-QL liposome will stimulate research in elimination of other bacteria that hide intracellularly acting as reservoirs and source of chronic infections and resistance strains.

1.7 Overview of dissertation

The research work performed is presented in this thesis in the publication format, according to University of Kwa-Zulu Natal, College of Health Sciences guidelines. It specifies the inclusion of a brief introductory chapter, published papers and a final chapter on the conclusions. A PhD study requires at least three first authored papers, two of which must be experimental.

CHAPTER 2. BOOK CHAPTER: This chapter is a first authored book chapter titled “Amphiphilic Dendrimers for Drug Delivery” in ‘Handbook of Materials for Nanomedicine’ 2nd Edition, that has been accepted and is in press, to be published by the internationally acclaimed publisher Pan Stanford Publishing Pte, Singapore 2018, with Professor Vladimir Torchillin as the book editor. This book chapter focuses on the medical applications of amphiphilic dendrimers, such as drug delivery in various diseases, including infectious diseases. The modification of dendrimers to acquire amphiphilicity that results in improved the toxicity profile, enhanced efficiency and solubility of the loaded drugs was also discussed. The book chapter also included the design of smart drug delivery systems, and translational potential of the resulting drug delivery systems which is part of the main objective this study which involves synthesis of amphiphilic dendrimer-based system, synthesis of advanced smart materials and enhancement of efficiency and solubility antibiotics using nanobased strategies.

CHAPTER 3. EXPERIMENTAL PAPER 1: This chapter addresses Aim 1, Objectives 1- 6 and is a first authored experimental article published in an ISI international journal: Journal of Controlled Release (Impact Factor = 7.877). This article highlights the

synthesis of a novel block copolymer dendrimer star polymer hybrid, the *in vitro* toxicity evaluation, formulation of the ultra-small vesicles (V-3-mPEA) to deliver VCM, molecular dynamics simulation of the self-assembly of a novel block copolymer dendrimer star polymer hybrid, and characterization of its physical and antibacterial properties both *in vitro* and *in vivo*.

CHAPTER 4. EXPERIMENTAL PAPER 3: This chapter addresses Aim 3, Objectives 1 – 6 and is a first authored experimental article communicated to Advanced Healthcare Materials (Impact Factor 5.76.) an ISI international journal (manuscript ID advhealthmat-S-18-01827). This article highlights the synthesis of a novel fatty acid quaternary lipid, the *in vitro* toxicity evaluation, formulation of a liposome with “On and Off” pH switches (OA-QL liposome) for targeted delivery of VCM, molecular dynamics simulation of the “On and Off” mechanism of the switches and binding affinity of the lipid on a model bacterial membrane, and characterization of its physical and antibacterial properties both *in vitro* and *in vivo* of the drug loaded liposome.

CHAPTER 5. EXPERIMENTAL PAPER 2: This chapter addresses Aim .2, Objectives 1 - 3 and is a first authored experimental article published in the ISI international journal ACS Molecular Pharmaceutics (Impact Factor = 4.556). This article highlights the formulation development of a novel FA-NS, and the characterization of its physical properties, aqueous solubility enhancement, enhanced antibacterial activity against methicillin sensitive and resistant *S. aureus* both *in vitro* and *in vivo*, and MD simulations on the formation of a stable nanosuspension.

CHAPTER 6. CO-AUTHORED PAPERS: In addition to the first authored experimental papers in Chapters, 3, 4 and 5 focusing on the aims 1, 2 and 3 I have also been involved in other research projects within our group as a team member. As these projects also focused on the broad aim of novel nanobased strategies to effectively treat bacterial infections, these papers have been included in the thesis. This chapter therefore includes two co-authored experimental papers and one review article published in ISI international journals: International Journal of Pharmaceutics (Impact Factor = 3.902), Journal of Biomolecular Structure & Dynamics (Impact Factor = 3.107) and Journal of Drug Delivery Science and Technology (Impact Factor = 2.297).

CHAPTER 7. CONCLUSION: This chapter includes the overall conclusions from research findings in the study, provides information on potential significance of the findings and makes recommendations for future research work in the field of strategic solutions to combat bacterial resistance to antibiotics.

1.8 References

- [1] M. Dan, Infectious diseases--the progress is huge--a lot remains to be done, in, 2009.
- [2] WHO, Diarrhoeal disease, in, world Health Organisation, 2017.
- [3] N.I. Nii-Trebi, Emerging and neglected infectious diseases: insights, advances, and challenges, *BioMed Research International*, 1 (2017) 1-15.
- [4] D. Kostova, M.J. Husain, D. Sugerman, Y. Hong, M. Saraiya, J. Keltz, S. Asma, Synergies between Communicable and Noncommunicable Disease Programs to Enhance Global Health Security, *Emerging Infectious Diseases*, 23 (2017) S40.
- [5] R.R. Roberts, B. Hota, I. Ahmad, R.D. Scott, S.D. Foster, F. Abbasi, S. Schabowski, L.M. Kampe, G.G. Ciavarella, M. Supino, Hospital and societal costs of antimicrobial-resistant infections in a Chicago teaching hospital: implications for antibiotic stewardship, *Clinical Infectious Diseases*, 49 (2009) 1175-1184.
- [6] R.R. Roberts, E.K. Mensah, R.A. Weinstein, A guide to interpreting economic studies in infectious diseases, *Clinical Microbiology and Infection*, 16 (2010) 1713-1720.
- [7] A. Fleming, Nobel Lecture, Penicillin, in, Nobel Foundation, 1945.
- [8] N. Rosenblatt-Farrell, The Landscape of Antibiotic Resistance, *Environmental Health Perspectives*, 117 (2009) A244-A250.
- [9] CDC, Antibiotic Resistance Threats in the United States, in, Centre for Disease Control, 2013.
- [10] R.o.A. Resistance, Tackling drug-resistant infections globally: final report and recommendations, in: J. O'Neill (Ed.), *Review on Antimicrobial Resistance*, 2016, pp. 1-84.
- [11] WHO, Urgent action needed to prevent a return to pre-antibiotic era: WHO, in, 2015.
- [12] M. Monaco, F.P. de Araujo, M. Cruciani, E.M. Coccia, A. Pantosti, Worldwide epidemiology and antibiotic resistance of *Staphylococcus aureus*, in: *Staphylococcus aureus*, Springer, 2016, pp. 21-56.
- [13] L.F. Reyes, S. Aliberti, P. Faverio, M.I. Restrepo, Global Burden Of Mrsa Pneumonia: An International Point-Prevalence Study, in: A62. clinical aspects of CAP, HCAP, HAP, AND VAP, *American Thoracic Society*, 2016, pp. A2089-A2089.
- [14] J. Cameron, D.L. Paterson, P.N. Britton, S.Y. Tong, L. Hall, G.R. Nimmo, C. Bennett, K. Halton, CO-MRSA Infections in Australia Cost \$3.5 B Per Annum, (2017).
- [15] WHO, WHO publishes list of bacteria for which new antibiotics are urgently needed, in, World Health Organisation, GENEVA, 2017.
- [16] L. Zhang, D. Pornpattananangkul, C.M. Hu, C.M. Huang, Development of nanoparticles for antimicrobial drug delivery, *Current Medicinal Chemistry*, 17 (2010) 585-594.
- [17] A. Sharma, D. Kumar Arya, M. Dua, G.S. Chhatwal, A.K. Johri, Nano-technology for targeted drug delivery to combat antibiotic resistance, in, Taylor & Francis, 2012, pp. 1325-1332.
- [18] D.Z. Kvesic, Product lifecycle management: marketing strategies for the pharmaceutical industry, *Journal of Medical Marketing*, 8 (2008) 293-301.
- [19] E. Power, Impact of antibiotic restrictions: the pharmaceutical perspective, *Clinical Microbiology and Infection*, 12 (2006) 25-34.
- [20] M.J. Renwick, D.M. Brogan, E. Mossialos, A systematic review and critical assessment of incentive strategies for discovery and development of novel antibiotics, *The Journal of Antibiotics*, 69 (2016) 73.
- [21] E. Cara, Novartis Becomes the Latest Pharma Company to Give Up on Antibiotics Research, in, Gizmodo, 2018.
- [22] M.S. Butler, M.A. Cooper, Antibiotics in the clinical pipeline in 2011, *The Journal of Antibiotics*, 64 (2011) 413-425.
- [23] M.S. Butler, M.A. Blaskovich, M.A. Cooper, Antibiotics in the clinical pipeline in 2013, *The Journal of Antibiotics*, 66 (2013) 571-591.
- [24] M.S. Butler, M.A.T. Blaskovich, M.A. Cooper, Antibiotics in the clinical pipeline at the end of 2015, *The Journal Of Antibiotics*, 70 (2016) 3.
- [25] B.C. Kataria, D.S. Mehta, S.J. Mehta, Trends in approval of new antimicrobial agents in India compared with the USA, *International Journal of Antimicrobial Agents*, 40 (2012) 85-86.
- [26] C. Cain, Rediscovering antibiotics, *SciBX: Science-Business eXchange*, 5 (2012).

- [27] B. Spellberg, R. Guidos, D. Gilbert, J. Bradley, H.W. Boucher, W.M. Scheld, J.G. Bartlett, J. Edwards Jr, I.D.S.o. America, The epidemic of antibiotic-resistant infections: a call to action for the medical community from the Infectious Diseases Society of America, *Clinical Infectious Diseases*, 46 (2008) 155-164.
- [28] S.B. Singh, K. Young, L.L. Silver, What is an "ideal" antibiotic? Discovery challenges and path forward, *Biochemical Pharmacology*, 133 (2017) 63-73.
- [29] M.S. Butler, M.A. Blaskovich, M.A. Cooper, Antibiotics in the clinical pipeline at the end of 2015, *The Journal of antibiotics*, 70 (2017) 3.
- [30] J.V. Barth, G. Costantini, K. Kern, Engineering atomic and molecular nanostructures at surfaces, in: *Nanoscience And Technology: A Collection of Reviews from Nature Journals*, World Scientific, 2010, pp. 67-75.
- [31] C.A. Omolo, R.S. Kalhapure, N. Agrawal, S. Rambharose, C. Mocktar, T. Govender, Formulation and Molecular Dynamics Simulations of a Fusidic Acid Nanosuspension for Simultaneously Enhancing Solubility and Antibacterial Activity, *Molecular Pharmaceutics*, 15 (2018) 3512-3526.
- [32] K.A. Hamblin, S.J. Armstrong, K.B. Barnes, C. Davies, T. Laws, J.D. Blanchard, S.V. Harding, H.S. Atkins, Inhaled Liposomal Ciprofloxacin Protects against a Lethal Infection in a Murine Model of Pneumonic Plague, *Frontiers in Microbiology*, 8 (2017) 91.
- [33] J.M. Caster, A.N. Patel, T. Zhang, A. Wang, Investigational nanomedicines in 2016: a review of nanotherapeutics currently undergoing clinical trials, *Wiley Interdisciplinary Reviews: Nanomedicine and Nanobiotechnology*, 9 (2017) e1416.
- [34] M. BioPharma, MAT2501: LNC Formulation of Amikacin, in, *Matinas BioPharma*.
- [35] B. Mukherjee, N.S. Dey, R. Maji, P. Bhowmik, P.J. Das, P. Paul, Current status and future scope for nanomaterials in drug delivery, in: *Application of Nanotechnology in Drug Delivery*, InTech, 2014, pp. 525-544.
- [36] H. Yang, J.J. Morris, S.T. Lopina, Polyethylene glycol–polyamidoamine dendritic micelle as solubility enhancer and the effect of the length of polyethylene glycol arms on the solubility of pyrene in water, *Journal of Colloid and Interface Science*, 273 (2004) 148-154.
- [37] Y. Wang, G. Qi, J. He, Unimolecular Micelles from Layered Amphiphilic Dendrimer-Like Block Copolymers, *ACS Macro Letters*, 5 (2016) 547-551.
- [38] J. Del Barrio, L. Oriol, C. Sánchez, J.L. Serrano, A.I. Di Cicco, P. Keller, M.-H. Li, Self-assembly of linear– dendritic diblock copolymers: from nanofibers to polymersomes, *Journal of the American Chemical Society*, 132 (2010) 3762-3769.
- [39] W. Jiang, Y. Zhou, D. Yan, Hyperbranched polymer vesicles: from self-assembly, characterization, mechanisms, and properties to applications, *Chemical Society Reviews*, 44 (2015) 3874-3889.
- [40] Y. Zhou, D. Yan, Supramolecular Self-Assembly of Giant Polymer Vesicles with Controlled Sizes, *Angewandte Chemie International Edition*, 43 (2004) 4896-4899.
- [41] S.J. Guillaudeu, M.E. Fox, Y.M. Haidar, E.E. Dy, F.C. Szoka, J.M. Fréchet, PEGylated dendrimers with core functionality for biological applications, *Bioconjugate Chemistry*, 19 (2008) 461-469.
- [42] S.A. McNelles, S.D. Knight, N. Janzen, J.F. Valliant, A. Adronov, Synthesis, radiolabeling, and in vivo imaging of PEGylated high-generation polyester dendrimers, *Biomacromolecules*, 16 (2015) 3033-3041.
- [43] X. Li, M. Takashima, E. Yuba, A. Harada, K. Kono, PEGylated PAMAM dendrimer–doxorubicin conjugate-hybridized gold nanorod for combined photothermal-chemotherapy, *Biomaterials*, 35 (2014) 6576-6584.
- [44] S. Aryal, M. Prabakaran, S. Pilla, S. Gong, Biodegradable and biocompatible multi-arm star amphiphilic block copolymer as a carrier for hydrophobic drug delivery, *International Journal of Biological Macromolecules*, 44 (2009) 346-352.
- [45] Y.-Y. Jiang, G.-T. Tang, L.-H. Zhang, S.-Y. Kong, S.-J. Zhu, Y.-Y. Pei, PEGylated PAMAM dendrimers as a potential drug delivery carrier: in vitro and in vivo comparative evaluation of covalently conjugated drug and noncovalent drug inclusion complex, *Journal of Drug Targeting*, 18 (2010) 389-403.

- [46] W. Xiao, J. Luo, T. Jain, J.W. Riggs, H.P. Tseng, P.T. Henderson, S.R. Cherry, D. Rowland, K.S. Lam, Biodistribution and pharmacokinetics of a telodendrimer micellar paclitaxel nanoformulation in a mouse xenograft model of ovarian cancer, *International Journal of Nanomedicine*, 7 (2012) 1587.
- [47] Y. Zhang, C. Xiao, M. Li, J. Ding, C. Yang, X. Zhuang, X. Chen, Co-delivery of doxorubicin and paclitaxel with linear-dendritic block copolymer for enhanced anti-cancer efficacy, *Science China Chemistry*, 57 (2014) 624-632.
- [48] P. Dineshkumar, T. Panneerselvam, K. Deepti Brundavani, K. Selvaraj, P. Vijayaraj Kumar, Formulation of Rifampicin Loaded PEGylated 5.0 G EDA-PAMAM Dendrimers as Effective Long-Duration Release Drug Carriers, *Current Drug Therapy*, 12 (2017) 115-126.
- [49] M.A. Mintzer, E.L. Dane, G.A. O'Toole, M.W. Grinstaff, Exploiting dendrimer multivalency to combat emerging and re-emerging infectious diseases, *Molecular Pharmaceutics*, 9 (2011) 342-354.
- [50] B.S. Pattni, V.V. Chupin, V.P. Torchilin, New developments in liposomal drug delivery, *Chemical Reviews*, 115 (2015) 10938-10966.
- [51] Y. Lee, D. Thompson, Stimuli-responsive liposomes for drug delivery, *Wiley Interdisciplinary Reviews: Nanomedicine and Nanobiotechnology*, 9 (2017).
- [52] H. Xing, C.L. Zhang, G. Ruan, J. Zhang, K. Hwang, Y. Lu, Multimodal Detection of a Small Molecule Target Using Stimuli-Responsive Liposome Triggered by Aptamer-Enzyme Conjugate, *Analytical Chemistry*, 88 (2016) 1506-1510.
- [53] C. Cordeiro, D.J. Wiseman, P. Lutwyche, M. Uh, J.C. Evans, B.B. Finlay, M.S. Webb, Antibacterial efficacy of gentamicin encapsulated in pH-sensitive liposomes against an in vivo *Salmonella enterica* serovar typhimurium intracellular infection model, *Antimicrobial Agents and Chemotherapy*, 44 (2000) 533-539.
- [54] M. Jadhav, R.S. Kalhapure, S. Rambharose, C. Mocktar, S. Singh, T. Kodama, T. Govender, Novel lipids with three C18-fatty acid chains and an amino acid head group for pH-responsive and sustained antibiotic delivery, *Chemistry and Physics of Lipids*, (2018).
- [55] D.J. Hackam, O.D. Rotstein, W.-J. Zhang, N. Demaurex, M. Woodside, O. Tsai, S. Grinstein, Regulation of Phagosomal Acidification DIFFERENTIAL TARGETING OF Na⁺/H⁺ EXCHANGERS, Na⁺/K⁺-ATPases, AND VACUOLAR-TYPE H⁺-ATPases, *Journal of Biological Chemistry*, 272 (1997) 29810-29820.
- [56] F.D. Lowy, *Staphylococcus aureus* infections, *New England journal of medicine*, 339 (1998) 520-532.
- [57] T.-T. Lãm, B. Giese, D. Chikkaballi, A. Kühn, W. Wolber, J. Pané-Farré, D. Schäfer, S. Engelmann, M. Fraunholz, B. Sinha, Phagolysosomal integrity is generally maintained after *Staphylococcus aureus* invasion of nonprofessional phagocytes but is modulated by strain 6850, *Infection and Immunity*, 78 (2010) 3392-3403.
- [58] S. Verma, D. Burgess, Solid nanosuspensions: the emerging technology and pharmaceutical applications as nanomedicine, in: *Pharmaceutical Suspensions*, Springer, 2010, pp. 285-318.
- [59] S. Kalepu, V. Nekkanti, Insoluble drug delivery strategies: review of recent advances and business prospects, *Acta Pharmaceutica Sinica B*, 5 (2015) 442-453.
- [60] K.R. Chu, E. Lee, S.H. Jeong, E.-S. Park, Effect of particle size on the dissolution behaviors of poorly water-soluble drugs, *Archives of Pharmacal Research*, 35 (2012) 1187-1195.
- [61] B. Van Eerdenbrugh, J. Vermant, J.A. Martens, L. Froyen, J.V. Humbeek, G. Van den Mooter, P. Augustijns, Solubility increases associated with crystalline drug nanoparticles: methodologies and significance, *Molecular pharmaceutics*, 7 (2010) 1858-1870.
- [62] B.E. Rabinow, Nanosuspensions in drug delivery, *Nature Reviews Drug Discovery*, 3 (2004) 785.
- [63] M. Ansari, M. Althubaiti, M. Ibnouf, M. Anwer, M. Ahmed, F. Fatima, S. Jamil, Enhanced anti-bacterial effects of ciprofloxacin enclosed in cyclodextrin and nano-suspension carrier systems, *Bulletin of Environment, Pharmacology and Life Sciences*, 4 (2015) 11-14.
- [64] J. Parmentier, E.H. Tan, A. Low, J.P. Möschwitzer, Downstream drug product processing of itraconazole nanosuspension: Factors influencing drug particle size and dissolution from nanosuspension-layered beads, *International Journal of Pharmaceutics*, 524 (2017) 443-453.

- [65] K. Tahara, M. Nishikawa, K. Matsui, K. Hisazumi, R. Onodera, Y. Tozuka, H. Takeuchi, In Vitro and In Vivo Characterization of Drug Nanoparticles Prepared Using PureNano™ Continuous Crystallizer to Improve the Bioavailability of Poorly Water Soluble Drugs, *Pharmaceutical Research*, 33 (2016) 2259-2268.
- [66] D.R. Sikwal, R.S. Kalhapure, M. Jadhav, S. Rambharose, C. Mocktar, T. Govender, Non-ionic self-assembling amphiphilic polyester dendrimers as new drug delivery excipients, *RSC Advances*, 7 (2017) 14233-14246.
- [67] S.P. Chakraborty, S.K. Sahu, P. Pramanik, S. Roy, In vitro antimicrobial activity of nanoconjugated vancomycin against drug resistant *Staphylococcus aureus*, *International Journal of Pharmaceutics*, 436 (2012) 659-676.
- [68] E. Bouza, M. Valerio, A. Soriano, L. Morata, E.G. Carus, C. Rodríguez-González, M.C. Hidalgo-Tenorio, A. Plata, P. Muñoz, A. Vena, Dalbavancin in the treatment of different gram-positive infections: a real-life experience, *International Journal of Antimicrobial Agents*, 51 (2018) 571-577.
- [69] R. Hasan, M. Acharjee, R. Noor, Prevalence of vancomycin resistant *Staphylococcus aureus* (VRSA) in methicillin resistant *S. aureus* (MRSA) strains isolated from burn wound infections, *Tzu-Chi Medical Journal*, 28 (2016) 49-53.
- [70] W.A. McGuinness, N. Malachowa, F.R. DeLeo, Vancomycin Resistance in *Staphylococcus aureus*, *The Yale Journal of Biology and Medicine*, 90 (2017) 269-281.
- [71] J. Turnidge, Fusidic acid pharmacology, pharmacokinetics and pharmacodynamics, *International Journal of Antimicrobial Agents*, 12 (1999) S23-S34.
- [72] A. Huttner, S. Harbarth, 149 - Miscellaneous Agents: Fusidic Acid, Nitrofurantoin and Fosfomycin, in: J. Cohen, W.G. Powderly, S.M. Opal (Eds.) *Infectious Diseases (Fourth Edition)*, Elsevier, 2017, pp. 1277-1279.e1271.
- [73] D.J. Farrell, R.E. Mendes, M. Castanheira, R.N. Jones, Activity of Fusidic Acid Tested Against *Staphylococci* Isolated From Patients in United States Medical Centers During 2014, *Antimicrobial Agents and Chemotherapy*, (2016) AAC. 00238-00216.
- [74] J.C. Craft, S.R. Moriarty, K. Clark, D. Scott, T.P. Degenhardt, J.G. Still, G.R. Corey, A. Das, P. Fernandes, A randomized, double-blind phase 2 study comparing the efficacy and safety of an oral fusidic acid loading-dose regimen to oral linezolid for the treatment of acute bacterial skin and skin structure infections, *Clinical Infectious Diseases*, 52 (2011) S520-S526.

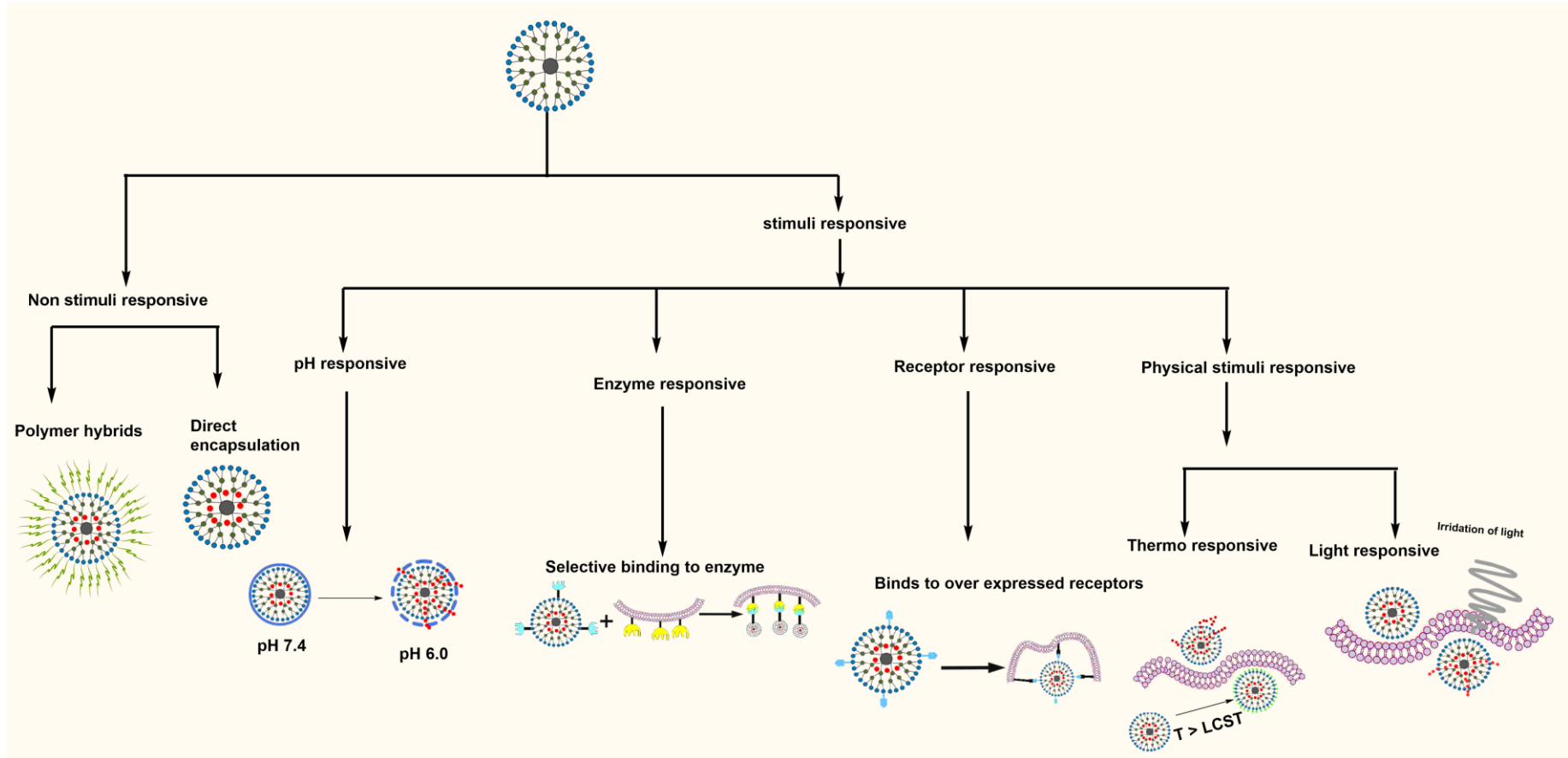
CHAPTER 2, BOOK CHAPTER

2.1 Introduction

This chapter is a first authored book chapter titled “Amphiphilic Dendrimers for Drug Delivery” in ‘Handbook of Materials for Nanomedicine’ 2nd Edition, that has been accepted (appendix I) and is in press, to be published by the internationally acclaimed publisher Pan Stanford Publishing Pte, Singapore 2018, with Professor Vladmir Torchillin as the book editor. This book chapter focuses on the medical applications of amphiphilic dendrimers, such as drug delivery in various diseases, including infectious diseases. The modification of dendrimers to acquire amphiphilicity that results improved the toxicity profile, enhanced efficiency and solubility of the loaded drugs was also discussed. The book chapter includes the design of smart drug delivery systems, and translational potential of the resulting drug delivery systems which is part of the main objective this study that involves synthesis of amphiphilic dendrimer-based system, synthesis of advanced smart materials and enhancement of efficiency and solubility antibiotics using nanobased strategies.

2.2 Graphical abstract

Amphiphilic dendrimers



2.3 Book Chapter

Amphiphilic Dendrimers for Drug Delivery

Calvin A. Omolo¹, Rahul S Kalhapure^{1,2,#}, Dhiraj R Sikwal^{1,3}, Thirumala Govender^{1,#}

1. Department of Pharmaceutical Sciences, University of KwaZulu-Natal, Private Bag X54001, Durban 4000, South Africa.
2. School of Pharmacy, The University of Texas at El Paso, 500 W. University Ave, El Paso, Texas, 79968, USA.
3. Shivlingeshwar College of Pharmacy, Deelip Nagar, Almala, Tq. Ausa, Dist. Latur, Maharashtra 513520, India.

corresponding author: Private Bag X54001 Durban, 4000, KwaZulu-Natal, South Africa.

Tel: 00 27 31 260 7358, Fax: 0027 31 260 7792

Email address: govenderth@ukzn.ac.za; rkalhapure@utep.edu, rahul.kalhapure@rediffmail.com

2.1 INTRODUCTION

The development of performance efficient and safe drug carriers for various purposes, such as reduced toxicity, controlled release and targeted delivery, is an active area of research among pharmaceutical and biomedical scientific communities. In this context, scientists have shown the potential of dendrimers, tree-like monodisperse polymers, as promising drug delivery vehicles. For instance, polyamidoamine (PAMAM) dendrimers have proven to be versatile vehicle candidates for nano drug delivery systems, especially in the field of diagnostics and cancer treatment (Márquez-Miranda et al., 2016). The main reasons that justify the use of dendrimers in drug delivery can be summarized as their multivalency, uniform size, water solubility, internal cavities and modifiable surface functionalities (Lin, Jiang and Tong, 2010). It is also possible that the nanometric size of dendrimers may induce enhanced permeation and retention effect (Caminade and Turrin, 2014). PAMAM dendrimers, were the first family of dendrimers brought into existence by Tomalia et al. in 1985. This class of materials have been widely studied as symmetrical conventional dendrimers for their applications in drug and gene delivery (Kesharwani et al., 2015; Kaur et al., 2016).

Despite well-defined properties, such as high-density terminal groups and globular architecture, symmetrical conventional dendrimers have several limitations, such as toxicity, rapid systemic clearance, poor drug loading and difficulty in achieving controlled drug release (Dhiraj R. Sikwal et al., 2017). Surface modification techniques have been used by several researchers to minimize toxicity and improve performance of conventional dendrimers for application in drug delivery and biomedical sciences. One example of such surface modification is PEGylation of the peripheral amine groups of PAMAM. Limitations of PAMAM dendrimers, such as immunogenicity, systemic cytotoxicity, haemolytic toxicity and drug leakage, could be addressed by PEGylation. In addition, PEGylated PAMAM dendrimers have shown the potential to enhance the solubility of hydrophobic drugs and facilitate the potential for DNA transfection, tumour targeting and siRNA delivery (Luong et al., 2016). However, the process of surface functionalization at times leads to batch-to-batch inconsistencies in the number of attached groups at the dendrimers' surface, resulting in varying biological activities (Caminade and Turrin, 2014; D.R. Sikwal, Kalhapure and Govender, 2017).

With an increasing interest in nanomedicine for controlled and targeted drug delivery applications, much attention has been paid to synthesizing polymeric materials that can be utilized in formulation of smart nano delivery systems. The most commonly used polymeric materials are amphiphilic block copolymers due to their ability to self-assemble in different media (Park et al., 2013; Rao, Hottinger and Khan, 2014; Avila-Salas et al., 2017). Recognizing the advantages of dendrimers over conventional block-copolymers, there has been considerable research on the synthesis and utilization of amphiphilic dendrimers in drug delivery during last the 15 years. Amphiphilic dendrimers reported so far are structural modifications of conventional dendrimers, or completely novel dendrimers synthesized using hydrophobic and hydrophilic chemical structures. These amphiphilic dendrimers have been reported to self-assemble into nano structures, such as micelles, unimolecular micelles, spherical aggregates, nanospheres and supramolecular aggregates, which can encapsulate a drug molecule. Advancements in the design, synthesis and applications of novel amphiphilic dendrimers in drug delivery sciences have also led to the introduction of novel Janus amphiphilic dendrimers that form different self-assembling structures such as dendrimersomes, and micelles. Flexibility their design has also resulted in the Janus dendrimers that are stimuli-responsive. This chapter discusses the synthesis and application of these amphiphilic dendrimers for drug and nucleic acid delivery. Emphasis has also been given on studies that will facilitate translating amphiphilic dendrimers into clinically used novel drug delivery systems.

2.2 CLASSIFICATION OF AMPHIPHILIC DENDRIMERS

Depending on the structural arrangement of hydrophilic and hydrophobic segments, amphiphilic dendrimers can be classified into: i) amphiphilic layered, ii) amphiphilic di-block or Janus, and iii) facially amphiphilic dendrimers (Fig. 1) (Wang and Scott M. Grayson, 2012).

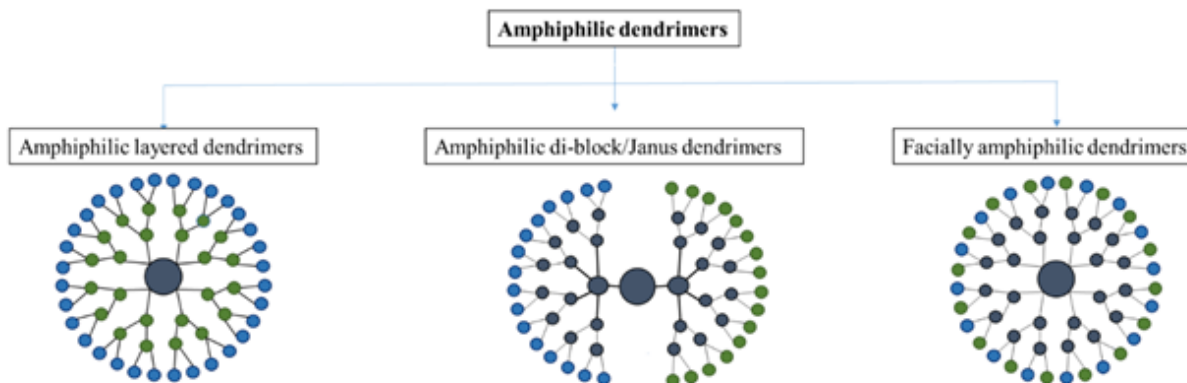


Fig.1. Classification of amphiphilic dendrimers depending on the structural arrangement of the hydrophilic and hydrophobic segments.

2.2.1 Amphiphilic layered dendrimers

Amphiphilic layered dendrimers are also known as dendritic core-shell and can be prepared by incorporating a contrasting block between different layers i.e. with hydrophobic core and hydrophilic corona or vice versa. These types of dendrimers were first synthesized by Newkome and co-workers in 1985 using a divergent technique through the functionalizing of the polar poly-ol corona on non-polar arborol core (Newkome et al., 1985). As a result of the layered structural arrangement, these amphiphilic dendrimers were able to self-assemble to form unimolecular micelles that could encapsulate hydrophobic guest molecules and maintain their carrier function under high dilution. With the introduction of these dendrimers, unimolecular self-assembly attracted attention, as single molecule can perform micelles-like properties without aggregating with other molecules. These types of unimolecular self-assemblies can be stable to various in vivo environmental changes, such as concentration variation, interaction with lipids and proteins, and flow stress, which could lead to disaggregation and early drug release (Hawker, Wooley and Frechet, 1993; Wang and Scott M Grayson, 2012). Frechet and co-workers also reported the

convergent synthesis of amphiphilic layered dendrimers with a 3,5- dihydroxybenzyl core and carboxylate end group at the periphery. These amphiphilic dendrimers were synthesized by the convergent method, where two polyether dendrons were grown convergently by using methyl p-bromomethyl benzoate as a starting material, which became a peripheral functional group with protected methyl esters. In the interior 3,5-dihydroxybenzyl alcohol as monomeric units were coupled to the methyl p-bromomethyl benzoate. This was followed by a twostep generation growth process that involved activation by bromination and propagation by alkylation. Furthermore, 2 two protected polyether dendrons were coupled together with the bifunctional core, 4,4-dihydroxybiphenyl, in the presence of K₂CO₃, after which the methyl ester groups were deprotected by alkaline hydrolysis to obtain hydrophilic carboxylate end groups (Hawker, Wooley and Frechet, 1993). Several other research groups later synthesized amphiphilic layered dendrimers, studied their self-assembly into unimolecular micelles and evaluated their capacity for encapsulating hydrophobic guest molecules (Hawker, Wooley and Frechet, 1993; Pan et al., 2005; Morgan et al., 2006).

2.2.2 Amphiphilic diblock or Janus dendrimers

Amphiphilic diblock dendrimers can be prepared by covalently bonding two different types of dendrons (hydrophobic and hydrophilic) in a single molecule. This functional arrangement provides hydrophilic and hydrophobic groups on the extreme end of the dendritic structure, that results in a broken symmetry with differing solubilities of the two contrasting regions. This offers new properties to form complexes of self-assembled structures, such as bilayer spherical assemblies that are known as dendrimersomes (Percec, Daniela A Wilson, et al., 2010). Janus dendrimers were first synthesized by Wooley and Frechet as unsymmetrically functionalized dendrimers, with the non-polar benzyl and polar benzoate functional groups possessing large dipole moments (Wooley, Hawker and Frechet, 1993). The Janus amphiphilic dendrimers could not form unimolecular micelles but acted as surfactants at oil-water interface and self-assembled into micellar aggregates. They can be synthesized by three synthetic methods: i) Chemoselective coupling, ii) heterogeneous double exponential growth method, and iii) mixed modular approach, details of which can be found elsewhere (Dhiraj R. Sikwal et al., 2017). It is envisaged that Janus dendrimers could revolutionize the drug delivery field, as their diverse applications are due to their unique characteristic features (Dhiraj R. Sikwal et al., 2017).

2.2.3 Facially amphiphilic dendrimers

Facially amphiphilic dendrimers are comprised of repeating amphiphilic monomeric units that create uniform amphiphilicity over the dendritic surface, thus polar and non-polar functionalities are distributed throughout the dendritic structure and are also referred to as amphiphilic dendritic homopolymers (Wang and Scott M. Grayson, 2012). These amphiphilic dendrimers were first described by Thayumanvan and coworkers in 2004, where they synthesized AB₂ functionalized facially amphiphilic dendrimers via a biaryl monomer composed of a carboxyl group as polar moiety, and dodecyl chain as the non-polar moiety. Fig. 2 represents the structure of facially amphiphilic dendrimer reported by Thayumanavan et al. (Vutukuri, Basu and Thayumanavan, 2004).

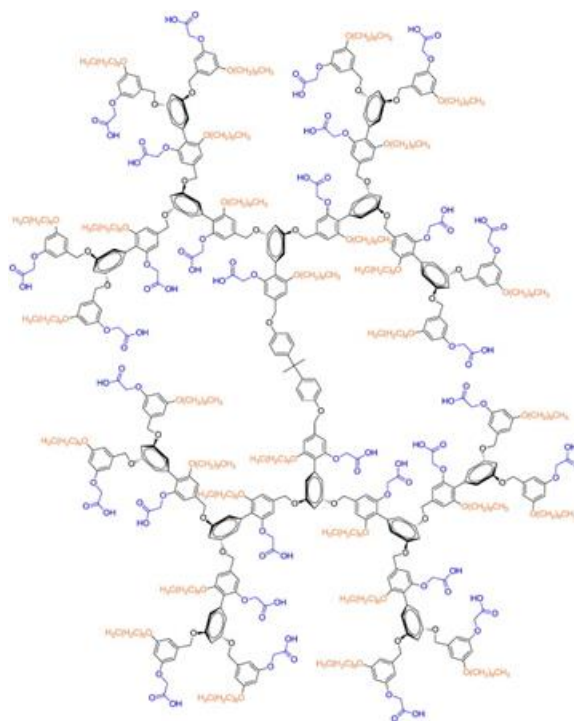


Fig 2. Facially amphiphilic dendrimer prepared by Thayumanavan and co-workers consisting of amphiphilic benzylic monomer with hydrophilic carboxylic group and hydrophobic dodecyl chains (Wang and Scott M Grayson, 2012). Reproduced with permission from Elsevier.

2.3.0 APPLICATIONS IN DRUG DELIVERY

With the advances in synthetic methodologies for dendrimers, and an increasing need by pharmaceutical scientists for controlled and targeted drug delivery, both stimuli and non-stimuli

responsive amphiphilic dendrimers have been reported in the literature for drug delivery applications. This section is divided into two major sections: non-stimuli responsive self-assembling dendrimers and stimuli-responsive self-assembling dendrimers. These major sections are both further divided into three sub-sections: i) amphiphilic layered, ii) Janus and iii) facially amphiphilic dendrimer-based drug delivery systems, depending on their classification. Finally, the section summarizes the application of low molecular weight dendritic amphiphiles in drug delivery.

2.3.1 Non-stimuli-responsive (NSR) self-assembling dendrimers

Polymeric materials based nano delivery systems provide several advantages over conventional dosage forms. For example, they protect encapsulated drugs from degradation due to acids or enzymes and minimize the required dose and side effects by providing targeted delivery (Wang and Scott M. Grayson, 2012). Self-assembly of the amphiphilic dendrimers have gained significant attention due to the formation of a wide array of morphologies, starting from simple micelles and vesicles to more complex hierarchical architectures, such as dendrimersomes, fibers, helices and tubes (Wang and Scott M Grayson, 2012). This section addresses the self-assembled architectures formed by non-stimuli responsive amphiphilic dendrimers and their utilization in drug delivery for the three classes of dendrimers discussed in this chapter. A summary of non-stimuli responsive amphiphilic dendrimers, the resulting self-assembling structures, drugs encapsulated, important findings of the studies and conclusion are given in Table 1.

2.3.1.1 Amphiphilic layered dendrimers based NSR delivery systems

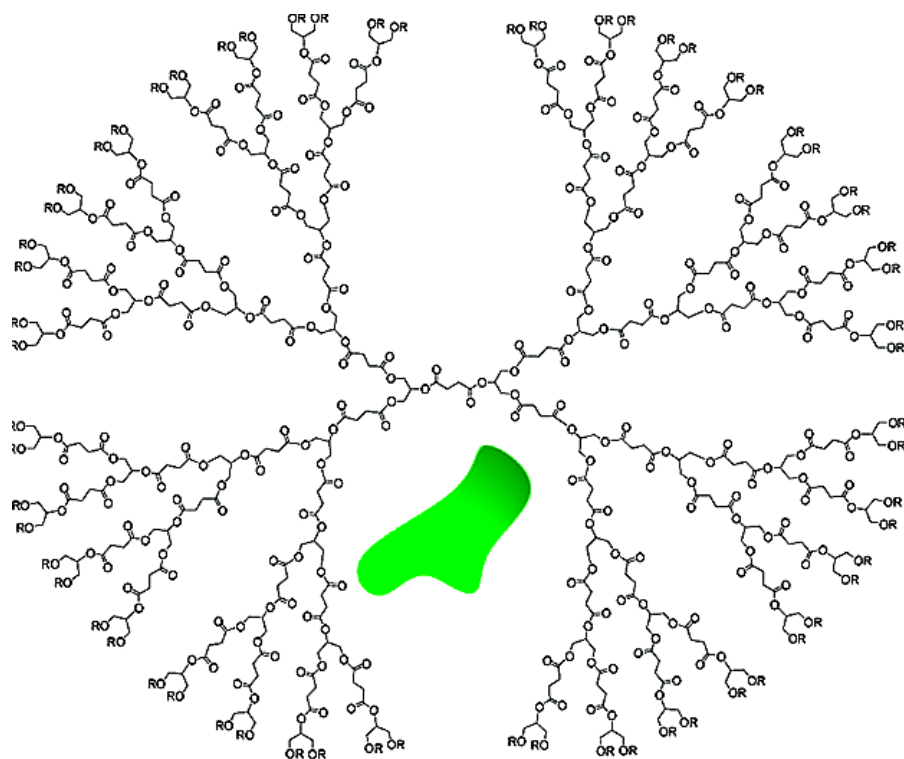
The structure of amphiphilic layered dendrimers utilizes layer-wise segregation of hydrophobic core and hydrophilic corona, thus creating specialized self-assembling structures known as unimolecular dendritic micelles (Hawker, Wooley and Frechet, 1993). These unimolecular micelles are considered to be effective micellar delivery vehicles due to their single molecular self-assembly pattern (Fan, Li and Loh, 2016).

Using the Fréchet and company design of a layer-wise segregation of hydrophobic and hydrophilic hydrophobic regions, Morgan and coworkers constructed an amphiphilic layered dendrimer from biocompatible polyester amphiphilic layered G3 and G4 poly(glycerol-succinic acid) (PGLSA) dendrimers from natural components, such as glycerol and succinic acid (Fig. 3). PGLSA-OH and

PGLSA-COONa (G3 & G4) dendrimers were synthesized divergently by propagating through esterification with 2-(cis-1,3-O-benzylidenglycerol) succinic acid and deprotecting with H₂/Pd/C (hydrogenolysis). To obtain PGLSA-COONa dendrimers, in the final synthesis step, hydroxyl terminals of PGLSA-OH were converted to carboxylate terminals by reaction with succinic anhydride in pyrene and the molecular weights for G4-PGLSA-OH and G4-PGLSA-COONa were found to be 10715 and 18500 Daltons respectively.

An aggregation study performed on G4-PGLSA-OH and G4-PGLSA-COONa by using quasi-elastic light scattering method showed the formation of unimolecular micelles. The hydrodynamic diameter of the PGLSA-OH (G4) dendrimer was found to be 7 nm, which was further reduced to 4 nm after encapsulation of Richard's dye, this decrease of the unimolecular micelles being attributed to the collapse of aliphatic the amphiphilic dendrimer around the hydrophobic dye. The G3 PGLSA amphiphilic dendrimers encapsulated approximately one dye molecule, while the G4 dendrimer showed encapsulation of two molecules of the dye, increasing the solubility of Richard's dye 2000-fold compared to water. These observations showed that an increase in glomerular structure of the amphiphilic dendrimer enhances the encapsulation efficiency.

Drug encapsulation studies were performed using 10-hydroxycamptothecin (10HCPT) as a model hydrophobic guest molecule. Encapsulation of 10HCPT was performed using G4-PGLSA-COONa, as solubilization with G4-PGLSA-OH amphiphilic dendrimers resulted in the formation of precipitate on storage. Results of the in-vitro anticancer activity against human breast cancer cell (MCF-7) demonstrated that dendrimers alone were inactive, whereas anticancer activity of 10HCPT was retained after encapsulation within the dendrimers (Cytotoxicity results as indicated in Fig. 4). The study concluded that the unimolecular micelles formed by these amphiphilic dendrimers were suitable as delivery vehicle for encapsulating hydrophobic anticancer drugs (Morgan et al., 2003).



[G4]-PGLSA-OH (1): R = H

[G4]-PGLSA-COONa (2): R = COCH₂CH₂COONa

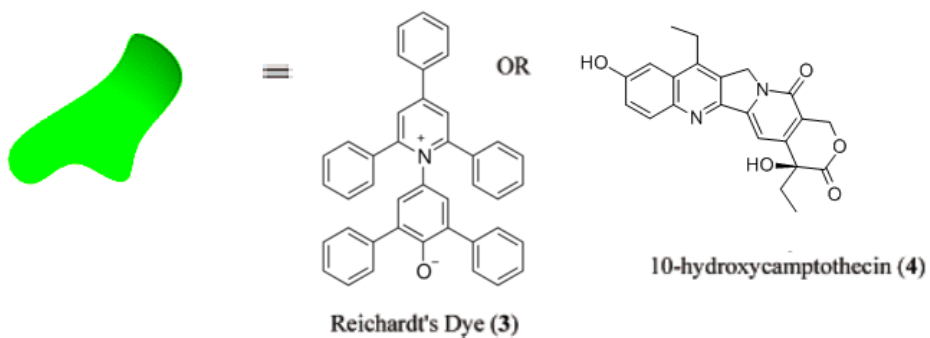


Fig. 3. Structure of G4-PGLSA dendrimers and hydrophobic guest molecules (Morgan et al., 2003). Reproduced with license from American Chemical Society.

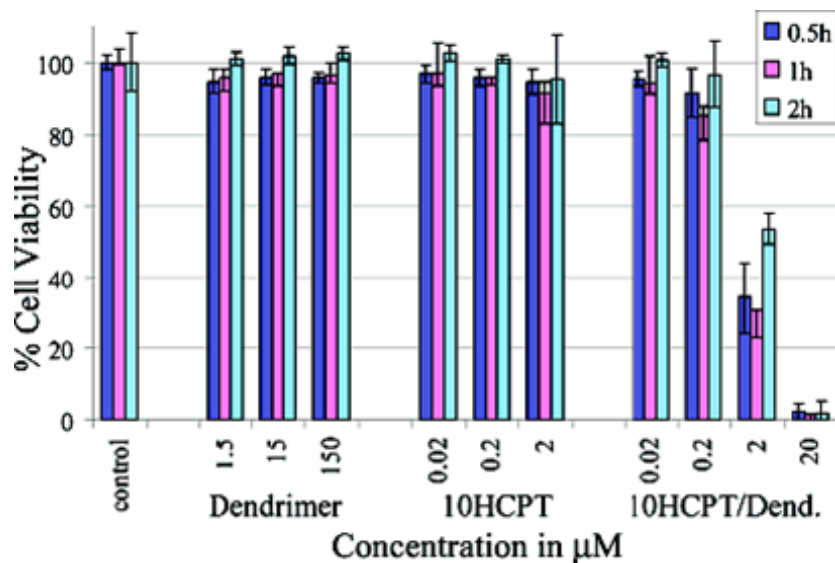


Fig. 4. Cytotoxicity assay with human breast cancer, MCF-7, cells (5000 cells/well; n) 8) (Morgan et al., 2003). Reproduced with license from American Chemical Society.

In another study, the same research group expanded the potential use of these PGLSA dendrimers to deliver poorly water soluble 7-butyl-10-aminocamptothecin (BACPT) along with 10HCPT (Morgan et al., 2006). Encapsulation studies were carried out using a solvent evaporation method, where G4-PGLSA-COONa amphiphilic dendrimers and camptothecins were used at a 1:1 ratio. The results of the encapsulation study indicated a 10 -fold solubility enhancement for 10HCPT and BACPT in amphiphilic dendrimer solution compared to water. The drug release profile of the encapsulated 10HCPT/G4-PGLSA-COONa vehicle was monitored by dialysis method using phosphate buffer solution (pH 7.4), with the drug release being complete within 6 h with linearity over the period of 2 h (release results are shown in Fig. 5. Encapsulation into the dendrimers enhanced the cytotoxic potency of both 10HCPT and BACPT towards human cancer cell lines [human breast adenocarcinoma (MCF-7), colorectal adenocarcinoma (HT-29), non-small cell lung carcinoma (NCI-H460), and glioblastoma (SF-268) (Morgan et al., 2006). The two studies reported by Morgan and co-workers provided information on the solubility and activity enhancement of the hydrophobic anticancer drug molecules by their encapsulation into self-assembled amphiphilic dendrimers, with the morphology of the formed self-assemblies not being investigated. Morphological investigations using scanning electron microscopy (SEM) and/or transmission electron microscopy (TEM) would have been helpful to understand the effect of size

and shape on encapsulation efficiency, as there were differences in the number of molecules encapsulated in the G3 and G4 PGLSA.

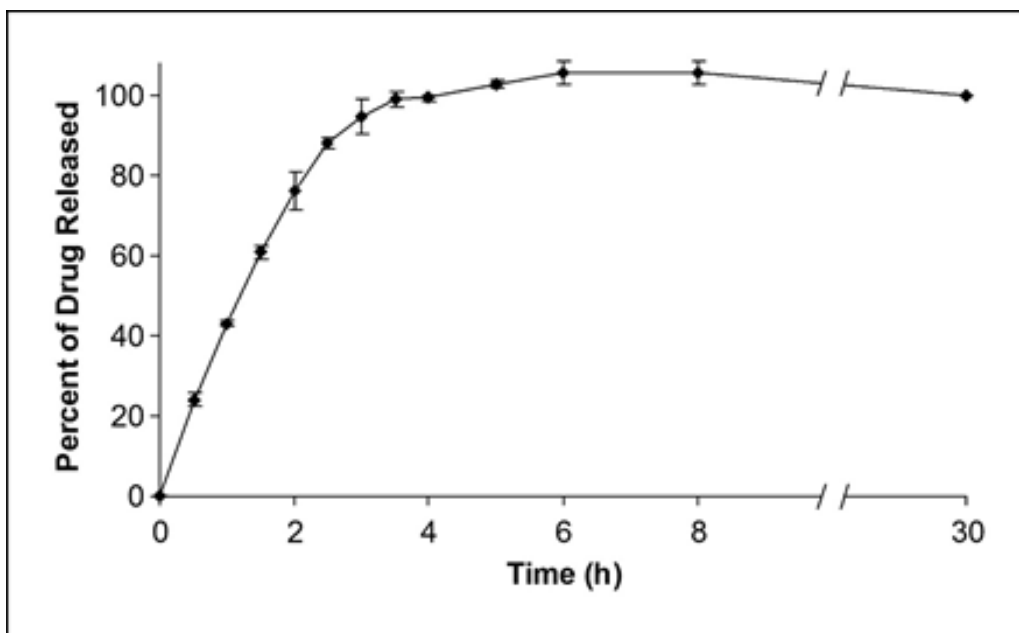


Fig. 5. Release profile of [G4.5]-PGLSA-COONa encapsulated 10HCPT. Points, mean; bars, range ($n = 2$) (Morgan et al., 2006). Reproduced with permission from American Association for Cancer Research.

Alternatively, amphiphilic layered dendrimers can also be constructed by coupling hydrophobic moieties to hydrophilic polyamidoamine (PAMAM) dendrimers to form different self-assembling nano structures. This approach was employed by Hung et al., who coupled a hydrophilic PAMAM dendron shell to the poly(L-lactide) (PLLA) core, which self-assembled to unimolecular micelles (Hung et al., 2013). Cao and Zhu applied a very similar strategy, where a hydrophilic segment of the amphiphilic PAMAM, G2 to G5 core, was attached to a hydrophobic shell of the aniline pentamer, whose self-assembled spherical aggregates formed bilayer vesicular structures (Cao and Zhu, 2011b).

Linking the block linear polymers to dendrimers has also resulted in amphiphilic layered dendrimers. Such a method was employed by Wang et al who designed a dendritic micellar system with a G2 PAMAM core, and a linear block copolymer from a poly(ϵ -caprolactone) (PCL) and poly(ethylene glycol) (PEG) shell. These PAMAM-PCL-PEG hybrids self-assembled to micelles that were able to encapsulate etoposide with 22% loading capacity. Furthermore, the cytotoxicity

assay of the hybrid against porcine kidney epithelial cells (LLC-PK) demonstrated that the PAMAM-PCL-PEG amphiphilic molecule was nontoxic, and that the entrapped drug produced significantly better anticancer effect than the free drug (Wang et al., 2005). These types of core shell assemblies could be employed to non-covalently entrap the drug within the dendrimer structure. The advantage of these systems is that the release process is not chemical dependent, but purely dependent on ‘soft-bonds’, such as the ionic pairing, hydrogen and halogen bonds, which requires lower energy interactions and more subtle conditions, such as shifts in local equilibria, to release the drug (Jain and Asthana, 2007).

2.3.1.2 Janus dendrimers based NSR delivery systems

The second sub-section will address NSR drug delivery from amphiphilic Janus dendrimers. Janus or amphiphilic segmented dendrimers consists of two dendritic blocks with different polarity, thereby providing asymmetry to the dendritic structure. This asymmetry offers the property of self-assembly into different kind of aggregates, such as micelles, supramolecular hydrogels and dendrimersomes (Dhiraj R. Sikwal, Kalhapure and Govender, 2017). In this section, aggregates with non-responsiveness will be highlighted.

Janus dendrimers that have the ability to self-assemble into micelles have been studied by Movellla et al. These Janus dendrimers based micellar drug delivery systems were employed as carriers for antimalarial drugs [chloroquine (CQ) and primaquine (PQ)]. They were developed by the self-assembly of two amphiphilic segmented dendrimers and two hybrids dendritic-linear-dendritic block co-polymer. Fig. 6 shows the structures of these amphiphilic dendrimers (A and B) and amphiphilic dendritic block copolymers (C and D), both being derived from 2,2-bis(hydroxymethyl) propionic acid (bis-MPA) monomers. The synthesis of these amphiphiles was accomplished by using the chemo selective coupling method through click chemistry, by coupling the hydrophilic glycine containing dendron with the azido end group and alkyne terminated hydrophobic stearic acid functionalized dendron. Hemolysis and in-vitro cytotoxicity studies performed on human umbilical vein endothelial cells (HUVEC) showed a very low value of IC₅₀ (1.2 to 3.5 mg/ml) for B and D. Copolymer C did not reach the IC₅₀ value even at high concentrations (14.2 mg/ml). At 2 mg/ml of the concentration, none of the amphiphiles showed hemolytic activity, indicating the biocompatibility of these structures. Micelles were prepared using these four amphiphilic dendritic derivatives by oil/water emulsification method and

encapsulated the antimalarial drugs (CQ and PQ) and fluorescent dye, Rhodamine B (rho B). High entrapment efficiency (%EE) was achieved (ca. 50 to 100) for both drugs at a drug/dendritic derivatives ratio of 5:1, with drugs %EE being highest in the Janus dendrimers A and B, whereas the %EE of rhoB was highest in dendritic polymer C and D (Movellan et al., 2014).

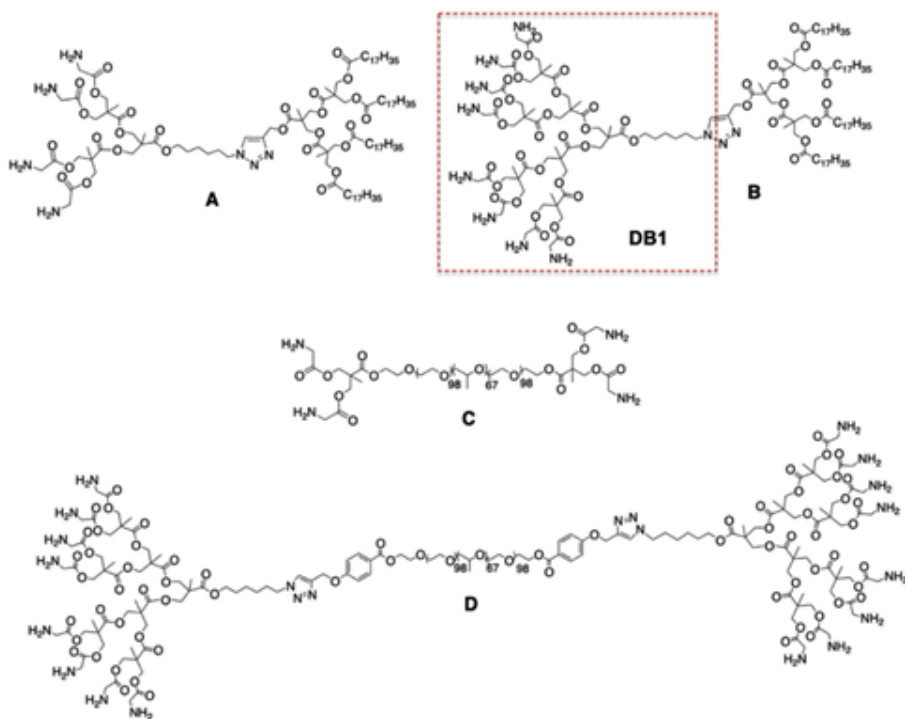


Fig 6. Structural representation of two Janus dendrimers (A, B) and two hybrid dendritic-linear-dendritic block copolymers (C and D) (Movellan et al., 2014). Scanning electron microscopy (SEM) studies showed ovoid or spherical morphologies for CQ and PQ encapsulated micelles with a mean long axes/diameters range of ca. 170 to 500 nm (Fig. 7). Reproduced with copyright permission from Elsevier

All the rhoB encapsulated nano-carriers were significantly smaller (100 to 300 nm) and more spherical compared to the antimalarial drugs encapsulated micelles. The *in vitro* activity against *P. falciparum* revealed intrinsic activity for all dendritic derivatives, and the cell targeting studies by fluorescence microscopy displayed selective targeting of these micelles to plasmodium infected RBCs compared to non-infected RBCs. These results can be accredited to the chemical interplay between the dendritic derivatives, the drug and elongated shape of the micelle (Movellan et al., 2014).

It has been reported that amphiphilic Janus dendrimers can self-assemble into fiber-like aggregates, which further arrange themselves into a supramolecular structure, as displayed in Fig. 8, and can trap water molecules to form hydrogels with outstanding mechanical properties. One such example is Janus dendrimers, which consists of G3 Bis-MPA hydrophilic dendron and alkyl gallate ether with various branching pattern [(3,4); (3, 5) and (3,4,5)] joined together via triazole linker (Fig. 9) (Nummelin et al., 2015).

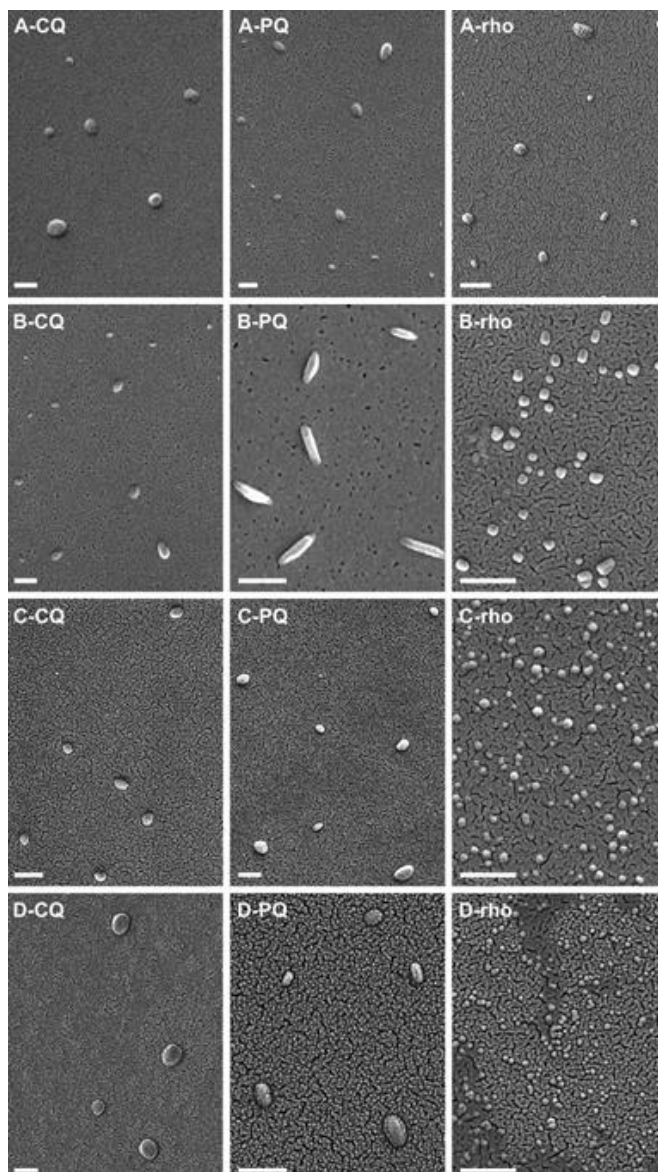


Fig. 7. Scanning electron microscopy analysis of the dendritic derivatives encapsulating chloroquine, primaquine, and rhodamine B (Movellan et al., 2014). Reproduced with copyright permission from Elsevier.

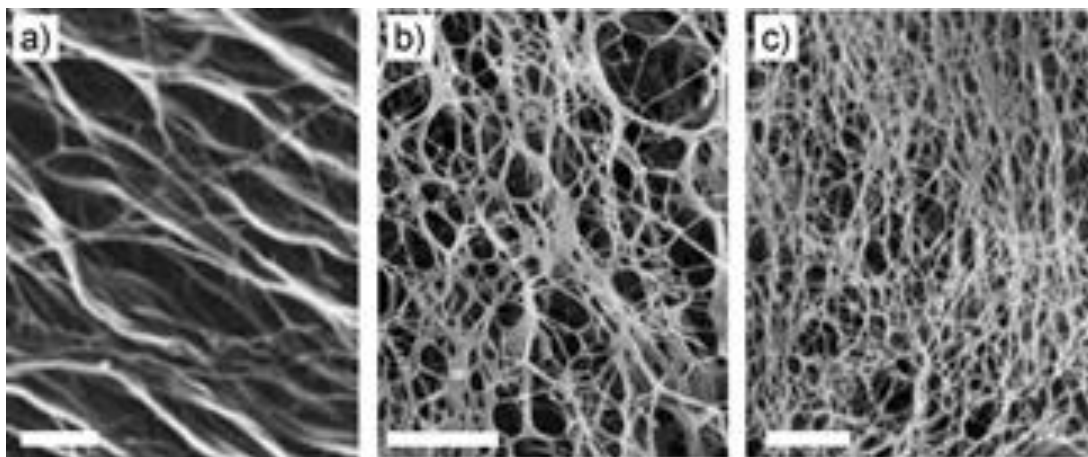


Fig. 8. SEM images of vitrified cold dried 1.0% amphiphilic dendritic hydrogel, prepared from a) (3,4), b) (3,5), and c) (3,4,5). Scale bars 1 mm (Nummelin et al., 2015). Copyright (2015) John Wiley and Sons.

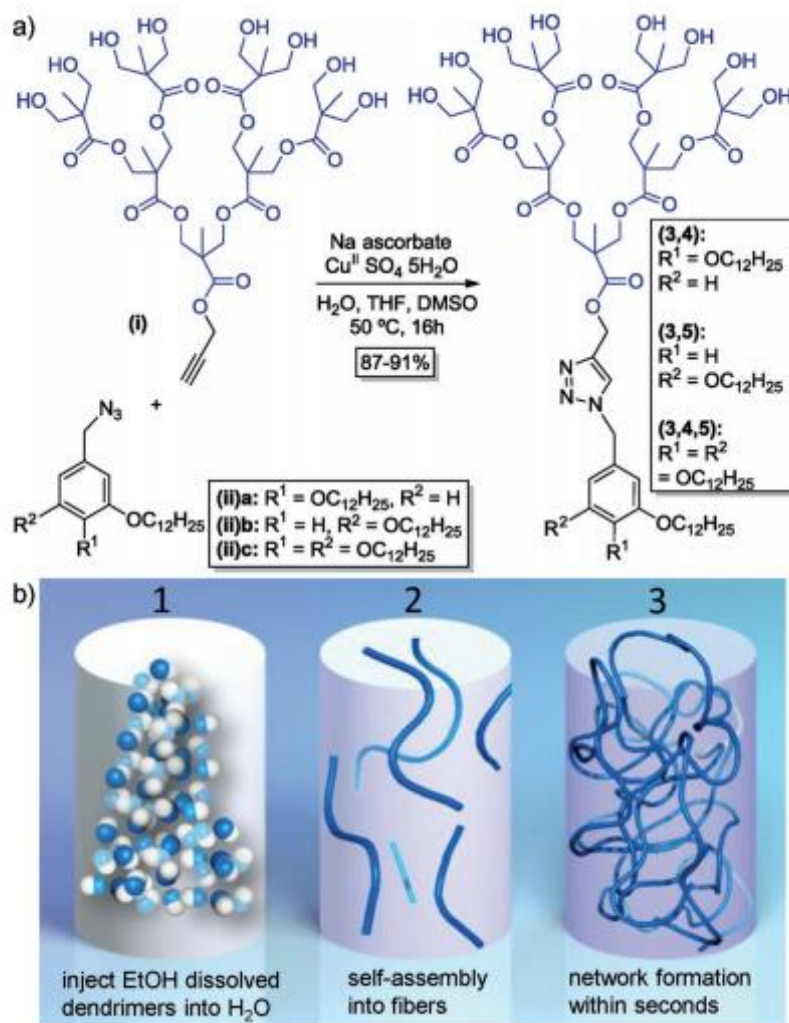


Fig. 9. a) Synthesis of amphiphilic Janus dendrimers through click chemistry, b) Schematic representation of hydrogel formation (Nummelin et al., 2015). Copyright (2015) John Wiley and Sons

The ethanolic injection of these Janus dendrimers into water caused self-assembly of the nanofibers with a thickness of 5-7 nm, which then bundled up and crosslinked with each other to form a three dimensional network (steps shown in Fig. 11b.), and further trap water molecules to form hydrogel. The authors further showed that these hydrogels were able to encapsulate a drug (nadalol), a dipeptide (gondoreline) and an active enzyme (horseradish peroxidase). Studies performed on these hydrogels showed that release of these cargo was by first order release kinetics, which was indicative of sustained release profile.

One important observation about self-assembly behavior of the Janus amphiphilic dendrimers is they can form uniform bilayered vesicular structure called dendrimersomes. Due to their unique properties, such as uniform size, tailored structure, higher vesicular stability, improved mechanical strength and easy functionalization, dendrimersomes are proposed to be more advantageous and stable nanostructures than liposomes and polymersomes (Percec et al., 2004). Percec et. al. studied the efficiency of these dendrimersomes to encapsulate drug molecules using the DOX as a model drug, and were formulated by a simple injection method, where the Janus dendrimer solution in ethanol was injected into water. The DOX was encapsulated in these structures with a film hydration technique, its release being found to be pH dependent due to the cleavage of the aromatic ester functional group present in the Janus dendrimers, which suggested their application for intracellular targeted delivery. Incorporating a pore forming protein (melittin) was also studied, with the results indicating that pore forming proteins could be successfully embedded in their bilayered structures, thus, confirming that the formed dendrimersomes mimicked the natural lipid bilayer cell membrane (Percec, Daniela A. Wilson, et al., 2010).

In another study, Zhang et al. reported the synthesis of isomeric amide containing 'Single-Single' Janus dendrimers (SS-JD), with a single hydrophilic and a single hydrophobic group compared with twin dendrons in conventional Percec type Janus dendrimers (Percec et al., 2004; S. Zhang et al., 2014). The simple direct or reverse injection of a SS-JD solution into organic solvents, such as tetrahydrofuran, acetone, acetonitrile and 1, 4-dioxane to Milli-Q water or phosphate and HEPES buffer, produces onion-like dendrimersomes. By controlling the final concentration of SS-JD in the solution, the size and numbers of the onion-like dendrimersomes can be tailored. These onion-like dendrimersomes can encapsulate different hydrophilic and hydrophobic cargoes within multiple layers. Time dependent release pattern can be achieved by encapsulating them in different layers of these onion-like dendrimersomes and can thus be regarded as "peeling of one onion-layer at a time" (S. Zhang et al., 2014). Although the authors stated that "these onion-like dendrimersomes can be used to encapsulate both hydrophilic and hydrophobic cargoes", there was no such cargo encapsulation study reported in the paper. Studies are needed regarding encapsulating drugs or drug-like molecules and evaluating their time dependent release pattern to pave the way for the introduction of onion-like dendrimersomes as smart carriers of both hydrophilic and lipophilic actives.

Table-1. Non-stimuli responsive self-assembling amphiphilic dendrimers as drug carriers.

Dendrimer	Structures formed	Drug/Payload	Key Findings and/or Conclusions	Reference
Amphiphilic layered dendrimers				
3, 5-dihydroxybenzyl alcohol based amphiphilic layered dendrimer with hydrophobic 3, 5- benzylic polyether core and hydrophilic carboxylate end groups	Unimolecular micelles	Pyrene Anthracene 1,4 diaminoanthraquinon 2,3,6,7-tetranitrofluorenone	<ul style="list-style-type: none"> Enhanced solubility of pyrene, anthracene, 1,4-diaminoanthraquinon, 2,3,6,7-tetranitrofluorenone by 120, 58, 56 and 258 -fold respectively compared to their water solubility. High solubilization was attributed to stabilizing π-π interactions between dendrimers and hydrophobic guest molecules. 	(Hawker, Wooley and Frechet, 1993)
G3 & G4 poly(glycerol-succinic acid) based polyester amphiphilic layered dendrimers (PGLSA) with carboxylate end groups as hydrophilic corona	Unimolecular micelles	Richard's dye Camptothecins	<ul style="list-style-type: none"> PGLSA dendrimers formed unimolecular micelles with average size of 7 nm. The hydrodynamic diameter decreased to 4 nm after encapsulating Richard's dye. Solubility of Richard's dye and camptothecins was enhanced by 2000 and 10 -folds respectively compared to their solubility in water. 	(Morgan et al., 2003, 2006)
Folate functionalized amphiphilic dendrimer-like star polymer (DLSP) from polyester dendrons	Unimolecular micelles	None	<ul style="list-style-type: none"> Unimolecular micelles with mean particle size of about 18 nm formed Increased cellular uptake of the folate- DLSP hybrid through overexpressed folate-receptor on KB cells Folate-DLSP hybrid showed potential as a carrier for targeted drug delivery. 	(Cao et al., 2010)
Amphiphilic dendrimer-like star polymers (DLSPs)	Unimolecular micelles	Doxorubicin (DOX)	<ul style="list-style-type: none"> Dendrimers had solubility of 10-25 mg/ml in water. Unimolecular micelles of 14-28 nm size and larger sized (205-344 nm) aggregates were formed. DOX loading was found to be 11.5 wt% DLSPs showed potential as candidates for controlled delivery of hydrophobic drugs. 	(Cao and Zhu, 2011a)
Folate functionalized amphiphilic dendrimer-like polymer	Micelles	DOX	<ul style="list-style-type: none"> Unimolecular micelles with mean particle size of .15 nm formed. DOX was released in a controlled sustained manner from the micelles. Unimolecular micelles could be promising nanosize anticancer drug carrier with excellent targeting property. 	(Cao et al., 2011)
Janus dendrimers				
11 distinct libraries of Janus dendrimers from six hydrophilic segments derived from oligoethylene oxide, dimethylolpropionic acid, glycerol, thioglycerol,	Various complex architectures such as vesicles, cubosomes, dendrimersomes, tubular vesicles, disks and helical ribbons	DOX	<ul style="list-style-type: none"> Bilayer dendrimersomes with varying size range of 33 to 732 nm were formed by ethanolic injection of Janus dendrimers in water. Bilayer structure thickness of 5 to 8 nm that could be imbedded in pore-forming proteins. System had high stability for 244 days. 	(Percec, Daniela A Wilson, et al., 2010)

tert butylcarbamate, and quaternary ammonium salts and with hydrophobic segments such as aliphatic and mixed aliphatic aromatic			<ul style="list-style-type: none"> • DOX was encapsulated in dendrimersomes using film hydration method. • System had high stability, mechanical strength, uniformity of size of particles formed, and easy chemical functionalization of the structures. 	
Amphiphilic Janus Glycodendrimers with D-mannose and D-galactose hydrophilic groups and n-alkyl hydrophobic chains	Bilayered glycodendrimersomes	None	<ul style="list-style-type: none"> • Glycodendrimersomes with average size of 114 to 126 nm uniformly assembled. • System offers possibility of lysine-mediated delivery of drugs, genes and imaging agents. 	(Percec et al., 2013)
Single–single” amphiphilic Janus dendrimers with polyethylene glycol and aliphatic hydrophobic chains	Onion like dendrimersomes	None	<ul style="list-style-type: none"> • Formation of multi layered onion-like dendrimersomes with size of 99 to 169 nm, and narrow size distribution achieved. • Transformation in number of layers was realized by changing concentration of Janus dendrimers. • Structures could offer time dependent multi layered delivery systems with multiple cargo loading 	(Shaodong Zhang et al., 2014)
Janus dendrimers with alkyl gallate ether dendron as hydrophobic part and hydroxyl terminated bis-MPA as hydrophilic dendron.	Supramolecular hydrogels	Nadolol Gonadorelin Horseradish peroxidase	<ul style="list-style-type: none"> • Supramolecular ribbon-like hydrogel with outstanding mechanical strength formulated. • Various drugs, active enzymes and peptide encapsulated in the hydrogel. • Hydrogel offers the potential for a sustained drug release drug delivery system. 	(Nummelin et al., 2015)
Bis-MPA based Janus dendrimer with amine groups as hydrophilic part and aliphatic hydrocarbon chains	Nanomicelles	Chloroquine Primaquine	<ul style="list-style-type: none"> • Spherical shaped nanomicelles with high entrapment efficiency for both chloroquine and primaquine were formulated. • Nanmicelles were non-toxic towards mammalian cells. • in vitro Studies showed intrinsic activity against P. falciparum. • Dendrimeric mediated transport of payloads was selectively achieved in plasmodium infected but not non-infected RBCs. 	(Movellan et al., 2014)
Facially amphiphilic dendrimers				
Amphiphilic dendrimers with repeating orthogonally placed biaryl units with hydrophilic (carboxylic acid) and hydrophobic (decyl chain) substituents and 3, 5-dihydroxy benzylic group as a backbone	Micelles in polar solvents and inverted micelles in non-polar solvents	Reichardt’s dye (pyridinium-N-phenoxide betaine) as hydrophobic guest, Proflavin dye as hydrophilic guest	<ul style="list-style-type: none"> • Formed micelles and inverted micelles depending on nature of solvent used: unimolecular micelles with average size of 2-4 nm in non-polar solvents; micellar aggregates with average size of 20-40 nm in polar solvents. • Dendrimers ability to sequester guests was generation dependent. • Formed structures were capable of encapsulating hydrophobic or hydrophilic guest molecules. 	(Vutukuri, Basu and Thayumanavan, 2004)

2.3.1.3 Facially amphiphilic dendrimer based NSR delivery systems

The third sub-section is on will emphasize on facially amphiphilic dendrimer based NSR delivery systems. Facially amphiphilic dendrimers, which are uniformly asymmetric over the entire globular surface. Therefore, unlike other amphiphilic dendrimers, these molecules can show solvent dependent conformational self-assembly. Bharathi P. and coworkers described the design and synthesis of such facially amphiphilic dendrimers and their solvent dependent self-assembly to form convex or concave interior structures (Bharathi, Zhao and Thayumanavan, 2001). The design of the facially amphiphilic dendrimers was based upon the orthogonally placed AB₂ functionalized biphenyl monomeric units containing triethylene glycol monomethyl ether and n-butyl group as hydrophilic and hydrophobic parts, were place placed oppositely to each other. (Fig. 10).

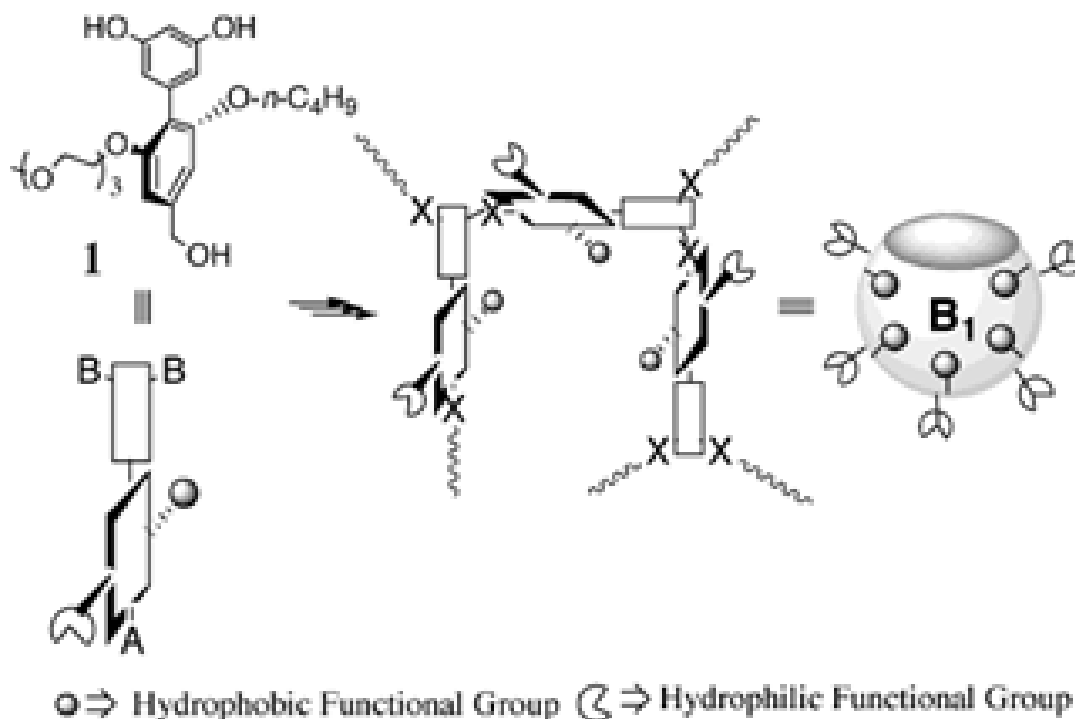
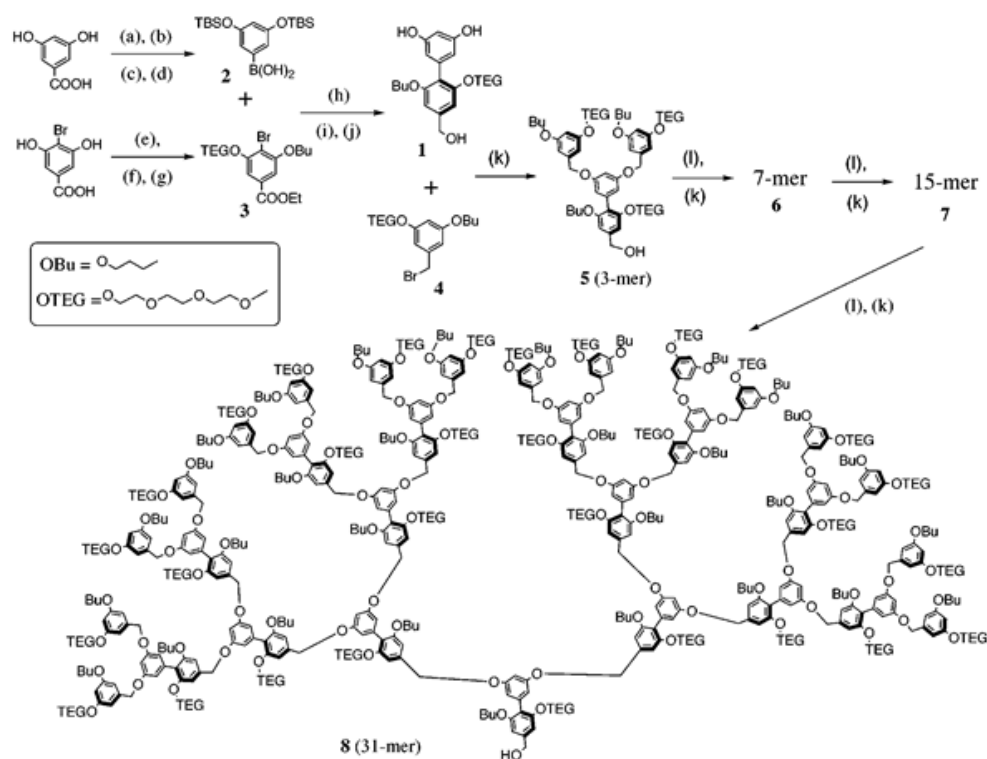


Fig. 10. Structure of biphenyl monomer (1) and orthogonal placement of the monomers in the dendrimers (Bharathi, Zhao and Thayumanavan, 2001). Reproduced with permission from American Chemical Society (2001)

Two phenolic and one hydroxymethyl group in the biphenyl monomeric unit (Fig. 10) provides an AB₂ branching motif similar to that of the Frechet type of the classical 3,5-dihydroxybenzyl alcohol monomeric units (Bharathi, Zhao and Thayumanavan, 2001). These amphiphilic dendrimers were synthesized following the synthetic steps depicted in Scheme 3. The biaryl monomeric unit was synthesized from the protected bis(O-*t*-butyldimethylsilyl) boronic acid (2) and bromoarene (3) by a palladium catalyzed coupling reaction. Furthermore, the dendron was constructed convergently using biaryl monomer 1, with monomer 4 being used for the periphery (Scheme 1).



Scheme 1. Synthesis of facially amphiphilic dendrimers (Bharathi, Zhao and Thayumanavan, 2001). Redrawn with permission from with permission from American Chemical Society. (a) TBS-Cl, imidazole, DMF, 81%; (b) SOCl₂, catalytic Me₃NHCl; (c) catalytic AIBN, 2-mercaptopyridine-N-oxide sodium salt, CBrCl₃, 62%; (d) (i) *t*-BuLi, (ii) B(OMe)₃, (iii) aqueous NH₄Cl; (e) catalytic H₂SO₄, EtOH, 95%; (f) K₂CO₃, 18-crown-6, acetone, Bu-I (0.8 equiv), 46%; (g) K₂CO₃, 18-crown-6, acetone, TEG-OTs, 92%; (h) catalytic Pd(PPh₃)₄, K₃PO₄, DME, reflux, 45%; (i) LiBH₄, THF, 88%; (j) TBAF, THF, 91%; (k) K₂CO₃ 1, 18-crown-6, THF; (l) Ph₃P, CBr₄ (5 72% from 4; 6 61% from 5; 7 21% from 6; 8 39% from 7).

These custom designed dendrimers can have either hydrophilic or hydrophobic functional groups that are selectively directed towards the concave interiors of the dendrimers, depending on the polarity of the solvent used. This relative placement of the functionality was a result of the solvophobic interactions, as seen in the case of amphiphilic globular proteins. These facially amphiphilic dendrimers can provide recognition sites at their concave surface, as seen in active binding sites in enzymes. In polar solvents, unimolecular micelles can be formed, while in nonpolar solvents, inverted micelles can be formed. These new amphiphilic scaffolds will provide such recognition and can mimic globular proteins and can also act as carries for various biological molecules. Furthermore, from the same group, extended application of these amphiphilic dendrimers for encapsulation of hydrophilic and hydrophobic guest molecules were investigated (Vutukuri, Basu and Thayumanavan, 2004). Biaryl dendrimeric structures were prepared with potassium carboxylate as the hydrophilic moiety and the same dodecyl chain as hydrophobic moiety. Due to the presence of carboxylate ions, these dendrimers were more soluble in water compared to the triethylene glycerol monomethyl ether structure. In the presence of polar solvents, such as water, these amphiphilic dendrimers formed unimolecular micelles and were able to harbor hydrophobic Reichardt's dye (pyridinium-N-phenoxide betaine), whereas in nonpolar solvents, such as toluene, they formed inverted micelles and were able to encapsulate the hydrophilic dye, proflavine (Fig. 11). The results of this study showed the potential of facially amphiphilic dendrimers to form either hydrophobic or hydrophilic unimolecular nanocontainers, depending upon polarity of the solvent used. The authors concluded that these amphiphilic multifunctional macromolecules could be considered as a first step toward structurally complex biomimetic assemblies (Vutukuri, Basu and Thayumanavan, 2004). However, more meaningful and useful information could have been obtained by performing morphological and biocompatibility studies to support the authors' claim of biomimetic assemblies.

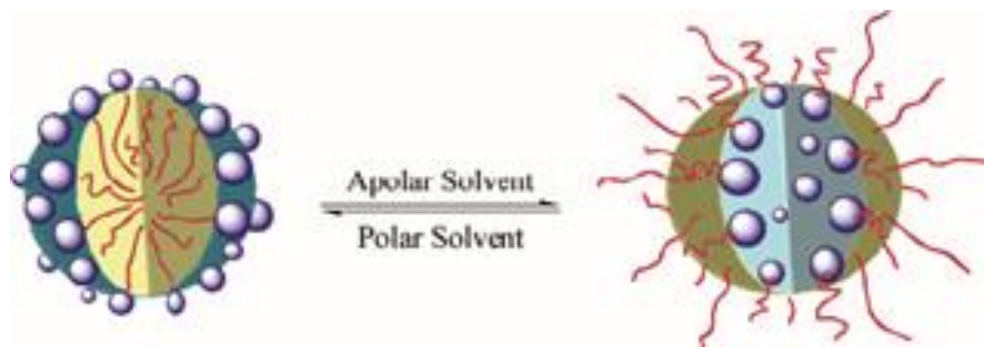


Fig. 11. Pictorial representation of self-assembly of facially amphiphilic dendrimers forming unimolecular micelles and inverted micelles in polar and nonpolar solvents respectively (Vutukuri, Basu and Thayumanavan, 2004). Reproduced with license from American Chemical Society

2.3.2 Stimuli-responsive (SR) self-assembling dendrimers

In this the second main section, stimuli-responsive (SR) self-assembling dendrimers and their application in drug delivery will be addressed. The targeted delivery of drug molecules to the diseased site for enhanced efficacy and to overcome resistance has become a focus research area for not only drug delivery scientists but also biomedical and material scientists. For triggered drug delivery, there are numerous reports in the literature on the synthesis of SR polymers and/or materials. By taking the advantages of their structure, scientists have focused on introducing SR functionalities into these dendrimers to achieve targeted and site-specific drug delivery. Various stimuli, which have been considered so far for synthesizing SR amphiphilic dendrimers, are pH, enzyme, UV and temperature. Various building blocks with different properties and functions have been effectively introduced to realize a programmable drug delivery system (Cheetham et al., 2013). SR systems are designed to take advantage of changes in different biological environments, such as the on and off switches for drug release (Mura, Nicolas and Couvreur, 2013). Depending upon the nature of the stimuli, the response to the SR self-assembling dendrimers can be classified as follows: i) physical stimuli, e.g. light, temperature, solvent, ionic strength, electric field and magnetic field strength, and ii) chemical stimuli, e.g. pH, redox microenvironment, enzyme over expression, host-guest recognition, antigen-antibody interactions and salts. Some of the stimuli responsive systems have been summarized in Table 2

2.3.2.1 Amphiphilic layered dendrimer based SR delivery systems

This sub section will deal with amphiphilic layered dendrimer based SR delivery system. Amphiphilic layered dendrimers can be transformed to SR by incorporating SR blocks between the layers. For example, Cho and Allcock introduced ion sensitive amphiphilic SR composed of phosphazene groups on the surface of a hydrophobic diaminobutane poly(propyleneimine) (PPI) dendrimer core, and then entrapped a hydrophobic payload (pyrene) in the functionalized dendrimer. While the pyrene release profile from the phosphazene modified dendrimer was similar to the parent, upon introduction of sodium chloride, the system triggered a faster release of pyrene than the parent dendrimer. It was concluded that the consequent increase in charge density due to the presence of salts caused an expansion of the ethyleneoxy coils in the polyphosphazene chains, causing swelling and increased wetting of the dendrimer, and resulting in solubilization of the hydrophobic payload and release (Cho and Allcock, 2007). Unlike the Cho and Allcock study, Paleos et al. also employed similar diaminobutane poly(propyleneimine) (PPI) salt responsive dendrimers to target the extracellular fluids that are usually composed of salts, such as NaCl and KCl. The betamethasone valerate was encapsulated in the dendrimer system, and in the presence of NaCl, the drug was released faster from the dendritic system (Paleos et al., 2004). This type of system could be of importance in bringing to life smart dendritic drug delivery systems that will selectively release the drugs in disease conditions that affect physiological ionic concentrations. However, further in vivo and in silico studies are required to establish the applicability of these salt responsive systems.

pH is also being widely employed as a trigger mechanism for the targeted release of drugs. Different ligands that are pH responsive are being attached to dendrimers to successfully deliver drugs without disrupting the healthy cells. The mechanism of these SR amphiphilic layered dendrimers includes protonation and deprotonation, which results in conformational changes and the subsequently release of drugs (Sideratou et al., 2000). As summarized in Table 2, another mechanism of pH response involves cleavage of acid labile bonds in acidic environment, resulting in drug release.

Advances in supramolecular chemistry have resulted in the design of systems that responds to more than one stimulus, which could result in highly specialized delivery systems that target more than one biomarker at the disease site. Such as system has been reported by Shaoqin Gong and

colleagues and has the ability to respond to pH and folate tumor receptor targeting. The synthesized SR amphiphilic layered dendrimer system self-assembled to a unimolecular micelle, its core comprising of a hyperbranched aliphatic polyester, Boltorn H40. The inner hydrophobic layer consisted of random copolymers of poly(ϵ -caprolactone) and poly(malic acid) (PMA-co-PCL) segments, while the outer hydrophilic shell was composed of poly(ethylene glycol) (PEG) segments. Folate, an active tumor-targeting ligands, were selectively conjugated to the distal ends of the PEG segments, while an anticancer drug, i.e., doxorubicin (DOX) molecules, was conjugated onto the poly(malic acid) (PMA) segments with pH-sensitive drug binding linkers for pH-triggered drug release (Fig. 12). The cellular uptake and distribution of micelles determined by means of flow cytometry and confocal laser scanning microscopy indicated that the folate-conjugated micelles had enhanced cellular uptake and cytotoxicity via folate-receptor-mediated endocytosis. At physiological pH, the DOX that had conjugated onto the unimolecular micelles exhibited excellent stability; however, once the micelles were internalized by the cancer cells, the pH-sensitive hydrazone linkages were cleaved by intracellular acidic environment, which caused a rapid release of DOX (Yuan, Yeudall and Yang, 2010). The versatility of amphiphilic layered dendrimers provides an opportunity to incorporate different stimuli molecules that can provide flexible drug delivery systems with a high efficiency and selectivity, and a low toxicity. While this provides a platform to design efficient drug delivery systems, more studies are needed to prove their applicability and upscaling potential for introducing them into the market as main-stream treatment options.

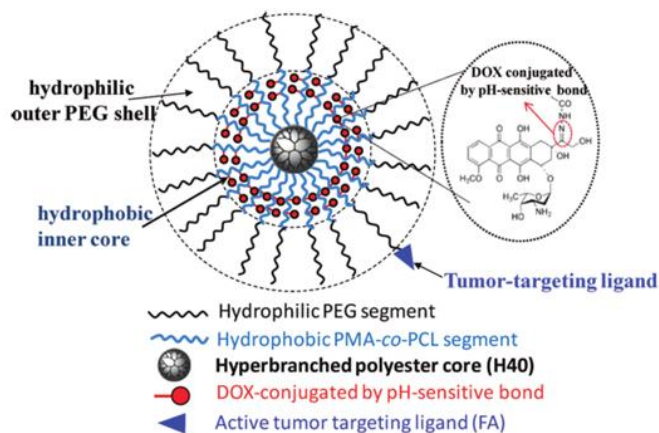


Fig 12. Multi stimuli responsive amphiphilic layered dendrimer (Yuan, Yeudall and Yang, 2010). Reproduced with permission from American Chemical Society.

2.3.2.2 Janus dendrimer based SR delivery systems

This subsection will discuss the applications of SR Janus based dendrimer. Janus dendrimers can be fine-tuned into smart materials by incorporating SR moieties in either the hydrophilic segments or hydrophobic parts. This incorporation has resulted in Janus dendrimer-based SR delivery systems that are responsive to an array of stimuli, such as light. As illustrated in Table 2, Janus dendrimer-based SR systems have been designed to self-assemble in aqueous media and disassemble when irradiated with certain light wavelength, such as near infrared and ultraviolet, to release drugs. Such systems are showing the potential for the on-demand targeted delivery of medicines (Sun et al., 2012).

Apart from light, enzyme response is also a stimulus of interest in designing drug delivery systems for disease site targeting. Zhongwei Gu et. al. designed such a smart polymeric vehicle for the hydrophobic drug paclitaxel (PTX), which was linked to the PEGylated Janus peptide dendrimer via enzyme sensitive tetrapeptide peptide linker glycyphenylalanylleucylglycine by efficient click reaction, resulting in a Janus dendritic prodrug with 20.9% PTX content (Fig. 13). The prodrug self-assembled into nanoscale particles with appropriate nanosizes, compact morphology and negative surface charge. The prepared amphiphilic Janus dendrimer-based SR delivery system allowed for the maximum steady-state circulation and enzyme triggered fast-intracellular PTX release in tumors. In the presence of cathepsin B enzyme, changes in size and morphology were observed, demonstrating the enzyme-sensitive property and enzyme-induced collapse of particles, thereby contributing to rapid drug release (Li et al., 2017). This similar principle of using enzymes' responsiveness as a mechanism to stimulate the release of payloads has also been reported, using Nile red dye as encapsulated payload in amphiphilic Janus dendritic systems, with Penicillin G amidase, esterase and amidase enzymes as triggers for the disassembly of the amphiphilic Janus dendritic micelles. (Harnoy et al., 2014, Harnoy et al., 2017, Rosenbaum et al., 2017). These studies are evidence that dendritic systems that respond to enzyme response could be a future prospective for efficacious targeted drug delivery.

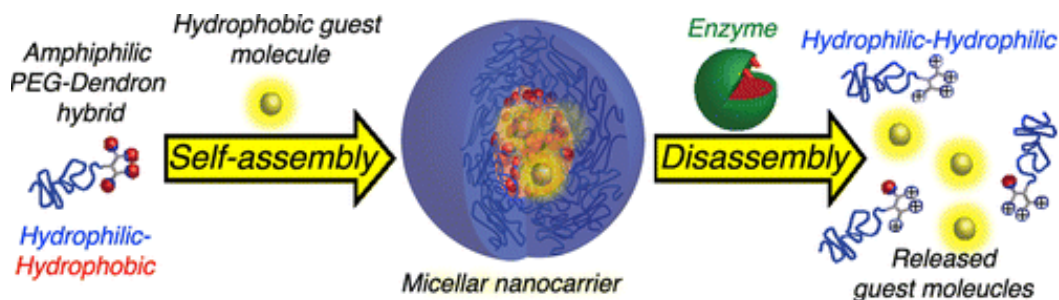


Fig. 13. Schematic representation of enzyme triggered disassembly of nano micelles releasing payloads (Harnoy et al., 2014) and reproduced with permission from American Chemical Society.

Self-assembly of SR Janus dendrimer provides a perfect platform for drug delivery, as payloads can be encapsulated in the dendritic free spaces, and in the presence of a stimuli, the system collapses, and the drug is released. As shown in Table 2, DOX is one of the most explored model drug encapsulations in these SR Janus dendrimer systems. pH as a stimulus has also been extensively reported in the literature as a trigger mechanism for breaking down the Janus dendrimer self-assembled systems, resulting in the localized release of drugs (Table 2). Qiao et al. also reported a series of Janus dendrimers consisting of hydrophilic polyamidoamine (PAMAM) and various ratios of hydrophobic poly(d,l-lactic acid) portions. The synthesized amphiphilic dendrimers were able to form micelles, with particle sizes in the range of 39 to 87 nm. In the resulting micellar systems, docetaxel, an antitumor drug, was successfully encapsulated, with an encapsulation efficiency of 29 to 80.4%. Furthermore, it was noted that as the hydrophobic segment increased, so did the size and encapsulation efficiencies. The prepared micelles were evaluated for pH-responsive drug release at pH 7.4, 6.8 and 5.5 in release media containing 0.1% polysorbate 80.

The results demonstrated pH-induced charge conversion and dimension changes, which were confirmed by TEM and AFM studies respectively. The in vitro drug release suggested susceptibility of docetaxel-loaded micelles to an acidic microenvironment, and the system was biocompatible. Furthermore, pharmacokinetic studies performed using Sprague-Dawley (SD) rat in vivo models showed that micelles enhanced the area under the curve (AUC) of docetaxel and prolonged drug clearance in comparison to conventional docetaxel injection. (Qiao et al., 2013). The stimuli responsive Janus dendritic systems clearly showed the potential for targeted delivery drug molecules; however, most applications have been for anticancer drugs. More studies are

needed for other diseases associated with pH changes, such as bacterial infections and diabetes, as well as an in-depth evaluation of the in vivo efficacy of these systems for future introduction into clinical practice.

2.3.2.3 Facially amphiphilic dendrimer based SR delivery systems

Application of Discussions involving facially amphiphilic dendrimer based SR delivery systems will be discussed in this subsection. Overexpression of proteins and enzymes has been frequently implicated in the diseased state of cells. Disruption of hydrophilic-lipophilic balance, using an external stimulus, could lead to disassembly of the aggregates, which can be utilized to cause an actuation event, such as guest molecule release (Raghupathi et al., 2014). Azagarsamy et. al. demonstrated enzyme-induced disassembly of amphiphilic nanocontainers based on dendrimers, with the system consisting of biaryl dendrimers composed of a hexyl ester as the lipophilic unit and PEG as a hydrophilic unit. The enzyme-induced disassembly tested using porcine liver esterase revealed that there was a systematic decrease with time in the size of the self-assembled nanoparticles (Azagarsamy et al., 2009).

In another study, enzyme responsive facially amphiphilic dendritic systems consisting of (i) a polyglycerol dendrimer core, (ii) a dipeptide Phe–Lys attached self-immolative enzyme responsive para amino benzyloxy carbonyl group, and (iii) the tetrapeptide Ala–Phe–Lys–Lys, to which either doxorubicin and methotrexate were attached. Size-exclusion chromatograms, after incubation with the cathepsin B enzyme, showed the individual mass of the conjugated drugs, indicating an effective release of the drugs after cleavage by the enzyme. The dendritic drug conjugates appeared to be biosafe after being evaluated on human tumor cell lines MDA-MB-231 and AsPC1 (Calderón et al., 2009). In the above studies, the efficacy and safety of these enzyme responsive systems were mostly performed using in vitro study models. However, studies on enzyme triggered release and pharmacokinetic evaluation in animal models will add value and open the door for further exploitation of this system, due to their ability to address difficulties in managing disease conditions and offer more efficient ways to deliver drugs.

Advancements in synthetic chemistry, and the development of technology for analysis and chemical characterization, have led to the design of elaborate dendritic systems that can respond to various disease biomarkers, including reactive oxygen species (ROS), which are often elevated in cancer cells. Using this biomarker in the pathogenesis of cancer cells, Fernandes, and Malkoch

synthesized a family of dendrimers with internally queued disulfide bridges that selectively rupture into a set of monomeric mercaptans in the presence of ROS. Their composition was dictated by three dendritic regions: (i) the symmetrical trithiol of the core (C3), (ii) the interior-asymmetric trithiols (CD2), and (iii) the periphery-asymmetric monothiols (DB2) (Fig. 14). In the dendritic system, sulfide bridges were specifically selected as they can undergo selective redox cleavage in a single step, and are involved in biological functions, such as the thioredoxin or glutaredoxin redox systems. To prove their concept of disassembly, the synthesized multi-stimuli responsive amphiphilic layered dendrimers-were evaluated in human lung carcinoma A549 cells to establish the effect of the ROS. Analysis by MALDI-TOF-MS showed that the mass fragmented dendrimers building blocks were isolated after incubation, and that there was a significant increase of ROS inside the cancer cells exposed to the dendrimers (Andrén et al., 2017). These dendrimer scaffolds can be considered as next generation precision polymers in the field of nanomedicines.

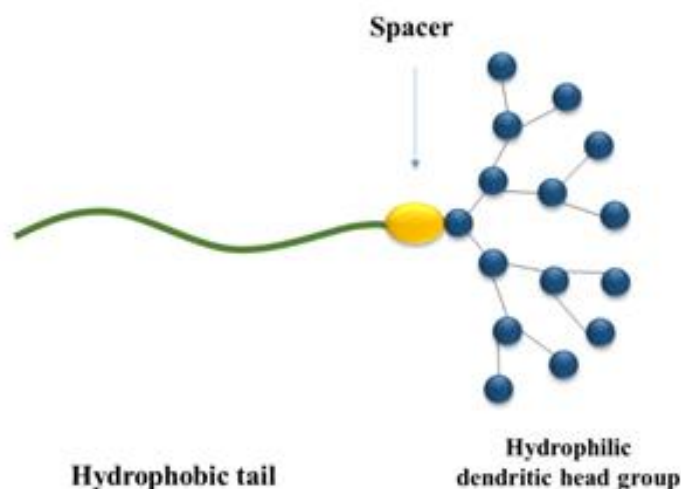


Fig 14. Synthetic strategy of rupturing amphiphilic dendrimers from (Andrén et al., 2017) and with permission from American Chemical Society.

Table 2 Stimuli-responsive self-assembling dendrimers for drug delivery.

Dendrimer	Stimuli	Drug/model molecule	Main findings	Reference
Amphiphilic layered dendrimers				
Poly (propyleneimine) (PPI) dendrimers with 64 amino ends protected with t-butoxycarbonyl (t-BOC)-protected phenylalanine groups to afford a dendrimer with a “sterically closed” shell	pH	Rose Bengal	<ul style="list-style-type: none"> • Box-like dendrimer steric entrapment of hydrophobic guest molecule witnessed. • t-butoxycarbonyl (t-BOC)-protected phenylalanine attached dendrimers formed sterically closed shell, while acid hydrolysis of amine end groups regenerated open-shell form after exposure to formic acid. • Sterically mediated release mechanism provided unique method for stimuli responsive and controlled drug delivery. 	(Jansen, Meijer and de Brabander-van den Berg, 1995)
Hyperbranched poly(ethylene imine) cores and different shells which contain aliphatic chains and poly(ethylene glycol) chains	pH	Congo red	<ul style="list-style-type: none"> • Higher capacities for polar dyes and drugs to be encapsulated and extracted from dendrimer observed. • pH labile shells were cleaved in 5–6 pH environments. 	(Xu, Krämer and Haag, 2006)
Amphiphilic layered dendrimers (DAB-PN) with hydrophobic diaminobutane poly(propyleneimine) core and with hydrophilic polyphosphazene outer segments	Salts (Sodium chloride)	Pyrene	<ul style="list-style-type: none"> • Dendrimers formed unimolecular micelles and sequestered hydrophobic pyrene molecules within nonpolar interiors. • Increase in pyrene solubility was observed as generations of DAB-PN increased. • Cationization of ethyleneoxy moieties by Na⁺ ions increased charge density causing expansion of ethyleneoxy coils, resulting in release of entrapped cargo. • Enhanced solubility and stimuli-dependent controlled release of hydrophobic molecules observed. 	(Cho and Allcock, 2007)
Janus dendrimers				
Polyester dendrimer functionalized with acetal shells (JDs)	pH	DOX	<ul style="list-style-type: none"> • Hydrolysis of acetal function at acidic pH resulted in release of entrapped DOX. • Hydrolysis at acidic pH caused disruption of the micelles and larger aggregates due to rearrangement. • Localization of DOX in intracellular organelles achieved. 	(Gillies and Fréchet, 2005)

Janus dendrimers prepared by coupling of G3 PAMAM dendron containing diazonaphthoquinone (DNQ) end groups and PAMAM dendron decorated with lactose groups.	Light [ultra violet light (UV) and near infra-red light (NIR)]	DOX	<ul style="list-style-type: none"> • DOX loaded micelle with average size of 59 to 70 nm and loading capacity of 8.3 to 15.6 wt% formed. • Wolff rearrangement of hydrophobic DNQ ends to hydrophilic 3-indenecarboxylic acid due to NIR and UV light resulted in destabilization of micellar structure and faster drug release. • Faster DOX release was observed after irradiation of micelles for 30 min with an 808 nm laser or 365 nm high pressure mercury lamp. • On-demand spatiotemporal delivery achieved for anticancer drug. 	(Sun et al., 2012)
Janus dendrimers consisting of G2 hydrophilic PAMAM dendron and two hydrophobic C18 alkyl chains bridged together via click chemistry.	pH	DOX	<ul style="list-style-type: none"> • Ultra-small micelles with average size of 10 nm with narrow PDI and DOX loading up to 42% formulated. • High drug loading was attributed to large void spaces within inner cores of the micellar structure. • pH dependent DOX release observed. 	(Wei et al., 2015)
mPEG-b-PAMAM-DOX Amphiphilic Janus dendrimer consisting of methoxypoly(ethylene glycol) (MPEG)-b poly(amidoamine) (PAMAM)-DOX prodrug	pH	10-hydroxycamptothecin (HCPT) and DOX	<ul style="list-style-type: none"> • Janus amphiphilic dendrimers with mPEG and PAMAM dendritic polymer attached to DOX through pH liable hydrazone linkages synthesized. • Self-assembly to formed nano-aggregates with size range of 49.0±5.4 and 59.1±7.8nm. • Encapsulation of HCPT was 19.2 to 21.6% and of DOX was 22.0 to 41.2%. • Degradation of hydrazone linkage occurred within acidic range (pH 4.5 to 5.5), releasing both drugs concurrently. • Co-delivery systems with pH responsive controlled release and enhanced anticancer activity drug delivery system was reported. 	(Zhang et al., 2013)
Janus type amphiphilic linear dendritic block copolymer, semi polyamidoamine-b poly(D,L-lactic acid) (PALA)	pH	Docetaxel (DTX)	<ul style="list-style-type: none"> • pH faster release of DTX loaded micelles in acidic microenvironment was observed. • In vivo studied in Sprague-Dawley (SD) rats model showed increased AUC and prolonged clearance of DTX compared to conventional DTX 	(Qiao et al., 2013)
Polyester dendrimers	UV light	Nile red and Fluorescein	<ul style="list-style-type: none"> • polyester dendrimers self-assembled to form dendrimersomes • UV light triggered release of both hydrophilic and hydrophobic payloads from the system. 	(Nazemi and Gillies, 2014)
PAMAM-co oligo(ethylene glycol) (PAG)	Temperature	Methotrexate	<ul style="list-style-type: none"> • Unimolecular and multimolecular aggregates with particle sizes of 8 and 200 nm were achieved. 	(Guo et al., 2014)

			<ul style="list-style-type: none"> • PAG exhibited only 10% release after 8 h at 37oC, while at 48oC faster release of 55% 1h observed. 	
Amphiphilic peptide dendrimer	Enzyme (Papain)	DOX	<ul style="list-style-type: none"> • DOX conjugated mPEGylated dendron with glycylphenylalanylleucylglycine tetra-peptide (GFLG) as enzyme sensitive linker was synthesized. • mPEGylated-GFLG-DOX dendritic conjugate self-assembled into nanoparticles with average size of 80 nm. • Incubation with papain triggered 50% release of DOX after 6h. • System showed effective killing of cancer cells in vitro when compared to conventional DOX. • No significant side effects to normal organs that amphiphilic dendrimer was exposed to. 	(Li et al., 2014)
Facially amphiphilic dendrimers				
Facially amphiphilic biaryl dendrimers with hexyl ester as hydrophobic moiety and pentaethylene glycol as hydrophilic group.	Enzyme [porcine liver esterase (PLE)]	Pyrene	<ul style="list-style-type: none"> • Dendrimer-based amphiphilic assemblies with 100 nm size that could noncovalently sequester hydrophobic guest molecules were formulated. • Hydrolysis of ester moieties in hydrophobic part in presence of PLE lead to destabilization and subsequent cargo release. 	(Azagarsamy, Sokkalingam and Thayumanavan, 2009)
Amphiphilic pentaethylene glycol unit and coumarin derivative based dendrimer	Enzyme (PLE)	1,1'-dioctadecyl-3,3,3'-tetramethylindo carbocyanine perchlorate	<ul style="list-style-type: none"> • PLE enzyme triggered the release of the lipophilic fluorophore from the dendritic backbone. 	(Raghupathi, Azagarsamy and Thayumanavan, 2011)

2.3.3. Low molecular weight dendritic amphiphiles in drug delivery

Low molecular weight dendritic amphiphiles are receiving considerable attention due to their simple structure and ease of self-assembly into well-defined and persistent micellar aggregates (Thota, Urner and Haag, 2016). The structure of these dendritic amphiphiles lie in between classical surfactants and amphiphilic polymers and consist of a hydrophilic multifunctional dendritic head group and a hydrophobic hydrocarbon tail. Their unique traits make them better building blocks for micellar systems than linear amphiphilic polymers. Table 3 Summarizes the applications of these low molecular weight dendritic amphiphiles as drug delivery systems.

These dendritic amphiphiles have been used as solubility enhancers (Richter et al., 2010; Dhiraj R. Sikwal et al., 2017), as micellar carriers (Trappmann et al., 2010), as non-viral gene delivery vectors (Malhotra et al., 2012), stearic stabilizers for colloidal drug delivery systems (D.R. Sikwal et al., 2017) and photo responsive delivery vehicles (Kördel, Popeney and Haag, 2011). Since the discovery of dendrimers, these architectures have been successfully employed as non-viral gene delivery vehicles, with polycationic dendritic structures, such as dendritic polylysine and polyglycerol amines, having demonstrated their potential in this field. However, despite preliminary successful attempts, these structures have not been used widely due to their toxicity profiles. This problem can be addressed by using dendritic amphiphiles, which self-assemble to form pseudodendrimer like structures, and are capable of condensing genetic materials and delivering them into the cells. Malhotra and coworkers reported the application of these dendritic amphiphiles in siRNA delivery (Malhotra et al., 2012). The hydrophilic segment of the dendritic amphiphiles were G1 and G2 glycine functionalized oligoglycerol with 1, 2, 4 and 8 amino groups and a C18 hydrophobic tail (Fig. 15).

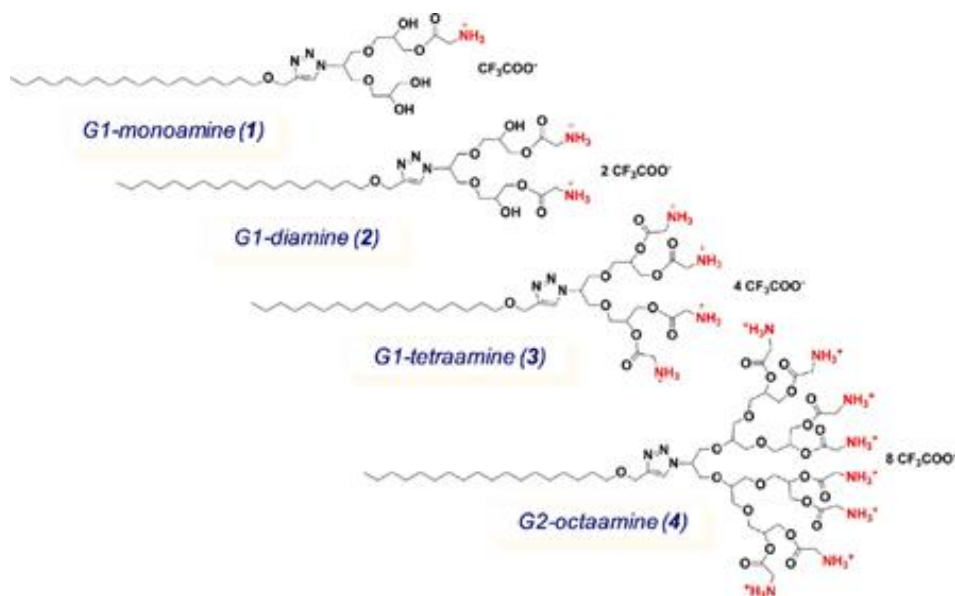
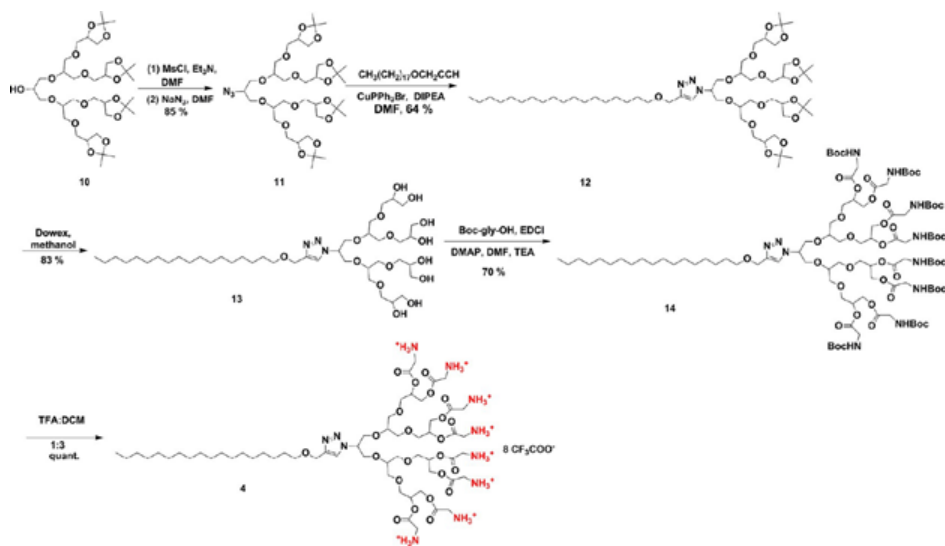


Fig. 15. Structure of dendritic amphiphiles for siRNA delivery obtained from (Malhotra et al., 2012) with permission from American Chemical Society.

The dendritic head group was grown divergently on azide focal point and then condensed to the hydrophobic chain by click chemistry. Thereafter, N-boc glycine was condensed to the hydroxyl terminal by using 4-(dimethylamino)pyridine and 1-ethyl-3-[3-(dimethylamino)propyl]carbodiimide hydrochloride (EDCI), and ionized with the help of trifluoroacetic acid (TFA) (Scheme. 2).



Scheme. 2. Synthesis of G2 octamine dendritic amphiphile redrawn from (Malhotra et al., 2012) with permission from American Chemical Society.

Physicochemical characterization of all these dendritic amphiphiles by determination of the CMC showed that all four amphiphiles aggregated in a low concentration range of 10 to 60 μM (Fig. 16). CMC values increased from G1 monoamine to G1 tetraamine due to an increase in positive charge that induced more repulsion in the head group of the amphiphiles. All these amphiphiles aggregated in the micelles, with the size range of 7 to 9 nm and a zeta potential values of 40-58 mV. The cationic glycine functional end groups complexed with the DNA and acted as an efficient gene delivery vehicle. Furthermore, the complexation ability of these amphiphiles with DNA was due to the combined effect of the hydrophobic alkyl chain and hydrophilic glycine molecules. This complexation results in the self-assembly of amphiphiles-DNA polyplexes of average size range of 69 to 306 nm. Cytotoxicity and siRNA transfection results confirmed the application of these dendritic amphiphiles as efficient vectors for siRNA transfection and cytotoxicity (Malhotra et al., 2012).

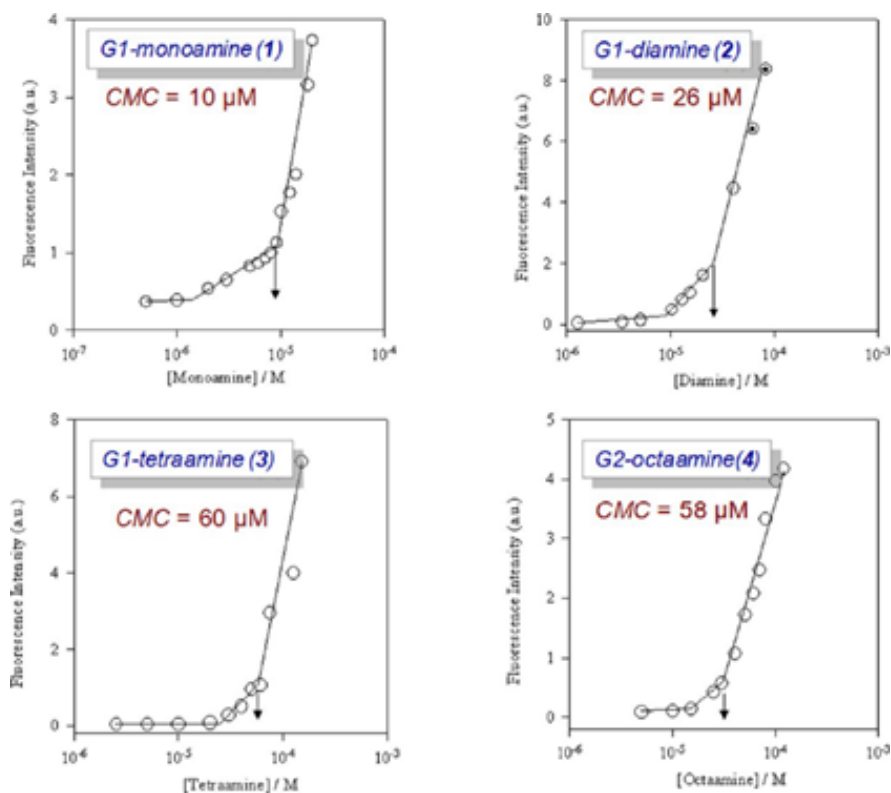


Fig. 16. Determination of CMC of glycine amphiphiles in 0.5 μM DPH (aqueous HEPES saline (pH 7.2, 9.4 mM NaCl) obtained from (Malhotra et al., 2012) with permission from American Chemical Society

Sikwal et al. also reported the synthesis of dendritic amphiphiles based glycerol monostearate (GMS-G2-OH, GMS-G3-OH) and glycerol monooleate derivatives (GMOA-G2-OH, GMOA-G3-OH). These amphiphiles were studied for their applications as both solubility enhancer and stearic stabilizers for nanoparticles (D.R. Sikwal et al., 2017). Biocompatible polyester dendritic amphiphiles were prepared using the OH terminated G2 and G3 Bis-MPA dendrons dendritic head group, and stearic acid or oleic acid as the hydrophobic tail. The synthesis of these dendritic amphiphiles involved simple protection and deprotection steps, where the hydrophilic dendrons were grown divergently with acetonide protected Bis-MPA on a focal point of glycerol monostearate or monooleate. Deprotection of the acetonide group was carried out by using acidic Dowex® H⁺ resin to produce a focal point for the next generation.

Cytotoxicity studies against MCF 7, Hep G2 and A549 human carcinoma cells using MTT assay indicated a biocompatibility (70% cell viability) for all derivatives and further studies showed that the amphiphiles had HLB values that were greater than 15. This confirmed that the synthesized dendritic amphiphiles could be good solubilizers, as shown by the higher solubilization of the hydrophobic fusidic acid when compared to water and Pluronic F-68. Aggregation behavior showed the formation of ultra-small micelles, with an average size range of 6.48-12.38 nm and narrow polydispersity indices. The reason for higher solubilization was attributed to the spatial arrangement of these dendritic amphiphiles, and chain kink confirmation of unsaturated bond in oleic acid. In-vitro antibacterial activity proved that the GMOA-G2-OH micellar carrier also enhanced the antibacterial potency of fusidic acid.

To prove the stearic stabilizing property of these dendritic amphiphiles, solid lipid nanoparticles (SLNs) were formulated using Compritol 888 ATO as solid lipids, and amphiphiles as surfactants. The results from the formulation studies proved that dendritic amphiphiles were capable of providing sufficient stability to the SLNs, as confirmed by an optimum particle size in the range of 133 to 291 nm, narrow polydispersity index values (0.296 to 0.485) and higher zeta potential values (-22.33 to -34.10). Overall results of this study indicated that these dendritic amphiphiles could be promising excipients for pharmaceutical application (Dhiraj R. Sikwal et al., 2017).

Table 3. Summary of low molecular weight dendritic amphiphiles based drug delivery systems.

Purpose	Structural components of dendritic amphiphile	Payload	Important finding	Reference
Micellar delivery	Non-ionic lower molecular weight dendritic amphiphiles with hydrophilic polyglycerol dendrons (G1-G3) and hydrophobic C11 or C16 alkyl chains joined together by mono or biaryl spacer	Nile red Pyrene	<ul style="list-style-type: none"> Dendritic head group influenced supramolecular self-assembly and aggregation number while biaryl spacer influenced transport capacity G1 amphiphile formed ring-like or worm-like micelles, G2 and G3 amphiphiles formed spherical micelles with average size of 8 nm. High entrapment of hydrophobic molecules was attributed to and 74% of empty space in the micelles composed of 15 amphiphilic molecules. Lower critical micellar concentration (CMC) was recorded. 	(Trappmann et al., 2010)
Solubilizing agents	Glycerol (G2) based amphiphiles with different hydrophobic moieties (C18 chain, C18 chain with naphthyl and biaryl end groups) with single or double aromatic linkers.	Sagopilone	<ul style="list-style-type: none"> All amphiphiles formed ultra-small micellar structures with size range 7 to 10 nm and polydispersity index of 0.04 to 0.2. All amphiphilic structure did not show any cytotoxicity up to concentration of 0.01g/ml after 24 h. The amphiphiles showed 2 to 3 -fold higher solubilization of sagopilone and greater stabilization of micellar structures than Cremophor® ELP and polysorbate-80. G2 amphiphile with diaromatic spacer and C18 chain showed highest solubilization capacity. 	(Trappmann et al., 2010)
Gene delivery	Oligoglycerol based dendritic amphiphiles with glycine terminals as hydrophilic part and stearic acid as hydrophobic chain.	siRNA/NDA	<ul style="list-style-type: none"> Amphiphiles formed micellar aggregates in size range of 7-9 nm and zeta potential of 40-58 mV. Amphiphiles were efficient vectors for siRNA transfection and cytotoxicity. First time in vitro siRNA transfection was achieved using dendritic amphiphiles. 	(Malhotra et al., 2012)
Pharmaceutical excipients	Polyester dendritic amphiphiles with G2 and G3 Bis-MPA based dendritic head group and stearic acid and oleic acid as hydrophobic tail.	Fusidic acid Vancomycin	<ul style="list-style-type: none"> Biocompatible amphiphilic dendrimers with low CMC values that self-assembled into ultra-small micellar aggregates. Micellization of fusidic acid through these amphiphiles enhanced solubility of fusidic acid. Amphiphiles also acted as good stearic stabilizers for solid lipid nanoparticles (SLNs) formulations. 	(Dhiraj R. Sikwal et al., 2017)
Photoresponsive delivery	Photoswitchable non-ionic dendritic amphiphiles with G2, G3 glycerol based dendrons and C11, C16 tail connected together with dibenzodiazepine connector.	Nile Red	<ul style="list-style-type: none"> All dendritic amphiphiles formed spherical micelles with size range of 7.2-10.2 nm. Amphiphiles undergo trans-cis photoisomerization under UV/Visible leading to disassembly of micelles. CMC of these amphiphiles changed effectively under influence of light, rendering structures photoresponsive. 	(Kördel, Popeney and Haag, 2011)

2.4 CONCLUSION AND FUTURE PERSPECTIVE

The studies in this chapter demonstrated promising preliminary results for amphiphilic dendrimers as drug delivery carriers. With advancements in synthetic chemistry, tailor made amphiphilic dendrimers, which can self-assemble into different structures such as vesicles, dendrimersomes and onion-like structures, are possible. Moreover, these formed structures can mimic biological architectures, and the different moieties that respond to various disease biomarkers can be incorporated into the nano systems for efficient and targeted drug delivery and biomedical applications. However, the field is in its infancy, and there is still a long way to go before any product becomes commercially available in the market for medical applications. Almost 30 years after the introduction of PAMAM dendrimers, no product has been introduced in the market. Further investigations that involve an in vivo evaluation of their performance, biosafety, long-term stability, and that explore their cost-effective and large-scale production, are required. Industry-academia collaborations hold the key to achieving a scale of synthesis that will provide economies of scale in production, as well as the preclinical and clinical trials to make these materials viable for market. While SR amphiphilic dendrimers are promising candidates, there is a need to explore and design dual or multi-stimuli responsiveness, such as a combination of pH and enzyme, or pH and temperature, as these studies will advance the field. Most of the studies undertaken for pH-responsive have been in oncology, while there is dearth of literature on other diseases, such as diabetes and bacterial infections, in this regard, stimuli-responsive systems from amphiphilic dendrimers could advance the field. It is also important to address the obstacles that emerge from technological, experimental and personnel limitations/errors at the initial stages of developing these materials, including stringent regulatory requirements to obtain amphiphilic dendrimers for future medical applications.

2.5 REFERENCES

- Andr n, O.C.J., Fernandes, A.P., Malkoch, M., 2017. Heterogeneous Rupturing Dendrimers. *Journal of the American Chemical Society* 139, 17660-17666. doi: 10.1021/jacs.7b10377.
- Avila-Salas, F., Pereira, A., Rojas, M.A., Saavedra-Torres, M., Montecinos, R., Bonardd, S., Quezada, C., Sald as, S., D az, D.D., Leiva, A. and Radic, D. (2017) 'An experimental and theoretical comparative study of the entrapment and release of dexamethasone from micellar and vesicular aggregates of PAMAM-PCL dendrimers', *European Polymer Journal*. Elsevier Ltd, 93, pp. 507-520. doi: 10.1016/j.eurpolymj.2017.06.023.
- Azagarsamy, M. A., Sokkalingam, P. and Thayumanavan, S. (2009) 'Enzyme-triggered disassembly of dendrimer-based amphiphilic nanocontainers', *Journal of the American Chemical Society*, 131(40), pp. 14184-14185. doi: 10.1021/ja906162u.
- Azagarsamy, M.A., Sokkalingam, P., Thayumanavan, S., 2009. Enzyme-Triggered Disassembly of Dendrimer-Based Amphiphilic Nanocontainers. *Journal of the American Chemical Society* 131, 14184-14185. doi: 10.1021/ja906162u.
- Bharathi, P., Zhao, H. and Thayumanavan, S. (2001) 'Toward globular macromolecules with functionalized interiors: Design and synthesis of dendrons with an interesting twist', *Organic Letters*, 3(12), pp. 1961-1964. doi: 10.1021/ol1016064b.
- Calder n, M., Graeser, R., Kratz, F., Haag, R., 2009. Development of enzymatically cleavable prodrugs derived from dendritic polyglycerol. *Bioorganic & medicinal chemistry letters* 19, 3725-3728. doi.org/10.1016/j.bmcl.2009.05.058
- Caminade, A.-M. and Turrin, C.-O. (2014) 'Dendrimers for drug delivery', *J. Mater. Chem. B*, 2(26), pp. 4055-4066. doi: 10.1039/C4TB00171K.
- Cao, W. and Zhu, L. (2011) 'Synthesis and unimolecular micelles of amphiphilic dendrimer-like star polymer with various functional surface groups', *Macromolecules*, 44(6), pp. 1500-1512. doi: 10.1021/ma1021242.
- Cao, W., Zhou†, J., Wang, Y. and Zhu, L.. (2010) 'Synthesis and In Vitro Cancer Cell Targeting of Folate-Functionalized Biodegradable Amphiphilic Dendrimer-Like Star Polymers', pp. 3680-3687. doi: 10.1021/bm101154r
- Cao, W., Zhou, J., Mann, A., Wang, Y., and Zhu, Y. (2011) 'Folate-functionalized unimolecular micelles based on a degradable amphiphilic dendrimer-like star polymer for cancer cell-targeted drug delivery', *Biomacromolecules*, 12(7), pp. 2697-2707. doi: 10.1021/bm200487h.
- Cheetham, A.G., Zhang, P., Lin, Y.A., Lock, L.L. and Cui, H. (2013) 'Supramolecular Nanostructures Formed by Anticancer Drug Assembly', *Journal of the American Chemical Society*, 135(8), pp. 2907-2910. doi: 10.1021/ja3115983.
- Cho, S. Y. and Allcock, H. R. (2007) 'Dendrimers derived from polyphosphazene - Poly(propyleneimine) systems: Encapsulation and triggered release of hydrophobic guest molecules', *Macromolecules*, 40(9), pp. 3115-3121. doi: 10.1021/ma062582w.
- Fan, X., Li, Z. and Loh, X. J. (2016) 'Recent development of unimolecular micelles as functional materials and applications', *Polymer Chemistry*, 7(38), pp. 5898-5919. doi: 10.1039/C6PY01006G.
- Gillies, E. R. and Fr chet, J. M. J. (2005) 'pH-responsive copolymer assemblies for controlled release of doxorubicin', *Bioconjugate Chemistry*, 16(2), pp. 361-368. doi: 10.1021/bc049851c.
- Guo, Y., Zhao, Y., Zhao, J., Han, M., Zhang, A. and Wang, X. (2014) 'Codendrimer from polyamidoamine (PAMAM) and oligoethylene dendron as a thermosensitive drug carrier', *Bioconjugate Chemistry*, 25(1), pp. 24-31. doi: 10.1021/bc300560p.
- Harnoy, A.J., Buzhor, M., Tirosh, E., Shaharabani, R., Beck, R., Amir, R.J., 2017. Modular Synthetic Approach for Adjusting the Disassembly Rates of Enzyme-Responsive Polymeric Micelles. *Biomacromolecules* 18, 1218-1228. doi: 10.1021/acs.biomac.6b01906
- Harnoy, A.J., Rosenbaum, I., Tirosh, E., Ebenstein, Y., Shaharabani, R., Beck, R., Amir, R.J., 2014. Enzyme-Responsive Amphiphilic PEG-Dendron Hybrids and Their Assembly into Smart Micellar Nanocarriers. *Journal of the American Chemical Society* 136, 7531-7534. doi: 10.1021/ja413036q.
- Hawker, C.J., Wooley, K.L. and Fr chet, J.M. (1993) 'Unimolecular micelles and globular amphiphiles: dendritic macromolecules as novel recyclable solubilization agents'. *Journal of the Chemical Society, Perkin Transactions 1*, (12), pp.1287-1297. doi: 10.1039/P19930001287.
- Hung, W.I., Chang, C.H., Chang, Y.H., Wu, P.S., Hung, C.B., Chang, K.C., Lai, M.C., Hsu, S.C., Wei, Y., Jia, X.R. and Yeh, J.M. (2013) 'Self-Assembly Behavior of Amphiphilic Poly(amidoamine) Dendrimers with a Shell of Aniline Pentamer', *Langmuir*, 29(39), pp. 12075-12083. doi: 10.1021/la403063t.

- Jain, N. K. and Asthana, A. (2007) 'Dendritic systems in drug delivery applications', *Expert Opinion on Drug Delivery*. Taylor & Francis, 4(5), pp. 495–512. doi: 10.1517/17425247.4.5.495.
- Jansen, J. F. G. A., Meijer, E. W. and de Brabander-van den Berg, E. M. M. (1995) 'The Dendritic Box: Shape-Selective Liberation of Encapsulated Guests', *Journal of the American Chemical Society*, 117(15), pp. 4417–4418. doi: 10.1021/ja00120a032.
- Kaur, D., Jain, K., Mehra, N. K., Kesharwani, P., & Jain, N. K. (2016). 'A review on comparative study of PPI and PAMAM dendrimers', *Journal of Nanoparticle Research*. Springer Netherlands, 18(6), pp. 1–14. doi: 10.1007/s11051-016-3423-0.
- Kesharwani, P., Banerjee, S., Gupta, U., Amin, M. C. I. M., Padhye, S., Sarkar, F. H., & Iyer, A. K. (2015). 'PAMAM dendrimers as promising nanocarriers for RNAi therapeutics', *Materials Today*. Elsevier Ltd., 18(10), pp. 565–572. doi: 10.1016/j.mattod.2015.06.003.
- Kördel, C., Popeney, C. S. and Haag, R. (2011) 'Photoresponsive amphiphiles based on azobenzene-dendritic glycerol conjugates show switchable transport behavior', *Chemical Communications*, 47(23), p. 6584. doi: 10.1039/c1cc11673h.
- Li, N., Cai, H., Jiang, L., Hu, J., Bains, A., Hu, J., Gong, Q., Luo, K., Gu, Z., 2017. Enzyme-Sensitive and Amphiphilic PEGylated Dendrimer-Paclitaxel Prodrug-Based Nanoparticles for Enhanced Stability and Anticancer Efficacy. *ACS Applied Materials & Interfaces* 9, 6865-6877. doi: 10.1021/acsami.6b15505.
- Li, N., Li, N., Yi, Q., Luo, K., Guo, C., Pan, D., & Gu, Z. (2014). 'Amphiphilic peptide dendritic copolymer-doxorubicin nanoscale conjugate self-assembled to enzyme-responsive anti-cancer agent', *Biomaterials*, 35(35), pp. 9529–9545. doi: 10.1016/j.biomaterials.2014.07.059.
- Lin, Q., Jiang, G. and Tong, K. (2010) 'Dendrimers in drug-delivery applications', *Designed Monomers and Polymers*, 13(4), pp. 301–324. doi: 10.1163/138577210X509552.
- Luong, D., Kesharwani, P., Deshmukh, R., Amin, M. C. I. M., Gupta, U., Greish, K., & Iyer, A. K.. (2016) 'PEGylated PAMAM dendrimers: Enhancing efficacy and mitigating toxicity for effective anticancer drug and gene delivery', *Acta Biomaterialia*. Acta Materialia Inc., 43, pp. 14–29. doi: 10.1016/j.actbio.2016.07.015.
- Malhotra, S., Bauer, H., Tschiche, A., Staedtler, A.M., Mohr, A., Calderón, M., Parmar, V.S., Hoeke, L., Sharbati, S., Einspanier, R. and Haag, R. (2012) 'Glycine-terminated dendritic amphiphiles for nonviral gene delivery', *Biomacromolecules*, 13(10), pp. 3087–3098. doi: 10.1021/bm300892v.
- Márquez-Miranda, V., Araya-Durán, I., Camarada, M.B., Comer, J., Valencia-Gallegos, J.A. and González-Nilo, F.D. (2016) 'Self-Assembly of Amphiphilic Dendrimers: The Role of Generation and Alkyl Chain Length in siRNA Interaction', *Scientific Reports*. Nature Publishing Group, 6(June), pp. 1–15. doi: 10.1038/srep29436.
- Morgan, M.T., Carnahan, M.A., Immoos, C.E., Ribeiro, A.A., Finkelstein, S., Lee, S.J. and Grinstaff, M.W. (2003) 'Dendritic Molecular Capsules for Hydrophobic Compounds', *Journal of the American Chemical Society*, 125(50), pp. 15485–15489. doi: 10.1021/ja0347383.
- Morgan, M.T., Nakanishi, Y., Kroll, D.J., Griset, A.P., Carnahan, M.A., Wathier, M., Oberlies, N.H., Manikumar, G., Wani, M.C. and Grinstaff, M.W. (2006) 'Dendrimer-Encapsulated Camptothecins: Increased Solubility, Cellular Uptake, and Cellular Retention Affords Enhanced Anticancer Activity In vitro', *Cancer Research*. American Association for Cancer Research, 66(24), pp. 11913–11921. doi: 10.1158/0008-5472.CAN-06-2066.
- Movellan, J., Urbán, P., Moles, E., Jesús, M., Sierra, T., Serrano, J.L. and Fernandez-Busquets, X. (2014) 'Amphiphilic dendritic derivatives as nanocarriers for the targeted delivery of antimalarial drugs', *Biomaterials*, 35(27), pp. 7940–7950. doi: 10.1016/j.biomaterials.2014.05.061.
- Mura, S., Nicolas, J. and Couvreur, P. (2013) 'Stimuli-responsive nanocarriers for drug delivery', *Nature materials*, 12, pp. 991–1003. doi:10.1038/nmat3776.
- Nazemi, A. and Gillies, E. R. (2014) 'Dendrimersomes with photodegradable membranes for triggered release of hydrophilic and hydrophobic cargo', *Chem. Commun. Royal Society of Chemistry*, 50(76), pp. 11122–11125. doi: 10.1039/C4CC05161K.
- Newkome, G.R., Yao, Z., Baker, G.R. and Gupta, V.K. (1985) 'Micelles. Part 1. Cascade molecules: a new approach to micelles. A [27]-arborol', *The Journal of Organic Chemistry*, 50(11), pp. 2003–2004. doi: 10.1021/jo00211a052.
- Nummelin, S., Liljeström, V., Saarikoski, E., Ropponen, J., Nykänen, A., Linko, V., Seppälä, J., Hirvonen, J., Ikkala, O., Bimbo, L.M. and Kostianen, M.A. (2015) 'Self-Assembly of Amphiphilic Janus Dendrimers into Mechanically Robust Supramolecular Hydrogels for Sustained Drug Release', *Chemistry - A European Journal*, 21(41), pp. 14433–14439. doi: 10.1002/chem.201501812.

Paleos, C.M., Tsiourvas, D., Sideratou, Z., Tziveleka, L., 2004. Acid- and Salt-Triggered Multifunctional Poly(propylene imine) Dendrimer as a Prospective Drug Delivery System. *Biomacromolecules* 5, 524-529. doi: 10.1021/bm030068h

Pan, G., Lemmouchi, Y., Akala, E.O. and Bakare, O. (2005) 'Studies on PEGylated and Drug-Loaded PAMAM Dendrimers', *Journal of Bioactive and Compatible Polymers*, 20(1), pp. 113–128. doi: 10.1177/0883911505049656.

Park, W.I., You, B.K., Mun, B.H., Seo, H.K., Lee, J.Y., Hosaka, S., Yin, Y., Ross, C.A., Lee, K.J. and Jung, Y.S. (2013) 'Self-assembled incorporation of modulated block copolymer nanostructures in phase-change memory for switching power reduction', *ACS Nano*, 7(3), pp. 2651–2658. doi: 10.1021/nn4000176.

Percec, V. et al. (2013) 'Modular synthesis of amphiphilic Janus glycodendrimers and their self-assembly into glycodendrimersomes and other complex architectures with bioactivity to biomedically relevant lectins', *Journal of the American Chemical Society*, 135(24), pp. 9055–9077. doi: 10.1021/ja403323y.

Percec, V., Dulcey, A.E., Balagurusamy, V.S., Miura, Y., Smidrkal, J., Peterca, M., Nummelin, S., Edlund, U., Hudson, S.D., Heiney, P.A. and Duan, H. (2004) 'Self-assembly of amphiphilic dendritic dipeptides into helical pores', *Nature*, 430(7001), pp. 764–768. doi: 10.1038/nature02770. doi:10.1038/nature02770.

Percec, V., Wilson, D. A., et al. (2010) 'Self-Assembly of Janus Dendrimers into Uniform Dendrimersomes and Other Complex Architectures', *Science*. American Association for the Advancement of Science, 328(5981), pp. 1009–1014. doi: 10.1126/science.1185547.

Qiao, H., Li, J., Wang, Y., Ping, Q., Wang, G. and Gu, X. (2013) 'Synthesis and characterization of multi-functional linear-dendritic block copolymer for intracellular delivery of antitumor drugs', *International Journal of Pharmaceutics*. Elsevier B.V., 452(1–2), pp. 563–573. doi: 10.1016/j.ijpharm.2013.05.003.

Qiao, H., Li, J., Wang, Y., Ping, Q., Wang, G., Gu, X., 2013. Synthesis and characterization of multi-functional linear-dendritic block copolymer for intracellular delivery of antitumor drugs. *International journal of pharmaceutics* 452, 363-373. doi: org/10.1016/j.ijpharm.2013.05.003.

Raghupathi, K. R., Azagarsamy, M. A. and Thayumanavan, S. (2011) 'Guest-release control in enzyme-sensitive, amphiphilic-dendrimer-based nanoparticles through photochemical crosslinking', *Chemistry - A European Journal*, 17(42), pp. 11752–11760. doi: 10.1002/chem.201101066.

Raghupathi, K.R., Guo, J., Munkhbat, O., Rangadurai, P., Thayumanavan, S., 2014. Supramolecular Disassembly of Facially Amphiphilic Dendrimer Assemblies in Response to Physical, Chemical, and Biological Stimuli. *Accounts of Chemical Research* 47, 2200-2211. doi: 10.1021/ar500143u.

Rao, J., Hottinger, C. and Khan, A. (2014) 'Enzyme-triggered cascade reactions and assembly of abiotic block copolymers into micellar nanostructures', *Journal of the American Chemical Society*, 136(16), pp. 5872–5875. doi: 10.1021/ja501632r.

Richter, A., Wiedekind, A., Krause, M., Kissel, T., Haag, R. and Olbrich, C. (2010) 'Non-ionic dendritic glycerol-based amphiphiles: Novel excipients for the solubilization of poorly water-soluble anticancer drug Sagopilone', *European Journal of Pharmaceutical Sciences*. Elsevier B.V., 40(1), pp. 48–55. doi: 10.1016/j.ejps.2010.02.008.

Rosenbaum, I., Avinery, R., Harnoy, A.J., Slor, G., Tirosh, E., Hananel, U., Beck, R., Amir, R.J., 2017. Reversible Dimerization of Polymeric Amphiphiles Acts as a Molecular Switch of Enzymatic Degradability. *Biomacromolecules* 18, 3457-3468. doi: 10.1021/acs.biomac.7b01150.

Sideratou, Z., Tsiourvas, D., Paleos, C.M., 2000. Quaternized Poly(propylene imine) Dendrimers as Novel pH-Sensitive Controlled-Release Systems. *Langmuir* 16, 1766-1769. doi: 10.1021/la990829v.

Sikwal, D. R., Kalhapure, R. S. and Govender, T. (2017) 'An emerging class of amphiphilic dendrimers for pharmaceutical and biomedical applications: Janus amphiphilic dendrimers', *European Journal of Pharmaceutical Sciences*, 97. doi: 10.1016/j.ejps.2016.11.013.

Sikwal, D.R., Kalhapure, R.S., Jadhav, M., Rambharose, S., Mocktar, C. and Govender, T. (2017) 'Non-ionic self-assembling amphiphilic polyester dendrimers as new drug delivery excipients', *RSC Advances*, 7(23). doi: 10.1039/c6ra28100a.

Sun, L., Ma, X., Dong, C.M., Zhu, B. and Zhu, X. (2012) 'NIR-responsive and lectin-binding doxorubicin-loaded nanomedicine from Janus-type dendritic PAMAM amphiphiles', *Biomacromolecules*, 13(11), pp. 3581–3591. doi: 10.1021/bm3010325.

Thota, B. N. S., Urner, L. H. and Haag, R. (2016) 'Supramolecular architectures of dendritic amphiphiles in water', *Chemical Reviews*, 116(4), pp. 2079–2102. doi: 10.1021/acs.chemrev.5b00417.

- Trappmann, B., Ludwig, K., Radowski, M.R., Shukla, A., Mohr, A., Rehage, H., Böttcher, C. and Haag, R. (2010) 'A New Family of Nonionic Dendritic Amphiphiles Displaying Unexpected Packing Parameters in Micellar Assemblies', *Journal of the American Chemical Society*, 132(32), pp. 11119–11124. doi: 10.1021/ja101523v.
- Vutukuri, D. R., Basu, S. and Thayumanavan, S. (2004) 'Dendrimers with Both Polar and Apolar Nanocontainer Characteristics', *Journal of the American Chemical Society*, 126(48), pp. 15636–15637. doi: 10.1021/ja0449628.
- Wang, F., Bronich, T.K., Kabanov, A.V., Rauh, R.D. and Roovers, J. (2005) 'Synthesis and Evaluation of a Star Amphiphilic Block Copolymer from Poly(ϵ -caprolactone) and Poly(ethylene glycol) as a Potential Drug Delivery Carrier', *Bioconjugate Chemistry*, 16(2), pp. 397–405. doi: 10.1021/bc049784m. doi: 10.1021/bc049784m.
- Wang, Y. and Grayson, S. M. (2012) 'Approaches for the preparation of non-linear amphiphilic polymers and their applications to drug delivery', *Advanced Drug Delivery Reviews*. Elsevier B.V., 64(9), pp. 852–865. doi: 10.1016/j.addr.2012.03.011.
- Wei, T., Chen, C., Liu, J., Liu, C., Posocco, P., Liu, X., Cheng, Q., Huo, S., Liang, Z., Fermeglia, M. and Pricl, S. (2015) 'Anticancer drug nanomicelles formed by self-assembling amphiphilic dendrimer to combat cancer drug resistance', *Proceedings of the National Academy of Sciences*, 112(10), pp. 2978–2983. doi: 10.1073/pnas.1418494112.
- Wooley, K. L., Hawker, C. J. and Frechet, J. M. J. (1993) 'Unsymmetrical three-dimensional macromolecules: preparation and characterization of strongly dipolar dendritic macromolecules', *Journal of the American Chemical Society*, 115(24), pp. 11496–11505. doi: 10.1021/ja00077a055.
- Xu, S., Krämer, M. and Haag, R. (2006) 'pH-Responsive dendritic core-shell architectures as amphiphilic nanocarriers for polar drugs', *Journal of Drug Targeting*, 14(6), pp. 367–374. doi: 10.1080/10611860600834011.
- Yuan, Q., Yeudall, W. A. and Yang, H. (2010) 'PEGylated Polyamidoamine Dendrimers with Bis-Aryl Hydrazone Linkages for Enhanced Gene Delivery', *Biomacromolecules*, 11, pp. 1940–1947. doi: 10.1021/bm100589g.
- Zhang, S., Sun, H.J., Hughes, A.D., Draghici, B., Lejnicks, J., Leowanawat, P., Bertin, A., Otero De Leon, L., Kulikov, O.V., Chen, Y. and Pochan, D.J. (2014) "'Single-Single" Amphiphilic Janus Dendrimers Self-Assemble into Uniform Dendrimersomes With Predictable Size', *ACS Nano*, 8(2), pp. 1554–1565. doi: 10.1021/nn405790x.
- Zhang, S., Sun, H.J., Hughes, A.D., Moussodia, R.O., Bertin, A., Chen, Y., Pochan, D.J., Heiney, P.A., Klein, M.L. and Percec, V. (2014) 'Self-assembly of amphiphilic Janus dendrimers into uniform onion-like dendrimersomes with predictable size and number of bilayers', *Proceedings of the National Academy of Sciences*, 111(25), pp. 9058–9063. doi: 10.1073/pnas.1402858111.
- Zhang, Y., Xiao, C., Li, M., Chen, J., Ding, J., He, C., Zhuang, X. and Chen, X. (2013) 'Co-delivery of 10-hydroxycamptothecin with doxorubicin conjugated prodrugs for enhanced anticancer efficacy', *Macromolecular Bioscience*, 13(5), pp. 584–594. doi: 10.1002/mabi.201200441.

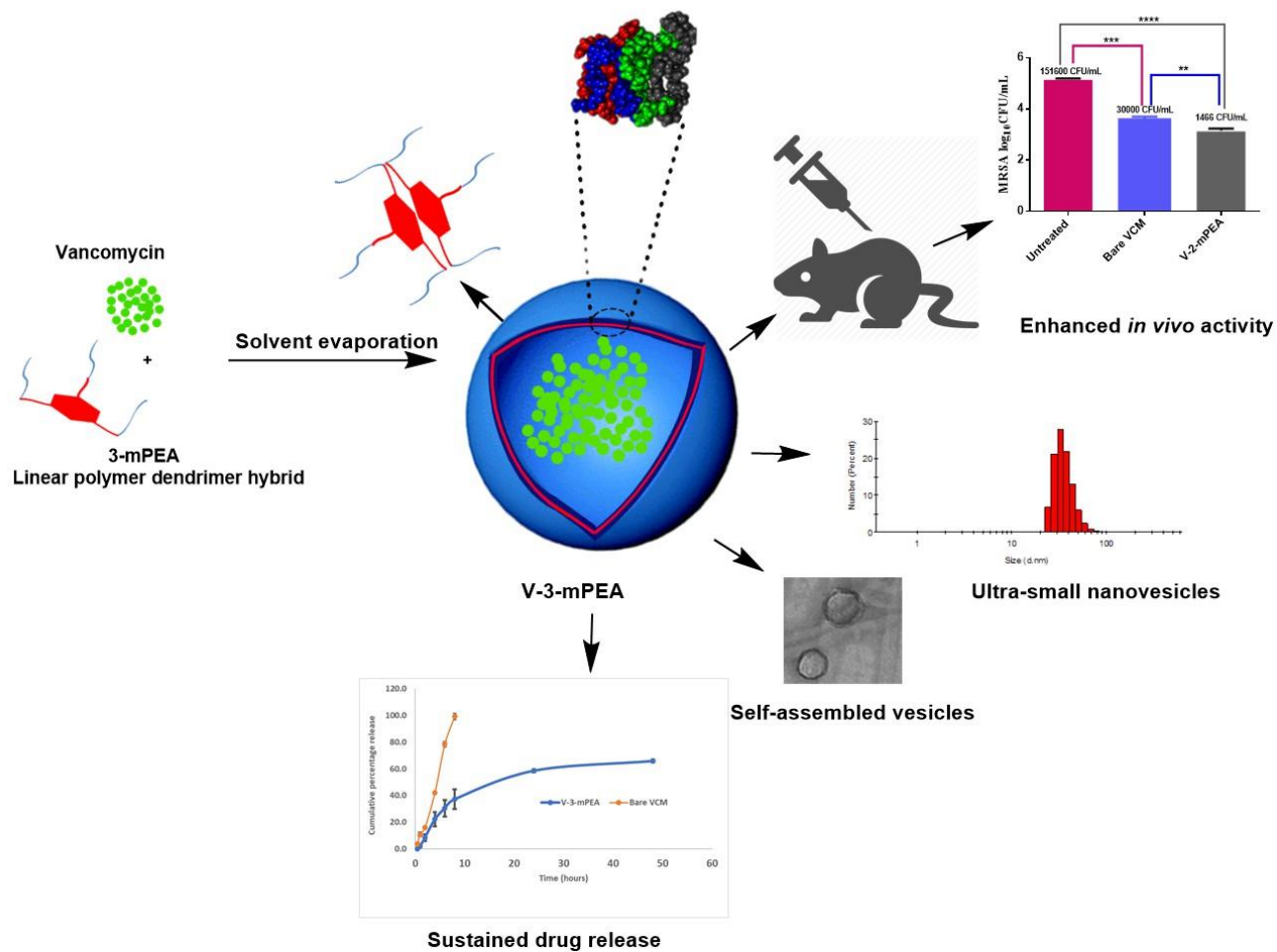
CHAPTER 3, EXPERIMENTAL PAPER 1

3.1 Introduction

This chapter addresses Aim 1, Objectives 1- 6 and is a first authored experimental article. This chapter highlights the synthesis of a novel block copolymer dendrimer star polymer hybrid, the in vitro toxicity evaluation, formulation of the ultra-small vesicles (V-3-mPEA) to deliver vancomycin, molecular dynamics simulation of the self-assembly of a novel block copolymer dendrimer star polymer hybrid, and characterization of its physical and antibacterial properties both in vitro and in vivo. Research outputs from the chapter includes; published in an ISI international journal: Journal of Controlled Release (Impact Factor = 7.877) and data from this chapter has also been presented in two international conferences:

- Calvin A. Omolo, Rahul S. Kalhapure, Sanjeev Rambharose, Chunderika Mocktar, Thirumala Govender, A novel six-armed PEG-b-PCL copolymer (6m-PEPEA) based on G1-PETIM dendrimer for nano delivery of vancomycin. The AAPS Annual Meeting and Exposition October 2, 2017, San Diego, USA. (poster presentation). (appendix IV)
- Calvin A. Omolo, Rahul S. Kalhapure, Mahantesh Jadhav, Sanjeev Rambharose, Chunderika Mocktar, Thirumala Govender, A novel six-armed PEG-b-PCL copolymer based on G1 PETIM dendrimer for nano delivery of vancomycin. International Conference on Nanomedicine and Nanobiotechnology, September 25, 2017 Barcelona, Spain (poster presentation). (appendix V)
- Calvin A. Omolo, Rahul S. Kalhapure, Mahantesh Jadhav, Sanjeev Rambharose, Chunderika Mocktar, Thirumala Govender, A novel six-armed PEG-b-PCL copolymer based on G1 PETIM dendrimer for nano delivery of vancomycin. College of Health Sciences Annual Research Symposium, University of KwaZulu Natal, 05-06 October 2017, Durban, South Africa. (Oral presentation).

3.2 Graphical abstract



3.4 Published manuscript

A Hybrid of mPEG-*b*-PCL and G1-PEA Dendrimer for Enhancing Delivery of Antibiotics

Calvin A. Omolo¹, Rahul S. Kalhapure^{1,2}, Nikhil Agrawal¹, Mahantesh Jadhav¹, Sanjeev
Rambharose^{1,3}, Chunderika Mocktar¹, Thirumala Govender^{1,#}

1. Discipline of Pharmaceutical Sciences, College of Health Sciences, University of KwaZulu-Natal, Private Bag X54001, Durban, South Africa.
2. School of Pharmacy, The University of Texas at El Paso, 500 W University Ave, El Paso, TX 79968, USA.
3. Division of Emergency Medicine, Department of Surgery, University of Cape Town, Cape Town, South Africa.

corresponding author: Private Bag X54001 Durban, 4000, KwaZulu-Natal, South Africa.
Tel: 00 27 31 260 7358, Fax: 0027 31 260 7792

Email address: govenderth@ukzn.ac.za; rkalhapure@utep.edu;
rahul.kalhapure@rediffmail.com

3.5 Abstract

The development of novel materials is essential for the efficient delivery of drugs. Therefore, the aim of the study was to synthesize a linear polymer dendrimer hybrid star polymer (3-mPEA) comprising of a generation one poly (ester-amine) dendrimer (G1-PEA) and a diblock copolymer of methoxy poly (ethylene glycol)-b-poly(ϵ -caprolactone) (mPEG-*b*-PCL) for formulation of nanovesicles for efficient drug delivery. The synthesized star polymer was characterized by FTIR, ^1H and ^{13}C NMR, HRMS, GPC and its biosafety was confirmed by MTT assays. Thereafter it was evaluated as a nanovesicle forming polymer. Vancomycin loaded nanovesicles were characterized using *in vitro*, molecular dynamics (MD) simulations and *in vivo* techniques. MTT assays confirmed the nontoxic nature of the synthesized polymer, the cell viability was 77.23 to 118.6 %. The nanovesicles were prepared with size, polydispersity index and zeta potential of 52.48 ± 2.6 nm, 0.103 ± 0.047 , -7.3 ± 1.3 mV respectively, with the encapsulation efficiency being $76.49 \pm 2.4\%$. MD simulations showed spontaneous self-aggregation of the dendritic star polymer and the interaction energy between the two monomers was -146.07 ± 4.92 , Van der Waals interactions playing major role for the aggregate's stability. Human serum albumin (HSA) binding studies with Microscale Thermophoresis (MST) showed that the 3-mPEA did not have any binding affinity to the HSA, which showed potential for long systemic circulation. The vancomycin (VCM) release from the drug loaded nanovesicles was found to be slower than bare VCM, with an 65.8% release over a period of 48 h. The *in vitro* antibacterial test revealed that the drug loaded nanovesicles had 8- and 16-fold lower minimum inhibitory concentration (MIC) against methicillin sensitive *Staphylococcus aureus* and methicillin-resistant *S. aureus* strains (MRSA) compared to free drug. The flow cytometry study showed 3.9-fold more dead cells of MRSA in the population when samples were treated with the drug loaded nanovesicles than the bare VCM at concentration $0.488 \mu\text{g/mL}$. An *in vivo* skin infection mice model showed a 20-fold reduction in the MRSA load in the drug loaded nanovesicles treated groups compared to bare VCM. These findings confirmed the potential of 3-mPEA as a promising biocompatible effective nanocarrier for antibiotic delivery.

Keywords: Resistance; MRSA; linear polymer dendrimer star polymer; biosafe, vancomycin; nanovesicles; antibacterial.

3.6 Introduction

Since the discovery of penicillin by Sir Alexander Fleming in 1928, many lives have been saved by antibiotics[1]. However, in the last decade, the world has witnessed a dramatic upsurge in the number of bacterial pathogens that are resistant to multiple antibacterial agents [2, 3], coupled with the drying up of the antibiotic pipeline [4-6], with major pharmaceutical companies leaving the antibiotic development field [2]. One of the bacteria that causes significant health care challenges is *Staphylococcus aureus* (SA) and its resistant strain, known as methicillin-resistant *Staphylococcus aureus* (MRSA), which is insensitive to a wide range of antibiotics[7]. Recent findings indicate that of the 385 MRSA isolates, 36 (9.35%) are resistant to the routinely used antibiotics [8]. The World Health Organization recognizes that the dearth of new and novel antibiotics, particularly those with new modes of action, as well as the need to identify innovative strategies to enhance, protect and potentiate those available in the market to avert returning to a pre-antibiotic era [9-12].

Antimicrobial resistance is a complex and a multifaceted problem. Some of the contributors to antibiotic resistance are sub-lethal concentrations of the antibiotics at the infection site, low patients' compliance due to high frequency of administration and side or adverse effects; some of which are dose dependent which leads to development of resistant strains in the population [13]. In addition to antibiotic stewardship and discovery of new potent drugs, novel drug delivery systems, are demonstrating the potential to solve some of the patient and dosage form factors related to the development of resistance by extending the circulation time, targeting infectious sites, protecting and enhancing antibacterial activity of pristine drugs with prominent examples such as Lipoquin®, Pulmaquin® and MAT2501, an encholeated formulation of amikacin [14-17].

Core-shell aggregates of linear polymers have both a hydrophobic (core) and hydrophilic (shell) parts that self-assembles in aqueous milieu to form micelles, which have the ability to encapsulate hydrophobic drugs in the core [18, 19]. However, premature dissociation of the self-assembled unimers during circulation in the bloodstream can cause a burst release, resulting in high concentration of drugs in the bloodstream [20, 21]. Dendrimers as drug delivery materials have widely been reported due to their attractive properties such as high degree of branching, multivalency, globular architecture and well-defined molecular weight. Their unique properties make them suitable materials for drug delivery [22]. They are being employed as alternative to linear block polymers [23]. However, there are some concerns about toxicity and biocompatibility of the dendritic nanostructures regarding their applications in

drug delivery such as damage to cell membrane integrity, chromosomes and mitochondria, oxidative stress, genotoxicity, and stimulates immune response [24].

To address the problem associated with dendrimer nanostructures and linear polymers, such as toxicity, biocompatibility and premature disassociation, several research groups have resorted to modifying the end groups of the dendrimers using linear polymers star results to hyperbranched polymers with dendrimer cores. This strategy embodies some positive traits from both dendrimers and the attached linear polymers for efficient drug delivery [25, 26]. Moreover, the ability to functionalize their end groups, fine-tunes dendrimers for targeted delivery, long circulation [27], biodegradability [28], and covalent attachment of the drugs for sustained release [29]. Most reports for this strategy have been for the delivery of anti-cancer drugs [30, 31], there is a dearth of literature on the evaluation of hybrids of linear polymer shells with dendrimer cores as carriers for enhancing antibiotic delivery despite their numerous advantages. There is therefore a need to develop and employ this strategy for antibacterial delivery as this could offer biosafe and effective drug delivery system for antibiotics.

Typically, linear polymer-dendrimer hybrids (LPDH) self-assemble to become core-shell aggregates, such as classical micelles [32] and unimolecular micelles [33] However, there is limited literature on vesicular self-assembly, and most of the reported vesicles have shown to be large in size with a poor polydispersity index (PI) [34-36]. Hence, there is a need for a synthesis of novel LPDHs that assemble into ultra-small nanovesicles with lower PI to advance the field by offering reproducible and predictable biodistribution and activity, and have wider applications, such as drug delivery, diagnostics and imaging.

The experimental, characterization and information for vesicles from polymers, such as their size, geometric structure, polydispersity is well understood [37]. However, there is a need to understand the self-assembly process and molecular dynamics (MD) simulations are being employed to explain self-assembly process of the polymers [38]. Thus, providing a detailed molecular insight at atomic level on how self-assembly occurs and the forces that play important roles for the stability of the formation of the structures are of paramount importance in drug delivery.

In this study, we therefore propose the use of generation one poly ester amine dendrimer (PEA) and methoxypoly(ethylene glycol)-b-poly(ϵ -caprolactone) (mPEG-b-PCL) linear block polymer to synthesize a novel LPDHs with ability to self-assemble into nanovesicles. PEA dendrimers have shown to have better characteristics, such as bio-compatibility, nontoxicity, biodegradability, a higher drug loading and drug encapsulation[39, 40], flexibility and sustained release properties than other dendritic polymer counterparts[41-43]. mPEG-*b*-PCL

linear has proven to have biocompatibility, non-toxicity and biodegradable excellent solvating properties [44], we envisage the resulting LPDHs to be efficient and safe biomaterial for drug delivery.

There are several reports on antimicrobial drug delivery using PEGylated PAMAM dendrimers to form LPDHs [45, 46]. This highlights the feasibility and importance of using this strategy to deliver antimicrobials. The aim of this study was therefore to explore the potential of delivering antimicrobials via nanovesicles formulated from the modification of generation one PEA dendrimer with mPEG-*b*-PCL block polymer to yield a 3-arm star polymer (3-mPEA) with a dendrimer core and block copolymer shell. Most of dendrimer modification with the linear polymers has been through PEGylation, however, we envisaged that the use of mPEG-*b*-PCL block polymer will offer a better drug delivery system as the hydrophobic PCL portion attached to the dendrimer core will offer stability, mechanical strength of the vesicle membrane and improved loading capacity while the mPEG shell will offer long circulation. This paper is the first report of a LPDHs from PEA dendrimer with mPEG-*b*-PCL block copolymer for delivery of any class of drug. The synthesis, *in vitro*, MD simulations and *in vivo* findings through end groups functionalization of PEA dendrimer with a linear block polymer mPEG-*b*-PCL, and formulation of VCM encapsulated nanovesicles are reported in this paper.

3.7 Materials, instrumentation and methods

3.7.1 Materials

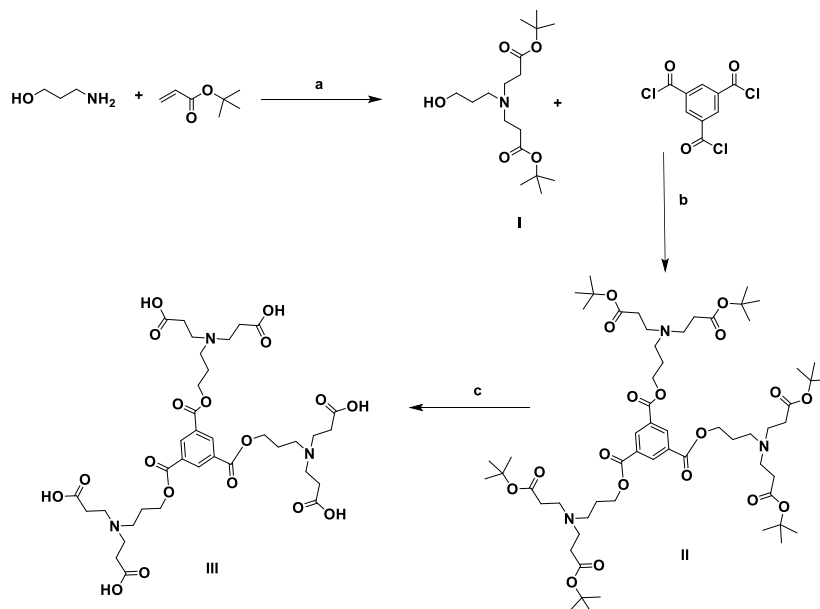
Acetylchloride (AcCl), *tert*-butyl acrylate, 3-amino-1-propanol, *p*-dimethylaminopyridine (DMAP), N,N'-Dicyclohexylcarbodiimide (DCC), 1,3,5-benzenetricarbonyl trichloride (Trimesoyl chloride), stannous octoate (Sn(Oct)₂), *tertiary* butyl acrylate, ϵ -caprolactone, tetrahydrofuran (THF), toluene, monomethoxy polyethylene glycol (mPEG) (MW 5,000), phosphatidyl choline, Human serum albumin (HSA) and silica gel were procured from Sigma-Aldrich (USA). Vancomycin (VCM) was obtained from Sinobright Import and Export Co., Ltd. (China), 3-(4,5-dimethylthiazol-2-yl)-2,5-diphenyltetrazolium bromide (MTT) was bought from Merck Chemicals (Germany). Nutrient Broth, Mueller-Hinton Broth (MHB) and Mueller-Hinton Agar (MHA) were acquired from Biolab (South Africa). Propidium iodide and Syto9 dyes cell viability kits were purchased from Thermofisher (USA). Monolith protein labelling kit RED-NHS, MST buffer supplement with 0.05 % Tween 20, Monolith NT.115 Standard Treated Capillaries were supplied by NanoTemper Technologies (Germany). The bacterial cultures used were *Staphylococcus aureus* ATCC 25923 and methicillin-resistant *S. aureus* (MRSA) (*S. aureus* Rosenbach ATCC BAA 1683).

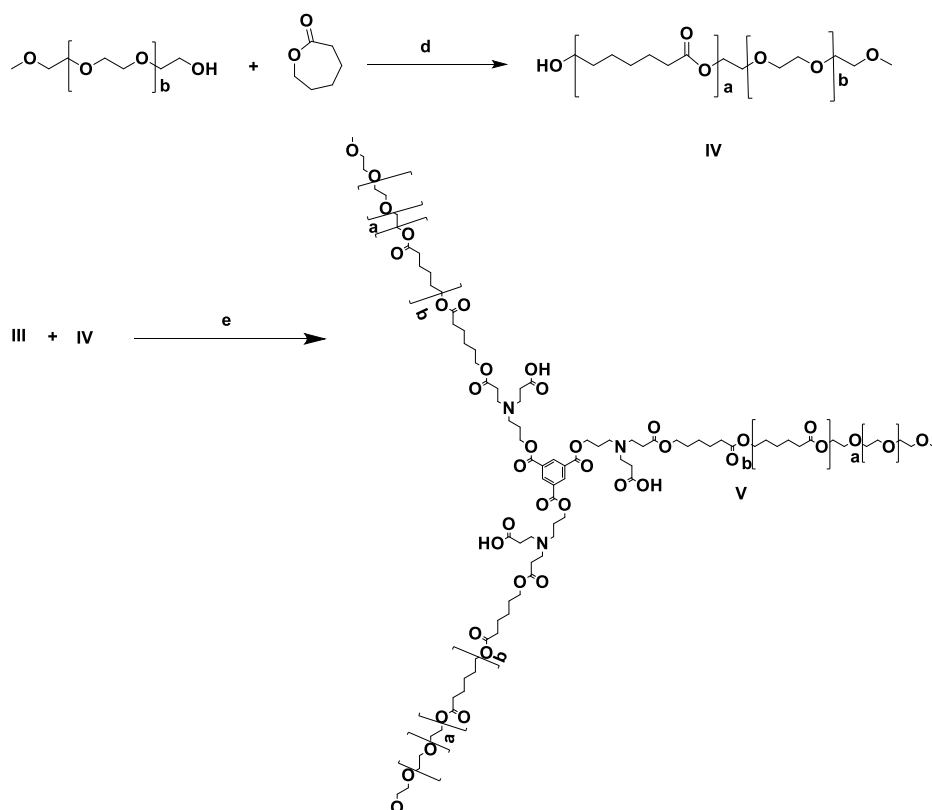
3.7.2. Instrumentation

Fourier-transform infrared spectroscopy (FT-IR) spectra of all the compounds were recorded on a Bruker Alpha-p spectrometer with a diamond ATR (Germany). Proton and Carbon nuclear magnetic resonance (^1H NMR and ^{13}C NMR) measurements were performed on a Bruker 400 and 600 Ultra shield™ (United Kingdom) NMR spectrometer. High Resolution Mass Spectrometry (HRMS) was performed on a Waters Micromass LCT Premier TOF-MS (United Kingdom). The matrix-assisted laser desorption ionization time-of-flight mass spectrometry (MALDI TOF) mass analysis was performed on a Bruker SmartBeam Autoflex III (Bruker Daltonics, Bremen, Germany). Gel permeation chromatography (GPC) was performed on a THF solvent system consisting of a Waters 1515 isocratic high-performance liquid chromatography (HPLC) pump, a Waters 717 plus auto-sampler, Waters 600E system controller (run by Breeze Version 3.30 SPA) with a Waters refractive index detector and mass was relative to a linear polystyrene calibration standard. Optical density (OD) was measured using a spectrophotometer (spectrostar nano, Germany)

3.7.3 Methods

3.7.3.1 Synthesis and characterization of the hybrid dendrimer





Scheme 1. a). methanol, stirring at room temperature 12 h, b). toluene, DMAP, 110 °C reflux, 6 h c). AcCl, H₂O, DCM, room temperature, 8 h, d). Sn(Oct)₂, toluene, 110 °C reflux 6 h, e). DCC, DMAP, DMF room temperature, 5 days.

3.7.3.1.1 Synthesis of di-*tert*-butyl 3,3'-((3-hydroxypropyl)azanediyl)dipropionate (compound I, Scheme 1a)

Compound I was synthesized following a reported procedure[40]. In brief, a solution of 3-Aminopropanol (1 g; 13.4 mmol) was dissolved in methanol (40 ml) then added slowly to *tertiary* butyl acrylate (14.0 g; 106.4 mmol), the mixture was left stirring overnight at 25 °C. Excess *tertiary* butyl acrylate and methanol were evaporated, and the product was dissolved in DCM and washed with brine solution. The organic layer was collected and dried over anhydrous sodium sulfate then concentrated to collect the product (7.4 g; yield 95%). FT-IR: 3432, 2933, 1722, 1151 cm⁻¹. ¹H NMR (400 MHz, CDCl₃): δ 1.37 (s, 18H), 1.62 – 1.64 (m, 2H), 2.33 – 2.36 (t, 2H), 2.56 – 2.57 (t, 4H), 2.58 – 2.69 (t, 4H), 3.67 – 3.68 (t, 2H). ¹³C NMR (400 MHz, CDCl₃): δ 28.06, 30.89, 33.09, 49.28, 52.91, 62.90, 80.71, 171.61; HRMS (ES-TOF): [M + H]⁺ calculated for C₁₇H₃₃NO₅: 331.24, found 331.24 (Appendix VI and VII).

3.7.3.1.2 Synthesis of tris(3-(bis(3-(tert-butoxy)-3-oxopropyl)amino)propyl) benzene-1,3,5-tricarboxylate (compound II, scheme 1b)

Compound II was synthesized following the reported procedure [40]. In summary, compound I (6 g; 18 mmol) and DMAP (6.6 g; 54 mmol) were dissolved in toluene (100 ml) and refluxed for 4 h and then cooled to room temperature. To the above reaction mixture, Trimesoyl chloride (1.2 g; 4.6 mmol) was added and refluxing continued for further 8 h. After reaction completion, toluene was removed by rotavap vacuum evaporation and the purification was done via column chromatography (hexane: ethyl acetate, 6 : 4) to obtain a yellowish thick oil ((4.4 g; yield 60%) compound 2 [47]. FT-IR: 2927, 2856, 1722, 1453, 1147 cm^{-1} . ^1H NMR (400 MHz, CDCl_3): δ 1.42 (s, 54), 1.95 (s, 6H), 2.37 (s, 12H), 2.58 (s, 6H), 2.75 (s, 12H), 4.4 (m, 6H), 8.82 (s, 3H). ^{13}C NMR (400 MHz, CDCl_3): δ 28.08, 33.47, 49.34, 50.14, 63.98, 80.41, 131.42, 134.42, 164.95, 171.80; HRMS (ES-TOF): $[\text{M} + \text{H}]^+$ calculated for $\text{C}_{60}\text{H}_{99}\text{N}_3\text{O}_{18}$: 1149.69, found 1149.63 (Appendix VI and VII).

3.7.3.1.3 Synthesis of 3,3',3'',3''',3''''',3''''''-((((benzene-1,3,5-tricarbonyl) tris (oxy)) tris (propane-3,1-diyl))tris(azanetriyl)) hexapropionic acid (compound III scheme 1c)

To a solution of compound II (2.12 g; 1.84 mmol) in DCM (60 ml), acetyl chloride (7.26 g; 92 mmol) and water (1.46 mL; 82 mmol) were reacted at ambient temperature, as reported in the literature [47]. The resulting reaction mass was stirred at 25 °C for 8 h and upon completion of the reaction solvents were then evaporated, and impurities from the product washed off with a mixture of DCM and hexane to obtain an off white foamy sticky compound III (G1-PEA) (1.12 g; yield 75%). FT-IR: 2958, 2610, 1710, 1403, 1334, 1178 cm^{-1} . ^1H NMR (400 MHz, D_2O): δ 2.25 – 2.23 (m, 6H), 2.84 – 2.87 (t, 12), 3.37 – 3.47 (m, 18H), 4.43 – 4.46 (t, 6H), 8.65 (s, 3). ^{13}C NMR (400 MHz, D_2O): δ 28.08, 33.47, 49.34, 50.14, 63.98, 80.41, 131.42, 134.42, 164.95, 171.80; HRMS (ES-TOF): $[\text{M} + \text{H}]^+$ calculated for $\text{C}_{36}\text{H}_{51}\text{N}_3\text{O}_{18}$: 814.32, found 814.33 (Appendix VI and VII).

3.7.3.1.4 Synthesis of methoxy poly (ethylene glycol)-b-poly(ϵ -caprolactone) (mPEG-b-PCL) (compound IV, scheme 1d)

Diblock mPEG-*b*-PCL copolymer (compound IV) was synthesized following a reported ring-opening polymerization procedure of ϵ -caprolactone using mPEG as a macroinitiator and Stannous Octoate ($\text{Sn}(\text{Oct})_2$) as a catalyst[48]. mPEG (5 g; 1 mmol) (Average molecular weight :5000Da) was dissolved in anhydrous toluene (100 ml) and azeotropically distilled for 6 h to remove any traces of water. To the above reaction mass, ϵ -caprolactone (5.7 g; 50 mmol) and of $\text{Sn}(\text{Oct})_2$ (0.04 g; 0.1mmol) were injected, after which the reaction mass was refluxed under nitrogen for 12h. The cooled reaction mass was added to excess cold diethyl ether to obtain a

white precipitate, which was filtered off. The filtration residue was washed several times with diethyl ether and then cold methanol and was kept for drying under vacuum for 48 h and a white solid was obtained with the yield of 85%.

The samples were detected on a Bruker SmartBeam Autoflex III (Bruker Daltonics, Bremen, Germany) MALDI TOF system. The samples were prepared in DCM (5mg/ml) spotted on a ground steel target with α -cyano-hydroxycinnamic acid (CHCA) matrix (1:1 ratio). The laser was set at 85%, with a detector voltage of 1850 V and sample digitizer rate of 2.00 GS/s in a mass range of 4000-8000 m/z. FT-IR :2942, 2868, 1723, 1347-1365, 1100 cm^{-1} . ^1H NMR (400 MHz, D_2O): δ 1.25 (m), 1.52 – 1.55(m), 2.19(t), 3.53 (s), 3.95(t). ^{13}C NMR (400 MHz, D_2O): δ 24.57, 25.52, 28.34, 34.11, 64.13, 70.56, 173.51(Appendix VI).

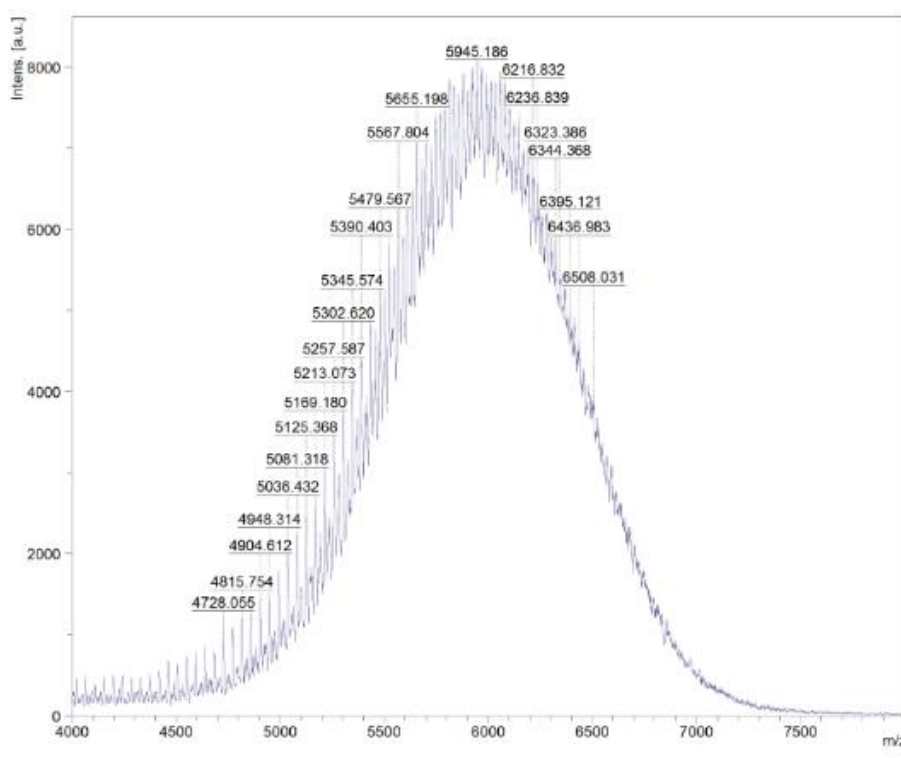


Figure 2. Mass peaks distribution as determined by MALDI TOF

Degree of polymerization was calculated using HNMR integration of the caprolactone repeating units against ethylene glycol repeating units[49] by the formula below

$$\text{PCL \%} = \left(\frac{\frac{ax}{mx}}{\frac{ax}{mx} + \frac{ay}{my}} \right) \times 100\%$$

Where ax is sum of caprolactone (CL) integrals, mx number of protons of repeating monomer unit of CL, ay sum of ethylene glycol (EG) integrals and my number of protons of repeating monomer unit of EG

3.7.3.1.5 Synthesis of G1 poly ester amine dendrimer core with 3 arm mPEG-b-PCL shell (3-mPEA) (compound V, Scheme 1e)

The telo-dendrimer (Compound V) was synthesized, as per a reported procedure [50]. In brief, compound III (0.2 g; 0.25mmol) was added to a mixture of mPEG-*b*-PCL copolymer (9.7 g; 4 mmol), DMAP (0.06 g; 2 mmol) and DCC (0.115 g; 2.2 mmol) were dissolved in DMF (10 ml), and the reaction mixture stirred at room temperature for five days. After completion of the reaction, the reaction mixture was filtered to remove dicyclohexylurea and the filtrate was diluted with water then loaded into a dialysis bag with a pore size of 14 to 18kDa. The reaction mass loaded bag was subsequently put in a receiver compartment filled with 20% methanolic water and dialyzed for 96 h. The receiver compartment phase was changed periodically to maintain the high concentration gradient in the donor compartment. After dialysis, the final pure product of PEA dendrimer core with 3 surface carboxylic groups have been attached with a linear block polymer mPEG-*b*-PCL (3-mPEA) compound V was isolated by freeze-drying the bag component (1.83 g; yield 40%). GPC was performed on a THF solvent system consisting of a Waters 1515 isocratic HPLC pump, a Waters 717 plus auto-sampler, Waters 600E system controller (run by Breeze Version 3.30 SPA) with a Waters refractive index detector, and mass was relative to a linear polystyrene calibration standard. FT-IR :2927, 2856, 1725, 1453,1105 cm^{-1} . ^1H NMR (600 MHz, CDCl_3): δ 1.31 – 1.32 (m), 1.58 (m), 1.84 (s), 2.23 – 2.24 (m), 3.4 – 3.42 (m), 3.98 – 3.99(m), 4.1 – 4.15(m), 8.12 (s). ^{13}C NMR (600 MHz, CDCl_3): δ 24.56, 25.52, 28.34, 34.11, 55.74, 59.01, 63.43 – 64.12, 69.11, 106.54, 173.51 – 173.72.8. GPC mass calculated for $\text{C}_{887}\text{H}_{16233}\text{N}_3\text{O}_{376}$: 18335.80, average molecular weight found 19115, Polydispersity:1.42 (Appendix VI and VII).

3.8.3.2 *In vitro* cytotoxicity

The *in vitro* cell viability of the synthesized material was assessed using a previously reported MTT assay method [51, 52] on human breast adenocarcinoma (MCF 7), adenocarcinomic alveolar basal epithelial cells (A 549), liver hepatocellular carcinoma (HepG 2) cell-lines and human embryonic kidney cells 293 (HEK 293). Each of the four cell lines containing 2.5×10^3 cells were seeded into 96-well plates and incubated for 24 h with different dilutions of 3-mPEA (20, 40, 60, 80 and 100 $\mu\text{g}/\text{mL}$). Wells with culture medium only and culture medium containing cells were considered as the negative and positive controls respectively. After 48 h of incubation, the culture medium and test materials were discarded and replaced with 100 μL of fresh culture medium and 100 μL of MTT solution (5 mg/mL in PBS) in each well. Cell viability was evaluated by measuring the mitochondrial-dependent conversion of the

the reaction, the reaction mixture was filtered to remove dicyclohexylurea and the filtrate was diluted with water then loaded into a dialysis bag with a pore size of 14 to 18kDa. The reaction mass loaded bag was subsequently put in a receiver compartment filled with 20% methanolic water and dialyzed for 96 h. The receiver compartment phase was changed periodically to maintain the high concentration gradient in the donor compartment. After dialysis, the final pure product of PEA dendrimer core with 3 surface carboxylic groups have been attached with a linear block polymer mPEG-*b*-PCL (3-mPEA) compound V was isolated by freeze-drying the bag component (1.83 g; yield 40%). GPC was performed on a THF solvent system consisting of a Waters 1515 isocratic HPLC pump, a Waters 717 plus auto-sampler, Waters 600E system controller (run by Breeze Version 3.30 SPA) with a Waters refractive index detector, and mass was relative to a linear polystyrene calibration standard. FT-IR :2927, 2856, 1725, 1453,1105 cm^{-1} . ^1H NMR (600 MHz, CDCl_3): δ 1.31 – 1.32 (m), 1.58 (m), 1.84 (s), 2.23 – 2.24 (m), 3.4 – 3.42 (m), 3.98 – 3.99(m), 4.1 – 4.15(m), 8.12 (s). ^{13}C NMR (600 MHz, CDCl_3): δ 24.56, 25.52, 28.34, 34.11, 55.74, 59.01, 63.43 – 64.12, 69.11, 106.54, 173.51 – 173.72.8. GPC mass calculated for $\text{C}_{887}\text{H}_{16233}\text{N}_3\text{O}_{376}$: 18335.80, average molecular weight found 19115, Polydispersity:1.42 (Appendix VI and VII).

3.8.3.2 *In vitro* cytotoxicity

The *in vitro* cell viability of the synthesized material was assessed using a previously reported MTT assay method [51, 52] on human breast adenocarcinoma (MCF 7), adenocarcinomic alveolar basal epithelial cells (A 549), liver hepatocellular carcinoma (HepG 2) cell-lines and human embryonic kidney cells 293 (HEK 293). Each of the four cell lines containing 2.5×10^3 cells were seeded into 96-well plates and incubated for 24 h with different dilutions of 3-mPEA (20, 40, 60, 80 and 100 $\mu\text{g}/\text{mL}$). Wells with culture medium only and culture medium containing cells were considered as the negative and positive controls respectively. After 48 h of incubation, the culture medium and test materials were discarded and replaced with 100 μL of fresh culture medium and 100 μL of MTT solution (5 mg/mL in PBS) in each well. Cell viability was evaluated by measuring the mitochondrial-dependent conversion of the tetrazolium salt MTT to formazan crystals. After 4 h of incubation with MTT, the media was

removed from the wells, and solubilization of formazan was achieved by adding 100 μ L of dimethyl sulfoxide. The optical density (proportional to the number of live cells) was assessed with a microplate spectrophotometer (spectrostar nano, Germany) at an absorbance wavelength of 540 nm. The percentage cell viability was calculated as follows;

$$\% \text{ Cell viability} = \left(\frac{\text{A540 nm treated cells}}{\text{A540 nm untreated cells}} \right) \times 100\%$$

3.8.4 Formulating VCM loaded 3-mPEA nanovesicles

The nanovesicles were prepared using a solvent evaporation method [53]. A solution of 10, 30, 40 and 50 mg of 3-mPEA each dissolved in 5 mL organic solvent (THF) was added drop-wise to 20 mL of the aqueous solution containing 10 mg of VCM under stirring (400 rpm). The resulting emulsions was left to stir overnight at room temperature to ensure the complete evaporation of the organic solvent. The non-drug loaded nanovesicles were prepared using the same procedure.

3.8.5 Characterisation of the nanoparticles

3.8.5.1 Size, Polydispersity Index (PI), Zeta Potential (ZP) and morphology.

The size, PI, and ZP of 3-mPEA nanovesicles were determined using dynamic light scattering technique on a Zetasizer Nano ZS90 (Malvern Instruments Ltd., UK), with all measurements being performed in triplicate. The Morphology was examined using transmission electron microscopy on a Jeol, JEM-1010 (Japan) transmission electron microscopy (TEM) with uranyl acetate (UA) negative staining [54]. The nanovesicles were diluted appropriately then mounted onto the surface of a copper grid, and the excess sample was removed by blotting off with filter paper, then dried at ambient temperature and stained using 2% uranyl acetate (UA) solution before measurement. The images were captured at an accelerating voltage of 100 kV.

3.8.5.2 Entrapment efficiency (% EE) and drug loading capacity (LC).

The EE and DL of V-3-mPEA were determined by an ultrafiltration method. Briefly, 2 mL of nanovesicles containing 500 μ g/mL, 1.5 mg/mL, 2 mg/mL, 2.5mg/mL of 3-mPEA loaded with 500 μ g/mL of VCM were placed in Amicon[®] Ultra-4 centrifugal filter tubes (Millipore Corp., USA) of 10 kDa pore size and centrifuged at 3000 rpm at 25 °C for 30 min. The filtrate was collected and the untrapped VCM in the filtrate was quantified using a high-pressure liquid chromatography (HPLC) (Shimadzu, Japan) method, with UV detection at a wavelength of 280 nm [55]. The mobile phase consisted of a mixture of water with 0.1 % TFA and acetonitrile (85/15 v/v), which was pumped through a Nucleosil 100-5 C18 column (150 mm X 4.6 mm

internal diameter) at a flow rate of 1 mL/min, with an injection volume of 100 μ L. The EE (%) and DL (%) were calculated using the following equations:

$$\%EE = \left(\frac{\text{Weight of VCM in nanoparticles}}{\text{Weight of VCM added}} \right) \times 100\%$$

$$\%LC = \left(\frac{\text{Weight of VCM in nanoparticles}}{\text{Total weight of nanoparticles}} \right) \times 100\%$$

3.8.5.3 Differential scanning calorimetry (DSC)

The VCM, 3-mPEA, physical mixture (drug and the polymer) and lyophilized formulation thermal profiles were determined by DSC (Shimadzu DSC-60, Japan). Briefly, samples (2 mg) were placed in an aluminum pan and sealed, which was then heated to 300 $^{\circ}$ C at a constant rate of 10 $^{\circ}$ C/min under a constant nitrogen flow of 20 mL/min using an empty pan as a reference [52].

3.8.5.4 All-atom MD simulations of 3-mPEA self-assembly

3.8.5.4.1 Methods

3-mPEA dendritic star polymer structure containing 3 arms of the block polymer comprising of 2 and 4 repeating monomer units of caprolactone and mPEG was constructed using ChemDraw[56]. The 3-mPEA dendritic star polymer was equilibrated for 2 ns before performing the self-assembly simulation. GROMACS insert-molecules tool was used for random insertion of 8 molecules of 3-mPEA and the polymers were solvated using TIP3P water model [57] and CHARMM General Force Field (CGenFF) [58]. The system containing a total of 29494 water molecules and 8 moles of 3-mPEA was first energy minimized using the steepest descent [59] method and self-assembly simulation was then performed using isobaric-isothermic ensemble (NPT) for 80 nanoseconds (ns). The velocity-rescale thermostat was used for temperature coupling and the Parrinello-Rahman method was used for pressure coupling [60]. The simulation was performed at 298.15 K temperature and 1 atm pressure using the coupling time of 0.1 ps and 2.0 ps, respectively. The Particle Mesh Ewald (PME) method [61] was used for long-range electrostatic interactions and VdW and short-range coulombic interactions were calculated using 10 \AA cut-off. MD simulations were performed using GROMACS 5.1.2 [62].

3.8.5.4.2 Data Analysis

Numbers of aggregates and the Com of Mass (COM) distances between two monomers were calculated using the g_aggregate tool [63] and in-house Tcl script respectively. The interaction

and binding energies between two monomers were computed using the *g_mmpbsa* tool [64], which employs the molecular mechanics Poisson–Boltzmann surface area (MM-PBSA) method and has been in the previous studies to calculate interaction and binding energies [65, 66]. The binding energy of two monomer complex in water environment was expressed as:

$$\Delta G_{binding} = \Delta G_{complex(dimer)} - (\Delta G_{monomer1} + \Delta G_{monomer2})$$

Where $\Delta G_{complex}$ is total energy of dimer complex and $\Delta G_{monomer1}$, $\Delta G_{monomer2}$ are total energy of both monomers individually. The energy of $\Delta G_{monomer1}$, and $\Delta G_{monomer2}$ were estimated using:

$$\Delta G_{monomer1} = \Delta E_{monomer1(MM)} + \Delta G_{monomer1(Solvation)}$$

$$\Delta G_{monomer2} = \Delta E_{monomer2(MM)} + \Delta G_{monomer2(Solvation)}$$

Where ΔE_{MM} is potential energy in the vacuum and estimated using:

$$\Delta E_{MM} = \Delta E_{bonded} + \Delta E_{nonbonded}$$

$$\Delta E_{MM} = \Delta E_{bonded} + (\Delta E_{vdw} + \Delta E_{elec})$$

The $\Delta G_{solvation}$ is solvation free energy and estimated using:

$$\Delta G_{solvation} = \Delta G_{polar} + \Delta G_{nonpolar}$$

ΔG_{polar} was calculated using the Poisson-Boltzmann (PB) equation and $\Delta G_{nonpolar}$ was estimated using:

$$\Delta G_{nonpolar} = \gamma SASA + b$$

Where SASA is the solvent accessible surface area, \AA radius of the probe boundary while γ is a coefficient related to the surface tension of the solvent and b is a fitting parameter

$$\gamma = 0.0226778 \text{ kJ/Mol/\AA}^2 \text{ and } b = 3.84928 \text{ kJ/Mol}$$

For binding energy calculation frames were extracted between 25 ns to 32 ns at interval of 500 ps. A bootstrap analysis was performed to calculate the standard error

3.8.6 Determination of the binding affinity of 3-mPEA nanovesicles on human serum albumin (HSA).

3.8.6.1 Microscale thermophoresis (MST) binding affinity studies.

The binding between 3-mPEA and HSA was measured using microscale thermophoresis (MST) on Monolith NT.115 (Germany) [67]. Human serum albumen (HSA) was labelled using the Monolith protein labelling kit RED-NHS according to the manufacturer's instructions. The labelled HSA was adjusted to 80 nM using an MST buffer supplemented with 0.05 % Tween 20. A 16-step serial dilution of 20 μ L solutions containing 25 μ M of mPEG 5000 (positive control), Phosphatidyl choline (negative control) and 3-mPEA with MST buffer was performed, with 10 μ L of the labelled HSA being added to each of the dilutions to form a ligand protein complex containing 40 nM HSA and ligand concentrations ranging from 12.5 μ M to 0.00038147 μ M. The ligand HSA complex was incubated for 15 min, then loaded into Monolith NT.115 Standard Treated Capillaries and the binding affinity measured on an MST instrument. Data of three independently pipetted measurements were analysed (MO-Affinity Analysis software version 2.1.3, NanoTemper Technologies). The strength of binding was evaluated by the dissociation constant K_d calculated by the equation:

$$K_d = \frac{([A][T])}{[AT]}$$

where [A] is the concentration of free fluorescent molecules, [T] is the concentration of titrant and [AT] is the concentration of complex formed by [A] and [T]. The smaller the K_d the stronger the binding force.

3.8.6.2 HSA protein adsorption studies

Human serum albumin adsorption studies were performed following a literature reported protocol [68, 69]. Nanoparticles were incubated in a solution of 400 μ g/ mL of HSA and stirred vigorously with a magnetic stirrer for 2 h at 37 $^{\circ}$ C. The nanoparticles were then centrifuged (14000 rpm, 4 $^{\circ}$ C for 20 min) to remove any unabsorbed proteins, after which the samples were diluted, and size and the surface charge was analysed by the Zeta Sizer.

3.8.7 *In vitro* drug release

Drug release of VCM was performed using the diffusion dialysis bag method, as per previously reported procedures [70, 71]. Dialysis bags (pore size: 8000–14,400 Da) were loaded with 2 mL of the drug loaded nanovesicles and non-drug loaded vesicles then placed in a 40 mL receiver compartment of PBS (pH 7.4) at 37 $^{\circ}$ C. This was then placed in shaking incubator (100 rpm) and at specific time intervals 3 mL of samples were drawn from the receiver solution and an equal amount of fresh PBS was replaced to keep a constant volume. Determination of the amount of the drug released was performed as per section 2.5.2 via a reported HPLC method

[55]. The experiments were performed in triplicate, with the release fraction of VCM from V-3-mPEA nanovesicles being calculated using the following equation:

$$\text{Cumulative release \%} = \left(\frac{M_t}{M_\infty} \right) \times 100\%$$

Where M_t is the amount of VCM released from the V-3-mPEA nanovesicles at time t , and M_∞ the amount of VCM pre-loaded in V-3-mPEA nanovesicles.

In addition, 60% cumulative *in vitro* drug release data was modeled and analyzed with DDSolver to determine the mechanism of release of VCM from the nanovesicles[51, 72, 73]. Zero order, first order, Higuchi, Weibull, Hixson-Crowell, and Korsmeyer–Peppas models were analyzed. Model with highest correlation coefficient (R^2) and lowest root mean square error (RMSE) was considered to be the best fit model. The ‘n’ exponent obtained after modeling the release data using the Korsmeyer-Peppas model and mean dissolution time (MDT) were parameters applied to deduce the kinetics and mechanism of drug release of the drug from the nanovesicles[74].

3.8.8 Stability studies

Short term stability studies of the V-3-mPEA nanovesicles were evaluated for 90 days at 4 °C and at room temperature by assessing, particle size, PI, and ZP parameters.

3.8.9 Antibacterial activity

3.8.9.1 Determination of the MIC

An *in vitro* antibacterial study was conducted using the broth microdilution method against SA and MRSA [75]. Both the bacterial cultures were grown in Mueller–Hinton Broth, with (MHB) appropriate dilutions being made to achieve 5×10^5 colony forming units per mL (CFU/mL) [76] of bacteria. V-3-mPEA nanovesicles and bare VCM were serially diluted in MHB broth and then incubated with bacterial cultures containing 5×10^5 colony forming units per mL (CFU/mL) for 18 h in a shaking incubator at 37 °C and 100 rpm. 10 μ L of the serial dilutions were spotted on Mueller–Hinton Agar (MHA) plates and incubated for a further 18 h. The minimum concentration at which no visible bacterial growth was observed was considered as the MIC.

3.8.9.2 Bacterial membrane disruption

Suspensions of MRSA 1.5×10^8 CFU/mL in phosphate saline buffer (PBS) were incubated with V-3-mPEA containing 250 μ g/mL of VCM in a 50:50 ratio for 4 h in an Eppendorf tube. The mixture of nanovesicles was diluted appropriately and mounted onto the surface of a copper grid. The excess sample was removed by blotting off with filter paper and was then dried at ambient temperature before measurement. The images were examined using High

Resolution Transmission Electron Microscope (brightfield, darkfield, STEM diffraction) - JEOL HRTEM 2100 [77].

3.8.9.3 Reduction of MRSA biofilm by V-3-mPEA

Inhibition of MRSA biofilms by V-3-mPEA was determined by fluorescence microscopy [78]. Microscope cover slips were placed at the bottom of 6 well plates. Then 2 mL of MRSA 1.5×10^8 CFU/mL suspensions in MHB were added to the wells and incubated for 3 days at 37 °C to form a fully mature biofilm. Prior to treatment, the media was sucked out of the wells with a Pasteur pipette and the wells were washed 3 times to remove non-adhered bacteria. 1 mL of bare VCM solution and nanovesicles formulation containing 125 µg/mL of VCM were added to the wells and incubated for 12 hours at 37 °C. The wells were then washed with Phosphate Buffer pH 7.4 to remove the treatments and non-adhered MRSA cells. While still in the wells the coverslips were stained with solution of Syto9 and propidium iodide (PI) containing 30 µL in 1 mL of distilled water for 30 mins in darkness. The wells were washed again to remove excess dye, then inverted on a microscope glass slide and the coverslips were carefully glued on the edges on the glass slides. The inhibition of biofilm formation by V-3-mPEA was viewed on a Fluorescence microscope (Nikon Eclipse 80i FM Japan). Syto9 and PI were sequentially excited at 488 nm and 543 nm, respectively, and their fluorescence emissions were collected between 500 and 600 nm for Syto9 and between 640 and 750 nm for PI. Microscopic observations were performed at least three times

in independent experiment.

3.8.9.4 Flow cytometry bacterial cell viability

Viable MRSA cells in the population after treatment with VCM and V-3-mPEA for 18 h was determined using flowcytometry method [79]. 15 µL containing 5×10^5 colony forming units (CFU)/mL of the bacterial suspension was added to a 96 well plate each containing 135 µL of bare VCM (positive control), and V-3-mPEA at the MIC concentration (15.65 µg/mL and 0.988 µg/mL respectively), which was further incubated at 37 °C in a shaking incubator (100 rpm). 50 µL of each VCM and V-3-mPEA mixture were added to the flow cytometry tubes each containing 350 µL of the sheath fluid and vortexed for 5 min. The mixture was incubated for 30 min with 5 µL of non-cell wall permeant propidium iodide (PI) and Syto9 cell permeant dye. PI fluorescence was excited by a 455-nm laser and collected through a 636 nm bandpass filter (red wavelength), while Syto9 excitation laser was at 485 nm laser and collected through a 498 nm band pass filter (green wave length). Untreated pure MRSA cells were used as a

negative control. The BD FACSCANTO II (Becton Dickinson, CA, USA) equipment was used for flow cytometry. Instrumentation settings included sheath fluid flow rate of 16 mL/min, a sample flow rate of 0.1 mL/min. Data with fixed cells were collected using a flow cytometer software (BD FACSDIVA V8.0.1 software [USA]). The voltage settings used for fluorescence-activated cell sorting (FACS) analysis were: 731 (forward scatter [FSC]), 538 (side scatter [SSC]), 451 (Syto9) and 444 for PI. The bacteria were initially gated using forward scatter, and cells of the appropriate size were then gated and at least 10,000 cells collected for each sample in triplicate, and their position as 'live' and 'dead' determined. To avoid any background signals from particles smaller than the bacteria, the detection threshold was set at 1,000 in SSC analyses [80].

3.8.9.5 Bacterial killing kinetics

An overnight culture of MRSA in MHB was diluted with phosphate buffer to a concentration of 5×10^5 CFU/ml. VM and VM loaded 3-mPEA were added at concentrations equivalent to 5x MIC. Sterile water was added in the bacterial broth with the test samples to serve as a negative control. Bacterial cell viability was monitored up to 24 h. Samples were removed at specific intervals, serially diluted in PBS, and plated in triplicate on MHA plates. After incubation of the plates for 24 h at 37°C, the CFU were counted and converted to \log_{10} values and plotted in a graph [81].

3.8.9.6 *In vivo* antibacterial activity

A BALB/c mouse skin infection model was used for *in vivo* antibacterial activity following a study protocol approved by the University of KwaZulu-Natal's Animal Research Ethics Committee (Approval number: AREC/104/015PD) [82, 83]. Humane care and use of the animals were in accordance with the guidelines of the AREC of UKZN and South African National Standard SANS 10386:2008. 18 – 20 g male BALB/c mice were obtained from the Biomedical Research Unit, University of KwaZulu-Natal. Mice back hairs were shaved carefully without bruising the skin then disinfected with 70% ethanol. After 24 h, 50 μ L of MRSA saline (1.5×10^8 CFU/mL) suspension was injected intradermally and the mice ($n = 4$) were divided into three treatment groups (positive control, negative control and V-3-mPEA groups). 30 minutes post infection with MRSA, 50 μ L of the different (V-3-mPEA formulation, free VCM and saline) treatments was administered to all the groups at the same site of infection. The mice were kept under observation for 48 h under the following conditions; a normal 12 h light and dark, temperature 19-23 °C, relative humidity $55 \pm 10\%$ and adequate ventilation. After 48 h the mice were euthanized with halothane and the infected area of the skin was

collected and homogenized in PBS of pH 7.4 (5 mL). Tissue homogenates were serially diluted in pH 7.4 phosphate buffer then 20 μ L were spotted on MHA plates, which were incubated at 37 °C for 24 h and the number of colonies forming units (CFU) were counted. The CFU/mL was calculated using the equation:

$$\text{CFU/mL} = \frac{\text{number of colonies} \times \text{dilution factor}}{\text{volume of culture plate}}$$

The infected skins were also collected and processed as per reported procedure [51] for further histological investigations. The Processed skin sections were collected on slides and stained with hematoxylin and eosin (H&E). Examinations and image capturing of the slide was performed on a Leica Microscope DM 500, fitted with a Leica ICC50 HD camera (Leica Biosystems, Germany).

3.8.10 Statistical analysis

One-way analysis of variance (ANOVA), followed by Bonferroni's multiple comparison test, was used for the statistical analysis. Individual groups were compared to each other using a paired *t*-test, with *p* values of <0.05 being considered statistically significant, and the values are represented as mean \pm SD.

3.9.0 Results and discussion

3.9.1 Synthesis and characterization

The surface end groups modified dendrimer was synthesized in four steps (supplementary materials). The first step involved bis-aza-Michael addition reaction, as depicted in scheme 1a, to synthesize a dendron (compound I), after which the 1st generation dendrimer (compound II) was synthesized by coupling the dendron with the 1,3,5-benzenetricarbonyl chloride as a central aromatic core using DMAP as a catalyst. The tertiary butyl ester protecting groups on compound II were hydrolyzed to give a poly (ester-amine) dendrimer with an aromatic core (compound III). mPEG-*b*-PCL (compound IV) was synthesized, as illustrated in scheme 1d via ring-opening polymerization chemistry [48]. The degree of polymerization of the block polymer was calculated by integrating the mPEG peaks at 3.53 ppm against the 1.52 – 2.199 poly caprolactone repeating units peak in the ¹H NMR spectrum [84] and the degree of polymerization was found to be 21.1% which was correlating with the mass analysis by MALDI TOF (supplementary material).

The dendrimer was further coupled to the diblock copolymer to afford the final compound V (3-mPEA). In the final Steglich esterification reaction, only 3 among the six carboxylic acid groups of the dendrimer were esterified or occupied with the mPEG-PCL. This limited

esterification was confirmed by observed practical mass by GPC analysis, with an average molecular weight 19115 Da and polydispersity index of 1.42. The partial esterification may be due to the high molecular weight of mPEG-*b*-PCL that caused steric hindrance [85], and more intra molecular hydrogen bonding in the dendrimer (carboxylic acid group) could have restricted the esterification reaction [86].

The diblock copolymer mPEG-*b*-PCL was chosen to functionalize the dendrimer as it has been shown to be safe with excellent solvating properties [44, 87]. Apart from being efficient nano materials, dendrimers are associated with toxicities that hinder their biomedical applications [43, 88]. However, the literature shows that PEA dendrimers are safe, biodegradable [89, 90], flexible, and provide sustained release properties when compared to other dendritic polymer counterparts [41-43]. This makes them a good candidate for drug delivery. Thus a hybrid of mPEG-*b*-PCL and PEA dendrimers would result in a material with inherent good properties from the parent blocks.

3.9.2 *In vitro* cytotoxicity

The *in vitro* cell viability of 3-mPEA was assessed by quantifying the viable mammalian cells after exposure of the synthesized material. Four cell lines MCF 7, A549, Hep G2 and HEK 293 were employed to determine the bio-safety of 3-mPEA in an *in vitro* cell culture system. The results showed that cell viability ranging from 77.23 to 118.6 % across all the concentrations in all cell lines that were tested. The percentage cell viability range obtained for the individual cell lines ranged from 77.41 to 83.57%, 77.29 to 82.68 %, 78.29 to 87.01 % and 87.3 to 118.6 % for MF7, A549, Hep G2 and HEK 293 respectively (**Figure 2**) with no dose-dependent toxicity within the concentrations of the polymer studied. This percentage viability displayed by 3-mPEA was above the requirements for biocompatibility and toxicity regulatory requirements for synthesized biomaterial [91-93]. Therefore, results from these findings shows 3-mPEA to be safe and nontoxic for biomedical applications.

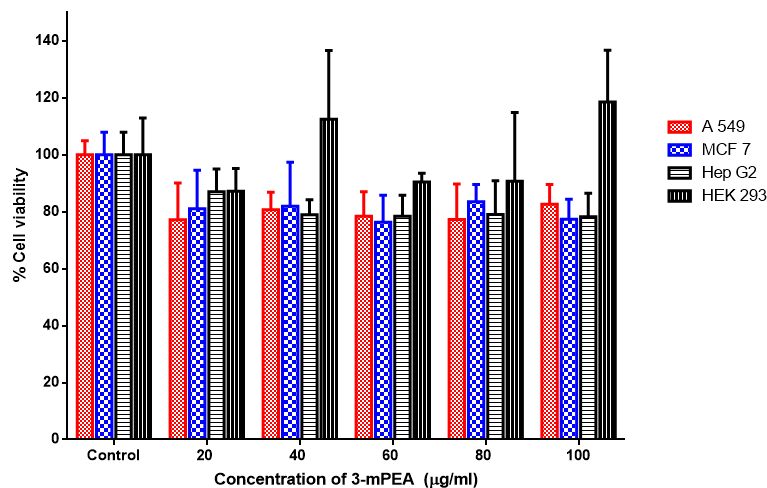


Figure 2. Cytotoxicity evaluation of various concentrations of 3-mPEA against on A 549, MCF 7 Hep G2 and HEK 293 cells

3.9.3 Preparation and characterisation of 3-mPEA nanovesicles

Self-assembled 3-mPEA nanovesicles were formulated by a solvent evaporation method. Solutions containing different concentrations of 3-mPEA in THF were added dropwise to the aqueous VCM solution under continuous stirring to optimize the concentrations of dendritic star polymer that will have the highest entrapment, size and PI (Table 1). As the organic solvent evaporated, the 3-mPEA molecules formed stable self-assembled nanovesicles while entrapping the VCM (**Figure 3**). The amphiphiles self-assembly might have been due to non-covalent interactions, such as hydrogen bond formation, π - π interactions, van der Waals interactions, electrostatic interactions, and the hydrophobic effects that lead to enhanced thermodynamic and kinetic stability of the vesicles [42, 94, 95].

There was no significant ($P > 0.5$) difference in the resulting sizes across all the concentrations. Although, there was an increase in PI with increasing concentration of the polymer however the increase was not significant ($P > 0.5$) (Table 1). It was observed that by increasing the polymer concentration above the ratio 3:1 the EE started to decrease. The polymer: drug ratio of 3:1 (w/w) was found to be the optimal concentration giving highest VCM encapsulation with nanovesicles of size, PI and, ZP of 52.48 ± 2.6 nm, 0.103 ± 0.047 and, -7.3 ± 1.3 mV respectively.

Table 1. Different ratio of drug polymer with their respective EE (n =3).

Polymer: drug	Size	PI	EE
1:1	54.07±0.291	0.199 ± 0.014	35.97 ±5.5 %
3:1	52.48± 2.6	0.103 ±0.047	76.49 ± 2.4%
5:1	53.89 ± 2.57	0.165 ± 0.028	60.74 ± 5.2 %
8:1	59.12± 0.54	0.23 ± 0.002	55.37 ± 0.8 %

The results were comparable to other nanovesicles from Janus dendrimers by Luis M. Bimbo and coworkers, who reported size ranges of 56–249 nm [96]. Percentage EE and LC for vesicles formed using 3:1 polymer to drug ratio were found to be 76.49 ± 2.4% and 19.1 ± 0.95 % ^{w/w} respectively. These results are better than other drug delivery systems from poly (ε-caprolactone) and poly (ethylene oxide) based vesicles where EE and LC were in the range of 45.5 to 69.33 % and 12 to 16 % respectively for clavulanic acid and methotrexate [87, 97, 98].. TEM images showed thin walled ring-shaped spherical structures (**Figure 4I**), with the population being discrete and in sizes that were comparable to the ones determined by DLS. The drug loaded vesicles were found to be physically stable in terms of size, PI and ZP both at room temperature and 4 °C for a period of 90 days.

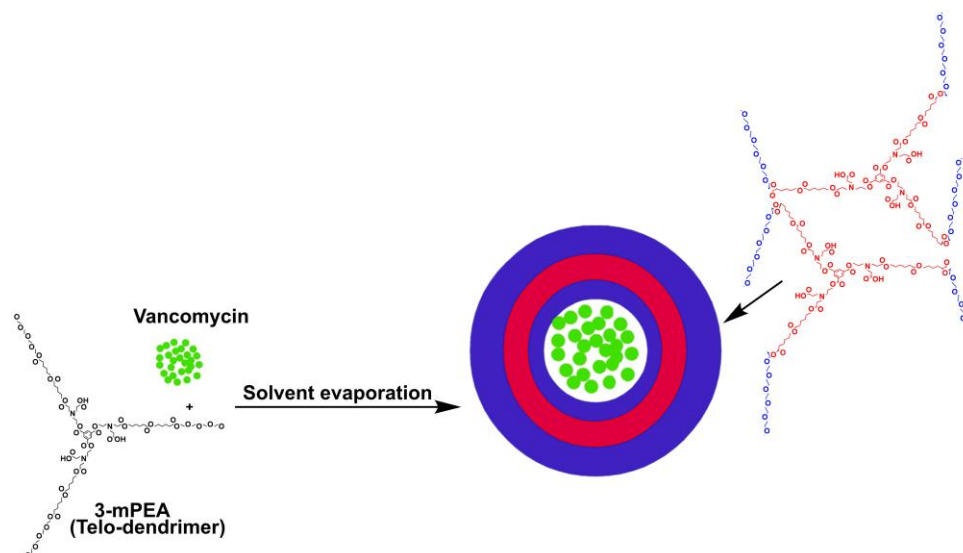


Figure 3. Schematic of drug encapsulation into nanovesicles.

3.9.3.2 Differential scanning calorimetry (DSC)

To determine the melting and crystallization behavior of VCM, 2m-PEA, lyophilized V-3-mPEA and the physical mixture, DSC studies were performed (**Figure 4III**). There was a broad endothermic peak at 105.93 °C for the bare VCM that presented the thermal decomposition of

the glycopeptide antibiotic, while for 3-mPEA, the peak was observed at 55.44 °C (**Figure 4III A**) [99]. The physical mixture showed the respective thermal peaks of VCM and 3-mPEA at temperature near to their individual peaks with a slight upward shift, while the thermogram of the lyophilized V-3-mPEA vesicles did not display any thermal peaks for neither VCM nor 3-mPEA. This disappearance suggested that VCM was encapsulated by vesicles in the non-crystalline form [100].

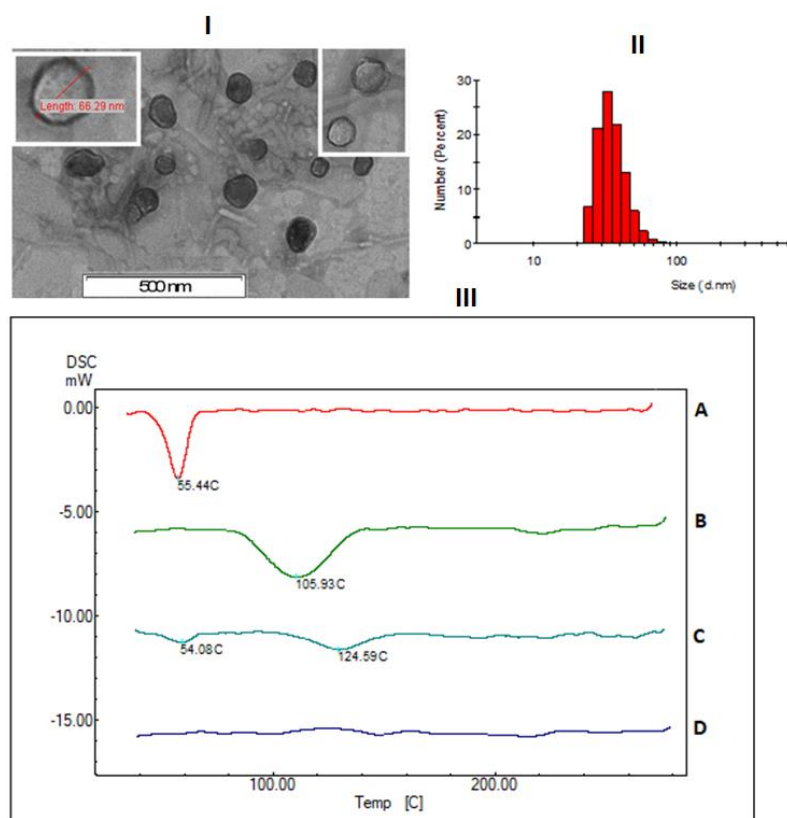


Figure 4. I) TEM of V-3-mPEA nanovesicles; II) size distribution of nanovesicles determined by DLS. III) thermogram of (A) 3-mPEA; (B) VCM; (C) physical mixture of VCM and 3-mPEA and (D) freeze dried V-3-mPEA

3.9.4 All-atom MD simulations of 3-mPEA self-assembly.

All-atom MD simulation was employed to understand the self-assembly of 3-mPEA star polymer. At time zero monomers were randomly apart, however a dimer was formed at time ~6.02 and ~10.14 ns respectively from aggregation of each of two molecules of the star polymer (**Figure 5E**). At times ~12.31, ~14.9 and ~51.93 aggregation of 3, 4 and 5 moles of the star polymer aggregated to form trimers, tetramers and pentamer respectively (**Figure 5A and B**). At time ~71.85 ns there was a rearrangement to form two tetramers for the short period of time and at ~79.11 ns all molecules aggregated to form an octamer (**Figure: 5D and E**). The arrangement included the hydrophilic portions (mPEG) of the linear block polymer facing on

the either side of the aggregates and in contact with water molecules, while the hydrophobic segment sandwiched in the middle (**Figure: 5C and D**). This aggregation could have been the possible arrangement that resulted in formation of the vesicle. Literature shows this arrangement is typical intermediate arrangement prior to the formation of a vesicle [35, 38, 101]. The general structure of 3-mPEA dendritic star polymer is a solvent-(philic-phobic-philic) (PHP) type sequence that contains hydrophobic connection between two hydrophilic ends that restricts the chain stretching in solvent-phobic core. The PHP structures have shown the ability to form complex structures such as vesicles, toroidal micelles, “Y” junctions, cylindrical micelles and disk-like membranes [102-104]. These structures have been successfully employed in drug delivery. Overall, results of this study supported the fact that 3-mPEA could self-assemble to stable aggregates.

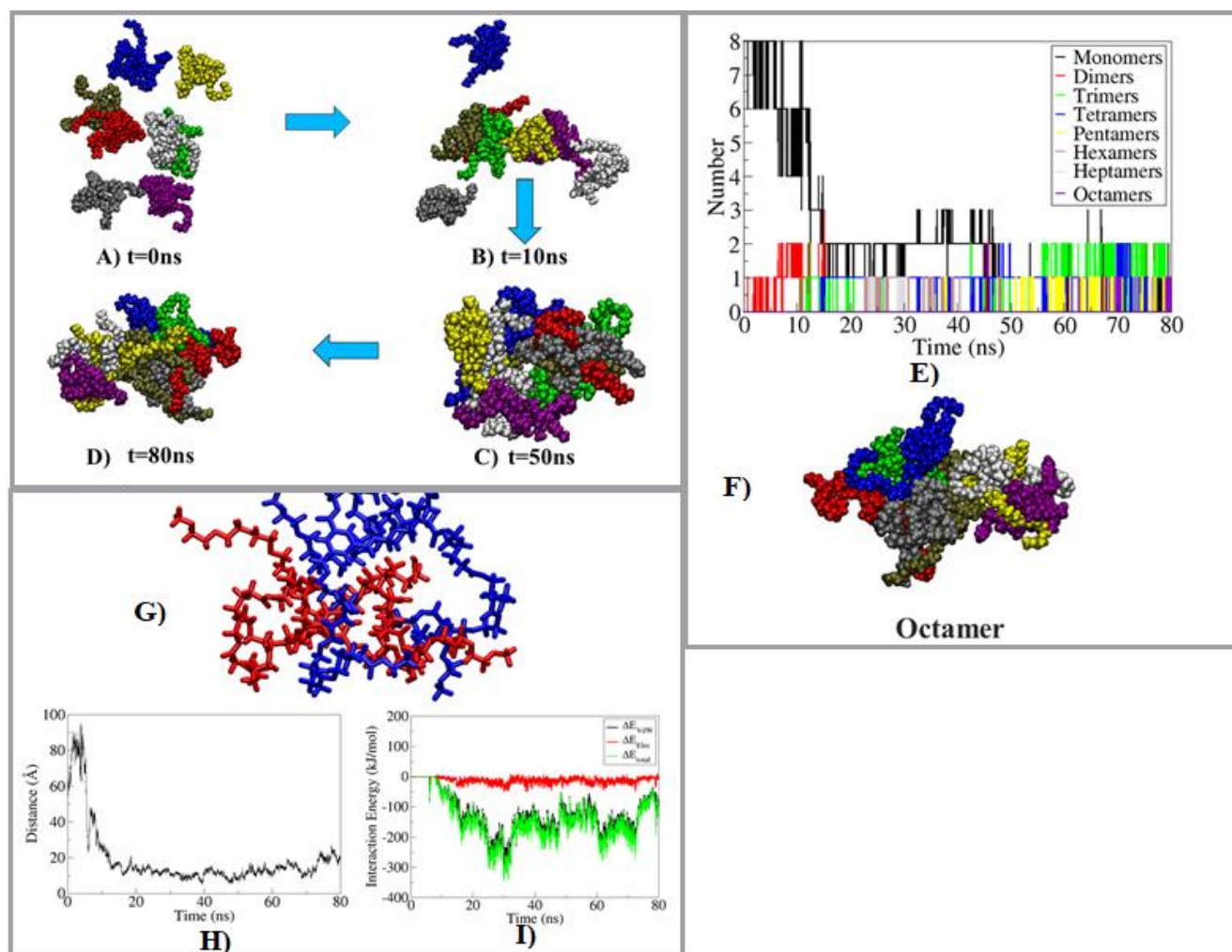


Figure 5. Self-assembly of 3-mPEA snapshots at t= A) 0, B) 10, C) 50 and D) 80 ns aggregation;. E) shows the time evolution self-assembly process; F) shows the arrangement

of octamer; G) shows the dimer in licorice representation, with monomers in blue, and red colours; H) shows the time evolution of distance between two monomers; I) shows the time evolution of interaction energy and its components

To understand the spontaneous interaction between 3-mPEA molecules, the type of interactions (VdW or electrostatics) that played a key role in their aggregation, binding energy and time evolution of COM distance we focused on one of the dimer (Figure 4G). It was observed that two monomers aggregated at ~8.32 ns and remained stably bound until the end of the simulation. Average interaction energy between both the monomers from ~8.32 ns to 80 ns was -159.58 kJ/mol (**Figure 4I**, green line) and decomposition of interaction energy in its components revealed that VdW interaction plays a curical role in the interaction between polymers. The average VdW and electrostatics interaction energies between polymers from ~8.32 to 80 ns were -145.85 kJ/mol and -13.74 kJ/mol respectively. Binding energy (**Table 2**) was calculated between the monomers from 25 ns to 32 ns when they were closest to each other. Binding energy components showed that polar solvation energy was highly unfavorable, however, favorable VdW energy, nonpolar energy, and electrostatic energies lead to the overall highly favorable binding energy.

Table 2. Average Binding Energy and its components obtained from the MM-PBSA Calculation for 3-mPEA dimer.

Contribution	Energy (kJ/mol)
ΔE_{vdw}	-241.49 ± 7.18
ΔE_{elec}	-26.78 ± 2.58
ΔG_{polar}	160.04 ± 8.49
$\Delta G_{nonpolar}$	-37.82 ± 0.83
ΔG_{total}	-146.07 ± 4.92

3.9.5 Human serum protein binding affinity.

To determine the binding affinity of 3-mPEA, mPEG 5000 polymer (positive control) and phosphatidyl choline (negative control) to HSA was performed using a Microscale Thermophoresis (MST) study. MST studies employ the motion of molecules due to changes in microscale temperature gradients [105]. The laser is usually focused onto the sample, which allows a temperature rise that induces thermophoresis of the molecules, which allows the MST signal to detect the binding by quantifying the change in the normalized fluorescence. The change in concentration between the initial and steady states is measured and can be plotted against the concentration of the added binding partner. From these data, the equilibrium

dissociation constant (K_d) is obtained [105-108]. In the study, a constant concentration HSA was labelled with NT-647 dye then incubated with increasing concentrations of the test samples (3-mPEA, mPEG 5000 and PC). Thermophoresis was then induced and detected due to a created temperature gradient (2–6 °C) by an infrared (IR) laser. The binding study on the mPEG 5000 did not display any binding affinity, which was similar to other results obtained using a different method [109]. However, binding studies for PC showed binding affinity to the HSA with a K_d of $39.997 \pm 0.1157 \mu\text{M}$ (Fig 4B). The 3-mPEA did not display any affinity to the HSA (**Figure 6**) [107] and there was no strong interaction of 3-mPEA with HSA to conclude any binding, and the data could not generate the dissociation constant.

The MST results were further confirmed by a zeta sizer study, where the nanovesicles were incubated with HSA, and its impact on the size, PDI and ZP were investigated [69]. There was no significant impact ($P>0.05$) of HSA on the nanovesicles before and after incubation (**Table 3**). This could be attributed to the 3-mPEA nanovesicles shell being composed of mPEG 5000, which is considered not to bind with HAS [110], which could suggest long circulating and offer stealth abilities to the nanovesicles [111, 112]. These studies indicated that the 3-mPEA nanovesicles could be utilized to formulate a long circulating drug delivery system.

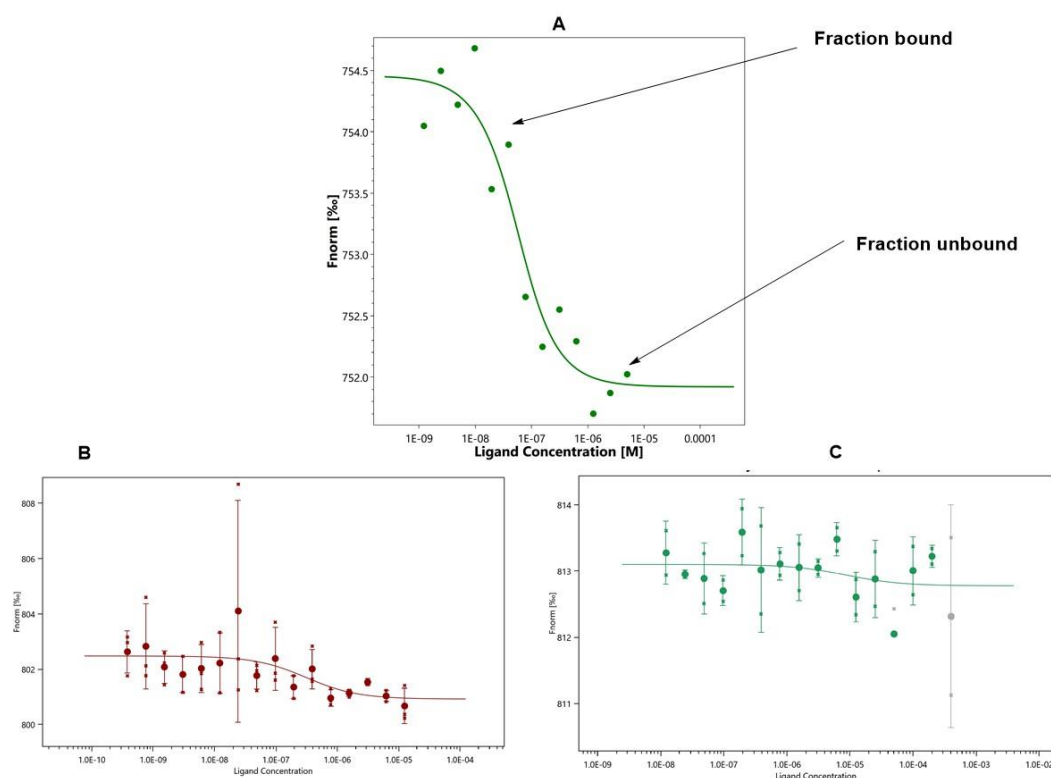


Figure 6. A) the change in the normalized fluorescence of PC which concludes binding, B and C) the change in the normalized fluorescence of 3-mPEA and mPEG 5000 respectively showing response to low to conclude binding.

Table 3. The effect of HSA on 3-mPEA nanovesicles after incubation.

Sample	Size	PDI	ZP
Before test	56.53 ± 2.822	0.190 ± 0.008	- 8.05 ± 1.6
After test	54.25 ± 1.73	0.228 ± 0.038	-6.23 ± 1.71

n = 3

3.9.6 *In vitro* drug release

In vitro drug release pattern of the bare drug and the nanovesicles formulation are represented in **Figure 7**. Release pattern after 1, 4 and 8 hours bare VCM had cumulative release of 10.63%, 42.2 % and 99.19% when compared to V-3-mPEA which was, 1.9 %, 22.2%, and 37.8% respectively After 24 and 48 hours cumulative drug release from the vesicles was 58.5 and 65.8 % respectively. The initial faster release could have been governed by diffusion, while later slower release phase after 8 hours might have been due to polymer erosion. The VCM release from the V-3-mPEA nanovesicles showed a slower drug release profile from the formulation when compared to the bare drug. This slower release of the drug from the V-3-mPEA nanovesicles could be beneficial as it could prolong exposure of bacteria to the lethal dose of

the drug and sustained antibacterial activity also could improve patients' compliance which could translate to reduced frequency of administration.

The release kinetics of VCM from the 3-mPEA nanovesicles was performed using different models (**Table 4**). Weibull model having shown a correlation coefficient of 0.9947 and mean square error of 2.14 was considered as the best fitting model for the release of VCM from nanovesicles. Korsmeyer-Peppas drug release n' exponent was 0.494 (**Table 4**), this indicated that non-Fickian diffusion was the responsible mechanism for the release of the drug from the nanovesicles. Basing on the n' exponent value more than one mechanism might have been involved [113, 114] in the release of the drug from the nanovesicles. Apart from diffusion, erosion and degradation might have played a role, as the 3-mPEA dendritic star polymer arms were coined from mPEG-*b*-PCL, which is a biodegradable synthetic polymer [115].

The mean dissolution time (MDT90 %) for the release of VCM from the drug solution and V-3-mPEA nanovesicles was calculated [116] and found to be 4.31 h and 11.29 h respectively from the nanovesicles and bare VCM respectively. These values further indicated that the rate at which the drug was released from the 3-mPEA nanovesicle was at a slower rate when compared to bare VCM. This value indicates that the release of the drug from the nanovesicles was sustained over an extended period of time and could translate into desired patient outcomes and improved patient compliance.

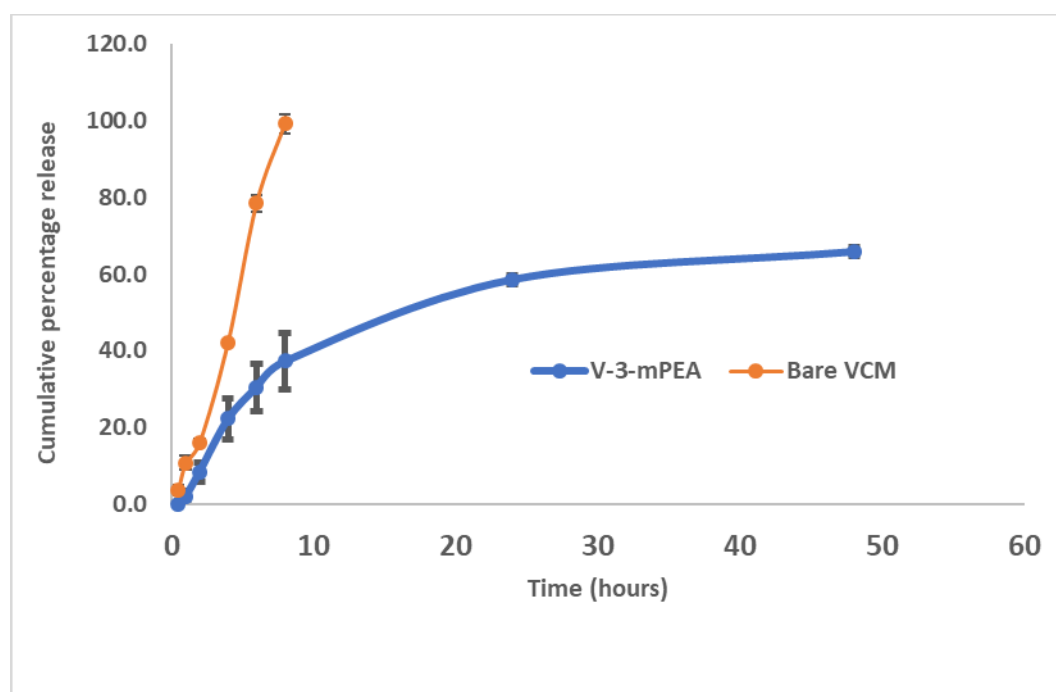


Figure 7. *In vitro* drug release profile of V-3-mPEA nanovesicles and bare VCM (n=3)

Table 4. Release kinetics data from different models

Model	R ²	RMSE	Release exponent (<i>n</i>)
Zero Order	0.5864	16.00	-
First Order	0.8563	9.4	-
Higuchi	0.9193	7.07	-
Korsmeyer-Peppas	0.9194	7.63	0.494
Hixson-crowell	0.7821	11.62	-
Weibull	0.9947	2.14	-

R² =linear regression coefficient, RMSE = Root mean square error

3..97 Antibacterial activity

3.9.7.1 Determination of the MIC

The broth dilution method was employed to determine the MIC values of the bare VCM and V-3-mPEA against *S. aureus* and MRSA. After 24 h of the study the MIC for VCM against *S. aureus* and MRSA was 3.9 µg/mL and 15.65 µg/mL respectively, whereas for V-3-mPEA nanovesicles against the same set of bacteria it was found to be 0.488 and 0.988 µg/mL respectively (**Table 5**). This was a 7- and 16-fold decrease in MIC against SA and MRSA after delivery of VCM via 3-mPEA nanovesicles (Table 3). Interestingly the activity continued up to 120 h, while the VCM was inactive after 24 h. The thicker cell walls of the MRSA could have been the reason for reduced activity towards MRSA than SA as more VCM molecules are needed to saturate the increased peptidoglycan layers before reaching the target site [117]. General enhanced activity of the 3-mPEA nanovesicles when compared to the bare VCM can be attributed to the small size of the nanovesicles, as literature shows that smaller particles sizes have a high surface area to volume ratio, which allows better distribution and adsorption to the bacterial surface [118, 119]. Furthermore, the slow release of the drug concentration for a relatively long time could also have been a contributing factor [120]. The lower MICs and prolonged activity attributed to the V-3-mPEA nanovesicles could result in a decrease in the effective the dose of treatment and less frequency of administration of VCM. This could go a long way in reducing dose-dependent nephrotoxicity [121], side effects and improved patients' compliance associated with vancomycin therapy without compromising their therapeutic outcomes. These findings highlight 3-mPEA star polymer as an efficient biomaterial for the delivery of VCM against SA and MRSA infections.

Table 5. MICs of bare VCM, blank and VCM loaded 3-mPEA, against *S. aureus* and MRSA

Time (hours)	24	48	72	96	120	24	48	72	96	120
	<i>S. aureus</i> (MIC $\mu\text{g/mL}$)					MRSA (MIC $\mu\text{g/mL}$)				
Bare VCM	3.9	NA	NA	NA	NA	15.65	NA	NA	NA	NA
V-3-mPEA	0.488	0.488	0.488	0.488	0.488	0.98	0.98	0.98	0.98	0.98
Blank	NA	NA	NA	NA	NA	NA	NA	NA	NA	NA

NA = No activity. The values are expressed as mean \pm SD, $n=3$.

3.9.7.2 Bacterial membrane disruption

The effect of V-3-mPEA membrane disruption on MRSA was determined by incubating the bacteria with V-3-mPEA for 4 hours. At initial stages of incubation, intact cocci can be seen (**Figure 8A**). After 1 hour, perforations on the bacteria membrane can be witnessed (**Figure 8B and C**). Following 4 hours of treatment, it can be seen that bacteria had lost all the membrane and intact vesicles can be see entering and surrounding the bacteria (Figure **8E and F**). Association of V-3-mPEA with the bacteria seems to be facilitated by the smaller sizes of the nanovesicles to cause maximum effective damage. This result supported the MIC data which showed effective killing of bacteria by V-3-mPEA and highlighted the plausible mechanism of action of V-3-mPEA.

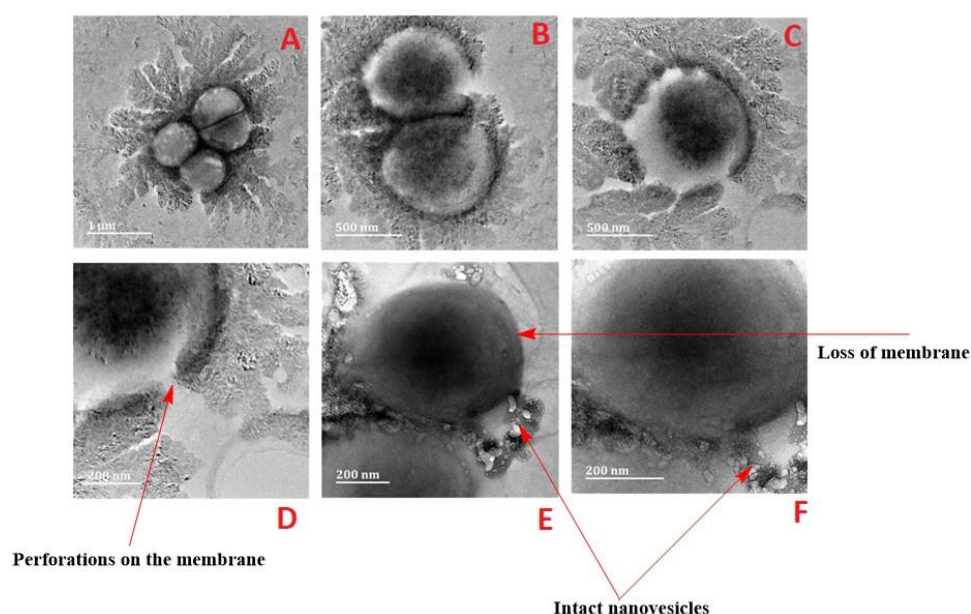


Figure 8. HRTEM images of MRSA after incubation with V-3-mPEA. A. At initial treatment; B. After 1 hour incubation, C. Single bacteria after 1 hour, D. Formation of pores on the bacterial membrane after treatment, E and F. Loss of the membrane of the MRSA after 4 hours with nanovesicles still intact.

3.9.7.3 Inhibition of MRSA biofilm

The ability of V-3-mPEA to eradicate biofilms was investigated. A 4 day fully mature biofilm of MRSA inhibition by V-3-mPEA and VCM was determined by fluorescence microscopy. The biofilms were grown on the cover slips and were stained with Syto9 and propidium iodide (PI) solution containing 30 μ L in 1 mL of distilled water for 30 mins in darkness, after which the dyes were washed off and cover slips were inverted on the glass slides (**Figure 9A**). Untreated biofilms showed high intensity of Syto9 fluorescence emanating from the whole of the cover slip. As Syto is a cell permeant dye, the high intensity is clearly due to the intact membrane of the high number of cells on the cover slip [122, 123]. When untreated cells were stained with the non-permeating dye PI, there was no intensity of the dye fluorescence as PI couldn't penetrate alive cells with an intact cell membrane (**Figure 9B**). Treatment of the biofilm with bare VCM and stained with Syto9 and PI, showed a slight decrease in the biofilm when compared to the untreated (**Figure 9C**) with some PI emission fluorescence emanating from the slide indicating some penetration of VCM in the biofilm and bacterial killing (**Figure 9D**). Unlike the previous treatments, when the biofilms were treated with V-3-mPEA nanovesicles there was a greater reduction of the biofilms. This was indicated by the reduction in the fluorescence intensity of Syto9 when compared to bare VCM treated and untreated biofilms, indicating fewer number of cells alive on the glass slide (**Figure 9E**). Interestingly there was very high intensity of PI emission fluorescence emanating from the slides of biofilms treated with the drug loaded nanovesicles. Despite PI being a non-cell permeant dye [122, 123], the high emission observed indicates that treatment with V-3-mPEA resulted in destruction of the biofilm and cell membrane of MRSA leading to high penetration of the PI which bound to DNA. Higher intensity therefore confirmed high killing percentage of V-3-mPEA compared to bare VCM that had a minimum effect on the biofilms. These results indicate that V-3-mPEA could be employed to also eliminate biofilms which cause detrimental health effects associated with surgical implants, chronic infections, urogenital infections, cystic fibrosis and dental infections.

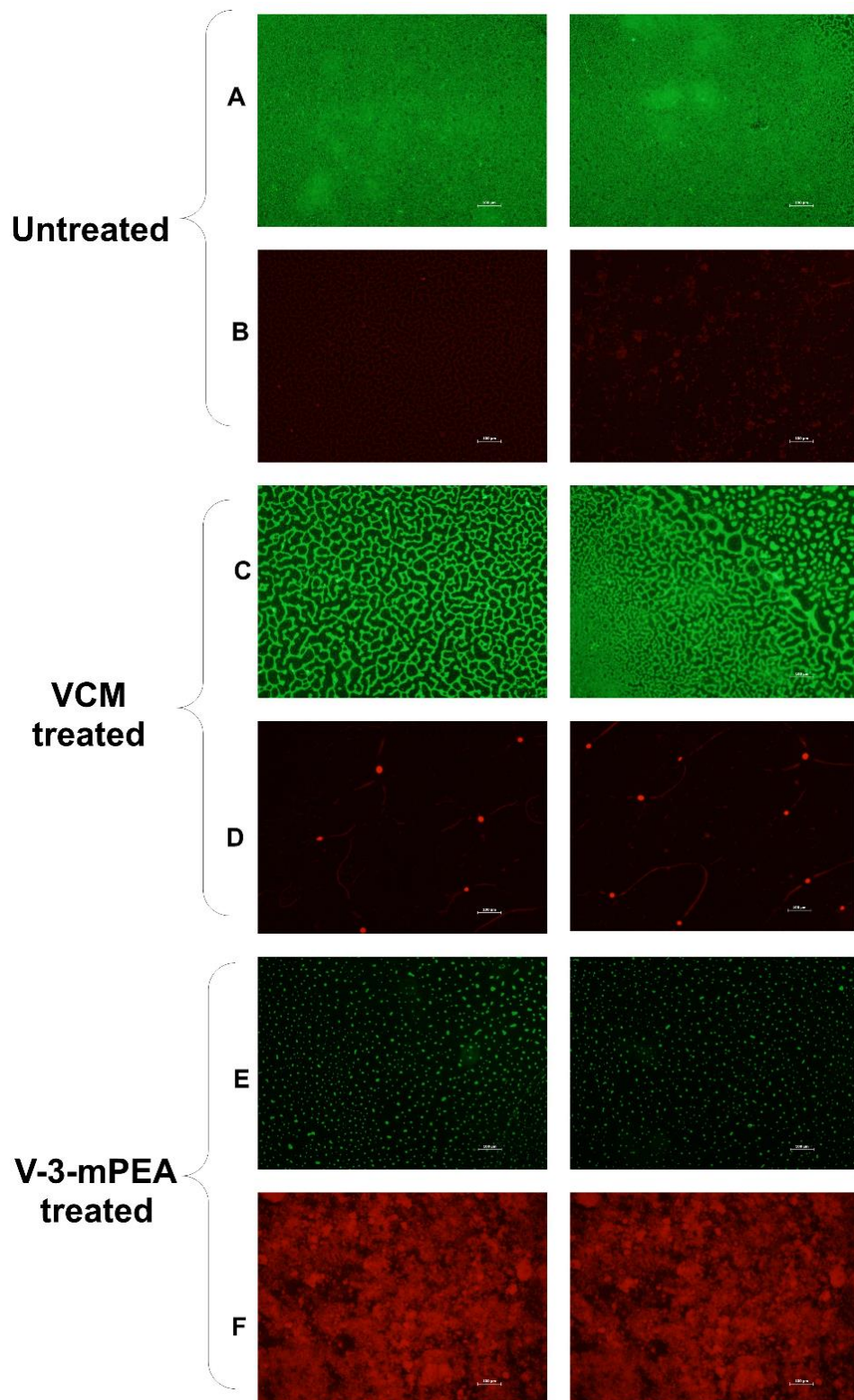


Figure 9. Fluorescence microscopy micrographs of the untreated, VCM treated and V-3-mPEA treated MRSA biofilms. A, and B untreated biofilm stained with Syto9 and PI respectively, B, C, D, E, F. VCM and V-3-mPEA treated biofilm stained with Syto9 and PI respectively (scale bar = 100 μm).

3.9.7.4 Flow cytometry bacterial cell viability

The rapid cell viability of the MRSA cells was determined using a flow cytometry method [79]. MRSA bacterial cells were incubated with bare VCM and V-3-mPEA mediums for 24 hours. The process of incubating bacteria in the presence of antibiotics induces changes in the bacteria morphology and cells cycle, which can be measured using special dyes [124]. The PI fluorescent dye, which is not cell wall permeating, is generally used to detect dead cells in the population, while Syto9 a non-selective cell wall permeant dye was used for alive cells [122, 123]. Data captured from flow cytometry were analyzed using Kaluza-1.5.20 (Beckman Coulter USA) flow cytometer software (**Figure 10I**). Two gates were created representing viable cells (green) and dead cells (red) in the population. VCM's mode of action compromises the integrity of the cell wall, which enhances the PI permeability and uptake and leads to intercalation with the DNA that results in a shift in PI fluorescence, this being an indication of bacterial cell death. After treating the MRSA cells with both bare VCM and V-3-mPEA, there was a shift in PI fluorescence (**Figure 10I B, C and D**). The bare VCM (**Figure 10IC**) and V-3-mPEA (**Figure 10I D**) at concentration of 0.488 and 3.9 $\mu\text{g/mL}$ respectively had $98.5 \pm 1.49\%$ and $99.59 \pm 0.55\%$ dead MRSA cells in the population. However, by treating the MRSA cells with bare VCM at the same concentration as the concentration of VCM in the drug-loaded nanovesicles (0.488 $\mu\text{g/mL}$), there were only $25.5 \pm 2.6\%$ dead cells in the population ($P < 0.0001$). From these results it can be deduced that the activity of VCM encapsulated 3-mPEA was the same as that of bare VCM but at a 16-fold lower concentration. These results could translate to lowering the amount of the dose required for treatment with V-3-mPEA without compromising the therapeutic outcomes. Furthermore, such a dose reduction could also go a long way to reducing dose-dependent vancomycin toxicity, such as nephrotoxicity [125], these results confirming the superiority of V-3-mPEA as a nano antibiotic.

3.9.7.5 Bacterial killing kinetics.

Figure 10II presents the rates of microbial killing by VCM, and VCM loaded 3-mPEA nanovesicles when exposed to MRSA at 5 times MIC of each treatment over a 24 h incubation period at 37°C. VM loaded 3-mPEA nanovesicles exhibited a rapid bactericidal effect, with a 3-log reduction (99.9% clearance) within 10 h in comparison to VCM which achieved its bactericidal effect within 24 h. The kill kinetics of vancomycin is similar to reports in the literature [81]. Noteworthy at 16 times lower concentration of VCM in the nanovesicles, they achieved faster killing rate (10 h) when compared to the bare drug. This could translate to quick

elimination of the bacteria in the body thus reducing the duration of treatment and the doses required to achieve successful therapy.

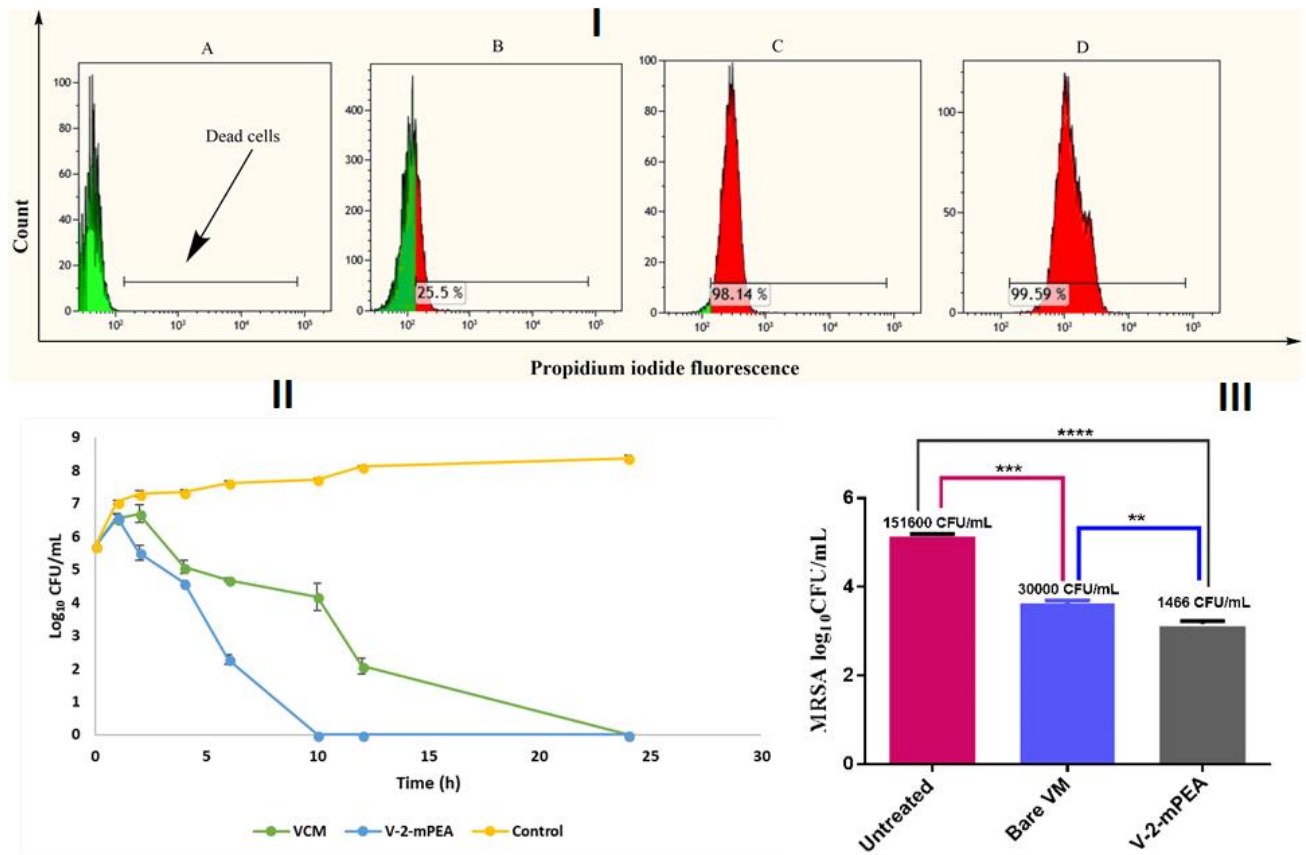


Figure 10 (I). cell counts vs PI uptake histogram where A, represents untreated MRSA (live cells); B, C and D represents percentage of dead cells in the population after incubation with VCM at its MIC (3.9 $\mu\text{g/mL}$) and V- 3-mPEA at its MIC (0.488 $\mu\text{g/mL}$) respectively; (II) the killing kinetics of MRSA exposed to 5x MIC of 3-mPEA nanovesicles, VCM and sterile water (control); (III) evaluation of MRSA burden post 48 h treatment. Data represented as mean \pm SD (n = 3). **denotes significant difference for V-3-mPEA versus bare VCM. ***denotes significant difference between untreated verses bare VCM and ****denotes significant difference between bare VCM free base and V-3-mPEA;

3.9.7.7 *In vivo* antibacterial activity

As a proof of concept, the antimicrobial activity and therapeutic efficacy of V-3-mPEA nanovesicles against MRSA infections were further assessed in a mouse skin infection model. The CFUs, from each treatment group were recovered and converted to log₁₀ CFU/mL as shown in **Figure 10III**. One-way ANOVA test showed a statistically significant ($P < 0.0001$)

reduction in the bacterial load of recovered bacteria in both V-3-mPEA and bare VCM treatment groups when compared to the untreated. The negative control (untreated), bare VCM and V-3-mPEA nanovesicles groups had the bacterial load (\log_{10} CFU/mL) of 5.18 ± 0.01 (151733.33 CFU/mL), 4.48 ± 0.05 (30000 CFU/ml) and 3.16 ± 0.07 (1466.7 CFU/mL) respectively. These findings established that the bare VCM and V-3-mPEA nanovesicles groups had a 20.5 ($P=0.0002$) and 103.5-fold($P<0.0001$) reduction of bacterial load when compared to untreated group. Furthermore, comparison between V-3-mPEA and bare VCM groups showed a 5.06-fold reduction of CFUs in nanovesicles group ($P = 0.0045$). These findings demonstrated V-3-mPEA nanovesicles as an effective drug delivery system for vancomycin.

Visual observations of the skin during harvesting revealed the formation of pus at the infection site of the untreated groups, while the treatment groups did not show pus formation (**Figure 11 A and B**). Microscopic morphological evaluations on the excised skin from the untreated, bare VCM and V-3-mPEA nanovesicles groups on the H&E stained slides revealed that the untreated skin samples displayed evidence of tissue inflammation and abscess formation (**Figure 11 C**). Although the bare VCM treatment group (**Figure 11 D**) displayed less degree of signs of swelling and abscess formation than the untreated group. However, comparatively, the V-3-mPEA group (**Figure 11 E**) displayed no signs of abscess formation, with minimal signs of tissue inflammation. Large quantities of white blood cells (WBCs) at the infection site was observed in the untreated and bare VCM groups indicating a greater immune response due to the high amount of isolated CFUs (**Figure 10 III**). The quantity of WBCs was minimal in the V-3-mPEA nanovesicles group (**Figure 11 E**). These histomorphological findings correlated with the recovered CFU/ml (**Figure 10 III**), which showed the skin samples (untreated and VCM treated groups) with the most number bacteria triggered higher degree of immune response that was manifested with the highest degree of inflammation, abscess formation and presence of white blood cells present at the infection site. Due to the lowest number of isolated bacteria in the V-3-mPEA nanovesicles group (**Figure 10 III**), minimal signs of inflammation and no abscess formation was observed. The histomorphological studies therefore confirm the antimicrobial advantage of the V-3-mPEA nanovesicles.

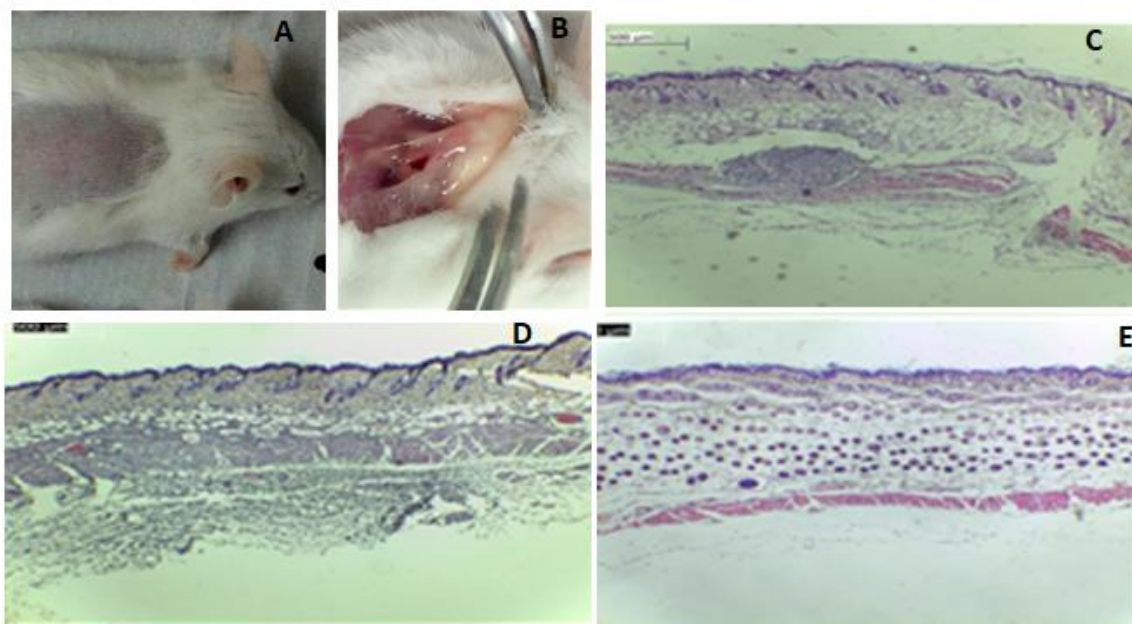


Figure 11. Histo-morphological evaluation post 48 h treatment- A) V-3-mPEA nanovesicles treatment, B) untreated group showing exudating pus, Light Microscopy (LM) micrographs of the control and the treated skin samples stained with H&E; (X40) (C) Untreated (MRSA and Saline); (D) Bare VCM; (E) V-3-mPEA nanovesicles (scale bar = 500 μm).

3.10 Conclusions

Generation one poly(ester-amine) dendrimer end groups were modified with mPEG-*b*-PCL linear polymer and evaluated for sustained delivery and enhanced activity of VCM. The hydrodynamic diameter of the nanovesicles was 52.48 ± 2.6 nm, as measured by the DLS and confirmed by the TEM. The nanovesicles exhibited a sustain release behavior of vancomycin over a period of 72 h. Studies performed with the MST and HSA binding showed that V-3-mPEA did not have any adsorption and binding affinity to the HSA, which indicated their potential for long systemic circulation. The *in vitro* antibacterial activity against the susceptible and resistance SA showed that V-3-mPEA had 8- and 16-fold greater activity when compared to the bare VCM. Further antibacterial studies using the flow cytometry method revealed that nanovesicles at MIC concentrations killed 99.5% of MRSA cells. Even at an 8-fold, lower concentrations of VCM in the nanovesicles compared to the bare VCM the nanovesicles were effective without compromising the efficacy of VCM. This was proof that the nanovesicles enhanced the activity of vancomycin. *In vivo* antibacterial test showed that V-3-mPEA had a 103 and 20-fold reduction in the MRSA load compared to the untreated and VCM treated mice respectively. These results indicated high efficacy of V-3-mPEA when compared to the bare drug. Findings of the study suggests promising development and translational potential of 3-

mPEA and V-3-mPEA for use as a drug delivery vehicle and nanoantibiotic against bacterial infections respectively.

Acknowledgments

The authors acknowledge the University of KwaZulu-Natal (UKZN), UKZN Nanotechnology Platform, Medical Research Council of South Africa and National Research Foundation of South Africa for financial support (Grant No. NRF Grant No. 87790 and 88453). The Microscopy and Microanalysis Unit, Biomedical Resource Unit, Department of Human Physiology and Sooraj Baijnath and Catalysis and Peptide Research Unit at UKZN and Department of Chemistry and Polymer Science and University of Stellenbosch are acknowledged for their technical assistance and CHPC Cape town for supercomputing resources.

Disclosure

The authors report no conflicts of interest in this work.

3.11References

- [1] R. Gaynes, The Discovery of Penicillin—New Insights After More Than 75 Years of Clinical Use, *Emerging Infectious Diseases*, 23 (2017) 849.
- [2] Shakeeb Asrar, K. Guimaraes, Global shortage of penicillin: Reasons and consequences, in, *Al Jazeera, US & Canada*, 2017.
- [3] I. Roca, M. Akova, F. Baquero, J. Carlet, M. Cavaleri, S. Coenen, J. Cohen, D. Findlay, I. Gyssens, O.E. Heur, G. Kahlmeter, H. Kruse, R. Laxminarayan, E. Liébana, L. López-Cerero, A. MacGowan, M. Martins, J. Rodríguez-Baño, J.M. Rolain, C. Segovia, B. Sigauque, E. Tacconelli, E. Wellington, J. Vila, The global threat of antimicrobial resistance: science for intervention, *New Microbes and New Infections*, 6 (2015) 22-29.
- [4] K.H. Luepke, K.J. Suda, H. Boucher, R.L. Russo, M.W. Bonney, T.D. Hunt, J.F. Mohr, Past, Present, and Future of Antibacterial Economics: Increasing Bacterial Resistance, Limited Antibiotic Pipeline, and Societal Implications, *Pharmacotherapy: The Journal of Human Pharmacology and Drug Therapy*, (2016).
- [5] K. Outtersson, New business models for sustainable antibiotics, Centre on Global health Security Working Group Papers, Chatham House (The Royal Institute of International Affairs), Working Groups on Antimicrobial Resistance, Paper, 1 (2014) 14-10.
- [6] K. Outtersson, U. Gopinathan, C. Clift, A.D. So, C.M. Morel, J.-A. Røttingen, Delinking Investment in Antibiotic Research and Development from Sales Revenues: The Challenges of Transforming a Promising Idea into Reality, *PLoS Med*, 13 (2016) e1002043.
- [7] R. Rath, R. Gupta, M.A. Rath, Antimicrobial Resistance: A Global Threat, *Imperial Journal of Interdisciplinary Research*, 2 (2016) 130-134.
- [8] D.C. Kaur, S.S. Chate, Study of Antibiotic Resistance Pattern in Methicillin Resistant Staphylococcus Aureus with Special Reference to Newer Antibiotic, *Journal of Global Infectious Diseases*, 7 (2015) 78-84.
- [9] M.S. Butler, M.A. Blaskovich, M.A. Cooper, Antibiotics in the clinical pipeline at the end of 2015, *The Journal of Antibiotics*, (2016) 3.
- [10] H.W. Boucher, J.S. Bakken, B.E. Murray, The United Nations and the Urgent Need for Coordinated Global Action in the Fight Against Antimicrobial Resistance Coordinated Global Action to Fight Against Antimicrobial Resistance, *Annals of Internal Medicine*, 165 (2016) 812-813.
- [11] WHO, Antimicrobial resistance, Fact sheet, in: WHO (Ed.) Fact sheet N°194, Geneva, 2015.
- [12] Who, Antimicrobial resistance: global report on surveillance 2014, in, WHO, 2014, pp. 257.
- [13] A.J. Huh, Y.J. Kwon, “Nanoantibiotics”: a new paradigm for treating infectious diseases using nanomaterials in the antibiotics resistant era, *Journal of Controlled Release*, 156 (2011) 128-145.

- [14] C.A. Omolo, R.S. Kalhapure, N. Agrawal, S. Rambharose, C. Mocktar, T. Govender, Formulation and Molecular Dynamics Simulations of a Fusidic Acid Nanosuspension for Simultaneously Enhancing Solubility and Antibacterial Activity, *Molecular Pharmaceutics*, 15 (2018) 3512-3526.
- [15] K.A. Hamblin, S.J. Armstrong, K.B. Barnes, C. Davies, T. Laws, J.D. Blanchard, S.V. Harding, H.S. Atkins, Inhaled Liposomal Ciprofloxacin Protects against a Lethal Infection in a Murine Model of Pneumonic Plague, *Frontiers in Microbiology*, 8 (2017) 91.
- [16] J.M. Caster, A.N. Patel, T. Zhang, A. Wang, Investigational nanomedicines in 2016: a review of nanotherapeutics currently undergoing clinical trials, *Wiley Interdisciplinary Reviews: Nanomedicine and Nanobiotechnology*, 9 (2017) e1416.
- [17] M. BioPharma, MAT2501: LNC Formulation of Amikacin, in, *Matinas BioPharma*, 2017.
- [18] C. Ma, P. Pan, G. Shan, Y. Bao, M. Fujita, M. Maeda, Core-shell structure, biodegradation, and drug release behavior of poly (lactic acid)/poly (ethylene glycol) block copolymer micelles tuned by macromolecular stereostructure, *Langmuir*, 31 (2015) 1527-1536.
- [19] Y. Lu, K. Park, Polymeric Micelles and Alternative Nanonized Delivery Vehicles for Poorly Soluble Drugs, *International Journal of Pharmaceutics*, 453 (2013) 198-214.
- [20] Y. Li, K. Xiao, W. Zhu, W. Deng, K.S. Lam, Stimuli-responsive cross-linked micelles for on-demand drug delivery against cancers, *Advanced Drug Delivery Reviews*, 66 (2014) 58-73.
- [21] Y.Q. Yang, B. Zhao, Z.D. Li, W.J. Lin, C.Y. Zhang, X.D. Guo, J.F. Wang, L.J. Zhang, pH-sensitive micelles self-assembled from multi-arm star triblock co-polymers poly (ϵ -caprolactone)-b-poly (2-(diethylamino) ethyl methacrylate)-b-poly (poly (ethylene glycol) methyl ether methacrylate) for controlled anticancer drug delivery, *Acta Biomaterialia*, 9 (2013) 7679-7690.
- [22] E.R. Gillies, J.M. Frechet, Dendrimers and dendritic polymers in drug delivery, *Drug Discovery Today*, 10 (2005) 35-43.
- [23] K. Madaan, S. Kumar, N. Poonia, V. Lather, D. Pandita, Dendrimers in drug delivery and targeting: Drug-dendrimer interactions and toxicity issues, *Journal of Pharmacy & Bioallied Sciences*, 6 (2014) 139-150.
- [24] S. Mignani, J. Rodrigues, H. Tomas, R. Roy, X. Shi, J.-P. Majoral, Bench-to-bedside translation of dendrimers: Reality or utopia? A concise analysis, *Advanced Drug Delivery Reviews*, (2017) In Press.
- [25] S.J. Guillaudeu, M.E. Fox, Y.M. Haidar, E.E. Dy, F.C. Szoka, J.M. Fréchet, PEGylated dendrimers with core functionality for biological applications, *Bioconjugate Chemistry*, 19 (2008) 461-469.
- [26] S.A. McNelles, S.D. Knight, N. Janzen, J.F. Valliant, A. Adronov, Synthesis, radiolabeling, and in vivo imaging of PEGylated high-generation polyester dendrimers, *Biomacromolecules*, 16 (2015) 3033-3041.
- [27] V.P. Torchilin, Multifunctional, stimuli-sensitive nanoparticulate systems for drug delivery, *Nat. Rev. Drug Discov.*, 13 (2014) 813.
- [28] S. Aryal, M. Prabakaran, S. Pilla, S. Gong, Biodegradable and biocompatible multi-arm star amphiphilic block copolymer as a carrier for hydrophobic drug delivery, *International Journal of Biological Macromolecules*, 44 (2009) 346-352.
- [29] Y.-Y. Jiang, G.-T. Tang, L.-H. Zhang, S.-Y. Kong, S.-J. Zhu, Y.-Y. Pei, PEGylated PAMAM dendrimers as a potential drug delivery carrier: in vitro and in vivo comparative evaluation of covalently conjugated drug and noncovalent drug inclusion complex, *Journal of Drug Targeting*, 18 (2010) 389-403.
- [30] W. Xiao, J. Luo, T. Jain, J.W. Riggs, H.P. Tseng, P.T. Henderson, S.R. Cherry, D. Rowland, K.S. Lam, Biodistribution and pharmacokinetics of a telodendrimer micellar paclitaxel nanoformulation in a mouse xenograft model of ovarian cancer, *International Journal of Nanomedicine*, 7 (2012) 1587.
- [31] Y. Zhang, C. Xiao, M. Li, J. Ding, C. Yang, X. Zhuang, X. Chen, Co-delivery of doxorubicin and paclitaxel with linear-dendritic block copolymer for enhanced anti-cancer efficacy, *Science China Chemistry*, 57 (2014) 624-632.
- [32] H. Yang, J.J. Morris, S.T. Lopina, Polyethylene glycol-polyamidoamine dendritic micelle as solubility enhancer and the effect of the length of polyethylene glycol arms on the solubility of pyrene in water, *Journal of Colloid and Interface science*, 273 (2004) 148-154.
- [33] Y. Wang, G. Qi, J. He, Unimolecular Micelles from Layered Amphiphilic Dendrimer-Like Block Copolymers, *ACS Macro Letters*, 5 (2016) 547-551.
- [34] J. Del Barrio, L. Oriol, C. Sánchez, J.L. Serrano, A.I. Di Cicco, P. Keller, M.-H. Li, Self-assembly of linear-dendritic diblock copolymers: from nanofibers to polymersomes, *Journal of the American Chemical Society*, 132 (2010) 3762-3769.
- [35] W. Jiang, Y. Zhou, D. Yan, Hyperbranched polymer vesicles: from self-assembly, characterization, mechanisms, and properties to applications, *Chemical Society Reviews*, 44 (2015) 3874-3889.
- [36] Y. Zhou, D. Yan, Supramolecular Self-Assembly of Giant Polymer Vesicles with Controlled Sizes, *Angewandte Chemie International Edition*, 43 (2004) 4896-4899.
- [37] C.G. Palivan, R. Goers, A. Najer, X. Zhang, A. Car, W. Meier, Bioinspired polymer vesicles and membranes for biological and medical applications, *Chemical Society Reviews*, 45 (2016) 377-411.

- [38] Y. Wang, B. Li, H. Jin, Y. Zhou, Z. Lu, D. Yan, Dissipative Particle Dynamics Simulation Study on Vesicles Self-Assembled from Amphiphilic Hyperbranched Multiarm Copolymers, *Chemistry—An Asian Journal*, 9 (2014) 2281-2288.
- [39] M.T. Morgan, M.A. Carnahan, C.E. Immoos, A.A. Ribeiro, S. Finkelstein, S.J. Lee, M.W. Grinstaff, Dendritic molecular capsules for hydrophobic compounds, *Journal of the American Chemical Society*, 125 (2003) 15485-15489.
- [40] D. Soto-Castro, J.A. Cruz-Morales, M.T.R. Apan, P. Guadarrama, Synthesis of Non-Cytotoxic Poly (Ester-Amine) Dendrimers as Potential Solubility Enhancers for Drugs: Methotrexate as a Case Study, *Molecules*, 15 (2010) 8082-8097.
- [41] J.d.A.K. Twibanire, T.B. Grindley, Polyester dendrimers, *Polymers*, 4 (2012) 794-879.
- [42] J.d.A. Twibanire, T.B. Grindley, Polyester Dendrimers: Smart Carriers for Drug Delivery, *Polymers*, 6 (2014) 179.
- [43] K. Jain, P. Kesharwani, U. Gupta, N.K. Jain, Dendrimer toxicity: Let's meet the challenge, *International Journal of Pharmaceutics*, 394 (2010) 122-142.
- [44] H. Pungkham, N. Swatdipakdi, M. Theerasilp, S. Karnkla, M. Chittchang, P. Ploypradith, N. Nasongkla, PEG-b-PCL and PEG-b-PLA polymeric micelles as nanocarriers for lamellarin N delivery, in: *Engineering in Medicine and Biology Society, EMBC, 2011 Annual International Conference of the IEEE, IEEE, 2011*, pp. 3245-3248.
- [45] P. Dineshkumar, T. Panneerselvam, K. Deepti Brundavani, K. Selvaraj, P. Vijayaraj Kumar, Formulation of Rifampicin Loaded PEGylated 5.0 G EDA-PAMAM Dendrimers as Effective Long-Duration Release Drug Carriers, *Current Drug Therapy*, 12 (2017) 115-126.
- [46] M.A. Mintzer, E.L. Dane, G.A. O'Toole, M.W. Grinstaff, Exploiting dendrimer multivalency to combat emerging and re-emerging infectious diseases, *Molecular Pharmaceutics*, 9 (2011) 342-354.
- [47] T.R. Krishna, N. Jayaraman, Synthesis of poly (propyl ether imine) dendrimers and evaluation of their cytotoxic properties, *The Journal of organic chemistry*, 68 (2003) 9694-9704.
- [48] W. Zhang, J. He, Z. Liu, P. Ni, X. Zhu, Biocompatible and pH-responsive triblock copolymer mPEG-b-PCL-b-PDMAEMA: Synthesis, self-assembly, and application, *Journal of Polymer Science Part A: Polymer Chemistry*, 48 (2010) 1079-1091.
- [49] J.U. Izunobi, C.L. Higginbotham, Polymer molecular weight analysis by ¹H NMR spectroscopy, *Journal of Chemical Education*, 88 (2011) 1098-1104.
- [50] B. Neises, W. Steglich, Simple method for the esterification of carboxylic acids, *Angewandte Chemie International Edition*, 17 (1978) 522-524.
- [51] C.A. Omolo, R.S. Kalhapure, M. Jadhav, S. Rambharose, C. Mocktar, V.M. Ndesendo, T. Govender, Pegylated oleic acid: A promising amphiphilic polymer for nano-antibiotic delivery, *European Journal of Pharmaceutics and Biopharmaceutics*, 112 (2017) 96-108.
- [52] R.S. Kalhapure, D.R. Sikwal, S. Rambharose, C. Mocktar, S. Singh, L. Bester, J.K. Oh, J. Renukuntla, T. Govender, Enhancing targeted antibiotic therapy via pH responsive solid lipid nanoparticles from an acid cleavable lipid, *Nanomedicine: Nanotechnology, Biology and Medicine*, (2017).
- [53] Z. Daman, S. Ostad, M. Amini, K. Gilani, Preparation, optimization and in vitro characterization of stearyl-gemcitabine polymeric micelles: A comparison with its self-assembled nanoparticles, *International Journal of Pharmaceutics*, 468 (2014) 142-151.
- [54] Y. Wang, J. Fang, D. Cheng, Y. Wang, X. Shuai, A pH-sensitive micelle for codelivery of siRNA and doxorubicin to hepatoma cells, *Polymer*, 55 (2014) 3217-3226.
- [55] K. Muppidi, A. Pumerantz, G. Betageri, J. Wang, Development and validation of a rapid high-performance liquid chromatography method with UV detection for the determination of vancomycin in mouse plasma, *J Chromat Separation Techniq*, 4 (2013) 1-5.
- [56] K.R. Cousins, Computer review of ChemDraw Ultra 12.0, in, *ACS Publications*, 2011, pp. 8388-8388.
- [57] P. Mark, L. Nilsson, Structure and dynamics of the TIP3P, SPC, and SPC/E water models at 298 K, *The Journal of Physical Chemistry A*, 105 (2001) 9954-9960.
- [58] K. Vanommeslaeghe, E. Hatcher, C. Acharya, S. Kundu, S. Zhong, J. Shim, E. Darian, O. Guvench, P. Lopes, I. Vorobyov, CHARMM general force field: A force field for drug-like molecules compatible with the CHARMM all-atom additive biological force fields, *Journal of Computational Chemistry*, 31 (2010) 671-690.
- [59] M. Bixon, S. Lifson, Potential functions and conformations in cycloalkanes, *Tetrahedron*, 23 (1967) 769-784.
- [60] M. Parrinello, A. Rahman, Polymorphic transitions in single crystals: A new molecular dynamics method, *Journal of Applied physics*, 52 (1981) 7182-7190.
- [61] T. Darden, D. York, L. Pedersen, Particle mesh Ewald: An $N \cdot \log(N)$ method for Ewald sums in large systems, *The Journal of Chemical Physics*, 98 (1993) 10089-10092.

- [62] M.J. Abraham, T. Murtola, R. Schulz, S. Páll, J.C. Smith, B. Hess, E. Lindahl, GROMACS: High performance molecular simulations through multi-level parallelism from laptops to supercomputers, *SoftwareX*, 1 (2015) 19-25.
- [63] J. Barnoud, G. Rossi, L. Monticelli, Lipid embranes as solvents for carbon nanoparticles, *Physical Review Letters*, 112 (2014) 068102.
- [64] R. Kumari, R. Kumar, O.S.D.D. Consortium, A. Lynn, g_mmpbsa A GROMACS tool for high-throughput MM-PBSA calculations, *Journal of chemical information and modeling*, 54 (2014) 1951-1962.
- [65] N. Agrawal, A.A. Skelton, Binding of 12-crown-4 with Alzheimer's A β 40 and A β 42 monomers and its effect on their conformation: insight from molecular dynamics simulations, *Molecular Pharmaceutics*, 15 (2017) 289-299.
- [66] N. Agrawal, A.A. Skelton, 12-Crown-4 Ether Disrupts the Patient Brain-Derived Amyloid- β -Fibril Trimer: Insight from All-Atom Molecular Dynamics Simulations, *ACS Chemical Neuroscience*, 7 (2016) 1433-1441.
- [67] Q.-S. Liu, R. Deng, Q.-F. Yan, L. Cheng, Y. Luo, K. Li, X. Yin, X. Qin, Novel Beta-Tubulin-Immobilized Nanoparticles Affinity Material for Screening β -Tubulin Inhibitors from a Complex Mixture, *ACS Applied Materials & Interfaces*, 9 (2017) 5725-5732.
- [68] S. Parveen, S.K. Sahoo, Corrigendum to "Long circulating chitosan/PEG blended PLGA nanoparticle for tumor drug delivery"[*Eur. J. Pharmacol.* 670 (2011) 372–383], *European Journal of Pharmacology*, (2014) 186.
- [69] L. Thiele, J.E. Diederichs, R. Reszka, H.P. Merkle, E. Walter, Competitive adsorption of serum proteins at microparticles affects phagocytosis by dendritic cells, *Biomaterials*, 24 (2003) 1409-1418.
- [70] X. Cheng, H. Yan, X. Jia, Z. Zhang, Preparation and in vivo/in vitro evaluation of formononetin phospholipid/vitamin E TPGS micelles, *Journal of Drug Targeting*, 24 (2016) 161-168.
- [71] S.J. Sonawane, R.S. Kalhapure, S. Rambharose, C. Mocktar, S.B. Vepuri, M. Soliman, T. Govender, Ultra-small lipid-dendrimer hybrid nanoparticles as a promising strategy for antibiotic delivery: In vitro and in silico studies, *International Journal of Pharmaceutics*, 504 (2016) 1-10.
- [72] T. Loftsson, B. Ilievska, G.M. Asgrimsdottir, O.T. Ormarsson, E. Stefansson, Fatty acids from marine lipids: Biological activity, formulation and stability, *Journal of Drug Delivery Science and Technology*, 34 (2016) 71-75.
- [73] Z. Karami, S. Sadighian, K. Rostamizadeh, M. Parsa, S. Rezaee, Naproxen conjugated mPEG-PCL micelles for dual triggered drug delivery, *Materials Science and Engineering: C*, 61 (2016) 665-673.
- [74] Y. Zhang, M. Huo, J. Zhou, A. Zou, W. Li, C. Yao, S. Xie, DDSolver: an add-in program for modeling and comparison of drug dissolution profiles, *The AAPS journal*, 12 (2010) 263-271.
- [75] J.H. Jorgensen, J.D. Turnidge, Susceptibility test methods: dilution and disk diffusion methods, in: *Manual of Clinical Microbiology*, Eleventh Edition, American Society of Microbiology, 2015, pp. 1253-1273.
- [76] C.a.L.S. Institute, *Methods for Dilution Antimicrobial Susceptibility Tests for Bacteria That Grow Aerobically; Approved Standard—Ninth Edition* in: C.a.L.S. Institute (Ed.), CLSI, Pennsylvania 19087, USA, 2012, pp. 63.
- [77] N. Chauhan, A.K. Tyagi, P. Kumar, A. Malik, Antibacterial potential of *Jatropha curcas* synthesized silver nanoparticles against food borne pathogens, *Frontiers in Microbiology*, 7 (2016) 1748.
- [78] F. Berlutti, A. Frioni, T. Natalizi, F. Pantanella, P. Valenti, Influence of sub-inhibitory antibiotics and flow condition on *Staphylococcus aureus* ATCC 6538 biofilm development and biofilm growth rate: BioTimer assay as a study model, *The Journal Of Antibiotics*, 67 (2014) 763.
- [79] N.M. O'Brien-Simpson, N. Pantarat, T.J. Attard, K.A. Walsh, E.C. Reynolds, A Rapid and Quantitative flow cytometry method for the analysis of membrane disruptive antimicrobial activity, *PloS One*, 11 (2016) e0151694.
- [80] S. Renggli, W. Keck, U. Jenal, D. Ritz, Role of autofluorescence in flow cytometric analysis of *Escherichia coli* treated with bactericidal antibiotics, *Journal of Bacteriology*, 195 (2013) 4067-4073.
- [81] M.F. Mohamed, M.I. Hamed, A. Panitch, M.N. Seleem, Targeting methicillin-resistant *Staphylococcus aureus* with short salt-resistant synthetic peptides, *Antimicrobial Agents and Chemotherapy*, 58 (2014) 4113-4122.
- [82] E. Kugelberg, T. Norström, T.K. Petersen, T. Duvold, D.I. Andersson, D. Hughes, Establishment of a superficial skin infection model in mice by using *Staphylococcus aureus* and *Streptococcus pyogenes*, *Antimicrobial Agents and Chemotherapy*, 49 (2005) 3435-3441.
- [83] R.S. Kalhapure, M. Jadhav, S. Rambharose, C. Mocktar, S. Singh, J. Renukuntla, T. Govender, pH-responsive chitosan nanoparticles from a novel twin-chain anionic amphiphile for controlled and targeted delivery of vancomycin, *Colloids and Surfaces B: Biointerfaces*, 158 (2017) 650-657.
- [84] X. Shuai, T. Merdan, F. Unger, M. Wittmar, T. Kissel, Novel biodegradable ternary copolymers hy-PEI-g-PCL-b-PEG: synthesis, characterization, and potential as efficient nonviral gene delivery vectors, *Macromolecules*, 36 (2003) 5751-5759.
- [85] S. Svenson, The dendrimer paradox - high medical expectations but poor clinical translation, *Chemical Society Reviews*, 44 (2015) 4131-4144.

- [86] P.I. Nagy, Competing Intramolecular vs. Intermolecular Hydrogen Bonds in Solution, *International Journal of Molecular Sciences*, 15 (2014) 19562-19633.
- [87] H. Nosrati, R. Adinehvand, H.K. Manjili, K. Rostamizadeh, H. Danafar, Synthesis, characterization, and kinetic release study of methotrexate loaded mPEG–PCL polymersomes for inhibition of MCF-7 breast cancer cell line, *Pharmaceutical Development and Technology*, (2018) 1-10.
- [88] J. Šebestík, M. Reiniš, J. Ježek, Biocompatibility and Toxicity of Dendrimers, in: J. Šebestík, M. Reiniš, J. Ježek (Eds.) *Biomedical Applications of Peptide-, Glyco- and Glycopeptide Dendrimers, and Analogous Dendrimeric Structures*, Springer Vienna, Vienna, 2012, pp. 111-114.
- [89] R.B. Arote, S.-K. Hwang, M.-K. Yoo, D. Jere, H.-L. Jiang, Y.-K. Kim, Y.-J. Choi, J.-W. Nah, M.-H. Cho, C.-S. Cho, Biodegradable poly(ester amine) based on glycerol dimethacrylate and polyethylenimine as a gene carrier, *The Journal of Gene Medicine*, 10 (2008) 1223-1235.
- [90] S.K. Prajapati, S.D. Maurya, M.K. Das, V.K. Tilak, K.K. Verma, R.C. Dhakar, Dendrimers in drug delivery, diagnosis and therapy: basics and potential applications, *Journal of Drug Delivery and Therapeutics*, 6 (2016) 67-92.
- [91] T.L. Riss, R.A. Moravec, A.L. Niles, S. Duellman, H.A. Benink, T.J. Worzella, L. Minor, *Cell Viability Assays*, National Institutes of Health, Bethesda, Maryland, 2016.
- [92] R. Hamid, Y. Rotshteyn, L. Rabadi, R. Parikh, P. Bullock, Comparison of alamar blue and MTT assays for high throughput screening, *Toxicology in vitro*, 18 (2004) 703-710.
- [93] T. Mosmann, Rapid colorimetric assay for cellular growth and survival: application to proliferation and cytotoxicity assays, *Journal of Immunological Methods*, 65 (1983) 55-63.
- [94] H. Cui, Z. Chen, S. Zhong, K.L. Wooley, D.J. Pochan, Block copolymer assembly via kinetic control, *Science*, 317 (2007) 647-650.
- [95] S. Zhang, Y. Zhao, Rapid release of entrapped contents from multi-functionalizable, surface cross-linked micelles upon different stimulation, *Journal of the American Chemical Society*, 132 (2010) 10642-10644.
- [96] S. Nummelin, M. Selin, S. Legrand, J. Ropponen, J. Seitsonen, A. Nykanen, J. Koivisto, J. Hirvonen, M.A. Kostianen, L.M. Bimbo, Modular synthesis of self-assembling Janus-dendrimers and facile preparation of drug-loaded dendrimersomes, *Nanoscale*, 9 (2017) 7189-7198.
- [97] I.N. Kurniasih, J. Keilitz, R. Haag, Dendritic nanocarriers based on hyperbranched polymers, *Chemical Society Reviews*, 44 (2015) 4145-4164.
- [98] H. Danafar, Preparation and characterization of PCL-PEG-PCL polymersomes for delivery of clavulanic acid, *Cogent Medicine*, 3 (2016) 1235245.
- [99] T.H. Hoang Thi, F. Chai, S. Leprêtre, N. Blanchemain, B. Martel, F. Siepman, H.F. Hildebrand, J. Siepman, M.P. Flament, Bone implants modified with cyclodextrin: Study of drug release in bulk fluid and into agarose gel, *International Journal of Pharmaceutics*, 400 (2010) 74-85.
- [100] C.G. Pupe, M. Villardi, C.R. Rodrigues, H.V.A. Rocha, L.C. Maia, V.P. de Sousa, L.M. Cabral, Preparation and evaluation of antimicrobial activity of nanosystems for the control of oral pathogens *Streptococcus mutans* and *Candida albicans*, *International Journal of Nanomedicine*, 6 (2011) 2581-2590.
- [101] S.J. Marrink, A.E. Mark, Molecular Dynamics Simulation of the Formation, Structure, and Dynamics of Small Phospholipid Vesicles, *Journal of the American Chemical Society*, 125 (2003) 15233-15242.
- [102] Q. Zhang, J. Lin, L. Wang, Z. Xu, Theoretical modeling and simulations of self-assembly of copolymers in solution, *Progress in Polymer Science*, 75 (2017) 1-30.
- [103] P. He, X. Li, D. Kou, M. Deng, H. Liang, Complex micelles from the self-assembly of amphiphilic triblock copolymers in selective solvents, *The Journal of Chemical Physics*, 132 (2010) 204905.
- [104] W. Kong, B. Li, Q. Jin, D. Ding, A.-C. Shi, Complex micelles from self-assembly of ABA triblock copolymers in B-selective solvents, *Langmuir*, 26 (2009) 4226-4232.
- [105] P. Baaske, C. Wienken, M. Willemsen, D. Braun, S. Duhr, Protein-binding assays in biological liquids using microscale thermophoresis, *Journal of Biomolecular Techniques: JBT*, 22 (2011) S55.
- [106] C.J. Wienken, P. Baaske, U. Rothbauer, D. Braun, S. Duhr, Protein-binding assays in biological liquids using microscale thermophoresis, *Nature Communications*, 1 (2010) ncomms1093.
- [107] M. Jerabek-Willemsen, T. André, R. Wanner, H.M. Roth, S. Duhr, P. Baaske, D. Breitsprecher, MicroScale Thermophoresis: Interaction analysis and beyond, *Journal of Molecular Structure*, 1077 (2014) 101-113.
- [108] J.M. Rainard, G.C. Pandarakalam, S.P. McElroy, Using Microscale Thermophoresis to Characterize Hits from High-Throughput Screening: A European Lead Factory Perspective, *SLAS Discovery: Advancing Life Sciences R&D*, 23 (2018) 225-241.

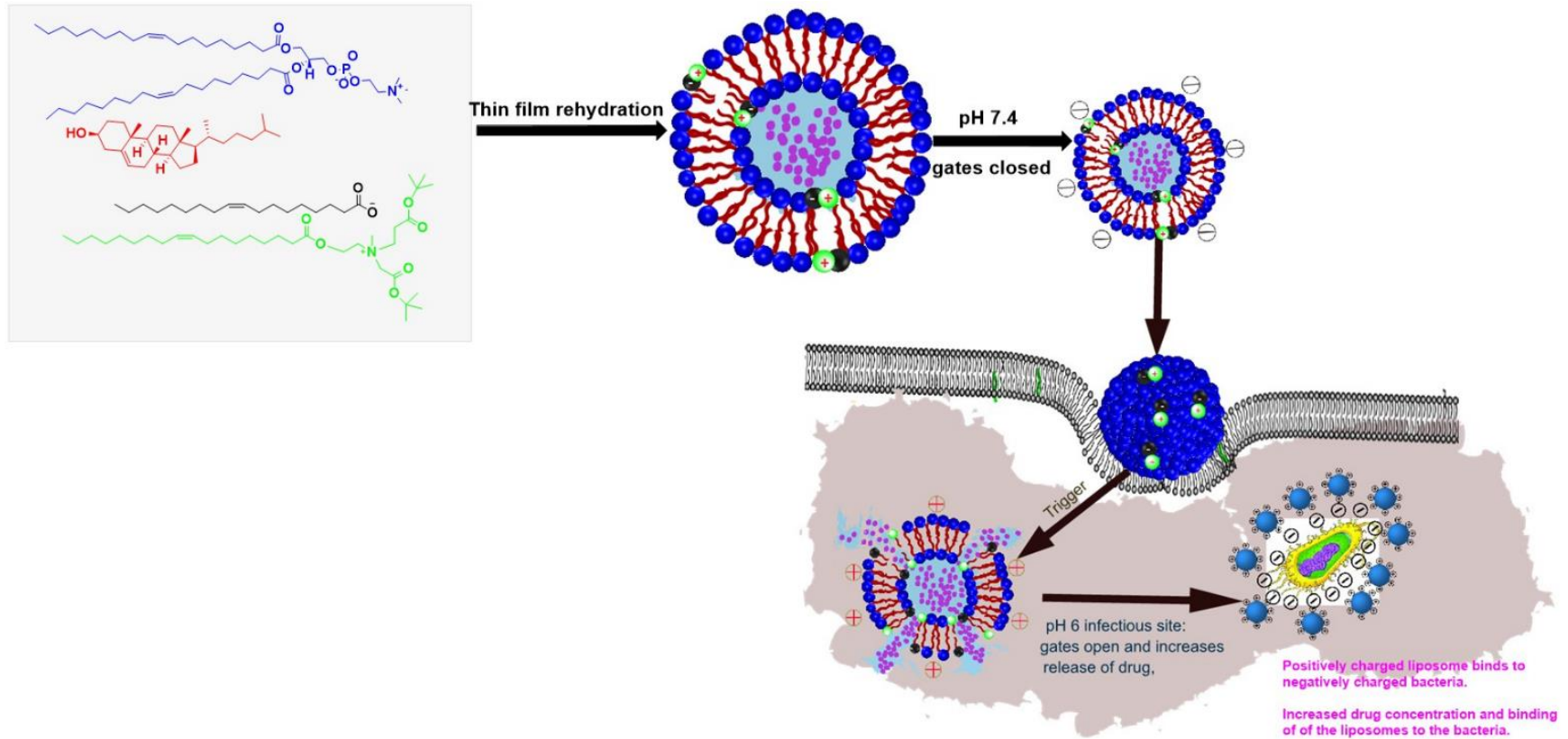
- [109] H. Du, P. Chandaroy, S.W. Hui, Grafted poly-(ethylene glycol) on lipid surfaces inhibits protein adsorption and cell adhesion, *Biochimica et Biophysica Acta (BBA) - Biomembranes*, 1326 (1997) 236-248.
- [110] D.E. Owens, N.A. Peppas, Opsonization, biodistribution, and pharmacokinetics of polymeric nanoparticles, *International Journal of Pharmaceutics*, 307 (2006) 93-102.
- [111] T. Verrecchia, G. Spenlehauer, D. Bazile, A. Murry-Brelier, Y. Archimbaud, M. Veillard, Non-stealth (poly (lactic acid/albumin)) and stealth (poly (lactic acid-polyethylene glycol)) nanoparticles as injectable drug carriers, *Journal of Controlled Release*, 36 (1995) 49-61.
- [112] A. Gabizon, R. Catane, B. Uziely, B. Kaufman, T. Safra, R. Cohen, F. Martin, A. Huang, Y. Barenholz, Prolonged circulation time and enhanced accumulation in malignant exudates of doxorubicin encapsulated in polyethylene-glycol coated liposomes, *Cancer research*, 54 (1994) 987-992.
- [113] P. Costa, J.M.S. Lobo, Modeling and comparison of dissolution profiles, *European Journal of Pharmaceutical Sciences*, 13 (2001) 123-133.
- [114] L. Tao, J.W. Chan, K.E. Uhrich, Drug loading and release kinetics in polymeric micelles: Comparing dynamic versus unimolecular sugar-based micelles for controlled release, *Journal of Bioactive and Compatible Polymers*, 31 (2015) 227-241.
- [115] W.B. Liechty, D.R. Kryscio, B.V. Slaughter, N.A. Peppas, Polymers for drug delivery systems, *Annual Review of Chemical and Biomolecular Engineering*, 1 (2010) 149.
- [116] Y. Weerapol, S. Limmatvapirat, C. Jansakul, H. Takeuchi, P. Sriamornsak, Enhanced dissolution and oral bioavailability of nifedipine by spontaneous emulsifying powders: effect of solid carriers and dietary state, *European Journal of Pharmaceutics and Biopharmaceutics*, 91 (2015) 25-34.
- [117] K. Hiramoto, Vancomycin-resistant *Staphylococcus aureus*: a new model of antibiotic resistance, *The Lancet Infectious Diseases*, 1 (2001) 147-155.
- [118] K.R. Raghupathi, R.T. Koodali, A.C. Manna, Size-Dependent Bacterial Growth Inhibition and Mechanism of Antibacterial Activity of Zinc Oxide Nanoparticles, *Langmuir*, 27 (2011) 4020-4028.
- [119] A. Thill, O. Zeyons, O. Spalla, F. Chauvat, J. Rose, M. Auffan, A.M. Flank, Cytotoxicity of CeO₂ nanoparticles for *Escherichia coli*. Physico-chemical insight of the cytotoxicity mechanism, *Environmental Science & Technology*, 40 (2006) 6151-6156.
- [120] M.-H. Xiong, Y. Bao, X.-Z. Yang, Y.-H. Zhu, J. Wang, Delivery of antibiotics with polymeric particles, *Advanced Drug Delivery Reviews*, 78 (2014) 63-76.
- [121] S. Van Hal, D.L. Paterson, T.P. Lodise, Systematic review and meta-analysis of vancomycin-induced nephrotoxicity associated with dosing schedules that maintain troughs between 15 and 20 milligrams per liter, *Antimicrobial Agents and Chemotherapy*, 57 (2013) 734-744.
- [122] M. Fittipaldi, A. Nocker, F. Codony, Progress in understanding preferential detection of live cells using viability dyes in combination with DNA amplification, *Journal of Microbiological Methods*, 91 (2012) 276-289.
- [123] M. Engel, Y. Hadar, S. Belkin, X. Lu, M. Elimelech, B. Chefetz, Bacterial inactivation by a carbon nanotube-iron oxide nanocomposite: a mechanistic study using *E. coli* mutants, *Environmental Science: Nano*, 5 (2018) 372-380.
- [124] Ž. Maglica, E. Özdemir, J.D. McKinney, Single-cell tracking reveals antibiotic-induced changes in mycobacterial energy metabolism, *MBio*, 6 (2015) e02236-02214.
- [125] P.R. Ingram, D.C. Lye, P.A. Tambyah, W.P. Goh, V.H. Tam, D.A. Fisher, Risk factors for nephrotoxicity associated with continuous vancomycin infusion in outpatient parenteral antibiotic therapy, *Journal of Antimicrobial Chemotherapy*, 62 (2008) 168-171.

CHAPTER 4, EXPERIMENTAL PAPER 2

4.1 Introduction

This chapter addresses Aim 3, Objectives 1 – 6 and is a first authored experimental article communicated to European Journal of Pharmaceutical Sciences (Impact Factor 3.466.) an ISI international journal (Manuscript ID EJPS-S-18-02306). This article highlights the synthesis of a novel fatty acid quaternary lipid, the in vitro toxicity evaluation, formulation of a liposome with On and Off pH switches (OA-QL liposome) for targeted delivery and intracellular delivery of vancomycin, molecular dynamics simulation of the On and Off mechanism of the switches and binding affinity of the lipid on a model bacterial membrane, and characterization of its physical and antibacterial properties both in vitro and in vivo of the drug loaded liposome.

4.2 Graphical abstract



4.3 Published manuscript

Liposomes with pH Responsive “On and Off” Switches for Targeted and Intracellular

Calvin A. Omolo¹, Nagia Megrab⁴, Rahul S. Kalhapure^{1,2,#}, Nikhil Agrawal¹, Mahantesh Jadhav¹, Chunderika Mocktar¹, Sanjeev Rambharose^{1,3}, Kaminee Maduray⁵, Bongani Nkambule⁵, Thirumala Govender^{1,#}.

1. Discipline of Pharmaceutical Sciences, College of Health Sciences, University of KwaZulu-Natal, Private Bag X54001, Durban, South Africa.
2. School of Pharmacy, The University of Texas at El Paso, 500 W University Ave, El Paso, TX 79968, USA.
3. Division of Emergency Medicine, Department of Surgery, University of Cape Town, Cape Town, South Africa.
4. Department of Pharmaceutics and Industrial Pharmacy, Zagazig University, Zagazig, Egypt.
5. Department of Physiology, School of Laboratory Medicine and Medical Sciences, College of Health Sciences, University of KwaZulu-Natal, Durban, South Africa.

. #corresponding author Private Bag X54001 Durban, 4000, KwaZulu-Natal, South Africa.
Tel: 00 27 31 260 7358, Fax: 0027 31 260 7792

Email address: govenderth@ukzn.ac.za; rkalhapure@utep.edu;
rahul.kalhapure@rediffmail.com

4.4 Abstract

Vancomycin (VCM) loaded liposomes with Oleic acid based ‘On’ and ‘Off’ pH responsive switches for infection site and intracellular bacteria targeting were formulated using thin layer rehydration technique and found to have size, of 98.88 ± 01.92 at pH 7.4. They showed surface charge switching from negative at pH 7.4 to positive charge at acidic pH accompanied by faster drug release at pH 6.0. Molecular dynamic studies of lipids forming the switches showed of spontaneous opening and closing of the gates at protonated and deprotonated states. Liposomes had 4-fold lower minimum inhibitory concentration (MIC) at pH 7.4 and 8- and 16-fold lower MICs at pH 6.0 compared to bare VCM against both Methicillin susceptible (MSSA) and resistant *Staphylococcus aureus* (MRSA) respectively. When tested for the intracellular infection in TPH-1 macrophage and HEK293 cells the liposome had a 1266.67- and 704.33-fold reduction in the intracellular MRSA respectively. *In vivo* studies showed a 189.67 and 6.33-fold lower MRSA burden from mice treated with formulations than the untreated and bare VCM treated groups respectively.

These studies demonstrated that the ‘On’ and ‘Off’ pH responsive liposomes enhanced the activity and targeted delivery of the loaded drug.

Keywords: Oleic acid, liposomes, pH response, vancomycin, intracellular infection.

4.5 Introduction

The success of antibiotics since the middle of the 20th century to manage infectious diseases has been immense, however bacterial infections continue to cause significant challenges worldwide ^[1]. Since the discovery of antibiotics, resistant bacterial strains have emerged against almost all the introduced newly antibiotics within a short period of time. ^[2, 3]. This is further compounded by the drying up of the antibiotic pipeline ^[4] and a short half-life between the introduction of new antibiotics and the development of resistant strains ^[5]. There is therefore a need for approaches to safeguard and enhance antibacterial activity of the existing antibiotics to greatly extend the period between the introduction of antibiotics and the development of resistance.

Since their introduction, antibiotics have been delivered via conventional dosage forms. Limitations of conventional dosage forms, such as sub-lethal concentrations at the infection site, lack of targeting that results in exposure to uninfected sites, elimination of the normal flora and the inability to extend the half-life of drugs, have been well documented ^[6-9]. Although antimicrobial resistance is a multifaced problem, the limitations of conventional dosage forms have been one of the underlining contributors to antimicrobial resistance. Recently, researchers have focused on the development of novel strategies, such as nano based drug delivery systems, which are showing potential in overcoming the limitations of conventional dosage forms while protecting the current antibiotics in the market by enhancing their activity and overcoming the resistance mechanisms of bacteria ^[10, 11].

Liposomes are one of the most widely used nano drug delivery systems, particularly for the delivery of antibiotics, due to their attractive attributes, such as membrane fusogenic ability ^[12-14], intracellular delivery and lowering toxicity of antibiotics ^[15-17]. They are usually composed of phospholipids, which assemble to form lipid bilayers vesicles with an aqueous core ^[18]. Drugs with different lipophilicities can be encapsulated into liposomes, which i.e. lipophilic

drugs can be entrapped in the lipid bilayer, while hydrophilic drugs can be encapsulated in the aqueous core. However, depending on the log P of the drug, it can partition between the lipid and aqueous phases ^[19]. Due to the versatility in the formulation of liposomes, stimuli-responsive biomaterials can be incorporated in them for the site-specific delivery of drugs. Liposomes have been engineered to possess distinctive properties, such as long systemic circulation, to target specific cells and receptors, and to respond to various stimuli, such as environmental pH and redox, and changes in temperature ^[20, 21].

pH is one of the common biomarkers for a number of diseases, such as Huntington's Disease ^[22], cancer ^[23], diabetes ^[24] and bacterial infections ^[25]. Nano drug delivery systems have been devised to achieve the programmable release of drugs due to pH changes at a target disease site with great success ^[26, 27] via micelles ^[28, 29], polymersomes^[30, 31], dendrimer based systems^[32, 33], peptides ^[34, 35] and liposomes ^[36, 37]. A survey of the literature shows that most of the reports of pH responsive liposomes have been in the field of cancer. However, there are limited reports regarding pH responsive liposomes to deliver antibiotics. The reported pH responsive liposomal systems for antibiotics delivery have been for gentamycin, ^[38] which employed phospholipid-cholesterol hemisuccinate as a pH responsive material, and for vancomycin, where intramolecular protonation and deprotonation of zwitterionic lipids were responsible for pH response, as reported by our group and other researchers ^[39]. With the current global crisis of antibiotic resistance, delivering antibiotics with pH responsive liposomes could prove to be a valuable tool. There is therefore a need for more studies to evaluate pH responsive systems for the targeted delivery of antibiotics.

Treatment of *Staphylococcus aureus* infections is often problematic due to the slow response to therapy and the high frequency of infection recurrence ^[40]. The intracellular persistence of *staphylococci* has been recognized as the reason for chronic and recurrence infections. Moreover, it is associated with a reduced expression of virulence factors that are important for

acute infection, which leads to the persistent and long-term survival of pathogens within their hosts. This intracellular reservoir is linked with treatment difficulties, such as a slow response to antibiotic treatment, an extended duration of antimicrobial therapy and treatment failure ^[41]. The presence of intracellular bacteria could offer a slow response or an inability of the antibiotics to clear this reservoir, as the bacteria might be shielded from the effects of antibiotics that have low intracellular penetration ^[42]. Moreover, bacteria have shown to localize the endosomes and phagolysosomes of the cells that are acidic and making them their reservoirs ^[43] which forms small colony variants in persistent infections (SCVs). Therefore, designing systems with pH stimuli responsive and having cell wall penetration could prove to be useful in eliminating the SCVs.

Compared to those reported in the literature so far, we herein report a liposome with a different mechanism of pH responsiveness by inserting ‘On’ and ‘Off’ switches within the bilayer membrane. The liposomes will be incorporated with a newly designed oleic acid derived quaternary lipid (QL) and parent Oleic acid (OA) as pH responsive components for site specific antibiotic delivery. We envisage that the novel QL can form a supra-molecular complex with OA in the lipid bilayer membrane of the liposome. Depending on the pH environment, the formed complex will form an “On and Off” switch to release the drug from the liposome. Under basic pH, the oleic acid will deprotonate and acquire a negative charge, thus forming a supramolecular complex with the quaternary nitrogen in the novel QL molecules (Off position of the liposome), and the negative charge will dominate, while in an acidic environment, oleic acid will be protonated, losing its charge, which will result in a slight repulsion between the positively charged QL and rearrangements (On position of the liposome) and the net charge of the liposomes will be positive. Thus, surface charge switching and increased drug release will be expected in an acidic pH, which will increase targeted drug release at the infection site,

while the positive charge will also potentiate the binding of the liposome to the negatively charged bacterial membrane.

To the best of our knowledge, this is the first report on delivery of antibiotics using liposomes having a pH triggered dependent “On and Off” switches. This kind of trigger mechanism can be of a better response and more sensitive in the acidic environment due to the noncovalent bond between the QL lipid and OA. This paper also reports, for the first time, on the delivery of any class of drug with the synthesized QL lipid, and the delivery of antibiotics with acid sensitive smart switches liposomes. This work could assist in helping to solve the current global antimicrobial crisis and SCVs, as the synthesized material will widen the pool of available material for drug delivery. The results and succinct discussions obtained from the synthesis of the QL lipid, *in vitro*, *in silico* and *in vivo* findings from the formulated liposome are herein reported in this paper.

4.6. Materials and Methods

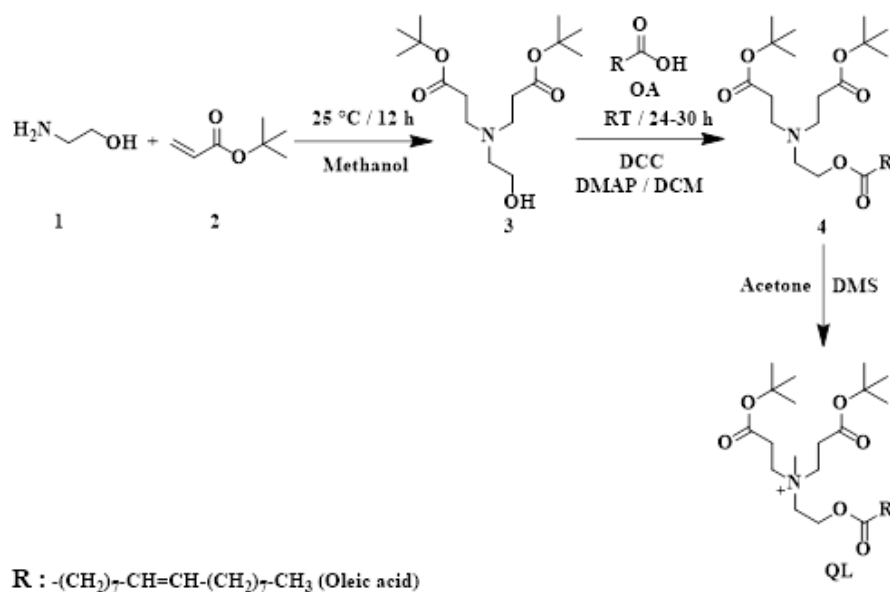
4.6.1 Materials

Vancomycin hydrochloride (VCM) was purchased from Sino-bright Import and Export Co., Ltd. (China). Phosphatidylcholine from soybean (PC) donated by Lipoid (USA). Cholesterol (Chol), *p*-dimethylamino pyridine (DMAP) and oleic acid (OA) were purchased from Sigma-Aldrich Co., Ltd. (USA). Ethanolamine and N, N'-dicyclohexylcarbodiimide (DCC) were purchased from Merck Co. Ltd. (Germany), and tert-butyl acrylate from Alfa Aesar (Germany). Dimethyl sulate (DMS) and 3-(4,5-dimethylthiazol-2-yl)-2,5- diphenyltetrazolium bromide (MTT) were purchased from Merck Co. Ltd. (Germany). Mueller Hinton Agar (MHA) and Nutrient Broth were obtained from Biolab Inc. (South Africa), and Mueller-Hinton broth (MHB) from Oxoid Ltd. (England), and the bacterial cultures *S. aureus* (ATCC 25922) and *S.*

aureus Rosenbach (ATCC®BAA-1683TM) (MRSA) cultures were used for antibacterial studies. All other reagents and solvents were of analytical grade.

4.6.2 Methods

4.6.2.1 Synthesis and characterization of QL



Scheme 1: QL synthesis scheme

4.6.2.1.1 Synthesis of 4-(tert-butoxy)-N-(3-(tert-butoxy)-3-oxopropyl)-N-(2-hydroxyethyl)-3-oxobutan-1-aminium (compound 3)

Solutions of *tertiary*-butyl acrylate **2** (26.26 g; 0.205 mol) and 2-aminoethanol **1** (100 mL), (6.11 g; 0.10 mol) in methanol were mixed at room temperature with stirring for 24 hours. Methanol and excess *tertiary*-butyl acrylate were removed by evaporation in vacuo, and the crude product was further purified by column chromatography (hexane and ethyl acetate 3:1) to form a thick oil (compound **3**) (yield 25.40 g; 80%). FTIR: 3487.09, 2977.13, 2933.06, 2826.27, 1722.76, 1456.78, 1392.00, 1366.55, 1247.77, 1151.59, 1027.13, 986.30, 950.40, 845.83, 755.11, 736.07, 591.66, 461.00, 434.60 cm^{-1} . ^1H NMR (CDCl_3) δ (ppm): 1.38 (s; 18H), 2.30 (t; 4H), 2.32-2.33

(m; 2H); 2.53-2.54 (t; 4H), 3.51-3.52(m; 2H). ^{13}C NMR (CDCl_3) δ (ppm): 27.9, 35.56, 53.35, 58.96, 80.38, 171.78. ESI-TOF MS m/z : $[\text{M} + \text{H}]^+$ - calculated 318.2280 found 318.2286.

4.6.2.1.2 Synthesis of 4-(tert-butoxy)-N-(3-(tert-butoxy)-3-oxopropyl)-N-(2-(oleoyloxy)ethyl)-3-oxobutan-1-aminium (compound 4)

Compound 4 was synthesized by reacting Oleic acid (2.34 g; 8.27 mmol) and compound 3 (2.5g; 7.88 mmol), with DCC (1.71 g; 8.27 mmol), and DMAP (0.062 g; 0.5 mmol) as catalysts in dry DCM (30 mL) under a nitrogen atmosphere at room temperature (RT) with stirring for 24 hours. The reaction mixture was filtered to remove dicyclohexylurea then filtrate was evaporated, and the residue was purified via column chromatography (ethyl acetate: hexane 20:80). The yield was 3.80 g (83%) FTIR: 2923.57,2853.60, 1727.95, 1458.10,1391.72,1367.26, 1244.84, 1154.22, 1092.26, 983.89, 951.57, 845.86, 722.44, 587.75, 457.74, cm^{-1} . ^1H NMR (CDCl_3) δ (ppm): 0.808 (t; 3H), 1.195-1.229 (m; 21H), 1.37 (s; 18H), 1.536 (q; 2H), 1.93-1.967 (m; 4H), 2.218 (t; 2H), 2.631 (m; 4H), 2.71(m; 2H),4.039-4.054 (m; 4H), 5.267 (t; 2H) ^{13}C NMR (CDCl_3) δ (ppm): 14.06, 22.63, 24.86, 27.13,27.16,28.05,31.86, 34.02, 52.11, 62.43, 80.24, 129.69-129.92, 171.70-171.65: ESI-TOF MS m/z : $[\text{M}]^+$ - calculated 581.88, found 581.4656

4.6.2.1.3 Synthesis of 4-(tert-butoxy)-N-(3-(tert-butoxy)-3-oxopropyl)-N-methyl-N-(2-(oleoyloxy)ethyl)-3-oxobutan-1-aminium (QL lipid(compound 5))

Compound 4 (2.0 g; 3.44 mmol) was dissolved in 15 mL acetone while stirring at 0 °C, dimethyl sulfate (0.653 mL; 6.88 mmol) was then added dropwise, and the reaction was allowed to slowly warm to room temperature, while it continued to stir for 24 h at room temperature. The solvent was removed by evaporation in vacuo, the crude oil was dispersed in 100 mL DCM washed with water (2 x 20 mL) and brine (25 mL) and dried over Na_2SO_4 . The

crude product was purified by column chromatography using a 0-25% methanol in hexane gradient to yield QL, 1.50 g, (73%). FTIR: 2922.93, 2853.55, 1709.29, 1457.52, 1392.22, 1245.30, 1148.64, 1035.47, 845.53, 722.73, 576.16, 470.76, 439.44, cm^{-1} . ^1H NMR (CDCl_3) δ (ppm): 0.866 (m; 3H), 1.25-1.283 (m; 21-), 1.44 (m; 18H), 1.546 -1.599 (m; 3H), 1.987-2.00(m; 4H), 2.300-2.333 (t; 2H), 2.764 (m; 2H), 2.851 -2.886 (t; 2H), 3.185-3.22 (t; 2H),, 3.443-3.440 (m; 4H), 3.676(m; 6H), 4.520 (t; 2H), 5.325 (t; 2H) ^{13}C NMR (CDCl_3) δ (ppm): 14.06, 22.64, 24.55, 27.16, 27.93-27.96, 28.71, 29.09-29.73, 31.87, 33.82, 49.07, 52.47, 57.55, 58.45, 61.76, 82.66, 129.65-129.99, 168.58, 172.79: ESI-TOF MS m/z : $[\text{M}]^+$ - calculated 596.4890, found 596.4882.

4.6.3. *In vitro* cytotoxicity

An MTT assay was employed to assess the biological safety of the synthesized QL, as per a previously reported method ^[44, 45] on three cell lines. Adenocarcinoma human alveolar basal epithelial cells (A549), human embryonic kidney cells 293 (HEK 293) and human liver hepatocellular carcinoma (Hep G 2). Cell lines were grown and seeded on Dulbecco's Modified Eagle's Medium (DMEM) supplemented with 10% Fetal Bovine Serum (FBS), (100U) 20 $\mu\text{g}/\text{ml}$ penicillin, and 100 $\mu\text{g}/\text{ml}$ streptomycin as per previously procedure ^[46]. At the end of the seeding time, cells were incubated with different concentrations of QL ^[44, 45]. After the 48 hours incubation, the test materials laden medium was removed and replaced with fresh DMEM media containing 5 mg/mL of MTT in each well for 4 hours, MTT was solubilized by adding 100 μL of dimethyl sulfoxide and absorbance was recorded at 540 nm using the microplate spectrophotometer (spectrometer nano, Germany). Results were analyzed and presented as percentage of the control values.

4.6.4 Preparation and characterization of liposomes

4.6.4.1 Preparation of liposomes

The liposomes were prepared by a previously reported method ^[47]. Briefly a mixture of different ratios of phospholipid, cholesterol, oleic acid and quaternary lipid making up a total weight of 100 mg, were dissolved in organic solvent (chloroform). Then the solvent was evaporated at reduced pressure forming a film on the flask. The film was hydrated at room temperature for 3 hours using 10 mL of pH 7.4 PBS buffer for blank liposomes and 10 mL of (1 mg/mL) VCM in pH 7.4 PBS buffer solution for drug-loaded liposomes, after which the formed liposomes dispersions were vortexed for seven minutes and sonicated for seven minutes using a probe sonicator at 30% amplitude.

4.6.4.2 Characterization of liposomes

4.6.4.2.1 Particle size (PS), polydispersity index (PDI) and zeta potential (ZP) of liposomes

The mean particle size (PS), polydispersity index (PDI) and zeta potential (ZP) of liposomes (n=3) were determined by dynamic light scattering technique using a Zetasizer Nano Series (Malvern Instruments Ltd., UK). Liposome dispersions (0.2 mL) were diluted with different phosphate buffer solution (1 mL) at different pHs then measured for PS, PDI and ZP.

4.6.4.2.2 Entrapment Efficiency (%EE) and Drug Loading (DL)

To determine the percentage of VCM encapsulated in the liposomes, an ultrafiltration method, using Amicon®Ultra-4, centrifugal filter tubes of 10 kDa molecular weight cut-off (Millipore Corp., USA), was used ^[39]. Liposomal suspension (2 mL) (n = 3) was placed into the upper chamber of the ultrafiltration centrifugal tube and centrifuged at 3000 rpm at 25°C for 30 min. The concentration of free VCM in the ultrafiltrate was detected by a UV spectrophotometer method (Schimadzu UV 1800, Japan) at 280.4 nm using a regression equation of $y = 0.00454x - 0.0014$ and R^2 coefficient of 0.99997 after appropriate dilution and appropriate blanks. The percentage entrapment efficiency and drug loading capacity were calculated using the following equation:

$$\%EE = \frac{W_{TD} - W_{FD}}{W_{TD}} \times 100$$

Where W_{TD} is total drug in the liposomal formulation and W_{FD} is total free drug in the filtrate obtained after ultrafiltration.

$$\%DL = \frac{W_{ED}}{W_T} \times 100$$

Where W_{ED} is the weight of drug entrapped and W_T is the total amount of lipids.

4.6.4.3 Transmission Electron Microscopy (TEM)

The surface morphology of prepared liposomes was examined using transmission electron microscopy^[48]. A drop of liposome dispersion (0.2 mL diluted to 1 mL) was placed on 3 mm forman (0.5% plastic powder in amyl acetate) coated copper grid (300 mesh). The excess aqueous solution was removed by blotting with filter paper, stained with 2% uranyl acetate (as a negative stain) for the 90s, then left to dry and visualized using a TEM (JEOL, JEM-1010, Japan) at an accelerating voltage of 100 kV.

4.6.4.4 Effect of storage

The effect of storage on the physical stability of the liposomes formulations was evaluated at room temperature (RT) and at 4°C over a period of three months. Physical appearance, PS, PDI, and ZP were monitored at zero time, and at the end of one, two and three months to assess the physical stability of the VCM loaded liposomes.

4.6.4.5 Differential Scanning Calorimetry (DSC)

Thermal profiles of VCM, Chol, PC, OA, QL, physical mixture and lyophilized liposome were determined via DCS on a Shimadzu-DSC-60 (Shimadzu, Corporation, Kyoto, Japan) as per previously reported method^[45].

4.6.5. MD simulations of QL with deprotonated (OAD) and protonated (OAP) oleic acid.

MD simulations are commonly used in drug delivery to evaluate proteins drug interaction, drug interaction with membranes, polymers interaction with drug and interactions between small molecules under various conditions ^[49]. The spontaneous binding of QL-OAD and QL-OAP was studied using MD simulations to understand the interactions that play a crucial role in the binding and interaction of the studied molecules.

4.6.5.1 MD simulations of QL with OAD and OAP

To understand the interactions between QL and OA at basic media (deprotonated state) and acid media (protonated state), MD simulations were done. The structure of OAD, OAP and QL was constructed using ChemDraw ^[50], and CHARMM General Force Field (CGenFF) ^[51] was used for all three molecules. The TIP3P water model was used for water molecules in the system ^[52]. The molecular dynamics (MD) simulation system of OAD-QL contained one molecule of OAD, one of QL and 6040 water molecules. The MD simulation system of OAP-QL containing one molecule of each OAP and QL, 4106 water molecules, and one Cl^- ion was added to neutralize the overall charge on the system. Both systems of OAD-QL and OAP-QL were energy minimized using the steepest descent algorithm ^[53]. Thereafter, two sequential equilibration simulations were performed using canonical ensemble (NVT), followed by an isobaric-isothermic ensemble (NPT) for 10 ps each, with further production simulations being performed using NPT ensemble for 100 ns for the QL-OAD system and 100 ns for QL-OAP system. The simulations were performed at room temperature using the velocity-rescale method ^[54] using a temperature with 0.1 ps coupling time. Pressure coupling was achieved via the Parrinello-Rahman method ^[55] using 2.0 ps as coupling time, with 1 atm pressure being used as a reference pressure. The Particle Mesh Ewald (PME) method ^[56] was employed for long-range electrostatic interactions, and the short-range electrostatic and vdw interactions were calculated using a 10 Å cut-off. The Leap-frog integrator ^[57] was used for the Newtown's equation of motion, using an integration step of 2 fs.

4.6.6 In vitro drug release

In vitro drug release from the liposomes was performed using dialysis methods [58]. Briefly, prior to adding the formulations, the dialysis tube (Membra-CEL® MD10 14x 100 CLR, USA) was rinsed with flowing water overnight. After the pre-treatment, an aliquot of 2 mL of VCM loaded liposomal suspension, blank liposomes and a free drug solution were added into the dialysis bags. The tubes were then suspended in 40 mL PBS of each pH 7.4 and pH 6.0 and incubated in a shaking incubator (100 rpm) at $37 \pm 0.5^\circ\text{C}$. Drug release was analyzed by extracting 3 mL aliquots of the immersion medium at intervals of 30 min, 1, 2, 3, 4, 5, 6, 7, 8 and 24 hours. To keep the volume of the solution constant, the supernatant was replaced with fresh PBS pre-equilibrated at 37°C at each time point. The amount of drug released at each time point was determined by a UV-visible spectrophotometer method (Schimadzu UV 1800, Japan) at 280.4 nm. The regression equation and linearity (r^2) were $y = 0.00454x - 0.0014$ and 0.9999 respectively. Drug release mechanism was determined by fitting 60% of the release data on various drug release models using DDSolver.^[44, 59-61]

4.6.7 Antibacterial Activity

4.6.7.1 In vitro Antibacterial Activity

Minimum inhibitory concentrations (MICs) for OA-QL liposomes and bare VCM was determined using micro broth dilution method, where test samples were serially diluted against 5×10^5 colony forming units per mL (CFU/mL) [62] of MSSA and MRSA as per our previously reported procedure [46, 63]. The concentration where there was no visible bacterial growth was regarded as the MIC.

4.6.7.2 Fluorescence Assisted Cell Sorting (FACS) bacterial cell viability

Viable cells in the MRSA population after incubation with OA-QL liposomes and bare VCM solution were determined by a previously reported fluorescence assisted cell sorting technique [46, 49]. Briefly bare VCM solution (positive control) and OA-QL liposomes at their respective

MIC concentrations (15.65 μ g/mL and 1.95 μ g/mL respectively) were incubated with 5×10^5 of the bacteria at 37 °C for 6 hours then analyzed following previously reported flow cytometry assay method [46, 49]. Cells of the appropriate size were then gated, and at least 10,000 cells collected for each sample in triplicate, with the position of the 'live' and 'dead' cells gates determined. To avoid a background signal from particles smaller than bacteria, the detection threshold was put to 1,000 in SSC analyses [64].

4.6.7.3 Assessment of intracellular activity OA-QL liposomes.

Experiments were performed on THP-1 a human myelomonocytic cell line displaying macrophage like activity and HEK 293 cells. THP-1 cells were cultured as a loose suspension in RPMI medium and were supplemented with 10% decompemented fetal calf serum and 2 mM glutamine in an atmosphere of 95% air–5% CO₂. The cells of 5×10^5 cells/mL concentration were infected by 2.5×10^6 CFU/mL of fresh MRSA inoculum, then incubated for 2 h at 37°C and washed four times successively by configuration at 1,500 rpm for seven minutes to remove any non-phagocytosed bacteria, followed by a gentle resuspension of the THP-1 cells sediment in a prewarmed RPMI 1640 medium. The cells were thereafter incubated in fresh medium with VCM loaded OA-QL liposomes (concentration of VCM 9.75 μ g/mL), bare VCM (39 μ g/mL) and cells that were untreated as negative control for 18 h [65-67]. To ensure the absence of extracellular bacteria, the culture medium that contained cells with phagocytosed MRSA, and that had not been exposed to antibiotics after the washing procedure described here, were incubated at 37°C for 48 hours and plated on nutrient agar plates, and no bacterial growth was detected. 24 hours post infection and treatment, the cells were collected by centrifugation, washed with ice-cold sterile phosphate buffered saline, and lysed with 0.1 % triton X in distilled water [67].

The evaluation of the intracellular activity of the OA-QL liposomes on the MRSA infected HEK 293 was carried out through a previously described method [68]. Briefly, HEK 293 cells were seeded in 96-well plates at a density of 5×10^4 cells/mL per well for 24 h in DMEM medium containing 10% DMEM without any antibiotics. Overnight culture of MRSA was washed with centrifugation at a 3000 rpm at 4 °C three times, resuspended and diluted with DMEM medium at a cell density of 10^{12} bacteria/mL and added to the wells with the adhered cells. After 2 h of incubation, the infected cells were washed seven times with a DMEM medium containing 10% FBS without any antibiotic to remove the extracellular bacteria. The last medium for washing was plated on nutrient agar plates to ensure that all the extracellular cells had been removed and no growth was observed. Fresh media was added to the infected cells in the wells, thereafter VCM loaded OA-QL liposomes, bare VCM at a of concentration of 9.75 µg/mL, and 39 µg/mL with respect to VCM (5 x MIC) and the negative control (untreated cells) were incubated for 22 h, after which the cells were lysed with 0.1 % triton X in distilled water [69]. The lysates for both cells were then plated on nutrient agar plates at appropriate dilutions for 24 h to determine the number of viable bacteria by counting the colony finding units (CFU) [67]. was determined as following:

$$\text{CFU/mL} = \frac{n \times f}{v}$$

Where: n =number of colonies, f = dilution factor and v = volume of the culture plate

4.6.7.4 *In vivo* antibacterial activity

Staphylococcus aureus have the ability to evade the immune system and resist conventional treatment by hiding intracellularly in skin tissues which has often resulted in resistant skin infections [70]. BALB/c skin infection model was employed to determine the ability of the OA-QL liposomes to eliminate MRSA skin infections [71, 72] using a study protocol (ethical clearance number AREC/104/015PD) that was performed as per by the guidelines of

University of KwaZulu-Natal's Animal Research Ethics Committee [73, 74]. Briefly male BALB/c mice weighing between 18 – 20 g were obtained and the hairs on their back was carefully shaved leaving the skin intact and then disinfected. 24 hours after shaving day, 50 μ L of MRSA containing 1.5×10^8 CFU/mL were administered via intradermal route then animals were clustered into 3 groups of four animals (treatment, positive control and negative control groups). 30 minutes after infection, 50 μ L of OA-QL liposomes formulation, free VCM and saline were injected at the same site of infection according to the respective groups. The animals were provided with normal 12 hours of light and dark condition at a temperature of 19-23°C and relative humidity of $55 \pm 10\%$ with adequate ventilation. 48 hours post infection, the mice were put down humanely with halothane and the area of infection was excised and homogenized in 5 mL pH 7.4 phosphate saline buffer. The homogenized tissues were serially diluted in pH 7.4 phosphate saline buffer, after which 20 μ L were spotted on nutrient agar plates, incubated for 24 hours at 37 °C, and the CFU were counted. The CFU/mL was determined as mentioned earlier (section 2.7.3)

For histological investigation, the skin samples from all the groups were fixed in formalin then dehydrated using ethanol followed by embedding in paraffin wax. Slides of the skin sections were then prepared and stained with hematoxylin and eosin (H&E). The slides were then examined on a Nikon 80i, (Japan) light microscope and bright field images were digitally captured by NIS Elements D software and a Nikon U2camera (Japan).

4.6.8 MD simulations of QL with POPC bilayer

QL lipid having both oleate moiety and positive charge MD simulations were performed on a POPC model membrane to understand the impact of the hydrophobicity and the positive charge on the bacterial membrane. POPC membranes are widely used to represent the gram-positive

bacterial membrane [75-77]. A 180 ns pre-equilibrated POPC bilayer was obtained from online repository [78, 79], and the QL molecule initially placed more than 20 Å from POPC bilayer (COM distance between QL and POPC upper leaflet PO4 atoms in Z-axis). For the POPC bilayer, charmm36 ff [80] was used, and for QL charmm general ff [51] was used. The QL-POPC system contains 6990 water molecules, with the TIP3P water model being used for solvation. In order to neutralize the charge on the system, one CL^- ion was added. The QL-POPC system was energy minimized using the steepest descent algorithm [53]. The simulated annealing simulation was performed for 500ps under the isobaric-isothermic (NPT) to equilibrate the water molecules around the POPC bilayer head group atoms. The QL-POPC system was equilibrated for 100 ps with a canonical (NVT) ensemble, followed by 1000ps with an NPT ensemble, with the QL molecule being restrained during the equilibration simulations. The Particle mesh Ewald (PME) method [56] was employed to calculate the long-range electrostatic interactions, while the van der Waals (vdW) and electrostatic interactions were calculated using a cut-off of 12 Å. The Nose-Hoover method [81] was employed, and the temperature coupling and the Parrinello -Rahman methods [55] were used for pressure coupling. For temperature coupling, 0.5 ps time constant and a 298.15 references temperature were used. For pressure semiisotropic, pressure coupling type, 2ps time constant and 1 bar reference pressure were used. The leap-frog integrator [57] was used to integrate the Newtown's law of motion using 2 fs integration time. The production run was performed for 20 ns without any restrains using an NPT ensemble. Periodic boundary conditions were applied in xyz dimensions, and the simulations were performed using the GROMACS package [82].

4.6.9 Statistical analysis

One-way analysis of variance (ANOVA), followed by Bonferroni's Multiple Comparison Test, was used for the statistical analysis. Individual groups were compared to each other using a

paired *t*-test, with *p* values of <0.05 being considered statistically significant, the values being represented as mean ± SD.

4.7. Results and Discussion

4.7.1 Synthesis of Quaternary lipid

The oleic acid derived quaternary lipid was synthesized by a three-step synthesis scheme (Scheme-1). The first step involved di-Michael addition reaction between an amino alcohol and tert-butyl acrylate, followed by a Steglich esterification reaction using oleic acid in the second step. The tertiary amine derivative (compound 4) was quaternarized by using dimethyl sulfate. Purification of the quaternary lipid and the intermediate products was achieved by column chromatography.

4.7.2 In vitro cytotoxicity assay

In vitro cytotoxicity assay was performed to confirm the bio-safety of the synthesized QL lipid by evaluating the viability of the cells after exposure to the test material. Quantification of viable cells was performed using MTT (tetrazolium) cytotoxicity assay, whereby exposure of the test material to mammalian viable cells leads to the reduction of tetrazolium to insoluble crystalline formazan. The quantity of formazan crystals formed in the cells is usually proportional to the number of viable cells. A549, HEK 293 and Hep G2 cell lines were seeded with different concentrations of QL lipid and the results showed cell viability ranging from 76.63 to 80.4% across all the concentrations in all cell lines tested (Figure 1). There was no dose-dependent toxicity towards all cell lines within the concentration range studied of the lipid. This percentage cell viability (76.63 to 80.4%) of the QL lipid met the biocompatibility and cytotoxicity requirements for the synthesized biomaterial [83-85]. These findings therefore revealed that the QL lipid is a bio-safe material for biomedical applications, considering that many quaternary lipids show toxicity or dose dependent toxicity.

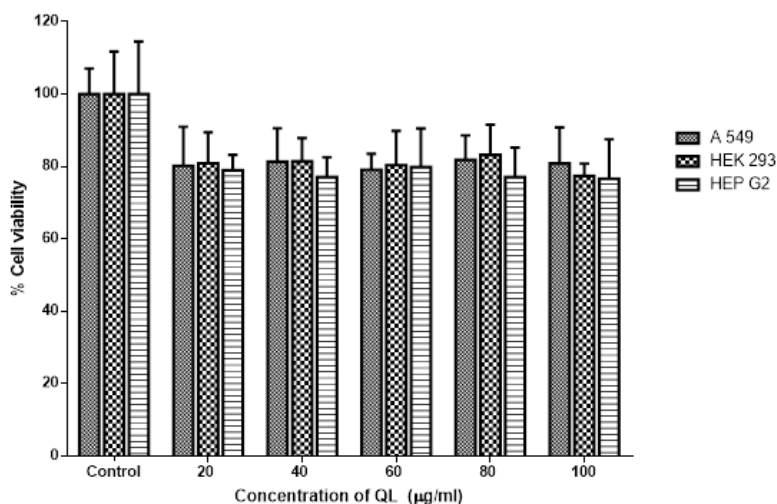


Figure 1. Cell viability of A 549, MCF 7 and Hep G2 cells against various concentrations of QL lipid

4.7.3 Preparation and characterization of liposomes

The thin-film hydration method was used to formulate liposomes from phosphatidylcholine (PC), cholesterol, OA and QL lipids, with the of ratios 60:30:5:5 % w/w respectively. Preliminary studies were done to achieve a ratio that gives the surface charge switch and the best encapsulation efficiency. A DLS study was used to determine the vesicle size, distribution and surface charge, the effect of different pH', encapsulation efficiency (EE) and loading capacity (LC). The size, PDI and ZP of the drug-loaded liposomes at pH 7.4 were 98.88 ± 1.92 , 0.204 ± 0.030 and -17.33 ± 2.95 respectively. The sizes were comparable to those obtained from the TEM images (**Fig 3B**), and the EE and LC were found to be 43.06 ± 5.86 and $4.31\% \pm 0.89\%$ respectively, the results were comparable to the other reported VCM loaded liposomes [39, 86, 87].

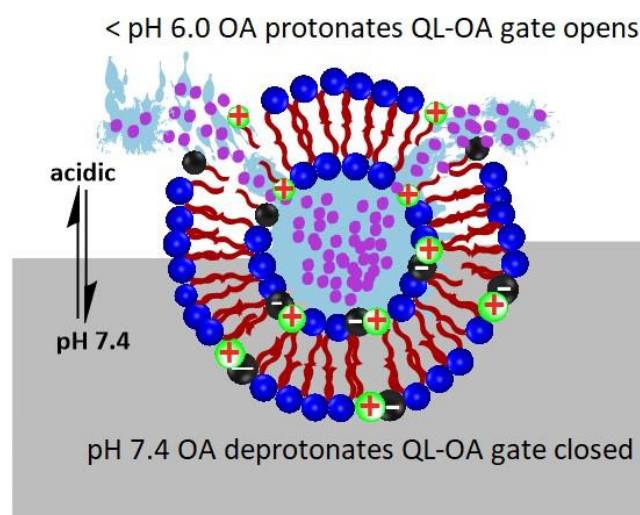


Figure 2. Opening and closing the gates in the liposome at pH 7.4 and acidic pH

The effect of pH on the liposomes was investigated by determining the change in size and surface charge in different pH media. There was a significant increase in size ($p < 0.00001$), from $98.88 \pm 01.927.4$ to 314.67 ± 44.06 , when the OA-QL liposomes were placed at pH 7.4 and pH 5.5 respectively (**Figure 3**). The ZP was negative at the biological pH and shifted towards a positive in acidic pH (**Figure 3C**). The increase in size and the switch in surface charge at acidic pH could be due to protonation of OA in the acid medium, resulting in a break in the link between the OA and QL lipids, with the quaternary nitrogen positive charge dominating, and the overall zeta potential of the liposome becoming positive (**Figure 2**). The increase in the size of the liposome in the acidic media (**Figure 3D**) was attributed to the slight repulsion between the positive charge of the QL lipid and the neutral charged protonated OA. These results are in agreement with the previous study of pH-sensitive liposome formulations that were based on the incorporation of a fatty alcohol, oleyl alcohol ^[88].

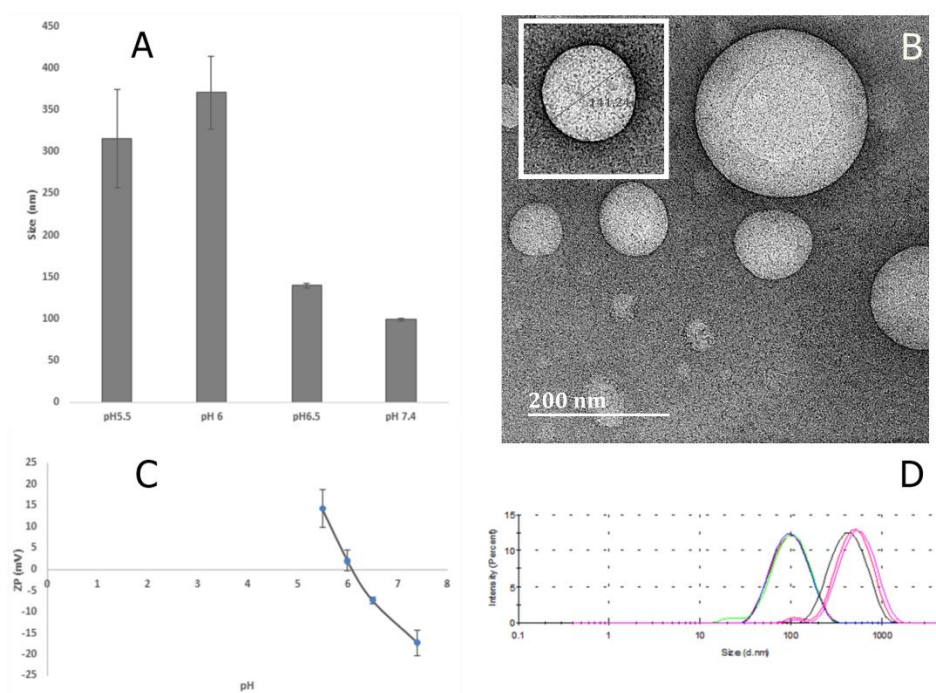


Figure 3. A) Increase in the size of liposomes with a decrease in pH, B) TEM images of the liposomes, C) Switch of surface charge from negative to positive, D) Difference in particle sizes distribution at pH 7.4 and pH 5.5

4.7.4 Differential Scanning Calorimetry (DSC)

The thermograms of the excipients used to formulate the OA-QL liposomes are presented in **Figure 4**, with the DSC thermogram of the bare VCM showing an endothermic peak at 111.86°C (**Figure 4A**). The phosphatidylcholine (PC) exhibited three endothermic peaks at 163.2°C, 183.3°C, and 247.6°C, whereas the cholesterol did not show any noticeable endothermic peak over the studied temperature range, and the OA showed a broad endothermic peak at 244.5 °C^[89]. Two endothermic peaks were observed in the thermogram of the QL, one was at 131.5°C and the other around 216.4°C (Fig. 5E). The physical mixtures demonstrated 4 sharp endothermic peaks at 133.5°C, 180.2°C, 212.87°C and 159.35 °C (**Figure 4F**). The DSC curves of the lyophilized formulations showed the disappearance of the endothermic peaks of the drug and lipid components (**Figure 4G**), which was an indication of VCM entrapment and its conversion from crystalline to amorphous form.

distribution at pH 7.4 and pH 5.5

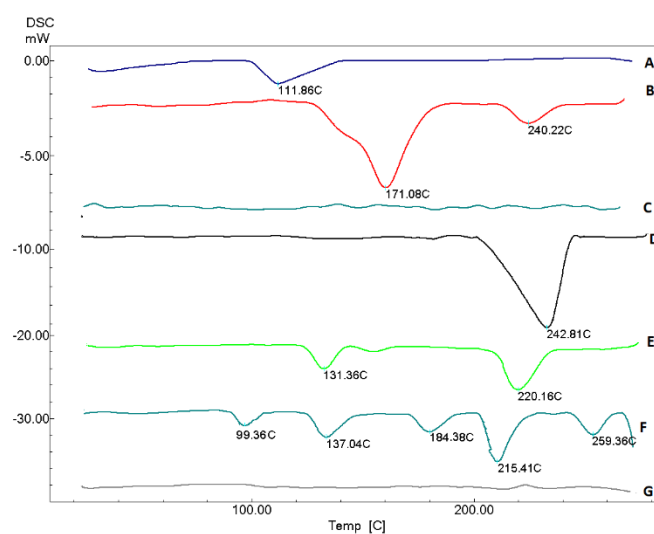


Figure 4. DSC thermograms of (A) vancomycin HCl; (B) phosphatidylcholine; (C) cholesterol; (D) oleic acid; (E) quaternary lipid; (F) physical mixture and (G) lyophilized liposomal formulations.

4.7.5 In vitro Drug Release

An *in vitro* drug release was performed to determine the release profile of the bare VCM and the OA-QL liposomes, with **Figure 5** illustrating the drug release profiles of free VCM solution, VCM loaded QL liposomes, and PC liposomes at pH 6.0 and pH 7.4. More than 90% of the drug was released from the free VCM solution at both pHs media after 24 h, with the responsive and non-responsive liposomes showing slower drug release profiles (**Figure 5**) than the VCM solution. The cumulative release of the VCM released from the OA-QL liposome formulation at the end of 24 h was $74.3 \pm 3.2\%$ at pH 6.0 and $50.0 \pm 3.1\%$ at pH 7.4. The release of VCM from the OA-QL liposomes was a significantly faster at pH 6.0. ($P=0.0048$). The faster release of the drug at pH 6.0 could be due to the protonation of the OA, which results in a break in the complex between the OA and QL lipid, leading to a destabilization of the liposome and resulting in a faster drug release. The faster release from the OA-QL liposomes at pH 6.0 than pH 7.4 could be used to effectively provide a localized release of the antibiotic

at the infection sites, which tend to be in acidic pH. This could be critical in effectively killing and eliminating the bacteria, which will reduce the development of resistant mutant species due to their sublethal exposure to antibiotics, a reduction of the side effects due to a narrowed volume distribution of the drug, and a lowered treatment dosage being required that can lead to improved patient compliance.

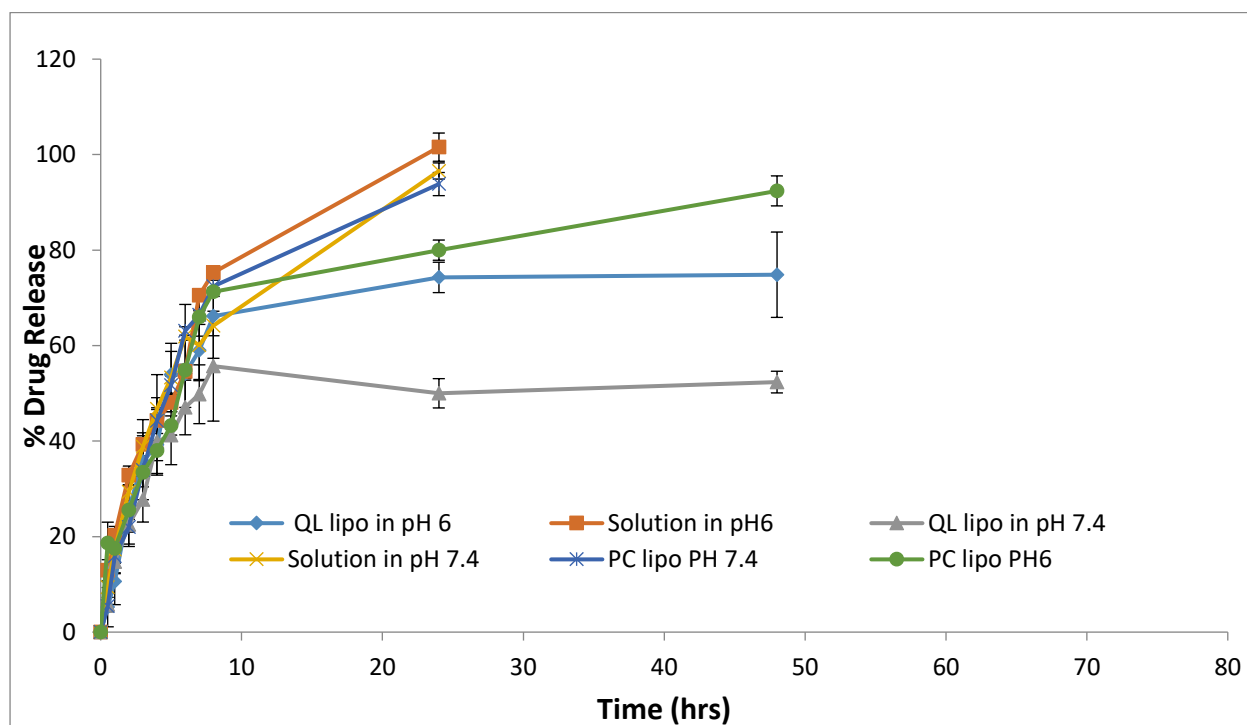


Figure 5. *In vitro* VCM release from Bare VCM solution, liposomal formulations and PC liposomes at pH 6 and pH 7.4. Error bar indicates SD (n=3).

Drug release mechanism was determined by modelling release data against various models. Korsmeyer-Peppas model was found to be the best fit model for VCM release from OA-QL liposomes at pH 6.0 with R^2 coefficient of 0.9740 and low RMSE of 4.519, while at pH 7.4 VCM release was found to fit the Weibull model with $R^2 = 0.9455$ and $RMSE = 7.003$ values compared to all other models (**Table 1**). The Korsmeyer-Peppas model 'n' exponent, which characterizes the drug release mechanisms was obtained and the value for release at pH 6.0 was found to be 0.626, while at pH 7.4 it was found to be 0.243. The release at pH 6.0 indicates

non-Fickian diffusion (Anomalous transport) suggesting that more than one release mechanism might have been involved [90,91]. Apart from diffusion at acidic pH, the protonation OA could have led to a break in the ionic pairing between the QL lipid and OA, which might have resulted in the leakage and destabilization of the liposome, leading to the release of the drug at pH 6.0 [92]. The release of drug from the OA-OL liposomes at pH 7.4 followed the Fickian release, with a diffusion-mediated release of the drug [93], the difference in release mechanism further indicated the pH responsive ability of OA-QL liposomes. The slower release of drug over an extended period of time for the OA-QL liposomes could lead to better therapy outcomes, as it would result in a lower frequency of administration, decreased side effects and improved patient compliance.

Table 1. Curve fitting of the *in vitro* VCM release data from the liposome formulation at pH6 and pH 7.4

pH 6				pH 7.4		
Model	R ²	RMSE	exponent (n)	R ²	RMSE	exponent (n)
Zero Order	0.8735	6.506	-	0.550	28.190	-
First Order	0.9054	5.627	-	0.451	18.781	-
Higuchi	0.9330	4.735	-	0.7648	15.629	-
Korsmeyer-Peppas	0.9740	4.519	0.626	0.8738	9.868	0.243
Hixson-crowell	0.8989	5.816	-	0.7920	20.804	-
Weibull	0.9704	5.100	-	0.9455	7.003	-

R² =linear regression coefficient, *RMSE* = Root mean square error

4.7.6 MD simulations of QL with deprotonated AO (AOD) and protonated OA (OAP)

To understand the interaction that might cause the closing and opening of the gates on the liposome at the physiological pH (7.4) and acidic pH (< 6), MD simulations of QL-OAD (100 ns) and QL-OAP (100 ns) were performed in water. Time evolution Center of mass (COM) distance, time evolution of interaction energies and binding energies between QL-OAD and

QL-OAP were calculated, with Figure 6 showing the interaction between them at different time points. The time evolution of the COM distance between QL-OAD (Figure 6 A-D) and QL-OAP (Figure 6 E-H) revealed that OAD and OAP interacted with QL at six different time periods (Table 2). The average COM distances between QL-OAD and QL-OAP at the different time points showed that OAD was closer to QL during binding compared to OAP. The shorter distance between OAD and QL was may be due to the attraction between the opposite charge of the two lipids i.e. negative charge of OAD and positive charge of QL, while in the protonated state, OA loses the charge, which may

Table2. Average distance between QL-OAD and QL-OAP during interaction time

Time of interactions (ns) QL-OAD	Average COM distance between QL-OAD (Å)	Time of interactions (ns) QL-OAP	Average COM distance between QL-OAP (Å)
~3.6 to ~14.1	10.71 ± 4.36	~5.9 to ~19.2	10.23 ± 2.70
~18 to ~27	9.07 ± 3.09	~27.3 to ~30.3	10.85 ± 2.91
~39.6 to ~45.3	9.55 ± 4.46	~34 to ~38.6	11.02 ± 3.19
~49.9 to 56.9	8.75 ± 2.33	~39.7 to ~62.6	10.63 ± 3.45
~61 to ~88.1	9.04 ± 3.91	~65.7 to ~75.8	10.44 ± 3.06
~92.3 to 100	8.69 ± 2.43	~80.1 to ~90.2	12.14 ± 4.76

The interaction energy components showed that spontaneous binding between QL and OAD was mainly governed by the electrostatic interactions (**Figure 7 B**, red line), and that the spontaneous binding between QL lipid and OAP was largely governed by the van der Waals (VdW) interactions (**Figure 7 D**, black line). The contribution to the binding energy (ΔG_{total}) from the VdW and electrostatic interactions was represented by ΔE_{vdw} and ΔE_{elec} . The contribution from polar and nonpolar solvation energy to ΔG_{total} was represented by ΔG_{polar} and $\Delta G_{\text{nonpolar}}$ respectively. The results for the QL-OAD showed that ΔE_{elec} , ΔE_{VdW} , and $\Delta G_{\text{nonpolar}}$ were favorable, but ΔG_{polar} was unfavorable, while a gain in the ΔE_{elec} and ΔE_{VdW} energies led

to the overall favorable ΔG_{total} (**Table 3**). The binding energy results for QL and OAP interactions showed that ΔE_{VdW} , ΔE_{elec} , and $\Delta G_{\text{nonpolar}}$ were favorable, but that ΔG_{polar} was unfavorable. However, a gain in intermolecular ΔE_{VdW} compensated for an increase in the polar solvation energy, which leads to the overall favorable ΔG_{total} (**Table 3**). Overall, the binding energy results suggest that the interaction between QL and OAD was stronger than between QL and OAP. This could be significant, as OAD was able to form both electrostatic and VdW interactions, while OAP mainly formed VdW interactions with QL. The energy interactions between QL, OAD and OAP could be the reason for the different behaviors exhibited by the liposomes in varying pH environments. At physiological pH, the supramolecular bonds between QL and OAD were stronger and the liposome released the drug slower. However, at acidic pH, OA is in the protonated state and loses its charge, which leads to weaker supramolecular interactions between OA and QL which could be the reason for the faster release of the drug from the liposome. Interestingly, throughout the MD simulation, the QL and OAD arrangement showed the polar head of all the lipids faced the same direction (**Figure 6A to D**), while at the end of the QL and OAD, MD simulation, the polar heads were in opposite directions. This rearrangement may be responsible for opening and closing the gates in the liposome that resulted in the increase in their sizes, release of the drug and the change in their surface charge (**Figure 6 E to G**). The MD simulations assisted in identifying the mechanistic behaviour of the OA-QL liposome in response to the pH and explaining the effect on drug release.lead to slight repulsion or weaker interactions with the always positively charged QL.

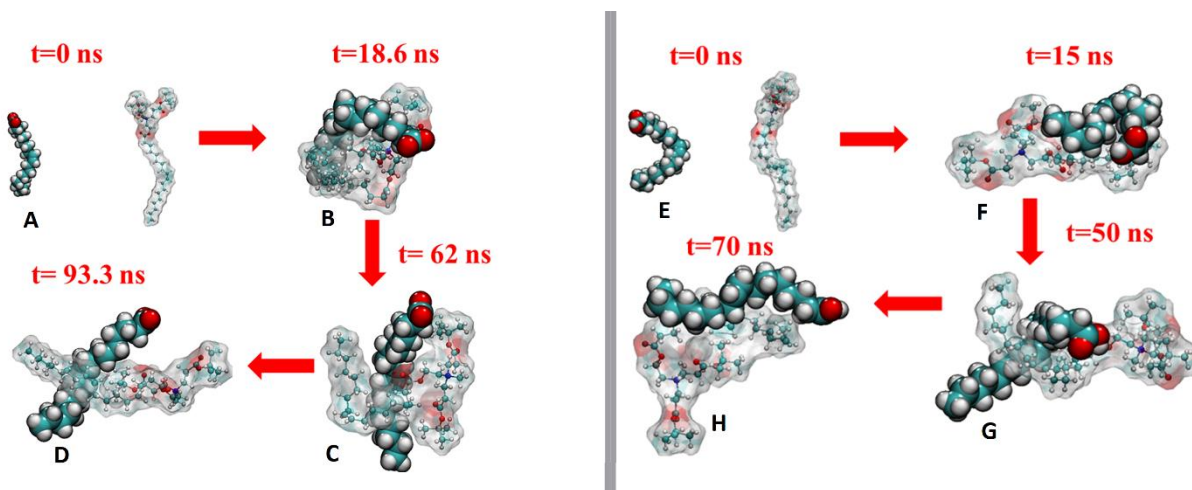


Figure 6. (A to D) Four representative images of QL interaction with deprotonated OA at four different time points A) $t=0$ ns. B) $t=18.6$ ns. C) $t=62$ ns. D) $t=93.3$ ns. From (E to H) are 4 representative images of QL interaction with protonated OA at 4 time points E) $t=0$ ns. F) $t=15$ ns. G) $t=50$ ns. H) $t=70$ ns.

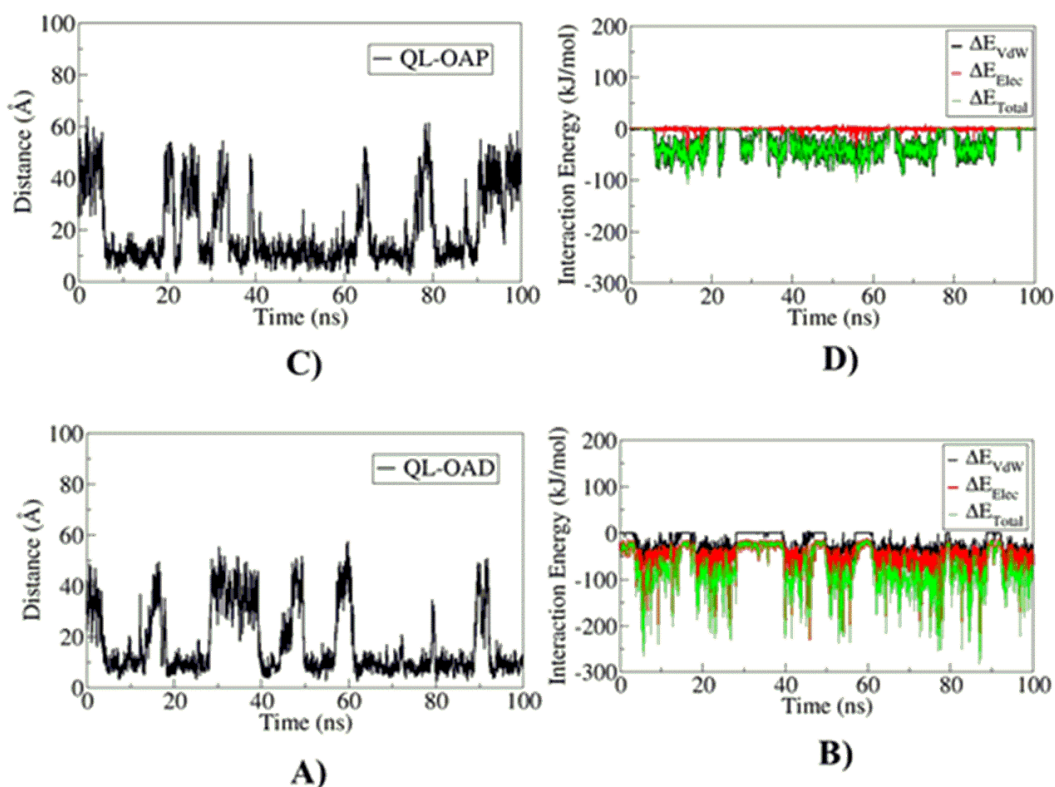


Figure 7 A) Time evolution of COM distance between QL-OAD. B) Time evolution of interaction energy between QL-OAD and its components (ΔE_{elec} and ΔE_{vdW}). C) Time

evolution of COM distance between QL-OAP. D) Time evolution of interaction energy between QL-OAP and its components (ΔE_{elec} and ΔE_{vdw}).

Table 3 Average Binding Energy and its Components Obtained from the MM-PBSA Calculation for the QL-OAD and QL-OAP complexes.

Components	Energy (kJ/mol)	
	QL-OAD (70-85 ns)	QL-OAP (45-60 ns)
ΔE_{vdw}	-40.01 ± 0.40	-43.61 ± 0.35
ΔE_{elec}	-65.25 ± 0.83	-1.51 ± 0.13
ΔG_{polar}	22.81 ± 0.91	11.05 ± 0.29
$\Delta G_{\text{nonpolar}}$	-7.39 ± 0.06	-8.06 ± 0.05
ΔG_{total}	-89.90 ± 0.54	-42.12 ± 0.31

4.7.7 Antibacterial Activity

4.7.7.1 Invitro Antibacterial Activity

The MIC values of bare VCM against SA and MRSA at pH 7.4 were 3.9 $\mu\text{g/mL}$ and 7.8 $\mu\text{g/mL}$ after 24 h respectively, while for the non-responsive liposomes and OA-QL liposomes they were 1.95 $\mu\text{g/mL}$ and 0.98 $\mu\text{g/mL}$, 3.9 and 1.95 $\mu\text{g/mL}$ respectively after 24 h (**Table 4**). It was observed that the OA-QL liposomes had a 4- and 2-fold increase in activity compared to the bare drug and non-responsive liposomes at pH 7.4 respectively, (**Table 5**) and was 8 and 16 times better than the bare VCM against SA and MRSA respectively. From the MIC data, the OA-QL liposomes displayed better anti-microbial activity in contrast to the bare VCM and non-responsive liposome, this enhanced antimicrobial activity possibly due to the fusion between the OA-QL liposomes and the membrane of the bacteria by fusing into the bacterial membranes, the OA-QL liposomes can induce a lethal dose of the drug, thereby killing the bacteria before they develop any possible resistance mechanisms. OA also has an inherent antimicrobial activity that could be a contributing factor ^[71, 94]. The enhanced activity at acid pH of the OA-QL liposomes can be ascribed to the switch of the surface charge of the liposome

to positive after protonation of OA. The positively charged OA-QL liposomes could have enhanced the fusion with the anionic bacterial cell wall, released higher VCM concentrations at the acidic infection site and reduced the total number of recovered bacteria [95, 96]. In addition to the charge and the presence of OA in the liposomes, studies have shown that the smaller sized liposomes tend to have better antimicrobial activity due to improved distribution on the bacteria and enhanced delivery of the drug, thus offering a better killing effect [97]. Therefore, targeting acidic bacterial site via pH-responsive liposomes represents an exciting platform to develop drug delivery systems that can enhance the drug localization at infections site and augment the antibacterial activity of antibiotics, which will go a long way towards reducing the emergence of bacterial resistance and improving treatment outcomes.

Table 4. MIC of QL lipids and controls at pH 7.4

Time (hours)	24	48	72	24	48	72
	<i>S. aureus</i> (MIC µg/mL)			MRSA (MIC µg/mL)		
Bare VCM	3.9	3.9	3.9	7.8	15.6	15.6
PC liposomes	1.95	7.8	250	3.9	3.9	15.6
VCM-OA-QL liposomes	0.98	0.98	0.98	1.95	1.95	1.95
Blank liposomes	NA	NA	NA	NA	NA	NA

NA = No activity. The values are expressed as mean ±SD, n=3.

Table 5. MIC of QL lipids and controls at pH6.0

Time (hours)	24	48	72	24	48	72
	<i>S. aureus</i> (MIC µg/mL)			MRSA (MIC µg/mL)		
Bare VCM	3.9	3.9	3.9	7.8	31.2	31.2
PC liposomes	1.95	7.8	7.8	3.9	3.9	15.6
VCM-OA-QL liposomes	0.488	1.95	3.9	0.488	1.95	3.9
Blank liposomes	NA	NA	NA	NA	NA	NA

NA = No activity. The values are expressed as mean ±SD, n=3.

4.7.7.2 Fluorescence Assisted Cell Sorting (FACS) bacterial cell viability

To determine cell viability of MRSA a flow cytometry method was used^[46,98]. Bare VCM and OA-QL liposomes were incubated for 6 hours with MRSA. PI fluorescent dye was used to detect bacterial membrane integrity and its permeation symbolized bacterial cell death, while Syto9 was employed to separate alive from dead cells^[99,100]. FACS Data was analyzed using Kaluza-1.5.20 (Beckman Coulter USA) fluorescence activated cell sorting software and were plotted as histograms of PI fluorescence versus the number of cells that internalized (**Figure 8**). Gating was done to separate dead cells (red) from alive cells (grey) in the MRSA population. VCM mechanism of action, results in loss of membrane integrity leading to permeability, uptake of and intercalation of PI with the DNA causing a shift in fluorescence. MRSA cells treatment with both bare VCM and OA-QL liposomes resulted a shift of PI fluorescence (**Figure 8 B, C and D**). The bare drug (**Figure 8C**) and OA-QL (**Figure 8D**) at their respective MIC concentration (7.8 µg/mL and 1.95 µg/mL respectively) had $58.17 \pm 5.79\%$ and $66.71 \pm 2.85\%$ dead MRSA cells in the population respectively. MRSA cells treated with bare VCM at a concentration of 1.95 µg/mL (OA-QL lipo MIC), there was only $16.86 \pm 2.6\%$ killing indicating the enhancement of VCM activity after encapsulation in OA-QL liposomes. These results can translate to a reduction in the amount of dose needed for the treatment with OA-QL liposomes without affecting the treatment outcomes and a reduction in the dose-dependent VCM side effects, such as nephrotoxicity and red man's syndrome^[101]. These results confirmed the enhanced activity of VCM after entrapping in OA-QL liposomes.

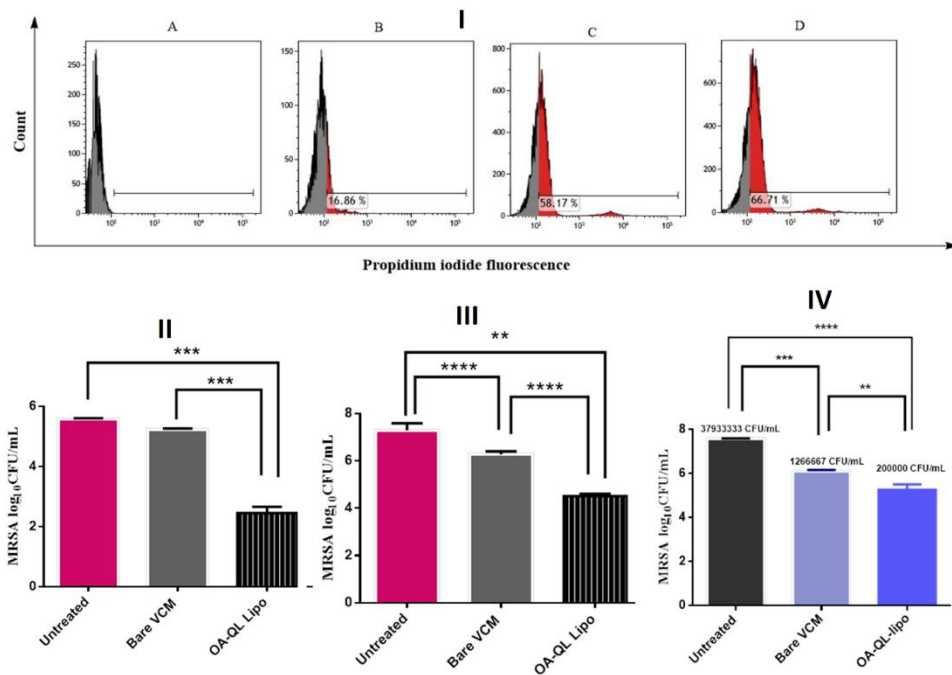


Figure 8. I. A) live cells (Untreated MRSA); B, and C, represents the percentage dead of MRSA cells after incubation with VCM solution at concentration 1.95 µg/mL and 7.8 µg/mL respectively, while D represents OA-QL lipo loaded 1.95µg/mL of VCM. II denotes intracellular MRSA CFU/mL recovered after treatment of infected TPH-1 cells. ***indicates the statistical difference for OA-QL liposome versus untreated and VCM solution. III represents **statistical difference of untreated versus bare VCM solution, **** is the statistical difference when OA-QL liposomes treated infected HEK 293 cells in comparison to the untreated and bare VCM. IV represent disease burden 48 hours after treatment of the mice. **represents statistical difference for OA-QL liposome versus bare VCM solution. ***represents statistical difference between untreated versus bare VCM solution. ****represents statistical difference between bare VCM solution and OA-QL liposome. In all the data n = 3.

4.7.7.3 Intracellular antibacterial activity

Evaluating the ability of the QL liposomes to eliminate intracellular bacterial infections was carried out on MRSA infected TPH-1 macrophage and HEK 293 cell lines. After the infection

and treatment process, the cells were lysed, the lysates plated on nutrient agar plates, and the CFU counted and quantified for each treatment group, being represented as \log_{10} (**Figure 8II**). The one-way ANOVA analysis among all the treatment groups revealed that there was a statistically significant ($P = 0.0003$ and $P < 0.0001$) reduction in bacterial load in both the TPH-1 macrophage and HEK 293 cells respectively. VCM had a 2.24- and 9-fold reduction of bacteria in the TPH-1 macrophage and HEK 293 cells ($P > 0.05$ and $P = 0.019$) respectively in comparison to the untreated. The OA-QL liposomes treated cells had a 1266.67- and 704.33-fold reduction in the infection ($P = 0.0003$ and $P < 0.0001$) for TPH-1 macrophage and HEK 293 cells respectively (**Figure 8 III**) compared to the untreated cells. Additionally, there was a 566.67 and 59.54-fold greater reduction in bacterial load after treatment with OA-QL liposomes compared with bare VCM ($P = 0.0005$ and $P < 0.0001$) respectively. Interestingly, the QL liposomes had better elimination of the intracellular MRSA, despite having a 4-fold lower concentration than the bare VCM. The better activity of the OA-QL liposomes in comparison to the bare drug may be ascribed to the capability of the liposome to penetrate the cell membrane and deliver the drug intracellularly^[102]. In addition, the acidic pH of the endosomes and phagolysosomes could have resulted in a breakdown of the OA and QL lipid ion pair, causing an increased drug release, as shown in **Figure 9**, which could prove effective in eliminating small colony variants in persistent infections (SCVs). The SCVs have been associated with chronic MRSA infections and long duration of treatments failure, and as a source of resistant bacteria strains^[103]. Localization of bacteria inside the host cells provides protection, and despite multiple antibacterial options being available to treat intracellular bacterial infections, more than two-thirds are ineffective against intracellular pathogens^[104]. These results demonstrated that OA-QL liposomes could be an effective drug delivery system for eliminating such intracellular infections.

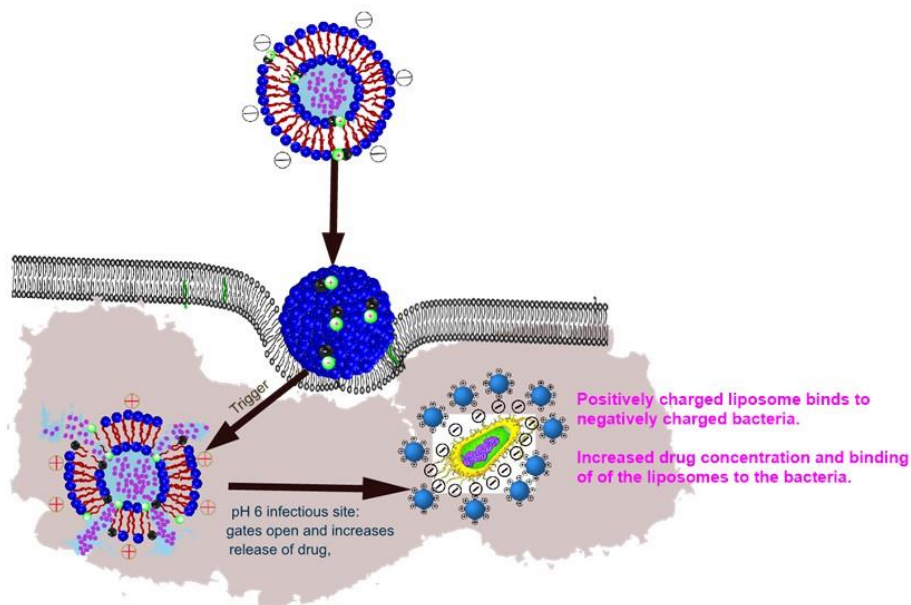


Figure 9. Proposed mechanism of intracellular delivery of VCM and enhancement of antibacterial activity by the pH responsive liposome OA-QL.

4.7.7.4 *In vivo* antibacterial activity

Staphylococcus aureus have been shown to readily internalize cells, thereby causing resistant intracellular infections of the skin, providing a source for chronic infections and the systemic dissemination of the pathogen [70]. A mouse skin infection model was used to evaluate if OA-QL liposomes can eliminate MRSA infections in an animal system. MRSA was administered intradermally and the CFUs quantified and represented as \log_{10} (**Figure 8 IV**). One-way ANOVA analysis among all the treatment groups revealed that there was a statistical significance ($P < 0.0001$) in the reduction of bacterial load in the skin samples (**Figure 6 IV**). The mean load of the bacteria (\log_{10} CFU) from the untreated and bare VCM groups was 7.58 ± 0.01 (37933333.33 CFU/mL) and 6.1 ± 0.05 (1266666.667 CFU/mL) respectively. The results demonstrated that bare VCM had a 29.95-fold reduction in bacterial load versus the untreated group ($P = 0.0005$). In the OA-QL liposomes treated group, the bacterial load was 5.26 ± 0.24 \log_{10} CFU/mL (200000 CFU/mL), translated to 189.67-times lower CFUs recovered in comparison to the untreated group ($P < 0.0001$). Furthermore, 6.33-fold reduction in bacterial

load was observed when OA-QL liposomes was compared to bare VCM ($P = 0.0041$). These findings demonstrated that OA-QL liposomes had better ability to treat MRSA skin infections than bare VCM.

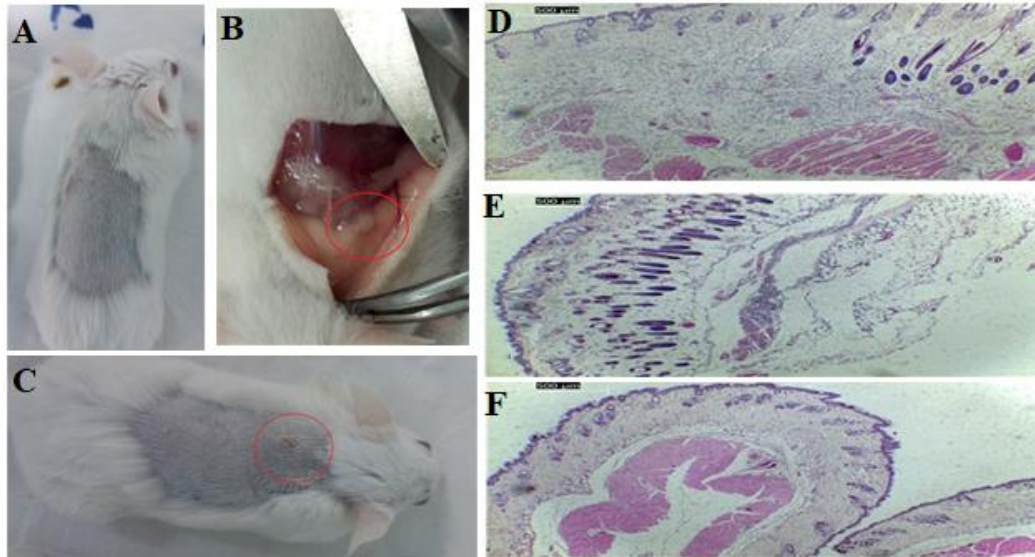


Figure 10. A) OA-QL VCM loaded liposomes treated mice, B) pus exudates from untreated mice; C) Skin of untreated mice showing infection, H&E stained micrographs photographs of the skin samples for the controls and different treatment groups (X40); D) negative control (saline and MRSA injected sample, E) Bare VCM treated, F) OA-QL VCM loaded liposomes treated.

Pus was observed in the untreated groups skin samples (**Figure 10A,B and C**) during skin excision upon physical examination. After H&E staining of the slides from the excised skin samples of untreated and bare VCM treatment group there was evidence of tissue inflammation and abscess formation (**Figure 10D and E**). However, the bare drug had lesser extend of tissue inflammation and abscess formation in comparison with to the untreated group. In the OA-QL group (**Figure 10E**) there was lack of abscess formation, but with minimal signs of tissue inflammation (**Figure 10F**). These observations were in line with the CFUs recovered from homegenised skin tissues (**Figure 8IV**), this is because immune response is directly propoirtinal

to the number of the bacteria present at the infection site as untreated and VCM treated groups displayed higher values of CFU/mL recovered. This histomorphological studies confirmed the antimicrobial advantage of the OA-QL liposomes.

4.7.8. MD simulation of QL with POPC bilayer

To understand the binding affinity of the QL lipid on gram positive bacteria, a 20 ns atomistic MD simulation was performed between the lipid and the POPC bilayer membrane. Atomistic modeling and molecular dynamics (MD) simulations have proven to be effective approaches for providing insight into experimental procedures and their results. The POPC bilayer membrane has been reported to study the surface interactions of bacteria and biomolecules ^[105]. Due to the QL lipid having both a hydrophobic tail and a positive charge, the effect of the positive charge and the hydrophobicity of the lipid were evaluated. Spontaneous binding, interaction and binding energy components involved in the binding between QL with POPC bilayer were also determined. **Figure 11 A and B** show two representative images from the QL-POPC bilayer simulation. QL formed the first interaction with POPC bilayer from ~6.3 to ~7.4 ns, while the second interaction between QL and POPC formed ~15ns and remained until the end of the simulations. However, during the second interaction, QLs close association to the POPC bilayer was observed from ~15 ns to ~17.5 ns, after which a slight increase in the COM distance between the QL and POPC upper leaflet PO4 atoms was observed (**Figure 11C**).

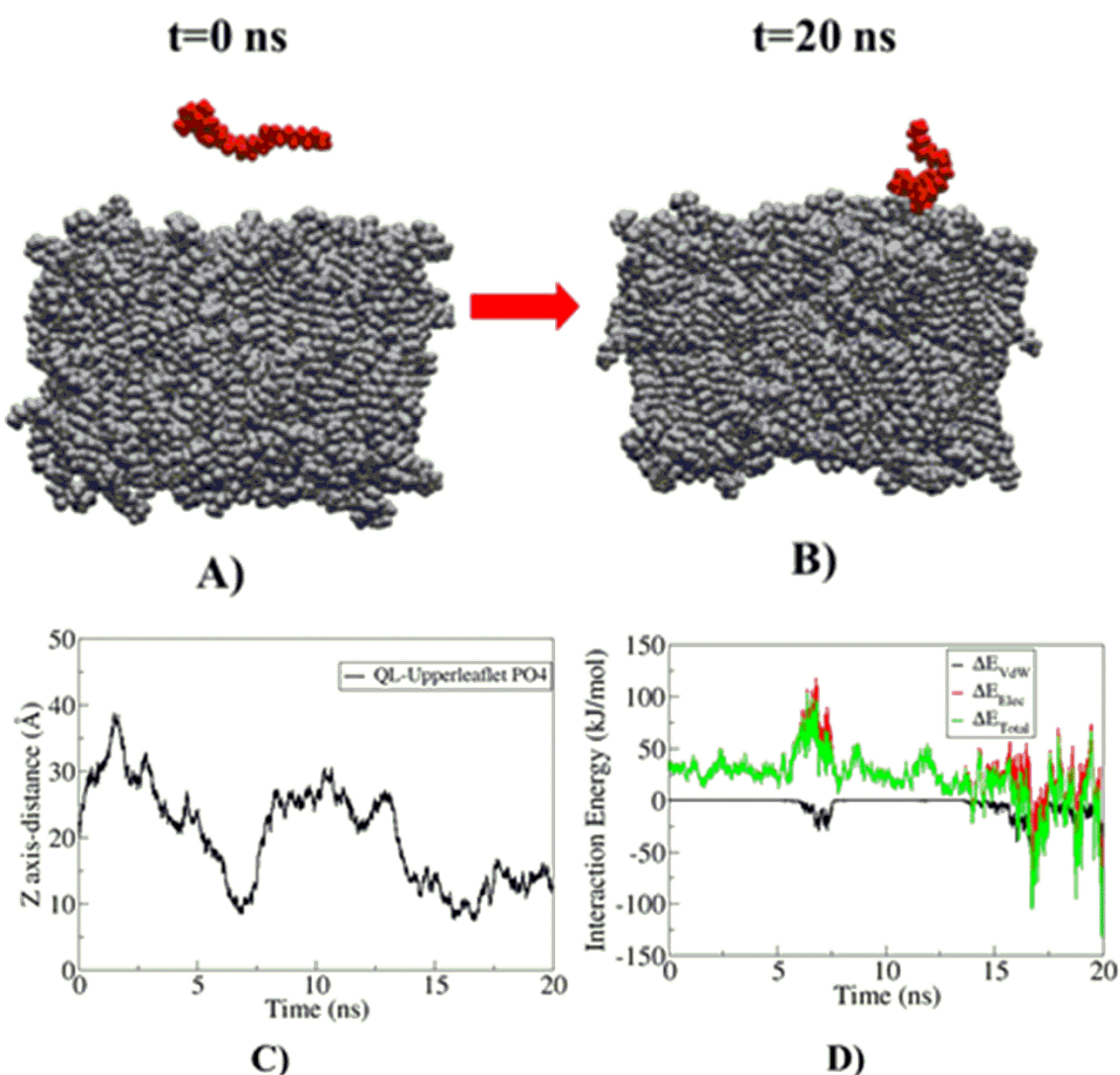


Figure 11. A) QL with POPC bilayer at $t=0$ ns. B) QL with POPC bilayer at $t=20$ ns. The QL molecule and POPC bilayer have been shown in VdW representation. C) Time evolution of COM distance of QL and upper leaflet PO4 atoms in the Z-axis. D) Time evolution of interaction energy and its components.

The time evolution of the interaction energy and its components revealed that during the first interaction, ΔE_{vdw} energy was favorable and ΔE_{elec} highly unfavorable, with ΔE_{total} therefore being unfavorable. During the second interaction, especially between ~ 16.5 ns to ~ 17.5 ns, it was observed that both ΔE_{vdw} and ΔE_{elec} were favorable, which led to an overall favorable ΔE_{total} , after which, fluctuations in ΔE_{elec} were observed (**Figure 11D**, red line). Binding energy

analysis was performed for the ~16.5 ns to ~17.5 ns and showed that ΔE_{vdw} , ΔE_{elec} and the highly favorable $\Delta G_{\text{nonpola}}$ energies lead to an overall favorable ΔG_{total} (**Table 6**). The ΔE_{vdw} and ΔE_{elec} were the most favorable binding force of the lipid to the membrane. This could have been the reason for the enhanced antibacterial activity of the QL liposomes, as the hydrophobicity of the liposome lipids enhanced their fusogenicity to the bacterial membrane,^[12, 106, 107] while the positive charge of the liposome at pH 6 might have led to electrostatic binding with the negatively charged bacterial membrane, resulting in increased release of the drug on the bacteria at lethal doses that lead to the annihilation of the bacteria^[95]. These results indicated that the hydrophobicity and the positive charge of the QL lipid might have been the reason for the increased bacterial targeting and enhanced activity of OA-QL liposome.

Table 6. Average Binding Energy and its Components Obtained from the MM-PBSA Calculation for the QL and POPC bilayer.

Components	Energy (kJ/mol) QL-POPC (16.5-17.5 ns)
ΔE_{vdw}	-27.33 ± 0.91
ΔE_{elec}	-9.80 ± 2.33
ΔG_{polar}	0.72 ± 8.36
$\Delta G_{\text{nonpolar}}$	-26.10 ± 0.42
ΔG_{total}	-62.48 ± 8.53

4.7.9 Effect of Storage

Stability studies were performed by storing samples at 4°C and RT for three months, during which their physical appearance, particle size, PDI, and ZP were evaluated (**Table 3**). The physical appearance of the liposome did not show any signs of color change, aggregation and phase separation throughout the storage period at specified storage conditions and time periods. There was a slight increase in size for the liposomes stored at room temperature from 109 nm

to 165nm. However, 4°C degree storage conditions were deemed to be more stable, as the size only increased from 109 nm to 124nm from time zero to 90 days of storage. This data confirmed the short-term physical stability potential of the VCM loaded OA-QL liposomes as a drug delivery system.

Table 7. Effect of storage on liposomal formulation over three months at 4°C and RT. All the samples were studied in triplicate and the data presented as mean \pm SD (n=3).

Time (days)	RT			4 °C		
	Size	PDI	ZP(mV)	Size	PDI	ZP(mV)
0	109.5 \pm 5.93	0.252 \pm 0.01	-17.83 \pm 1.05	109.5 \pm 5.93	0.252 \pm 0.01	-17.83 \pm 1.05
30	114.8 \pm 1.01	0.256 \pm 0.045	-16.33 \pm 2.91	113.76 \pm 1.39	0.259 \pm 0.012	-17.90 \pm 2.13
60	133.8 \pm 10.88	0.311 \pm 0.04	-16.20 \pm 3.78	125.5 \pm 12.03	0.376 \pm 0.010	-16.58 \pm 5.71
90	164.7 \pm 43.8	0.366 \pm 0.072	-15.14 \pm 1.96	124.7 \pm 7.97	0.309 \pm 0.09	-16.33 \pm 2.95

4.8 Conclusion

Fast-emerging resistant bacteria threaten the extraordinary health benefits that have been achieved with antibiotics and highlight the need for innovative strategies to combat the problem. Thus, a new oleic acid based novel quaternary lipid, as a pH stimulant component of a liposomal system for infection site-specific delivery of vancomycin (VCM), was synthesized and incorporated into a liposome to render it pH responsive. The *in vitro* MTT assay showed the QL lipid to be biosafe. *In vitro* pH differentials (6.0 and 7.4) of the drug release were obtained, and the system showed the ability to eliminate intracellular antibacterial in both HEK 293 and THP-1 microphage cells. The *in vitro* antibacterial activity showed that the pH responsive liposomes had superior activity both at pH 7.4 and pH 6.0 compared to vancomycin. The *in vivo* studies showed that the amount of MRSA recovered from mice treated with formulations was approximately 189.67 and 6.33-fold lower than the untreated groups and bare VCM treated mice respectively. MD simulation of the QL lipid and POPC membrane showed the lipid spontaneously binding to the bilayer membrane, with both electrostatic and Vander

Waals interactions playing a major role. These studies demonstrated that the inclusion of the ‘On’ and ‘Off’ pH responsive switches in the liposomes enhanced the activity and targeted delivery of the loaded drug as well as enhanced the elimination of the intracellular MRSA infections.

Acknowledgments

The authors acknowledge the University of KwaZulu-Natal (UKZN), UKZN Nanotechnology Platform, Medical Research Council and National Research Foundation of South Africa for financial support (NRF Grant No. 87790 and 88453). The Microscopy and Microanalysis and Biomedical Resource Unit of UKZN are acknowledged for their technical assistance, Ms Carrin Martin for proofreading and CHPC Cape town for their supercomputing resources.

Disclosure

The authors report no conflicts of interest in this work.

Supporting information

NMR and Mass spec analysis for synthesis of QL lipid (appendix IX).

4.9 References

- [1] W. Gao, S. Thamphiwatana, P. Angsantikul, L. Zhang, Wiley Interdiscip. Rev. Nanomed Nanobiotechnol. **2014**, 6, 532.
- [2] R. I. Aminov, Front. Microbiol. **2010**, 1, 134.
- [3] M. O. A. Sommer, C. Munck, R. V. Toft-Kehler, D. I. Andersson, Nat. Rev. Microbiol. **2017**, 15, 689.
- [4] A. MacGowan, E. Macnaughton, Medicine **2017**, 45, 622.
- [5] A. Coates, Y. Hu, R. Bax, C. Page, Nat. Rev. Drug Discov. **2002**, 1, 895.
- [6] M. Chidambaram, R. Manavalan, K. Kathiresan, J. Pharm. Pharm. Sci. **2011**, 14, 67.
- [7] E. Blanco, H. Shen, M. Ferrari, Nat. Biotechnol. **2015**, 33, 941.
- [8] R. Laxminarayan, A. Duse, C. Wattal, A. K. Zaidi, H. F. Wertheim, N. Sumpradit, E. Vlieghe, G. L. Hara, I. M. Gould, H. Goossens, Lancet Infect. Dis. **2013**, 13, 1057.
- [9] A. Malani, R. Laxminarayan, D. Howard, D. Smith, Earthscan. **2007**, 25.
- [10] D. R. Sikwal, R. S. Kalhapure, M. Jadhav, S. Rambharose, C. Mocktar, T. Govender, RSC Advances **2017**, 7, 14233.

- [11] R. S. Kalhapure, N. Suleman, C. Mocktar, N. Seedat, T. Govender, *J. Pharm. Sci.* **2015**, 104, 872.
- [12] D. Nicolosi, S. Cupri, C. Genovese, G. Tempera, R. Mattina, R. Pignatello, *Int. J. Antimicrob. Agents* **2015**, 45, 622.
- [13] C. B. Garcia, D. Shi, T. J. Webster, *Int. J. Nanomedicine* **2017**, 12, 3009.
- [14] D. Nicolosi, M. Scalia, V. M. Nicolosi, R. Pignatello, *Int. J. Antimicrob. Agents* **2010**, 35, 553.
- [15] H. Pinto-Alphandary, A. Andremont, P. Couvreur, *Int. J. Antimicrob. Agents* **2000**, 13, 155.
- [16] J. P. Wong, H. Yang, K. L. Blasetti, G. Schnell, J. Conley, L. N. Schofield, *J. Control. Release* **2003**, 92, 265.
- [17] R. S. Santos, G. R. Dakwar, E. Zagato, T. Brans, C. Figueiredo, K. Raemdonck, N. F. Azevedo, S. C. De Smedt, K. Braeckmans, *Biomaterials* **2017**, 138, 1.
- [18] B. S. Pattni, V. V. Chupin, V. P. Torchilin, *Chem. Rev.* **2015**, 115, 10938.
- [19] R. P. Austin, A. M. Davis, C. N. Manners, *J. Pharm. Sci.* **1995**, 84, 1180.
- [20] Y. Lee, D. Thompson, *Wiley Interdiscip. Rev. Nanomed Nanobiotechnol.* **2017**, 9.
- [21] H. Xing, C. L. Zhang, G. Ruan, J. Zhang, K. Hwang, Y. Lu, *Anal. Chem.* **2016**, 88, 1506.
- [22] M. M. Chaumeil, J. Valette, C. Baligand, E. Brouillet, P. Hantraye, G. Bloch, V. Gaura, A. Rialland, P. Krystkowiak, C. Verny, P. Damier, P. Remy, A.-C. Bachoud-Levi, P. Carlier, V. Lebon, *J. Cereb. Blood Flow Metab.* **2012**, 32, 771.
- [23] J. Nam, N. Won, H. Jin, H. Chung, S. Kim, *J. Am. Chem. Soc.* **2009**, 131, 13639.
- [24] D. Bruen, C. Delaney, L. Florea, D. Diamond, *Sensors* **2017**, 17, 1866.
- [25] B. Horev, M. I. Klein, G. Hwang, Y. Li, D. Kim, H. Koo, D. S. Benoit, *ACS nano* **2015**, 9, 2390.
- [26] Y. J. Zhu, F. Chen, *Chem. Asian J.* **2015**, 10, 284.
- [27] J. Liu, Y. Huang, A. Kumar, A. Tan, S. Jin, A. Mozhi, X.-J. Liang, *Biotechnol. Adv.* **2014**, 32, 693.
- [28] Y. Zhao, Y. Zhou, D. Wang, Y. Gao, J. Li, S. Ma, L. Zhao, C. Zhang, Y. Liu, X. Li, *Acta Biomater.* **2015**, 17, 182.
- [29] T. Woraphatphadung, W. Sajomsang, P. Gonil, A. Treetong, P. Akkaramongkolporn, T. Ngawhirunpat, P. Opanasopit, *Int. J. Pharm.* **2016**, 497, 150.
- [30] L. Wang, G. Liu, X. Wang, J. Hu, G. Zhang, S. Liu, *Macromolecules* **2015**, 48, 7262.
- [31] B. Iyisan, J. r. Kluge, P. Formanek, B. Voit, D. Appelhans, *Chem. Mater.* **2016**, 28, 1513.
- [32] H. Wang, Q. Huang, H. Chang, J. Xiao, Y. Cheng, *Biomater. Sci.* **2016**, 4, 375.
- [33] L. Chen, W. Cao, N. Grishkewich, R. Berry, K. Tam, *J. Colloid Interface Sci.* **2015**, 450, 101.
- [34] M. Paternostre, F. Artzner, *Biophys. J.* **2017**, 112, 359a.
- [35] J. Liang, W.-L. Wu, X.-D. Xu, R.-X. Zhuo, X.-Z. Zhang, *Colloids Surf. B* **2014**, 114, 398.
- [36] M. Kanamala, W. R. Wilson, M. Yang, B. D. Palmer, Z. Wu, *Biomaterials* **2016**, 85, 152.
- [37] V. P. Torchilin, *Nat. Rev. Drug Discov.* **2014**, 13, 813.

- [38] C. Cordeiro, D. J. Wiseman, P. Lutwyche, M. Uh, J. C. Evans, B. B. Finlay, M. S. Webb, *Antimicrob. Agents Chemother.* **2000**, 44, 533.
- [39] M. Jadhav, R. S. Kalhapure, S. Rambharose, C. Mocktar, S. Singh, T. Kodama, T. Govender, *Chem. Phys. Lipids* **2018**, 212, 12.
- [40] F. D. Lowy, *N. Engl. J. Med.* **1998**, 339, 520.
- [41] B. C. Kahl, K. Becker, B. Löffler, *Clin. Microbiol. Rev.* **2016**, 29, 401.
- [42] A. Sandberg, J. H. R. Hessler, R. L. Skov, J. Blom, N. Frimodt-Møller, *Antimicrob. Agents Chemother.* **2009**, 53, 1874.
- [43] D. J. Hackam, O. D. Rotstein, W.-J. Zhang, N. Demaurex, M. Woodside, O. Tsai, S. Grinstein, *J. Biol. Chem.* **1997**, 272, 29810.
- [44] C. A. Omolo, R. S. Kalhapure, M. Jadhav, S. Rambharose, C. Mocktar, V. M. Ndesendo, T. Govender, *Eur. J. Pharm. Biopharm.* **2017**, 112, 96.
- [45] R. S. Kalhapure, D. R. Sikwal, S. Rambharose, C. Mocktar, S. Singh, L. Bester, J. K. Oh, J. Renukuntla, T. Govender, *Nanomedicine* **2017**, 13, 2067.
- [46] C. A. Omolo, R. S. Kalhapure, N. Agrawal, M. Jadhav, S. Rambharose, C. Mocktar, T. Govender, *J. Control. Release* 2018, 290, 112.
- [47] A. Samad, Y. Sultana, M. Aqil, *Curr. Drug Deliv.* **2007**, 4, 297.
- [48] S. Anabousi, M. Laue, C.-M. Lehr, U. Bakowsky, C. Ehrhardt, *Eur. J. Pharm. Biopharm.* **2005**, 60, 295.
- [49] C. A. Omolo, R. S. Kalhapure, N. Agrawal, S. Rambharose, C. Mocktar, T. Govender, *Mol. Pharm.* **2018**, 15, 3512.
- [50] K. R. Cousins, *J. Am. Chem. Soc.* **2011**, 133, 8388.
- [51] K. Vanommeslaeghe, E. Hatcher, C. Acharya, S. Kundu, S. Zhong, J. Shim, E. Darian, O. Guvench, P. Lopes, I. Vorobyov, *J. Comput. Chem.* **2010**, 31, 671.
- [52] P. Mark, L. Nilsson, *J. Phys. Chem. A* **2001**, 105, 9954.
- [53] M. Bixon, S. Lifson, *Tetrahedron* 1967, 23, 769.
- [54] G. Bussi, D. Donadio, M. Parrinello, *J. Chem. Phys.* **2007**, 126, 014101.
- [55] M. Parrinello, A. Rahman, *Journal of Applied physics* **1981**, 52, 7182.
- [56] T. Darden, D. York, L. Pedersen, *J. Chem. Phys.* **1993**, 98, 10089.
- [57] M. A. Cuendet, W. F. van Gunsteren, *J. Chem. Phys.* **2007**, 127, 184102.
- [58] S. S. D'souza, P. P. DeLuca, *Pharm. Res.* **2006**, 23, 460.
- [59] T. Loftsson, B. Ilievska, G. M. Asgrimsdottir, O. T. Ormarsson, E. Stefansson, *J. Drug Del. Sci. Tech.* **2016**, 34, 71.
- [60] Z. Karami, S. Sadighian, K. Rostamizadeh, M. Parsa, S. Rezaee, *Mater. Sci. Eng. C.* **2016**, 61, 665.
- [61] Y. Zhang, M. Huo, J. Zhou, A. Zou, W. Li, C. Yao, S. Xie, *The AAPS journal* **2010**, 12, 263.
- [62] C. a. L. S. Institute, Vol. 32 (Ed: C. a. L. S. Institute), CLSI, Pennsylvania 19087, USA **2012**, 63.

- [63] J. H. Jorgensen, J. D. Turnidge, in *Manual of Clinical Microbiology, Eleventh Edition*, American Society of Microbiology, **2015**, 1253.
- [64] S. Renggli, W. Keck, U. Jenal, D. Ritz, *J. Bacteriol.* **2013**, 195, 4067.
- [65] N. Sémiramoth, C. D. Meo, F. Zouhiri, F. Saïd-Hassane, S. Valetti, R. Gorges, V. Nicolas, J. H. Poupaert, S. Chollet-Martin, D. Desmaële, R. Gref, P. Couvreur, *ACS Nano* **2012**, 6, 3820.
- [66] C. Seral, F. Van Bambeke, P. M. Tulkens, *Antimicrob. Agents Chemother.* **2003**, 47, 2283.
- [67] S. Carryn, F. Van Bambeke, M.-P. Mingeot-Leclercq, P. M. Tulkens, *Antimicrob. Agents Chemother.* **2002**, 46, 2095.
- [68] S. Maya, S. Indulekha, V. Sukhithasri, K. Smitha, S. V. Nair, R. Jayakumar, R. Biswas, *Int. J. Biol. Macromol* **2012**, 51, 392.
- [69] N. Abed, F. Saïd-Hassane, F. Zouhiri, J. Mougin, V. Nicolas, D. Desmaële, R. Gref, P. Couvreur, *Sci. Rep.* **2015**, 5, 13500.
- [70] A. H. Abu-Humaidan, M. Elvén, A. Sonesson, P. Garred, O. E. Sørensen, *Front. Immunol.* **2018**, 9, 396.
- [71] C.-M. Huang, C.-H. Chen, D. Pornpattananangkul, L. Zhang, M. Chan, M.-F. Hsieh, L. Zhang, *Biomaterials* **2011**, 32, 214.
- [72] L. R. Martinez, G. Han, M. Chacko, M. R. Mihu, M. Jacobson, P. Gialanella, A. J. Friedman, J. D. Nosanchuk, J. M. Friedman, *J. Investig. Dermatol.* **2009**, 129, 2463.
- [73] E. Kugelberg, T. Norström, T. K. Petersen, T. Duvold, D. I. Andersson, D. Hughes, *Antimicrob. Agents Chemother.* **2005**, 49, 3435.
- [74] R. S. Kalhapure, M. Jadhav, S. Rambharose, C. Mocktar, S. Singh, J. Renukuntla, T. Govender, *Colloids Surf. B* **2017**, 158, 650.
- [75] C. L. Friedrich, A. Rozek, A. Patrzykat, R. E. Hancock, *J. Biol. Chem.* **2001**, 276, 24015.
- [76] M. Dathe, T. Wieprecht, *Biochim. Biophys. Acta Biomembr.* **1999**, 1462, 71.
- [77] R. Yang, G. Zhang, F. Zhang, Z. Li, C. Huang, *Biochimie* 2018, 146, 139.
- [78] J. Melcr, **2016**, 2018.
- [79] J. Melcr, Vol. 5.1.2 *Zenodo*, **2016**. (https://zenodo.org/record/153944#W_QbEegzbIV)
- [80] J. Huang, S. Rauscher, G. Nawrocki, T. Ran, M. Feig, B. L. de Groot, H. Grubmüller, A. D. MacKerell Jr, *Nat. Methods* **2016**, 14, 71.
- [81] C. Braga, K. P. Travis, *J. Chem. Phys.* **2005**, 123, 134101.
- [82] M. J. Abraham, T. Murtola, R. Schulz, S. Páll, J. C. Smith, B. Hess, E. Lindahl, *SoftwareX* **2015**, 1, 19.
- [83] T. L. Riss, R. A. Moravec, A. L. Niles, S. Duellman, H. A. Benink, T. J. Worzella, L. Minor, *Assay Guidance Manual*, Eli Lilly & Company and the National Center for Advancing Translational Sciences, Bethesda (MD) **2004**.
- [84] R. Hamid, Y. Rotshteyn, L. Rabadi, R. Parikh, P. Bullock, *Toxicology in vitro* **2004**, 18, 703.
- [85] T. Mosmann, *J. Immunol. Methods* **1983**, 65, 55.
- [86] V. Rane, *pH sensitive liposomes for targeted delivery of antibiotics to localized internal bacterial infection sites*, Rutgers The State University of New Jersey-New Brunswick, **2016**.

- [87] J. Liu, Z. Wang, F. Li, J. Gao, L. Wang, G. Huang, *Asian J. Pharm.* **2015**, 10, 212.
- [88] J. J. Sudimack, W. Guo, W. Tjarks, R. J. Lee, *Biochim. Biophys. Acta Biomembr.* **2002**, 1564, 31.
- [89] S. Verma, A. Bhardwaj, M. Vij, P. Bajpai, N. Goutam, L. Kumar, *Artif. Cells Nanomed. Biotechnol.* **2014**, 42, 95.
- [90] P. Costa, J. M. S. Lobo, *Eur. J. Pharm. Sci.* **2001**, 13, 123.
- [91] L. Tao, J. W. Chan, K. E. Uhrich, *J. Bioact. Compat. Polym.* **2015**, 31, 227.
- [92] H. Zhao, H. Lu, T. Gong, Z. Zhang, *Int. J. Nanomedicine* 2013, 8, 1959.
- [93] N. Seedat, R. S. Kalhapure, C. Mocktar, S. Vepuri, M. Jadhav, M. Soliman, T. Govender, *Mater. Sci. Eng. C.* **2016**, 61, 616.
- [94] D. Yang, D. Pornpattananangkul, T. Nakatsuji, M. Chan, D. Carson, C.-M. Huang, L. Zhang, *Biomaterials* **2009**, 30, 6035.
- [95] A. F. Radovic-Moreno, T. K. Lu, V. A. Puscasu, C. J. Yoon, R. Langer, O. C. Farokhzad, *ACS Nano* **2012**, 6, 4279.
- [96] Q. Yu, Z. Wu, H. Chen, *Acta Biomater.* **2015**, 16, 1.
- [97] D. Dong, N. Thomas, B. Thierry, S. Vreugde, C. A. Prestidge, P.-J. Wormald, *PLoS One* **2015**, 10, e0131806.
- [98] N. M. O'Brien-Simpson, N. Pantarat, T. J. Attard, K. A. Walsh, E. C. Reynolds, *PloS One* **2016**, 11, e0151694.
- [99] M. Fittipaldi, A. Nocker, F. Codony, *J. Microbiol. Methods* **2012**, 91, 276.
- [100] M. Engel, Y. Hadar, S. Belkin, X. Lu, M. Elimelech, B. Chefetz, *Environ. Sci. Nano* **2018**, 5, 372.
- [101] P. R. Ingram, D. C. Lye, P. A. Tambyah, W. P. Goh, V. H. Tam, D. A. Fisher, *J. Antimicrob. Chemother.* **2008**, 62, 168.
- [102] M. Costanzo, F. Carton, A. Marengo, G. Berlier, B. Stella, S. Arpicco, M. Malatesta, *Eur. J. Histochem.* **2016**, 60, 2640.
- [103] B. G. J. Surewaard, J. F. Deniset, F. J. Zemp, M. Amrein, M. Otto, J. Conly, A. Omri, R. M. Yates, P. Kubes, *J. Exp. Med.* **2016**, 213, 1141.
- [104] N. Abed, P. Couvreur, *Int. J. Antimicrob. Agents* **2014**, 43, 485.
- [105] S. Mukherjee, R. K. Kar, R. P. R. Nanga, K. H. Mroue, A. Ramamoorthy, A. Bhunia, *Phys. Chem. Chem. Phys.* **2017**, 19, 19289.
- [106] D. Nicolosi, M. Scalia, V. M. Nicolosi, R. Pignatello, *Int. J. Antimicrob. Agents* **2010**, 35, 553.
- [107] F. Versluis, J. Voskuhl, B. van Kolck, H. Zope, M. Bremmer, T. Albrecht, A. Kros, *J. Am. Chem. Soc.* **2013**, 135, 8057.

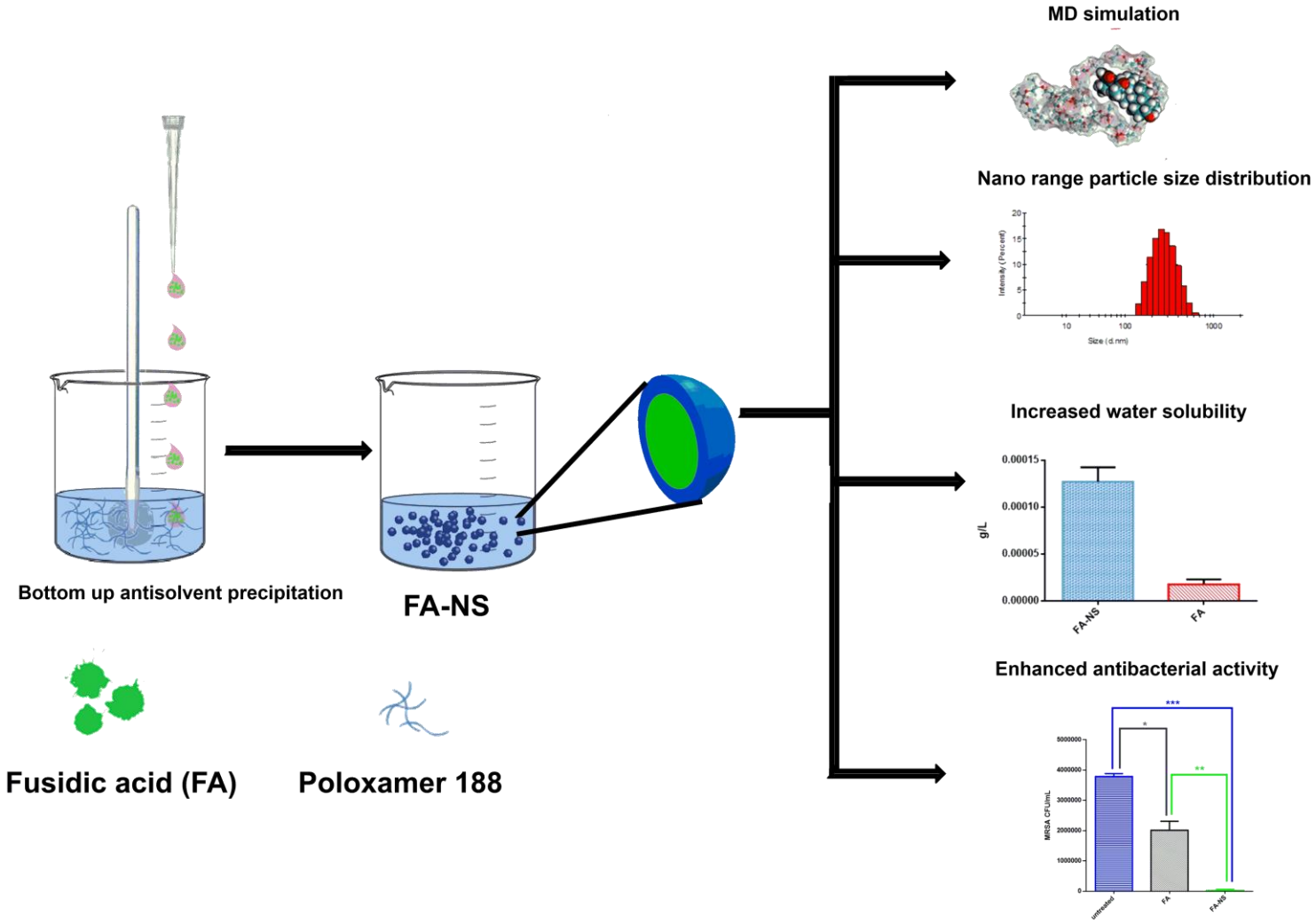
CHAPTER 5, EXPERIMENTAL PAPER 3

5.1 Introduction

This chapter addresses Aim .2, Objectives 1 - 3 and it highlights the formulation development of a novel FA-NS, and the characterization of its physical properties, aqueous solubility enhancement, enhanced antibacterial activity against sensitive and resistant *S. aureus* both in vitro and in vivo, and MD simulations on the formation of a stable nanosuspension. Data from this study has resulted to a first authored experimental article published in the ISI international journal ACS Molecular Pharmaceutics (Impact Factor = 4.556) and two conference presentations:

- Omolo, C. A., Kalhapure, R. S., Agrawal, N., Rambharose, S., Mocktar, C., & Govender, T. (2018). Formulation and Molecular Dynamics Simulations of a Fusidic Acid Nanosuspension for Simultaneously Enhancing Solubility and Antibacterial activity. Applied Nanotechnology and Nanoscience International conference. October 22-24 Berlin Germany. (Oral presentation).
- Omolo, C. A., Kalhapure, R. S., Agrawal, N., Rambharose, S., Mocktar, C., & Govender, T. (2018). Formulation and Molecular Dynamics Simulations of a Fusidic Acid Nanosuspension for Simultaneously Enhancing Solubility and Antibacterial activity. 38th Annual Conference of the Academy of Pharmaceutical Sciences, 06-08 July 2017, Johannesburg, South Africa (appendix viii)

5.2 Graphical abstract



5.3 Published manuscript

Formulation and Molecular Dynamics Simulations of a Fusidic Acid Nanosuspension for Simultaneously Enhancing Solubility and Antibacterial activity.

Calvin A. Omolo¹, Rahul S. Kalhapure^{1,2#}, Nikhil Agrawal¹, Sanjeev Rambharose^{1,3}, Chunderika Mocktar¹, Thirumala Govender^{1,#}

1. Discipline of Pharmaceutical Sciences, College of Health Sciences, University of KwaZulu-Natal, Private Bag X54001, Durban, South Africa.
2. School of Pharmacy, The University of Texas at El Paso, 500 W. University Ave, El Paso, Texas, 79968, USA.
3. Division of Emergency Medicine, Department of Surgery, University of Cape Town, Cape Town, South Africa

*Corresponding Author: Private Bag X54001 Durban, 4000, KwaZulu-Natal, South Africa.
Tel: 00 27 31 260 7358, Fax: 0027 31 260 7792

E-mail addresses: govenderth@ukzn.ac.za (T. Govender); rahul.kalhapure@rediffmail.com; kalhapure@ukzn.ac.za; rkalhapure@utep.edu (R.S. Kalhapure).

5.4 Abstract

The aim of the present study was to formulate a nanosuspension (FA-NS) of fusidic acid (FA) to enhance its aqueous solubility and antibacterial activity. The nanosuspension was characterized using various *in vitro*, *in silico* and *in vivo* techniques. Size, PI and ZP of the optimized FA-NS were 265 ± 2.25 nm, 0.158 ± 0.026 and -16.9 ± 0.794 mV respectively. Molecular dynamics simulation of FA and Poloxamer-188 showed an interaction and binding energy of -74.42 kJ/mol and -49.764 ± 1.298 kJ/mol, respectively with Van der Waals interactions playing a major role in the spontaneous binding. There was an 8-fold increase in solubility of FA in nanosuspension compared to the bare drug. MTT assays showed cell viability of 75%-100 % confirming the nontoxic nature of FA-NS. *In vitro* antibacterial activity revealed a 16- and 18-fold enhanced activity against *Staphylococcus aureus* (SA) and methicillin-resistant SA (MRSA) respectively when compared to bare FA. Flowcytometry showed MRSA cells treated with FA-NS had almost twice the percentage of dead bacteria in the population, despite having an 8-fold lower MIC in comparison to bare drug. *In vivo* skin infected mice showed a 76-fold reduction in the MRSA load for FA-NS treated group compared to bare FA. These results show that nanosuspension of antibiotics can enhance their solubility and antibacterial activity simultaneously.

Keywords: Nanosuspension, improved solubility, enhanced antibacterial activity, molecular dynamics, MRSA

5.5 Introduction

Despite the global spread of antimicrobial resistance, development and regulatory approval of new antibiotics has declined by 90% over the past 30 years due to the excessive cost of antibiotic research¹⁻³. Scientists are therefore focusing on enhancing the efficacy of old antibiotics through structural modifications⁴ and reformulating them into nano systems⁵. It is widely reported in the literature that nanonization of antibiotics enhances their activity⁵⁻⁶ through sustained release⁷⁻⁸, thereby lowering the minimum inhibitory concentration (MIC)⁹ and targeting the infection sites¹⁰. Thus, revisiting older antibiotics, such as fusidic acid (FA), is of importance to expanding and protecting the shrinking armamentarium available to clinicians to treat illnesses caused by resistant bacteria.

FA is a fusidane antibiotic that is derived from *Fusidium coccineum* and is a tetracyclic triterpenoid that is structurally related to cephalosporin P1 (Figure 1)¹¹, active against a wide range of bacteria¹², has low toxicity and a unique mechanism of action that lacks significant cross resistance to other antibacterial classes¹³. An Increase in the rate of global antimicrobial resistance has promogulated research interest in FA, even in markets where it lacked registration, for example the United States of America (USA), and is in clinical trials for approval as a potentially valuable therapeutic option¹³⁻¹⁴.

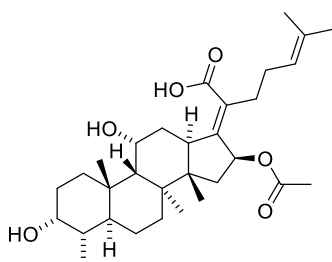


Figure 1. Chemical structure of FA. IUPAC name: (E)-2-((3R,4S,5S,8S,9S,10S,11R,13R,14S,16S)-16acetoxy-3,11-dihydroxy-4,8,10,14-tetramethylhexadecahydro-17H-cyclopenta[a]phenanthren-17-ylidene)-6-methylhept-5-enoic acid.

High hydrophobicity of biopharmaceutical classification system class (BCS) II drugs, such as fusidic acid hemihydrate, partitions well through biological membranes, which can translate to high bioavailability¹⁵⁻²⁰. However, their bio-absorption process is rate-limited by their low rate of dissolution, which results in low absorption for oral dosage and difficulty in formulating parenteral dosage forms¹⁵⁻²⁰, with poor aqueous solubility often resulting in poor bioavailability. A previously prepared FA suspension displayed only 22.5% bioavailability in pediatric patients following a 20 mg/kg dose^{11, 21}. There is therefore a need for innovative strategies to improve solubility and bioavailability of FA.

To solve the problem of poor aqueous solubility of drugs, several techniques, such as micronization^{15, 22}, solubilization²³ and salt formation, have been explored²⁴, although they have a number of limitations. The micronization technique results in very fine powders that affects the flow and wettability properties of the drug due to enhanced electrostatic forces²⁵. Solubilization techniques require the formulation to be in liquid form, which has stability problems²⁶, and salt formation is a complicated process, not being feasible for neutral compounds²⁷. As much as it enhances solubility, sodium salts, like sodium fusidate, undergoes precipitation in acid media, and their solubility also tends to vary with change in pH, which changes along the gastrointestinal tract²⁸.

Nanotechnology has been used to successfully deliver and improve the activity of a wide range of antibiotics^{6, 10, 29-30}. However, nanocarriers require the use of matrix material to encapsulate the compound, thereby reducing the maximum possible drug loading³¹. Recent advancements in technologies for reducing particles sizes to nanoparticulate level have stimulated the formulation of nanosuspensions, these being solid dispersions of the drug in the sub-micron scale that are stabilized with surfactants, polymers or both³². Nanosuspensions offer increased dissolution rates, enhanced bioavailability and activity, and complete entrapment of insoluble

drugs by forming stable solid dispersions in their amorphous state ³³. As described by the Noyes–Whitney, and Kelvin and Ostwald-Freundlich equations, particle size reduction can lead to increased dissolution rate and absorption due to greater surface area, amplified dissolution pressure and increased adhesiveness to surfaces/cell membranes ³⁴⁻³⁶. Nanosuspensions have been successfully used to improve the activity of a wide range of anti-infectives, such as triclosan ³¹, ciprofloxacin³⁷, itraconazole ³⁸ and miconazole ³⁹. To the best of our knowledge, there are no reports on FA nanosuspension as a drug delivery system. Despite FA being an effective agent against gram positive bacteria, there has been only one report for enhancing its solubility and activity using nanomicelles, which further involved the use of a newly synthesized material i.e. polyester dendrimers⁴⁰. Nano precipitation antisolvent technique, used to formulate nanosuspensions, has shown to have advantages, such as little energy input, readily available machinery and easy scale-up. It also allows for the preparation of nanosuspensions without the use of additional specialized materials like the study reported by Sikwal et al ⁴⁰.

Development of pharmaceutical dosage forms requires an understanding of the *in vitro* and *in vivo* performance of the dosage forms. *In vitro* studies have been shown to be convenient as they: (a) reduce costs, (b) provides an opportunity to more directly assess product performance, and (c) offer benefits in terms of ethical considerations ⁴¹. As useful as *in vitro* assays are, they could fail to replicate the results in living conditions of an organism ⁴² as some studies have shown *in vivo* results were better than *in vitro* outcomes. There have been also reports where studies have been effective *in vitro* but when introduced into living organism they cause a cascade of events that have turned out to be toxic and incompatible with the animal ⁴³. Therefore, to increase confidence in the effectiveness of pharmaceuticals, *in vivo* studies are usually recommended as the field is moving from formulation based to disease focus research.

In addition to their physicochemical properties and *in vitro* and *in vivo* performance, understanding the underlying behavior and mechanism of formation of drug delivery systems is essential for formulation optimization, and requires an examination under spatial and sequential resolutions. Molecular dynamics (MD) simulations are being employed in drug delivery studies as they can track the systems behavior changes across considerable spatial-sequential domain lengths with atomic precision and high resolutions⁴⁴. Thus, providing a detailed molecular insight into the formation of nanosuspensions for drug delivery applications is of paramount importance. The MD simulations in this paper has not been reported previously.

Thus, the aim of this study was to formulate a stable FA nanosuspension (FA-NS) by employing a bottom-up antisolvent precipitation technique and characterizing it with various *in vitro*, MD simulations and *in vivo* studies. We envisaged that the formulated nanosuspension would enhance aqueous solubility and antibacterial activity of FA against *S. aureus* and MRSA.

5.6. Materials and methods

5.6.1 Materials

Fusidic acid (FA), Polyvinylpyrrolidone (PVP), Poloxamer 188 (P188), sodium dodecyl sulfate (SDS), Cremophore (RH40), Solutol® (HS15), Tween 80 and Cremophor® EL (EL) were purchased from Sigma–Aldrich Co. Ltd (USA). Propidium iodide and Syto9 dyes cell viability kits were purchased from Thermofisher (USA), 3-(4,5-dimethylthiazol-2-yl)-2,5-diphenyltetrazolium bromide (MTT) was bought from Merck Chemicals (Germany), Fetal bovine serum (FBS) was obtained from Life Technologies (USA) and penicillin streptomycin (pen/strep) was purchased from Lonza (USA). An Elix 10 water purification system (Millipore Corp.,USA) was used to obtain milli-Q water. Mueller Hinton Agar (MHA) (Biolab, South Africa), Nutrient Broth (Biolab, South Africa), Nutrient Agar (Biolab, South Africa) and

Mueller Hinton Broth 2 (MHB) (Sigma-Aldrich, USA) were used in the antibacterial testing studies and tested against *Staphylococcus aureus* (ATCC 25922) and *Staphylococcus aureus* Rosenbach (ATCC BAA-1683TM) (MRSA).

5.6.2 Screening and preparation of FA-NS

A bottom-up antisolvent ultrasonication-precipitation technique was employed to prepare FA-NS. A solution of FA in organic solvent was prepared and added dropwise to a surfactant solution in milli-Q water under vigorous stirring. The resulting mixture was further sonicated for a determined time period under ice ⁴⁵. Initially a surfactant solution (0.1% w/v) was prepared and 1mL of FA solution (10 mg/mL) in water miscible organic solvent was added dropwise under vigorous stirring, sonicated at 30% amplitude for 5 min. Thereafter, the suspension was stirred overnight at room temperature to completely evaporate the organic solvent. Various parameters, such as surfactant type, surfactant concentration, drug concentration, solvents (methanol, ethanol and acetone), sonication time and amplitude, were evaluated to obtain a stable FA-NS nanosuspension. Potential surfactants were screened to provide a stable system: Polyvinylpyrrolidone (PVP), Poloxamer 188 (P188), sodium dodecyl sulfate (SDS), Macrogol (RH40), Solutol® HS 15 (HS15), Tween 80 and Cremophor® EL (EL). Following the evaporation of organic solvent, the FA-NS was immediately lyophilized using 3% mannitol as a cryoprotectant ⁴⁶.

5.6.3 Characterization of Fusidic acid nanosuspension

5.6.3.1 In silico studies

MD simulations is a widely applied technique in the field of drug delivery to accomplish tasks such as understanding the drug interaction with proteins^{47,48} membranes^{49,50} and polymers^{51,52}. The spontaneous binding of P188 with FA was studied using MD simulations to allow us to understand: 1) the FA spontaneously binding with P188, 2) interactions that play a crucial role in FA interaction with P188 (whether VdW or electrostatics), and 3) if the binding free energy

of the complex is favorable. The structure of FA (Figure 2A) was taken from PDB id: 2VUF⁵³, and 10 monomer units of each P188 blocks were constructed using ChemDraw⁵⁴ (Figure 2 B) (Figure: 1A). CHARMM General Force Field (CGenFF)⁵⁵ parameters were used for both of the molecules, and the TIP3P model⁵⁶ was used for water. The molecular dynamics simulation system contains one Fusidic acid molecule, a polymer of P188 and 30235 water molecules. The system was first energy minimized using the 5000 steps of steepest descent method⁵⁷, after which equilibration simulations were performed using canonical ensemble (NVT), followed by an isobaric-isothermic ensemble (NPT) for 10 ps each, with the production run being performed using an NPT ensemble for 30 ns. The simulation was performed at 300K temperature using the velocity-rescale method and at 1 atm pressure using the Parrinello-Rahman method⁵⁸, with the coupling time for the temperature being 0.1 and for pressure 2.0 ps. The Particle Mesh Ewald (PME) method⁵⁹ was used for long-range electrostatic interactions, with 10Å cut-off being used to calculate the VdW and short-range coulombic interactions. The Com of Mass (COM) distances between P188 and FA were calculated using in-house Tcl script. The interaction and binding energy between P188 and FA was calculated using the g_mmpbsa tool, which uses the molecular mechanics poisson–boltzmann surface area (MM-PBSA) method⁶⁰, while the Simulation was performed using GROMACS 5.1.2⁶¹. The binding free energy of P188-FA complex in solvent was expressed as:

$$\Delta G_{binding} = \Delta G_{complex(p188+FA)} - (\Delta G_{P188} + \Delta G_{FA})$$

Where $\Delta G_{complex}$ is free energy of p188 and FA complex and $\Delta G_{p188}, \Delta G_{FA}$ are total energy of P188 and FA individually. Free energy of $\Delta G_{complex}, \Delta G_{p188}$ and ΔG_{FA} were estimated using:

$$\Delta G_{p188} = \Delta E_{p188(MM)} + \Delta G_{p188(Solvation)}$$

$$\Delta G_{FA} = \Delta E_{FA(MM)} + \Delta G_{FA(Solvation)}$$

Where ΔE_{MM} is potential energy in vacuum and estimated using:

$$\Delta E_{MM} = \Delta E_{bonded} + \Delta E_{nonbonded}$$

$$\Delta E_{MM} = \Delta E_{bonded} + (\Delta E_{vdw} + \Delta E_{elec})$$

The $\Delta G_{solvation}$ is solvation free energy and estimated using:

$$\Delta G_{Solvation} = \Delta G_{polar} + \Delta G_{nonpolar}$$

ΔG_{polar} was calculated using the Poisson-Boltzmann (PB) equation and $\Delta G_{nonpolar}$ was estimated using:

$$\Delta G_{nonpolar} = \gamma SASA + b$$

here γ is a coefficient related to surface tension of the solvent and b is fitting parameter

$$\gamma = 0.0226778 \text{ kJ/Mol/\AA}^2 \text{ and } b = 3.84928 \text{ kJ/Mol}$$

A bootstrap analysis was performed to calculate the standard error.

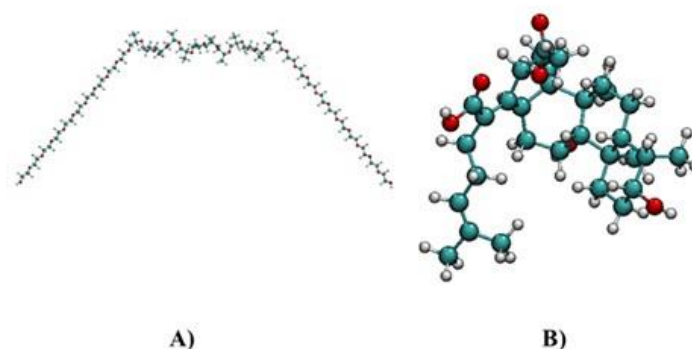


Figure 2. Structure of A) monomer units of P188, B) FA (PDB:2VUF).

5.6.3.2 Size, polydispersity index (PI), zeta potential (ZP) and morphology

The size, PI and ZP of FA-NS were analyzed by dynamic light scattering (DLS) using a Zetasizer Nano ZS90 (Malvern Instruments Ltd., UK). The FA-NS were diluted with milli-Q water in such a way that the scattering intensity was within the instrument's sensitivity range, after which it was analyzed. All measurements were performed in triplicate on three different batches that were prepared separately. The morphological investigations were performed using Jeol, JEM-1010 (Japan) transmission electron microscopy (TEM). The FA-NS suspension was diluted appropriately and mounted onto the surface of a copper grid, with the excess sample

being removed by blotting off with filter paper, after which it was dried at ambient temperature and stained using 2% uranyl acetate solution before measurement⁶². The images were captured at an accelerating voltage of 100 kV

5.6.3.3. Differential scanning calorimetry (DSC)

The thermal profiles of the FA, P188 physical mixture and lyophilized FA-NS were determined by DSC (Shimadzu DSC-60, Japan). Briefly, samples (2 mg) were placed in an aluminum pan and sealed using a crimper, then heated to 300 °C at a constant rate of 10 °C/min under a constant nitrogen flow of 20 mL/min using an empty pan as a reference.

5.6.3.4 X-ray diffraction (XRD) analysis

The XRD patterns were obtained using Bruker D8 advance diffractometer (Bruker, Karlsruhe, Baden-Württemberg, Germany) equipped with a graphite monochromator operated at 40 kV and 40 mA. CuK α radiation was used as the X-ray source with $\lambda=1.5406 \text{ \AA}$.

5.6.3.5 Fourier transform-infrared (FT-IR)

A Bruker Alfa spectrophotometer (Germany) was used for the FT-IR analysis of FA, Poloxamer 188 (P188) and lyophilized FA-NS in order to determine any chemical changes that occurred during formulation.

5.6.4 Rheology of the suspension

The rheological properties of the FA-NS suspension were measured by the MCR 302 Rheometer® (Anton Parr, Graz, Austria) using a 49.96 mm plate (0.995 °, shear rate from 0.01 to 100/s) at room temperature, with the experiments being performed in triplicate.

5.6.5 Physical stability study

Stability studies of both the wet and lyophilized nanosuspensions were performed at 4 °C and room temperature over a 3-month period. The parameters evaluated for confirming the stability were particle size, PI, ZP, settling behavior and physical appearance.

5.6.6 Solubility studies

A shake-flask method was used to determine the solubility of FA-NS and FA in water. Excess quantities of FA and lyophilized FA-NS were added to the milli-Q water (10 mL) and placed in a shaking incubator at a temperature of 25 °C for 24 hours. The undissolved FA was removed by filtering through syringe filters (cellulose acetate membrane, 0.2 µm, GVS filter technology, USA)^{40, 63}, with the FA content being determined by HPLC (Shimadzu, Japan) using a reported method⁶⁴. The mobile phase was composed of acetonitrile and water (70:30, v/v) that was adjusted to pH 3.5 with acetic acid. The flow rate and detection wavelength were 1.0 mL min⁻¹, and 210 nm respectively. The injection volume was 20 µL and was pumped through a Nucleosil 100-5 C18 column (150 mm X 4.6 mm internal diameter). The regression equation for the calibration curve was $y = 186436x - 10635$, and the linearity correlation coefficient r^2 was 0.9994.

5.6.7 In vitro cytotoxicity

The biosafety of FA-NS suspension was assessed using a MTT assay method⁶⁵. Adenocarcinoma human alveolar epithelial cell line (A549) and Human embryonic kidney cells (HEK 293) were plated in T-25 cell culture flasks at a density of 104 cells/mL and cultured in DMEM media supplemented with 10% FBS (v/v) and 1% Pen-Strep (v/v). The cells were grown at 37 °C in a humidified incubator with 5% CO₂. The medium was exchanged every two days. Each of the two cell lines containing 3000 cells were seeded into 96-well plates and were further incubated for 24 h and the media was discarded and replaced with 100 µL of fresh media. Thereafter, different dilutions of FA-NS containing 20, 40, 60, 80 and 100 µg of P188 were added to the 96-well plates (n=6 per concentration). After 48 h of incubation, sample-laden medium was then removed from each well, discarded and replaced with 100 µL of fresh culture medium and 20 µL of MTT solution (5 mg/mL in PBS) in each well. Cell viability was

assessed on a microplate spectrophotometer (Spectrostar Nano, Germany) at an absorbance wavelength of 540 nm. The percentage cell viability was calculated as follows.

$$\% \text{ Cell viability} = \left(\frac{\text{A540 nm treated cells}}{\text{A540 nm untreated cells}} \right) \times 100\%$$

5.6.8 Antibacterial activity

5.6.8.1 *In vitro* antibacterial activity

The broth microdilution method was used to determine the minimum inhibitory concentration (MIC) values. *S. aureus* and MRSA were grown overnight in Nutrient Broth at 37 °C in a shaking incubator at 100 rpm and diluted with sterile deionized water to achieve a concentration equivalent to 0.5 McFarland standard using a DEN-1B McFarland densitometer (Latvia). In a 96 well plate 135 µL of MHB was added followed by addition of 135 µL of bare FA (1.5 mg/mL) (positive control) and FA-NS (1 mg/mL) in the first well then it was then serially diluted. Both the bacterial cultures grown in Mueller–Hinton Broth (MHB) were further diluted to 5×10^5 colony forming units per mL (CFU/mL)⁶⁶ and 15 µL was added to the sample and MHB laden 96 well plate and incubated at 37 °C in a shaking incubator (100 rpm). After 24 h, 10 µL of the incubated broth was spotted on Mueller-Hinton (MHA) plates and incubated for 24 h at 37 °C to determine the MIC values. The studies were performed in triplicate using 1 % v/v DMSO solution as a negative control^{30, 67}.

5.6.8.2 Flow cytometry bacterial cell viability

Cell viability studies on the MRSA cells were performed following a flow cytometry assay method. A volume of 15 µL of the bacterial suspension containing 5×10^5 colony forming units (CFU)/mL was added to each well containing 135 µL of bare FA (positive control), and FA-NS at their respective MICs, were incubated at 37 °C in a shaking incubator (100 rpm). Percentage cell viability after 24 hours was determined using the flow cytometry method on a BD FACSCANTO II (Becton Dickinson, CA, USA) fluorescence activated cell sorter⁶⁸⁻⁶⁹. 50 µL of each FA and FA-NS treated with bacterial cultures in each well were added to the flow

cytometry tubes, each containing 350 μL of the sheath fluid, and vortexed for 5 min. The mixture was incubated for 30 min with 5 μL of propidium iodide (PI), which is a non-cell wall permeant dye, as well as the Syto9 cell permeant dye. PI fluorescence was excited by a 455 nm laser and collected through a 636 nm bandpass filter, while Syto9 excitation was at 485 nm laser and collection was through a 498 nm band pass filter⁷⁰⁻⁷². Untreated pure MRSA cells were used as a negative control. Instrumentation settings included a sheath fluid flow rate of 16 mL/min, and a sample flow rate of 0.1 mL/min. Data with fixed cells were collected using flow cytometer software (BD FACSDIVA V8.0.1 software [USA]). The voltage settings used for the fluorescence-activated cell sorting (FACS) analysis were: 731 (forward scatter [FSC]), 538 (side scatter [SSC]), 451 (Syto9) and 444 for PI. Bacteria were initially gated using forward scatter, with the cells of the appropriate size being gated and at least 10,000 cells collected for each sample in triplicate, and their position as 'live' and 'dead' cells being determined. To avoid any background signal from particles smaller than bacteria, the detection threshold was set at 1,000 events in SSC analyses⁷³.

5.6.8.3 *In vivo* antibacterial activity

A mouse skin infection model was used for *in vivo* antibacterial activity following a study protocol approved by University of KwaZulu-Natal's (UKZN) Animal Research Ethics Committee (AREC) (Approval number: AREC/104/015PD). Humane care and use of animals were in accordance with the guidelines of the AREC of UKZN and the South African National Standard SANS 10386:2008. BALB/c male mice weighing 18 – 20 g were used in the study. The back hair of mice was removed 24 h prior to the experiment, and the intact exposed skin disinfected using 70% ethanol. 50 μL of MRSA saline suspension containing 1.5×10^8 CFU/mL was injected intradermally the following day. The mice were then divided into three groups; treatment, positive and negative control (n = 4). After 30 minutes of infection, 50 μL (0.05 mg of FA) of FA-NS (treatment), bare FA (0.25 mg) in 1% DMSO (positive control),

and saline (negative control) were injected at the same site of infection for each treatment group respectively^{10, 30, 74-75}.

The mice were kept under observation for 48 h with a normal 12 h of light and darkness conditions at 19-23 °C and 55 ± 10% relative humidity with adequate ventilation, after which they were euthanized with halothane and the infected area of the skin harvested and homogenized in 5 mL PBS (pH 7.4). Tissue homogenates were serially diluted in PBS (pH 7.4) and 20 µL of the diluted homogenates were spotted on nutrient agar plates followed by incubation at 37 °C for 24 h, after which the number of colonies were counted. The CFU/mL was calculated using the equation:

$$\text{CFU/mL} = \frac{\text{number of colonies} \times \text{dilution factor}}{\text{volume of culture plate}}$$

Histomorphological assessments were performed on the freshly harvested excised skin from the injection site. The skin samples were transferred directly after harvesting and the excisions from the normal saline skin samples were fixed into 10% buffered formalin at 25°C for seven days, dehydrated using ethanol and implanted in paraffin wax. The tissue wax blocks were sectioned using a microtome (Leica RM2235, Leica Biosystems, Germany), the sections being collected on slides, then dried and stained with hematoxylin and eosin (H&E). The sections were examined and captured with a Leica Microscope DM 500 that was fitted with a Leica ICC50 HD camera (Leica Biosystems, Germany).

5.6.9 Statistical analysis

One-way analysis of variance (ANOVA), followed by Bonferroni's multiple comparison test, was used for statistical analysis. Individual groups were compared against each other using paired t-test, with *p* values of <0.05 being considered statistically significant. Values are represented as mean ± SD. GraphPad Prism® software (Graph Pad Software Inc., Version 6, San Diego, CA) was used for statistical analysis.

5.7. Results

5.7.1 Formulation of the nanosuspension

The FA-NS nanosuspension was prepared by bottom up antisolvent precipitation, with the FA being dissolved in a water miscible organic solvent to form a solution, then added to the aqueous (antisolvent) phase containing a suitable stabilizer (surfactant) under vigorous stirring, and sonication under ice. As the drug solution was added to the antisolvent, precipitation of the drug molecules occurred, forming a new solid phase of drug nuclei, as per Kelvin's Law⁷⁶. The formed nuclei have the tendency to condense into larger particles, which is energetically favored due to Ostwald ripening, as shown in TEM images (Figure 3), resulting in various formulation parameters being optimized before achieving a stable nanosuspension.

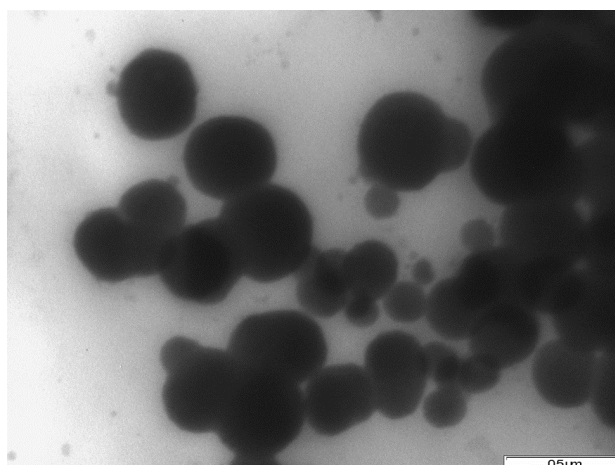


Figure 3. TEM image of smaller particles showing coalescence to form larger thermodynamically stable larger particles before optimum FA-NS suspension was achieved.

5.7.2 Evaluation of the formulation variables to obtain optimized FA-NS

5.7.2.1 Effect of surfactants

A potential surfactant to provide a stable nanosuspension was identified from screening several surfactants, the results being displayed in Table 1. FA drug concentration of 10 mg/mL, organic solvent (methanol), sonication of 30% amplitude and sonication time of 5 min were fixed, while different types of surfactants were varied. The effect of surfactant type on size, PI and ZP was investigated, with the particle sizes ranging from 200 nm to 1400 nm, and the PI from

0.1 to 0.6. The SDS produced FA-NS with the lowest particle sizes, followed by PVP and P188. However, nanoprecipitation in the presence of P188 consistently generated nanosuspensions with significantly lower PI when compared to PVP ($p = 0.0113$) and SDS ($p = 0.0288$), with P188 being chosen as the surfactant of choice.

Table 1. Effect of surfactant type on stabilizing the nanosuspension (n=3)

Surfactant	Average size	PI	ZP
PVP	563.5 ± 6.18	0.354 ± 0.031	- 10.6 ± 0.24
P188	590.0 ± 7.92	0.254 ± 0.017	-13.1 ± 2.70
SDS	388.6 ± 58.00	0.592 ± 0.124	-62.5 ± 6.34
RH 40	1159 ± 21.36	0.330 ± 0.045	-10.0 ± 0.16
HS15	1289 ± 28.00	0.412 ± 0.230	-7.21 ± 1.67
Tween 80	772.4 ± 4.71	0.375 ± 0.049	-11.1 ± 0.07
EL	1403 ± 18.69	0.462 ± 0.004	-08.57 ± 1.16

Having chosen P188 as surfactant of choice, nanosuspensions with various concentrations of P188 (0.1, 0.2, 0.4, 0.8, 1.6 and 2 % w/v) were prepared in order to determine the concentration of the surfactant that offered FA-NS with the lowest possible size, PI and a ZP in an acceptable range.

As the concentration of surfactant increased from 0.1 % w/v to 0.8 % w/v, the particle size decreased from 590 nm to 518.4 nm respectively (Figure 4). However, above the 1 % w/v the size started to increase.

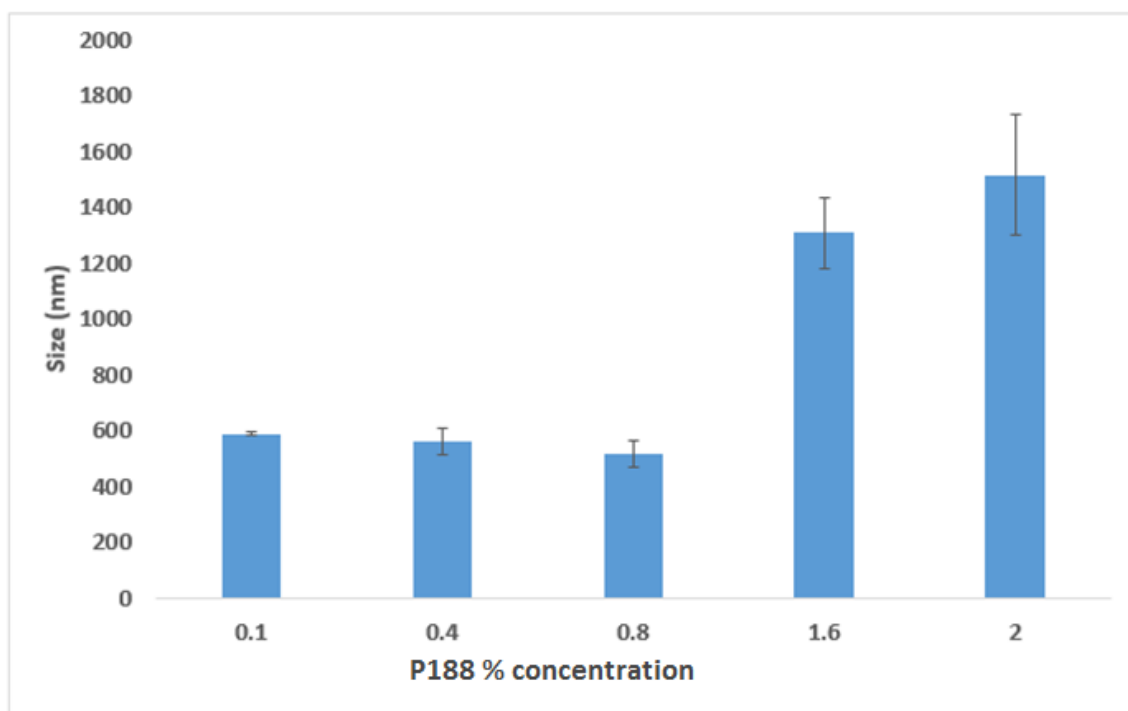


Figure 4. Effect of surfactant concentration on particle size (n = 3).

5.7.2.2 Effect of organic solvent

Having determined the concentration of P188 suitable to formulate the nanosuspension, solvents were evaluated for their effect on the size of the formed FA-NS. the FA concentration of 10 mg/mL, sonication time (5 min) and 30 % amplitude were fixed. Methanol was considered to be a suitable solvent as it produced FA-NA with lowest particle size (Table 2) compared to ethanol ($p = 0.0001$) and acetone ($p = 0001$). It was also observed that FA-NS formulated using methanol had a better PI than acetone and ethanol.

Table 2. Effect of organic solvents on nanosuspension formation (n=3)

Solvent	Average size	PI	ZP
Ethanol	950.0 ± 21.13	0.307 ± 0.036	- 14.6 ± 1.08
Acetone	896.0 ± 17.37	0.384 ± 0.058	-12.8 ± 0.85
Methanol	590.0 ± 07.92	0.254 ± 0.017	-13.1 ± 2.70

5.7.2.3 Effect of drug concentration

To achieve an optimum size and distribution of the FA nanocrystals, the effect of the drug concentration was evaluated. The concentration of the drug was varied from 10 mg/mL to 30 mg/mL, while keeping the concentration of P188 at 1 mg/mL, methanol as the solvent, a fixed sonication amplitude of 30 % and time a of 5 min. As the drug concentration increased from 10 mg/mL to 30 mg/mL, the particles sizes increased from 552 ± 13.3 nm to 1336 ± 89.4 nm and the PI increased from 0.198 ± 0.017 to 0.498 ± 0.042 (Figure 5)

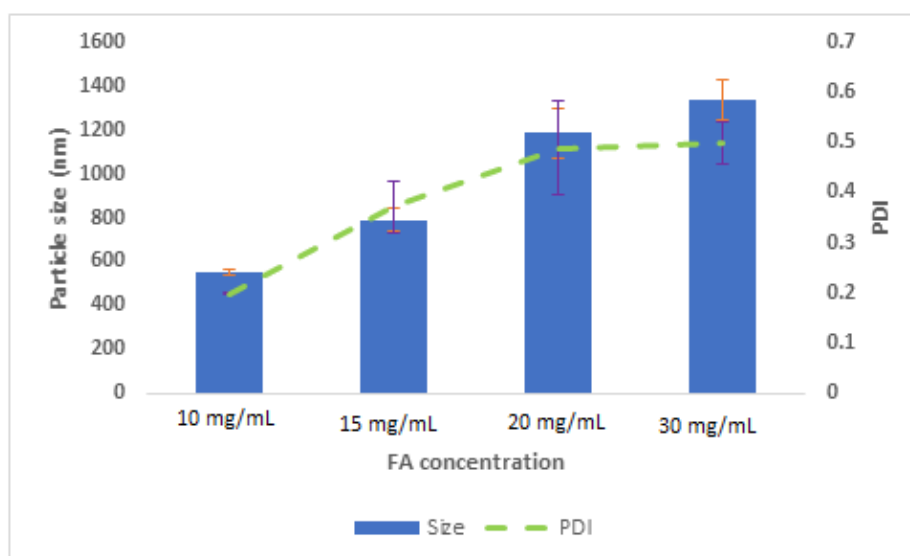


Figure 5. The effect of increasing drug concentration on particle sizes and homogeneity of the formed particles.

5.7.2.4 Effect of sonication time and amplitude

By fixing the concentration of the surfactant (P188 = 1 % w/v), drug concentration (FA = 10 mg/mL) and methanol as the solvent, the effect of ultrasonication was studied by changing the sonication time and amplitude. Fixing the sonication amplitude at 30%, ultrasonication times of 5, 7, 10, 15 and 20 min were employed to determine their effect. The particle sizes showed the tendencies to decrease with increasing time. However, after 15 min, increasing the sonication time did not show any significant ($p > 0.05$) change in the particle size. Consequently, the effect of ultrasonication amplitude (5 %, 10 %, 20 %, 30 %, 40 %) was also investigated

by fixing the time at 15 min. The trend similar to sonication time was witnessed, where initially increasing ultrasonication amplitude led to reduced particle sizes, while above an amplitude of 30% there was no significant decrease in particle sizes

5.7.3 Characterization of FA-NS

The above screening studies identified the following: the surfactant (P188 = 1 % w/v), drug concentration (FA = 10 mg/mL), methanol as an organic solvent, ultrasonication time and amplitude of 15 min and 30 % respectively as the optimal conditions for preparing FA-NS that resulted in monodisperse nanosuspension. The formulation was then subjected to detailed characterization, as reflected below.

5.7.3.1 *In silico* studies

MD simulation of 30 nanosecond (ns) of FA and P188 (10 units per polymer block) molecule in the presence of water molecules was performed to investigate the spontaneous binding, interaction energy and free energy binding between P188 and FA. Figure 6 shows the interaction between p188 and FA at different time points. The time evolution of the COM distance between the P188 and FA revealed that there was spontaneous interaction between both molecules starting from ~9 ns (Figure 6A). After interacting, the two molecules remained in a stable complex until ~16.9 ns. From ~17 ns to ~17.3 ns of MD simulation for 300 ps, a momentary break in the interaction between both the molecules was observed. However, at ~17.4 ns, the interaction was re-established between both the molecules and remained stable until the end of the simulation. The average COM distance between the P188 and FA was ~14.37 Å, and the average interaction energy between the P188 and FA was ~ -74.42 kJ/mol from 9 ns to 30 ns (Figure 7B, black line). The interaction energy components showed that the spontaneous binding between the P188 and FA was largely governed by VdW interactions (Figure 7B, green line). The representative images from the trajectory revealed (Figure 6) that after the binding of the FA, the P188 rearranged its conformations to establish stable

interactions. The contribution to the ΔG_{total} from the van der Waals (VdW) and electrostatic interactions was represented by ΔE_{vdw} and ΔE_{elec} . The polar and nonpolar solvation energy contributions to ΔG_{total} were represented by ΔG_{polar} and $\Delta G_{\text{nonpolar}}$ respectively. The P188-FA binding was largely governed by hydrophobic interactions, with ΔE_{vdw} being the most favourable contributor. ΔG_{polar} was unfavourable for the binding, while favourable $\Delta G_{\text{nonpolar}}$ and a gain in intermolecular VdW compensated for an increase in the polar solvation energy, and which lead to an overall favourable binding energy. The binding energy (ΔG_{total}) of P188 with FA (Table: 3) was calculated using the MM-PBSA method from 9 ns to 30 ns, and the binding energy was found to be -49.764 ± 1.298 .

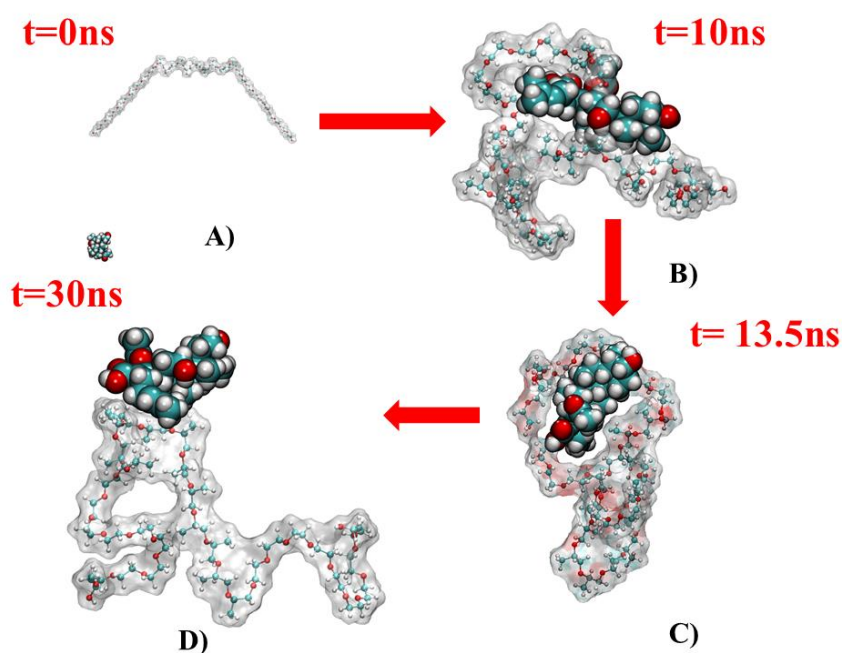


Figure 6. Structures of FA and P188 at four different time points of simulations. A) at $t=0$ ns. B) at $t=10$ ns. C) at $t=13.5$ ns. D) at $t=30$ ns. P188 has been represented in CPK model and FA is represented in the VdW model.

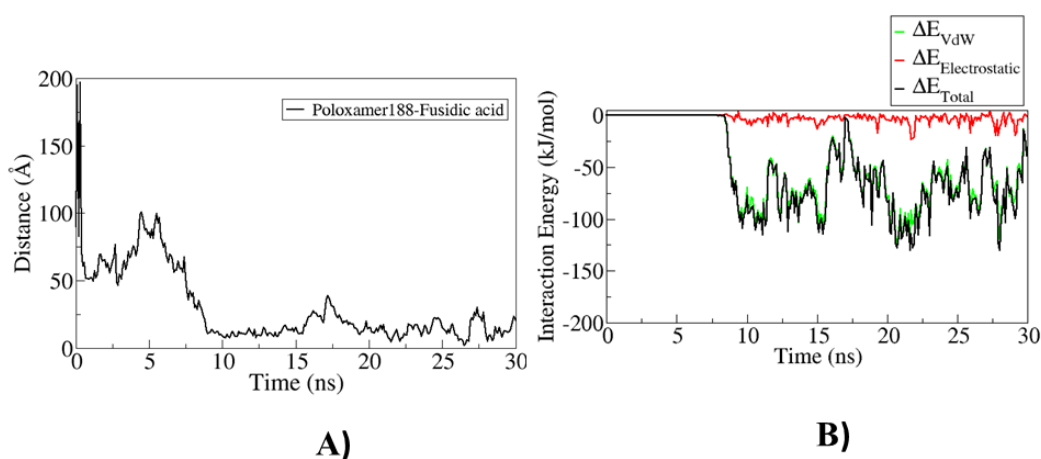


Figure 7. A) time evolution of COM distance between P188 and FA; B) Time evolution of interaction energy between the molecules and its non-bonded components.

Table: 3 Average Binding Energy and its Components Obtained from the MM-PBSA Calculation for the P188-FA complex.

Contribution	Energy (kJ/mol)
ΔE_{vdw}	-70.664 ± 1.680
ΔE_{elec}	-3.810 ± 0.314
ΔG_{polar}	36.075 ± 1.151
$\Delta G_{nonpolar}$	-11.416 ± 0.233
ΔG_{total}	-49.764 ± 1.298

5.7.3.2 Size, Polydispersity Index (PI), Zeta Potential (ZP) and Morphology of the optimal formulation

The optimal formulation, using the above variables, generated monodisperse FA-NS with size, PI and ZP of 265 ± 2.25 nm 0.158 ± 0.026 and -16.9 ± 0.794 respectively. The lyophilized and water re-dispersed samples did not have significant changes in size, PI and ZP (262.9 ± 2.59 nm, 0.179 ± 0.030 and -17.0 ± 1.01 mV respectively). The TEM images showed discrete spherical particles (Figure 8), with most of the population sizes being in the ranges that were comparable to the sizes observed in the DLS study.

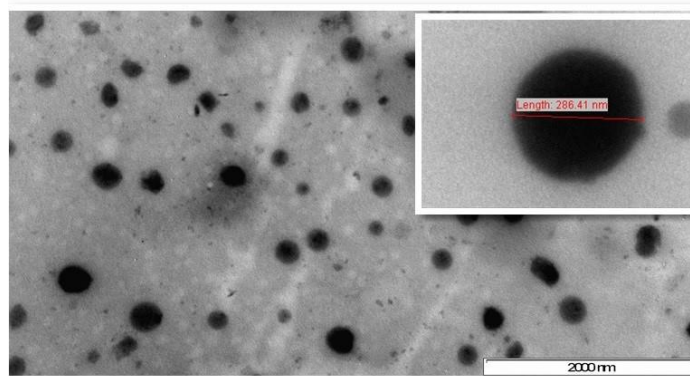


Figure 8. Morphology of the optimized FA-NS particles

5.7.3.2 DSC, XRD and FTIR analyses

A DSC investigation was performed to establish the melting and crystallization behavior of FA-NS and the formulation excipients. Endothermic peaks of P188 and bare FA were detected at 54.48 °C and 118.68 °C respectively (Figure. 9(II) A and B), while the Lyophilized FA-NS only showed a sharp endothermic peak at 42.46 °C (Figure 9(II) D). The XRD diffractograms pattern of P188 and FA showed 2 and 1 sharp peaks respectively (Figure 9(III)). The diffractogram pattern of the FA-NS nanosuspension showed no peaks for FA, however, it contained two sharp peaks in similar ranges to those of P188. The physical mixture was analyzed and the peaks for all the respective excipients and FA were observed (Figure 9(II) C). An FT-IR was also conducted to evaluate if there were chemical changes in the drug during formulation. The peaks for C=O stretch for both lyophilized FA-NS and bare FA were observed in the region of 1713 and 1645 cm^{-1} respectively, although the peak in the FA-NS was attenuated (Figure 9(I)). Carboxylic OH stretching groups were also present at the region of 3435 and 3395, both for the lyophilized and bare FA. The ester peak was missing in the FA-NS but was present in the bare drug at 1253.46 cm^{-1} . The disappearance might have been due to hydrogen bonding between P188 and FA during formulation of the FA-NS, as these kinds of interactions play a vital role in solubilizing the drug ⁷⁶. Finger print region spectra of the FA-NS was almost similar to FA alone, with the broad sharp peaks at 1079 and 1101 cm^{-1} for FA-

NS and P188 that were lacking in the bare FA possibly being due to a C-O stretch of the ether bonds present in P188.

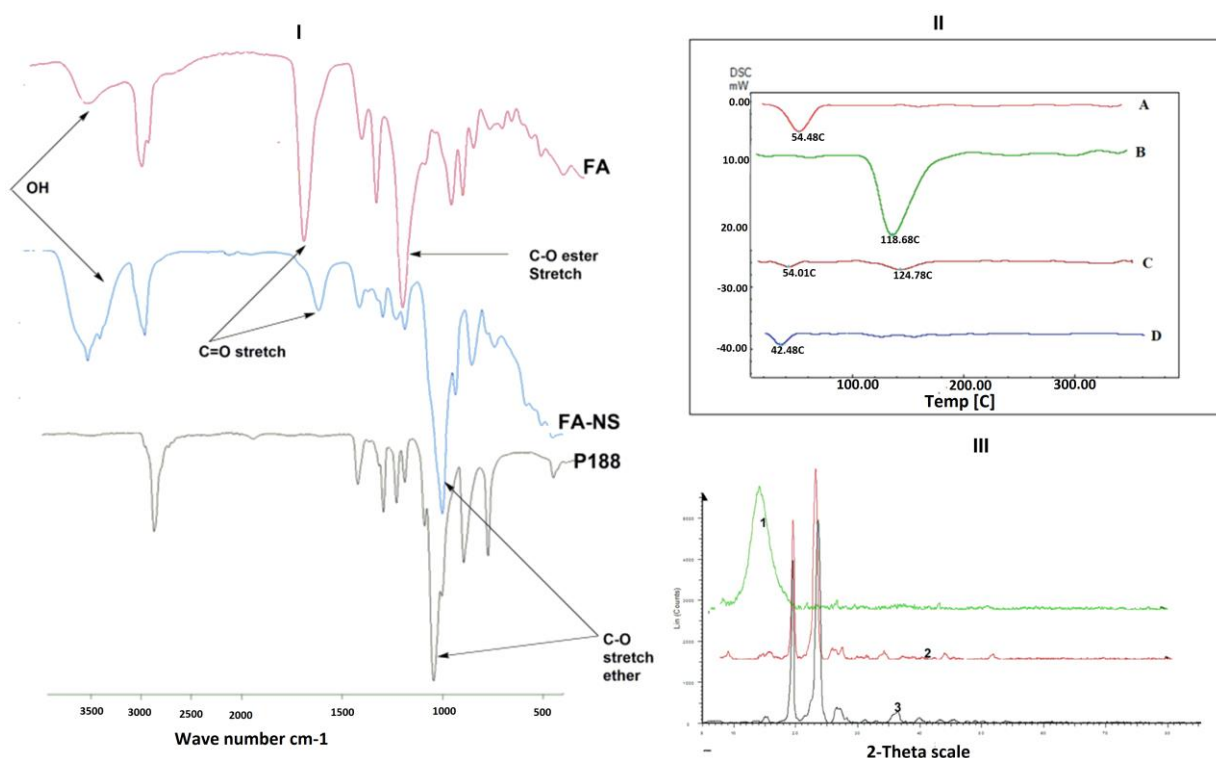


Figure 9. I) FT-IR of bare FA, FA-NS and P188, II) DSC thermogram of (A) P188; (B) FA (C) physical mixture and (D) lyophilized FA-NS, III) Diffractogram for (1) FA, (2) FA-NS and (3) P188.

5.7.4 Stability studies

5.7.4.1 Rheology

Rheology of the optimized FA-NS demonstrated a Newtonian flow with a relative viscosity of 1.335 ± 0.049 mPa-s. After seven days the nanosuspension had a viscosity of 1.371 ± 0.079 , which was 1.492 ± 0.095 mPa-s after one month, indicating no significant change in the viscosity of FA-NS ($p > 0.05$) during the storage period.

5.7.4.2 Physical stability study

The optimized formulation was further assessed for stability as both wet and lyophilized formulations for three months at room temperature (rt) and 4 °C. The FA-NS was found to be stable in both the lyophilized and wet states stored at 4 °C for the whole 3-month period of

evaluation, with particle sizes below 300 nm. Furthermore, the nanosuspension did not show any signs of coalescing and caking (Table 4). Room temperature studies revealed that the lyophilized formulations were more stable than the wet ones, with particle sizes below 300 nm after 60 days, increasing up to 500 nm after 90 days. The wet formulation was stable for two months and at the end of the 90 days, the particles sizes were found to be above the nano ranges.

Table 4. Stability studies of FA-NS

Formulation	Average size	PI	ZP
Time 0			
Wet	251.1 ± 11.9	0.126 ± 0.044	- 15.2 ± 1.73
Lyophilized rt	262.9 ± 2.59	0.179 ± 0.030	-17.0 ± 1.01
30 days			
Wet rt	386 ± 5.4	0.094 ± 0.015	- 21.2 ± 1.6
Wet 4 °C	274 ± 3.33	0.179 ± 0.042	- 15.4 ± 2.3
Lyophilized rt	296.4 ± 6.29	0.327 ± 0.072	-21.6 ± 1.1
Lyophilized 4°C	276.4 ± 5.7	0.087 ± 0.007	-20.8 ± 2.96
60 days			
Wet rt	426.8 ± 13.53	0.263 ± 0.164	- 19.7 ± 1.24
Wet 4 °C	267.6 ± 52.94	0.176 ± 0.07	- 15.6 ± 1.02
Lyophilized rt	280.5 ± 38.79	0.286 ± 0.04	- 16.5 ± 1.74
Lyophilized 4 °C	298.3 ± 43.96	0.321 ± 0.04	-15.04 ± 4.08
90 days			
Wet rt	1437.4 ± 681.2	0.908 ± 0.11	- 16.42 ± 4.2
Wet 4 °C	221.3 ± 7.9	0.307 ± 0.045	- 16.42 ± 4.2
Lyophilized rt	481.53 ± 70.70	0.50 ± 0.039	- 15.7 ± 12.9
Lyophilized 4 °C	292.4 ± 50.8	0.361 ± 0.04	-10.35 ± 0.43

5.7.4 Solubility studies

Solubility studies were conducted to determine the effect of formulating the FA into a nanosuspension on aqueous solubility. The solubility of the FA and FA-NS was found to be $17.81 \pm 5.30 \mu\text{g/mL}$ and $127.23 \pm 5.30 \mu\text{g/mL}$ respectively (Figure 10).

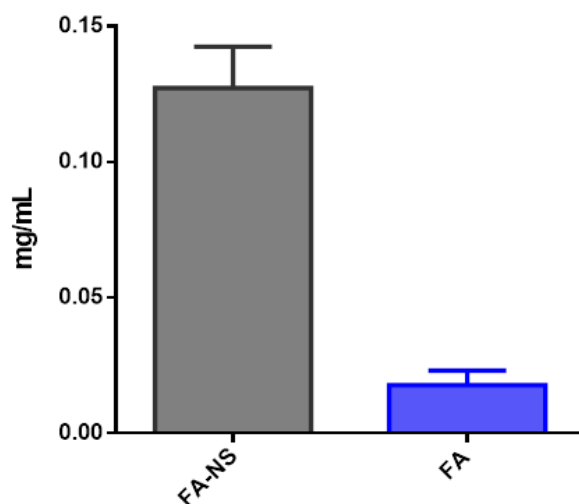


Figure 10. Solubility of FA-NS and FA in water (n = 3)

5.7.5 In vitro cytotoxicity

Biosafety of FA-NS was assessed by quantifying viable mammalian cells after exposure of the synthesized material. Two cell lines A549 and HEK 293 were employed to determine the biosafety of FA-NS in an *in vitro* cell culture system. The results showed cell viability ranging from 75.71 to 100.89% across all concentrations in all cell lines tested (Figure 11) with no dose-dependent toxicity within the concentrations studied.

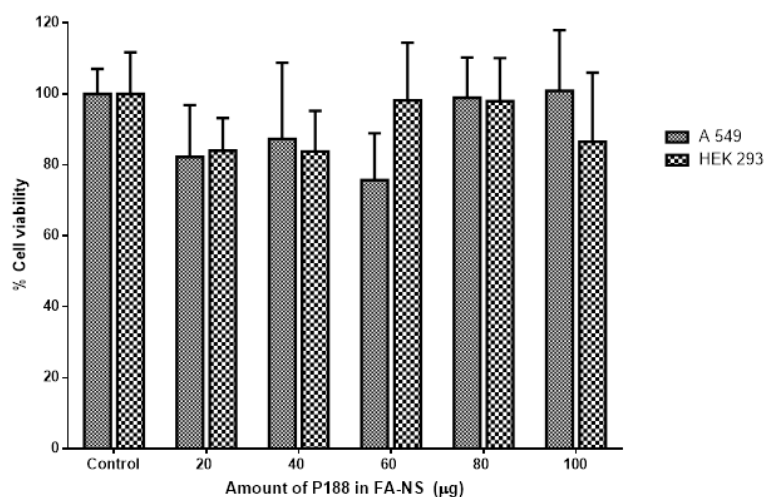


Figure 11. Cytotoxicity evaluation of FA-NS against various concentrations of P188 on A 549 and HEK 293 cells (n=6).

5.7.6 Antibacterial activity

5.7.6.1 *In vitro* antibacterial activity

To evaluate the efficacy of the FA-NS, the MIC values of the bare FA and FA-NS MIC values were determined against *S. aureus* and MRSA, with the results presented in Table 5. The MICs for FA and FA-NS were 62.5 µg/mL and 3.9 µg/mL respectively against *S. aureus*, whereas for MRSA, the values were 250 and 31.25 µg/mL respectively (Table 4).

Table 5. MIC of FA, FA-NS

	SA (µg/mL)	MRSA (µg/mL)
FA	62.5	250
FA-NS	3.9	31.25
1% v/v DMSO	NA	NA

NA = No activity. The values are expressed as mean ±SD, n=3

5.6.6.2 Flow cytometry bacterial cell viability

To quantify the number of bacterial cells killed at the MIC concentration of bare the FA and FA-NS, a flow cytometry method was employed. MRSA was incubated in an FA and FA-NS containing medium for 24 hours. PI fluorescent dye, which does not penetrate the cell wall, and Syto9 cell wall permeant dye was used to differentiate the live from dead cells in the population. The histograms showing the count of cells that internalized PI after 24 h of incubation are presented in (Supplementary information). The dead cells were sorted from the population using a gate created beyond the fluorescence of viable cells (Figure 12)⁷⁷. When the cells were incubated with the bare FA and FA-NS at their respective MIC, the average dead cells in the bacteria population were 38.8 % ± 2.35 and 73.14 ± 1.35 % respectively, indicating a significant difference ($p < 0.0001$). Furthermore, when the MRSA cells were treated with FA at the concentration similar to the MIC of FA-NS, the mean dead cells in the population were found to be only 4.66 ± 0.52 %. The FA and FA-NS dot plots of PI verses syto9 fluorescence^{69,71} showed similar results.

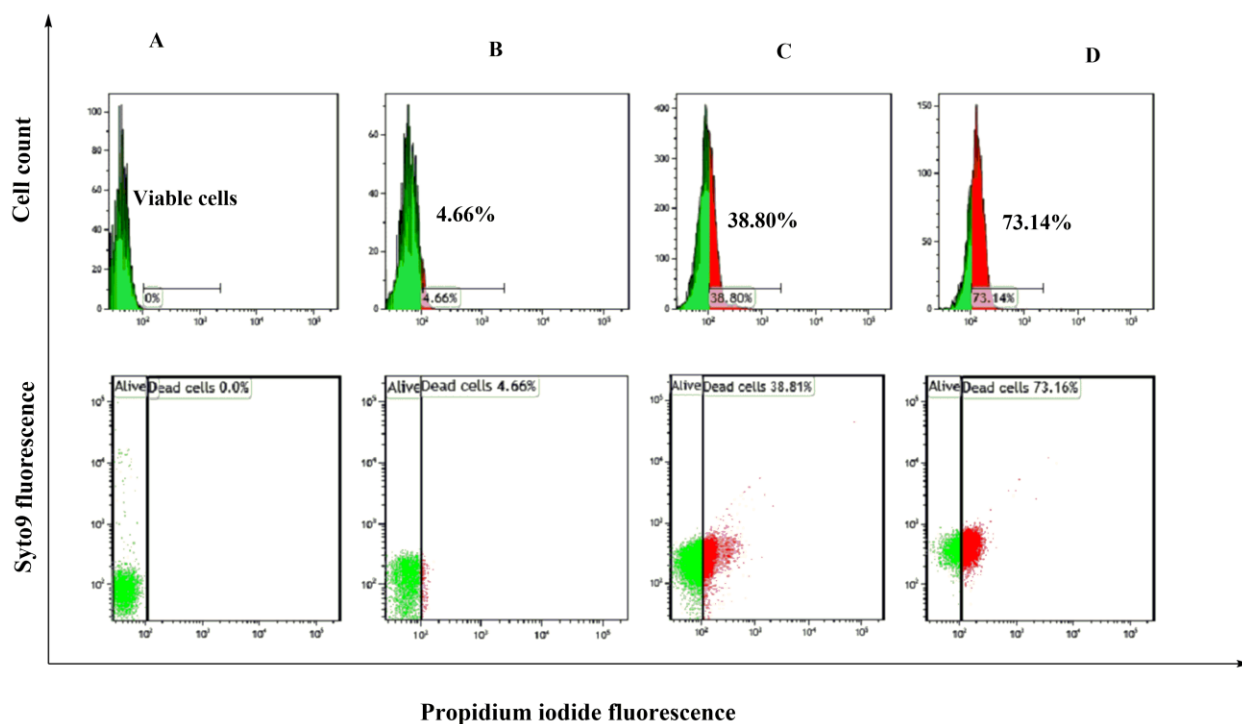


Figure 12. A) represents viable cells (negative events), Red colour represents dead cells percentage of dead cells in the population. B), C) and D) represents percentage dead cells after treatment with 31.25 $\mu\text{g}/\text{mL}$ of bare, bare FA and FA-NS at their respective MIC.

5.6.6.3 *In vivo* antibacterial activity

The efficacy of FA-NS was further evaluated *in vivo* using a mouse skin infection model. Intradermal injections of MRSA were administered with to causing short-term localization of the bacteria within the dermis skin layer without systemic infection. The number of colony-forming units (CFUs) was quantified for each treatment group and converted to \log_{10} CFU/mL, as represented in Figure 10. The mean bacterial load for untreated, FA and FA-NS groups were 6.58 ± 0.01 (3,790,000 CFU/mL), 6.30 ± 0.062 (2,016,667 CFU/mL), and $4.35 \pm 3.12 \log_{10}$ CFU/mL (26,667 CFU/mL) respectively.

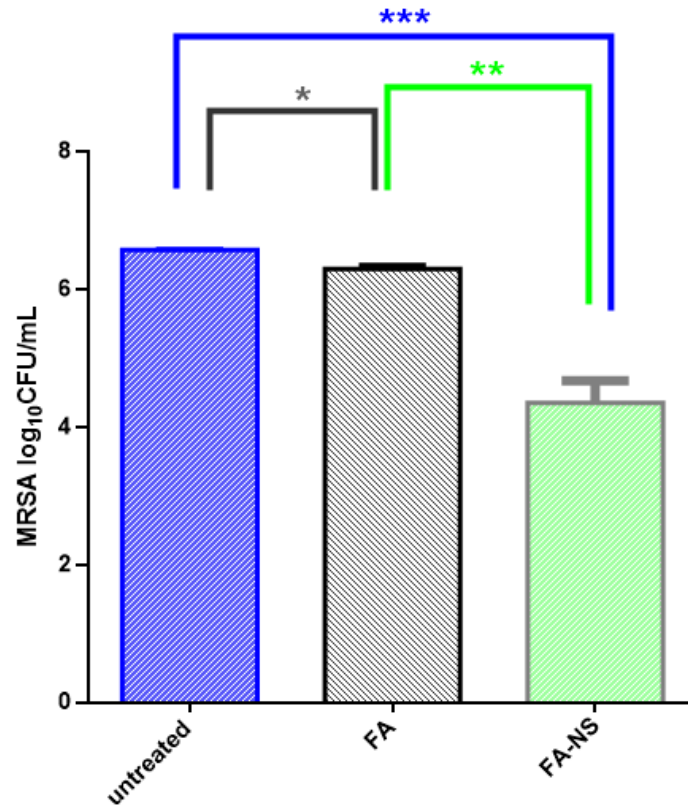


Figure 13. MRSA burden after 48 hours of treatment. *denotes significant difference for FA versus the untreated group. **denotes significant difference between bare FA versus FA-NS and ***denotes significant difference between bare FA-NS versus the untreated (n=4).

During tissue harvesting, fluid filled abscesses at the injection site were visually observed in skin samples from the MRSA injected control and the FA treated groups only, while none were seen for the FA-NS treated groups (Figure 13). Histological analysis was also performed to further assess the skin integrity and histomorphological changes after the MRSA intradermal infection. The H&E images from the MRSA injected control group confirmed inflammation and the formation of an abscess at the injection site (Figure 14B). The MRSA injected control tissue image also displayed evidence of inflammation, as represented by the excessive swelling of the dermal layer in the control image and the presence of white blood cells. The FA-NS treated tissue did not display any definite abscess formation, although there was evidence of minimal inflammation in the dermal layer (Figure 14D). In the MRSA injected control group, there were signs that a high number of cells were infiltrated by the bacteria, as evidenced by the large area of the abscess.

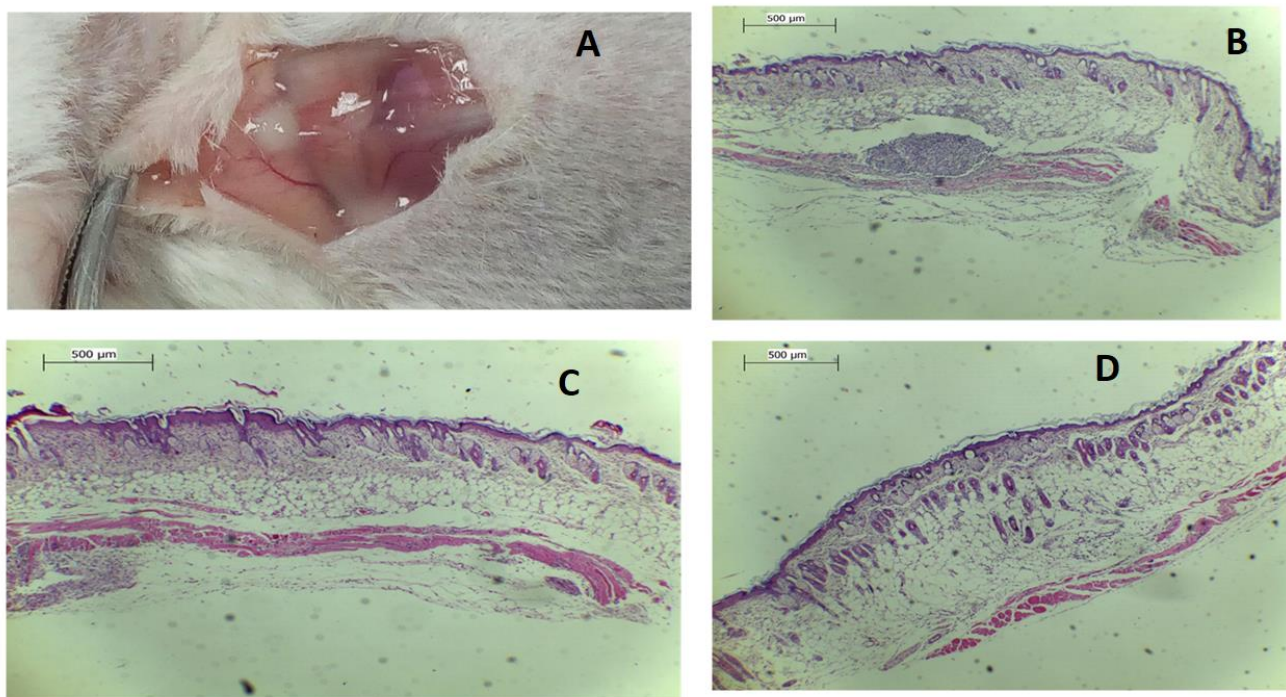


Figure 14. A) Abscesses from untreated mice, Photomicrographs of the control and the treated skin selections for light microscopy (LM) stained with H&E; (X40) (Scale bar = 500 μm) B) Control (MRSA injected, untreated (Saline) C) Treated (FA), E) Treated (FA-NS).

5.7. Discussion

This study explored formulating a FA antibiotic (BCS class II drug) into a nanosuspension (FA-NS), and its ability to enhance aqueous solubility and antibiotic activity due to the small sized particles. MD simulations were done to understand, at atomic level, the interaction between FA and P188. FA-NS nanosuspension was prepared using bottom up antisolvent precipitation technique. To achieve a stable nanosuspension, surfactants available in the market, various organic solvents and other formulation parameters, such as sonication time and amplitude, were screened. PVP, SDS and p188 were surfactants that provided nanosuspensions with small particle sizes, with P188 being found to be the surfactant of choice, as it consistently generated nanosuspensions with significantly low PI than PVP ($p = 0.0113$) and SDS ($p = 0.0288$). This may be due to the high hydrophilic–lipophilic balance (HLB value = 29) of the

amphiphilic block copolymer that may have led to better interactions with hydrophobic FA during the nanosuspension formation ⁷⁸.

Having chosen P188 as the surfactant of choice, various surfactant concentrations were screened to determine a suitable concentration that offers a stable nanosuspension. However, it was witnessed that when the surfactant concentration was > 1 % w/v, the particle sizes and the PI of the system increased. Studies have shown that increasing the surfactant above certain concentrations favors micelle formation due to the self-assembly of the surfactant, rather than providing stability to the nanosuspension, leading to the Ostwald ripening of the nanocrystals in the antisolvent. ⁷⁹⁻⁸¹. The formation of micelles at higher concentration of the surfactant resulted in a decreased amount of the surfactant available at the aqueous/ FA crystals interface to coat the surface of the formed solid phase, thus leading to Ostwald's ripening of the crystals. Various organic solvents were also screened to identify the one that provides the better antisolvent effect for precipitating the FA once the organic solvent FA solution comes in contact with water. Of the screened solvents, methanol was found to be the suitable as it generated a nanosuspension with better particle sizes, PI and ZP, although we could not conclusively state why it gave better particle sizes. These results could be ascribed to a higher rate of mixing of the solvent/antisolvent per unit time and easy crystal drawing out, which results in shorter time of nucleation and crystal growth, subsequently resulting in smaller crystals ⁸²

Drug concentration is also a critical variable in the formulation of the nanosuspensions, as increasing the drug concentration could result in an increased number of primary particles per unit volume and shorter interparticle distance ⁸³. Consequently, this may lead to a chance of forming an aggregate mass of loosely adhered particles by electrostatic charges, which can give rise to increased sizes and lack of uniformity amongst the particles formed ⁸⁴. This was also witnessed in the formulation of FA-NS, as the drug concentration increased from 10 mg/mL to

30 mg/mL, particles sizes increased from 552 ± 13.3 nm to 1336 ± 89.4 nm, and the PI increased from 0.198 ± 0.017 to 0.498 ± 0.042 . This phenomenon has also been previously reported for norfloxacin, griseofulvin, ampicillin, amoxicillin, and tetracycline nanosuspensions⁸⁵⁻⁸⁶, where above certain concentration of the drug particles coalesced to larger particles.

To further reduce the particles sizes, sonication time and amplitude were evaluated. Increase in sonication time and amplitude further reduced the particles sizes. However, above 15 min and an amplitude 30% of sonication there was no significant decrease in the particle size. The findings were in agreement with the work reported by Dengning et al in formulating a nifedipine nanosuspension⁸⁷. After screening to optimize all the parameters, a stable formulation was achieved. During formulation stirring provided a shear force that kept the particles in constant Brownian motion⁸⁸, sonication that broke down the aggregating solid phase, while the surfactant coated the particles, resulting in electrostatic repulsion of neighboring like-charged particles⁸⁹ and packing of the crystals into amorphous state that resulted in a stable colloidal system that had particle size, PI and ZP of 265 ± 2.25 nm 0.158 ± 0.026 and -16.9 ± 0.794 respectively.

MD simulations of 30 nanosecond (ns) between P188 (10 units per polymer block) and FA were performed. The negative free Gibbs energy change ($\Delta G_{\text{total}} -49.764 \pm 1.298$) indicated the degree of spontaneity of the binding process, and a higher negative value reflected a more energetically favorable adsorption⁹⁰. The favorable higher value of binding energy was also an indication of a strong binding between the molecules, which would require a higher repulsive energy to break the binding between the two molecules⁹¹. Furthermore, the energy components of the complex showed that the P188-FA binding was mainly governed by the hydrophobic interactions, with van der Waals (VdW) energy ΔE_{vdw} as the major contributor to binding energy (Table 3). Previous studies on ABA triblock polymer, such as P188, have

shown that, via its hydrophobic central block, the polymer forms strong interactions with the hydrophobic drug at the core, resulting in non-solvent assessable regions, while the hydrophilic blocks shell consequently forms water accessible regions. This arrangement leads to a stable complex and increased water solubility of the hydrophobic drug ⁹². Figure 6 and a video available in supplementary materials showed similar arrangements, thus the stabilization of the nanosuspension and the increased solubility of the FA in water could have occurred via this phenomenon of (ABA) triblock polymer solubilization ⁹³. These results were in agreement with experimental studies that showed an increased solubility of the drug in water at the simultaneously formation of a stable nanosuspension between P188 and FA.

DSC, XRD and F-TIR analyses were performed to investigate the melting and crystallization behavior of FA-NS and its formulation excipients. The DSC results showed the absence of a FA peak in the thermogram of the FA-NS, with a peak similar to the pure P188 being witnessed. This was an indication that the P188 was coating the surface of the FA, which was transformed into an amorphous state during the formulation process. The XRD diffractograms showed similar results to DSC, with the absence of FA peaks in the formulation diffractograms. The FT-IR analysis showed that both the formulation and physical mixture had the characteristic peaks of P188 and FA, and that the resultant FT-IR patterns were in line with the previous literature for nanosuspensions ⁹⁴⁻⁹⁶. The transformation of FA into FA-NS could have been due to the rapid drawing out of the drug particles from the organic solvent, as the aqueous solution with P188 as stabilizer coated the nascent drug particles nuclei, resulting in fast nucleation termination, leading to amorphous nanoparticles ⁹⁷. The patterns of the DCS thermograms, XRD diffractograms and FT-IR wave numbers of P188 and FA in the formulation and the crystalline pure P188 and bare drug was an indication that no new chemical compound was formed ⁹⁸.

The possibility of interactions between like and unlike particles in the system define the stability of a suspension⁹⁹. Ree and Eyring theory stated that viscosity is the sum of the contribution of an indefinite number of unspecified units of flow^{100, 101}. Therefore, Ostwald ripening, which might occur during the storage of a suspension, could result in viscosity changes that can be used to determine the stability of a suspension. The FA-NS viscosity was evaluated for a period of one month and showed that the nanosuspension had no significant ($p>0.05$) change of its viscosity. This might have been due to constant Brownian motion as a result of the small particle sizes that kept the system in a suspended state, the stabilizing effect of the surfactant and the high similar zeta potential values within the particles that causes repulsion, thus preventing Ostwald's ripening¹⁰². A further assessment of stability for wet and lyophilized formulations were performed for three months at room temperature and 4 °C. FA-NS was found to be stable in both lyophilized and wet state stored at 4 °C for the whole 3-month, however, room temperature studies revealed that lyophilized formulations were more stable than wet ones. These findings confirmed that the optimal storage conditions for the FA-NS suspension was at 4 °C for both wet and lyophilized formulations.

The applicability of the optimized formulation was evaluated for solubility enhancement and antimicrobial activity. Using a shake-flask method, the solubility was determined, there was a 7-fold increase in solubility of FA when formulated as FA-NS when compared to the bare drug. This phenomenon could be explained using various theories, such as that of Ostwald–Freundlich, in which the solubility of particles is inversely proportional to their radius¹⁰³⁻¹⁰⁵; Mihranyan and Strømme, who proposes increased solubility of nanoparticles due to surface fractal dimension;¹⁰⁶ and Letellier et al, who postulated that the improved solubility of nanoparticles is attributed to thermodynamic descriptions involving the internal energy of the particles¹⁰⁷. An increase in the aqueous solubility of the BCS Class II drugs, such as FA, is significant for their efficiency. Due to their hydrophobicity, they partition well through

biological membranes, although this does not translate to high bioavailability, as their partition from the dosage form is limited due to their low water solubility. Therefore, formulating FA as a nanosuspension could enhance the activity of the drug.

With the increase in application of nanoparticles there is a need for determination of their safety before application. The biosafety of FA-NS nanosuspension was determined using an *in vitro* MTT assay that quantifies viable cells upon exposure of the test materials to the two cell lines. Since cell viability upon exposure to FA-NS was above 75%, this indicated that the formulation met the requirements for biocompatibility and toxicity regulatory requirements for biomaterials¹⁰⁸. These results were in line with the findings in the literature where P188 has been reported to be biosafe and has been for 50 years approved by FDA as a surfactant and therapeutically used to reduce viscosity of blood before transfusion¹⁰⁹. Therefore, these findings show FA-NS to be a biosafe and nontoxic nanosuspension.

The impact on antibacterial activity of formulating FA in a nanosuspension was evaluated using the broth microdilution method. MIC values for the bare drug and FA-NS against *S. aureus* and MRSA showed that FA-NS had a 16- and 8-fold lower activity against *S. aureus* and MRSA respectively when compared to bare FA.

Generally, there was better activity against *S. aureus* than MRSA, which can be attributed to its thicker cell walls. This thickened cell wall is due to multiple peptidoglycan layers that limit the drug molecules from crossing the membrane. Enhanced activity of the antibacterial agents after formulation as a nanosuspension have been reported elsewhere¹¹⁰⁻¹¹². This enhanced activity by the FA-NS can be attributed to the nanoparticulate sizes of the nanosuspension that lead to an increase in the surface area, which resulted in an increased solubility for better penetration and higher uptake by the cells¹¹³. In addition, drug adsorption efficiency is directly proportional to the specific surface area of the adsorbent and inversely proportional to the particle size¹¹⁴⁻¹¹⁵. Smaller FA-NS nanoparticles may therefore have been effectively

distributed and adsorbed on the bacteria surface than bare FA, thus enhancing activity. Enhanced FA activity via the FA-NS underlines the use of nanosuspensions as a strategy to formulate BCS class II antibiotics as prospective drug delivery systems.

The viability of the surviving MRSA cells was determined using a flowcytometry method after incubating the bacteria with bare FA and FA-NS. Cells treated with FA-NS had almost twice the percentage population of dead bacterial cells, despite having an 8-fold lower MIC compared to bare FA. Furthermore, when the MRSA cells were treated with FA at the concentration similar to the MIC of FA-NS, the dead cells in the population were found to be $4.66 \pm 0.52 \%$, which confirmed its efficacy. The minimal effect of the bare FA on MRSA at low concentration was due to it having a bacteria static effect ¹¹⁶.

This result could translate to lowering amount the dosage amount required for treatment, with fewer dose dependent side effects that are related to FA, such as hepatic and hematological toxicities ¹¹⁷, thus showing FA-NS nanosuspension's superiority over FA.

Further evaluation of the efficacy of FA-NS was performed following a BALB/c mouse MRSA *in vivo* skin infection model. After infection and treatment periods, the mice were euthanized, their skin harvested and the number of CFUs quantified for each treatment group. A statistically significant ($p < 0.0001$) reduction in bacterial load was recovered from the treatment groups treated with FA-NS and FA when compared to the untreated group (Figure 14). Bacterial load recovered from the groups treated with bare FA compared to the untreated groups showed that the former had a significantly lowered ($p = 0.0133$) load of MRSA. The FA-NS treated samples had a 142.12-fold decrease in bacterial burden compared to the untreated groups ($p = 0.0002$). In comparing the bare FA and FA-NS, a 76-fold greater reduction of MRSA load in the groups treated with FA-NS ($p = 0.0081$) was observed compared to the bare FA. These results confirmed the ability of FA to enhance antibacterial activity when it is formulated as a nanosuspension, which can prove critical in treating infections of MRSA origin.

Histomorphological changes were also investigated as a suggestive means of identifying the extent of tissue destruction in the dermal layers that were infected with MRSA during the 48 h study. As all bacteria are recognized as foreign to the body, there is an innate immune response after their introduction into the intradermal layers¹¹⁸, which causes inflammation upon entry of the bacteria into the tissue, the degree of the response being proportional to the bacterial load. The histomorphological evaluations directly correlated with the findings of the bacterial load from each group of the *in vivo* antibacterial study, as the FA-NS treated tissue displayed a low isolated bacterial load and showed the least histomorphological signs of tissue inflammation. However, the MRSA injected negative control group and the FA treated group displayed a statistically significantly larger number of isolated bacteria, more histomorphological signs, and evidence of tissue inflammation and abscess formation. These histomorphological evaluations further confirmed the antimicrobial superiority of the novel FA-NS.

5.8 Conclusion

Nanotechnology derived novel formulations are showing significant potential for improving the efficacy of existing antibiotics. More than 40% of NCEs (new chemical entities) developed in the pharmaceutical industry are practically insoluble in water, this being a major challenge for formulation scientists. In this study, a new FA-NS formulation was successfully formulated using a bottom-up antisolvent precipitation with the goal of simultaneously enhancing solubility and antibacterial activity. After screening of various surfactants, solvents and formulation parameters an optimized nanosuspension, FA-NS with a particle size in the range of 200 nm was obtained. MD simulations revealed that there was spontaneous binding between FA and P188 in the aqueous milieu, with the average interaction energy and distance between the molecules being ~ -74.42 kJ/mol and ~ 14.37 Å. Further investigation on contributions of various energy components of the complex showed that Vander Waals interactions was the

major contributor, and that the binding energy between FA and P188 was -49.764 ± 1.298 kJ/mol. This further supported the experimental work of the formation of a stable nanosuspension between FA and P188. The formulation of FA as a FA-NS improved its solubility by 8-fold. The assessment of the *in vitro* antibacterial activity proved the superiority of the FA-NS over the bare FA to control the growth of susceptible and resistant *S. aureus*. *In vivo* antibacterial activity against MRSA using mice a skin infection model showed that FA-NS was more efficient in killing MRSA compared to bare FA. With these promising results, the formulated novel FA-NS nanosuspension can therefore be further exploited as a nanoantibiotic to fight against other bacteria, and this method possibly being employed to enhance the efficacy of other BCS class II drugs for various disease conditions.

Acknowledgments

The authors acknowledge the College of Health Sciences, University of KwaZulu-Natal (UKZN), the UKZN Nanotechnology Platform and the National Research Foundation of South Africa for financial support (Grant No. NRF Grant No. 87790 and 88453). The Microscopy and Microanalysis Unit, Biomedical Resource Unit, Department of Human Physiology and Flow Cytometry Research Laboratory at UKZN are also acknowledged as well as Mrs. Carrin Martin for proof reading and CHPC, Cape Town for supercomputing resources.

Disclosure

The authors report no conflicts of interest in this work.

5.9 References

1. Lewis, K., Platforms for antibiotic discovery. *Nat. Rev. Drug* **2013**, *12* (5), 371-387.
2. Boucher, H. W.; Ambrose, P. G.; Chambers, H.; Ebright, R. H.; Jezek, A.; Murray, B. E.; Newland, J. G.; Ostrowsky, B.; Rex, J. H.; America, I. D. S. o., White paper: developing antimicrobial drugs for resistant pathogens, narrow-spectrum indications, and unmet needs. *J. Infect. Dis.* **2017**, *jix211*.
3. Laxminarayan, R.; Duse, A.; Wattal, C.; Zaidi, A. K.; Wertheim, H. F.; Sumpradit, N.; Vlieghe, E.; Hara, G. L.; Gould, I. M.; Goossens, H., Antibiotic resistance—the need for global solutions. *Lancet Infect. Dis.* **2013**, *13* (12), 1057-1098.

4. Okano, A.; Isley, N. A.; Boger, D. L., Peripheral modifications of [Ψ [CH₂NH] Tpg₄] vancomycin with added synergistic mechanisms of action provide durable and potent antibiotics. *Proc. Natl. Acad. Sci. U. S. A.* **2017**, 114(26), E5052-E5061.
5. Kalhapure, R. S.; Suleman, N.; Mocktar, C.; Seedat, N.; Govender, T., Nanoengineered drug delivery systems for enhancing antibiotic therapy. *J. Pharm. Sci.* **2015**, 104 (3), 872-905.
6. Huh, A. J.; Kwon, Y. J., "Nanoantibiotics": a new paradigm for treating infectious diseases using nanomaterials in the antibiotics resistant era. *J. Control. Release.* **2011**, 156 (2), 128-145.
7. Jamil, B.; Habib, H.; Abbasi, S. A.; Ihsan, A.; Nasir, H.; Imran, M., Development of cefotaxime impregnated chitosan as nano-antibiotics: De novo strategy to combat biofilm forming multi-drug resistant pathogens. *Front. Microbiol.* **2016**, 7, 330
8. Zaidi, S.; Misba, L.; Khan, A. U., Nano-therapeutics: A revolution in infection control in post antibiotic era. *Nanomed. Nanotechnol. Biol. Med.* **2017**, 13(7), 2281-301.
9. Sonawane, S. J.; Kalhapure, R. S.; Rambharose, S.; Mocktar, C.; Vepuri, S. B.; Soliman, M.; Govender, T., Ultra-small lipid-dendrimer hybrid nanoparticles as a promising strategy for antibiotic delivery: In vitro and in silico studies. *Int. J. Pharm.* **2016**, 504 (1–2), 1-10.
10. Kalhapure, R. S.; Sikwal, D. R.; Rambharose, S.; Mocktar, C.; Singh, S.; Bester, L.; Oh, J. K.; Renukuntla, J.; Govender, T., Enhancing targeted antibiotic therapy via pH responsive solid lipid nanoparticles from an acid cleavable lipid. *Nanomed. Nanotechnol. Biol. Med* **2017**, 13(6), 2067-77.
11. Turnidge, J., Fusidic acid pharmacology, pharmacokinetics and pharmacodynamics. *Int. J. Antimicrob. Agents* **1999**, 12, S23-S34.
12. Huttner, A.; Harbarth, S., Miscellaneous Agents: Fusidic Acid, Nitrofurantoin and Fosfomycin. In *Infectious Diseases (Fourth Edition)*, Elsevier: 2017; pp 1277-1279. e1.
13. Farrell, D. J.; Mendes, R. E.; Castanheira, M.; Jones, R. N., Activity of Fusidic Acid Tested Against Staphylococci Isolated From Patients in United States Medical Centers During 2014. *Antimicrob. Agents Chemother.* **2016**, AAC. 00238-16.
14. Craft, J. C.; Moriarty, S. R.; Clark, K.; Scott, D.; Degenhardt, T. P.; Still, J. G.; Corey, G. R.; Das, A.; Fernandes, P., A Randomized, Double-Blind Phase 2 Study Comparing the Efficacy and Safety of an Oral Fusidic Acid Loading-Dose Regimen to Oral Linezolid for the Treatment of Acute Bacterial Skin and Skin Structure Infections. *Clin. Infect. Dis.* **2011**, 52 (suppl_7), S520-S526.
15. Zhang, Z.-B.; Shen, Z.-G.; Wang, J.-X.; Zhang, H.-X.; Zhao, H.; Chen, J.-F.; Yun, J., Micronization of silybin by the emulsion solvent diffusion method. *Int. J. Pharm.* **2009**, 376 (1-2), 116-122.
16. Hosey, C. M.; Chan, R.; Benet, L. Z., BDDCS Predictions, Self-Correcting Aspects of BDDCS Assignments, BDDCS Assignment Corrections, and Classification for more than 175 Additional Drugs. *AAPS. J.* **2016**, 18 (1), 251-260.
17. Hogben C.A.M. Biological Membranes and Their Passage by Drugs. Concepts in Biochemical Pharmacology. In *handbook of Experimental Pharmacology* vol 28 / 1.; Brodie B.B., Gillette J.R., Ackerman H.S. (eds); pp 1-8, Springer: Berlin, 1971; Heidelberg.
18. Merisko-Liversidge, E.; Liversidge, G. G.; Cooper, E. R., Nanosizing: a formulation approach for poorly-water-soluble compounds. *Eur. J. Pharm. Sci.* **2003**, 18 (2), 113-120.
19. Merisko-Liversidge, E. M.; Liversidge, G. G., Drug nanoparticles: formulating poorly water-soluble compounds. *Toxicol. Pathol.* **2008**, 36 (1), 43-48.
20. O'driscoll, C.; Griffin, B., Biopharmaceutical challenges associated with drugs with low aqueous solubility—the potential impact of lipid-based formulations. *Adv. Drug Del. Rev.* **2008**, 60 (6), 617-624.

21. Wishart, D. S.; Feunang, Y. D.; Guo, A. C.; Lo, E. J.; Marcu, A.; Grant, J. R.; Sajed, T.; Johnson, D.; Li, C.; Sayeeda, Z., DrugBank 5.0: a major update to the DrugBank database for 2018. *Nucleic Acids Res.* **2017**, *46* (D1), D1074-D1082.
22. Vasconcelos, T.; Sarmiento, B.; Costa, P., Solid dispersions as strategy to improve oral bioavailability of poor water soluble drugs. *Drug Discov. Today.* **2007**, *12* (23), 1068-1075.
23. Chen, H.; Khemtong, C.; Yang, X.; Chang, X.; Gao, J., Nanonization strategies for poorly water-soluble drugs. *Drug Discov. Today.* **2011**, *16* (7), 354-360.
24. Serajuddin, A. T., Salt formation to improve drug solubility. *Adv. Drug Del. Rev.* **2007**, *59* (7), 603-616.
25. Vandana, K. R.; Prasanna Raju, Y.; Harini Chowdary, V.; Sushma, M.; Vijay Kumar, N., An overview on in situ micronization technique – An emerging novel concept in advanced drug delivery. *Saudi Pharm J.* **2014**, *22* (4), 283-289.
26. Khadka, P.; Ro, J.; Kim, H.; Kim, I.; Kim, J. T.; Kim, H.; Cho, J. M.; Yun, G.; Lee, J., Pharmaceutical particle technologies: an approach to improve drug solubility, dissolution and bioavailability. *Asian J. Pharm.* **2014**, *9* (6), 304-316.
27. Qiu, Y.; Chen, Y.; Zhang, G. G.; Yu, L.; Mantri, R. V., 2nd ed.; *Developing solid oral dosage forms: Pharmaceutical Theory and Practice*; Academic press: Boston, 2016; pp 1127-1160.
28. Hamed, R.; Awadallah, A.; Sunoqrot, S.; Tarawneh, O.; Nazzal, S.; AlBaraghthi, T.; Al Sayyad, J.; Abbas, A., pH-Dependent Solubility and Dissolution Behavior of Carvedilol—Case Example of a Weakly Basic BCS Class II Drug. *AAPS PharmSciTech.* **2016**, *17* (2), 418-426.
29. Kalhapure, R. S.; Mocktar, C.; Sikwal, D. R.; Sonawane, S. J.; Kathiravan, M. K.; Skelton, A.; Govender, T., Ion pairing with linoleic acid simultaneously enhances encapsulation efficiency and antibacterial activity of vancomycin in solid lipid nanoparticles. *Colloids Surf. B. Biointerfaces.* **2014**, *117*, 303-311.
30. Omolo, C. A.; Kalhapure, R. S.; Jadhav, M.; Rambharose, S.; Mocktar, C.; Ndesendo, V. M.; Govender, T., Pegylated oleic acid: A promising amphiphilic polymer for nano-antibiotic delivery. *Eur. J. Pharm. Biopharm.* **2017**, *112*, 96-108.
31. McDonald, T. O.; Tatham, L. M.; Southworth, F. Y.; Giardiello, M.; Martin, P.; Liptrott, N. J.; Owen, A.; Rannard, S. P., High-throughput nanoprecipitation of the organic antimicrobial triclosan and enhancement of activity against Escherichia coli. *J. Mater. Chem. B.* **2013**, *1* (35), 4455-4465.
32. Verma, S.; Burgess, D., Solid Nanosuspensions: The Emerging Technology and Pharmaceutical Applications as Nanomedicine. In *Pharmaceutical Suspensions: From Formulation Development to Manufacturing*, Kulshreshtha, A. K.; Singh, O. N.; Wall, G. M., Eds. Springer: New York, 2010; pp 285-318.
33. Kalepu, S.; Nekkanti, V., Insoluble drug delivery strategies: review of recent advances and business prospects. *Acta Pharm. Sinica. B.* **2015**, *5* (5), 442-453.
34. Chu, K. R.; Lee, E.; Jeong, S. H.; Park, E.-S., Effect of particle size on the dissolution behaviors of poorly water-soluble drugs. *Arch. Pharm. Res.* **2012**, *35* (7), 1187-1195.
35. Van Eerdenbrugh, B.; Vermant, J.; Martens, J. A.; Froyen, L.; Humbeeck, J. V.; Van den Mooter, G.; Augustijns, P., Solubility Increases Associated with Crystalline Drug Nanoparticles: Methodologies and Significance. *Mol. Pharm.* **2010**, *7* (5), 1858-1870.
36. Rabinow, B. E., Nanosuspensions in drug delivery. *Nat. Rev. Drug. Discov.* **2004**, *3* (9), 785-796.
37. Ansari, M.; Althubaiti, M.; Ibnouf, M.; Anwer, M.; Ahmed, M.; Fatima, F.; Jamil, S., Enhanced anti-bacterial effects of ciprofloxacin enclosed in cyclodextrin and nano-suspension carrier systems. *Bull. Env. Pharmacol. Life Sci.* **2015**, *4* (11).

38. Parmentier, J.; Tan, E. H.; Low, A.; Möschwitzer, J. P., Downstream drug product processing of itraconazole nanosuspension: Factors influencing drug particle size and dissolution from nanosuspension-layered beads. *Int. J. Pharm.* **2017**, *524* (1), 443-453.
39. Tahara, K.; Nishikawa, M.; Matsui, K.; Hisazumi, K.; Onodera, R.; Tozuka, Y.; Takeuchi, H., In Vitro and In Vivo Characterization of Drug Nanoparticles Prepared Using PureNano™ Continuous Crystallizer to Improve the Bioavailability of Poorly Water Soluble Drugs. *Pharm. Res.* **2016**, *33* (9), 2259-2268.
40. Sikwal, D. R.; Kalhapure, R. S.; Jadhav, M.; Rambharose, S.; Mocktar, C.; Govender, T., Non-ionic self-assembling amphiphilic polyester dendrimers as new drug delivery excipients. *RSC Adv.* **2017**, *7* (23), 14233-14246.
41. Polli J.E. In vitro studies are sometimes better than conventional human pharmacokinetic in vivo studies in assessing bioequivalence of immediate-release solid oral dosage forms. *The AAPS journal*, **2008**, *1*;10(2), 289-99.
42. De Groote M.A.; Gruppo V; Woolhiser L.K; Orme I.M; Gilliland J.C.; Lenaerts A.J., Importance of confirming data on the in vivo efficacy of novel antibacterial drug regimens against various strains of Mycobacterium tuberculosis. *Antimicrob. Agents Chemother.*, **2012**, *56*(2),731-8
43. Hare J.I.; Lammers T.; Ashford M.B.; Puri S.; Storm G.; Barry ST., Challenges and strategies in anti-cancer nanomedicine development: An industry perspective. *Adv. Drug. Deliv. Rev.*, **2017** Jan 1;108:25-38
44. Borhani, D. W.; Shaw, D. E., The future of molecular dynamics simulations in drug discovery. *J. Comput.-Aided Mol. Des.* **2012**, *26* (1), 15-26.
45. Mohyeldin, S. M.; Mehanna, M. M.; Elgindy, N. A., The relevancy of controlled nanocrystallization on rifampicin characteristics and cytotoxicity. *Int J Nanomedicine.* **2016**, *11*, 2209.
46. Lee, M. K.; Kim, M. Y.; Kim, S.; Lee, J., Cryoprotectants for freeze drying of drug nanosuspensions: Effect of freezing rate. *Int J Nanomedicine.* **2009**, *98* (12), 4808-4817.
47. Agrawal, N.; Skelton, A. A., 12-Crown-4 Ether Disrupts the Patient Brain-Derived Amyloid- β -Fibril Trimer: Insight from All-Atom Molecular Dynamics Simulations. *ACS Chem. Neurosci.* **2016**, *7* (10), 1433-1441.
48. Agrawal, N.; Skelton, A. A., Binding of 12-Crown-4 with Alzheimer's A β 40 and A β 42 Monomers and Its Effect on Their Conformation: Insight from Molecular Dynamics Simulations. *Mol. Pharm.* **2018**, *15* (1), 289-299.
49. Bemporad, D.; Luttmann, C.; Essex, J. W., Behaviour of small solutes and large drugs in a lipid bilayer from computer simulations. *Biochim. Biophys. Acta.* **2005**, *1718* (1), 1-21.
50. Bemporad, D.; Luttmann, C.; Essex, J., Computer simulation of small molecule permeation across a lipid bilayer: dependence on bilayer properties and solute volume, size, and cross-sectional area. *Biophys. J.* **2004**, *87* (1), 1-13.
51. Subashini, M.; Devarajan, P. V.; Sonavane, G. S.; Doble, M., Molecular dynamics simulation of drug uptake by polymer. *J. Mol. Model.* **2011**, *17* (5), 1141-1147.
52. Gao, Y.; Olsen, K. W., Drug-polymer Interactions at Water-Crystal Interfaces and Implications for Crystallization Inhibition: Molecular Dynamics Simulations of Amphiphilic Block Copolymer Interactions with Tolazamide Crystals. *J. Pharm. Sci.* **2015**, *104* (7), 2132-2141.
53. Zunszain, P. A.; Ghuman, J.; McDonagh, A. F.; Curry, S., Crystallographic analysis of human serum albumin complexed with 4Z, 15E-bilirubin-IX α . *J. Mol. Biol.* **2008**, *381* (2), 394-406.
54. Cousins, K. R., Computer review of ChemDraw Ultra 12.0. *J. Am. Chem. Soc.* **2011**, *133* (21), 8388-8388.
55. Vanommeslaeghe, K.; Hatcher, E.; Acharya, C.; Kundu, S.; Zhong, S.; Shim, J.; Darian, E.; Guvench, O.; Lopes, P.; Vorobyov, I., CHARMM general force field: A force field for drug-like

molecules compatible with the CHARMM all-atom additive biological force fields. *J. Comput. Chem.* **2010**, *31* (4), 671-690.

56. Mark, P.; Nilsson, L., Structure and dynamics of the TIP3P, SPC, and SPC/E water models at 298 K. *J. Phys. Chem. A* **2001**, *105* (43), 9954-9960.

57. Bixon, M.; Lifson, S., Potential functions and conformations in cycloalkanes. *Tetrahedron* **1967**, *23* (2), 769-784.

58. Parrinello, M.; Rahman, A., Polymorphic transitions in single crystals: A new molecular dynamics method. *J. Appl. Phys.* **1981**, *52* (12), 7182-7190.

59. Darden, T.; York, D.; Pedersen, L., Particle mesh Ewald: An $N \cdot \log(N)$ method for Ewald sums in large systems. *J. Chem. Phys.* **1993**, *98* (12), 10089-10092.

60. Kumari, R.; Kumar, R.; Lynn, A., g_mmpbsa—A GROMACS Tool for High-Throughput MM-PBSA Calculations. *J. Chem. Inf. Model.* **2014**, *54* (7), 1951-1962.

61. Abraham, M. J.; Murtola, T.; Schulz, R.; Páll, S.; Smith, J. C.; Hess, B.; Lindahl, E., GROMACS: High performance molecular simulations through multi-level parallelism from laptops to supercomputers. *SoftwareX* **2015**, *1*, 19-25.

62. Ali, H. S. M.; York, P.; Ali, A. M. A.; Blagden, N., Hydrocortisone nanosuspensions for ophthalmic delivery: A comparative study between microfluidic nanoprecipitation and wet milling. *J. Control. Release* **2011**, *149* (2), 175-181.

63. Zhou, L.; Yang, L.; Tilton, S.; Wang, J., Development of a high throughput equilibrium solubility assay using miniaturized shake-flask method in early drug discovery. *J. Pharm. Sci.* **2007**, *96* (11), 3052-3071.

64. Curbete, M. M.; Salgado, H. R. N., Stability-indicating RP-LC method for quantification of fusidic acid in cream. *Braz. J. Pharm. Sci.* **2016**, *52* (3), 447-457.

65. Institute, C. a. L. S., Methods for Dilution Antimicrobial Susceptibility Tests for Bacteria That Grow Aerobically; *Approved Standard 9th ed*, C. a. L. S., Ed. CLSI: Pennsylvania 19087, USA, 2012; Vol. 32, p 63.

66. European Committee for Antimicrobial Susceptibility Testing of the European Society of Clinical, M.; Infectious, D., Determination of minimum inhibitory concentrations (MICs) of antibacterial agents by broth dilution. *Clin. Microbiol. Infect.* **2003**, *9* (8), ix-xv.

67. O'Brien-Simpson, N. M.; Pantarat, N.; Attard, T. J.; Walsh, K. A.; Reynolds, E. C., A Rapid and Quantitative flow cytometry method for the analysis of membrane disruptive antimicrobial activity. *Plos One.* **2016**, *11* (3), e0151694.

68. Rügner, M.; Bensch, G.; Tüngler, R.; Reichl, U., A flow cytometric method for viability assessment of *Staphylococcus aureus* and *Burkholderia cepacia* in mixed culture. *Cytometry A* **2012**, *81* (12), 1055-1066.

69. Bexfield, A.; Bond, A. E.; Roberts, E. C.; Dudley, E.; Nigam, Y.; Thomas, S.; Newton, R. P.; Ratcliffe, N. A., The antibacterial activity against MRSA strains and other bacteria of a < 500Da fraction from maggot excretions/secretions of *Lucilia sericata* (Diptera: Calliphoridae). *Microb. Infect.* **2008**, *10* (4), 325-333.

70. Shrestha, N. K.; Scalera, N. M.; Wilson, D. A.; Procop, G. W., Rapid differentiation of methicillin-resistant and methicillin-susceptible *Staphylococcus aureus* by flow cytometry after brief antibiotic exposure. *J. Clin. Microbiol.* **2011**, *49* (6), 2116-2120.

71. Arndt-Jovin, D. J.; Jovin, T. M., Fluorescence labeling and microscopy of DNA. *Methods Cell Biol.* **1989**, *30*, 417-448.

72. Renggli, S.; Keck, W.; Jenal, U.; Ritz, D., Role of autofluorescence in flow cytometric analysis of *Escherichia coli* treated with bactericidal antibiotics. *J. Bacteriol.* **2013**, *195* (18), 4067-4073.

73. Kugelberg, E.; Norström, T.; Petersen, T. K.; Duvold, T.; Andersson, D. I.; Hughes, D., Establishment of a superficial skin infection model in mice by using *Staphylococcus aureus* and *Streptococcus pyogenes*. *Antimicrob. Agents Chemother.* **2005**, *49* (8), 3435-3441.
74. Vingsbo Lundberg, C.; Frimodt-Møller, N., Efficacy of topical and systemic antibiotic treatment of methicillin-resistant *Staphylococcus aureus* in a murine superficial skin wound infection model. *Int. J. Antimicrob. Agents* **2013**, *42* (3), 272-275.
75. Fall, A.; Bertrand, F.; Ovarlez, G.; Bonn, D., Shear thickening of cornstarch suspensions. *J. Rheol.* **2012**, *56* (3), 575-591.
76. Riekens, M. K.; Kuminek, G.; Rauber, G. S.; de Campos, C. E. M.; Bortoluzzi, A. J.; Stulzer, H. K., HPMC as a potential enhancer of nimodipine biopharmaceutical properties via ball-milled solid dispersions. *Carbohydr. Polym.* **2014**, *99*, 474-482.
77. Novo, D. J.; Perlmutter, N. G.; Hunt, R. H.; Shapiro, H. M., Multiparameter Flow Cytometric Analysis of Antibiotic Effects on Membrane Potential, Membrane Permeability, and Bacterial Counts of *Staphylococcus aureus* and *Micrococcus luteus*. *Antimicrob. Agents Chemother.* **2000**, *44* (4), 827-834.
78. Tuomela, A.; Hirvonen, J.; Peltonen, L., Stabilizing Agents for Drug Nanocrystals: Effect on Bioavailability. *Pharmaceutics* **2016**, *8* (2), 16.
79. Sharma, N.; Madan, P.; Lin, S., Effect of process and formulation variables on the preparation of parenteral paclitaxel-loaded biodegradable polymeric nanoparticles: A co-surfactant study. *Asian J. Pharm.* **2016**, *11* (3), 404-416.
80. Zweers, M. L.; Grijpma, D. W.; Engbers, G. H.; Feijen, J., The preparation of monodisperse biodegradable polyester nanoparticles with a controlled size. *J. Biomed. Mater. Res. B Appl. Biomater.* **2003**, *66* (2), 559-566.
81. LaGrow, A. P.; Ingham, B.; Toney, M. F.; Tilley, R. D., Effect of Surfactant Concentration and Aggregation on the Growth Kinetics of Nickel Nanoparticles. *J. Phys. Chem. C* **2013**, *117* (32), 16709-16718.
82. Pina, C.; Fernández-Díaz, L.; Prieto, M.; Veintemillas-Verdaguer, S., Metastability in drowning-out crystallisation: precipitation of highly soluble sulphates. *J. Cryst. Growth* **2001**, *222* (1), 317-327.
83. Van Eerdenbrugh, B.; Van den Mooter, G.; Augustijns, P., Top-down production of drug nanocrystals: Nanosuspension stabilization, miniaturization and transformation into solid products. *Int. J. Pharm.* **2008**, *364* (1), 64-75.
84. Yoon, T. J.; Son, W.-S.; Park, H. J.; Seo, B.; Kim, T.; Lee, Y.-W., Tetracycline nanoparticles precipitation using supercritical and liquid CO₂ as antisolvents. *J. Supercrit. Fluids* **2016**, *107*, 51-60.
85. Panagiotou, T.; Mesite, S. V.; Fisher, R. J., Production of Norfloxacin Nanosuspensions Using Microfluidics Reaction Technology through Solvent/Antisolvent Crystallization. *Ind. Eng. Chem. Res.* **2009**, *48* (4), 1761-1771.
86. Reverchon, E.; Della Porta, G., Production of antibiotic micro- and nano-particles by supercritical antisolvent precipitation. *Powder Technol.* **1999**, *106* (1), 23-29.
87. Xia, D.; Quan, P.; Piao, H.; Piao, H.; Sun, S.; Yin, Y.; Cui, F., Preparation of stable nitrendipine nanosuspensions using the precipitation-ultrasonication method for enhancement of dissolution and oral bioavailability. *Eur. J. Pharm. Sci.* **2010**, *40* (4), 325-334.
88. Cherry, R. S.; Kwon, K.-Y., Transient shear stresses on a suspension cell in turbulence. *Biotechnol. Bioeng.* **1990**, *36* (6), 563-571.
89. Yang, D.; Ye, S.; Ge, J., Solvent Wrapped Metastable Colloidal Crystals: Highly Mutable Colloidal Assemblies Sensitive to Weak External Disturbance. *J. Am. Chem. Soc.* **2013**, *135* (49), 18370-18376.

90. Liu, Y., Is the Free Energy Change of Adsorption Correctly Calculated? *J. Chem. Eng. Data* **2009**, *54* (7), 1981-1985.
91. Deng, Y.; Roux, B., Computations of Standard Binding Free Energies with Molecular Dynamics Simulations. *J. Phys. Chem. B* **2009**, *113* (8), 2234-2246.
92. Torchilin, V. P., Structure and design of polymeric surfactant-based drug delivery systems. *J. Control. Release* **2001**, *73* (2), 137-172.
93. Nakashima, K.; Bahadur, P., Aggregation of water-soluble block copolymers in aqueous solutions: Recent trends. *Adv. Colloid Interface Sci.* **2006**, *123-126*, 75-96.
94. Liu, J.; Zou, M.; Piao, H.; Liu, Y.; Tang, B.; Gao, Y.; Ma, N.; Cheng, G., Characterization and Pharmacokinetic Study of Aprepitant Solid Dispersions with Soluplus®. *Molecules* **2015**, *20* (6), 11345.
95. Zhang, K.; Yu, H.; Luo, Q.; Yang, S.; Lin, X.; Zhang, Y.; Tian, B.; Tang, X., Increased dissolution and oral absorption of itraconazole/Soluplus extrudate compared with itraconazole nanosuspension. *Eur. J. Pharm. Biopharm.* **2013**, *85* (3), 1285-1292.
96. Raval, A. J.; Patel, M. M., Preparation and characterization of nanoparticles for solubility and dissolution rate enhancement of meloxicam. *Intl Res J Pharm* **2011**, *1* (2), 42-49.
97. Sarkari, M.; Brown, J.; Chen, X.; Swinnea, S.; Williams, R. O.; Johnston, K. P., Enhanced drug dissolution using evaporative precipitation into aqueous solution. *Int. J. Pharm.* **2002**, *243* (1), 17-31.
98. Gao, L.; Liu, G.; Wang, X.; Liu, F.; Xu, Y.; Ma, J., Preparation of a chemically stable quercetin formulation using nanosuspension technology. *Int. J. Pharm.* **2011**, *404* (1), 231-237.
99. Hogg, R.; Healy, T. W.; Fuerstenau, D. W., Mutual coagulation of colloidal dispersions. *Trans. Faraday Society* **1966**, *62*, 1638-1651.
100. Krieger, I. M.; Dougherty, T. J., A mechanism for non-Newtonian flow in suspensions of rigid spheres. *Trans. Soc. Rheol.* **1959**, *3* (1), 137-152.
101. Ree, F.; Ree, T.; Eyring, H., Relaxation Theory of Transport Problems in Condensed Systems. *Ind. Eng. Chem.* **1958**, *50* (7), 1036-1040.
102. Rudyak, V. Y.; Belkin, A. A.; Egorov, V. V., On the effective viscosity of nanosuspensions. *Tech. Phys.* **2009**, *54* (8), 1102-1109.
103. Sun, J.; Wang, F.; Sui, Y.; She, Z.; Zhai, W.; Wang, C.; Deng, Y., Effect of particle size on solubility, dissolution rate, and oral bioavailability: evaluation using coenzyme Q(10) as naked nanocrystals. *Int. J. Nanomedicine.* **2012**, *7*, 5733-5744.
104. Wais, U.; Jackson, A. W.; He, T.; Zhang, H., Nanoformulation and encapsulation approaches for poorly water-soluble drug nanoparticles. *Nanoscale* **2016**, *8* (4), 1746-1769.
105. Jindřich, L.; David, S., Enhanced solubility of nanostructured paracetamol. *Biomed. Phys. Eng. Express* **2016**, *2* (5), 055007.
106. Mhraryan, A.; Strømme, M., Solubility of fractal nanoparticles. *Surf Sci.* **2007**, *601* (2), 315-319.
107. Pierre, L.; Alain, M.; Mireille, T., Solubility of nanoparticles: nonextensive thermodynamics approach. *J. Phys.: Condens. Matter* **2007**, *19* (43), 436229.
108. Riss, T. L.; Moravec, R. A.; Niles, A. L.; Duellman, S.; Benink, H. A.; Worzella, T. J.; Minor, L.; *Cell viability assays*. NIH, Bethesda (MD), 2016, pp. 1-34.
109. G Moloughney, J.; Weisleder, N., Poloxamer 188 (p188) as a membrane resealing reagent in biomedical applications. *Pat. Biotechnol.* **2012**, *6* (3), 200-211.

110. Guo, J.-j.; Yue, P.-F.; Lv, J.-l.; Han, J.; Fu, S.-s.; Jin, S.-x.; Jin, S.-y.; Yuan, H.-L., Development and in vivo/in vitro evaluation of novel herpentrione nanosuspension. *Int. J. Pharm.* **2013**, *441* (1), 227-233.
111. Ambhore, N. P.; Dandagi, P. M.; Gadad, A. P., Formulation and comparative evaluation of HPMC and water soluble chitosan-based sparfloxacin nanosuspension for ophthalmic delivery. *Drug Deliv Transl Res.* **2016**, *6* (1), 48-56.
112. Rabinow, B.; Kipp, J.; Papadopoulos, P.; Wong, J.; Glosson, J.; Gass, J.; Sun, C.-S.; Wielgos, T.; White, R.; Cook, C., Itraconazole IV nanosuspension enhances efficacy through altered pharmacokinetics in the rat. *Int. J. Pharm.* **2007**, *339* (1), 251-260.
113. Bhawana; Basniwal, R. K.; Buttar, H. S.; Jain, V. K.; Jain, N., Curcumin Nanoparticles: Preparation, Characterization, and Antimicrobial Study. *J. Agric. Food Chem.* **2011**, *59* (5), 2056-2061.
114. Chen, Y.; Lan, T.; Duan, L.; Wang, F.; Zhao, B.; Zhang, S.; Wei, W., Adsorptive Removal and Adsorption Kinetics of Fluoroquinolone by Nano-Hydroxyapatite. *Plos One* **2015**, *10* (12), e0145025.
115. Wang, L.; Hu, C.; Shao, L., The antimicrobial activity of nanoparticles: present situation and prospects for the future. *Int J Nanomedicine.* **2017**, *12*, 1227-1249.
116. Dobie, D.; Gray, J., Fusidic acid resistance in Staphylococcus aureus. *Arch. Dis. Child.* **2004**, *89* (1), 74-77.
117. Christiansen, K., Fusidic acid adverse drug reactions. *Int. J. Antimicrob. Agents.*, **1999**, *12*, S3-S9.
118. Chaplin, D. D., Overview of the Immune Response. *J. Allergy Clin. Immunol.* **2010**, *125* (2 Suppl 2), S3-23.

CHAPTER 6, CO-AUTHORED PAPERS

6.1 Introduction

In addition to the first authored experimental papers in Chapters, 3, 4 and 5 focusing on the aims 1, 2 and 3. I have also been involved in other research projects within our group as a team member. These projects also focused on the broad aim of novel nanobased strategies to effectively treat bacterial infections, these papers have been included in the thesis. This chapter therefore includes two co-authored experimental papers and one review article published in ISI international journals: International Journal of Pharmaceutics (Impact Factor = 3.902), Journal of Biomolecular Structure & Dynamics (Impact Factor = 3.107) and Journal of Drug Delivery Science and Technology (Impact Factor = 2.297).

6.2 Published co-authored paper 1

Synthesis of an oleic acid-based pH-responsive lipid and its application in nanodelivery of vancomycin

Mhule D., Kalhapure, R. S., Jadhav, M., Omolo, C. A., Rambharose, S., Waddad, A. Y., Mocktar, C., & Govender, T. (2018). *International Journal of Pharmaceutics*, 550(1-2), 149-159. (appendix X)

6.2.1 Abstract

Stimuli-responsive nano-drug delivery systems can optimize antibiotic delivery to infection sites. Identifying novel lipids for pH responsive delivery to acidic conditions of infection sites will enhance the performance of nano-drug delivery systems. The aim of the present investigation was to synthesize and characterize a biosafe novel pH-responsive lipid for vancomycin delivery to acidic conditions of infection sites. A pH-responsive solid lipid, N-(2-morpholinoethyl) oleamide (NMEO) was synthesized and used to prepare vancomycin (VCM)-loaded solid lipid nanoparticles (VCM_NMEO SLNs). The particle size (PS), polydispersity index (PDI), zeta potential (ZP) and entrapment efficiency (EE) of the formulation were 302.8 ± 0.12 nm, 0.23 ± 0.03 , -6.27 ± 0.017 mV and $81.18 \pm 0.57\%$ respectively. The study revealed that drug release and antibacterial activity were significantly greater at pH 6.0 than at pH 7.4, while the *in silico* studies exposed the molecular mechanisms for improved stability and drug release. Moreover, the reduction of MRSA load was 4.14 times greater ($p < 0.05$) in the skin of VCM_NMEO SLNs treated mice than that of bare VCM treated specimens. Thus, this study confirmed that NMEO can successfully be used to formulate pH-responsive SLNs with potential to enhance the treatment of bacterial infections.

6.3 Published co-authored paper 2

Antimicrobial cell penetrating peptides with bacterial cell specificity: pharmacophore modelling, quantitative structure activity relationship and molecular dynamics simulation

Mbuso F., Kalhapure, R. S., Agrawal, N., Dhumal D., Omolo C.A., Akamanchi K.G., and Govender T. (2018), *Journal of Biomolecular Structure & Dynamics*,1-31 (Just accepted), DOI:10.1080/07391102.2018.1484814 (Impact factor 3.107). (appendix XI)

6.3.1 Abstract

Current research has shown cell-penetrating peptides and antimicrobial peptides (AMPs) as probable vectors for use in drug delivery and as novel antibiotics. It has been reported that the higher the therapeutic index (TI) the higher would be the bacterial cell penetrating ability. To the best of our knowledge, no in-silico study has been performed to determine bacterial cell specificity of the antimicrobial cell penetrating peptides (aCPP's) based on their TI. The aim of this study was to develop a quantitative structure activity relationship (QSAR) model, which can estimate antimicrobial potential and cell-penetrating ability of aCPPs against *S. aureus*, to confirm the relationship between the TI and aCPPs and to identify specific descriptors responsible for aCPPs penetrating ability. Molecular dynamics (MD) simulation was also performed to confirm the membrane insertion of the most active aCPPs obtained from the QSAR study. The most appropriate pharmacophore was identified to predict the aCPP's activity. The statistical results confirmed the validity of the model. The QSAR model was successful in identifying the optimal aCPP with high activity prediction and provided insights into the structural requirements to correlate their TI to cell penetrating ability. MD simulation of the best aCPP with 1-palmitoyl-2-oleoyl-sn-glycero-3-phosphocholine (POPC) bilayer confirmed its interaction with the membrane and the C-terminal residues of the aCPP played a key role in membrane penetration. The strategy of combining QSAR and molecular dynamics, allowed for optimal estimation of ligand-target interaction and confirmed the importance of Trp and Lys in interacting with the POPC bilayer.

6.4 Published co-authored paper 3

Conjugates and nano-delivery of antimicrobial peptides for enhancing therapeutic activity.

Faya, M., Kalhapure, R. S., Kumalo, H. M., Waddad, A. Y., Omolo, C., & Govender, T. (2017). *Journal of Drug Delivery Science and Technology*, 44, 153-171. (Impact factor 2.297 (appendix XII))

6.4.1 Abstract

The current global crisis of antibiotic drug resistance is driving the search for novel treatment approaches. Antimicrobial peptides (AMPs) are small molecular weight proteins with varying number of amino acids found in both eukaryotes and prokaryotes. They have recently been targeted as novel antimicrobial agents with the potential to treat multiple-drug resistant infections. Their conjugation with various classes of materials such as antibiotics, polymers, DNA, salts, phenolic derivatives and their delivery via nano carrier systems are strategies being used to enhance their therapeutic efficacy. An update and understanding of their applicability as conjugates and nano delivery are essential to optimise their development and activity. This review focuses on computational studies depicting their permeation through model membranes and identification of physicochemical descriptors for activity. It also highlights the potential of AMPs and their conjugates and encapsulation into nano delivery systems for improving activity. Further, research to realise their potential as conjugates and delivery via nano carrier systems are also identified. To our knowledge, this current review presents the first account that comprehensively highlights AMPs targeting various microorganisms, and their conjugation to different compounds to showcase the potential for nano delivery alone or in their respective conjugates for enhanced activity.

CHAPTER 7, CONCLUSION

7.1 General conclusions

Nanotechnology derived formulation development approaches are showing great potential to improve the efficacy of existing antibiotics. The current global crisis of bacterial resistance demands new materials to develop novel drug delivery systems that alter the physical chemical properties of drugs that can counteract antibacterial resistance and improve efficiency of drugs. The broad aim of this study was to design and synthesize advanced materials, formulate nano-based strategies and explore their potential for enhancing antibacterial activity and targeting infection sites. The specific research aims of this study were therefore: (1) explore the potential of delivering antimicrobials via nanovesicles formulated from the modification of generation one Poly ester amine dendrimer (G1-PEA) with a diblock copolymer of methoxy poly (ethylene glycol)-b-poly(ϵ -caprolactone) (mPEG-b-PCL) to yield linear block copolymer dendrimer hybrid 3 arm star polymer (3-mPEA), (2) to synthesize novel fatty acid quaternary lipid and employ it in formulation of liposomes with “On and Off” pH responsive switches for infection site-specific delivery of antibiotics, and (3) to prepare a nanosuspension (FA-NS) of FA to simultaneously enhance its aqueous solubility and antibacterial activity against *S. aureus* and MRSA.

The main conclusions generated from the research data are summarised below:

Aim 1:

- A novel linear polymer dendrimer hybrid star polymer (3-mPEA) was successfully synthesized, and FT-IR, ^1H NMR and ^{13}C NMR, HRMS, gel permeation chromatography and MALDI-TOF analyses confirmed the successful synthesis and structure of 3-mPEA.
- Cytotoxicity studies were performed using an MTT assay on four mammalian cell lines i.e. human breast adenocarcinoma (MCF 7), adenocarcinoma alveolar basal epithelial cells (A 549), liver hepatocellular carcinoma (HepG 2) cell-lines and human embryonic kidney cells 293 (HEK 293), which revealed the linear polymer dendrimer hybrid star polymer to be non-cytotoxic.
- 3-mPEA was employed to formulate vancomycin loaded nanovesicles., which exhibited size PI and ZP of 52.48 ± 2.6 nm, 0.103 ± 0.047 , -7.3 ± 1.3 mV respectively, with the encapsulation efficiency being $76.49 \pm 2.4\%$. The VCM release from the drug loaded nanovesicles was found to be sustained, with a 65.8 % release over a period of 48 h.

- The *in vitro* antibacterial test revealed that the drug loaded nanovesicles had 8- and 16-fold lower minimum effective concentration (MIC) against *S. aureus* strains and MRSA compared to the free drug. The flow cytometry study showed 3.9-fold more dead cells of MRSA in the population when samples were treated with the drug loaded nanovesicles than the bare VCM at a concentration of 0.488 $\mu\text{g/mL}$ of the drug. An *in vivo* skin infection mouse model showed a 20-fold reduction in the MRSA load in the drug loaded nanovesicles treated groups as compared to bare VCM.
- The MD simulations showed spontaneous self-aggregation of 3-mPEA, with interaction energy between the two monomers being -146.07 ± 4.92 kJ/mol, and Van der Waals interactions playing a major role for the aggregates' stability. The *in silico* experiments explained the stability of the nanovesicles and the arrangement of 3-mPEA that led to the formation of unique ultra-small vesicles.
- Human serum albumin (HSA) binding studies with Microscale Thermophoresis (MST) showed that the 3-mPEA did not have any binding affinity to the HSA when compared to the control, which showed its potential for long systemic circulation properties.

Aim 2:

- A novel quaternary fatty acid-based lipid (QL) was synthesized and FT-IR, ^1H NMR, ^{13}C NMR and HRMS analyses, confirmed the successful synthesis and structure of the lipid.
- Cytotoxicity studies performed using an MTT assay on three mammalian cell lines HELA, A549 and HEK-293 revealed that QL was a biosafe lipid.
- QL lipid was employed in the formulation of liposome with pH responsive “On and Off” switches. The formulated VCM loaded liposomes were found to have size, PDI and ZP of 98.88 ± 01.92 , 0.204 ± 0.030 and -17.33 ± 2.95 at pH 7.4 respectively. The QL-liposomes had a negative ZP at pH 7.4 that shifted to positive charge accompanied by breakdown of the system at acidic pH. The encapsulation efficiency was found to be 43.06 ± 5.86 %. The *in vitro* VCM release of the liposome was faster at acidic pH than at the physiological pH.
- The *in vitro* antibacterial studies against Methicillin susceptible *Staphylococcus aureus* (MSSA) and MRSA showed lower MICs and extended activity over 72 h for all the formulations compared to the bare VCM, which showed no activity after 24 hrs. The liposome had 4-fold lower MIC at pH 7.4 and 8- and 16-fold at pH 6.0 against both MSSA

and MRSA when compared to the bare drug. Flow cytometry studies indicated that the QL-liposomes had similar killing percentage of MRSA cells compared to the bare VCM, despite them having a 4-fold lower MIC in comparison to the bare drug. *In vivo* studies showed that the amount of MRSA recovered from mice treated with formulations was approximately 189.67 and 6.33-fold lower than the untreated and bare VCM treated mice respectively.

- MD simulation of QL lipid and the POPC membrane showed that the lipid spontaneously bonded to the bilayer membrane, with both electrostatic and Van der Waals interactions playing a major role for the binding.
- The efficacy of the OA-QL liposome in clearing the intracellular MRSA was determined by infecting the macrophages (TPH-1) and Human embryonic kidney cells (HEK-293). The OA-QL liposomes showed 567 and 60- fold reduction of intracellular bacteria when compared to bare VCM respectively.

Aim 3:

- Fusidic acid nanosuspension (FA-NS) with particle size, PI and ZP of 265 ± 2.25 nm, 0.158 ± 0.026 and -16.9 ± 0.794 respectively was successfully formulated from Poloxamer 188(P188) after screening different surfactant available in the market.
- Further characterisation of FA-NS by DSC, XRD and FT-IR showed that during formulation, no new chemical compound was formed and that the FA was converted into amorphous form in the suspension.
- FA-NS successfully increased the water solubility of FA by a 7-fold when compared to the bare drug.
- *In vitro* antibacterial activity revealed there was a 16- and 18-fold enhancement in activity of the FA-NS against *S. aureus* and MRSA respectively compared to the bare FA. A flow cytometry study showed that the MRSA cells treated with FA-NS had almost twice the percentage population of dead bacteria, despite having an 8-fold lower MIC compared to bare FA. The *in vivo* skin infected mice showed a 142- and a 76-fold reduction in the MRSA load in skin treated with FA-NS when compared to that of the untreated and bare FA respectively.
- Molecular dynamics (MD) simulation showed spontaneous binding between FA and P188, with the free binding and interaction energy between them being -74.42 kJ/mol and -49.764

± 1.298 kJ/mol, respectively, with the Van der Waal's interactions playing a major role in the spontaneous binding.

The findings of this study therefore confirmed that the newly synthesized material as biosafe for biomedical application and their potential to develop novel drug delivery systems, which enhanced the activity of the antibiotics against the MSSA and MRSA. Furthermore, the studies also converted FA into a novel nanosuspension. The nanobased systems reported in this study include: V-3-mPEA, OA-OA-QL lipo and FA-NS as approaches to treat susceptible and resistant *S. aureus* infections. The studies presented in Chapter 6 as a co-author on other publications by the group also confirmed the potential of pH responsive solid lipid nanoparticles loaded for efficient treatment of bacterial infections and designing antimicrobial cell penetrating peptides for bacterial membrane specificity.

7.2 Significance of the findings in the study

The newly synthesized material and designed Nano formulations V-3-mPEA, vancomycin loaded OA-OA-QL lipo and FA-NS were successfully employed to address the limitations associated with conventional dosage forms of antibiotics and antibacterial resistance. The significance of the findings in this study include the following:

New pharmaceutical products: The novel materials 3-mPEA and QL lipid were synthesized.

This will widen the pool of available pharmaceutical excipient for preparing new medicines.

This study also introduced three pharmaceutical products V-3-mPEA, OA-OA-QL lipo, and FA-NS. This can stimulate local pharmaceutical industries to manufacture cost-effective superior medicines.

Improved patient therapy and disease treatment: The newly designed V-3-mPEA, OA-OA-QL lipo and FA-NS, nano systems were formulated successfully with improved antibacterial potential against *S. aureus* and MRSA. The novel systems lowered the MIC of the loaded drugs significantly. This could lead to lowering the treatment doses and dosages without affecting therapeutic outcomes. These findings therefore prove the potential of these systems in improving patient therapy and treatment of bacterial infections, and thereby ultimately improving the quality of life as well as saving lives.

Creation of new knowledge to the scientific community: The various studies and their findings have contributed to the pharmaceutical sciences knowledge database in several ways. These include the following:

- New knowledge in the synthesis, characterisation and determination of the toxicity profile of the hybrid star polymer and QL lipid was generated. The properties of the drug loaded 3-mPEA nanovesicles, drug delivery systems were generated using various *in vitro*, *in silico* and *in vivo* techniques.
- Atomistic mechanism of interaction, and the process of spontaneous binding between the fusidic acid and the surfactant P188, was successfully identified. The effect of pH on the switches inserted in the liposome, the binding of the OA-QL liposome on the model bacterial membrane, and the self-assembly of 3-mPEA in water was also identified via MD simulations.
- Formulation parameters and processes of 3-mPEA nanovesicles, OA-QL liposome and FANS were identified using various experimental techniques.
- The in-depth antimicrobial testing from MIC determination, flow cytometry and *in vivo* antibacterial infection models successfully showed the *in vitro* and *in vivo* correlation of the 3-mPEA nanovesicles, OA-QL liposome and the FA-NS nano drug delivery systems.

Stimulation of new research: The research findings of the various studies and the successful development of V-3-mPEA, OA-QL lipo and FA-NS can stimulate new research areas, including the following:

- The newly synthesized 3-mPEA and QL can be utilized for delivering other classes of drugs to treat various disease conditions, such as cardiovascular diseases, HIV/AIDS, pain treatments (central nervous system related conditions), gene therapy related diseases, metabolic diseases etc.
- The successful formulation and *in vitro* and *in vivo* characterisation of the reported nano-drug delivery systems in this study could stimulate research into the formulation of other nano-drug delivery system for other classes of drugs to treat other diseases.
- The newly designed FA-NS, due to its ability to enhance the solubility of FA, could lead to the application of this strategy to stimulate research to develop nanosuspensions in other BCS class II drugs.
- The successful elimination of intracellular MRSA with the novel OA-QL lipo demonstrated the potential of applying pH responsive liposomes to eliminate intracellular bacteria and can stimulate research in the synthesis of other classes of pH

responsive lipids and novel drug delivery systems to treat bacteria that hide inside the cells, thereby acting as reservoirs and a source of resistance strains.

7.3 Recommendations for future studies

Although these approaches have demonstrated the potential of V-3-mPEA, FA-NS and OA-QL lipo as novel nano-drug delivery systems to eradicate the problem of bacterial resistance, additional studies are necessary to improve their formulations to ensure eventual regulatory approval for patient use.

The following studies are proposed:

- In the case of V-3-mPEA, there is a need for coarse grain MD simulations to build a system that can completely self-assemble into drug loaded nano-vesicles and to simulate the release of drug from the system.
- The qualitative analysis of the bacterial cell protein degradation performed using SDS-PAGE technique to understand the mechanism of antibacterial action of V-3-mPEA and OA-OA-QL lipo can be upgraded with a quantitative determination of a specific protein using techniques, such as western blot or dot blot analysis.
- The successfully developed nano-vesicles system for vancomycin delivery can be loaded with different classes of antibiotics and tested against various bacteria to evaluate its advantages over different antibiotics.
- In the case of the FA-Ns study, the next phase would be to formulate other BCS class II drugs using this simple technique, as well as surfactants in the market to further enhance their activity and water solubility.
- Long-term stability studies using ICH conditions to assess the physical and chemical stability of optimised formulations must be undertaken to confirm their shelf life.
- *In vivo* IV infection model, bioavailability and pharmacokinetic studies followed by clinical trials on both the developed nano-systems could be performed in order to achieve approval for market introduction.
- *In vivo* acute, intermediate and long-term toxicity studies models can be performed to determine the full toxicological profile of the material and the formulations reported in this study.

- A method for the bulk production of the nano-systems presented in this study could be developed in order to enable their applications for pharmaceutical industries.

7.4 Conclusion

The findings of this study therefore confirm the potential of the various newly developed nano-based approaches studied for improving the treatment of susceptible and resistant bacterial infections. This study has made a significant contribution to the field of drug delivery in addressing problems associated with current antibiotic therapy. The ultimate realisation of nano-technology to address the current global antibiotic drug therapy crisis will be dependent on future intensive and multidisciplinary research. This strategic approach will play a pivotal role towards improving globally the treatment of diseases associated with bacterial infections, thereby saving lives and improving the quality of lives of communities.

APPENDIXES



Northeastern

09/12/18

To whom it may concern

This letter is to confirm that the contribution entitled AMPHIPHILIC DENDRIMERS FOR DRUG DELIVERY by Calvin A. Omolo, Rahul S. Kalhapure, Dhiraj R. Sikwal, and Thirumala Govender has been accepted by me as the Editor for the inclusion into the Handbook of Materials for Nanomedicine and will now be forwarded to the Publisher (Pan Stanford Publications), who will make the final decision on book production.

Vladimir P. Torchilin
Ph.D., D.Sc.

University Distinguished
Professor,
Director, Center for
Pharmaceutical
Biotechnology and
Nanomedicine

*Bouve College
of Health Sciences
School of Pharmacy
Department of
Pharmaceutical Sciences*

*140 The Fenway
Room 214
360 Huntington Ave.
Boston, MA 02115*

*617-373-3206
F 617-373-7509*

v.torchilin@northeastern.edu

Sincerely,

A handwritten signature in blue ink, appearing to read "V. Torchilin".

Vladimir Torchilin, PhD, DSc
Volume Editor



Contents lists available at ScienceDirect

Journal of Controlled Release

journal homepage: www.elsevier.com/locate/jconrel

A hybrid of mPEG-*b*-PCL and G1-PEA dendrimer for enhancing delivery of antibiotics



Calvin A. Omolo^a, Rahul S. Kalhapure^{a,b}, Nikhil Agrawal^a, Mahantesh Jadhav^a, Sanjeev Rambharose^{a,c}, Chunderika Mocktar^a, Thirumala Govender^{a,*}

^a Discipline of Pharmaceutical Sciences, College of Health Sciences, University of KwaZulu-Natal, Private Bag X54001, Durban, South Africa

^b School of Pharmacy, The University of Texas at El Paso, 500 W University Ave, El Paso, TX 79968, USA

^c Division of Emergency Medicine, Department of Surgery, University of Cape Town, Cape Town, South Africa

ARTICLE INFO

Keywords:

Resistance
MRSA
Linear polymer dendrimer star polymer
Biosafe
Vancomycin
Nanovesicles
Antibacterial

ABSTRACT

The development of novel materials is essential for the efficient delivery of drugs. Therefore, the aim of the study was to synthesize a linear polymer dendrimer hybrid star polymer (3-mPEA) comprising of a generation one poly (ester-amine) dendrimer (G1-PEA) and a diblock copolymer of methoxy poly (ethylene glycol)-*b*-poly(ϵ -caprolactone) (mPEG-*b*-PCL) for formulation of nanovesicles for efficient drug delivery. The synthesized star polymer was characterized by FTIR, ¹H and ¹³C NMR, HRMS, GPC and its biosafety was confirmed by MTT assays. Thereafter it was evaluated as a nanovesicle forming polymer. Vancomycin loaded nanovesicles were characterized using *in vitro*, molecular dynamics (MD) simulations and *in vivo* techniques. MTT assays confirmed the nontoxic nature of the synthesized polymer, the cell viability was 77.23 to 118.6%. The nanovesicles were prepared with size, polydispersity index and zeta potential of 52.48 ± 2.6 nm, 0.103 ± 0.047 , -7.3 ± 1.3 mV respectively, with the encapsulation efficiency being $76.49 \pm 2.4\%$. MD simulations showed spontaneous self-aggregation of the dendritic star polymer and the interaction energy between the two monomers was -146.07 ± 4.92 , Van der Waals interactions playing major role for the aggregates stability. Human serum albumin (HSA) binding studies with Microscale Thermophoresis (MST) showed that the 3-mPEA did not have any binding affinity to the HSA, which showed potential for long systemic circulation. The vancomycin (VCM) release from the drug loaded nanovesicles was found to be slower than bare VCM, with an 65.8% release over a period of 48 h. The *in vitro* antibacterial test revealed that the drug loaded nanovesicles had 8- and 16-fold lower minimum inhibitory concentration (MIC) against methicillin sensitive *Staphylococcus aureus* and methicillin-resistant *S. aureus* strains (MRSA) compared to free drug. The flow cytometry study showed 3.9-fold more dead cells of MRSA in the population when samples were treated with the drug loaded nanovesicles than the bare VCM at concentration 0.488 μ g/mL. An *in vivo* skin infection mice model showed a 20-fold reduction in the MRSA load in the drug loaded nanovesicles treated groups compared to bare VCM. These findings confirmed the potential of 3-mPEA as a promising biocompatible effective nanocarrier for antibiotic delivery.

1. Introduction

Since the discovery of penicillin by Sir Alexander Fleming in 1928, many lives have been saved by antibiotics [1]. However, in the last decade, the world has witnessed a dramatic upsurge in the number of bacterial pathogens that are resistant to multiple antibacterial agents [2,3], coupled with the drying up of the antibiotic pipeline [4–6], with major pharmaceutical companies leaving the antibiotic development field [2]. One of the bacteria that causes significant health care challenges is *Staphylococcus aureus* (SA) and its resistant strain, known as methicillin-resistant *Staphylococcus aureus* (MRSA), which is insensitive

to a wide range of antibiotics [7]. Recent findings indicate that of the 385 MRSA isolates, 36 (9.35%) are resistant to the routinely used antibiotics [8]. The World Health Organization recognizes that the dearth of new and novel antibiotics, particularly those with new modes of action, as well as the need to identify innovative strategies to enhance, protect and potentiate those available in the market to avert returning to a pre-antibiotic era [9–12].

Antimicrobial resistance is a complex and a multifaceted problem. Some of the contributors to antibiotic resistance are sub-lethal concentrations of the antibiotics at the infection site, low patients' compliance due to high frequency of administration and side or adverse

* Corresponding author.

E-mail addresses: rkalhapure@utep.edu (R.S. Kalhapure), govenderth@ukzn.ac.za (T. Govender).

<https://doi.org/10.1016/j.jconrel.2018.10.005>

Received 30 May 2018; Received in revised form 17 September 2018; Accepted 6 October 2018

Available online 10 October 2018

0168-3659/© 2018 Elsevier B.V. All rights reserved.

effects; some of which are dose dependent which leads to development of resistant strains in the population [13]. In addition to antibiotic stewardship and discovery of new potent drugs, novel drug delivery systems, are demonstrating the potential to solve some of the patient and dosage form factors related to the development of resistance by extending the circulation time, targeting infectious sites, protecting and enhancing antibacterial activity of pristine drugs with prominent examples such as Lipoquin®, Pulmaquin® and MAT2501, an enochloated formulation of amikacin [14–17].

Core-shell aggregates of linear polymers have both a hydrophobic (core) and hydrophilic (shell) parts that self-assembles in aqueous milieu to form micelles, which have the ability to encapsulate hydrophobic drugs in the core [18,19]. However, premature dissociation of the self-assembled unimers during circulation in the bloodstream can cause a burst release, resulting in high concentration of drugs in the bloodstream [20,21]. Dendrimers as drug delivery materials have widely been reported due to their attractive properties such as high degree of branching, multivalency, globular architecture and well-defined molecular weight. Their unique properties make them suitable materials for drug delivery [22]. They are being employed as alternative to linear block polymers [23]. However, there are some concerns about toxicity and biocompatibility of the dendritic nanostructures regarding their applications in drug delivery such as damage to cell membrane integrity, chromosomes and mitochondria, oxidative stress, genotoxicity, and stimulates immune response [24].

To address the problem associated with dendrimer nanostructures and linear polymers, such as toxicity, biocompatibility and premature disassociation, several research groups have resorted to modifying the end groups of the dendrimers using linear polymers star results to hyperbranched polymers with dendrimer cores. This strategy embodies some positive traits from both dendrimers and the attached linear polymers for efficient drug delivery [25,26]. Moreover, the ability to functionalize their end groups, fine-tunes dendrimers for targeted delivery, long circulation [27], biodegradability [28], and covalent attachment of the drugs for sustained release [29]. Most reports for this strategy have been for the delivery of anti-cancer drugs [30,31], there is a dearth of literature on the evaluation of hybrids of linear polymer shells with dendrimer cores as carriers for enhancing antibiotic delivery despite their numerous advantages. There is therefore a need to develop and employ this strategy for antibacterial delivery as this could offer biosafe and effective drug delivery system for antibiotics.

Typically, linear polymer-dendrimer hybrids (LPDH) self-assemble to become core-shell aggregates, such as classical micelles [32] and unimolecular micelles [33] However, there is limited literature on vesicular self-assembly, and most of the reported vesicles have shown to be large in size with a poor polydispersity index (PI) [34–36]. Hence, there is a need for a synthesis of novel LPDHs that assemble into ultra-small nanovesicles with lower PI to advance the field by offering reproducible and predictable biodistribution and activity, and have wider applications, such as drug delivery, diagnostics and imaging.

The experimental, characterization and information for vesicles from polymers, such as their size, geometric structure, polydispersity is well understood [37]. However, there is a need to understand the self-assembly process and molecular dynamics (MD) simulations are being employed to explain self-assembly process of the polymers [38]. Thus, providing a detailed molecular insight at atomic level on how self-assembly occurs and the forces that play important roles for the stability of the formation of the structures are of paramount importance in drug delivery.

In this study, we therefore propose the use of generation one poly ester amine dendrimer (PEA) and methoxypoly(ethylene glycol)-b-poly (ϵ -caprolactone) (mPEG-b-PCL) linear block polymer to synthesize a novel LPDHs with ability to self-assemble into nanovesicles. PEA dendrimers have shown to have better characteristics, such as biocompatibility, nontoxicity, biodegradability, a higher drug loading and drug encapsulation [39,40], flexibility and sustained release properties than

other dendritic polymer counterparts [41–43]. mPEG-b-PCL linear has proven to have biocompatibility, non-toxicity and biodegradable excellent solvating properties [44], we envisage the resulting LPDHs to be efficient and safe biomaterial for drug delivery.

There are several reports on antimicrobial drug delivery using PEGylated PAMAM dendrimers to form LPDHs [45,46]. This highlights the feasibility and importance of using this strategy to deliver antimicrobials. The aim of this study was therefore to explore the potential of delivering antimicrobials via nanovesicles formulated from the modification of generation one PEA dendrimer with mPEG-b-PCL block polymer to yield a 3-arm star polymer (3-mPEA) with a dendrimer core and block copolymer shell. Most of dendrimer modification with the linear polymers has been through PEGylation, however, we envisaged that the use of mPEG-b-PCL block polymer will offer a better drug delivery system as the hydrophobic PCL portion attached to the dendrimer core will offer stability, mechanical strength of the vesicle membrane and improved loading capacity while the mPEG shell will offer long circulation. This paper is the first report of a LPDHs from PEA dendrimer with mPEG-b-PCL block copolymer for delivery of any class of drug. The synthesis, *in vitro*, MD simulations and *in vivo* findings through end groups functionalization of PEA dendrimer with a linear block polymer mPEG-b-PCL, and formulation of VCM encapsulated nanovesicles are reported in this paper.

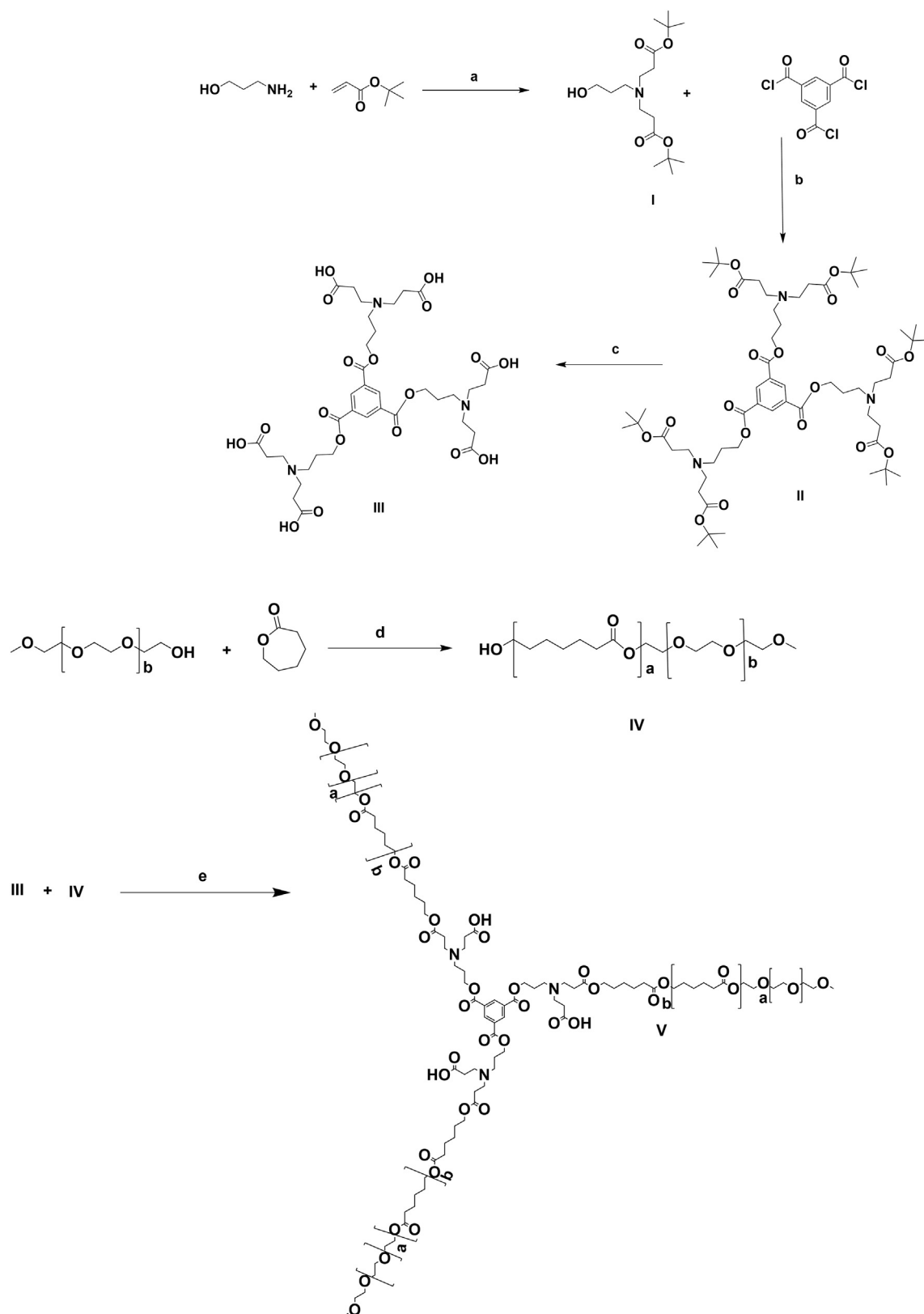
2. Materials, instrumentation and methods

2.1. Materials

Acetylchloride (AcCl), *tert*-butyl acrylate, 3-amino-1-propanol, *p*-dimethylaminopyridine (DMAP), *N,N'*-Dicyclohexylcarbodiimide (DCC), 1,3,5-benzenetricarbonyl trichloride (Trimesoyl chloride), stannous octoate (Sn(Oct)₂), *tertiary* butyl acrylate, ϵ -caprolactone, tetrahydrofuran (THF), toluene, monomethoxy polyethylene glycol (mPEG) (MW 5000), phosphatidyl choline, Human serum albumin (HSA) and silica gel were procured from Sigma-Aldrich (USA). Vancomycin (VCM) was obtained from Sinobright Import and Export Co., Ltd. (China), 3-(4,5-dimethylthiazol-2-yl)-2,5-diphenyltetrazolium bromide (MTT) was bought from Merck Chemicals (Germany). Nutrient Broth, Mueller-Hinton Broth (MHB) and Mueller-Hinton Agar (MHA) were acquired from Biolab (South Africa). Propidium iodide and Syto9 dyes cell viability kits were purchased from ThermoFisher (USA). Monolith protein labelling kit RED-NHS, MST buffer supplement with 0.05% Tween 20, Monolith NT.115 Standard Treated Capillaries were supplied by NanoTemper Technologies (Germany). The bacterial cultures used were *Staphylococcus aureus* ATCC 25923 and methicillin-resistant *S. aureus* (MRSA) (*S. aureus* Rosenbach ATCC BAA 1683).

2.2. Instrumentation

Fourier-transform infrared spectroscopy (FT-IR) spectra of all the compounds were recorded on a Bruker Alpha-p spectrometer with a diamond ATR (Germany). Proton and Carbon nuclear magnetic resonance (¹H NMR and ¹³C NMR) measurements were performed on a Bruker 400 and 600 Ultra shield™ (United Kingdom) NMR spectrometer. High Resolution Mass Spectrometry (HRMS) was performed on a Waters Micromass LCT Premier TOF-MS (United Kingdom). The matrix-assisted laser desorption ionization time-of-flight mass spectrometry (MALDI TOF) mass analysis was performed on a Bruker SmartBeam Autoflex III (Bruker Daltonics, Bremen, Germany). Gel permeation chromatography (GPC) was performed on a THF solvent system consisting of a Waters 1515 isocratic high-performance liquid chromatography (HPLC) pump, a Waters 717 plus auto-sampler, Waters 600E system controller (run by Breeze Version 3.30 SPA) with a Waters refractive index detector and mass was relative to a linear polystyrene calibration standard. Optical density (OD) was measured using a



Scheme 1. Synthesis of 3-mPEA. a). methanol, stirring at room temperature 12 h; b). toluene, DMAP, 110 °C, 6 h; c). AcCl, H₂O, DCM, room temperature, 8 h; d). Sn (Oct)₂, toluene, 110 °C, 6 h; e). DCC, DMAP, DMF, room temperature, 5 days.

spectrophotometer (spectrostar nano, Germany).

2.3. Methods

2.3.1. Synthesis and characterization of the hybrid dendrimer

The dendritic star polymer was synthesized using Scheme 1. Details of synthesis can be found in the supplementary material.

2.3.2. In vitro cytotoxicity

The *in vitro* cell viability of the synthesized material was assessed using a previously reported MTT assay method [47,48] on human breast adenocarcinoma (MCF 7), adenocarcinomic alveolar basal epithelial cells (A 549), liver hepatocellular carcinoma (HepG 2) cell-lines and human embryonic kidney cells 293 (HEK 293). Each of the four cell lines containing 2.5×10^3 cells were seeded into 96-well plates and incubated for 24 h with different dilutions of 3-mPEA (20, 40, 60, 80 and 100 $\mu\text{g/mL}$). Wells with culture medium only and culture medium containing cells were considered as the negative and positive controls respectively. After 48 h of incubation, the culture medium and test materials were discarded and replaced with 100 μL of fresh culture medium and 100 μL of MTT solution (5 mg/mL in PBS) in each well. Cell viability was evaluated by measuring the mitochondrial-dependent conversion of the tetrazolium salt MTT to formazan crystals. After 4 h of incubation with MTT, the media was removed from the wells, and solubilization of formazan was achieved by adding 100 μL of dimethyl sulfoxide. The optical density (proportional to the number of live cells) was assessed with a microplate spectrophotometer (spectrostar nano, Germany) at an absorbance wavelength of 540 nm. The percentage cell viability was calculated as follows;

$$\% \text{Cell viability} = \left(\frac{\text{A540 nm treated cells}}{\text{A540 nm untreated cells}} \right) \times 100\%$$

2.4. Formulating VCM loaded 3-mPEA nanovesicles

The nanovesicles were prepared using a solvent evaporation method [49]. A solution of 10, 30, 40 and 50 mg of 3-mPEA each dissolved in 5 mL organic solvent (THF) was added drop-wise to 20 mL of the aqueous solution containing 10 mg of VCM under stirring (400 rpm). The resulting emulsions was left to stir overnight at room temperature to ensure the complete evaporation of the organic solvent. The non-drug loaded nanovesicles were prepared using the same procedure.

2.5. Characterization of the nanoparticles

2.5.1. Size, Polydispersity Index (PI), Zeta Potential (ZP) and morphology

The size, PI, and ZP of 3-mPEA nanovesicles were determined using dynamic light scattering technique on a Zetasizer Nano ZS90 (Malvern Instruments Ltd., UK), with all measurements being performed in triplicate. The Morphology was examined using transmission electron microscopy on a Jeol, JEM-1010 (Japan) transmission electron microscopy (TEM) with uranyl acetate (UA) negative staining [50]. The nanovesicles were diluted appropriately then mounted onto the surface of a copper grid, and the excess sample was removed by blotting off with filter paper, then dried at ambient temperature and stained using 2% uranyl acetate (UA) solution before measurement. The images were captured at an accelerating voltage of 100 kV.

2.5.2. Entrapment efficiency (% EE) and drug loading capacity (LC)

The EE and DL of V-3-mPEA were determined by an ultrafiltration method. Briefly, 2 mL of nanovesicles containing 500 $\mu\text{g/mL}$, 1.5 mg/mL, 2 mg/mL, 2.5 mg/mL of 3-mPEA loaded with 500 $\mu\text{g/mL}$ of VCM were placed in Amicon® Ultra-4 centrifugal filter tubes (Millipore Corp., USA) of 10 kDa pore size and centrifuged at 3000 rpm at 25 °C for 30 min. The filtrate was collected and the untrapped VCM in the filtrate was quantified using a high-pressure liquid chromatography

(HPLC) (Shimadzu, Japan) method, with UV detection at a wavelength of 280 nm [51]. The mobile phase consisted of a mixture of water with 0.1% TFA and acetonitrile (85/15 v/v), which was pumped through a Nucleosil 100–5 C18 column (150 mm \times 4.6 mm internal diameter) at a flow rate of 1 mL/min, with an injection volume of 100 μL . The EE (%) and DL (%) were calculated using the following equations:

$$\% \text{EE} = \left(\frac{\text{Weight of VCM in nanoparticles}}{\text{Weight of VCM added}} \right) \times 100\%$$

$$\% \text{LC} = \left(\frac{\text{Weight of VCM in nanoparticles}}{\text{Total weight of nanoparticles}} \right) \times 100\%$$

2.5.3. Differential scanning calorimetry (DSC)

The VCM, 3-mPEA, physical mixture (drug and the polymer) and lyophilized formulation thermal profiles were determined by DSC (Shimadzu DSC-60, Japan). Briefly, samples (2 mg) were placed in an aluminum pan and sealed, which was then heated to 300 °C at a constant rate of 10 °C/min under a constant nitrogen flow of 20 mL/min using an empty pan as a reference [48].

2.5.4. All-atom MD simulations of 3-mPEA self-assembly

2.5.4.1. Methods. 3-mPEA dendritic star polymer structure containing 3 arms of the block polymer comprising of 2 and 4 repeating monomer units of caprolactone and mPEG was constructed using ChemDraw [52]. The 3-mPEA dendritic star polymer was equilibrated for 2 ns before performing the self-assembly simulation. GROMACS insert-molecules tool was used for random insertion of 8 molecules of 3-mPEA and the polymers were solvated using TIP3P water model [53] and CHARMM General Force Field (CGenFF) [54]. The system containing a total of 29,494 water molecules and 8 mol of 3-mPEA was first energy minimized using the steepest descent [55] method and self-assembly simulation was then performed using isobaric-isothermic ensemble (NPT) for 80 ns (ns). The velocity-rescale thermostat was used for temperature coupling and the Parrinello-Rahman method was used for pressure coupling [56]. The simulation was performed at 298.15 K temperature and 1 atm pressure using the coupling time of 0.1 ps and 2.0 ps, respectively. The Particle Mesh Ewald (PME) method [57] was used for long-range electrostatic interactions and VdW and short-range coulombic interactions were calculated using 10 Å cut-off. MD simulations were performed using GROMACS 5.1.2 [58].

2.5.4.2. Data analysis. Numbers of aggregates and the Com of Mass (COM) distances between two monomers were calculated using the g_aggregate tool [59] and in-house Tcl script respectively. The interaction and binding energies between two monomers were computed using the g_mmpbsa tool [60], which employs the molecular mechanics Poisson–Boltzmann surface area (MM-PBSA) method and has been in the previous studies to calculated interaction and binding energies [61,62]. The binding energy of two monomer complex in water environment was expressed as:

$$\Delta G_{\text{binding}} = \Delta G_{\text{complex(dimer)}} - (\Delta G_{\text{monomer1}} + \Delta G_{\text{monomer2}})$$

Where $\Delta G_{\text{complex}}$ is total energy of dimer complex and $\Delta G_{\text{monomer 1}}$, $\Delta G_{\text{monomer2}}$ are total energy of both monomers individually. The energy of $\Delta G_{\text{monomer1}}$, and $\Delta G_{\text{monomer2}}$ were estimated using:

$$\Delta G_{\text{monomer1}} = \Delta E_{\text{monomer1(MM)}} + \Delta G_{\text{monomer1(Solvation)}}$$

$$\Delta G_{\text{monomer2}} = \Delta E_{\text{monomer2(MM)}} + \Delta G_{\text{monomer2(Solvation)}}$$

Where ΔE_{MM} is potential energy in the vacuum and estimated using:

$$\Delta E_{\text{MM}} = \Delta E_{\text{bonded}} + \Delta E_{\text{nonbonded}}$$

$$\Delta E_{\text{MM}} = \Delta E_{\text{bonded}} + (\Delta E_{\text{vdw}} + \Delta E_{\text{elec}})$$

The $\Delta G_{\text{solvation}}$ is solvation free energy and estimated using:

$$\Delta G_{\text{Solvation}} = \Delta G_{\text{polar}} + \Delta G_{\text{nonpolar}}$$

ΔG_{polar} was calculated using the Poisson-Boltzmann (PB) equation and $\Delta G_{\text{nonpolar}}$ was estimated using:

$$\Delta G_{\text{nonpolar}} = \gamma \text{SASA} + b$$

Where SASA is the solvent accessible surface area, Å radius of the probe boundary while γ is a coefficient related to the surface tension of the solvent and b is a fitting parameter.

$$\gamma = 0.0226778 \text{ kJ/Mol/Å}^2 \text{ and } b = 3.84928 \text{ kJ/Mol}$$

For binding energy calculation frames were extracted between 25 ns to 32 ns at interval of 500 ps. A bootstrap analysis was performed to calculate the standard error.

2.6. Determination of the binding affinity of 3-mPEA nanovesicles on human serum albumin (HSA)

2.6.1. Microscale thermophoresis (MST) binding affinity studies

The binding between 3-mPEA and HSA was measured using microscale thermophoresis (MST) on Monolith NT.115 (Germany) [63]. Human serum albumin (HSA) was labelled using the Monolith protein labelling kit RED-NHS according to the manufacturer's instructions. The labelled HSA was adjusted to 80 nM using an MST buffer supplemented with 0.05% Tween 20. A 16-step serial dilution of 20 µL solutions containing 25 µM of mPEG 5000 (positive control), Phosphatidyl choline (negative control) and 3-mPEA with MST buffer was performed, with 10 µL of the labelled HSA being added to each of the dilutions to form a ligand protein complex containing 40 nM HSA and ligand concentrations ranging from 12.5 µM to 0.00038147 µM. The ligand HSA complex was incubated for 15 min, then loaded into Monolith NT.115 Standard Treated Capillaries and the binding affinity measured on an MST instrument. Data of three independently pipetted measurements were analyzed (MO-Affinity Analysis software version 2.1.3, Nano-Temper Technologies). The strength of binding was evaluated by the dissociation constant K_d calculated by the equation:

$$K_d = \frac{[A][X(T)]}{[AT]}$$

where $[A]$ is the concentration of free fluorescent molecules, $[T]$ is the concentration of titrant.

and $[AT]$ is the concentration of complex formed by $[A]$ and $[T]$. The smaller the K_d the stronger the binding force.

2.6.2. HSA protein adsorption studies

Human serum albumin adsorption studies were performed following a literature reported protocol [64,65]. Nanoparticles were incubated in a solution of 400 µg/mL of HSA and stirred vigorously with a magnetic stirrer for 2 h at 37 °C. The nanoparticles were then centrifuged (14,000 rpm, 4 °C for 20 min) to remove any unabsorbed proteins, after which the samples were diluted, and size and the surface charge was analyzed by the Zeta Sizer.

2.7. *In vitro* drug release

Drug release of VCM was performed using the diffusion dialysis bag method, as per previously reported procedures [66,67]. Dialysis bags (pore size: 8000–14,400 Da) were loaded with 2 mL of the drug loaded nanovesicles and non-drug loaded vesicles then placed in a 40 mL receiver compartment of PBS (pH 7.4) at 37 °C. This was then placed in shaking incubator (100 rpm) and at specific time intervals 3 mL of samples were drawn from the receiver solution and an equal amount of fresh PBS was replaced to keep a constant volume. Determination of the amount of the drug released was performed as per section 3.5.2 via a reported HPLC method [51]. The experiments were performed in triplicate, with the release fraction of VCM from V-3-mPEA nanovesicles

being calculated using the following equation:

$$\text{Cumulative release\%} = \left(\frac{Mt}{M_{\infty}} \right) \times 100\%$$

Where M_t is the amount of VCM released from the V-3-mPEA nanovesicles at time t , and M_{∞} the amount of VCM pre-loaded in V-3-mPEA nanovesicles.

In addition, 60% cumulative *in vitro* drug release data was modeled and analyzed with DDSolver to determine the mechanism of release of VCM from the nanovesicles [47,68,69]. Zero order, first order, Higuchi, Weibull, Hixson-Crowell, and Korsmeyer–Peppas models were analyzed. Model with highest correlation coefficient (R^2) and lowest root mean square error (RMSE) was considered to be the best fit model. The 'n' exponent obtained after modeling the release data using the Korsmeyer–Peppas model and mean dissolution time (MDT) were parameters applied to deduce the kinetics and mechanism of drug release of the drug from the nanovesicles [70].

2.8. Stability studies

Short term stability studies of the V-3-mPEA nanovesicles were evaluated for 90 days at 4 °C and at room temperature by assessing, particle size, PI, and ZP parameters.

2.9. Antibacterial activity

2.9.1. Determination of the MIC

An *in vitro* antibacterial study was conducted using the broth microdilution method against SA and MRSA [71]. Both the bacterial cultures were grown in Mueller–Hinton Broth, with (MHB) appropriate dilutions being made to achieve 5×10^5 colony forming units per mL (CFU/mL) [72] of bacteria. V-3-mPEA nanovesicles and bare VCM were serially diluted in MHB broth and then incubated with bacterial cultures containing 5×10^5 colony forming units per mL (CFU/mL) for 18 h in a shaking incubator at 37 °C and 100 rpm. 10 µL of the serial dilutions were spotted on Mueller–Hinton Agar (MHA) plates and incubated for a further 18 h. The minimum concentration at which no visible bacterial growth was observed was considered as the MIC.

2.9.2. Bacterial membrane disruption

Suspensions of MRSA 1.5×10^8 CFU/mL in phosphate saline buffer (PBS) were incubated with V-3-mPEA containing 250 µg/mL of VCM in a 50:50 ratio for 4 h in an Eppendorf tube. The mixture of nanovesicles was diluted appropriately and mounted onto the surface of a copper grid. The excess sample was removed by blotting off with filter paper and was then dried at ambient temperature before measurement. The images were examined using High Resolution Transmission Electron Microscope (brightfield, darkfield, STEM diffraction) - JEOL HRTEM 2100 [73].

2.9.3. Reduction of MRSA biofilm by V-3-mPEA

Inhibition of MRSA biofilms by V-3-mPEA was determined by fluorescence microscopy [74]. Microscope cover slips were placed at the bottom of 6 well plates. Then 2 mL of MRSA 1.5×10^8 CFU/mL suspensions in MHB were added to the wells and incubated for 3 days at 37 °C to form a fully mature biofilm. Prior to treatment, the media was sucked out of the wells with a Pasteur pipette and the wells were washed 3 times to remove non-adhered bacteria. 1 mL of bare VCM solution and nanovesicles formulation containing 125 µg/mL of VCM were added to the wells and incubated for 12 h at 37 °C. The wells were then washed with Phosphate Buffer pH 7.4 to remove the treatments and non-adhered MRSA cells. While still in the wells the coverslips were stained with solution of Syto9 and propidium iodide (PI) containing 30 µL in 1 mL of distilled water for 30 mins in darkness. The wells were washed again to remove excess dye, then inverted on a microscope glass slide and the coverslips were carefully glued on the edges on the glass

slides. The inhibition of biofilm formation by V-3-mPEA was viewed on a Fluorescence microscope (Nikon Eclipse 80i FM Japan). Syto9 and PI were sequentially excited at 488 nm and 543 nm, respectively, and their fluorescence emissions were collected between 500 and 600 nm for Syto9 and between 640 and 750 nm for PI. Microscopic observations were performed at least three times in independent experiment.

2.9.4. Flow cytometry bacterial cell viability

Viable MRSA cells in the population after treatment with VCM and V-3-mPEA for 18 h was determined using flowcytometry method [75]. 15 μ L containing 5×10^5 colony forming units (CFU)/mL of the bacterial suspension was added to a 96 well plate each containing 135 μ L of bare VCM (positive control), and V-3-mPEA at the MIC concentration (15.65 μ g/mL and 0.988 μ g/mL respectively), which was further incubated at 37 °C in a shaking incubator (100 rpm). 50 μ L of each VCM and V-3-mPEA mixture were added to the flow cytometry tubes each containing 350 μ L of the sheath fluid and vortexed for 5 min. The mixture was incubated for 30 min with 5 μ L of non-cell wall permeant propidium iodide (PI) and Syto9 cell permeant dye. PI fluorescence was excited by a 455-nm laser and collected through a 636 nm bandpass filter (red wavelength), while Syto9 excitation laser was at 485 nm laser and collected through a 498 nm band pass filter (green wave length). Untreated pure MRSA cells were used as a negative control. The BD FACSCANTO II (Becton Dickinson, CA, USA) equipment was used for flow cytometry. Instrumentation settings included sheath fluid flow rate of 16 mL/min, a sample flow rate of 0.1 mL/min. Data with fixed cells were collected using a flow cytometer software (BD FACSDIVA V8.0.1 software [USA]). The voltage settings used for fluorescence-activated cell sorting (FACS) analysis were: 731 (forward scatter [FSC]), 538 (side scatter [SSC]), 451 (Syto9) and 444 for PI. The bacteria were initially gated using forward scatter, and cells of the appropriate size were then gated and at least 10,000 cells collected for each sample in triplicate, and their position as 'live' and 'dead' determined. To avoid any background signals from particles smaller than the bacteria, the detection threshold was set at 1000 in SSC analyses [76].

2.9.5. Bacterial killing kinetics

An overnight culture of MRSA in MHB was diluted with phosphate buffer to a concentration of 5×10^5 CFU/mL. VM and VM loaded 3-mPEA were added at concentrations equivalent to $5 \times$ MIC. Sterile water was added in the bacterial broth with the test samples to serve as a negative control. Bacterial cell viability was monitored up to 24 h. Samples were removed at specific intervals, serially diluted in PBS, and plated in triplicate on MHA plates. After -incubation of the plates for 24 h at 37 °C, the CFU were counted and converted to \log_{10} values and plotted in a graph [77].

2.9.6. In vivo antibacterial activity

A BALB/c mouse skin infection model was used for *in vivo* antibacterial activity following a study protocol approved by the University of KwaZulu-Natal's Animal Research Ethics Committee (Approval number: AREC/104/015PD) [78,79]. Humane care and use of the animals were in accordance with the guidelines of the AREC of UKZN and South African National Standard SANS 10386:2008. 18–20 g male BALB/c mice were obtained from the Biomedical Research Unit, University of KwaZulu-Natal. Mice back hairs were shaved carefully without bruising the skin then disinfected with 70% ethanol. After 24 h, 50 μ L of MRSA saline (1.5×10^8 CFU/mL) suspension was injected intradermally and the mice ($n = 4$) were divided into three treatment groups (positive control, negative control and V-3-mPEA groups). 30 min post infection with MRSA, 50 μ L of the different (V-3-mPEA formulation, free VCM and saline) treatments was administered to all the groups at the same site of infection. The mice were kept under observation for 48 h under the following conditions; a normal 12 h light and dark, temperature 19–23 °C, relative humidity $55 \pm 10\%$ and adequate ventilation. After 48 h the mice were euthanized with

halothane and the infected area of the skin was collected and homogenized in PBS of pH 7.4 (5 mL). Tissue homogenates were serially diluted in pH 7.4 phosphate buffer then 20 μ L were spotted on MHA plates, which were incubated at 37 °C for 24 h and the number of colonies forming units (CFU) were counted. The CFU/mL was calculated using the equation:

$$\text{CFU/mL} = \frac{\text{number of colonies} \times \text{dilution factor}}{\text{volume of culture plate}}$$

The infected skins were also collected and processed as per reported procedure [47] for further histological investigations. The Processed skin sections were collected on slides and stained with hematoxylin and eosin (H&E). Examinations and image capturing of the slide was performed on a Leica Microscope DM 500, fitted with a Leica ICC50 HD camera (Leica Biosystems, Germany).

2.10. Statistical analysis

One-way analysis of variance (ANOVA), followed by Bonferroni's multiple comparison test, was used for the statistical analysis. Individual groups were compared to each other using a paired *t*-test, with *p* values of < 0.05 being considered statistically significant, and the values are represented as mean \pm SD.

3. Results and discussion

3.1. Synthesis and characterization

The surface end groups modified dendrimer was synthesized in four steps (supplementary materials). The first step involved bis-aza-Michael addition reaction, as depicted in Scheme 1a, to synthesize a dendron (compound I), after which the 1st generation dendrimer (compound II) was synthesized by coupling the dendron with the 1,3,5-benzenetricarbonyl chloride as a central aromatic core using DMAP as a catalyst. The tertiary butyl ester protecting groups on compound II were hydrolyzed to give a poly (ester-amine) dendrimer with an aromatic core (compound III). mPEG-*b*-PCL (compound IV) was synthesized, as illustrated in Scheme 1d via ring-opening polymerization chemistry [80]. The degree of polymerization of the block polymer was calculated by integrating the mPEG peaks at 3.53 ppm against the 1.52–2.199 poly caprolactone repeating units peak in the ^1H NMR spectrum [81] and the degree of polymerization was found to be 21.1% which was correlating with the mass analysis by MALDI TOF (supplementary material).

The dendrimer was further coupled to the diblock copolymer to afford the final compound V (3-mPEA). In the final Steglich esterification reaction, only 3 among the six carboxylic acid groups of the dendrimer were esterified or occupied with the mPEG-PCL. This limited esterification was confirmed by observed practical mass by GPC analysis, with an average molecular weight 19,115 Da and polydispersity index of 1.42. The partial esterification may be due to the high molecular weight of mPEG-*b*-PCL that caused steric hindrance [82], and more intra molecular hydrogen bonding in the dendrimer (carboxylic acid group) could have restricted the esterification reaction [83].

The diblock copolymer mPEG-*b*-PCL was chosen to functionalize the dendrimer as it has been shown to be safe with excellent solvating properties [44,84]. Apart from being efficient nano materials, dendrimers are associated with toxicities that hinder their biomedical applications [43,85]. However, the literature shows that PEA dendrimers are safe, biodegradable [86,87], flexible, and provide sustained release properties when compared to other dendritic polymer counterparts [41–43]. This makes them a good candidate for drug delivery. Thus a hybrid of mPEG-*b*-PCL and PEA dendrimers would result in a material with inherent good properties from the parent blocks.

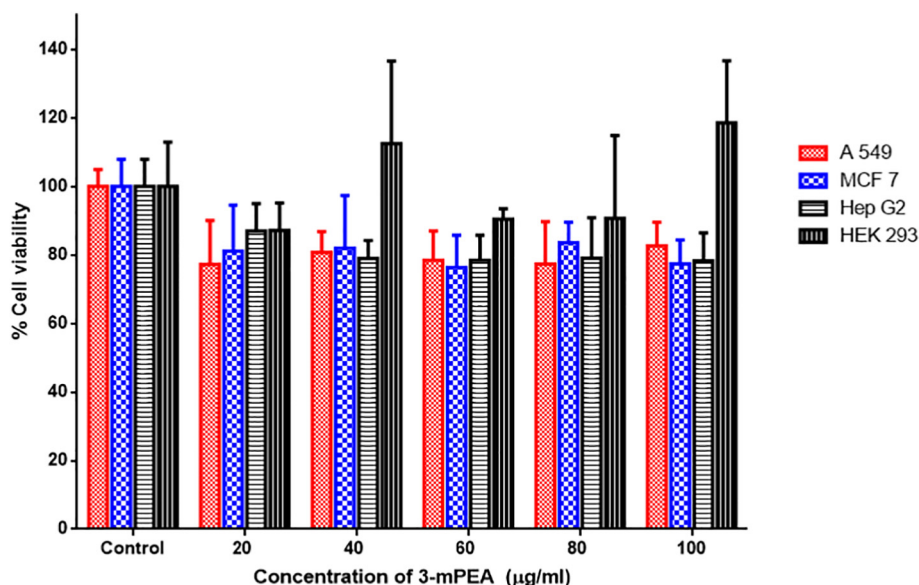


Fig. 1. Cytotoxicity evaluation of various concentrations of 3-mPEA against on A 549, MCF 7 Hep G2 and HEK 293 cells.

3.2. *In vitro* cytotoxicity

The *in vitro* cell viability of 3-mPEA was assessed by quantifying the viable mammalian cells after exposure of the synthesized material. Four cell lines MCF 7, A549, Hep G2 and HEK 293 were employed to determine the bio-safety of 3-mPEA in an *in vitro* cell culture system. The results showed that cell viability ranging from 77.23 to 118.6% across all the concentrations in all cell lines that were tested. The percentage cell viability range obtained for the individual cell lines ranged from 77.41 to 83.57%, 77.29 to 82.68%, 78.29 to 87.01% and 87.3 to 118.6% for MF7, A549, Hep G2 and HEK 293 respectively (Fig. 1) with no dose-dependent toxicity within the concentrations of the polymer studied. This percentage viability displayed by 3-mPEA was above the requirements for biocompatibility and toxicity regulatory requirements for synthesized biomaterial [88–90]. Therefore, results from these findings shows 3-mPEA to be safe and nontoxic for biomedical applications.

3.3. Preparation and characterization of 3-mPEA nanovesicles

Self-assembled 3-mPEA nanovesicles were formulated by a solvent evaporation method. Solutions containing different concentrations of 3-mPEA in THF were added dropwise to the aqueous VCM solution under continuous stirring to optimize the concentrations of dendritic star polymer that will have the highest entrapment, size and PI (Table 1). As the organic solvent evaporated, the 3-mPEA molecules formed stable self-assembled nanovesicles while entrapping the VCM (Fig. 2). The amphiphiles self-assembly might have been due to non-covalent interactions, such as hydrogen bond formation, π - π interactions, van der Waals interactions, electrostatic interactions, and the hydrophobic effects that lead to enhanced thermodynamic and kinetic stability of the vesicles [42,91,92].

There was no significant ($P > .5$) difference in the resulting sizes

Table 1
Different ratio of drug polymer with their respective EE ($n = 3$).

Polymer: drug	Size	PI	EE
1:1	54.07 \pm 0.291	0.199 \pm 0.014	35.97 \pm 5.5%
3:1	52.48 \pm 2.6	0.103 \pm 0.047	76.49 \pm 2.4%
5:1	53.89 \pm 2.57	0.165 \pm 0.028	60.74 \pm 5.2%
8:1	59.12 \pm 0.54	0.23 \pm 0.002	55.37 \pm 0.8%

across all the concentrations. Although, there was an increase in PI with increasing concentration of the polymer however the increase was not significant ($P > .5$) (Table 1). It was observed that by increasing the polymer concentration above the ratio 3:1 the EE started to decrease. The polymer: drug ratio of 3:1 (w/w) was found to be the optimal concentration giving highest VCM encapsulation with nanovesicles of size, PI and, ZP of 52.48 \pm 2.6 nm, 0.103 \pm 0.047 and, -7.3 ± 1.3 mV respectively.

The results were comparable to other nanovesicles from Janus dendrimers by Luis M. Bimbo and coworkers, who reported size ranges of 56–249 nm [93]. Percentage EE and LC for vesicles formed using 3:1 polymer to drug ratio were found to be 76.49 \pm 2.4% and 19.1 \pm 0.95% w/w respectively. These results are better than other drug delivery systems from poly (ϵ -caprolactone) and poly (ethylene oxide) based vesicles where EE and LC were in the range of 45.5 to 69.33% and 12 to 16% respectively for clavulanic acid and methotrexate [84,94,95].

TEM images showed thin walled ring-shaped spherical structures (Fig. 3I), with the population being discrete and in sizes that were comparable to the ones determined by DLS. The drug loaded vesicles were found to be physically stable in terms of size, PI and ZP both at room temperature and 4 °C for a period of 90 days.

3.3.1. Differential scanning calorimetry (DSC)

To determine the melting and crystallization behavior of VCM, 2-mPEA, lyophilized V-3-mPEA and the physical mixture, DSC studies were performed (Fig. 3III). There was a broad endothermic peak at 105.93 °C for the bare VCM that presented the thermal decomposition of the glycopeptide antibiotic, while for 3-mPEA, the peak was observed at 55.44 °C (Fig. 3III A) [96]. The physical mixture showed the respective thermal peaks of VCM and 3-mPEA at temperature near to their individual peaks with a slight upward shift, while the thermogram of the lyophilized V-3-mPEA vesicles did not display any thermal peaks for neither VCM nor 3-mPEA. This disappearance suggested that VCM was encapsulated by vesicles in the non-crystalline form [97].

3.4. All-atom MD simulations of 3-mPEA self-assembly

All-atom MD simulation was employed to understand the self-assembly of 3-mPEA dendritic star polymer. At time zero monomers were randomly apart, however a dimer was formed at time \sim 6.02 and \sim 10.14 ns respectively from aggregation of each of two molecules of

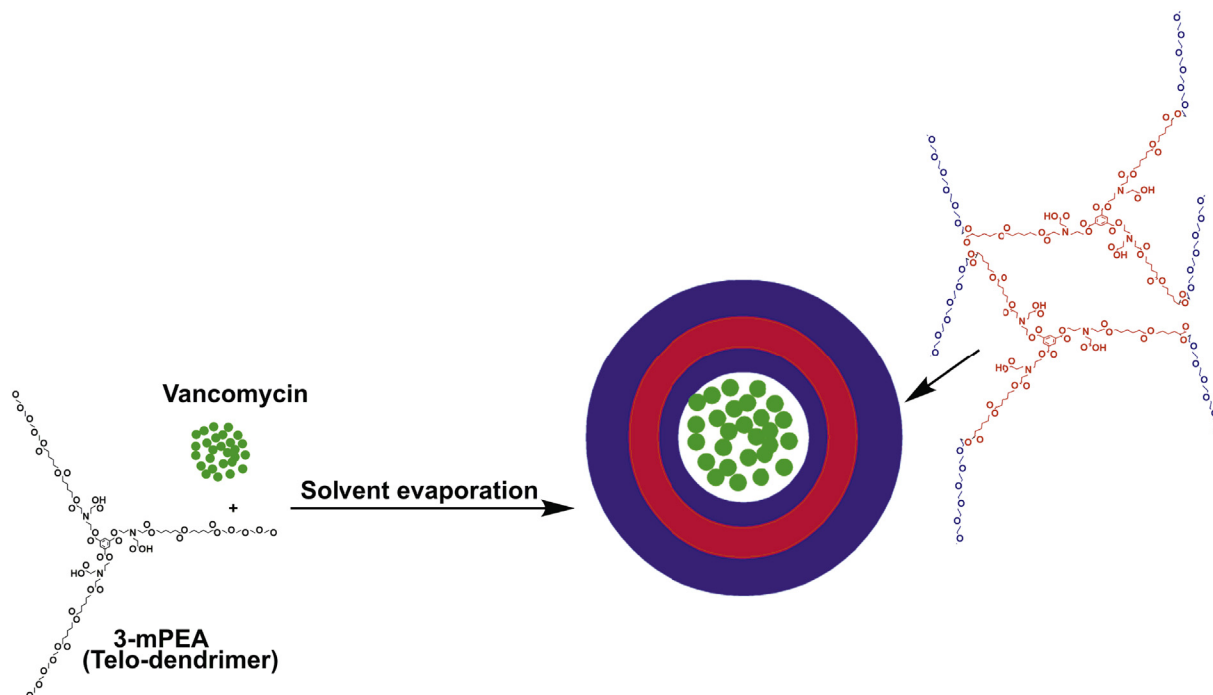


Fig. 2. Schematic of drug encapsulation into nanovesicles.

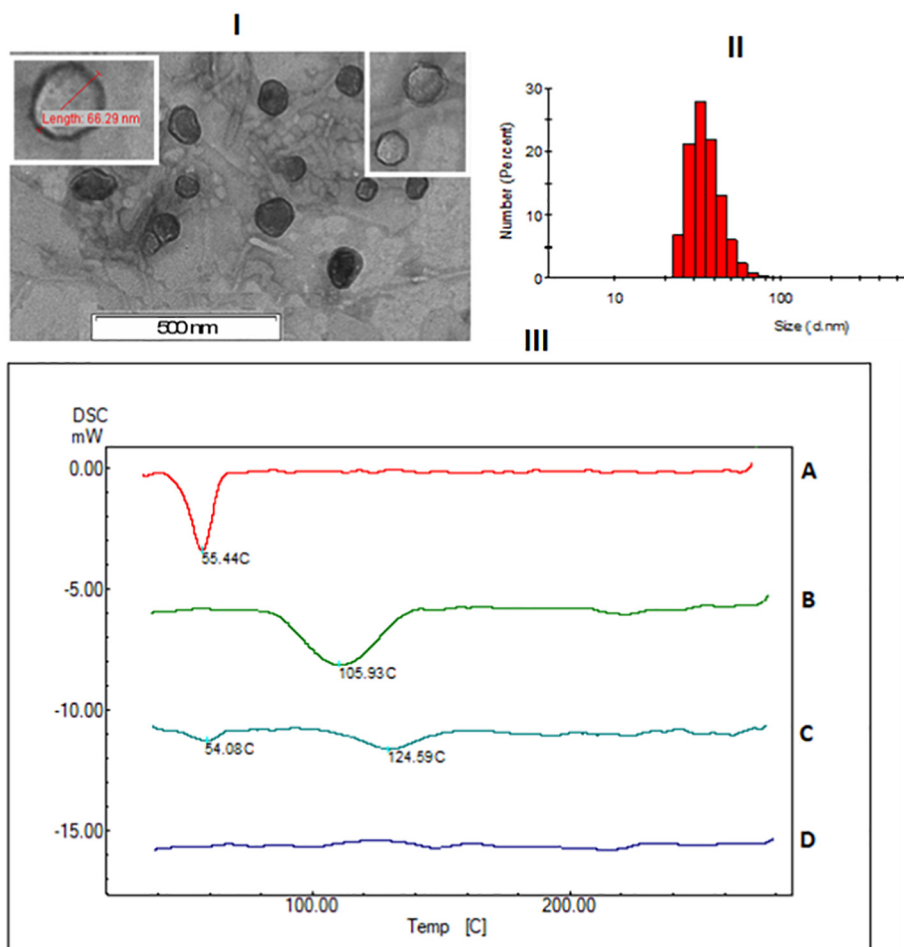


Fig. 3. I) TEM of V-3-mPEA nanovesicles; II) size distribution of nanovesicles determined by DLS. III) thermogram of (A) 3-mPEA; (B) VCM; (C) physical mixture of VCM and 3-mPEA and (D) freeze dried V-3-mPEA.

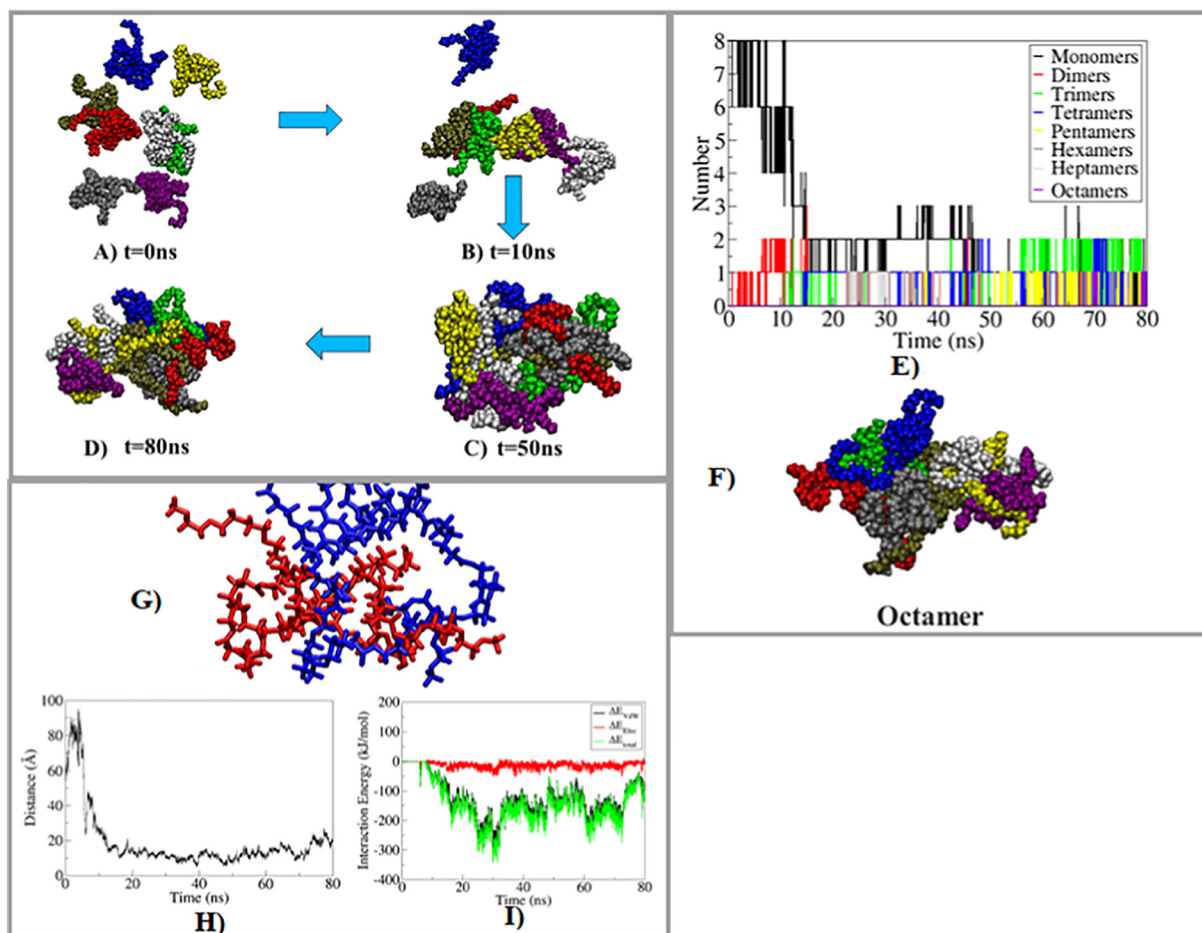


Fig. 4. Self-assembly of 3-mPEA snapshots at $t =$ A) 0, B) 10, C) 50 and D) 80 ns aggregation; E) shows the time evolution self-assembly process; F) shows the arrangement of octamer; G) shows the dimer in licorice representation, with monomers in blue and red colours; H) shows the time evolution of distance between two monomers; I) shows the time evolution of interaction energy and its components. (For interpretation of the references to colour in this figure legend, the reader is referred to the web version of this article.)

the star polymer (Fig. 4E). At times ~ 12.31 , ~ 14.9 and ~ 51.93 aggregation of 3, 4 and 5 mol of the star polymer aggregated to form trimers, tetramers and pentamer respectively (Fig. 4 A and B). At time ~ 71.85 ns there was a rearrangement to form two tetramers for the short period of time and at ~ 79.11 ns all molecules aggregated to form an octamer (Fig. 4 D and E). The arrangement included the hydrophilic portions (mPEG) of the linear block polymer facing on the either side of the aggregates and in contact with water molecules, while the hydrophobic segment sandwiched in the middle (Fig. 4C and D). This aggregation could have been the possible arrangement that resulted in formation of the vesicle. Literature shows this arrangement is typical intermediate arrangement prior to the formation of a vesicle [35,38,98]. The general structure of 3-mPEA dendritic star polymer is a solvent-(philic-phobic-philic) (PHP) type sequence that contains hydrophobic connection between two hydrophilic ends that restricts the chain stretching in solvent-phobic core. The PHP structures have shown the ability to form complex structures such as vesicles, toroidal micelles, “Y” junctions, cylindrical micelles and disk-like membranes [99–101]. These structures have been successfully employed in drug delivery. Overall, results of this study supported the fact that 3-mPEA could self-assemble to stable aggregates.

To understand the spontaneous interaction between 3-mPEA molecules, the type of interactions (VdW or electrostatics) that played a key role in their aggregation, binding energy and time evolution of COM distance we focused on one of the dimer (Fig. 4G). It was observed that two monomers aggregated at ~ 8.32 ns and remained stably bound until

Table 2

Average Binding Energy and its components obtained from the MM-PBSA Calculation for 3-mPEA dimer.

Contribution	Energy (kJ/mol)
ΔE_{vdw}	-241.49 ± 7.18
ΔE_{elec}	-26.78 ± 2.58
ΔG_{polar}	160.04 ± 8.49
$\Delta G_{nonpolar}$	-37.82 ± 0.83
ΔG_{total}	-146.07 ± 4.92

the end of the simulation. Average interaction energy between both the monomers from ~ 8.32 ns to 80 ns was -159.58 kJ/mol (Fig. 4I, green line) and decomposition of interaction energy in its components revealed that VdW interaction plays a crucial role in the interaction between polymers. The average VdW and electrostatics interaction energies between polymers from ~ 8.32 to 80 ns were -145.85 kJ/mol and -13.74 kJ/mol respectively. Binding energy (Table 2) was calculated between the monomers from 25 ns to 32 ns when they were closest to each other. Binding energy components showed that polar solvation energy was highly unfavorable, however, favorable VdW energy, nonpolar energy, and electrostatic energies lead to the overall highly favorable binding energy.

3.5. Human serum protein binding affinity

To determine the binding affinity of 3-mPEA, mPEG 5000 polymer

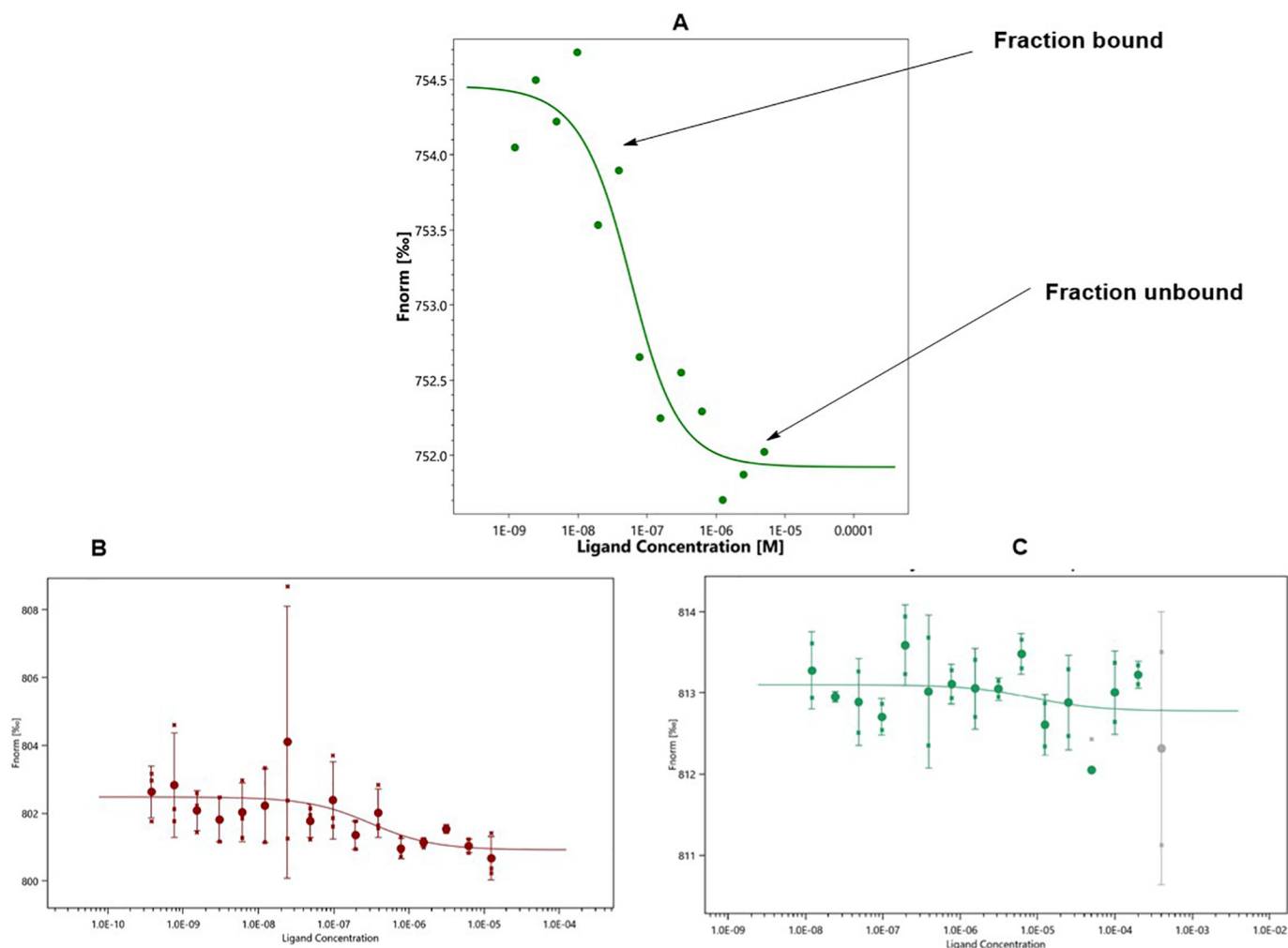


Fig. 5. A) the change in the normalized fluorescence of PC which concludes binding, B and C) the change in the normalized fluorescence of 3-mPEA and mPEG 5000 respectively showing response to low to conclude binding.

Table 3
The effect of HSA on 3-mPEA nanovesicles after incubation.

Sample	Size	PDI	ZP
Before test	56.53 ± 2.822	0.190 ± 0.008	- 8.05 ± 1.6
After test	54.25 ± 1.73	0.228 ± 0.038	- 6.23 ± 1.71
n = 3			

Table 4
Release kinetics data from different models.

Model	R ²	RMSE	Release exponent (n)
Zero Order	0.5864	16.00	-
First Order	0.8563	9.4	-
Higuchi	0.9193	7.07	-
Korsmeyer-Peppas	0.9194	7.63	0.494
Hixson-crowell	0.7821	11.62	-
Weibull	0.9947	2.14	-

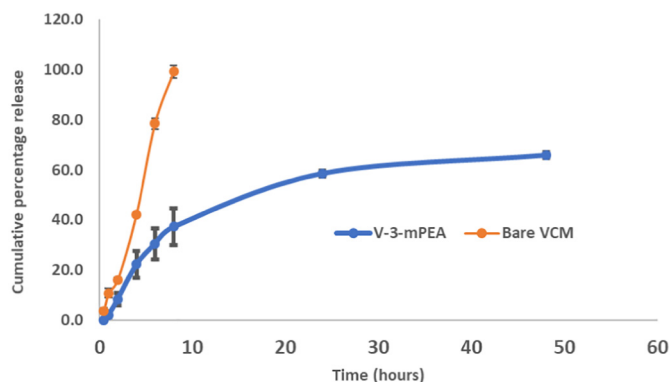


Fig. 6. *In vitro* drug release profile of V-3-mPEA nanovesicles and bare VCM (n = 3).

(positive control) and phosphatidyl choline (negative control) to HSA was performed using a Microscale Thermophoresis (MST) study. MST studies employ the motion of molecules due to changes in microscale temperature gradients [102]. The laser is usually focused onto the sample, which allows a temperature rise that induces thermophoresis of the molecules, which allows the MST signal to detect the binding by quantifying the change in the normalized fluorescence. The change in concentration between the initial and steady states is measured and can be plotted against the concentration of the added binding partner. From these data, the equilibrium dissociation constant (K_d) is obtained [102–105]. In the study, a constant concentration HSA was labelled with NT-647 dye then incubated with increasing concentrations of the test samples (3-mPEA, mPEG 5000 and PC). Thermophoresis was then induced and detected due to a created temperature gradient (2–6 °C) by an infrared (IR) laser. The binding study on the mPEG 5000 did not

Table 5
MICs of bare VCM, blank and VCM loaded 3-mPEA, against *S. aureus* and MRSA.

Time (hours)	24	48	72	96	120	24	48	72	96	120
	<i>S. aureus</i> (MIC µg/mL)					MRSA (MIC µg/mL)				
Bare VCM	3.9	NA	NA	NA	NA	15.65	NA	NA	NA	NA
V-3-mPEA	0.488	0.488	0.488	0.488	0.488	0.98	0.98	0.98	0.98	0.98
Blank	NA	NA	NA	NA	NA	NA	NA	NA	NA	NA

NA = No activity. The values are expressed as mean \pm SD, n = 3.

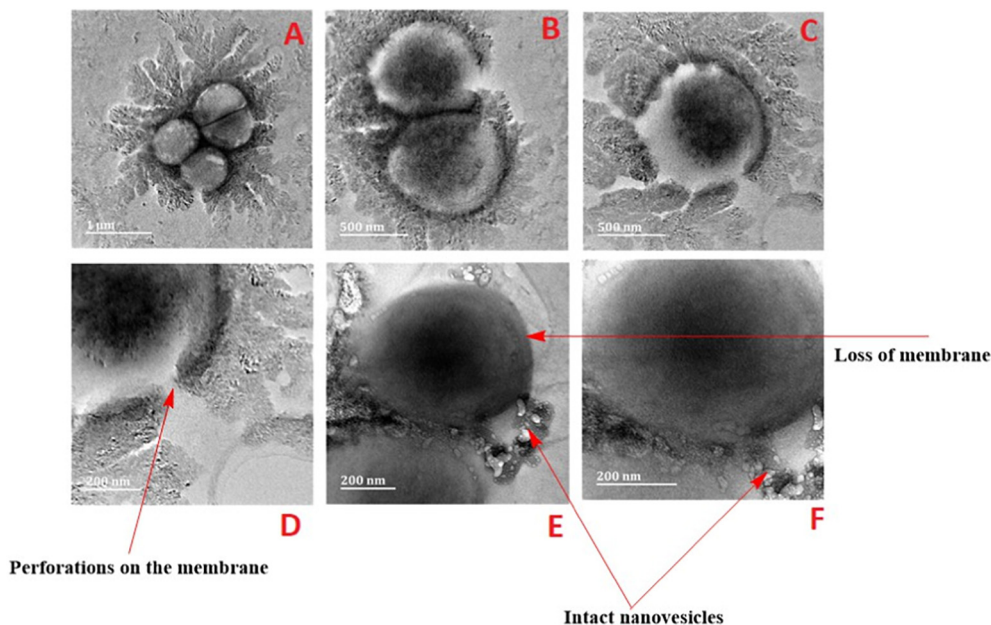


Fig. 7. HRTEM images of MRSA after incubation with V-3-mPEA. A. At initial treatment; B. After 1 h incubation, C. Single bacteria after 1 h, D. Formation of pores on the bacterial membrane after treatment, E and F. Loss of the membrane of the MRSA after 4 h with nanovesicles still intact.

display any binding affinity, which was similar to other results obtained using a different method [106]. However, binding studies for PC showed binding affinity to the HSA with a K_d of $39.997 \pm 0.1157 \mu\text{M}$ (Fig. 4B). The 3-mPEA did not display any affinity to the HSA (Fig. 5) [104] and there was no strong interaction of 3-mPEA with HSA to conclude any binding, and the data could not generate the dissociation constant.

The MST results were further confirmed by a zeta sizer study, where the nanovesicles were incubated with HSA, and its impact on the size, PDI and ZP were investigated [65]. There was no significant impact ($P > .05$) of HSA on the nanovesicles before and after incubation (Table 3). This could be attributed to the 3-mPEA nanovesicles shell being composed of mPEG 5000, which is considered not to bind with HAS [107], which could suggest long circulating and offer stealth abilities to the nanovesicles [108,109]. These studies indicated that the 3-mPEA nanovesicles could be utilized to formulate a long circulating drug delivery system.

3.6. *In vitro* drug release

In vitro drug release pattern of the bare drug and the nanovesicles formulation are represented in Fig. 6. Release pattern after 1, 4 and 8 h bare VCM had cumulative release of 10.63%, 42.2% and 99.19% when compared to V-3-mPEA which was, 1.9%, 22.2%, and 37.8% respectively. After 24 and 48 h cumulative drug release from the vesicles was 58.5 and 65.8% respectively. The initial faster release could have been governed by diffusion, while later slower release phase after 8 h might have been due to polymer erosion. The VCM release from the V-3-mPEA nanovesicles showed a slower drug release profile from the formulation

when compared to the bare drug. This slower release of the drug from the V-3-mPEA nanovesicles could be beneficial as it could prolong exposure of bacteria to the lethal dose of the drug and sustained antibacterial activity also could improve patients' compliance which could translate to reduced frequency of administration.

The release kinetics of VCM from the 3-mPEA nanovesicles was performed using different models (Table 4). Weibull model having shown a correlation coefficient of 0.9947 and mean square error of 2.14 was considered as the best fitting model for the release of VCM from nanovesicles. Korsmeyer-Peppas drug release n' exponent was 0.494 (Table 4), this indicated that non-Fickian diffusion was the responsible mechanism for the release of the drug from the nanovesicles. Basing on the n' exponent value more than one mechanism might have been involved [110,111] in the release of the drug from the nanovesicles. Apart from diffusion, erosion and degradation might have played a role, as the 3-mPEA dendritic star polymer arms were coined from mPEG-*b*-PCL, which is a biodegradable synthetic polymer [112].

The mean dissolution time (MDT90%) for the release of VCM from the drug solution and V-3-mPEA nanovesicles was calculated [113] and found to be 4.31 h and 11.29 h respectively from the nanovesicles and bare VCM respectively. These values further indicated that the rate at which the drug was released from the 3-mPEA nanovesicle was at a slower rate when compared to bare VCM. This value indicates that the release of the drug from the nanovesicles was sustained over an extended period of time and could translate into desired patient outcomes and improved patient compliance.

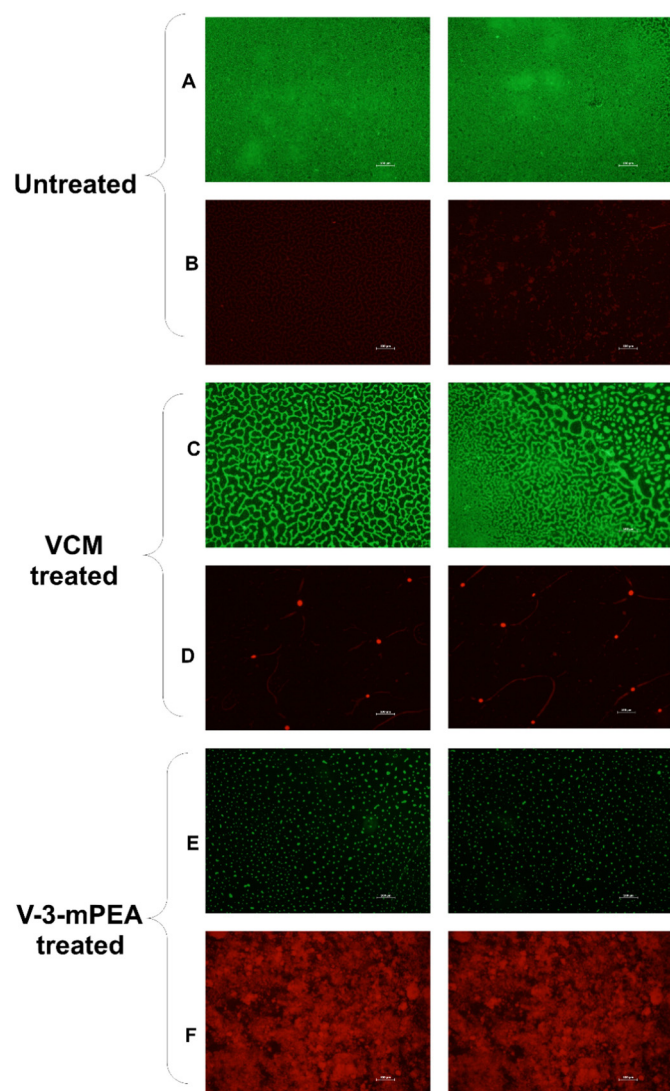


Fig. 8. Fluorescence microscopy micrographs of the untreated, VCM treated and V-3-mPEA treated MRSA biofilms. A, and B untreated biofilm stained with Syto9 and PI respectively, B, C, D, E, F. VCM and V-3-mPEA treated biofilm stained with Syto9 and PI respectively (scale bar = 100 μm).

3.7. Antibacterial activity

3.7.1. Determination of the MIC

The broth dilution method was employed to determine the MIC values of the bare VCM and V-3-mPEA against *S. aureus* and MRSA. After 24 h of the study the MIC for VCM against *S. aureus* and MRSA was 3.9 $\mu\text{g}/\text{mL}$ and 15.65 $\mu\text{g}/\text{mL}$ respectively, whereas for V-3-mPEA nanovesicles against the same set of bacteria it was found to be 0.488 and 0.988 $\mu\text{g}/\text{mL}$ respectively (Table 5). This was a 7- and 16-fold decrease in MIC against SA and MRSA after delivery of VCM via 3-mPEA nanovesicles (Table 3). Interestingly the activity continued up to 120 h, while the VCM was inactive after 24 h. The thicker cell walls of the MRSA could have been the reason for reduced activity towards MRSA than SA as more VCM molecules are needed to saturate the increased peptidoglycan layers before reaching the target site [114]. General enhanced activity of the 3-mPEA nanovesicles when compared to the bare VCM can be attributed to the small size of the nanovesicles, as literature shows that smaller particles sizes have a high surface area to volume ratio, which allows better distribution and adsorption to the bacterial surface [115,116]. Furthermore, the slow release of the drug concentration for a relatively long time could also have been a

contributing factor [117]. The lower MICs and prolonged activity attributed to the V-3-mPEA nanovesicles could result in a decrease in the effective dose of treatment and less frequency of administration of VCM. This could go a long way in reducing dose-dependent nephrotoxicity [118], side effects and improved patients' compliance associated with vancomycin therapy without compromising their therapeutic outcomes. These findings highlight 3-mPEA star polymer as an efficient biomaterial for the delivery of VCM against SA and MRSA infections.

3.7.2. Bacterial membrane disruption

The effect of V-3-mPEA membrane disruption on MRSA was determined by incubating the bacteria with V-3-mPEA for 4 h. At initial stages of incubation, intact cocci can be seen (Fig. 7A). After 1 h, perforations on the bacteria membrane can be witnessed (Fig. 7B and C). Following 4 h of treatment, it can be seen that bacteria had lost all the membrane and intact vesicles can be seen entering and surrounding the bacteria (Fig. 7E and F). Association of V-3-mPEA with the bacteria seems to be facilitated by the smaller sizes of the nanovesicles to cause maximum effective damage. This result supported the MIC data which showed effective killing of bacteria by V-3-mPEA and highlighted the plausible mechanism of action of V-3-mPEA.

3.7.3. Inhibition of MRSA biofilm

The ability of V-3-mPEA to eradicate biofilms was investigated. A 4 day fully mature biofilm of MRSA inhibition by V-3-mPEA and VCM was determined by fluorescence microscopy. The biofilms were grown on the cover slips and were stained with Syto9 and propidium iodide (PI) solution containing 30 μL in 1 mL of distilled water for 30 mins in darkness, after which the dyes were washed off and cover slips were inverted on the glass slides (Fig. 8A). Untreated biofilms showed high intensity of Syto9 fluorescence emanating from the whole of the cover slip. As Syto is a cell permeant dye, the high intensity is clearly due to the intact membrane of the high number of cells on the cover slip [119,120]. When untreated cells were stained with the non-permeating dye PI, there was no intensity of the dye fluorescence as PI couldn't penetrate alive cells with an intact cell membrane (Fig. 8B). Treatment of the biofilm with bare VCM and stained with Syto9 and PI, showed a slight decrease in the biofilm when compared to the untreated (Fig. 8C) with some PI emission fluorescence emanating from the slide indicating some penetration of VCM in the biofilm and bacterial killing (Fig. 8D). Unlike the previous treatments, when the biofilms were treated with V-3-mPEA nanovesicles there was a greater reduction of the biofilms. This was indicated by the reduction in the fluorescence intensity of Syto9 when compared to bare VCM treated and untreated biofilms, indicating fewer number of cells alive on the glass slide (Fig. 8E). Interestingly there was very high intensity of PI emission fluorescence emanating from the slides of biofilms treated with the drug loaded nanovesicles. Despite PI being a non-cell permeant dye [119,120], the high emission observed indicates that treatment with V-3-mPEA resulted in destruction of the biofilm and cell membrane of MRSA leading to high penetration of the PI which bound to DNA. Higher intensity therefore confirmed high killing percentage of V-3-mPEA compared to bare VCM that had a minimum effect on the biofilms. These results indicate that V-3-mPEA could be employed to also eliminate biofilms which cause detrimental health effects associated with surgical implants, chronic infections, urogenital infections, cystic fibrosis and dental infections.

3.7.4. Flow cytometry bacterial cell viability

The rapid cell viability of the MRSA cells was determined using a flow cytometry method [75]. MRSA bacterial cells were incubated with bare VCM and V-3-mPEA mediums for 24 h. The process of incubating bacteria in the presence of antibiotics induces changes in the bacteria morphology and cells cycle, which can be measured using special dyes [121]. The PI fluorescent dye, which is not cell wall permeating, is generally used to detect dead cells in the population, while Syto9 a non-

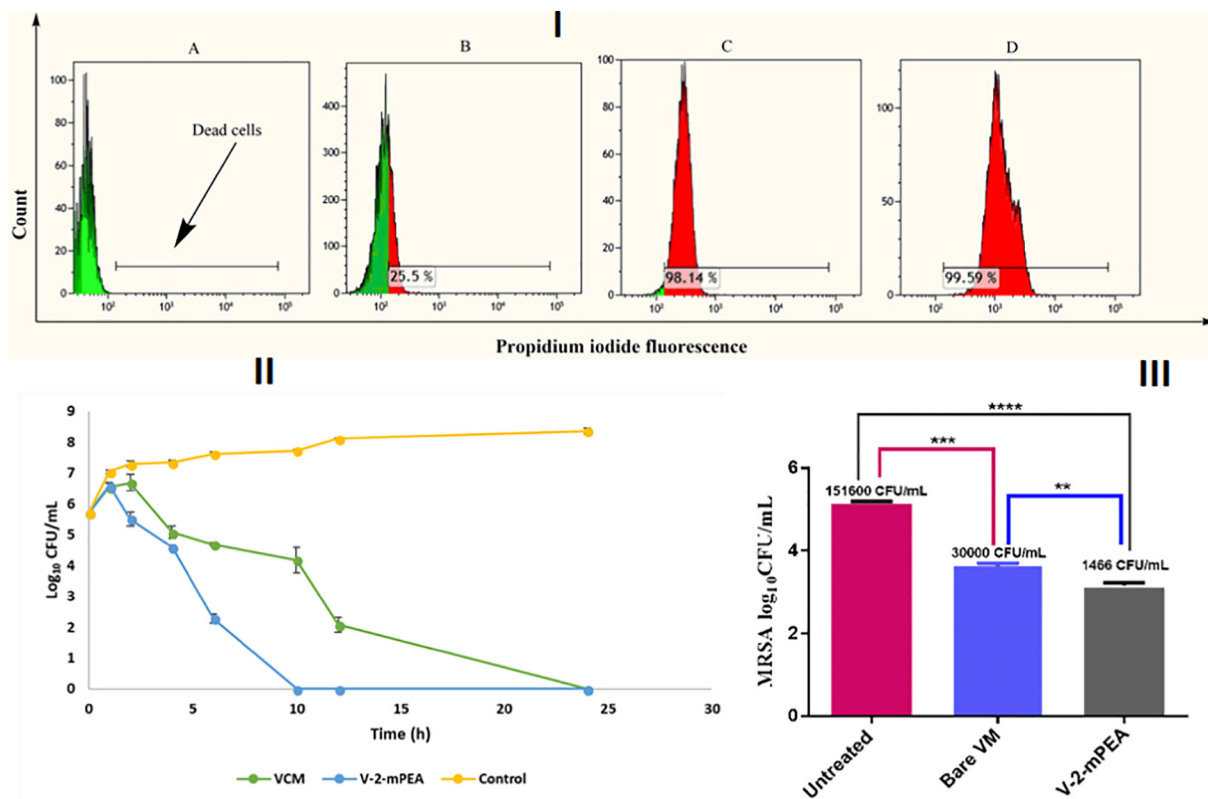


Fig. 9. (I). cell counts vs PI uptake histogram where A, represents untreated MRSA (live cells); B, C and D represents percentage of dead cells in the population after incubation with VCM at its MIC (3.9 $\mu\text{g}/\text{mL}$) and V-3-mPEA at its MIC (0.488 $\mu\text{g}/\text{mL}$) respectively; (II) the killing kinetics of MRSA exposed to $5\times$ MIC of 3-mPEA nanovesicles, VCM and sterile water (control); (III) evaluation of MRSA burden post 48 h treatment. Data represented as mean \pm SD ($n = 3$). **denotes significant difference for V-3-mPEA versus bare VCM. ***denotes significant difference between untreated versus bare VCM and ****denotes significant difference between bare VCM free base and V-3-mPEA;

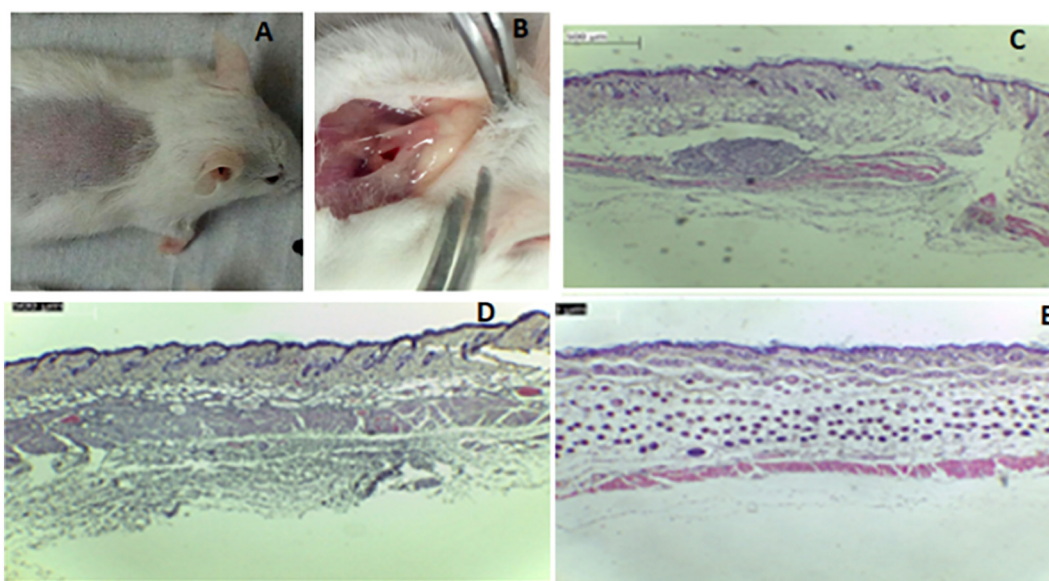


Fig. 10. Histo-morphological evaluation post 48 h treatment- A) V-3-mPEA nanovesicles treatment, B) untreated group showing exudating pus, Light Microscopy (LM) micrographs of the control and the treated skin samples stained with H&E; (X40) (C) Untreated (MRSA and Saline); (D) Bare VCM; (E) V-3-mPEA nanovesicles (scale bar = 500 μm).

selective cell wall permeant dye was used for alive cells [119,120]. Data captured from flow cytometry were analyzed using Kaluza-1.5.20 (Beckman Coulter USA) flow cytometer software (Fig. 9I). Two gates were created representing viable cells (green) and dead cells (red) in the population. VCM's mode of action compromises the integrity of the

cell wall, which enhances the PI permeability and uptake and leads to intercalation with the DNA that results in a shift in PI fluorescence, this being an indication of bacterial cell death. After treating the MRSA cells with both bare VCM and V-3-mPEA, there was a shift in PI fluorescence (Fig. 9I B, C and D). The bare VCM (Fig. 9IC) and V-3-mPEA (Fig. 9ID)

at concentration of 0.488 and 3.9 µg/mL respectively had $98.5 \pm 1.49\%$ and $99.59 \pm 0.55\%$ dead MRSA cells in the population. However, by treating the MRSA cells with bare VCM at the same concentration as the concentration of VCM in the drug-loaded nanovesicles (0.488 µg/mL), there were only $25.5 \pm 2.6\%$ dead cells in the population ($P < .0001$). From these results it can be deduced that the activity of VCM encapsulated 3-mPEA was the same as that of bare VCM but at a 16-fold lower concentration. These results could translate to lowering the amount of the dose required for treatment with V-3-mPEA without compromising the therapeutic outcomes. Furthermore, such a dose reduction could also go a long way to reducing dose-dependent vancomycin toxicity, such as nephrotoxicity [122], these results confirming the superiority of V-3-mPEA as a nano antibiotic.

3.7.5. Bacterial killing kinetics

Fig. 9II presents the rates of microbial killing by VCM, and VCM loaded 3-mPEA nanovesicles when exposed to MRSA at 5 times MIC of each treatment over a 24 h incubation period at 37 °C. VM loaded 3-mPEA nanovesicles exhibited a rapid bactericidal effect, with a 3-log reduction (99.9% clearance) within 10 h in comparison to VCM which achieved its bactericidal effect within 24 h. The kill kinetics of vancomycin is similar to reports in the literature [77]. Noteworthy at 16 times lower concentration of VCM in the nanovesicles, they achieved faster killing rate (10h) when compared to the bare drug. This could translate to quick elimination of the bacteria in the body thus reducing the duration of treatment and the doses required to achieve successful therapy.

3.7.6. In vivo antibacterial activity

As a proof of concept, the antimicrobial activity and therapeutic efficacy of V-3-mPEA nanovesicles against MRSA infections were further assessed in a mouse skin infection model. The CFUs, from each treatment group were recovered and converted to \log_{10} CFU/mL as shown in Fig. 9III. One-way ANOVA test showed a statistically significant ($P < .0001$) reduction in the bacterial load of recovered bacteria in both V-3-mPEA and bare VCM treatment groups when compared to the untreated. The negative control (untreated), bare VCM and V-3-mPEA nanovesicles groups had the bacterial load (\log_{10} CFU/mL) of 5.18 ± 0.01 (151,733.33 CFU/mL), 4.48 ± 0.05 (30,000 CFU/mL) and 3.16 ± 0.07 (1466.7 CFU/mL) respectively. These findings established that the bare VCM and V-3-mPEA nanovesicles groups had a 20.5 ($P = .0002$) and 103.5-fold ($P < .0001$) reduction of bacterial load when compared to untreated group. Furthermore, comparison between V-3-mPEA and bare VCM groups showed a 5.06-fold reduction of CFUs in nanovesicles group ($P = .0045$). These findings demonstrated V-3-mPEA nanovesicles as an effective drug delivery system for vancomycin.

Visual observations of the skin during harvesting revealed the formation of pus at the infection site of the untreated groups, while the treatment groups did not show pus formation (Fig. 10 A and B). Microscopic morphological evaluations on the excised skin from the untreated, bare VCM and V-3-mPEA nanovesicles groups on the H&E stained slides revealed that the untreated skin samples displayed evidence of tissue inflammation and abscess formation (Fig. 10 C). Although the bare VCM treatment group (Fig. 10 D) displayed less degree of signs of swelling and abscess formation than the untreated group. However, comparatively, the V-3-mPEA group (Fig. 10 E) displayed no signs of abscess formation, with minimal signs of tissue inflammation. Large quantities of white blood cells (WBCs) at the infection site was observed in the untreated and bare VCM groups indicating a greater immune response due to the high amount of isolated CFUs (Fig. 9 III). The quantity of WBCs was minimal in the V-3-mPEA nanovesicles group (Fig. 10 E). These histomorphological findings correlated with the recovered CFU/mL (Fig. 9 III), which showed the skin samples (untreated and VCM treated groups) with the most number bacteria triggered higher degree of immune response that was

manifested with the highest degree of inflammation, abscess formation and presence of white blood cells present at the infection site. Due to the lowest number of isolated bacteria in the V-3-mPEA nanovesicles group (Fig. 9 III), minimal signs of inflammation and no abscess formation was observed. The histomorphological studies therefore confirm the antimicrobial advantage of the V-3-mPEA nanovesicles.

4. Conclusions

Generation one poly(ester-amine) dendrimer end groups were modified with mPEG-*b*-PCL linear polymer and evaluated for sustained delivery and enhanced activity of VCM. The hydrodynamic diameter of the nanovesicles was 52.48 ± 2.6 nm, as measured by the DLS and confirmed by the TEM. The nanovesicles exhibited a sustain release behavior of vancomycin over a period of 72 h. Studies performed with the MST and HSA binding showed that V-3-mPEA did not have any adsorption and binding affinity to the HSA, which indicated their potential for long systemic circulation. The *in vitro* antibacterial activity against the susceptible and resistance SA showed that V-3-mPEA had 8- and 16-fold greater activity when compared to the bare VCM. Further antibacterial studies using the flow cytometry method revealed that nanovesicles at MIC concentrations killed 99.5% of MRSA cells. Even at an 8-fold, lower concentrations of VCM in the nanovesicles compared to the bare VCM the nanovesicles were effective without compromising the efficacy of VCM. This was proof that the nanovesicles enhanced the activity of vancomycin. *In vivo* antibacterial test showed that V-3-mPEA had a 103 and 20-fold reduction in the MRSA load compared to the untreated and VCM treated mice respectively. These results indicated high efficacy of V-3-mPEA when compared to the bare drug. Findings of the study suggests promising development and translational potential of 3-mPEA and V-3-mPEA for use as a drug delivery vehicle and nanoantibiotic against bacterial infections respectively.

Acknowledgments

The authors acknowledge the University of KwaZulu-Natal (UKZN), UKZN Nanotechnology Platform, Medical Research Council and National Research Foundation of South Africa for financial support (Grant No. NRF Grant No. 87790 and 88453). The Microscopy and Microanalysis Unit, Biomedical Resource Unit, Department of Human Physiology and Sooraj Bajinath and Catalysis and Peptide Research Unit at UKZN and Department of Chemistry and Polymer Science at University of Stellenbosch are acknowledged for their technical assistance and CHPC Cape town for supercomputing resources.

Disclosure

The authors report no conflicts of interest in this work.

Appendix A. Supplementary data

Supplementary data to this article can be found online at <https://doi.org/10.1016/j.jconrel.2018.10.005>.

References

- [1] R. Gaynes, The Discovery of Penicillin—New Insights After More Than 75 Years of Clinical Use, *Emerg. Infect. Dis.* 23 (2017) 849.
- [2] K. Shakeeb Asrar, Guimaraes, Global shortage of penicillin: Reasons and consequences, *Al Jazeera*, US & Canada, 2017.
- [3] I. Roca, M. Akova, F. Baquero, J. Carlet, M. Cavaleri, S. Coenen, J. Cohen, D. Findlay, I. Gyssens, O.E. Heur, G. Kahlmeter, H. Kruse, R. Laxminarayan, E. Liébana, L. López-Cerero, A. MacGowan, M. Martins, J. Rodríguez-Baño, J.M. Rolain, C. Segovia, B. Sigauque, E. Taconelli, E. Wellington, J. Vila, The global threat of antimicrobial resistance: science for intervention, *New Microbes and New Infections* 6 (2015) 22–29.
- [4] K.H. Luepke, K.J. Suda, H. Boucher, R.L. Russo, M.W. Bonney, T.D. Hunt, J.F. Mohr, Past, Present, and Future of Antibacterial Economics: Increasing

- Bacterial Resistance, Limited Antibiotic Pipeline, and Societal Implications, *Pharmacotherapy* 37 (1) (2016) 71–84.
- [5] K. Outterson, New business models for sustainable antibiotics, Centre on Global Health Security Working Group Papers, Chatham House (The Royal Institute of International Affairs), Working Groups on Antimicrobial Resistance, Paper 1 (2014) 10–14.
- [6] K. Outterson, U. Gopinathan, C. Clift, A.D. So, C.M. Morel, J.-A. Røttingen, Delinking Investment in Antibiotic Research and Development from Sales Revenues: The Challenges of Transforming a Promising Idea into Reality, *PLoS Med.* 13 (2016) e1002043.
- [7] R. Rath, R. Gupta, M.A. Rath, Antimicrobial Resistance: A Global Threat, *Imperial J. Interdisc. Res.* 2 (2016) 130–134.
- [8] D.C. Kaur, S.S. Chate, Study of Antibiotic Resistance Pattern in Methicillin Resistant *Staphylococcus Aureus* with Special Reference to Newer Antibiotic, *J. Global Infect. Dis.* 7 (2015) 78–84.
- [9] M.S. Butler, M.A. Blaskovich, M.A. Cooper, Antibiotics in the clinical pipeline at the end of 2015, *J. Antibiotics* 3 (2016).
- [10] H.W. Boucher, J.S. Bakken, B.E. Murray, The United Nations and the Urgent Need for Coordinated Global Action in the Fight Against Antimicrobial Resistance, *Ann. Intern. Med.* 165 (2016) 812–813.
- [11] WHO, Antimicrobial resistance, Fact sheet, in: WHO (Ed.) Fact sheet N°194, Geneva, 2015.
- [12] WHO, Antimicrobial resistance: global report on surveillance 2014, WHO, 2014, p. 257.
- [13] A.J. Huh, Y.J. Kwon, “Nanoantibiotics”: a new paradigm for treating infectious diseases using nanomaterials in the antibiotics resistant era, *J. Control. Release* 156 (2011) 128–145.
- [14] C.A. Omolo, R.S. Kalhapse, N. Agrawal, S. Rambharose, C. Mocktar, T. Govender, Formulation and Molecular Dynamics Simulations of a Fusidic Acid Nanosuspension for Simultaneously Enhancing Solubility and Antibacterial Activity, *Mol. Pharm.* 15 (2018) 3512–3526.
- [15] K.A. Hamblin, S.J. Armstrong, K.B. Barnes, C. Davies, T. Laws, J.D. Blanchard, S.V. Harding, H.S. Atkins, Inhaled Liposomal Ciprofloxacin Protects against a Lethal Infection in a Murine Model of Pneumonic Plague, *Front. Microbiol.* 8 (2017) 91.
- [16] J.M. Caster, A.N. Patel, T. Zhang, A. Wang, Investigational nanomedicines in 2016: a review of nanotherapeutics currently undergoing clinical trials, *Wiley Interdisciplinary Rev.* 9 (2017) e1416.
- [17] M. BioPharma, MAT2501: LNC Formulation of Amikacin, in: *Matinas BioPharma*, 2017.
- [18] C. Ma, P. Pan, G. Shan, Y. Bao, M. Fujita, M. Maeda, Core-shell structure, biodegradation, and drug release behavior of poly (lactic acid)/poly (ethylene glycol) block copolymer micelles tuned by macromolecular stereostructure, *Langmuir* 31 (2015) 1527–1536.
- [19] Y. Lu, K. Park, Polymeric Micelles and Alternative Nanonized Delivery Vehicles for Poorly Soluble Drugs, *Int. J. Pharm.* 453 (2013) 198–214.
- [20] Y. Li, K. Xiao, W. Zhu, W. Deng, K.S. Lam, Stimuli-responsive cross-linked micelles for on-demand drug delivery against cancers, *Adv. Drug Deliv. Rev.* 66 (2014) 58–73.
- [21] Y.Q. Yang, B. Zhao, Z.D. Li, W.J. Lin, C.Y. Zhang, X.D. Guo, J.F. Wang, L.J. Zhang, pH-sensitive micelles self-assembled from multi-arm star triblock co-polymers poly (ε-caprolactone)-b-poly (2-(diethylamino) ethyl methacrylate)-b-poly (poly (ethylene glycol) methyl ether methacrylate) for controlled anticancer drug delivery, *Acta Biomater.* 9 (2013) 7679–7690.
- [22] E.R. Gillies, J.M. Fréchet, Dendrimers and dendritic polymers in drug delivery, *Drug Discov. Today* 10 (2005) 35–43.
- [23] K. Madaan, S. Kumar, N. Poonia, V. Lather, D. Pandita, Dendrimers in drug delivery and targeting: Drug-dendrimer interactions and toxicity issues, *J. Pharm. Bioallied Sci.* 6 (2014) 139–150.
- [24] S. Mignani, J. Rodrigues, H. Tomas, R. Roy, X. Shi, J.-P. Majoral, Bench-to-bedside translation of dendrimers: Reality or utopia? A concise analysis, *Adv. Drug Deliv. Rev.* (2017), <https://www.sciencedirect.com/science/article/pii/S0169409X17302697> (In Press).
- [25] S.J. Guillaudeu, M.E. Fox, Y.M. Haidar, E.E. Dy, F.C. Szoka, J.M. Fréchet, PEGylated dendrimers with core functionality for biological applications, *Bioconjug. Chem.* 19 (2008) 461–469.
- [26] S.A. McNelles, S.D. Knight, N. Janzen, J.F. Valliant, A. Adronov, Synthesis, radiolabeling, and in vivo imaging of PEGylated high-generation polyester dendrimers, *Biomacromolecules* 16 (2015) 3033–3041.
- [27] X. Li, M. Takashima, E. Yuba, A. Harada, K. Kono, PEGylated PAMAM dendrimer-doxorubicin conjugate-hybridized gold nanorod for combined photothermal-chemotherapy, *Biomaterials* 35 (2014) 6576–6584.
- [28] S. Aryal, M. Prabhakaran, S. Pilla, S. Gong, Biodegradable and biocompatible multi-arm star amphiphilic block copolymer as a carrier for hydrophobic drug delivery, *Int. J. Biol. Macromol.* 44 (2009) 346–352.
- [29] Y.-Y. Jiang, G.-T. Tang, L.-H. Zhang, S.-Y. Kong, S.-J. Zhu, Y.-Y. Pei, PEGylated PAMAM dendrimers as a potential drug delivery carrier: in vitro and in vivo comparative evaluation of covalently conjugated drug and noncovalent drug inclusion complex, *J. Drug Target.* 18 (2010) 389–403.
- [30] W. Xiao, J. Luo, T. Jain, J.W. Riggs, H.P. Tseng, P.T. Henderson, S.R. Cherry, D. Rowland, K.S. Lam, Biodistribution and pharmacokinetics of a telodendrimer micellar paclitaxel nanoformulation in a mouse xenograft model of ovarian cancer, *Int. J. Nanomedicine* 7 (2012) 1587.
- [31] Y. Zhang, C. Xiao, M. Li, J. Ding, C. Yang, X. Zhuang, X. Chen, Co-delivery of doxorubicin and paclitaxel with linear-dendritic block copolymer for enhanced anti-cancer efficacy, *SCIENCE CHINA Chem.* 57 (2014) 624–632.
- [32] H. Yang, J.J. Morris, S.T. Lopina, Polyethylene glycol-polyamidoamine dendritic micelle as solubility enhancer and the effect of the length of polyethylene glycol arms on the solubility of pyrene in water, *J. Colloid Interface Sci.* 273 (2004) 148–154.
- [33] Y. Wang, G. Qi, J. He, Unimolecular Micelles from Layered Amphiphilic Dendrimer-Like Block Copolymers, *ACS Macro Lett.* 5 (2016) 547–551.
- [34] J. Del Barrio, L. Oriol, C. Sánchez, J.L. Serrano, A.L. Di Cicco, P. Keller, M.-H. Li, Self-assembly of linear–dendritic diblock copolymers: from nanofibers to polymersomes, *J. Am. Chem. Soc.* 132 (2010) 3762–3769.
- [35] W. Jiang, Y. Zhou, D. Yan, Hyperbranched polymer vesicles: from self-assembly, characterization, mechanisms, and properties to applications, *Chem. Soc. Rev.* 44 (2015) 3874–3889.
- [36] Y. Zhou, D. Yan, Supramolecular Self-Assembly of Giant Polymer Vesicles with Controlled Sizes, *Angew. Chem. Int. Ed.* 43 (2004) 4896–4899.
- [37] C.G. Palivan, R. Goers, A. Najer, X. Zhang, A. Car, W. Meier, Bioinspired polymer vesicles and membranes for biological and medical applications, *Chem. Soc. Rev.* 45 (2016) 377–411.
- [38] Y. Wang, B. Li, H. Jin, Y. Zhou, Z. Lu, D. Yan, Dissipative Particle Dynamics Simulation Study on Vesicles Self-Assembled from Amphiphilic Hyperbranched Multiarm Copolymers, *Chemistry–An Asian J.* 9 (2014) 2281–2288.
- [39] M.T. Morgan, M.A. Carnahan, C.E. Immoos, A.A. Ribeiro, S. Finkelstein, S.J. Lee, M.W. Grinstaff, Dendritic molecular capsules for hydrophobic compounds, *J. Am. Chem. Soc.* 125 (2003) 15485–15489.
- [40] D. Soto-Castro, J.A. Cruz-Morales, M.T.R. Apan, P. Guadarrama, Synthesis of Non-Cytotoxic Poly (Ester-Amine) Dendrimers as Potential Solubility Enhancers for Drugs: Methotrexate as a Case Study, *Molecules* 15 (2010) 8082–8097.
- [41] J.D.A.K. Twibanire, T.B. Grindley, Polyester dendrimers, *Polymer* 4 (2012) 794–879.
- [42] J.D.A. Twibanire, T.B. Grindley, Polyester Dendrimers: Smart Carriers for Drug Delivery, *Polymer* 6 (2014) 179.
- [43] K. Jain, P. Kesharwani, U. Gupta, N.K. Jain, Dendrimer toxicity: Let's meet the challenge, *Int. J. Pharm.* 394 (2010) 122–142.
- [44] H. Pungkhom, N. Swatdipakdi, M. Theerasilp, S. Karnkla, M. Chittchang, P. Ploypradith, N. Nasongkla, PEG-b-PCL and PEG-b-PLA polymeric micelles as nanocarriers for lamellarin N delivery, *Engineering in Medicine and Biology Society, EMBC, 2011 Annual International Conference of the IEEE, IEEE, 2011*, pp. 3245–3248.
- [45] P. Dineshkumar, T. Panneerselvam, K. Deepthi Brundavani, K. Selvaraj, P. Vijayaraj Kumar, Formulation of Rifampicin Loaded PEGylated 5.0 G EDA-PAMAM Dendrimers as Effective Long-Duration Release Drug Carriers, *Current Drug Therapy* 12 (2017) 115–126.
- [46] M.A. Mintzer, E.L. Dane, G.A. O'Toole, M.W. Grinstaff, Exploiting dendrimer multivalency to combat emerging and re-emerging infectious diseases, *Mol. Pharm.* 9 (2011) 342–354.
- [47] C.A. Omolo, R.S. Kalhapse, M. Jadhav, S. Rambharose, C. Mocktar, V.M. Ndesendo, T. Govender, Pegylated oleic acid: A promising amphiphilic polymer for nano-antibiotic delivery, *Eur. J. Pharm. Biopharm.* 112 (2017) 96–108.
- [48] R.S. Kalhapse, D.R. Sikwal, S. Rambharose, C. Mocktar, S. Singh, L. Bester, J.K. Oh, J. Renukuntla, T. Govender, Enhancing targeted antibiotic therapy via pH responsive solid lipid nanoparticles from an acid cleavable lipid, *Nanomedicine* 13 (6) (2017) 2067–2077.
- [49] Z. Daman, S. Ostad, M. Amini, K. Gilani, Preparation, optimization and in vitro characterization of stearyl-gemcitabine polymeric micelles: A comparison with its self-assembled nanoparticles, *Int. J. Pharm.* 468 (2014) 142–151.
- [50] Y. Wang, J. Fang, D. Cheng, Y. Wang, X. Shuai, A pH-sensitive micelle for code-livery of siRNA and doxorubicin to hepatoma cells, *Polymer* 55 (2014) 3217–3226.
- [51] K. Muppidi, A. Pumerantz, G. Betageri, J. Wang, Development and validation of a rapid high-performance liquid chromatography method with UV detection for the determination of vancomycin in mouse plasma, *J. Chromat Separation Techniq* 4 (2013) 1–5.
- [52] K.R. Cousins, Computer review of ChemDraw Ultra 12.0, ACS Publications, 2011, p. 8388.
- [53] P. Mark, L. Nilsson, Structure and dynamics of the TIP3P, SPC, and SPC/E water models at 298 K, *J. Phys. Chem. A* 105 (2001) 9954–9960.
- [54] K. Vanommeslaeghe, E. Hatcher, C. Acharya, S. Kundu, S. Zhong, J. Shim, E. Darian, O. Guvench, P. Lopes, I. Vorobyov, CHARMM general force field: A force field for drug-like molecules compatible with the CHARMM all-atom additive biological force fields, *J. Comput. Chem.* 31 (2010) 671–690.
- [55] M. Bixon, S. Lifson, Potential functions and conformations in cycloalkanes, *Tetrahedron* 23 (1967) 769–784.
- [56] M. Parrinello, A. Rahman, Polymorphic transitions in single crystals: A new molecular dynamics method, *J. Appl. Phys.* 52 (1981) 7182–7190.
- [57] T. Darden, D. York, L. Pedersen, Particle mesh Ewald: An N² log (N) method for Ewald sums in large systems, *J. Chem. Phys.* 98 (1993) 10089–10092.
- [58] M.J. Abraham, T. Murtola, R. Schulz, S. Páll, J.C. Smith, B. Hess, E. Lindahl, GROMACS: High performance molecular simulations through multi-level parallelism from laptops to supercomputers, *SoftwareX* 1 (2015) 19–25.
- [59] J. Barnoud, G. Rossi, L. Monticelli, Lipid membranes as solvents for carbon nanoparticles, *Phys. Rev. Lett.* 112 (2014) 068102.
- [60] R. Kumari, R. Kumar, O.S.D.D. Consortium, A. Lynn, g_mmpbsa A GROMACS tool for high-throughput MM-PBSA calculations, *J. Chem. Inf. Model.* 54 (2014) 1951–1962.
- [61] N. Agrawal, A.A. Skelton, Binding of 12-crown-4 with Alzheimer's Aβ40 and Aβ42

- monomers and its effect on their conformation: insight from molecular dynamics simulations, *Mol. Pharm.* 15 (2017) 289–299.
- [62] N. Agrawal, A.A. Skelton, 12-Crown-4 Ether Disrupts the Patient Brain-Derived Amyloid- β -Fibril Trimer: Insight from All-Atom Molecular Dynamics Simulations, *ACS Chem. Neurosci.* 7 (2016) 1433–1441.
- [63] Q.-S. Liu, R. Deng, Q.-F. Yan, L. Cheng, Y. Luo, K. Li, X. Yin, X. Qin, Novel Beta-Tubulin-Immobilized Nanoparticles Affinity Material for Screening β -Tubulin Inhibitors from a Complex Mixture, *ACS Appl. Mater. Interfaces* 9 (2017) 5725–5732.
- [64] S. Parveen, S.K. Sahoo, Corrigendum to Long circulating chitosan/PEG blended PLGA nanoparticle for tumor drug delivery, *Eur. J. Pharmacol.* (2014) 372–383 186.
- [65] L. Thiele, J.E. Diederichs, R. Reszka, H.P. Merkle, E. Walter, Competitive adsorption of serum proteins at microparticles affects phagocytosis by dendritic cells, *Biomaterials* 24 (2003) 1409–1418.
- [66] X. Cheng, H. Yan, X. Jia, Z. Zhang, Preparation and in vivo/in vitro evaluation of formononetin phospholipid/vitamin E TPGS micelles, *J. Drug Target.* 24 (2016) 161–168.
- [67] S.J. Sonawane, R.S. Kalhapure, S. Rambharose, C. Mocktar, S.B. Vepuri, M. Soliman, T. Govender, Ultra-small lipid-dendrimer hybrid nanoparticles as a promising strategy for antibiotic delivery: In vitro and in silico studies, *Int. J. Pharm.* 504 (2016) 1–10.
- [68] T. Loftsson, B. Ilievskaja, G.M. Asgrimsdottir, O.T. Ormarsson, E. Stefansson, Fatty acids from marine lipids: Biological activity, formulation and stability, *J. Drug Deliv. Sci. Technol.* 34 (2016) 71–75.
- [69] Z. Karami, S. Sadighian, K. Rostamizadeh, M. Parsa, S. Rezaee, Naproxen conjugated mPEG–PCL micelles for dual triggered drug delivery, *Mater. Sci. Eng. C* 61 (2016) 665–673.
- [70] Y. Zhang, M. Huo, J. Zhou, A. Zou, W. Li, C. Yao, S. Xie, DDSolver: an add-in program for modeling and comparison of drug dissolution profiles, *AAPS J.* 12 (2010) 263–271.
- [71] J.H. Jorgensen, J.D. Turnidge, Susceptibility test methods: dilution and disk diffusion methods, *Manual of Clinical Microbiology*, Eleventh Edition, American Society of Microbiology, 2015, pp. 1253–1273.
- [72] Methods for dilution antimicrobial susceptibility tests for bacteria that grow aerobically, in: C.A.L.S. Institute, C.A.L.S. Institute (Eds.), *Approved Standard—Ninth Edition*, CLSI, Pennsylvania 19087, USA, 2012, p. 63.
- [73] N. Chauhan, A.K. Tyagi, P. Kumar, A. Malik, Antibacterial potential of *Jatropha curcas* synthesized silver nanoparticles against food borne pathogens, *Front. Microbiol.* 7 (2016) 1748.
- [74] F. Berlutti, A. Frioni, T. Natalizi, F. Pantanella, P. Valenti, Influence of sub-inhibitory antibiotics and flow condition on *Staphylococcus aureus* ATCC 6538 biofilm development and biofilm growth rate: BioTimer assay as a study model, *J. Antibiot.* 67 (2014) 763.
- [75] N.M. O'Brien-Simpson, N. Pantarat, T.J. Attard, K.A. Walsh, E.C. Reynolds, A Rapid and Quantitative flow cytometry method for the analysis of membrane disruptive antimicrobial activity, *PLoS One* 11 (2016) e0151694.
- [76] S. Renggli, W. Keck, U. Jenal, D. Ritz, Role of autofluorescence in flow cytometric analysis of *Escherichia coli* treated with bactericidal antibiotics, *J. Bacteriol.* 195 (2013) 4067–4073.
- [77] M.F. Mohamed, M.I. Hamed, A. Panitch, M.N. Seleem, Targeting methicillin-resistant *Staphylococcus aureus* with short salt-resistant synthetic peptides, *Antimicrob. Agents Chemother.* 58 (2014) 4113–4122.
- [78] E. Kugelberg, T. Norström, T.K. Petersen, T. Duvold, D.I. Andersson, D. Hughes, Establishment of a superficial skin infection model in mice by using *Staphylococcus aureus* and *Streptococcus pyogenes*, *Antimicrob. Agents Chemother.* 49 (2005) 3435–3441.
- [79] R.S. Kalhapure, M. Jadhav, S. Rambharose, C. Mocktar, S. Singh, J. Renukuntla, T. Govender, pH-responsive chitosan nanoparticles from a novel twin-chain anionic amphiphile for controlled and targeted delivery of vancomycin, *Colloids Surf. B: Biointerfaces* 158 (2017) 650–657.
- [80] W. Zhang, J. He, Z. Liu, P. Ni, X. Zhu, Biocompatible and pH-responsive triblock copolymer mPEG-b-PCL-b-PDMAEMA: Synthesis, self-assembly, and application, *J. Polym. Sci. A Polym. Chem.* 48 (2010) 1079–1091.
- [81] X. Shuai, T. Merdan, F. Unger, M. Wittmar, T. Kissel, Novel biodegradable ternary copolymers hy-PEI-g-PCL-b-PEG: synthesis, characterization, and potential as efficient nonviral gene delivery vectors, *Macromolecules* 36 (2003) 5751–5759.
- [82] S. Svenson, The dendrimer paradox - high medical expectations but poor clinical translation, *Chem. Soc. Rev.* 44 (2015) 4131–4144.
- [83] P.I. Nagy, Competing Intramolecular vs. Intermolecular Hydrogen Bonds in Solution, *Int. J. Mol. Sci.* 15 (2014) 19562–19633.
- [84] H. Nosrati, R. Adinehvand, H.K. Manjili, K. Rostamizadeh, H. Danafar, Synthesis, characterization, and kinetic release study of methotrexate loaded mPEG–PCL polymersomes for inhibition of MCF-7 breast cancer cell line, *Pharm. Dev. Technol.* (2018) 1–10.
- [85] J. Šebestík, M. Reiniš, J. Ježek, Biocompatibility and toxicity of dendrimers, in: J. Šebestík, M. Reiniš, J. Ježek (Eds.), *Biomedical Applications of Peptide-, Glyco- and Glycopeptide Dendrimers, and Analogous Dendrimeric Structures*, Springer Vienna, Vienna, 2012, pp. 111–114.
- [86] R.B. Arote, S.-K. Hwang, M.-K. Yoo, D. Jere, H.-L. Jiang, Y.-K. Kim, Y.-J. Choi, J.-W. Nah, M.-H. Cho, C.-S. Cho, Biodegradable poly(ester amine) based on glycerol dimethacrylate and polyethylenimine as a gene carrier, *J. Gene Med.* 10 (2008) 1223–1235.
- [87] S.K. Prajapati, S.D. Maurya, M.K. Das, V.K. Tilak, K.K. Verma, R.C. Dhakar, Dendrimers in drug delivery, diagnosis and therapy: basics and potential applications, *J. Drug Deliv. Therap.* 6 (2016) 67–92.
- [88] T.L. Riss, R.A. Moravec, A.L. Niles, S. Duellman, H.A. Benink, T.J. Worzella, L. Minor, *Cell Viability Assays*, National Institutes of Health, Bethesda, Maryland, 2016.
- [89] R. Hamid, Y. Rotshteyn, L. Rabadi, R. Parikh, P. Bullock, Comparison of alamar blue and MTT assays for high through-put screening, *Toxicol. in Vitro* 18 (2004) 703–710.
- [90] T. Mosmann, Rapid colorimetric assay for cellular growth and survival: application to proliferation and cytotoxicity assays, *J. Immunol. Methods* 65 (1983) 55–63.
- [91] H. Cui, Z. Chen, S. Zhong, K.L. Wooley, D.J. Pochan, Block copolymer assembly via kinetic control, *Science* 317 (2007) 647–650.
- [92] S. Zhang, Y. Zhao, Rapid release of entrapped contents from multi-functionalizable, surface cross-linked micelles upon different stimulation, *J. Am. Chem. Soc.* 132 (2010) 10642–10644.
- [93] S. Nummelin, M. Selin, S. Legrand, J. Ropponen, J. Seitsonen, A. Nykanen, J. Koivisto, J. Hirvonen, M.A. Kostiaainen, L.M. Bimbo, Modular synthesis of self-assembling Janus-dendrimers and facile preparation of drug-loaded dendrimersomes, *Nanoscale* 9 (2017) 7189–7198.
- [94] I.N. Kurniasih, J. Keilitz, R. Haag, Dendritic nanocarriers based on hyperbranched polymers, *Chem. Soc. Rev.* 44 (2015) 4145–4164.
- [95] H. Danafar, Preparation and characterization of PCL-PEG-PCL polymersomes for delivery of clavulanic acid, *Cogent Med.* 3 (2016) 1235245.
- [96] T.H. Hoang Thi, F. Chai, S. Leprêtre, N. Blanchemain, B. Martel, F. Siepmann, H.F. Hildebrand, J. Siepmann, M.P. Flament, Bone implants modified with cyclodextrin: Study of drug release in bulk fluid and into agarose gel, *Int. J. Pharm.* 400 (2010) 74–85.
- [97] C.G. Pupe, M. Villardi, C.R. Rodrigues, H.V.A. Rocha, L.C. Maia, V.P. de Sousa, L.M. Cabral, Preparation and evaluation of antimicrobial activity of nanosystems for the control of oral pathogens *Streptococcus mutans* and *Candida albicans*, *Int. J. Nanomedicine* 6 (2011) 2581–2590.
- [98] S.J. Marrink, A.E. Mark, Molecular Dynamics Simulation of the Formation, Structure, and Dynamics of Small Phospholipid Vesicles, *J. Am. Chem. Soc.* 125 (2003) 15233–15242.
- [99] Q. Zhang, J. Lin, L. Wang, Z. Xu, Theoretical modeling and simulations of self-assembly of copolymers in solution, *Prog. Polym. Sci.* 75 (2017) 1–30.
- [100] P. He, X. Li, D. Kou, M. Deng, H. Liang, Complex micelles from the self-assembly of amphiphilic triblock copolymers in selective solvents, *J. Chem. Phys.* 132 (2010) 204905.
- [101] W. Kong, B. Li, Q. Jin, D. Ding, A.-C. Shi, Complex micelles from self-assembly of ABA triblock copolymers in B-selective solvents, *Langmuir* 26 (2009) 4226–4232.
- [102] P. Baaske, C. Wienken, M. Willemsen, D. Braun, S. Duhr, Protein-binding assays in biological liquids using microscale thermophoresis, *J. Biomolecular Techniques* 22 (2011) S55.
- [103] C.J. Wienken, P. Baaske, U. Rothbauer, D. Braun, S. Duhr, Protein-binding assays in biological liquids using microscale thermophoresis, *Nat. Commun.* 1 (2010) ncomms1093.
- [104] M. Jerabek-Willemsen, T. André, R. Wanner, H.M. Roth, S. Duhr, P. Baaske, D. Breitsprecher, MicroScale Thermophoresis: Interaction analysis and beyond, *J. Mol. Struct.* 1077 (2014) 101–113.
- [105] J.M. Rainard, G.C. Pandarakalam, S.P. McElroy, Using microscale thermophoresis to characterize hits from high-throughput screening: A European lead factory perspective, *SLAS Discovery* 23 (2018) 225–241.
- [106] H. Du, P. Chandaroy, S.W. Hui, Grafted poly(ethylene glycol) on lipid surfaces inhibits protein adsorption and cell adhesion, *Biochim. Biophys. Acta Biomembr.* 1326 (1997) 236–248.
- [107] D.E. Owens, N.A. Peppas, Opsonization, biodistribution, and pharmacokinetics of polymeric nanoparticles, *Int. J. Pharm.* 307 (2006) 93–102.
- [108] T. Verrecchia, G. Spenlehauer, D. Bazile, A. Murry-Brelrier, Y. Archimbaud, M. Veillard, Non-stealth (poly(lactic acid/albumin)) and stealth (poly(lactic acid-polyethylene glycol)) nanoparticles as injectable drug carriers, *J. Control. Release* 36 (1995) 49–61.
- [109] A. Gabizon, R. Catane, B. Uzieli, B. Kaufman, T. Safra, R. Cohen, F. Martin, A. Huang, Y. Barenholz, Prolonged circulation time and enhanced accumulation in malignant exudates of doxorubicin encapsulated in polyethylene-glycol coated liposomes, *Cancer Res.* 54 (1994) 987–992.
- [110] P. Costa, J.M.S. Lobo, Modeling and comparison of dissolution profiles, *Eur. J. Pharm. Sci.* 13 (2001) 123–133.
- [111] L. Tao, J.W. Chan, K.E. Uhrich, Drug loading and release kinetics in polymeric micelles: Comparing dynamic versus unimolecular sugar-based micelles for controlled release, *J. Bioact. Compat. Polym.* 31 (2015) 227–241.
- [112] W.B. Liechty, D.R. Kryscio, B.V. Slaughter, N.A. Peppas, Polymers for drug delivery systems, *Annual Review of Chemical and Biomolecular Engineering* 1 (2010) 149.
- [113] Y. Weerapol, S. Limmatvapirat, C. Jansakul, H. Takeuchi, P. Sriamornsak, Enhanced dissolution and oral bioavailability of nifedipine by spontaneous emulsifying powders: effect of solid carriers and dietary state, *Eur. J. Pharm. Biopharm.* 91 (2015) 25–34.
- [114] K. Hiramatsu, Vancomycin-resistant *Staphylococcus aureus*: a new model of antibiotic resistance, *Lancet Infect. Dis.* 1 (2001) 147–155.
- [115] K.R. Raghupathi, R.T. Koodali, A.C. Manna, Size-Dependent Bacterial Growth Inhibition and Mechanism of Antibacterial Activity of Zinc Oxide Nanoparticles, *Langmuir* 27 (2011) 4020–4028.
- [116] A. Thill, O. Zeyons, O. Spalla, F. Chauvat, J. Rose, M. Auffan, A.M. Flank, Cytotoxicity of CeO₂ nanoparticles for *Escherichia coli*. Physico-chemical insight of the cytotoxicity mechanism, *Environ. Sci. Technol.* 40 (2006) 6151–6156.
- [117] M.-H. Xiong, Y. Bao, X.-Z. Yang, Y.-H. Zhu, J. Wang, Delivery of antibiotics with

- polymeric particles, *Adv. Drug Deliv. Rev.* 78 (2014) 63–76.
- [118] S. Van Hal, D.L. Paterson, T.P. Lodise, Systematic review and meta-analysis of vancomycin-induced nephrotoxicity associated with dosing schedules that maintain troughs between 15 and 20 milligrams per liter, *Antimicrob. Agents Chemother.* 57 (2013) 734–744.
- [119] M. Fittipaldi, A. Nocker, F. Codony, Progress in understanding preferential detection of live cells using viability dyes in combination with DNA amplification, *J. Microbiol. Methods* 91 (2012) 276–289.
- [120] M. Engel, Y. Hadar, S. Belkin, X. Lu, M. Elimelech, B. Chefetz, Bacterial inactivation by a carbon nanotube-iron oxide nanocomposite: a mechanistic study using *E. coli* mutants, *Environ. Sci.* 5 (2018) 372–380.
- [121] Ž. Maglica, E. Özdemir, J.D. McKinney, Single-cell tracking reveals antibiotic-induced changes in mycobacterial energy metabolism, *MBio* 6 (2015) e02236–02214.
- [122] P.R. Ingram, D.C. Lye, P.A. Tambyah, W.P. Goh, V.H. Tam, D.A. Fisher, Risk factors for nephrotoxicity associated with continuous vancomycin infusion in outpatient parenteral antibiotic therapy, *J. Antimicrob. Chemother.* 62 (2008) 168–171.

Formulation and Molecular Dynamics Simulations of a Fusidic Acid Nanosuspension for Simultaneously Enhancing Solubility and Antibacterial Activity

Calvin A. Omolo,[†] Rahul S. Kalhapure,^{*,†,‡} Nikhil Agrawal,[†] Sanjeev Rambharose,^{†,§} Chunderika Mocktar,[†] and Thirumala Govender^{*,†}

[†]Discipline of Pharmaceutical Sciences, College of Health Sciences, University of KwaZulu-Natal, Private Bag, X54001 Durban, South Africa

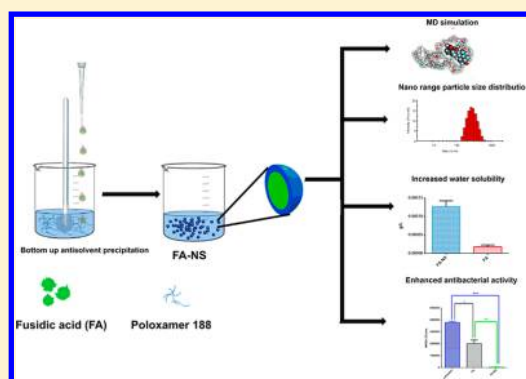
[‡]School of Pharmacy, The University of Texas at El Paso, 500 W. University Avenue, El Paso, Texas 79968, United States

[§]Division of Emergency Medicine, Department of Surgery, University of Cape Town, Cape Town 7700, South Africa

Supporting Information

ABSTRACT: The aim of the present study was to formulate a nanosuspension (FA-NS) of fusidic acid (FA) to enhance its aqueous solubility and antibacterial activity. The nanosuspension was characterized using various *in vitro*, *in silico*, and *in vivo* techniques. The size, polydispersity index, and zeta potential of the optimized FA-NS were 265 ± 2.25 nm, 0.158 ± 0.026 , and -16.9 ± 0.794 mV, respectively. The molecular dynamics simulation of FA and Poloxamer-188 showed an interaction and binding energy of -74.42 kJ/mol and -49.764 ± 1.298 kJ/mol, respectively, with van der Waals interactions playing a major role in the spontaneous binding. There was an 8-fold increase in the solubility of FA in a nanosuspension compared to the bare drug. The MTT assays showed a cell viability of 75–100% confirming the nontoxic nature of FA-NS. *In vitro* antibacterial activity revealed a 16- and 18-fold enhanced activity against *Staphylococcus aureus* (SA) and methicillin-resistant SA (MRSA), respectively, when compared to bare FA. Flowcytometry showed that MRSA cells treated with FA-NS had almost twice the percentage of dead bacteria in the population, despite having an 8-fold lower MIC in comparison to the bare drug. The *in vivo* skin-infected mice showed a 76-fold reduction in the MRSA load for the FA-NS treated group compared to that of the bare FA. These results show that the nanosuspension of antibiotics can enhance their solubility and antibacterial activity simultaneously.

KEYWORDS: nanosuspension, improved solubility, enhanced antibacterial activity, molecular dynamics, MRSA



INTRODUCTION

Despite the global spread of antimicrobial resistance, development and regulatory approval of new antibiotics has declined by 90% over the past 30 years due to the excessive cost of antibiotic research.^{1–3} Scientists are therefore focusing on enhancing the efficacy of old antibiotics through structural modifications⁴ and reformulating them into nano systems.⁵ It is widely reported in the literature that the nanonization of antibiotics enhances their activity^{5,6} through sustained release,^{7,8} thereby lowering the minimum inhibitory concentration (MIC)⁹ and targeting the infection sites.¹⁰ Thus, revisiting older antibiotics, such as fusidic acid (FA), is of importance to expand and protect the shrinking armamentarium available to clinicians to treat illnesses caused by resistant bacteria.

FA is a fusidane antibiotic that is derived from *Fusidium coccineum* and is a tetracyclic triterpenoid that is structurally related to cephalosporin P1 (Figure 1),¹¹ active against a wide range of bacteria,¹² has low toxicity, and a unique mechanism

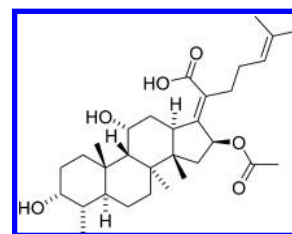


Figure 1. Chemical structure of FA. IUPAC name: (*E*)-2-((3*R*,4*S*,5*S*,8*S*,9*S*,10*S*,11*R*,13*R*,14*S*,16*S*)-16acetoxy-3,11-dihydroxy-4,8,10,14-tetramethylhexadecahydro-17*H*-cyclopenta[*a*]phenanthren-17-ylidene)-6-methylhept-5-enoic acid.

of action that lacks significant cross resistance to other antibacterial classes.¹³ An increase in the rate of global

Received: May 14, 2018

Revised: June 26, 2018

Accepted: June 28, 2018

Published: June 28, 2018

antimicrobial resistance has promulgated research interest in FA, even in markets where it lacked registration, for example the USA, and is in clinical trials for approval as a potentially valuable therapeutic option.^{13,14}

The high hydrophobicity of biopharmaceutical classification system class (BCS) II drugs, such as fusidic acid hemihydrate, partitions well through biological membranes, which can translate to high bioavailability.^{15–20} However, their bioabsorption process is rate-limited by their low rate of dissolution, which results in the low absorption for the oral dosage and the difficulty in formulating parenteral dosage forms,^{15–20} with poor aqueous solubility often resulting in poor bioavailability. A previously prepared FA suspension displayed only 22.5% bioavailability in pediatric patients following a 20 mg/kg dose.^{11,21} There is therefore a need for innovative strategies to improve solubility and bioavailability of FA.

To solve the problem of poor aqueous solubility of drugs, several techniques, such as micronization,^{15,22} solubilization,²³ and salt formation, have been explored,²⁴ although they have a number of limitations. The micronization technique results in very fine powders that affects the flow and wettability properties of the drug due to enhanced electrostatic forces.²⁵ Solubilization techniques require the formulation to be in liquid form, which has stability problems,²⁶ and salt formation is a complicated process, not being feasible for neutral compounds.²⁷ As much as they enhance solubility, sodium salts, like sodium fusidate, undergo precipitation in acid media, and their solubility also tends to vary with change in pH, which changes along the gastrointestinal tract.²⁸

Nanotechnology has been used to successfully deliver and improve the activity of a wide range of antibiotics.^{6,10,29,30} However, nanocarriers require the use of matrix material to encapsulate the compound, thereby reducing the maximum possible drug loading.³¹ Recent advancements in technologies for reducing particles sizes to nanoparticulate level have stimulated the formulation of nanosuspensions, these being solid dispersions of the drug in the submicron scale that are stabilized with surfactants, polymers, or both.³² Nanosuspensions offer increased dissolution rates, enhanced bioavailability, and activity, and complete entrapment of insoluble drugs by forming stable solid dispersions in their amorphous state.³³ As described by the Noyes–Whitney, and Kelvin and Ostwald–Freundlich equations, particle size reduction can lead to an increased dissolution rate and absorption due to greater surface area, amplified dissolution pressure, and increased adhesiveness to surfaces/cell membranes.^{34–36} Nanosuspensions have been successfully used to improve the activity of a wide range of anti-infectives, such as triclosan,³¹ ciprofloxacin,³⁷ itraconazole,³⁸ and miconazole.³⁹ To the best of our knowledge, there are no reports on FA nanosuspension as a drug delivery system. Despite FA being an effective agent against Gram-positive bacteria, there has been only one report for enhancing its solubility and activity using nanomicelles, which further involved the use of a newly synthesized material, i.e., polyester dendrimers.⁴⁰ A nano precipitation antisolvent technique, which was used to formulate nanosuspensions, has been shown to have advantages, such as little energy input, readily available machinery, and easy scale-up. It also allows for the preparation of nanosuspensions without the use of additional specialized materials, like the study reported by Sikwal et al.⁴⁰

Development of pharmaceutical dosage forms requires an understanding of the in vitro and in vivo performance of the dosage forms. In vitro studies have been shown to be convenient as they (a) reduce costs, (b) provide an opportunity to more directly assess product performance, and (c) offer benefits in terms of ethical considerations.⁴¹ As useful as in vitro assays are, they could fail to replicate the results in living conditions of an organism;⁴² as some studies have shown, in vivo results were better than in vitro outcomes. There have been also reports where studies have been effective in vitro, but when introduced into a living organism, they cause a cascade of events that have turned out to be toxic and incompatible with the animal.⁴³ Therefore, to increase the confidence in the effectiveness of pharmaceuticals, in vivo studies are usually recommended as the field is moving from the formulation-based to disease-focused research.

In addition to their physicochemical properties and in vitro and in vivo performance, understanding the underlying behavior and mechanism of the formation of drug delivery systems is essential for formulation optimization, and it requires an examination under spatial and sequential resolutions. Molecular dynamics (MD) simulations are being employed in drug delivery studies, as they can track the systems behavior changes across considerable spatial-sequential domain lengths with atomic precision and high resolutions.⁴⁴ Thus, providing a detailed molecular insight into the formation of nanosuspensions for drug delivery applications is of paramount importance. The MD simulations in this article have not been reported previously.

Thus, the aim of this study was to formulate a stable FA nanosuspension (FA-NS) by employing a bottom-up antisolvent precipitation technique and characterizing it with various in vitro, MD simulations, and in vivo studies. We envisaged that the formulated nanosuspension would enhance aqueous solubility and antibacterial activity of FA against *S. aureus* and MRSA.

■ MATERIALS AND METHODS

Materials. FA, polyvinylpyrrolidone (PVP), Poloxamer-188 (P188), sodium dodecyl sulfate (SDS), Cremophore (RH40), Solutol (HS15), Tween-80, and Cremophor EL (EL) were purchased from Sigma-Aldrich Co. Ltd. (USA). Propidium iodide and Syto9 dye cell viability kits were purchased from Thermofisher (USA). 3-(4,5-Dimethylthiazol-2-yl)-2,5-diphenyltetrazolium bromide (MTT) was bought from Merck Chemicals (Germany). Fetal bovine serum (FBS) was obtained from Life Technologies (USA), and penicillin streptomycin (pen/strep) was purchased from Lonza (USA). An Elix 10 water purification system (Millipore Corp., USA) was used to obtain Milli-Q water. Mueller Hinton Agar (MHA) (Biolab, South Africa), nutrient broth (Biolab, South Africa), nutrient agar (Biolab, South Africa), and Mueller Hinton broth 2 (MHB) (Sigma-Aldrich, USA) were used in the antibacterial testing studies and tested against *Staphylococcus aureus* (ATCC 25922) and *Staphylococcus aureus* Rosenbach (ATCC BAA-1683) (MRSA).

Screening and Preparation of FA-NS. A bottom-up antisolvent ultrasonication-precipitation technique was employed to prepare FA-NS. A solution of FA in organic solvent was prepared and added dropwise to a surfactant solution in Milli-Q water under vigorous stirring. The resulting mixture was further sonicated for a determined time period under ice.⁴⁵ Initially, a surfactant solution (0.1% w/v) was prepared and 1

mL of FA solution (10 mg/mL) in water miscible organic solvent was added dropwise under vigorous stirring, sonicated at 30% amplitude for 5 min. Thereafter, the suspension was stirred overnight at room temperature to completely evaporate the organic solvent. Various parameters, such as surfactant type, surfactant concentration, drug concentration, solvents (methanol, ethanol and acetone), sonication time, and amplitude, were evaluated to obtain a stable FA-NS nanosuspension. Potential surfactants were screened to provide a stable system: PVP, P188, SDS, Macrogol (RH40), HS15, Tween-80, and EL. Following the evaporation of the organic solvent, the FA-NS was immediately lyophilized using 3% mannitol as a cryoprotectant.⁴⁶

Characterization of Fusidic Acid Nanosuspension. *In Silico Studies.* MD simulations are a widely applied technique in the field of drug delivery to accomplish tasks such as understanding the drug interaction with proteins,^{47,48} membranes,^{49,50} and polymers.^{51,52} The spontaneous binding of P188 with FA was studied using MD simulations to allow us to understand (1) the FA spontaneously binding with P188, (2) interactions that play a crucial role in the FA interaction with P188 (whether VdW or electrostatics), and (3) if the binding energy of the complex is favorable. The structure of FA (Figure 2A) was taken from PDB id 2VUF,⁵³ and 10 monomer units of

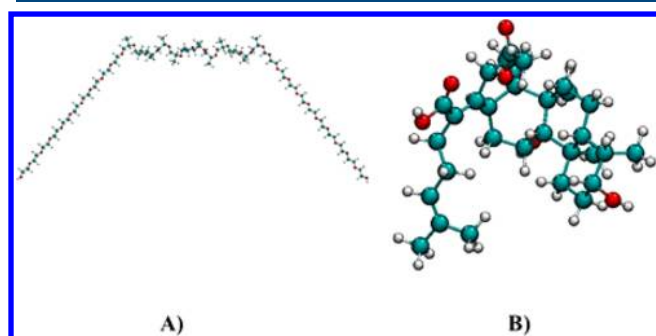


Figure 2. Structure of (A) monomer units of P188 and (B) FA (PDB: 2VUF).

each P188 block were constructed using ChemDraw⁵⁴ (Figure 2 B and 1A). The CHARMM general force field (CGenFF)⁵⁵ parameters were used for both of the molecules, and the TIP3P model⁵⁶ was used for water. The MD simulation system contains one FA molecule, a polymer of P188, and 30 235 water molecules. The system was first energy minimized using the 5000 steps of the steepest descent method,⁵⁷ after which the equilibration simulations were performed using a canonical ensemble (NVT), followed by an isobaric-isothermic ensemble (NPT) for 10 ps each, with the production run being performed using an NPT ensemble for 30 ns. The simulation was performed at 300 K temperature using the velocity-rescale method and at 1 atm pressure using the Parrinello–Rahman method,⁵⁸ with the coupling time for the temperature being 0.1 and for pressure 2.0 ps. The particle mesh Ewald (PME) method⁵⁹ was used for long-range electrostatic interactions, with a 10 Å cutoff being used to calculate the VdW and short-range Coulombic interactions. The COM of mass (COM) distances between P188 and FA were calculated using an in-house Tcl script. The interaction and binding energy between P188 and FA were calculated using the g_mmpbsa tool, which uses the molecular mechanics Poisson–Boltzmann surface area (MM-PBSA) method,⁶⁰ while the simulation was performed

using GROMACS 5.1.2.⁶¹ The binding energy of the P188–FA complex in solvent was expressed as

$$\Delta G_{\text{total}} = \Delta G_{\text{complex(P188+FA)}} - (\Delta G_{\text{P188}} + \Delta G_{\text{FA}})$$

where $\Delta G_{\text{complex}}$ is the binding energy of the P188–FA complex, and ΔG_{P188} , and ΔG_{FA} are the total energies of P188 and FA individually. The total energy of $\Delta G_{\text{complex}}$, ΔG_{P188} , and ΔG_{FA} were estimated using

$$\Delta G_{\text{P188}} = \Delta E_{\text{P188(MM)}} + \Delta G_{\text{P188(Solvation)}}$$

$$\Delta G_{\text{FA}} = \Delta E_{\text{FA(MM)}} + \Delta G_{\text{FA(Solvation)}}$$

where ΔE_{MM} is the potential energy in vacuum, and it was estimated using

$$\Delta E_{\text{MM}} = \Delta E_{\text{bonded}} + \Delta E_{\text{nonbonded}}$$

$$\Delta E_{\text{MM}} = \Delta E_{\text{bonded}} + (\Delta E_{\text{vdw}} + \Delta E_{\text{elec}})$$

$\Delta G_{\text{solvation}}$ is the solvation free energy, and it was estimated using

$$\Delta G_{\text{Solvation}} = \Delta G_{\text{polar}} + \Delta G_{\text{nonpolar}}$$

ΔG_{polar} was calculated using the Poisson–Boltzmann (PB) equation, and $\Delta G_{\text{nonpolar}}$ was estimated using

$$\Delta G_{\text{nonpolar}} = \gamma \text{SASA} + b$$

where γ is a coefficient related to the surface tension of the solvent, and b is the fitting parameter

$$\gamma = 0.0226778 \text{ kJ/Mol}/\text{\AA}^2 \text{ and } b = 3.84928 \text{ kJ/Mol}$$

A bootstrap analysis was performed to calculate the standard error.

Size, Polydispersity Index (PI), Zeta Potential (ZP), and Morphology. The size, PI, and ZP of FA-NS were analyzed by dynamic light scattering (DLS) using a Zetasizer Nano ZS90 (Malvern Instruments Ltd., UK). The FA-NS were diluted with Milli-Q water in such a way that the scattering intensity was within the instrument's sensitivity range, after which it was analyzed. All of the measurements were performed in triplicate on three different batches that were prepared separately. The morphological investigations were performed using Jeol, JEM-1010 (Japan) transmission electron microscopy (TEM). The FA-NS suspension was diluted appropriately and mounted onto the surface of a copper grid, with the excess sample being removed by blotting off with filter paper, after which it was dried at ambient temperature and stained using 2% uranyl acetate solution before measurement.⁶² The images were captured at an accelerating voltage of 100 kV.

Differential Scanning Calorimetry (DSC). The thermal profiles of the FA–P188 physical mixture and lyophilized FA-NS were determined by DSC (Shimadzu DSC-60, Japan). Briefly, samples (2 mg) were placed in an aluminum pan and sealed using a crimper; then, they were heated to 300 °C at a constant rate of 10 °C/min under a constant nitrogen flow of 20 mL/min using an empty pan as a reference.

X-ray Diffraction (XRD) Analysis. The XRD patterns were obtained using a Bruker D8 advance diffractometer (Bruker, Karlsruhe, Baden-Württemberg, Germany) equipped with a graphite monochromator operated at 40 kV and 40 mA. Cu K α radiation was used as the X-ray source with $\lambda = 1.5406 \text{ \AA}$.

Fourier Transform-Infrared (FT-IR). A Bruker Alfa spectrophotometer (Germany) was used for the FT-IR analysis of

FA, P188, and lyophilized FA-NS in order to determine any chemical changes that occurred during formulation.

Rheology of the Suspension. The rheological properties of the FA-NS suspension were measured by the MCR 302 rheometer (Anton Parr, Graz, Austria) using a 49.96 mm plate (0.995°, shear rate from 0.01 to 100/s) at room temperature, with the experiments being performed in triplicate.

Physical Stability Study. Stability studies of both the wet and lyophilized nanosuspensions were performed at 4 °C and room temperature over a 3-month period. The parameters evaluated for confirming the stability were particle size, PI, ZP, settling behavior, and physical appearance.

Solubility Studies. A shake-flask method was used to determine the solubility of FA-NS and FA in water. Excess quantities of FA and lyophilized FA-NS were added to the Milli-Q water (10 mL) and placed in a shaking incubator at a temperature of 25 °C for 24 h. The undissolved FA was removed by filtering through syringe filters (cellulose acetate membrane, 0.2 µm, GVS Filter Technology, USA),^{40,63} with the FA content being determined by HPLC (Shimadzu, Japan) using a reported method.⁶⁴ The mobile phase was composed of acetonitrile and water (70:30, v/v) that was adjusted to pH 3.5 with acetic acid. The flow rate and detection wavelength were 1.0 mL min⁻¹, and 210 nm, respectively. The injection volume was 20 µL and was pumped through a Nucleosil 100-5 C18 column (150 mm × 4.6 mm internal diameter). The regression equation for the calibration curve was $y = 186436x - 10635$, and the linearity correlation coefficient r^2 was 0.9994.

In Vitro Cytotoxicity. The biosafety of the FA-NS suspension was assessed using a MTT assay method.⁶⁵ The adenocarcinoma human alveolar epithelial cell line (A549) and human embryonic kidney cells (HEK 293) were plated in T-25 cell culture flasks at a density of 104 cells/mL and cultured in DMEM media supplemented with 10% FBS (v/v) and 1% Pen-Strep (v/v). The cells were grown at 37 °C in a humidified incubator with 5% CO₂. The medium was exchanged every 2 days. Each of the two cell lines containing 3000 cells were seeded into 96-well plates and were further incubated for 24 h, and the media was discarded and replaced with 100 µL of fresh media. Thereafter, different dilutions of FA-NS containing 20, 40, 60, 80, and 100 µg of P188 were added to the 96-well plates ($n = 6$ per concentration). After 48 h of incubation, sample-laden medium was then removed from each well, discarded, and replaced with 100 µL of fresh culture medium and 20 µL of MTT solution (5 mg/mL in PBS) in each well. Cell viability was assessed on a microplate spectrophotometer (Spectrostar Nano, Germany) at an absorbance wavelength of 540 nm. The percentage cell viability was calculated as follows

$$\text{Cell viability} = \left(\frac{\text{A540 nm treated cells}}{\text{A540 nm untreated cells}} \right) \times 100\%$$

Antibacterial Activity. In Vitro Antibacterial Activity. The broth microdilution method was used to determine the MIC values. *S. aureus* and MRSA were grown overnight in nutrient broth at 37 °C in a shaking incubator at 100 rpm and diluted with sterile deionized water to achieve a concentration equivalent to 0.5 McFarland standard using a DEN-1B McFarland densitometer (Latvia). In a 96-well plate 135 µL of MHB was added followed by the addition of 135 µL of bare FA (1.5 mg/mL) (positive control) and FA-NS (1 mg/mL) in the first well; then, it was serially diluted. Both of the bacterial cultures grown in MHB were further diluted to 5×10^5 colony

forming units per mL (CFU/mL),⁶⁶ and 15 µL was added to the sample and the MHB-laden 96-well plate and incubated at 37 °C in a shaking incubator (100 rpm). After 24 h, 10 µL of the incubated broth was spotted on MHA plates and incubated for 24 h at 37 °C to determine the MIC values. The studies were performed in triplicate using the 1% v/v DMSO solution as a negative control.^{30,67}

Flow Cytometry Bacterial Cell Viability. Cell viability studies on the MRSA cells were performed following a flow cytometry assay method. A volume of 15 µL of the bacterial suspension containing 5×10^5 CFU/mL was added to each well containing 135 µL of bare FA (positive control), and FA-NS at their respective MICs were incubated at 37 °C in a shaking incubator (100 rpm). The percentage cell viability after 24 h was determined using the flow cytometry method on a BD FACSCANTO II (Becton Dickinson, CA, USA) fluorescence activated cell sorter.^{68,69} Both FA and FA-NS treated with bacterial cultures (50 µL) in each well were added to the flow cytometry tubes, each containing 350 µL of the sheath fluid, and vortexed for 5 min. The mixture was incubated for 30 min with 5 µL of propidium iodide (PrI), which is a noncell wall permeant dye, as well as the Syto9 cell permeant dye. PrI fluorescence was excited by a 455 nm laser and collected through a 636 nm bandpass filter, while Syto9 excitation was at a 485 nm laser and collected through a 498 nm band-pass filter.^{70–72} Untreated pure MRSA cells were used as a negative control. Instrumentation settings included a sheath fluid flow rate of 16 mL/min and a sample flow rate of 0.1 mL/min. Data with fixed cells were collected using flow cytometer software (BD FACSDIVA V8.0.1 software, USA). The voltage settings used for the fluorescence-activated cell sorting (FACS) analysis were 731 (forward scatter [FSC]), 538 (side scatter [SSC]), 451 (Syto9), and 444 for PrI. Bacteria were initially gated using forward scatter, with the cells of the appropriate size being gated. At least 10 000 cells were collected for each sample in triplicate, and their position as “live” and “dead” cells were determined. To avoid any background signal from particles smaller than bacteria, the detection threshold was set at 1000 events in SSC analyses.⁷³

In Vivo Antibacterial Activity. A mouse skin infection model was used for in vivo antibacterial activity following a study protocol approved by the University of KwaZulu-Natal's (UKZN) Animal Research Ethics Committee (AREC) (Approval number: AREC/104/01SPD). Humane care and use of animals were in accordance with the guidelines of the AREC of UKZN and the South African National Standard SANS 10386:2008. BALB/c male mice weighing 18–20 g were used in the study. The back hair of mice was removed 24 h prior to the experiment, and the intact exposed skin was disinfected using 70% ethanol. MRSA saline suspension containing 1.5×10^8 CFU/mL (50 µL) was injected intradermally the following day. The mice were then divided into three groups: treatment, positive, and negative control ($n = 4$). After 30 min of infection, 50 µL (0.05 mg FA) of FA-NS (treatment), bare FA (0.25 mg) in 1% DMSO (positive control), and saline (negative control) were injected at the same site of infection for each treatment group, respectively.^{10,30,74,75}

The mice were kept under observation for 48 h with a normal 12 h of light and darkness condition at 19–23 °C and $55 \pm 10\%$ relative humidity with adequate ventilation, after which they were euthanized with halothane, and the infected area of the skin was harvested and homogenized in 5 mL of

PBS (pH 7.4). Tissue homogenates were serially diluted in PBS (pH 7.4), and 20 μL of the diluted homogenates were spotted on nutrient agar plates followed by incubation at 37 °C for 24 h, after which the number of colonies were counted. The CFU/mL was calculated using the following equation:

$$\text{CFU/mL} = \frac{\text{number of colonies} \times \text{dilution factor}}{\text{volume of culture plate}}$$

Histomorphological assessments were performed on the freshly harvested excised skin from the injection site. The skin samples were transferred directly after harvesting, and the excisions from the normal saline skin samples were fixed into a 10% buffered formalin at 25 °C for 7 days; they were dehydrated using ethanol and were implanted in paraffin wax. The tissue wax blocks were sectioned using a microtome (Leica RM2235, Leica Biosystems, Germany); the sections were collected on slides, dried, and then stained with hematoxylin and eosin (H&E). The sections were examined and captured with a Leica Microscope DM 500 that was fitted with a Leica ICC50 HD camera (Leica Biosystems, Germany).

Statistical Analysis. One-way analysis of variance (ANOVA), followed by Bonferroni's multiple comparison test, was used for statistical analysis. Individual groups were compared against each other using a paired *t* test, with *p* values < 0.05 being considered statistically significant. Values are represented as mean \pm SD. GraphPad Prism software (Graph Pad Software Inc., Version 6, San Diego, CA) was used for statistical analysis.

RESULTS

Formulation of the Nanosuspension. The FA-NS nanosuspension was prepared by bottom up antisolvent precipitation, with the FA being dissolved in a water miscible organic solvent to form a solution, then added to the aqueous (antisolvent) phase containing a suitable stabilizer (surfactant) under vigorous stirring, and sonicated under ice. As the drug solution was added to the antisolvent, precipitation of the drug molecules occurred, forming a new solid phase of drug nuclei, as per Kelvin's Law.⁷⁶ The formed nuclei have the tendency to condense into larger particles, which is energetically favored due to Ostwald ripening, as shown in the TEM images (Figure 3), resulting in various formulation parameters being optimized before achieving a stable nanosuspension.

Evaluation of the Formulation Variables To Obtain Optimized FA-NS. *Effect of Surfactants.* A potential surfactant to provide a stable nanosuspension was identified from screening several surfactants, the results being displayed in Table 1. The FA drug concentration of 10 mg/mL, organic solvent (methanol), sonication of 30% amplitude, and sonication time of 5 min were fixed, while different types of surfactants were varied. The effect of the surfactant type on the size, PI, and ZP was investigated, with the particle sizes ranging from 200 to 1400 nm, and the PI from 0.1 to 0.6. The SDS produced FA-NS with the lowest particle sizes, followed by PVP and P188. However, nanoprecipitation in the presence of P188 consistently generated nanosuspensions with significantly lower PI when compared to that of PVP (*p* = 0.0113) and SDS (*p* = 0.0288), with P188 being chosen as the surfactant of choice.

Having chosen P188 as the surfactant of choice, nanosuspensions with various concentrations of P188 (0.1, 0.2, 0.4,

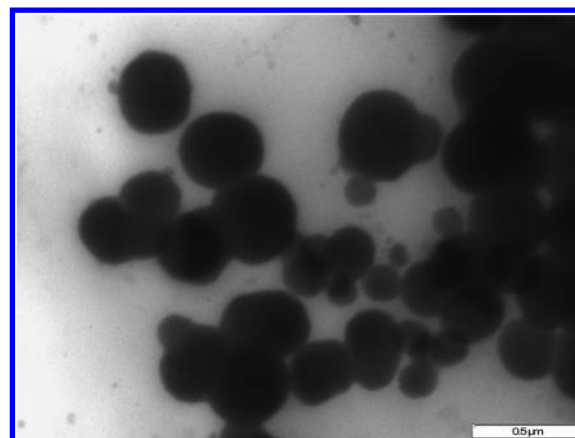


Figure 3. TEM image of smaller particles showing coalescence to form larger thermodynamically stable larger particles before optimum FA-NS suspension was achieved.

Table 1. Effect of Surfactant Type on Stabilizing the Nanosuspension (*n* = 3)

surfactant	average size	PI	ZP
PVP	563.5 \pm 6.18	0.354 \pm 0.031	- 10.6 \pm 0.24
P188	590.0 \pm 7.92	0.254 \pm 0.017	-13.1 \pm 2.70
SDS	388.6 \pm 58.00	0.592 \pm 0.124	-62.5 \pm 6.34
RH40	1159 \pm 21.36	0.330 \pm 0.045	-10.0 \pm 0.16
HS15	1289 \pm 28.00	0.412 \pm 0.230	-7.21 \pm 1.67
Tween-80	772.4 \pm 4.71	0.375 \pm 0.049	-11.1 \pm 0.07
EL	1403 \pm 18.69	0.462 \pm 0.004	-08.57 \pm 1.16

0.8, 1.6, and 2% w/v) were prepared in order to determine the concentration of the surfactant that offered FA-NS with the lowest possible size, PI, and a ZP in an acceptable range.

As the concentration of the surfactant increased from 0.1% w/v to 0.8% w/v, the particle size decreased from 590 to 518.4 nm, respectively (Supporting Information). However, above the 1% w/v, the size started to increase.

Effect of Organic Solvent. Having determined the concentration of P188 suitable to formulate the nanosuspension, solvents were evaluated for their effect on the size of the formed FA-NS. The FA concentration of 10 mg/mL, sonication time (5 min), and 30% amplitude were fixed. Methanol was considered to be a suitable solvent, as it produced FA-NS with the lowest particle size (Table 2) compared to that of ethanol (*p* = 0.0001) and acetone (*p* = 0.0001). It was also observed that FA-NS formulated using methanol had a better PI than that of acetone and ethanol.

Table 2. Effect of Organic Solvents on Nanosuspension Formation (*n* = 3)

solvent	average size	PI	ZP
ethanol	950.0 \pm 21.13	0.307 \pm 0.036	- 14.6 \pm 1.08
acetone	896.0 \pm 17.37	0.384 \pm 0.058	-12.8 \pm 0.85
methanol	590.0 \pm 07.92	0.254 \pm 0.017	-13.1 \pm 2.70

Effect of Drug Concentration. To achieve an optimum size and distribution of the FA nanocrystals, the effect of the drug concentration was evaluated. The concentration of the drug was varied from 10 to 30 mg/mL, while keeping the concentration of P188 at 1 % w/v, methanol as the solvent, a fixed sonication amplitude of 30%, and a time of 5 min. As

the drug concentration increased from 10 to 30 mg/mL, the particles sizes increased from 552 ± 13.3 to 1336 ± 89.4 nm, and the PI increased from 0.198 ± 0.017 to 0.498 ± 0.042 (Supporting Information).

Effect of Sonication Time and Amplitude. By fixing the concentration of the surfactant (P188 = 1% w/v), drug concentration (FA = 10 mg/mL), and methanol as the solvent, the effect of ultrasonication was studied by changing the sonication time and amplitude. Fixing the sonication amplitude at 30%, ultrasonication times of 5, 7, 10, 15, and 20 min were employed to determine their effect. The particle sizes showed the tendency to decrease with increasing time. However, after 15 min, increasing the sonication time did not show any significant ($p > 0.05$) change in the particle size. Consequently, the effect of ultrasonication amplitude (5%, 10%, 20%, 30%, 40%) was also investigated by fixing the time at 15 min. A trend similar to the sonication time was witnessed, where initially increasing the ultrasonication amplitude led to reduced particle sizes, while above an amplitude of 30%, there was no significant decrease in particle sizes

Characterization of FA-NS. The above screening studies identified the following as the optimal conditions for preparing FA-NS that resulted in monodisperse nanosuspension: the surfactant (P188 = 1% w/v), drug concentration (FA = 10 mg/mL), methanol as an organic solvent, and ultrasonication time and amplitude of 15 min and 30%, respectively. The formulation was then subjected to detailed characterization, as reflected below.

In Silico Studies. An MD simulation of 30 ns of the FA and P188 (10 units per polymer block) molecules in the presence of water molecules was performed to investigate the spontaneous binding, interaction energy, and binding energy between P188 and FA. Figure 4 shows the interaction between

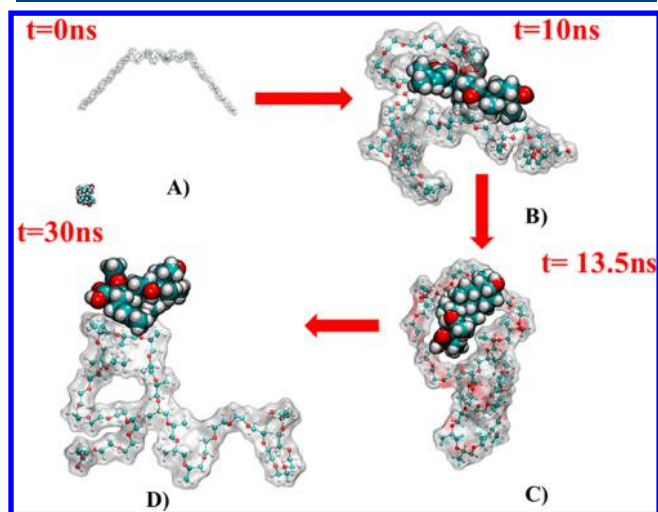


Figure 4. Structures of FA and P188 at four different time points of simulations: (A) at $t = 0$ ns; (B) at $t = 10$ ns; (C) at $t = 13.5$ ns; and (D) at $t = 30$ ns. P188 has been represented in a CPK model, and FA is represented in the VdW model.

P188 and FA at different time points. The time evolution of the COM distance between the P188 and FA revealed that there was spontaneous interaction between both molecules starting from ~ 9 ns (Figure 7A). After interacting, the two molecules remained in a stable complex until ~ 16.9 ns. From ~ 17 to ~ 17.3 ns of MD simulation for 300 ps, a momentary

break in the interaction between both of the molecules was observed. However, at ~ 17.4 ns, the interaction was re-established between both of the molecules and remained stable until the end of the simulation. The average COM distance between the P188 and FA was ~ 14.37 Å, and the average interaction energy between the P188 and FA was ~ -74.42 kJ/mol from 9 to 30 ns (Figure 5B, black line). The interaction energy components showed that the spontaneous binding between the P188 and FA was largely governed by van der Waals (VdW) interactions (Figure 5B, green line). The representative images from the trajectory revealed (Figure 4) that after the binding of the FA, the P188 rearranged its conformations to establish stable interactions. The contribution to the ΔG_{total} from the VdW and electrostatic interactions was represented by ΔE_{vdw} and ΔE_{elec} . The polar and nonpolar solvation energy contributions to ΔG_{total} were represented by ΔG_{polar} and $\Delta G_{\text{nonpolar}}$ respectively. The P188-FA binding was largely governed by hydrophobic interactions, with ΔE_{vdw} being the most favorable contributor. ΔG_{polar} was unfavorable for the binding, while favorable $\Delta G_{\text{nonpolar}}$ and a gain in intermolecular VdW compensated for an increase in the polar solvation energy, which lead to an overall favorable binding energy. The binding energy (ΔG_{total}) of P188 with FA (Table 3) was calculated using the MM-PBSA method from 9 to 30 ns, and the binding energy was found to be -49.764 ± 1.298 .

Size, PI, ZP, and Morphology of the Optimal Formulation. The optimal formulation, which used the above variables, generated monodisperse FA-NS with the size, PI, and ZP of 265 ± 2.25 nm, 0.158 ± 0.026 and -16.9 ± 0.794 , respectively. The lyophilized and water redispersed samples did not have significant changes in the size, PI, and ZP (262.9 ± 2.59 nm, 0.179 ± 0.030 , and -17.0 ± 1.01 mV, respectively). The TEM images show discrete spherical particles (Figure 6), with most of the population sizes being in ranges that were comparable to the sizes observed in the DLS study.

DSC, XRD, and FTIR Analyses. A DSC investigation was performed to establish the melting and crystallization behavior of FA-NS and the formulation excipients. Endothermic peaks of P188 and bare FA were detected at 54.48 and 118.68 °C, respectively (Figure 7(II)A,B), while the lyophilized FA-NS only showed a sharp endothermic peak at 42.46 °C (Figure 7(II)D). The XRD diffractograms pattern of P188 and FA showed 2 and 1 sharp peaks, respectively (Figure 7(III)). The diffractogram pattern of the FA-NS nanosuspension showed no peaks for FA; however, it contained two sharp peaks in similar ranges to those of P188. The physical mixture was analyzed, and the peaks for all of the respective excipients and FA were observed (Figure 7(II)C). An FT-IR was also conducted to evaluate if there were chemical changes in the drug during formulation. The peaks for the C=O stretch for both lyophilized FA-NS and bare FA were observed in the region of 1713 and 1645 cm^{-1} , respectively, although the peak in the FA-NS was attenuated (Figure 7(I)). Carboxylic OH stretching groups were also present at the region of 3435 and 3395 , both for the lyophilized and bare FA. The ester peak was missing in the FA-NS but was present in the bare drug at 1253.46 cm^{-1} . The disappearance might have been due to the hydrogen bonding between P188 and FA during the formulation of the FA-NS, as these kinds of interactions play a vital role in solubilizing the drug.⁷⁶ The fingerprint region spectra of the FA-NS was almost similar to FA alone, with the broad sharp peaks at 1079 and 1101 cm^{-1} for FA-NS and P188 that were

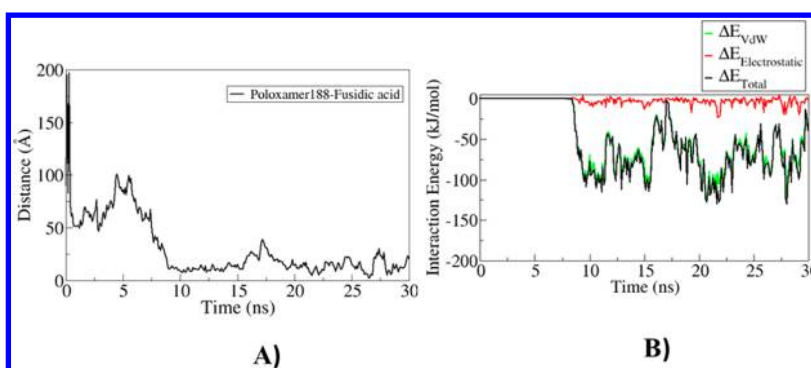


Figure 5. (A) Time evolution of COM distance between P188 and FA. B) Time evolution of interaction energy between the molecules and its nonbonded components.

Table 3. Average Binding Energy and Its Components Obtained from the MM-PBSA Calculation for the P188–FA Complex

contribution	energy (kJ/mol)
ΔE_{vdw}	-70.664 ± 1.680
ΔE_{elec}	-3.810 ± 0.314
ΔG_{polar}	36.075 ± 1.151
$\Delta G_{\text{nonpolar}}$	-11.416 ± 0.233
ΔG_{total}	-49.764 ± 1.298

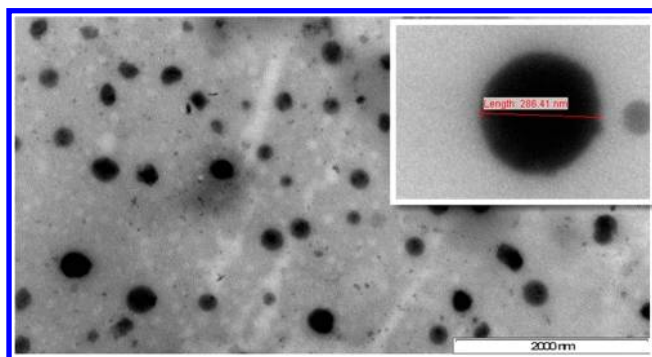


Figure 6. Morphology of the optimized FA-NS particles.

lacking in the bare FA, possibly due to a C–O stretch of the ether bonds present in P188.

Stability Studies. Rheology. Rheology of the optimized FA-NS demonstrated a Newtonian flow with a relative viscosity of 1.335 ± 0.049 mPa·s. After seven days and one month the nanosuspension had viscosity of 1.371 ± 0.079 and 1.492 ± 0.095 mPa·s respectively indicating no significant change in the viscosity of FA-NS ($p > 0.05$) during the storage period.

Physical Stability Study. The optimized formulation was further assessed for stability as both wet and lyophilized formulations for three months at room temperature (rt) and 4 °C. The FA-NS was found to be stable in both the lyophilized and wet states stored at 4 °C for the whole 3-month period of evaluation, with particle sizes below 300 nm. Furthermore, the nanosuspension did not show any signs of coalescing and caking (Table 4). Room temperature studies revealed that the lyophilized formulations were more stable than the wet ones, with particle sizes below 300 nm after 60 days, increasing up to 500 nm after 90 days. The wet formulation was stable for two months, and at the end of the 90 days, the particles sizes were found to be above the nano ranges.

Solubility Studies. Solubility studies were conducted to determine the effect of formulating the FA into a nano-suspension on an aqueous solubility. The solubility of the FA and FA-NS was found to be 17.81 ± 5.30 and 127.23 ± 5.30 $\mu\text{g}/\text{mL}$ respectively (Figure 8).

In Vitro Cytotoxicity. Biosafety of FA-NS was assessed by quantifying viable mammalian cells after exposure to the synthesized material. Two cell lines, A549 and HEK 293, were employed to determine the biosafety of FA-NS in an in vitro cell culture system. The results showed cell viability ranging from 75.71% to 100.89% across all of the concentrations in all of the cell lines tested (Figure 9) with no dose-dependent toxicity within the concentrations studied.

Antibacterial Activity. In Vitro Antibacterial Activity. To evaluate the efficacy of the FA-NS, the MIC values of the bare FA and FA-NS MIC values were determined against *S. aureus* and MRSA, with the results presented in Table 5. The MICs for FA and FA-NS were 62.5 and 3.9 $\mu\text{g}/\text{mL}$, respectively, against *S. aureus*, whereas for MRSA, the values were 250 and 31.25 $\mu\text{g}/\text{mL}$, respectively (Table 4).

Flow Cytometry Bacterial Cell Viability. To quantify the number of bacterial cells killed at the MIC concentration of the bare FA and FA-NS, a flow cytometry method was employed. MRSA was incubated in an FA and FA-NS containing medium for 24 h. PrI fluorescent dye, which does not penetrate the cell wall, and Syto9 cell wall permeant dye were used to differentiate the live from the dead cells in the population. The histograms showing the count of cells that internalized PrI after 24 h of incubation are presented in the Supporting Information. The dead cells were sorted from the population using a gate created beyond the fluorescence of viable cells (Supporting Information).⁷⁷ When the cells were incubated with the bare FA and FA-NS at their respective MIC, the average dead cells in the bacteria population were $38.8 \pm 2.35\%$ and $73.14 \pm 1.35\%$, respectively, indicating a significant difference ($p < 0.0001$). Furthermore, when the MRSA cells were treated with FA at the concentration similar to that of the MIC of FA-NS, the mean dead cells in the population were found to be only $4.66 \pm 0.52\%$. The FA and FA-NS dot plots of PrI versus Syto9 fluorescence^{69,71} showed similar results.

In Vivo Antibacterial Activity. The efficacy of FA-NS was further evaluated in vivo using a mouse skin infection model. Intradermal injections of MRSA were administered causing short-term localization of the bacteria within the dermis skin layer without systemic infection. The number of CFUs was quantified for each treatment group and converted to \log_{10} CFU/mL, as represented in Figure 10. The mean bacterial load

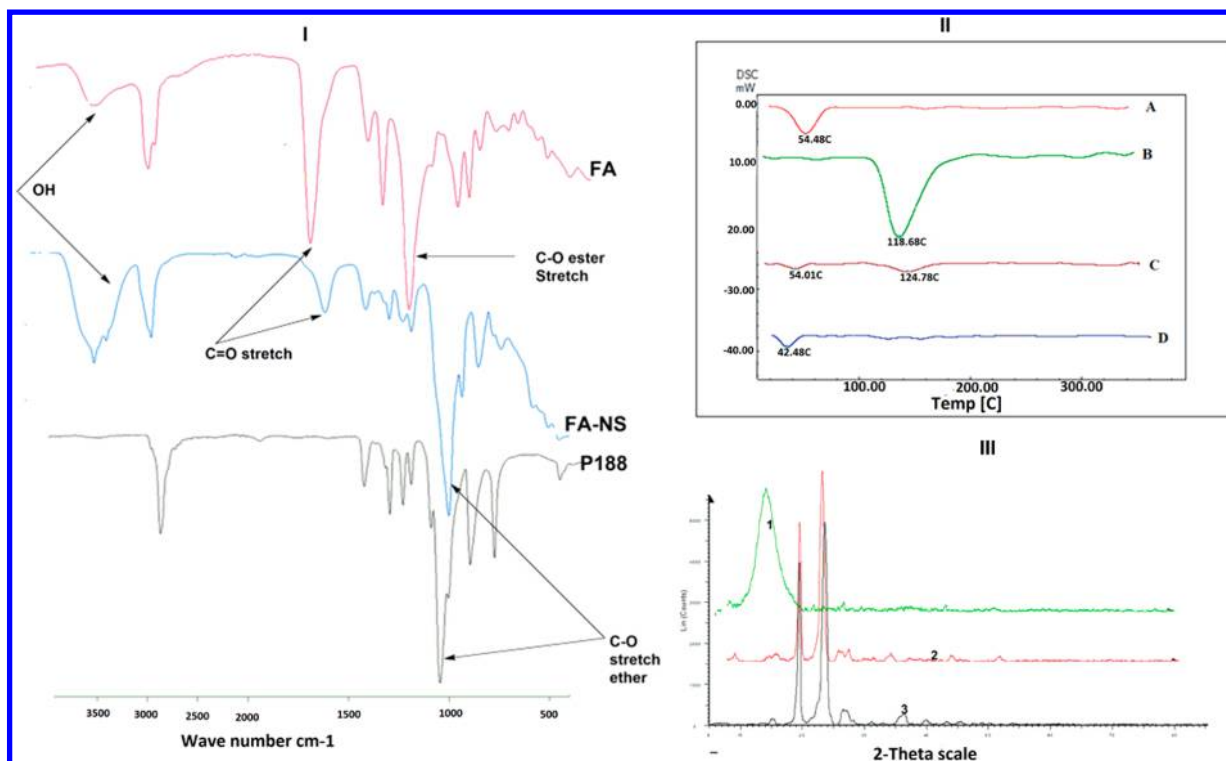


Figure 7. (I) FT-IR of bare FA, FA-NS, and P188. (II) DSC thermogram of (A) P188, (B) FA, (C) physical mixture, and (D) lyophilized FA-NS. (III) Diffractogram for (1) FA, (2) FA-NS, and (3) P188.

Table 4. Stability Studies of FA-NS

formulation	average size	PI	ZP
Time 0			
wet	251.1 ± 11.9	0.126 ± 0.044	-15.2 ± 1.73
lyophilized rt	262.9 ± 2.59	0.179 ± 0.030	-17.0 ± 1.01
30 days			
wet rt	386 ± 5.4	0.094 ± 0.015	-21.2 ± 1.6
wet 4 °C	274 ± 3.33	0.179 ± 0.042	-15.4 ± 2.3
lyophilized rt	296.4 ± 6.29	0.327 ± 0.072	-21.6 ± 1.1
lyophilized 4 °C	276.4 ± 5.7	0.087 ± 0.007	-20.8 ± 2.96
60 days			
wet rt	426.8 ± 13.53	0.263 ± 0.164	-19.7 ± 1.24
wet 4 °C	267.6 ± 52.94	0.176 ± 0.07	-15.6 ± 1.02
lyophilized rt	280.5 ± 38.79	0.286 ± 0.04	-16.5 ± 1.74
lyophilized 4 °C	298.3 ± 43.96	0.321 ± 0.04	-15.04 ± 4.08
90 days			
wet rt	1437.4 ± 681.2	0.908 ± 0.11	-16.42 ± 4.2
wet 4 °C	221.3 ± 7.9	0.307 ± 0.045	-16.42 ± 4.2
lyophilized rt	481.53 ± 70.70	0.50 ± 0.039	-15.7 ± 12.9
lyophilized 4 °C	292.4 ± 50.8	0.361 ± 0.04	-10.35 ± 0.43

for untreated, FA, and FA-NS groups were 6.58 ± 0.01 (3 790 000 CFU/mL), 6.30 ± 0.062 (2 016 667 CFU/mL), and $4.35 \pm 3.12 \log_{10}$ CFU/mL (26 667 CFU/mL), respectively.

During tissue harvesting, fluid-filled abscesses at the injection site were visually observed in skin samples from the MRSA-injected control and the FA-treated groups only, while none were seen for the FA-NS treated groups (Figure 11A). Histological analysis was also performed to further assess the skin integrity and histomorphological changes after the MRSA intradermal infection. The H&E images from the MRSA-injected control group confirmed inflammation and the

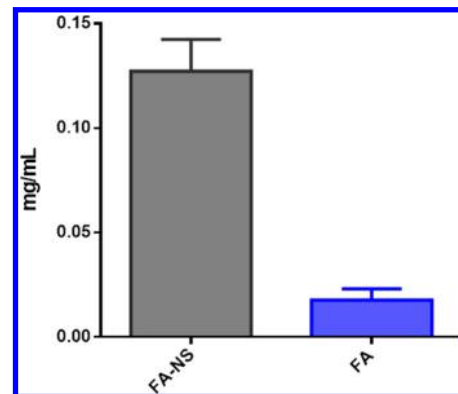


Figure 8. Solubility of FA-NS and FA in water ($n = 3$).

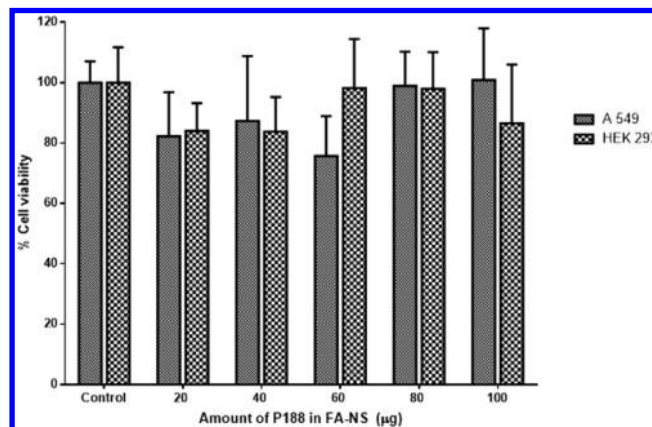


Figure 9. Cytotoxicity evaluation of FA-NS against various concentrations of P188 on A549 and HEK 293 cells ($n = 6$).

Table 5. MIC of FA and FA-NS^a

	SA ($\mu\text{g}/\text{mL}$)	MRSA ($\mu\text{g}/\text{mL}$)
FA	62.5	250
FA-NS	3.9	31.25
1% v/v DMSO	NA	NA

^aNA = No activity. The values are expressed as mean \pm SD, $n = 3$

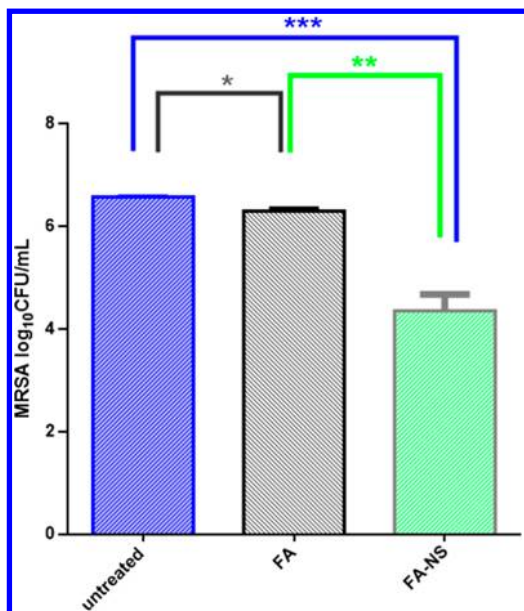


Figure 10. MRSA burden after 48 h of treatment. * denotes significant difference for FA versus the untreated group. ** denotes significant difference between bare FA versus FA-NS. *** denotes significant difference between bare FA-NS versus the untreated ($n = 4$).

formation of an abscess at the injection site (Figure 11B). The MRSA-injected control tissue image also displayed evidence of inflammation, as represented by the excessive swelling of the dermal layer in the control image and the presence of white

blood cells. The FA-NS-treated tissue did not display any definite abscess formation, although there was evidence of minimal inflammation in the dermal layer (Figure 11D). In the MRSA-injected control group, there were signs that a high number of cells were infiltrated by the bacteria, as evidenced by the large area of the abscess.

DISCUSSION

This study explored formulating a FA antibiotic (BCS class II drug) into a nanosuspension (FA-NS), and its ability to enhance aqueous solubility and antibiotic activity due to the small sized particles. MD simulations were done to understand, at an atomic level, the interaction between FA and P188. FA-NS nanosuspension was prepared using a bottom-up antisolvent precipitation technique. To achieve a stable nanosuspension, surfactants available in the market, various organic solvents, and other formulation parameters, such as sonication time and amplitude, were screened. PVP, SDS, and P188 were surfactants that provided nanosuspensions with small particle sizes, with P188 being found to be the surfactant of choice, as it consistently generated nanosuspensions with significantly lower PI than that of PVP ($p = 0.0113$) and SDS ($p = 0.0288$). This may be due to the high hydrophilic–lipophilic balance (HLB value = 29) of the amphiphilic block copolymer, which may have led to better interactions with hydrophobic FA during the nanosuspension formation.⁷⁸

Having chosen P188 as the surfactant of choice, various surfactant concentrations were screened to determine a suitable concentration that offers a stable nanosuspension. However, it was witnessed that when the surfactant concentration was $>1\%$ w/v, the particles sizes and the PI of the system increased. Studies have shown that increasing the surfactant above certain concentrations favors micelles formation due to the self-assembly of the surfactant, rather than providing stability to the nanosuspension, leading to the Ostwald ripening of the nanocrystals in the antisolvent.^{79–81} The formation of micelles at a higher concentration of the surfactant resulted in a decreased amount of the surfactant available at the aqueous/FA crystals interface to coat the

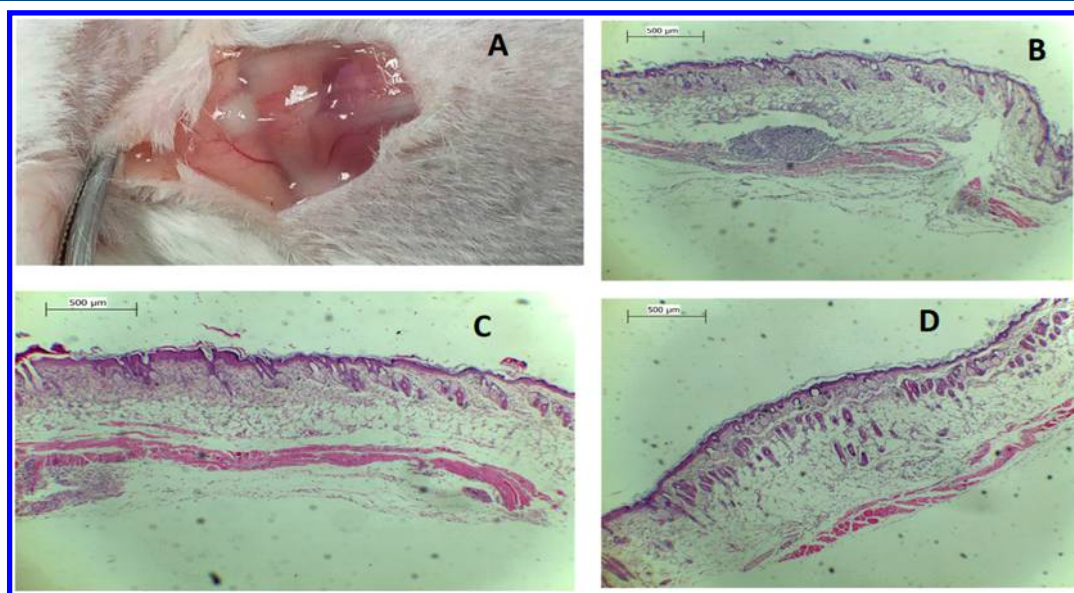


Figure 11. (A) Abscesses from untreated mice. Photomicrographs of the control and the treated skin selections for light microscopy (LM) stained with H&E ($\times 40$) (scale bar = 500 μm). (B) Control (MRSA-injected, untreated (saline)). (C) Treated (FA). (D) Treated (FA-NS).

surface of the formed solid phase, thus leading to Ostwald's ripening of the crystals. Various organic solvents were also screened to identify the one that provides the better antisolvent effect for precipitating the FA once the organic solvent FA solutions come in contact with water. Of the screened solvents, methanol was found to be the most suitable as it generated a nanosuspension with better particle sizes, PI, and ZP; although, we could not conclusively state why it gave better particles sizes. These results could be ascribed to a higher rate of mixing of the solvent/antisolvent per unit time and easy crystal drawing out, which results in a shorter time of nucleation and crystal growth, subsequently resulting in smaller crystals⁸²

Drug concentration is also a critical variable in the formulation of the nanosuspensions, as increasing the drug concentration could result in an increased number of primary particles per unit volume and a shorter interparticle distance.⁸³ Consequently, this may lead to a chance of forming an aggregate mass of loosely adhered particles by electrostatic charges, which can give rise to increased sizes and lack of uniformity among the particles formed.⁸⁴ This was also witnessed in the formulation of FA-NS, as the drug concentration increased from 10 to 30 mg/mL, particle sizes increased from 552 ± 13.3 to 1336 ± 89.4 nm, and the PI increased from 0.198 ± 0.017 to 0.498 ± 0.042 . This phenomenon has also been previously reported for norfloxacin, griseofulvin, ampicillin, amoxicillin, and tetracycline nanosuspensions,^{85,86} where the above certain concentration of the drug particles coalesced to larger particles.

To further reduce the particle sizes, sonication time and amplitude were evaluated. Increase in the sonication time and amplitude further reduced the particles sizes. However, above 15 min and an amplitude 30% of sonication, there was no significant decrease in the particle size. The findings were in agreement with the work reported by Dengning et al. in formulating a nifedipine nanosuspension.⁸⁷ After screening to optimize all of the parameters, a stable formulation was achieved. During formulation, stirring provided a shear force that kept the particles in constant Brownian motion,⁸⁸ sonication broke down the aggregating solid phase, while the surfactant coated the particles, resulting in electrostatic repulsion of neighboring like-charged particles⁸⁹ and packing of the crystals into an amorphous state that resulted in a stable colloidal system that had a particle size, PI, and ZP of 265 ± 2.25 nm, 0.158 ± 0.026 , and -16.9 ± 0.794 , respectively.

MD simulations of 30 ns between P188 (10 units per polymer block) and FA were performed. The negative binding energy ($\Delta G_{\text{total}} -49.764 \pm 1.298$) indicated the degree of spontaneity of the binding process, and a higher negative value reflected a more energetically favorable adsorption.⁹⁰ The favorable higher value of the binding energy was also an indication of a strong binding between the molecules, which would require a higher repulsive energy to break the binding between the two molecules.⁹¹ Furthermore, the energy components of the complex showed that the P188-FA binding was mainly governed by the hydrophobic interactions, with VdW energy ΔE_{vdw} as the major contributor to the binding energy (Table 3). Previous studies on the ABA triblock polymer, such as P188, have shown that, via its hydrophobic central block, the polymer forms strong interactions with the hydrophobic drug at the core, resulting in nonsolvent assessable regions, while the hydrophilic block shell consequently forms water accessible regions. This

arrangement leads to a stable complex and increased water solubility of the hydrophobic drug.⁹² Figure 6 and a video available in the Supporting Information show similar arrangements; thus, the stabilization of the nanosuspension and the increased solubility of the FA in water could have occurred via this phenomenon of the ABA triblock polymer solubilization.⁹³ These results were in agreement with experimental studies that showed an increased solubility of the drug in water at the simultaneous formation of a stable nanosuspension between P188 and FA.

DSC, XRD, and F-TIR analyses were performed to investigate the melting and crystallization behavior of FA-NS and its formulation excipients. The DSC results showed the absence of an FA peak in the thermogram of the FA-NS, with a peak similar to that of the pure P188 being witnessed. This was an indication that the P188 was coating the surface of the FA, which was transformed into an amorphous state during the formulation process. The XRD diffractograms showed similar results to DSC, with the absence of the FA peaks in the formulation diffractograms. The FT-IR analysis showed that both the formulation and physical mixture had the characteristic peaks of P188 and FA, and that the resultant FT-IR patterns were in line with the previous literature for nanosuspensions.⁹⁴⁻⁹⁶ The transformation of FA into FA-NS could have been due to the rapid drawing out of the drug particles from the organic solvent, as the aqueous solution with P188 as stabilizer coated the nascent drug particles nuclei, resulting in fast nucleation termination, leading to amorphous nanoparticles.⁹⁷ The patterns of the DCS thermograms, XRD diffractograms, and FT-IR wave numbers of P188 and FA in the formulation and the crystalline pure P188 and bare drug was an indication that no new chemical compound was formed.⁹⁸

The possibility of interactions between like and unlike particles in the system defines the stability of a suspension.⁹⁹ The Ree and Eyring theory stated that viscosity is the sum of the contribution of an indefinite number of unspecified units of flow.^{100,101} Therefore, Ostwald ripening, which might occur during the storage of a suspension, could result in viscosity changes that can be used to determine the stability of a suspension. The FA-NS viscosity was evaluated for a period of one month and showed that the nanosuspension had no significant ($p > 0.05$) change of its viscosity. This might have been due to constant Brownian motion as a result of the small particle sizes that kept the system in a suspended state, the stabilizing effect of the surfactant, and the high similar zeta potential values within the particles that causes repulsion, thus preventing Ostwald's ripening.¹⁰² A further assessment of the stability for wet and lyophilized formulations was performed for three months at room temperature and 4 °C. FA-NS was found to be stable in both lyophilized and wet state stored at 4 °C for the entire three months; however, room temperature studies revealed that lyophilized formulations were more stable than wet ones. These findings confirmed that the optimal storage conditions for the FA-NS suspension was at 4 °C for both wet and lyophilized formulations.

The applicability of the optimized formulation was evaluated for solubility enhancement and antimicrobial activity. Using a shake-flask method, the solubility was determined, there was a 7-fold increase in the solubility of FA when formulated as FA-NS when compared to the bare drug. This phenomenon could be explained using various theories, such as that of Ostwald-Freundlich, in which the solubility of particles is inversely

proportional to their radius;^{103–105} Mihranyan and Strømme, who propose an increased solubility of nanoparticles due to surface fractal dimension;¹⁰⁶ and Letellier et al, who postulated that the improved solubility of nanoparticles is attributed to thermodynamic descriptions involving the internal energy of the particles.¹⁰⁷ An increase in the aqueous solubility of the BCS class II drugs, such as FA, is significant for their efficiency. Due to their hydrophobicity, they partition well through biological membranes, although this does not translate to high bioavailability, as their partition from the dosage form is limited due to their low water solubility. Therefore, formulating FA as a nanosuspension could enhance the activity of the drug.

With the increase in the application of nanoparticles, there is a need for the determination of their safety before application. The biosafety of FA-NS nanosuspension was determined using an in vitro MTT assay that quantifies viable cells upon exposure of the test materials to the two cell lines. Since cell viability upon exposure to FA-NS was above 75%, this indicated that the formulation met the requirements for the biocompatibility and toxicity regulatory requirements for biomaterials.¹⁰⁸ These results were in line with the findings in the literature where P188 has been reported to be biosafe and has been approved by the FDA for 50 years as a surfactant and therapeutically has been used to reduce the viscosity of blood before transfusion.¹⁰⁹ Therefore, these findings show FA-NS to be a biosafe and nontoxic nanosuspension.

The impact on the antibacterial activity of formulating FA in a nanosuspension was evaluated using the broth microdilution method. MIC values for the bare drug and FA-NS against *S. aureus* and MRSA showed that FA-NS had a 16- and 8-fold lower activity against *S. aureus* and MRSA, respectively, when compared those of the bare FA.

Generally, there was better activity against *S. aureus* than MRSA, which can be attributed to its thicker cell walls. This thickened cell wall is due to multiple peptidoglycan layers that limit the drug molecules from crossing the membrane. Enhanced activity of the antibacterial agents after formulation as a nanosuspension have been reported elsewhere.^{110–112} This enhanced activity by the FA-NS can be attributed to the nanoparticulate sizes of the nanosuspension that led to an increase in the surface area, which resulted in an increased solubility for better penetration and higher uptake by the cells.¹¹³ In addition, drug adsorption efficiency is directly proportional to the specific surface area of the adsorbent and inversely proportional to the particle size.^{114,115} Smaller FA-NS nanoparticles may therefore have been effectively distributed and adsorbed on the bacteria surface than bare FA, thus enhancing activity. Enhanced FA activity via the FA-NS underlines the use of nanosuspensions as a strategy to formulate BCS class II antibiotics as prospective drug delivery systems.

The viability of the surviving MRSA cells was determined using a flowcytometry method after incubating the bacteria with bare FA and FA-NS. Cells treated with FA-NS had almost twice the percentage population of dead bacterial cells, despite having an 8-fold lower MIC compared to bare FA. Furthermore, when the MRSA cells were treated with FA at the concentration similar to that of the MIC of FA-NS, the dead cells in the population were found to be $4.66 \pm 0.52\%$, which confirmed its efficacy. The minimal effect of the bare FA on MRSA at a low concentration was due to it having a bacteria static effect.¹¹⁶

This result could translate to the decreased amount of the dosage amount required for treatment, with fewer dose dependent side effects that are related to FA, such as hepatic and hematological toxicities,¹¹⁷ thus showing FA-NS nanosuspension's superiority over FA.

Further evaluation of the efficacy of FA-NS was performed following a BALB/c mouse MRSA in vivo skin infection model. After infection and treatment periods, the mice were euthanized, their skin harvested, and the number of CFUs quantified for each treatment group. A statistically significant ($p < 0.0001$) reduction in bacterial load was recovered from the treatment groups treated with FA-NS and FA when compared to that of the untreated group (Figure 14). Bacterial load recovered from the groups treated with bare FA compared to that of the untreated groups showed that the former had a significantly lower ($p = 0.0133$) load of MRSA. The FA-NS treated samples had a 142.12-fold decrease in the bacterial burden compared to the untreated groups ($p = 0.0002$). In comparing the bare FA and FA-NS, a 76-fold greater reduction of the MRSA load in the groups treated with FA-NS ($p = 0.0081$) was observed compared to that of the bare FA. These results confirmed the ability of FA to enhance antibacterial activity when it is formulated as a nanosuspension, which can prove critical in treating infections of MRSA origin.

Histomorphological changes were also investigated as a suggestive means of identifying the extent of tissue destruction in the dermal layers that were infected with MRSA during the 48 h study. As all bacteria are recognized as foreign to the body, there is an innate immune response after their introduction into the intradermal layers,¹¹⁸ which causes inflammation upon entry of the bacteria into the tissue, the degree of the response being proportional to the bacterial load. The histomorphological evaluations directly correlated with the findings of the bacterial load from each group of the in vivo antibacterial study, as the FA-NS treated tissue displayed a low isolated bacterial load and showed the least histomorphological signs of tissue inflammation. However, the MRSA-injected negative control group and the FA-treated group displayed a statistically significantly larger number of isolated bacteria, more histomorphological signs, and evidence of tissue inflammation and abscess formation. These histomorphological evaluations further confirmed the antimicrobial superiority of the novel FA-NS.

CONCLUSION

Nanotechnology-derived novel formulations are showing significant potential for improving the efficacy of existing antibiotics. More than 40% of NCEs (new chemical entities) developed in the pharmaceutical industry are practically insoluble in water, this being a major challenge for formulation scientists. In this study, a new FA-NS formulation was successfully formulated using a bottom-up antisolvent precipitation with the goal of simultaneously enhancing solubility and antibacterial activity. After various surfactants were screened, solvents and formulation parameters of an optimized nanosuspension, FA-NS with a particle size in the range of 200 nm, were obtained. MD simulations revealed that there was spontaneous binding between FA and P188 in the aqueous milieu, with the average interaction energy and distance between the molecules being ~ -74.42 kJ/mol and ~ 14.37 Å. Further investigation on the contributions of various energy components of the complex showed that van der Waals interactions were the major contributor, and that the binding

energy between FA and P188 was -49.764 ± 1.298 kJ/mol. This further supported the experimental work of the formation of a stable nanosuspension between FA and P188. The formulation of FA as a FA-NS improved its solubility by 8-fold. The assessment of the in vitro antibacterial activity proved the superiority of the FA-NS over the bare FA to control the growth of susceptible and resistant *S. aureus*. In vivo antibacterial activity against MRSA using a mouse skin infection model showed that FA-NS was more efficient in killing MRSA compared to bare FA. With these promising results, the formulated novel FA-NS nanosuspension can therefore be further exploited as a nanoantibiotic to fight against other bacteria, and this method can possibly be employed to enhance the efficacy of other BCS class II drugs for various disease conditions.

■ ASSOCIATED CONTENT

📄 Supporting Information

The Supporting Information is available free of charge on the ACS Publications website at DOI: [10.1021/acs.molpharmaceut.8b00505](https://doi.org/10.1021/acs.molpharmaceut.8b00505).

Video of an MD simulation between FA and P188 (MPG)

Graphs representing the effect of the surfactant concentration on the particle size and the effect of the increasing drug concentration on particle sizes and homogeneity of the formed particles, as well as FACS data of bare FA and FA-NS (PDF)

■ AUTHOR INFORMATION

Corresponding Authors

*Tel: 00 27 31 260 7358; Fax: 0027 31 260 7792; E-mail: rahul.kalhature@rediffmail.com, kalhature@ukzn.ac.za, rkalhature@utep.edu.

*Tel: 00 27 31 260 7358; Fax: 0027 31 260 7792; E-mail: govenderth@ukzn.ac.za.

ORCID

Calvin A. Omolo: [0000-0002-4421-3783](https://orcid.org/0000-0002-4421-3783)

Rahul S. Kalhature: [0000-0003-4627-9628](https://orcid.org/0000-0003-4627-9628)

Nikhil Agrawal: [0000-0002-5365-6332](https://orcid.org/0000-0002-5365-6332)

Thirumala Govender: [0000-0002-4968-4779](https://orcid.org/0000-0002-4968-4779)

Notes

The authors declare no competing financial interest.

■ ACKNOWLEDGMENTS

The authors acknowledge the College of Health Sciences, University of KwaZulu-Natal (UKZN), the UKZN Nanotechnology Platform, and the National Research Foundation of South Africa for financial support (Grant NRF, 87790, and 88453). The Microscopy and Microanalysis Unit, Biomedical Resource Unit, Department of Human Physiology, and Flow Cytometry Research Laboratory at UKZN are also acknowledged, as well as Mrs. Carrin Martin for proofreading, and CHPC, Cape Town, for supercomputing resources.

■ REFERENCES

- (1) Lewis, K. Platforms for antibiotic discovery. *Nat. Rev. Drug Discovery* **2013**, *12* (5), 371–387.
- (2) Boucher, H. W.; Ambrose, P. G.; Chambers, H.; Ebright, R. H.; Jezek, A.; Murray, B. E.; Newland, J. G.; Ostrowsky, B.; Rex, J. H. White paper: developing antimicrobial drugs for resistant pathogens,

narrow-spectrum indications, and unmet needs. *J. Infect. Dis.* **2017**, *216*, 228.

- (3) Laxminarayan, R.; Duse, A.; Wattal, C.; Zaidi, A. K.; Wertheim, H. F.; Sumpradit, N.; Vlieghe, E.; Hara, G. L.; Gould, I. M.; Goossens, H. Antibiotic resistance—the need for global solutions. *Lancet Infect. Dis.* **2013**, *13* (12), 1057–1098.

- (4) Okano, A.; Isley, N. A.; Boger, D. L. Peripheral modifications of [Ψ [CH₂NH] Tpg₄] vancomycin with added synergistic mechanisms of action provide durable and potent antibiotics. *Proc. Natl. Acad. Sci. U. S. A.* **2017**, *114* (26), E5052–E5061.

- (5) Kalhapure, R. S.; Suleman, N.; Mocktar, C.; Seedat, N.; Govender, T. Nanoengineered drug delivery systems for enhancing antibiotic therapy. *J. Pharm. Sci.* **2015**, *104* (3), 872–905.

- (6) Huh, A. J.; Kwon, Y. J. Nanoantibiotics[®]: a new paradigm for treating infectious diseases using nanomaterials in the antibiotics resistant era. *J. Controlled Release* **2011**, *156* (2), 128–145.

- (7) Jamil, B.; Habib, H.; Abbasi, S. A.; Ihsan, A.; Nasir, H.; Imran, M. Development of cefotaxime impregnated chitosan as nano-antibiotics: De novo strategy to combat biofilm forming multi-drug resistant pathogens. *Front. Microbiol.* **2016**, *7*, 330.

- (8) Zaidi, S.; Misba, L.; Khan, A. U. Nano-therapeutics: A revolution in infection control in post antibiotic era. *Nanomedicine* **2017**, *13* (7), 2281–301.

- (9) Sonawane, S. J.; Kalhapure, R. S.; Rambharose, S.; Mocktar, C.; Vepuri, S. B.; Soliman, M.; Govender, T. Ultra-small lipid-dendrimer hybrid nanoparticles as a promising strategy for antibiotic delivery: In vitro and in silico studies. *Int. J. Pharm.* **2016**, *504* (1–2), 1–10.

- (10) Kalhapure, R. S.; Sikwal, D. R.; Rambharose, S.; Mocktar, C.; Singh, S.; Bester, L.; Oh, J. K.; Renukuntla, J.; Govender, T. Enhancing targeted antibiotic therapy via pH responsive solid lipid nanoparticles from an acid cleavable lipid. *Nanomedicine* **2017**, *13* (6), 2067–77.

- (11) Turnidge, J. Fusidic acid pharmacology, pharmacokinetics and pharmacodynamics. *Int. J. Antimicrob. Agents* **1999**, *12*, S23–S34.

- (12) Huttner, A.; Harbarth, S. Miscellaneous Agents: Fusidic Acid, Nitrofurantoin and Fosfomycin. In *Infectious Diseases*, Fourth ed.; Elsevier, 2017; pp 1277–1279

- (13) Farrell, D. J.; Mendes, R. E.; Castanheira, M.; Jones, R. N. Activity of Fusidic Acid Tested Against Staphylococci Isolated From Patients in United States Medical Centers During 2014. *Antimicrob. Agents Chemother.* **2016**, *60*, 3827.

- (14) Craft, J. C.; Moriarty, S. R.; Clark, K.; Scott, D.; Degenhardt, T. P.; Still, J. G.; Corey, G. R.; Das, A.; Fernandes, P. A Randomized, Double-Blind Phase 2 Study Comparing the Efficacy and Safety of an Oral Fusidic Acid Loading-Dose Regimen to Oral Linezolid for the Treatment of Acute Bacterial Skin and Skin Structure Infections. *Clin. Infect. Dis.* **2011**, *52*, S520–S526.

- (15) Zhang, Z.-B.; Shen, Z.-G.; Wang, J.-X.; Zhang, H.-X.; Zhao, H.; Chen, J.-F.; Yun, J. Micronization of silybin by the emulsion solvent diffusion method. *Int. J. Pharm.* **2009**, *376* (1–2), 116–122.

- (16) Hosey, C. M.; Chan, R.; Benet, L. Z. BDDCS Predictions, Self-Correcting Aspects of BDDCS Assignments, BDDCS Assignment Corrections, and Classification for more than 175 Additional Drugs. *AAPS J.* **2016**, *18* (1), 251–260.

- (17) Hogben, C. A. M. Biological Membranes and Their Passage by Drugs. Concepts in Biochemical Pharmacology. In *handbook of Experimental Pharmacology*; Brodie, B. B., Gillette, J. R., Ackerman, H. S., Eds.; Springer: Berlin, Heidelberg, 1971; pp 1–8, Vol. 28/1.

- (18) Merisko-Liversidge, E.; Liversidge, G. G.; Cooper, E. R. Nanosizing: a formulation approach for poorly-water-soluble compounds. *Eur. J. Pharm. Sci.* **2003**, *18* (2), 113–120.

- (19) Merisko-Liversidge, E. M.; Liversidge, G. G. Drug nanoparticles: formulating poorly water-soluble compounds. *Toxicol. Pathol.* **2008**, *36* (1), 43–48.

- (20) O'driscoll, C.; Griffin, B. Biopharmaceutical challenges associated with drugs with low aqueous solubility—the potential impact of lipid-based formulations. *Adv. Drug Delivery Rev.* **2008**, *60* (6), 617–624.

- (21) Wishart, D. S.; Feunang, Y. D.; Guo, A. C.; Lo, E. J.; Marcu, A.; Grant, J. R.; Sajed, T.; Johnson, D.; Li, C.; Sayeeda, Z. DrugBank 5.0: a major update to the DrugBank database for 2018. *Nucleic Acids Res.* **2018**, *46* (D1), D1074–D1082.
- (22) Vasconcelos, T.; Sarmiento, B.; Costa, P. Solid dispersions as strategy to improve oral bioavailability of poor water soluble drugs. *Drug Discovery Today* **2007**, *12* (23), 1068–1075.
- (23) Chen, H.; Khemtong, C.; Yang, X.; Chang, X.; Gao, J. Nanonization strategies for poorly water-soluble drugs. *Drug Discovery Today* **2011**, *16* (7), 354–360.
- (24) Serajuddin, A. T. Salt formation to improve drug solubility. *Adv. Drug Delivery Rev.* **2007**, *59* (7), 603–616.
- (25) Vandana, K. R.; Prasanna Raju, Y.; Harini Chowdary, V.; Sushma, M.; Vijay Kumar, N. An overview on in situ micronization technique – An emerging novel concept in advanced drug delivery. *Saudi Pharm. J.* **2014**, *22* (4), 283–289.
- (26) Khadka, P.; Ro, J.; Kim, H.; Kim, I.; Kim, J. T.; Kim, H.; Cho, J. M.; Yun, G.; Lee, J. Pharmaceutical particle technologies: an approach to improve drug solubility, dissolution and bioavailability. *Asian J. Pharm. Sci.* **2014**, *9* (6), 304–316.
- (27) Qiu, Y.; Chen, Y.; Zhang, G. G.; Yu, L.; Mantri, R. V. *Developing solid oral dosage forms: Pharmaceutical Theory and Practice*, 2nd ed.; Academic Press: Boston, 2016; pp 1127–1160.
- (28) Hamed, R.; Awadallah, A.; Sunoqrot, S.; Tarawneh, O.; Nazzal, S.; AlBaraghthi, T.; Al Sayyad, J.; Abbas, A. pH-Dependent Solubility and Dissolution Behavior of Carvedilol—Case Example of a Weakly Basic BCS Class II Drug. *AAPS PharmSciTech* **2016**, *17* (2), 418–426.
- (29) Kalhapure, R. S.; Mocktar, C.; Sikwal, D. R.; Sonawane, S. J.; Kathiravan, M. K.; Skelton, A.; Govender, T. Ion pairing with linoleic acid simultaneously enhances encapsulation efficiency and antibacterial activity of vancomycin in solid lipid nanoparticles. *Colloids Surf., B* **2014**, *117*, 303–311.
- (30) Omolo, C. A.; Kalhapure, R. S.; Jadhav, M.; Rambharose, S.; Mocktar, C.; Ndesendo, V. M.; Govender, T. Pegylated oleic acid: A promising amphiphilic polymer for nano-antibiotic delivery. *Eur. J. Pharm. Biopharm.* **2017**, *112*, 96–108.
- (31) McDonald, T. O.; Tatham, L. M.; Southworth, F. Y.; Giardiello, M.; Martin, P.; Liptrott, N. J.; Owen, A.; Rannard, S. P. High-throughput nanoprecipitation of the organic antimicrobial triclosan and enhancement of activity against *Escherichia coli*. *J. Mater. Chem. B* **2013**, *1* (35), 4455–4465.
- (32) Verma, S.; Burgess, D., Solid Nanosuspensions: The Emerging Technology and Pharmaceutical Applications as Nanomedicine. In *Pharmaceutical Suspensions: From Formulation Development to Manufacturing*; Kulshreshtha, A. K., Singh, O. N., Wall, G. M., Eds.; Springer: New York, 2010; pp 285–318.
- (33) Kalepu, S.; Nekkanti, V. Insoluble drug delivery strategies: review of recent advances and business prospects. *Acta Pharm. Sin. B* **2015**, *5* (5), 442–453.
- (34) Chu, K. R.; Lee, E.; Jeong, S. H.; Park, E.-S. Effect of particle size on the dissolution behaviors of poorly water-soluble drugs. *Arch. Pharmacol. Res.* **2012**, *35* (7), 1187–1195.
- (35) Van Eerdenbrugh, B.; Vermant, J.; Martens, J. A.; Froyen, L.; Humbeek, J. V.; Van den Mooter, G.; Augustijns, P. Solubility Increases Associated with Crystalline Drug Nanoparticles: Methodologies and Significance. *Mol. Pharmaceutics* **2010**, *7* (5), 1858–1870.
- (36) Rabinow, B. E. Nanosuspensions in drug delivery. *Nat. Rev. Drug Discovery* **2004**, *3* (9), 785–796.
- (37) Ansari, M.; Althubaiti, M.; Ibnouf, M.; Anwer, M.; Ahmed, M.; Fatima, F.; Jamil, S. Enhanced anti-bacterial effects of ciprofloxacin enclosed in cyclodextrin and nano-suspension carrier systems. *Bull. Env. Pharmacol. Life Sci.* **2015**, *4* (11), 14.
- (38) Parmentier, J.; Tan, E. H.; Low, A.; Möschwitzter, J. P. Downstream drug product processing of itraconazole nanosuspension: Factors influencing drug particle size and dissolution from nanosuspension-layered beads. *Int. J. Pharm.* **2017**, *524* (1), 443–453.
- (39) Tahara, K.; Nishikawa, M.; Matsui, K.; Hisazumi, K.; Onodera, R.; Tozuka, Y.; Takeuchi, H. In Vitro and In Vivo Characterization of Drug Nanoparticles Prepared Using PureNano Continuous Crystallizer to Improve the Bioavailability of Poorly Water Soluble Drugs. *Pharm. Res.* **2016**, *33* (9), 2259–2268.
- (40) Sikwal, D. R.; Kalhapure, R. S.; Jadhav, M.; Rambharose, S.; Mocktar, C.; Govender, T. Non-ionic self-assembling amphiphilic polyester dendrimers as new drug delivery excipients. *RSC Adv.* **2017**, *7* (23), 14233–14246.
- (41) Polli, J. E. In vitro studies are sometimes better than conventional human pharmacokinetic in vivo studies in assessing bioequivalence of immediate-release solid oral dosage forms. The AAPS journal. *AAPS J.* **2008**, *10* (2), 289–299.
- (42) De Groote, M. A.; Gruppo, V.; Woolhiser, L. K.; Orme, I. M.; Gilliland, J. C.; Lenaerts, A. J. Importance of confirming data on the in vivo efficacy of novel antibacterial drug regimens against various strains of *Mycobacterium tuberculosis*. *Antimicrob. Agents Chemother.* **2012**, *56* (2), 731–8.
- (43) Hare, J. I.; Lammers, T.; Ashford, M. B.; Puri, S.; Storm, G.; Barry, S. T. Challenges and strategies in anti-cancer nanomedicine development: An industry perspective. *Adv. Drug Delivery Rev.* **2017**, *108*, 25–38.
- (44) Borhani, D. W.; Shaw, D. E. The future of molecular dynamics simulations in drug discovery. *J. Comput.-Aided Mol. Des.* **2012**, *26* (1), 15–26.
- (45) Mohyeldin, S. M.; Mehanna, M. M.; Elgindy, N. A. The relevancy of controlled nanocrystallization on rifampicin characteristics and cytotoxicity. *Int. J. Nanomed.* **2016**, *11*, 2209.
- (46) Lee, M. K.; Kim, M. Y.; Kim, S.; Lee, J. Cryoprotectants for freeze drying of drug nano-suspensions: Effect of freezing rate. *J. Pharm. Sci.* **2009**, *98* (12), 4808–4817.
- (47) Agrawal, N.; Skelton, A. A. 12-Crown-4 Ether Disrupts the Patient Brain-Derived Amyloid- β -Fibril Trimer: Insight from All-Atom Molecular Dynamics Simulations. *ACS Chem. Neurosci.* **2016**, *7* (10), 1433–1441.
- (48) Agrawal, N.; Skelton, A. A. Binding of 12-Crown-4 with Alzheimer's $A\beta$ 40 and $A\beta$ 42 Monomers and Its Effect on Their Conformation: Insight from Molecular Dynamics Simulations. *Mol. Pharmaceutics* **2018**, *15* (1), 289–299.
- (49) Bemporad, D.; Luttmann, C.; Essex, J. W. Behaviour of small solutes and large drugs in a lipid bilayer from computer simulations. *Biochim. Biophys. Acta, Biomembr.* **2005**, *1718* (1), 1–21.
- (50) Bemporad, D.; Luttmann, C.; Essex, J. Computer simulation of small molecule permeation across a lipid bilayer: dependence on bilayer properties and solute volume, size, and cross-sectional area. *Biophys. J.* **2004**, *87* (1), 1–13.
- (51) Subashini, M.; Devarajan, P. V.; Sonavane, G. S.; Doble, M. Molecular dynamics simulation of drug uptake by polymer. *J. Mol. Model.* **2011**, *17* (5), 1141–1147.
- (52) Gao, Y.; Olsen, K. W. Drug-polymer Interactions at Water-Crystal Interfaces and Implications for Crystallization Inhibition: Molecular Dynamics Simulations of Amphiphilic Block Copolymer Interactions with Tolazamide Crystals. *J. Pharm. Sci.* **2015**, *104* (7), 2132–2141.
- (53) Zunszain, P. A.; Ghuman, J.; McDonagh, A. F.; Curry, S. Crystallographic analysis of human serum albumin complexed with 4Z, 15E-bilirubin-IX α . *J. Mol. Biol.* **2008**, *381* (2), 394–406.
- (54) Cousins, K. R. Computer review of ChemDraw Ultra 12.0. *J. Am. Chem. Soc.* **2011**, *133* (21), 8388–8388.
- (55) Vanommeslaeghe, K.; Hatcher, E.; Acharya, C.; Kundu, S.; Zhong, S.; Shim, J.; Darian, E.; Guvench, O.; Lopes, P.; Vorobyov, I.; Mackerell, A. D. CHARMM general force field: A force field for drug-like molecules compatible with the CHARMM all-atom additive biological force fields. *J. Comput. Chem.* **2009**, *31* (4), 671–690.
- (56) Mark, P.; Nilsson, L. Structure and dynamics of the TIP3P, SPC, and SPC/E water models at 298 K. *J. Phys. Chem. A* **2001**, *105* (43), 9954–9960.
- (57) Bixon, M.; Lifson, S. Potential functions and conformations in cycloalkanes. *Tetrahedron* **1967**, *23* (2), 769–784.

- (58) Parrinello, M.; Rahman, A. Polymorphic transitions in single crystals: A new molecular dynamics method. *J. Appl. Phys.* **1981**, *52* (12), 7182–7190.
- (59) Darden, T.; York, D.; Pedersen, L. Particle mesh Ewald: An $N \log(N)$ method for Ewald sums in large systems. *J. Chem. Phys.* **1993**, *98* (12), 10089–10092.
- (60) Kumari, R.; Kumar, R.; Lynn, A. g_mmpbsa—A GROMACS Tool for High-Throughput MM-PBSA Calculations. *J. Chem. Inf. Model.* **2014**, *54* (7), 1951–1962.
- (61) Abraham, M. J.; Murtola, T.; Schulz, R.; Páll, S.; Smith, J. C.; Hess, B.; Lindahl, E. GROMACS: High performance molecular simulations through multi-level parallelism from laptops to supercomputers. *SoftwareX* **2015**, *1*, 19–25.
- (62) Ali, H. S. M.; York, P.; Ali, A. M. A.; Blagden, N. Hydrocortisone nanosuspensions for ophthalmic delivery: A comparative study between microfluidic nanoprecipitation and wet milling. *J. Controlled Release* **2011**, *149* (2), 175–181.
- (63) Zhou, L.; Yang, L.; Tilton, S.; Wang, J. Development of a high throughput equilibrium solubility assay using miniaturized shake-flask method in early drug discovery. *J. Pharm. Sci.* **2007**, *96* (11), 3052–3071.
- (64) Curbete, M. M.; Salgado, H. R. N. Stability-indicating RP-LC method for quantification of fusidic acid in cream. *Braz. J. Pharm. Sci.* **2016**, *52* (3), 447–457.
- (65) Clinical and Laboratory Standards Institute, *Methods for Dilution Antimicrobial Susceptibility Tests for Bacteria That Grow Aerobically*; Approved Standard, 9th ed.; CLSI: Pennsylvania, USA, 2012; Vol. 32, p 63.
- (66) European Committee for Antimicrobial Susceptibility Testing of the European Society of Clinical Microbiology and Infectious Disease (ESCMID). Determination of minimum inhibitory concentrations (MICs) of antibacterial agents by broth dilution. *Clin. Microbiol. Infect.* **2003**, *9* (8), ix–xv.
- (67) O'Brien-Simpson, N. M.; Pantarat, N.; Attard, T. J.; Walsh, K. A.; Reynolds, E. C. A Rapid and Quantitative flow cytometry method for the analysis of membrane disruptive antimicrobial activity. *PLoS One* **2016**, *11* (3), e0151694.
- (68) Rüger, M.; Bensch, G.; Tüngler, R.; Reichl, U. A flow cytometric method for viability assessment of *Staphylococcus aureus* and *Burkholderia cepacia* in mixed culture. *Cytometry, Part A* **2012**, *81A* (12), 1055–1066.
- (69) Bexfield, A.; Bond, A. E.; Roberts, E. C.; Dudley, E.; Nigam, Y.; Thomas, S.; Newton, R. P.; Ratcliffe, N. A. The antibacterial activity against MRSA strains and other bacteria of a < 500 Da fraction from maggot excretions/secretions of *Lucilia sericata* (Diptera: Calliphoridae). *Microbes Infect.* **2008**, *10* (4), 325–333.
- (70) Shrestha, N. K.; Scalera, N. M.; Wilson, D. A.; Procop, G. W. Rapid differentiation of methicillin-resistant and methicillin-susceptible *Staphylococcus aureus* by flow cytometry after brief antibiotic exposure. *J. Clin. Microbiol.* **2011**, *49* (6), 2116–2120.
- (71) Arndt-Jovin, D. J.; Jovin, T. M. Fluorescence labeling and microscopy of DNA. *Methods Cell Biol.* **1989**, *30*, 417–448.
- (72) Renggli, S.; Keck, W.; Jenal, U.; Ritz, D. Role of autofluorescence in flow cytometric analysis of *Escherichia coli* treated with bactericidal antibiotics. *J. Bacteriol.* **2013**, *195* (18), 4067–4073.
- (73) Kugelberg, E.; Norström, T.; Petersen, T. K.; Duvold, T.; Andersson, D. I.; Hughes, D. Establishment of a superficial skin infection model in mice by using *Staphylococcus aureus* and *Streptococcus pyogenes*. *Antimicrob. Agents Chemother.* **2005**, *49* (8), 3435–3441.
- (74) Vingsbo Lundberg, C.; Frimodt-Møller, N. Efficacy of topical and systemic antibiotic treatment of methicillin-resistant *Staphylococcus aureus* in a murine superficial skin wound infection model. *Int. J. Antimicrob. Agents* **2013**, *42* (3), 272–275.
- (75) Fall, A.; Bertrand, F.; Ovarlez, G.; Bonn, D. Shear thickening of cornstarch suspensions. *J. Rheol.* **2012**, *56* (3), 575–591.
- (76) Riekes, M. K.; Kuminek, G.; Rauber, G. S.; de Campos, C. E. M.; Bortoluzzi, A. J.; Stulzer, H. K. HPMC as a potential enhancer of nimodipine biopharmaceutical properties via ball-milled solid dispersions. *Carbohydr. Polym.* **2014**, *99*, 474–482.
- (77) Novo, D. J.; Perlmutter, N. G.; Hunt, R. H.; Shapiro, H. M. Multiparameter Flow Cytometric Analysis of Antibiotic Effects on Membrane Potential, Membrane Permeability, and Bacterial Counts of *Staphylococcus aureus* and *Micrococcus luteus*. *Antimicrob. Agents Chemother.* **2000**, *44* (4), 827–834.
- (78) Tuomela, A.; Hirvonen, J.; Peltonen, L. Stabilizing Agents for Drug Nanocrystals: Effect on Bioavailability. *Pharmaceutics* **2016**, *8* (2), 16.
- (79) Sharma, N.; Madan, P.; Lin, S. Effect of process and formulation variables on the preparation of parenteral paclitaxel-loaded biodegradable polymeric nanoparticles: A co-surfactant study. *Asian J. Pharm. Sci.* **2016**, *11* (3), 404–416.
- (80) Zweers, M. L.; Grijpma, D. W.; Engbers, G. H.; Feijen, J. The preparation of monodisperse biodegradable polyester nanoparticles with a controlled size. *J. Biomed. Mater. Res.* **2003**, *66B* (2), 559–566.
- (81) LaGrow, A. P.; Ingham, B.; Toney, M. F.; Tilley, R. D. Effect of Surfactant Concentration and Aggregation on the Growth Kinetics of Nickel Nanoparticles. *J. Phys. Chem. C* **2013**, *117* (32), 16709–16718.
- (82) Pina, C.; Fernández-Díaz, L.; Prieto, M.; Veintemillas-Verdaguer, S. Metastability in drowning-out crystallisation: precipitation of highly soluble sulphates. *J. Cryst. Growth* **2001**, *222* (1), 317–327.
- (83) Van Eerdenbrugh, B.; Van den Mooter, G.; Augustijns, P. Top-down production of drug nanocrystals: Nanosuspension stabilization, miniaturization and transformation into solid products. *Int. J. Pharm.* **2008**, *364* (1), 64–75.
- (84) Yoon, T. J.; Son, W.-S.; Park, H. J.; Seo, B.; Kim, T.; Lee, Y.-W. Tetracycline nanoparticles precipitation using supercritical and liquid CO₂ as antisolvents. *J. Supercrit. Fluids* **2016**, *107*, 51–60.
- (85) Panagiotou, T.; Mesite, S. V.; Fisher, R. J. Production of Norfloxacin Nanosuspensions Using Microfluidics Reaction Technology through Solvent/Antisolvent Crystallization. *Ind. Eng. Chem. Res.* **2009**, *48* (4), 1761–1771.
- (86) Reverchon, E.; Della Porta, G. Production of antibiotic micro- and nano-particles by supercritical antisolvent precipitation. *Powder Technol.* **1999**, *106* (1), 23–29.
- (87) Xia, D.; Quan, P.; Piao, H.; Piao, H.; Sun, S.; Yin, Y.; Cui, F. Preparation of stable nitrendipine nanosuspensions using the precipitation-ultrasonication method for enhancement of dissolution and oral bioavailability. *Eur. J. Pharm. Sci.* **2010**, *40* (4), 325–334.
- (88) Cherry, R. S.; Kwon, K.-Y. Transient shear stresses on a suspension cell in turbulence. *Biotechnol. Bioeng.* **1990**, *36* (6), 563–571.
- (89) Yang, D.; Ye, S.; Ge, J. Solvent Wrapped Metastable Colloidal Crystals: Highly Mutable Colloidal Assemblies Sensitive to Weak External Disturbance. *J. Am. Chem. Soc.* **2013**, *135* (49), 18370–18376.
- (90) Liu, Y. Is the Free Energy Change of Adsorption Correctly Calculated? *J. Chem. Eng. Data* **2009**, *54* (7), 1981–1985.
- (91) Deng, Y.; Roux, B. Computations of Standard Binding Free Energies with Molecular Dynamics Simulations. *J. Phys. Chem. B* **2009**, *113* (8), 2234–2246.
- (92) Torchilin, V. P. Structure and design of polymeric surfactant-based drug delivery systems. *J. Controlled Release* **2001**, *73* (2), 137–172.
- (93) Nakashima, K.; Bahadur, P. Aggregation of water-soluble block copolymers in aqueous solutions: Recent trends. *Adv. Colloid Interface Sci.* **2006**, *123–126*, 75–96.
- (94) Liu, J.; Zou, M.; Piao, H.; Liu, Y.; Tang, B.; Gao, Y.; Ma, N.; Cheng, G. Characterization and Pharmacokinetic Study of Aprepitant Solid Dispersions with Soluplus®. *Molecules* **2015**, *20* (6), 11345.
- (95) Zhang, K.; Yu, H.; Luo, Q.; Yang, S.; Lin, X.; Zhang, Y.; Tian, B.; Tang, X. Increased dissolution and oral absorption of itraconazole/Soluplus extrudate compared with itraconazole nanosuspension. *Eur. J. Pharm. Biopharm.* **2013**, *85* (3), 1285–1292.

- (96) Raval, A. J.; Patel, M. M. Preparation and characterization of nanoparticles for solubility and dissolution rate enhancement of meloxicam. *Intl Res. J. Pharm.* **2011**, *1* (2), 42–49.
- (97) Sarkari, M.; Brown, J.; Chen, X.; Swinnea, S.; Williams, R. O.; Johnston, K. P. Enhanced drug dissolution using evaporative precipitation into aqueous solution. *Int. J. Pharm.* **2002**, *243* (1), 17–31.
- (98) Gao, L.; Liu, G.; Wang, X.; Liu, F.; Xu, Y.; Ma, J. Preparation of a chemically stable quercetin formulation using nanosuspension technology. *Int. J. Pharm.* **2011**, *404* (1), 231–237.
- (99) Hogg, R.; Healy, T. W.; Fuerstenau, D. W. Mutual coagulation of colloidal dispersions. *Trans. Faraday Soc.* **1966**, *62*, 1638–1651.
- (100) Krieger, I. M.; Dougherty, T. J. A mechanism for non-Newtonian flow in suspensions of rigid spheres. *Trans. Soc. Rheol.* **1959**, *3* (1), 137–152.
- (101) Ree, F.; Ree, T.; Eyring, H. Relaxation Theory of Transport Problems in Condensed Systems. *Ind. Eng. Chem.* **1958**, *50* (7), 1036–1040.
- (102) Rudyak, V. Y.; Belkin, A. A.; Egorov, V. V. On the effective viscosity of nanosuspensions. *Tech. Phys.* **2009**, *54* (8), 1102–1109.
- (103) Sun, J.; Wang, F.; Sui, Y.; She, Z.; Zhai, W.; Wang, C.; Deng, Y. Effect of particle size on solubility, dissolution rate, and oral bioavailability: evaluation using coenzyme Q(10) as naked nanocrystals. *Int. J. Nanomed.* **2012**, *7*, 5733–5744.
- (104) Wais, U.; Jackson, A. W.; He, T.; Zhang, H. Nanoformulation and encapsulation approaches for poorly water-soluble drug nanoparticles. *Nanoscale* **2016**, *8* (4), 1746–1769.
- (105) Leitner, J.; Sedmidubský, D. Enhanced solubility of nanostructured paracetamol. *Biomed. Phys. Eng. Express* **2016**, *2* (5), 055007.
- (106) Mihranyan, A.; Strømme, M. Solubility of fractal nanoparticles. *Surf. Sci.* **2007**, *601* (2), 315–319.
- (107) Letellier, P.; Mayaffre, A.; Turmine, M. Solubility of nanoparticles: nonextensive thermodynamics approach. *J. Phys.: Condens. Matter* **2007**, *19* (43), 436229.
- (108) Riss, T. L.; Moravec, R. A.; Niles, A. L.; Duellman, S.; Benink, H. A.; Worzella, T. J.; Minor, L. Cell viability assays. *Assay Guidance Manual* **2016**, 2016, 1–34.
- (109) Moloughney, J. G.; Weisleder, N. Poloxamer 188 (p188) as a membrane resealing reagent in biomedical applications. *Recent Pat. Biotechnol.* **2012**, *6* (3), 200–211.
- (110) Guo, J.-j.; Yue, P.-F.; Lv, J.-L.; Han, J.; Fu, S.-s.; Jin, S.-x.; Jin, S.-y.; Yuan, H.-L. Development and in vivo/in vitro evaluation of novel herpetic nanosuspension. *Int. J. Pharm.* **2013**, *441* (1), 227–233.
- (111) Ambhore, N. P.; Dandagi, P. M.; Gadad, A. P. Formulation and comparative evaluation of HPMC and water soluble chitosan-based sparfloxacin nanosuspension for ophthalmic delivery. *Drug Delivery Transl. Res.* **2016**, *6* (1), 48–56.
- (112) Rabinow, B.; Kipp, J.; Papadopoulos, P.; Wong, J.; Glosson, J.; Gass, J.; Sun, C.-S.; Wielgos, T.; White, R.; Cook, C.; Barker, K.; Wood, K. Itraconazole IV nanosuspension enhances efficacy through altered pharmacokinetics in the rat. *Int. J. Pharm.* **2007**, *339* (1), 251–260.
- (113) Bhawana; Basniwal, R. K.; Buttar, H. S.; Jain, V. K.; Jain, N. Curcumin Nanoparticles: Preparation, Characterization, and Antimicrobial Study. *J. Agric. Food Chem.* **2011**, *59* (5), 2056–2061.
- (114) Chen, Y.; Lan, T.; Duan, L.; Wang, F.; Zhao, B.; Zhang, S.; Wei, W. Adsorptive Removal and Adsorption Kinetics of Fluoroquinolone by Nano-Hydroxyapatite. *PLoS One* **2015**, *10* (12), e0145025.
- (115) Wang, L.; Hu, C.; Shao, L. The antimicrobial activity of nanoparticles: present situation and prospects for the future. *Int. J. Nanomed.* **2017**, *12*, 1227–1249.
- (116) Dobie, D. Fusidic acid resistance in *Staphylococcus aureus*. *Arch. Dis. Child.* **2004**, *89* (1), 74–77.
- (117) Christiansen, K. Fusidic acid adverse drug reactions. *Int. J. Antimicrob. Agents* **1999**, *12*, S3–S9.
- (118) Chaplin, D. D. Overview of the Immune Response. *J. Allergy Clin. Immunol.* **2010**, *125* (2), S3–S23.

AM-17-0300

Six-armed PEG-*b*-PCL copolymer based on G1-PETIM dendrimer for nano delivery of vancomycin

Calvin A. Omolo¹, Rahul S. Kalhapure^{1,2}, Sanjeev Rambharose¹, Chunderika Mocktar¹, Thirumala Govender¹.

¹Discipline of Pharmaceutical Sciences, School of Health Sciences, University of KwaZulu-Natal, Private Bag X54001, Durban 4000, South Africa.

²School of Pharmacy, The University of Texas at El Paso, 500 W. University Ave, El Paso, Texas 79968, USA.



2017
AAPS ANNUAL
MEETING & EXPOSITION

Email: govenderth@ukzn.ac.za; (T. Govender); kalhapure@ukzn.ac.za, rkalhapure@utep.edu, rahul.kalhapure@rediffmail.com (R.S. Kalhapure).

DEVELOPING SCIENCE. IMPACTING HEALTH.

PURPOSE

Bacterial infections and antibiotic resistance is becoming a major health concern globally. Nanocarrier systems is an innovative strategy to overcome the limitations with conventional dosage forms for improved delivery and efficacy of antibiotics and also to overcome resistance. The synthesis of novel materials for the design of nanoantibiotics with enhanced performance is therefore essential.¹ Whilst, micelles have been employed to deliver drug, their disadvantage like their dissociation in concentrations below the CMC has highlighted the need to design unimolecular micelles².

OBJECTIVES

The objectives of present work were to: (1) synthesize a nontoxic hybrid dendrimer block 6 arm star polymer (G1-PETIM-PEG-*b*-PCL) (2) utilize the synthesized novel G1-PETIM-PEG-*b*-PCL star polymer to prepare unimolecular micelles for sustained nano delivery of vancomycin to address the problem of bacterial resistance.

METHODS

Synthesis of 6m-PEPEA

G1-PETIM-PEG-*b*-PCL was synthesized by coupling G1-poly(propyl ether imine) dendrimer (G1-PETIM) to mPEG-*b*-PCL block polymer (Figure 1) using EDC/DMAP chemistry. The polymer was purified by dialysis method using dialysis bags of pore size 14kDa.



Figure 1. Scheme for synthesis G1-PETIM-PEG-*b*-PCL.

Aggregation behaviour and cytotoxicity

Aggregation behaviour of G1-PETIM-PEG-*b*-PCL was determined by dynamic light scattering (DLS) and in vitro cytotoxicity was performed on A549, MCF 7 and Hep G2 cells using 3-(4,5-dimethylthiazol-2-yl)-2,5-diphenyltetrazolium bromide (MTT) assay.

Preparation and characterization of Vancomycin loaded unimolecular micelles (VM-G1-PETIM-PEG-*b*-PCL)

VM-G1-PETIM-PEG-*b*-PCL micelles were prepared by solvent evaporation method and characterized for size, polydispersity index (PDI), zeta potential (ZP), entrapment efficiency (%EE), surface morphology, in vitro drug release, in vitro and in vivo antibacterial activity.

RESULTS

In vitro cytotoxicity

MTT assay confirmed non-toxicity of synthesized polymer as % cell viability was > 77 % at all the tested concentrations against all the cell lines.

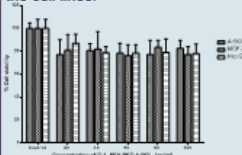


Figure 2. Cytotoxicity evaluation of G1-PETIM-PEG-*b*-PCL.

Aggregation behaviour

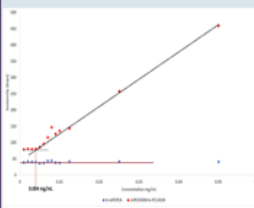


Figure 3. Plot of concentration (mg/mL) against intensity (kcps) for G1-PETIM-PEG-*b*-PCL and mPEG-*b*-PCL.

Size and surface morphology

VM-G1-PETIM-PEG-*b*-PCL micelles were spherical with, size, PDI and ZP of 52.48 ± 2.6 nm, 0.103 ± 0.047 , and -7.3 ± 1.3 mV respectively and %EE of $62.24 \pm 3.8\%$.

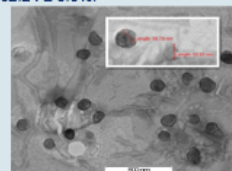


Figure 4. TEM image of VM-G1-PEA-PEG-*b*-PCL micelles.

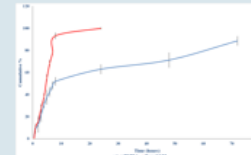


Figure 5. In vitro release pattern of VM-G1-PEA-PEG-*b*-PCL and VM solution at pH 7.4 (n = 3).

In vitro antibacterial activity

VM-G1-PETIM-PEG-*b*-PCL had 8 and 16-fold greater activity against *S. aureus* and MRSA when compared to bare VM. The activity of VM-G1-PETIM-PEG-*b*-PCL was sustained up to 120 hours.

In vivo antibacterial activity

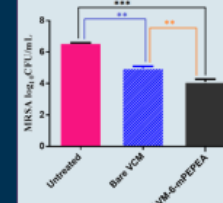


Figure 6. MRSA burden post 48 h treatment. Data represents mean \pm SD (n = 3). **denotes significant for untreated versus bare VM. ***denotes significant difference between untreated and VM-G1-PETIM-PEG-*b*-PCL micelles and **denotes significant difference between bare VM free base and VM-G1-PETIM-PEG-*b*-PCL micelles.

There was a significant difference ($p = 0.0017$) in the bacterial colony forming units per ml (CFU/ml) remaining in the skin of mice treated with bare VM and those treated with VM-G1-PETIM-PEG-*b*-PCL. The MRSA burden in VM-G1-PETIM-PEG-*b*-PCL micelles treated mice was almost 7-fold less compared to the bare VM.

CONCLUSION

In conclusion, this study has introduced:

- G1-PETIM-PEG-*b*-PCL, a novel safe biodegradable hybrid star polymer, for pharmaceutical and biological applications, and
- VM loaded G1-PETIM-PEG-*b*-PCL micelles with high drug loading capacity, sustained drug release profile and enhanced antibacterial activity.

Therefore, G1-PETIM-PEG-*b*-PCL can be of major significance in improving the therapeutic efficacy of antibacterial drugs, thereby addressing drug resistance challenges by resistant bacteria.

REFERENCES

- Kalhapure, R.S., et al., J. Pharm. Sc., 2015, 52, 6265-6268.
- Zhang, C., et al., Macromolecules, 2017, 50(4), 1657-1665.

Acknowledgements

The authors thank College of Health Sciences (CHS), University of KwaZulu-Natal (UKZN), UKZN Nanotechnology Platform and the National Research Foundation (NRF) of South Africa (NRF Grant No. 87790 and 88453) for financial support.



Activate Windows



Calvin A. Omoto¹, Rahul S. Kalhapure¹, Sanjeev Rambharose¹, Chunderika Mocktar¹, Sanil Singh², Thirumala Govender^{1*}

1. Discipline of Pharmaceutical Sciences, School of Health Sciences, University of KwaZulu-Natal, Private Bag X54001, Durban, South Africa.
 2. Biomedical Resource Unit, University of KwaZulu-Natal, Westville Campus, Durban, 4000, South Africa.
- *Corresponding author.

INTRODUCTION AND AIMS

- Staphylococcus aureus (S.A) is a pathogen of major concern due to its immense ability to cause wide range of infections and change its genome. This has resulted in a resistant isolates Methicillin-resistant Staphylococcus aureus (MRSA), that is resistant to a wide range of antibiotics.¹
- Nanotechnology has shown with significant success to enhance and prevent antibiotic resistance.¹
- The synthesis of novel materials for the design of nanoantibiotics with enhanced performance is therefore essential.
- Whilst, micelles have been employed to deliver drug, their disadvantage like their dissociation in concentrations below the CMC has called the need to fashion out unimolecular micelles.²
- The aim of this study was to synthesize a novel six arm star polymer star to offer unimolecular micelles with high loading capacity and sustained delivery of vancomycin against susceptible and resistant Staphylococcus aureus

MATERIALS AND METHODS

Preparation and characterization of VM-6m-PEPEA

- Synthesis of 6m-PEPEA was achieved via five step synthesis and characterized for FTIR, ¹H and ¹³C NMR, aggregation behavior and MTT assay for biosafety.
- Vancomycin (VM) loaded Unimolecular micelles from (6m-PEPEA VM-6m-PEPEA) were prepared using solvent evaporation and characterized for particle size, polydispersity index (PDI) and zeta potential (ZP) using a Zetasizer Nano ZS90 (Malvern Instruments Ltd., UK).
- Morphology was examined using a TEM (Jeol, JEM-1010, Japan)
- Entrapment efficiency and drug loading was determined by an ultrafiltration method.
- Thermoprofiles of 6m-PEPEA, VM and lyophilized micelles was determined using Shimadzu DSC-60, (Japan)
- In vitro drug release profile was performed using the diffusion dialysis bag method.
- The minimum inhibitory concentration (MIC) values for VM-6m-PEPEA micelles were determined against S.A and MRSA by a broth dilution method.
- A mouse skin infection model was used to determine in-vivo antibacterial activity (Protocol approval number. AREC/104/015PD)

REFERENCES & ACKNOWLEDGMENT

- Refer
1. Kalhapure RS, et al. (2017) A novel six-armed PEG-b-PCL copolymer (6m-PEPEA) based on G1 PETIM dendrimer for nano delivery of vancomycin. Journal of pharmaceutical sciences 104:872-905.
 2. Zhang, C., et al., Self-Assembly Kinetics of Amphiphilic Dendritic Copolymers. Macromolecules, 2017. 50(4): p. 1657-1665.

Acknowledgment

College of Health Sciences, UKZN Nanotechnology Platform and National Research Foundation of South Africa.

RESULTS AND DISCUSSION

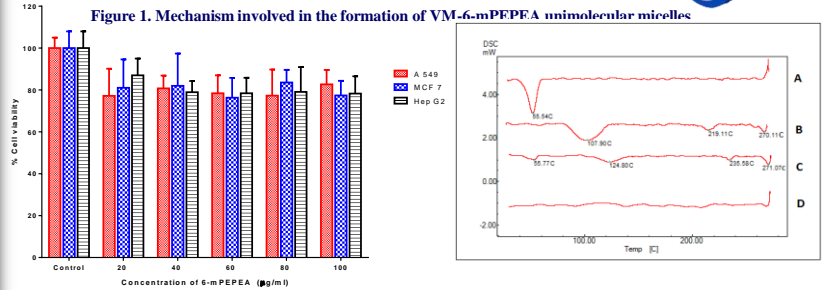
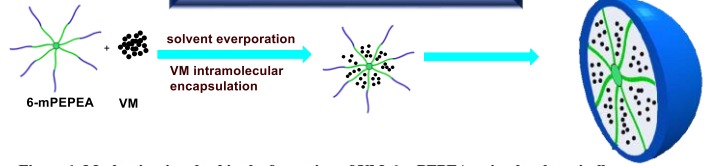


Figure 2. MTT assays showed 6-mPEPEA as nontoxic with a high cell viability (77%-85%).

Figure 5. DSC thermogram of A= 6m-PEPEA, B= VM C= physical mixture, E= VM-6mPEPEA

- Unimolecular spherical micelles were prepared. Size, PI and ZP was 52.48±2.6 nm, 0.103 ± 0.047, -7.3±1.3 mV, respectively and drug loading was

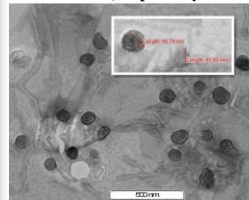


Figure 4. Morphology of the unimolecular micelles

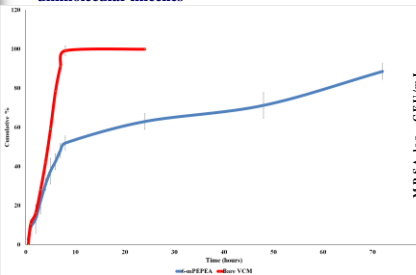


Figure 3. release profile of the VM-6-mPEPEA and bare VM

Time (hours)	S. aureus (MIC µg/mL)				MRSA (MIC µg/mL)			
	24	48	72	96	24	48	72	96
Bare VCM	3.9	NA	NA	NA	15.65	NA	NA	NA
VCM-6-mPEPEA	0.488	0.488	0.488	0.488	0.98	0.98	0.98	0.98
Blank	NA	NA	NA	NA	NA	NA	NA	NA

NA = No activity. The values are expressed as mean ±SD, n=3.

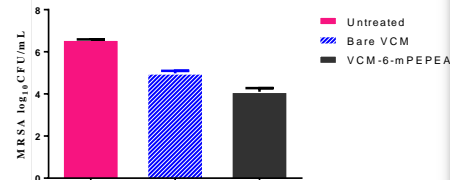


Figure 6. Disease burden of MRSA in treatment groups

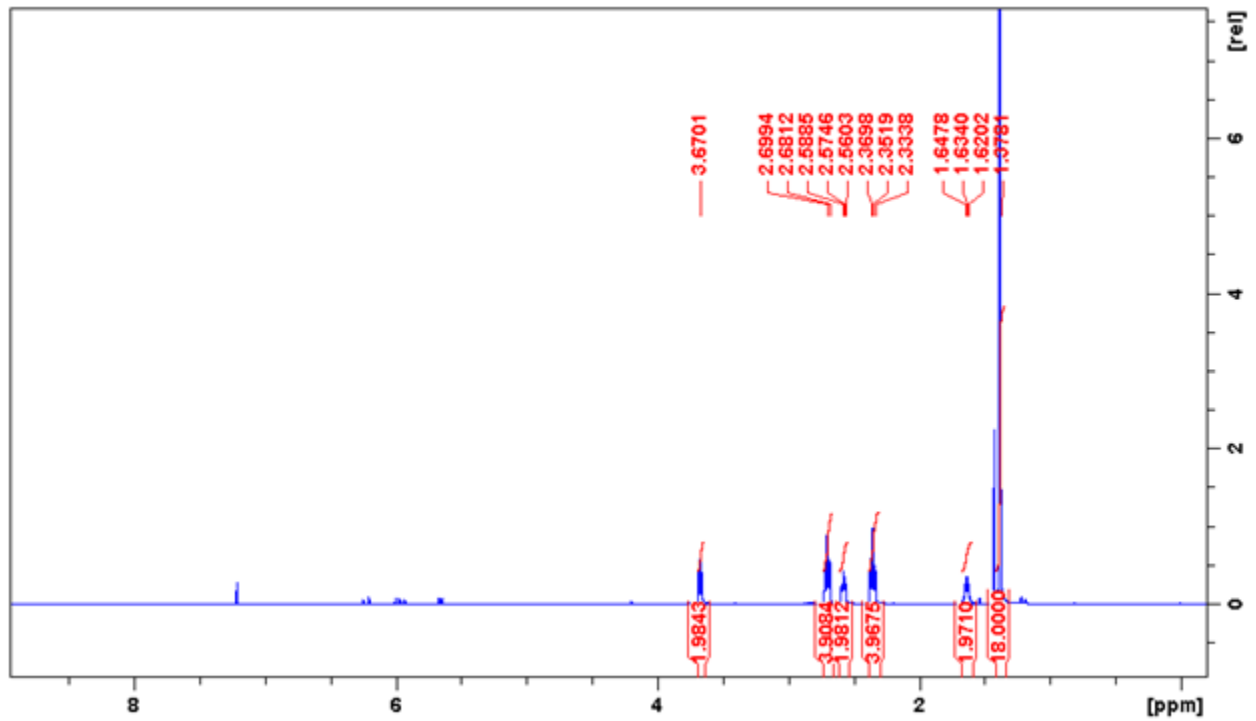
- 6-mPEPEA star polymer was successfully synthesized.
- The synthesized polymer was evaluated from cytotoxicity and the cell viability proved the polymer to be safe
- VM loaded micelles were formulated from the star polymer and were found to be in ultra small size of 52.48±2.6 with low polydispersity index.
- In vitro drug release from the micelles and VM solution showed that VM release from the micelles was at 88% after 72 hours while VM solution was 99% after 8 hours
- There was 7 and 16 times lower MIC in S.A and MRSA respectively for VM-6-mPEPEA when compared to bare VM
- Mice treated with VM-6-mPEPEA had a 7 and 284 times lower disease burden when compared to when treated with bare VM and untreated test groups
- VM-6-mPEPEA was stable for 3month when stored at 4 °C and at room temperature

CONCLUSIONS

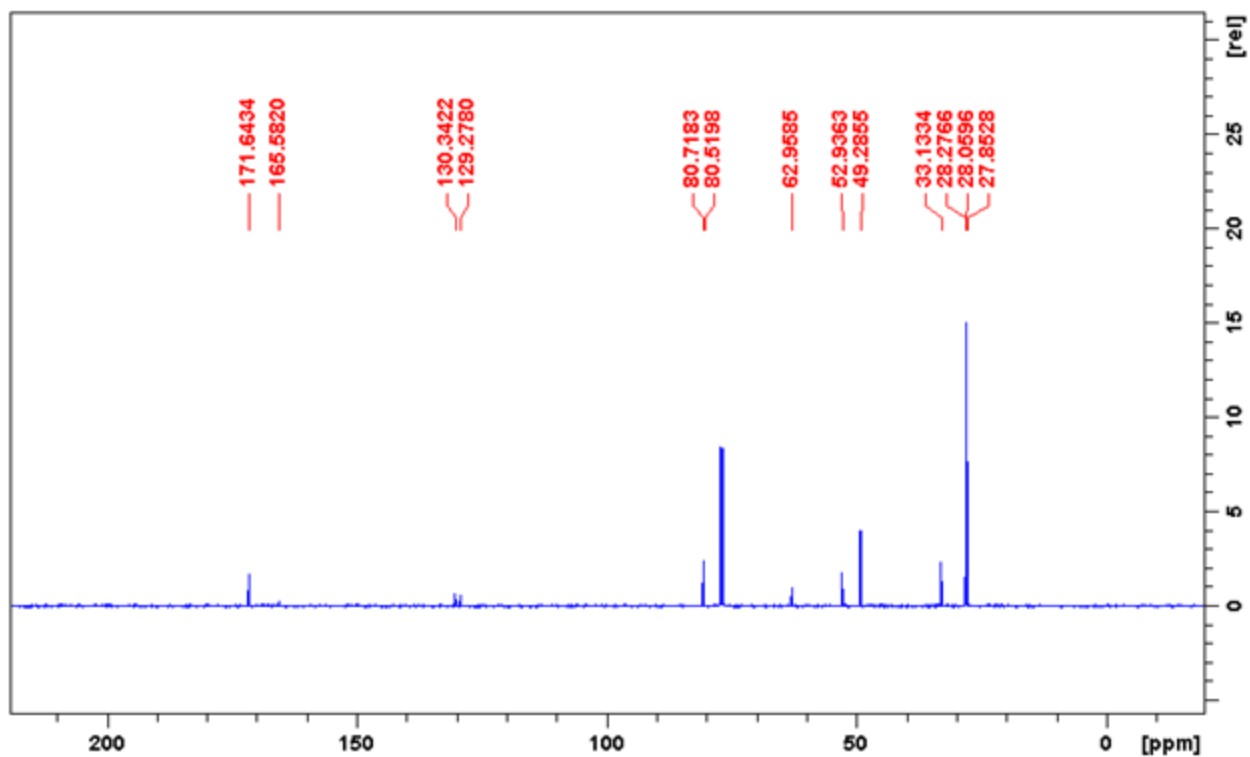
- The VM-6-mPEPEA star polymer proved to be safe. Release VM from VM-6-mPEPEA the micelles showed sustained release and the enhanced antibacterial activity of VM against sensitive and resistant S. aureus in both in vitro and in vivo studies. Therefore, this study suggest that VM-6-mPEPEA can be an effective formulation to combat resistant infections .

APPENDIX VI

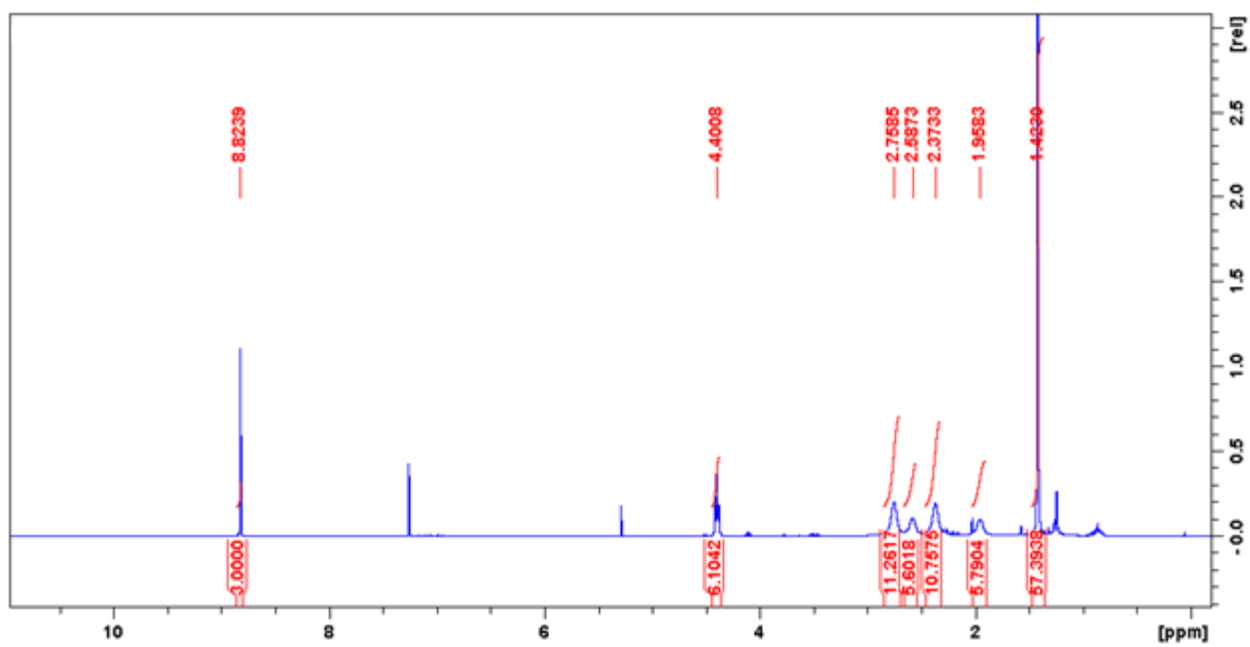
1.0 Synthesis and characterization of the hybrid dendrimer (NMR)



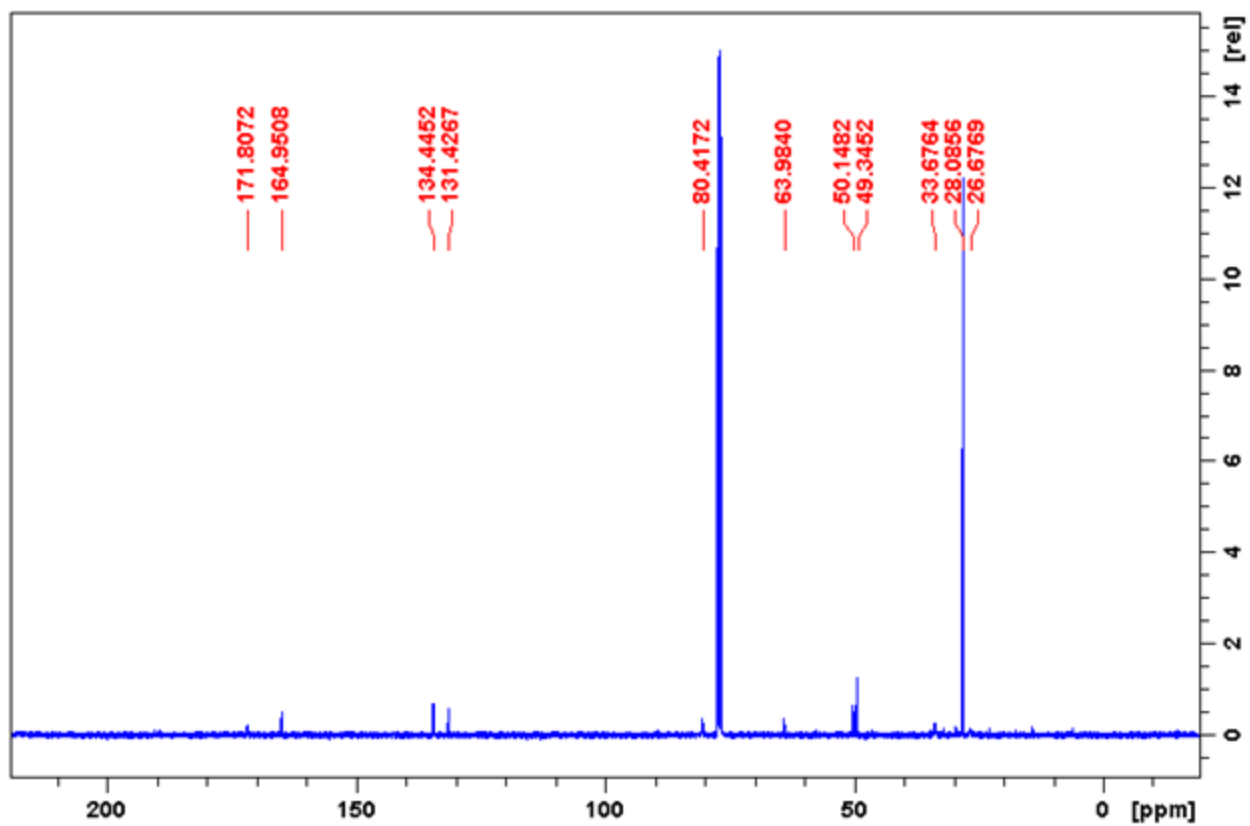
Compound I proton NMR



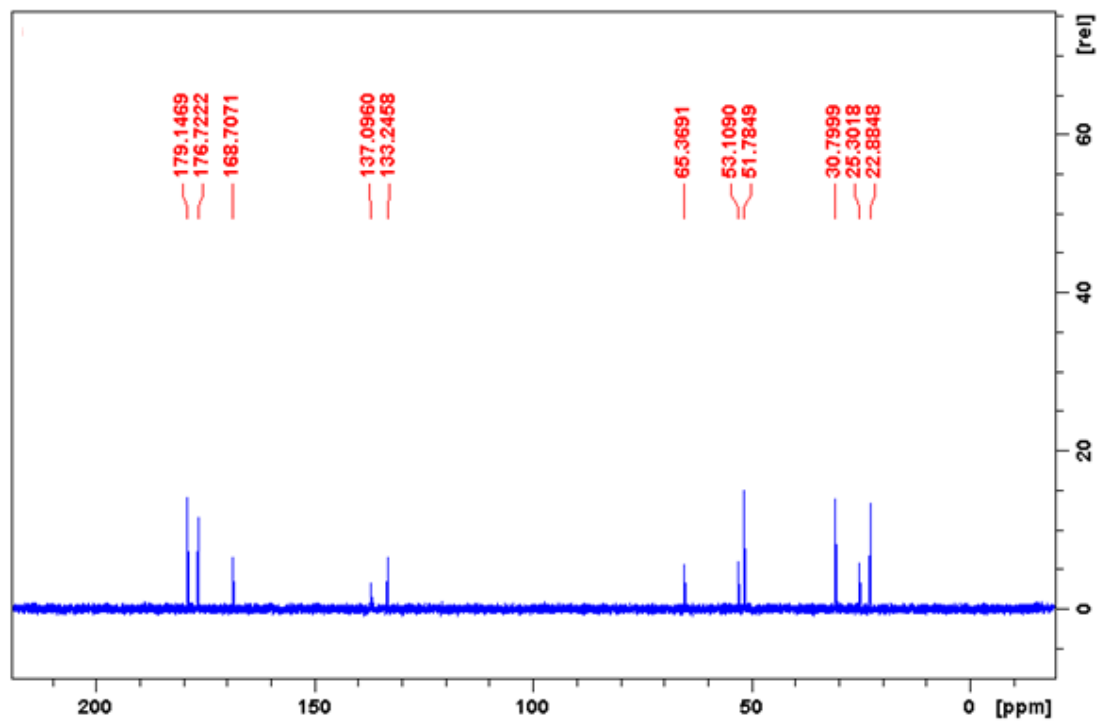
Compound I ¹³C NMR



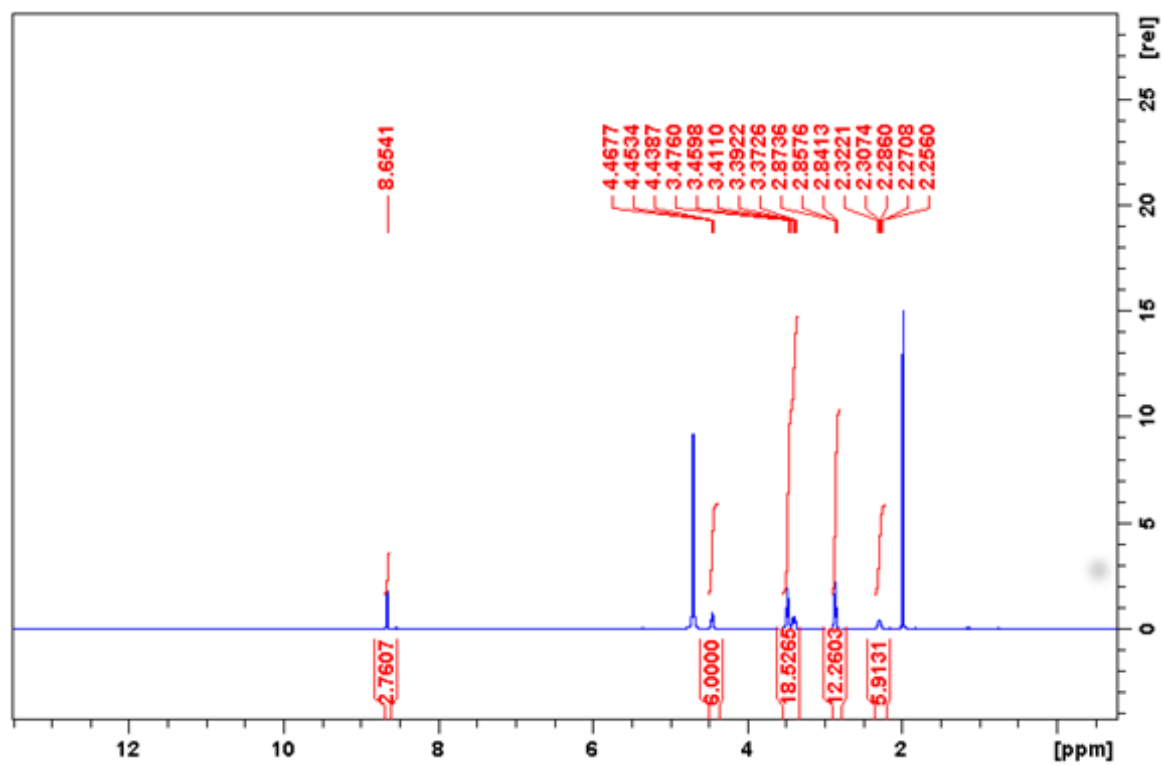
Compound II proton NMR



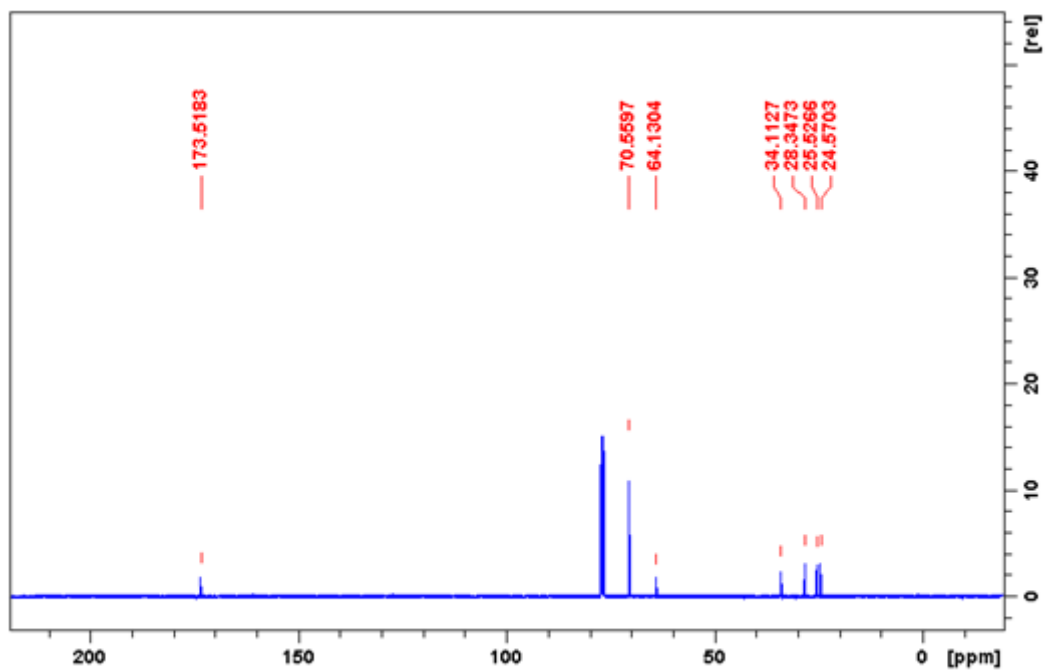
Compound II ^{13}C NMR



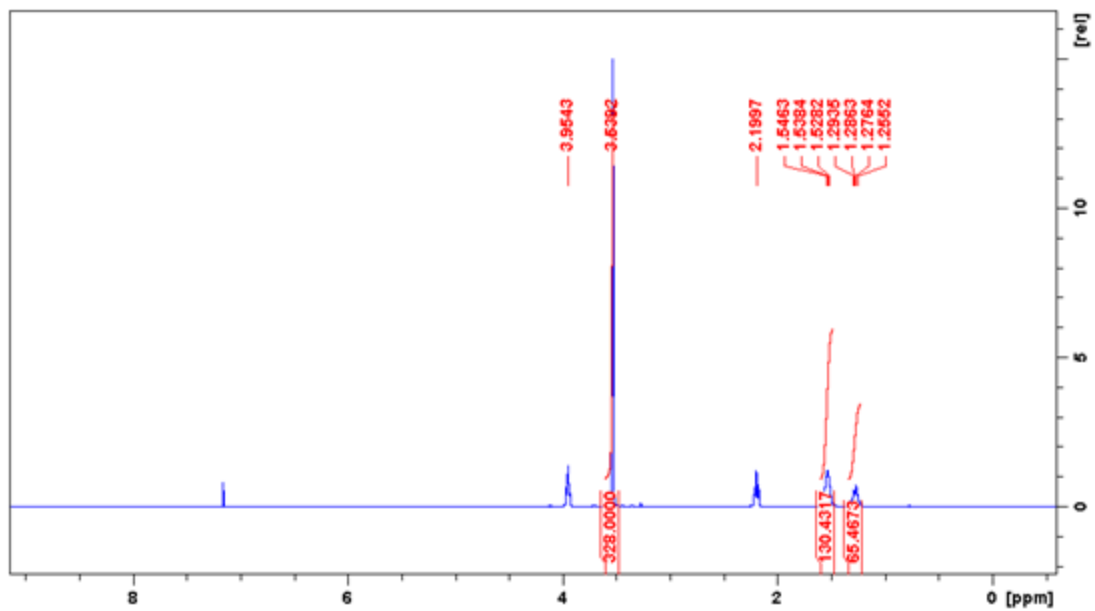
Compound III ^{13}C NMR



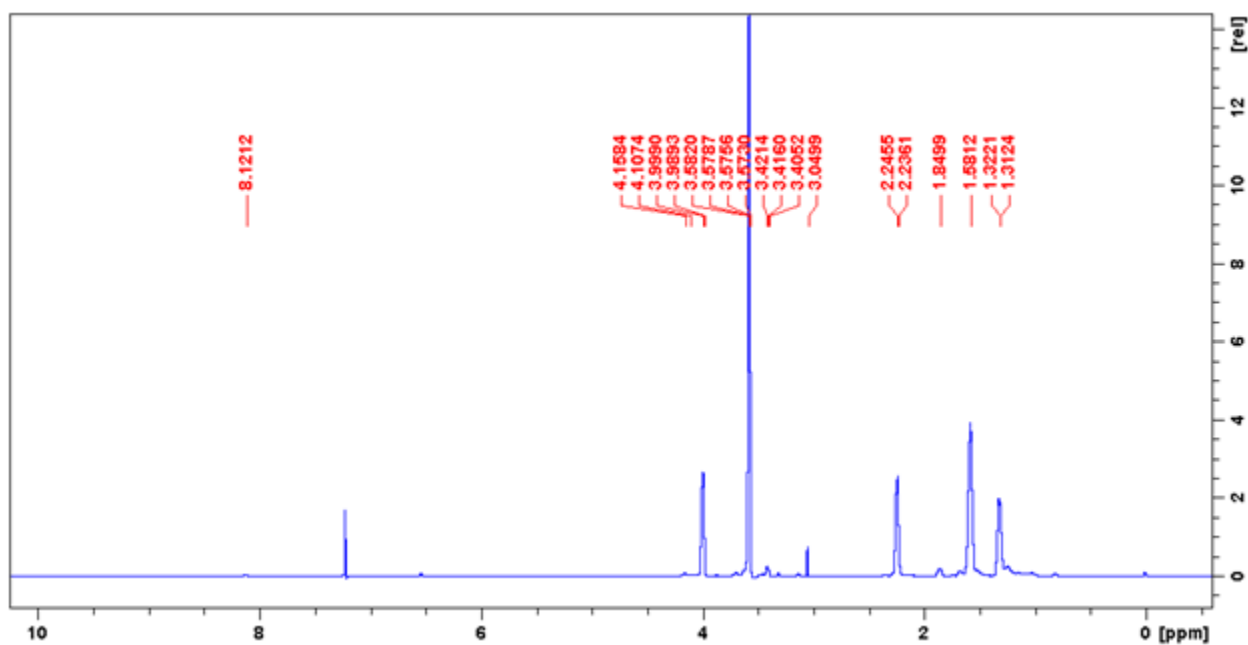
Compound III proton NMR



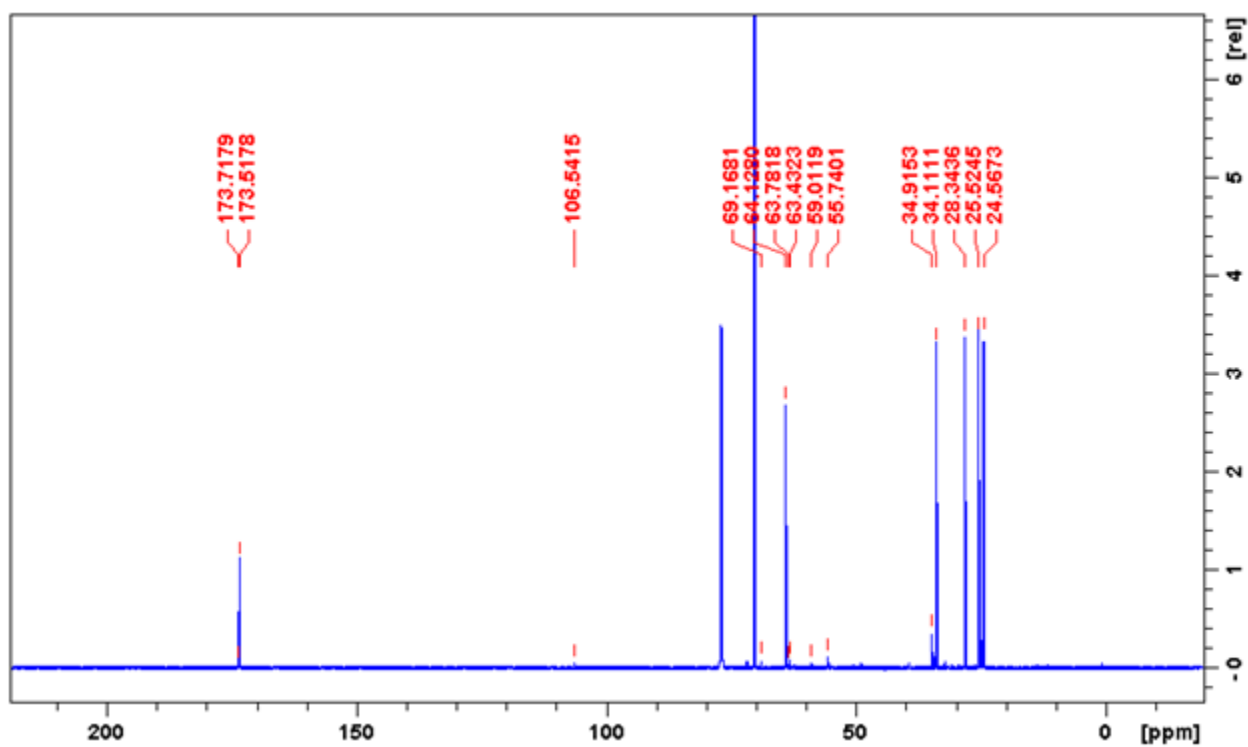
Compound IV Proton NMR



Compound IV ¹³C NMR



Compound 5 proton NMR



Compound V ¹³C NMR

References

Appendix VII

Elemental Composition Report

Single Mass Analysis

Tolerance = 5.0 PPM / DBE: min = -1.5, max = 50.0

Element prediction: Off

Number of isotope peaks used for i-FIT = 2

Monoisotopic Mass, Even Electron Ions

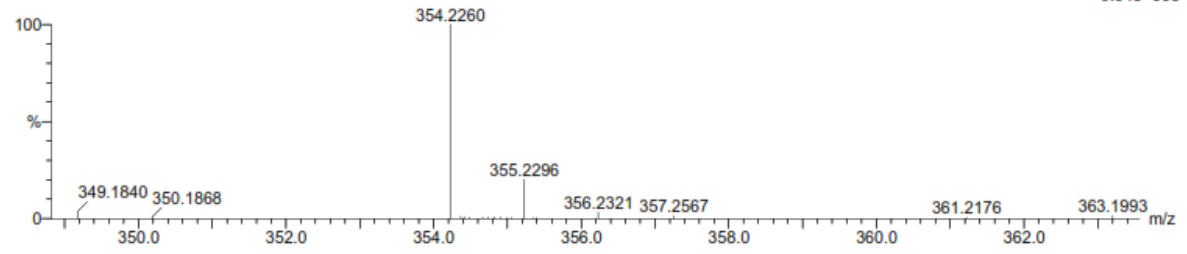
28 formula(e) evaluated with 1 results within limits (up to 20 best isotopic matches for each mass)

Elements Used:

C: 15-20 H: 30-35 N: 0-5 O: 0-5 Na: 0-1

AEDTAE 53 (1.754) Cm (1.61)

TOF MS ES+



Minimum: -1.5
Maximum: 5.0 5.0 50.0

Mass	Calc. Mass	mDa	PPM	DBE	i-FIT	i-FIT (Norm)	Formula
354.2260	354.2256	0.4	1.1	1.5	195.0	0.0	C17 H33 N O5 Na

HRMS compound I

Elemental Composition Report

Single Mass Analysis

Tolerance = 4.0 PPM / DBE: min = -1.5, max = 50.0

Element prediction: Off

Number of isotope peaks used for i-FIT = 2

Monoisotopic Mass, Even Electron Ions

8 formula(e) evaluated with 1 results within limits (up to 20 best isotopic matches for each mass)

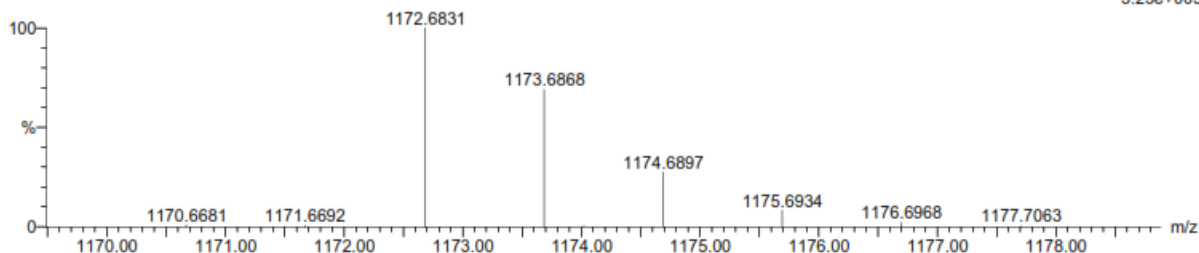
Elements Used:

C: 55-60 H: 95-100 N: 0-5 O: 15-20 Na: 1-1

6-PEAPE 6 (0.169) Cm (1.61)

TOF MS ES+

3.23e+005



Minimum:

Maximum: 5.0 4.0 -1.5

50.0

Mass	Calc. Mass	mDa	PPM	DBE	i-FIT	i-FIT (Norm)	Formula
1172.6831	1172.6821	1.0	0.9	12.5	28.9	0.0	C60 H99 N3 O18 Na

HRMS compound II

Elemental Composition Report

Single Mass Analysis

Tolerance = 4.0 PPM / DBE: min = -1.5, max = 50.0

Element prediction: Off

Number of isotope peaks used for i-FIT = 2

Monoisotopic Mass, Even Electron Ions

12 formula(e) evaluated with 1 results within limits (up to 20 best isotopic matches for each mass)

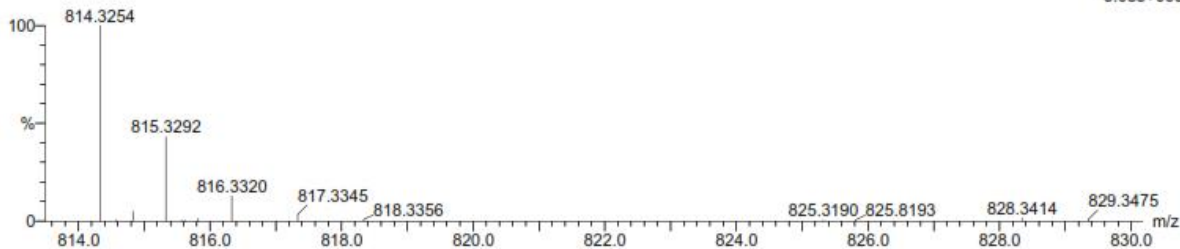
Elements Used:

C: 35-40 H: 50-55 N: 0-5 O: 15-20

6-PEA 50 (1.652) Cm (1.61)

TOF MS ES+

3.05e+005



Minimum:

Maximum: 5.0 4.0 -1.5

50.0

Mass	Calc. Mass	mDa	PPM	DBE	i-FIT	i-FIT (Norm)	Formula
814.3254	814.3246	0.8	1.0	12.5	89.6	0.0	C36 H52 N3 O18

HRMS Compound III

Elemental Composition Report

Single Mass Analysis

Tolerance = 4.0 PPM / DBE: min = -1.5, max = 50.0

Element prediction: Off

Number of isotope peaks used for i-FIT = 2

Monoisotopic Mass, Even Electron Ions

8 formula(e) evaluated with 1 results within limits (up to 20 best isotopic matches for each mass)

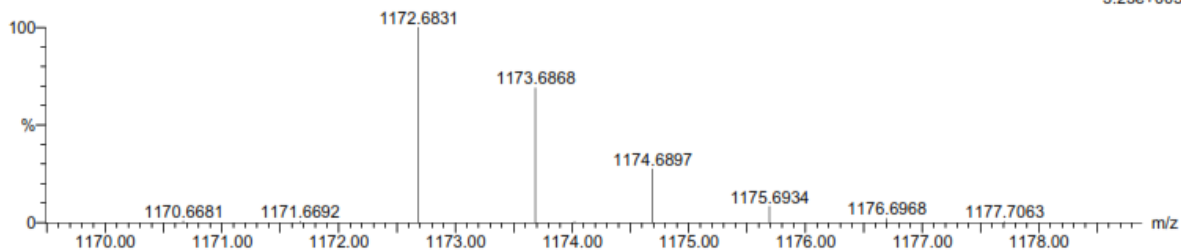
Elements Used:

C: 55-60 H: 95-100 N: 0-5 O: 15-20 Na: 1-1

6-PEAPE 6 (0.169) Cm (1:61)

TOF MS ES+

3.23e+005



Minimum: -1.5
Maximum: 5.0 4.0 50.0

Mass	Calc. Mass	mDa	PPM	DBE	i-FIT	i-FIT (Norm)	Formula
1172.6831	1172.6821	1.0	0.9	12.5	28.9	0.0	C60 H99 N3 O18 Na

HRMS compound IV

Calvin A. Omolo¹, Rahul S. Kalhapure¹, Sanjeev Rambharose¹, Chunderika Mocktar¹, Sanil Singh², Thirumala Govender^{3*}

1. Discipline of Pharmaceutical Sciences, School of Health Sciences, University of KwaZulu-Natal, Private Bag X54001, Durban, South Africa.
2. Biomedical Resource Unit, University of KwaZulu-Natal, Westville Campus, Durban, 4000, South Africa.
3. *Corresponding author.

INTRODUCTION AND AIMS

- Staphylococcus aureus (S.A) is a pathogen of major concern due to its immense ability to cause wide range of infections and change its genome. This has resulted in a resistant isolates Methicillin-resistant Staphylococcus aureus (MRSA), that is resistant to a wide range of antibiotics.¹
- Nanotechnology has shown with significant success to enhance and prevent antibiotic resistance.¹
- Nanosuspensions are among nanosystems that increase surface area of drugs leading to enhanced solubility and activity of poorly soluble drugs.²
- Whilst, fusidic acid has been formulated into various nanosystems, its formulation as a nanosuspension has not been previously explored despite it being a simple nanosystem containing 100% drug and stabilizing agent.
- The aim of this study was to prepare and characterize fusidic acid nanosuspension (FA-NS) and evaluate its activity against SA and MRSA.

MATERIALS AND METHODS

Preparation and characterization of FA-NS

- Antisolvent Sono-precipitation technique was employed to prepare FA-NS.
- Prepared FA-NS were characterized for particle size, polydispersity index (PDI) and zeta potential (ZP) using a Zetasizer Nano ZS90 (Malvern Instruments Ltd., UK).
- An optimum formulation was achieved through screening for type and concentration of surfactant, solvent, drug concentration, and sonication power and time.
- Morphology was examined using a TEM (Jeol, JEM-1010, Japan).
- The minimum inhibitory concentration (MIC) values for FA-NS were determined against S.A and MRSA by a broth dilution method.
- Solubility of FA was determined by a shaking incubator technique at 37 °C for 24 hours. Undissolved FA was removed by filtering through syringe filters (cellulose acetate membrane, 0.2 mm, GVS filter technology, USA)
- FA content was determined using a reported HPLC method (Shimadzu Prominence DGU-20A3)
- A mouse skin infection model was used to determine *in-vivo* antibacterial activity (Protocol approval number. AREC/104/015PD)
- Wet and lyophilized FA-NS were evaluated for their stability for a period of three months by storing then at

REFERENCES

1. Kalhapure et al. 2015, Nanoengineered drug delivery systems for enhancing antibiotic therapy. Journal of pharmaceutical sciences 104:872-905.
2. Kesiosoglou et al. 2007, Nanosizing Oral formulation development and biopharmaceutical evaluation. Advanced Drug Delivery Reviews, 59(7), 631-644. .

ACKNOWLEDGMENT

College of Health Sciences, UKZN Nanotechnology Platform and National Research Foundation of South Africa.

RESULTS

Table 1. Effect of Surfactant type on the formulation (n = 3)

Surfactant	Size (nm)	PDI	ZP (mV)
PVP	563.5± 6.18	0.354 ± 0.031	- 10.6 ± 0.243
LF68	590.0± 7.92	0.254 ± 0.017	-13.1 ± 2.7
SDS	388.6 ± 58	0.592 ± 0.124	-62.5 ± 6.34
RH 40	1159±21.36	0.33 ± 0.045	-10 ± 0.163
HS15	1289 ± 28	0.412 ± 0.23	-7.21 ± 1.67
Tween 80	772.4± 4.71	0.375 ± 0.049	-11.1± 0.0707
EL	1403±18.69	0.462 ± 0.004	-8.57 ± 1.16

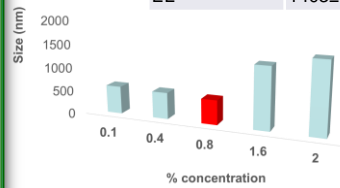


Fig 1. Effect of poloxamer 188 surfactant on the formulation (n = 3).

Table 3. The Effect of sonication time (n = 3)

Sonication n (min)	Size (nm)	PDI	ZP (mV)
5	552.3±13.2	0.198±0.02	-11.6±0.7
10	357.6±5.11	0.14±0.03	-18.1± 7.9
15	265 ± 2.25	0.16±0.03	-16.9± 0.8

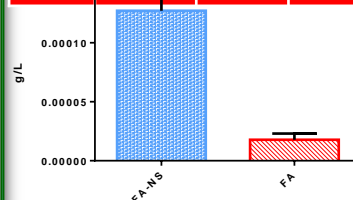


Fig 3. Solubility of FA-NS and FA in water

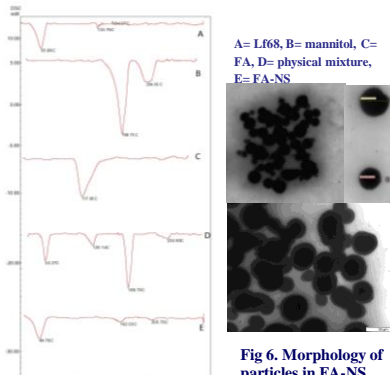


Fig 5. DSC thermogram of FA-NS and excipients

Fig 6. Morphology of particles in FA-NS

Table 2. Effect of different concentration of FA (n = 3)

FA	size (nm)	PDI	ZP (mV)
10mg/ml	552.3±13.2	0.198±0.002	-11.6±0.7
15mg/ml	788.5±52.8	0.371±0.052	-10.5± 1.1
20mg/ml	1183±111.0	0.488±0.093	-62.5± 6.3
30mg/ml	1336±89.4	0.498±0.042	-5.19± 2.19

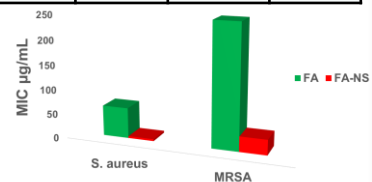


Fig 2. *In vitro* activity of FA-NS and FA against SA and MRSA

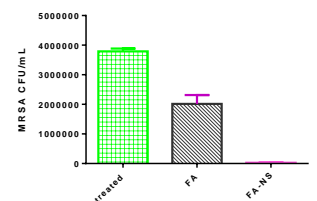


Fig 4. Disease burden of MRSA in treatment groups

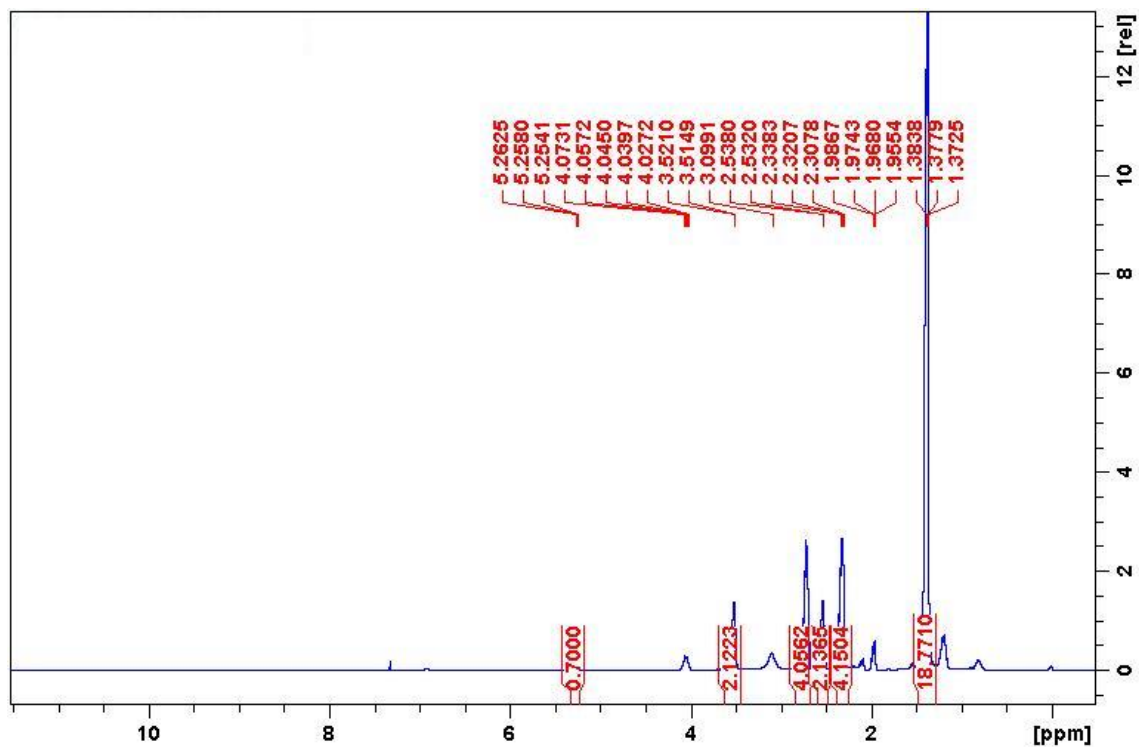
DISCUSSIONS

- Poloxamer 188 stabilized the system better compared to other surfactants. This is probably due to hydrophobic polyoxypropylene in the surfactant.
- There was an increase in particle size with increase of FA concentration due to saturation that supported crystal growth.
- FA-NS had a significant ($p=0.0093$) 8-fold increase of solubility in water when compared to water.
- There was 16 and 8 times lower MIC in S.A and MRSA respectively for FA-NS when compared to FA
- Mice treated with FA-NS had a 76 and 142 times lower disease burden when compared to when treated with FA and untreated test groups
- FA-NS was stable for 3 months for both lyophilized and wet formulations stored at 4 °C and 2 months stability for formulations stored at room temperature

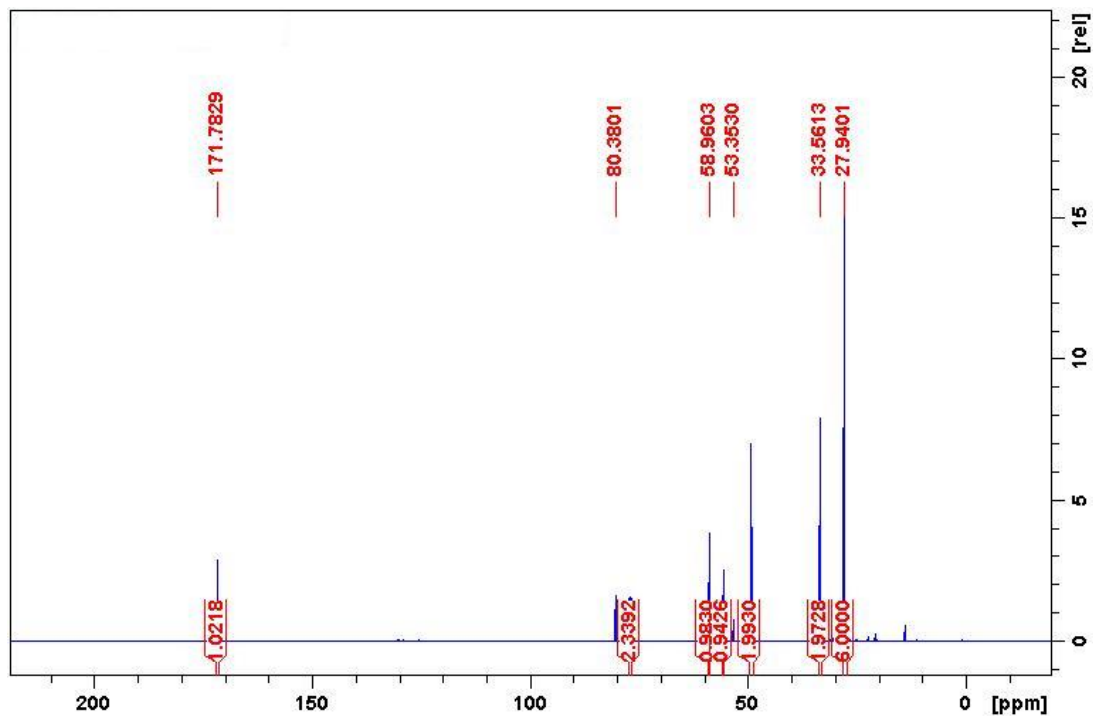
CONCLUSIONS

- The FA-NS formulation improved solubility and enhanced antibacterial activity of FA against sensitive and resistant *S. aureus* in both *in vitro* and *in vivo* studies. Therefore, this study suggest that nanosuspensions can be an effective formulation to combat resistant infections by improving activity of poorly water soluble antibiotics.

APPENDIX IX



S Figure 1. 4-(tert-butoxy)-N-(3-(tert-butoxy)-3-oxopropyl)-N-(2-hydroxyethyl)-3-oxobutan-1-aminium (**compound 3**) proton NMR.



S Figure 2. 4-(tert-butoxy)-N-(3-(tert-butoxy)-3-oxopropyl)-N-(2-hydroxyethyl)-3-oxobutan-1-aminium (**compound 3**) ^{13}C NMR.

APPENDIX IX

Elemental Composition Report

Compound 3

Page 1

Single Mass Analysis

Tolerance = 5.0 PPM / DBE: min = -1.5, max = 100.0

Element prediction: Off

Number of isotope peaks used for i-FIT = 2

Monoisotopic Mass, Even Electron Ions

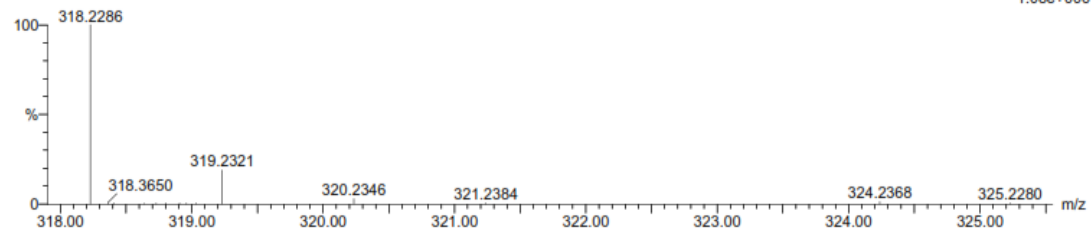
16 formula(e) evaluated with 1 results within limits (up to 20 best isotopic matches for each mass)

Elements Used:

C: 15-20 H: 30-35 N: 0-5 O: 0-5

Ethanolamine tertbutyl 23 (0.776) Cm (1.60)

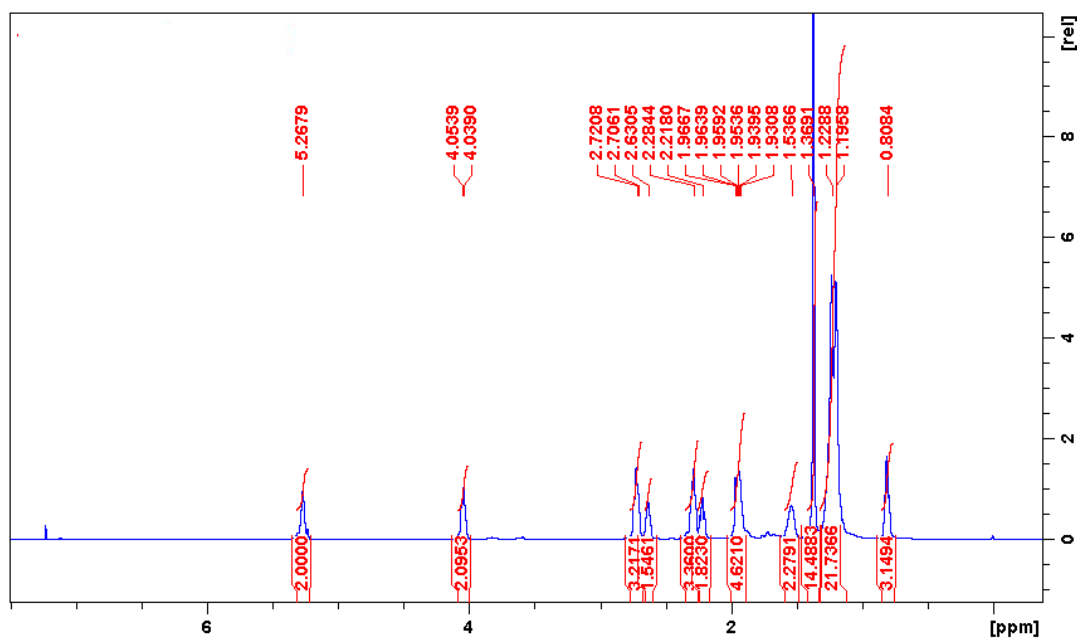
TOF MS ES+



Minimum: -1.5
Maximum: 5.0 5.0 100.0

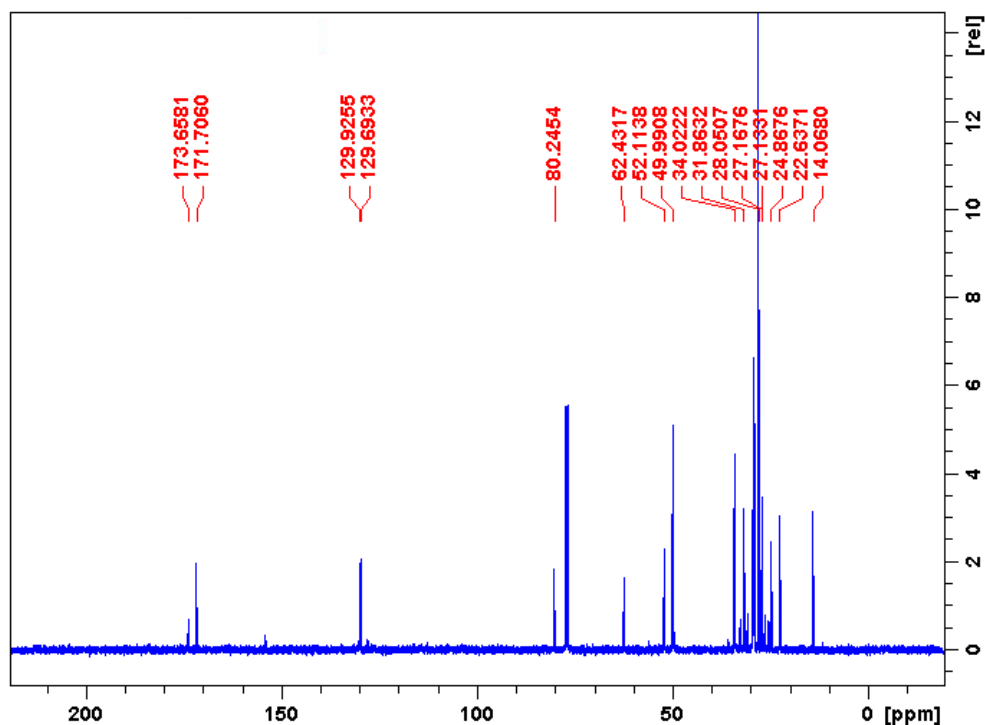
Mass	Calc. Mass	mDa	PPM	DBE	i-FIT	i-FIT (Norm)	Formula
318.2286	318.2280	0.6	1.9	1.5	143.2	0.0	C16 H32 N O5

S Figure 3. 4-(tert-butoxy)-N-(3-(tert-butoxy)-3-oxopropyl)-N-(2-hydroxyethyl)-3-oxobutan-1-aminium (compound 3) HRMS.



S Figure 4. 4-(tert-butoxy)-N-(3-(tert-butoxy)-3-oxopropyl)-N-(2-(oleoyloxy)ethyl)-3-oxobutan-1-aminium (compound 4) proton NMR

APPENDIX IX



S Figure 5. 4-(tert-butoxy)-N-(3-(tert-butoxy)-3-oxopropyl)-N-(2-(oleoyloxy)ethyl)-3-oxobutan-1-aminium (compound 4) ^{13}C NMR

Elemental Composition Report

Compound 4

Page 1

Single Mass Analysis

Tolerance = 5.0 PPM / DBE: min = -1.5, max = 100.0

Element prediction: Off

Number of isotope peaks used for i-FIT = 2

Monoisotopic Mass, Even Electron Ions

12 formula(e) evaluated with 1 results within limits (up to 20 best isotopic matches for each mass)

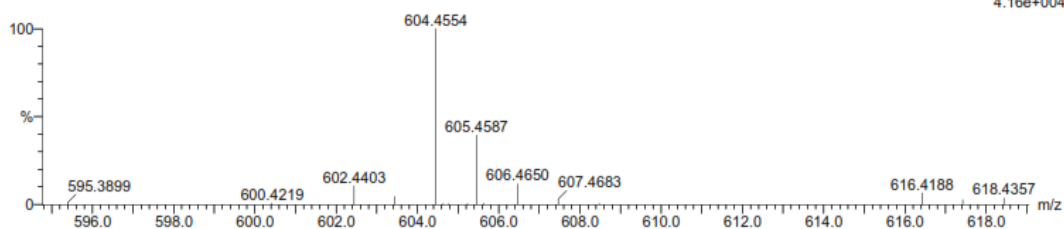
Elements Used:

C: 30-35 H: 60-65 N: 0-5 O: 5-10 Na: 1-1

OA Ethanolamine tertbutyl 10 (0.304) Cm (1:61)

TOF MS ES+

4.16e+004

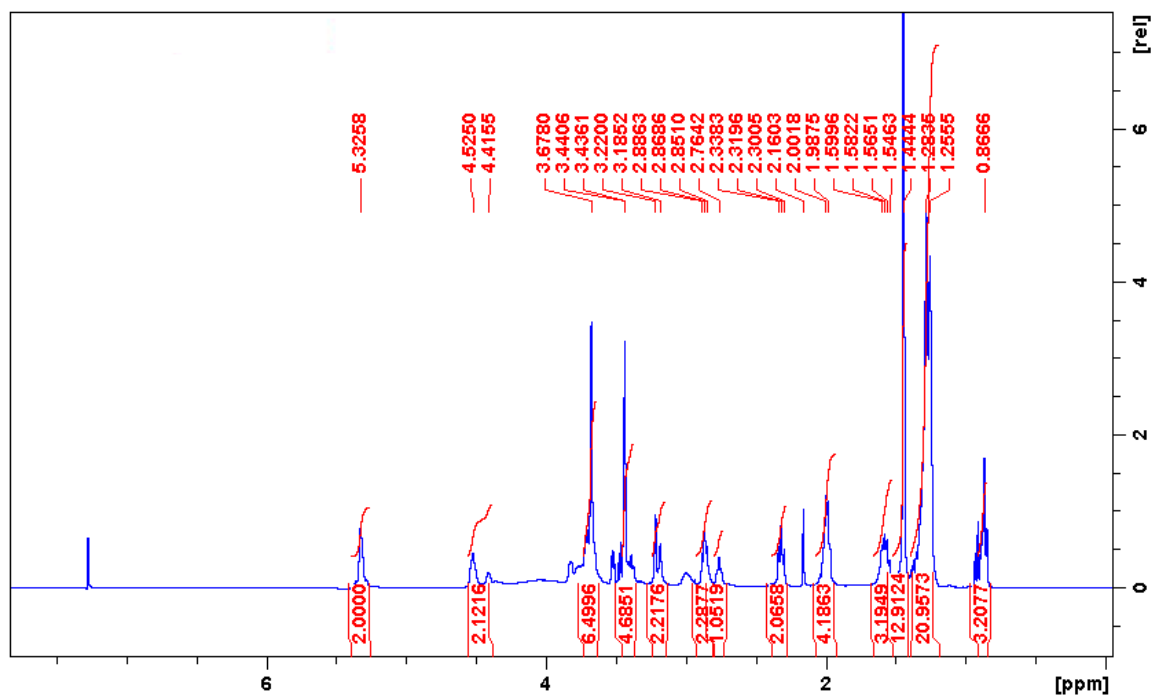


Minimum: -1.5
Maximum: 100.0

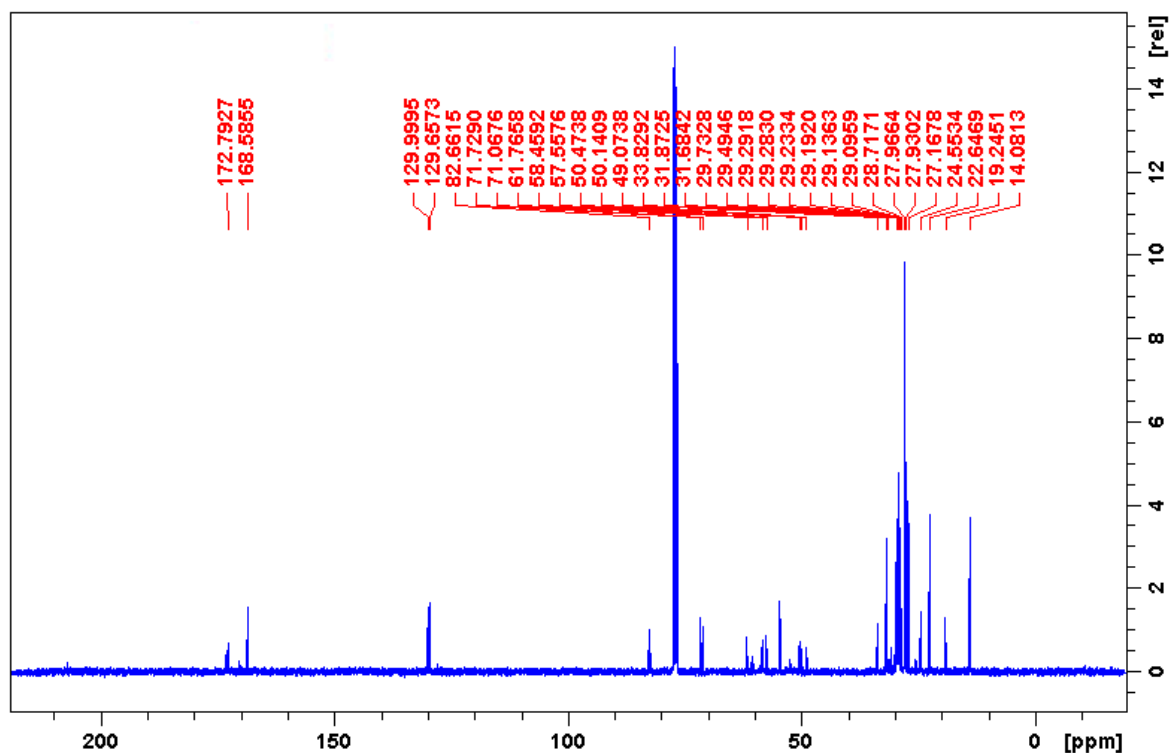
Mass	Calc. Mass	mDa	PPM	DBE	i-FIT	i-FIT (Norm)	Formula
604.4554	604.4553	0.1	0.2	3.5	48.7	0.0	C34 H63 N O6 Na

APPENDIX IX

S Figure 6. 4-(tert-butoxy)-N-(3-(tert-butoxy)-3-oxopropyl)-N-(2-(oleoyloxy)ethyl)-3-oxobutan-1-amium (compound 4) HRMS



S Figure 7. 4-(tert-butoxy)-N-(3-(tert-butoxy)-3-oxopropyl)-N-methyl-N-(2-(oleoyloxy)ethyl)-3-oxobutan-1-amium (QL lipid (compound 5)) proton NMR



APPENDIX IX

S Figure 8. 4-(tert-butoxy)-N-(3-(tert-butoxy)-3-oxopropyl)-N-methyl-N-(2-(oleoyloxy)ethyl)-3-oxobutan-1-aminium (QL lipid (compound 5)) ¹³C NMR

Elemental Composition Report

Compound 5

Page 1

Single Mass Analysis

Tolerance = 5.0 PPM / DBE: min = -1.5, max = 100.0

Element prediction: Off

Number of isotope peaks used for i-FIT = 3

Monoisotopic Mass, Even Electron Ions

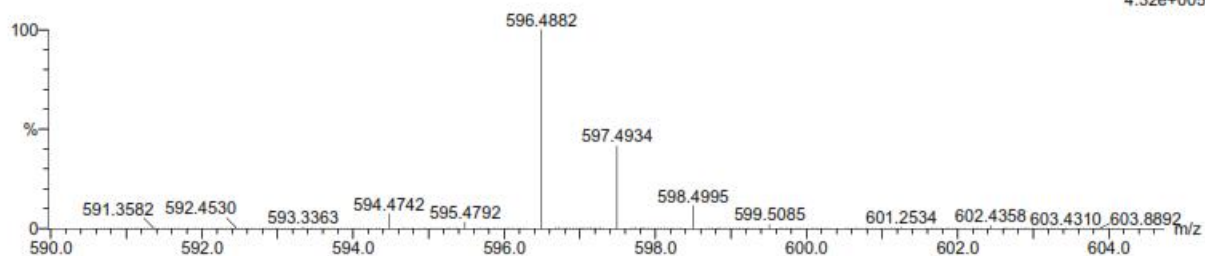
11 formula(e) evaluated with 1 results within limits (up to 20 closest results for each mass)

Elements Used:

C: 30-35 H: 65-70 N: 0-5 O: 5-10

OADPEQ 56 (1.857) Cm (1.61)

TOF MS ES+



Minimum:

Maximum: 5.0 5.0 -1.5 100.0

Mass	Calc. Mass	mDa	PPM	DBE	i-FIT	i-FIT (Norm)	Formula
596.4882	596.4890	-0.8	-1.3	3.5	546.6	0.0	C35 H66 N O6

S Figure 8. 4-(tert-butoxy)-N-(3-(tert-butoxy)-3-oxopropyl)-N-methyl-N-(2-(oleoyloxy)ethyl)-3-oxobutan-1-aminium (QL lipid (compound 5)) HRMS



ELSEVIER

Contents lists available at ScienceDirect

International Journal of Pharmaceutics

journal homepage: www.elsevier.com/locate/ijpharm

Synthesis of an oleic acid based pH-responsive lipid and its application in nanodelivery of vancomycin

Danford Mhule^a, Rahul S. Kalhapure^{a,*}, Mahantesh Jadhav^a, Calvin A. Omolo^a, Sanjeev Rambharose^a, Chunderika Mocktar^a, Sanil Singh^b, Ayman Y. Waddad^a, Valence M.K. Ndesendo^c, Thirumala Govender^{a,*}

^a Discipline of Pharmaceutical Sciences, School of Health Sciences, University of KwaZulu-Natal, Private Bag X54001, Durban 4000, South Africa

^b Biomedical Resource Unit, University of KwaZulu-Natal, Westville Campus, Durban 4000, South Africa

^c School of Pharmacy and Pharmaceutical Sciences, St. John's University of Tanzania, P.O. Box 47, Dodoma, Tanzania

ARTICLE INFO

Keywords:

NMEO
pH responsive SLNs
Antibiotic
Nanotechnology
Antibiotic resistance
Methicillin-resistant *S. aureus*

ABSTRACT

Stimuli-responsive nano-drug delivery systems can optimize antibiotic delivery to infection sites. Identifying novel lipids for pH responsive delivery to acidic conditions of infection sites will enhance the performance of nano-drug delivery systems. The aim of the present investigation was to synthesize and characterize a biosafe novel pH-responsive lipid for vancomycin delivery to acidic conditions of infection sites. A pH-responsive solid lipid, N-(2-morpholinoethyl) oleamide (NMEO) was synthesized and used to prepare vancomycin (VCM)-loaded solid lipid nanoparticles (VCM_NMEO SLNs). The particle size (PS), polydispersity index (PDI), zeta potential (ZP) and entrapment efficiency (EE) of the formulation were 302.8 ± 0.12 nm, 0.23 ± 0.03 , -6.27 ± 0.017 mV and $81.18 \pm 0.57\%$ respectively. The study revealed that drug release and antibacterial activity were significantly greater at pH 6.0 than at pH 7.4, while the *in silico* studies exposed the molecular mechanisms for improved stability and drug release. Moreover, the reduction of MRSA load was 4.14 times greater ($p < 0.05$) in the skin of VCM_NMEO SLNs treated mice than that of bare VCM treated specimens. Thus, this study confirmed that NMEO can successfully be used to formulate pH-responsive SLNs with potential to enhance the treatment of bacterial infections.

1. Introduction

The emergence of resistance against antibiotics has given rise to many problematic strains of bacteria, one of them being methicillin-resistant *Staphylococcus aureus* (MRSA) (Sonawane et al., 2016), a bacterium responsible for a wide range of infections in community and hospital settings (Ma et al., 2014; Song et al., 2011). It is resistant to several antibiotics and is also threatening vancomycin, which is considered a drug of last resort for combating MRSA infections (Kali et al., 2013; Mandal et al., 2017; Zetola et al., 2005). This makes its infections difficult and costly to treat, and associated with high mortality globally (Boucher and Corey, 2008).

A major contributory factor for resistance development is the limitations associated with the current dosage forms of antibiotics (Sharma et al., 2012), which include inadequate concentrations of the drug at infection sites and increased drug exposure to normal flora (Priya et al., 2009). In addition, their high doses and frequency of administration lead to toxicity, which affects patients' adherence to treatment

regimens (Xiong et al., 2014). Nanosized drug delivery systems are a strategy receiving increasing attention for their enhancing antibiotic therapy (Andrade et al., 2013). Nanocarriers are considered suitable for managing antimicrobial resistance as they are capable of ensuring both targeted and controlled/sustained delivery of antibiotics at infection sites as well as decreased exposure to normal tissues (Zazo et al., 2016). In this way, a constant and effective drug concentration is maintained above the minimum inhibitory concentration (MIC) at the site of infection. Consequently, the frequency of administration is lowered, side effects are decreased, and patient compliance is increased (Gao et al., 2011; Huh and Kwon, 2011). Advances in nanoscience have enabled researchers to design delivery systems that target biomarkers associated with specific pathological conditions/tissues, and include the over expression of specific molecules or changes in physiological conditions, such as pH and temperature (Kullberg et al., 2009; Timko et al., 2010; Wang et al., 2008).

Of these biomarkers, pH is useful for targeting various disease conditions such as cancer, inflammation and infection which are

* Corresponding authors at: School of Pharmacy, The University of Texas at El Paso, 500 W. University Ave, El Paso, TX 79968, USA (R.S. Kalhapure).
E-mail addresses: kalhapure@ukzn.ac.za, rkalhapure@utep.edu (R.S. Kalhapure), govenderth@ukzn.ac.za (T. Govender).

<https://doi.org/10.1016/j.ijpharm.2018.08.025>

Received 24 November 2017; Received in revised form 6 August 2018; Accepted 16 August 2018

Available online 17 August 2018

0378-5173/ © 2018 Elsevier B.V. All rights reserved.

accompanied by a change in pH in comparison to normal physiological pH (Lu et al., 2016; Sonawane et al., 2017). Thus, novel materials can be designed to specifically respond to pH changes resulting into targeted delivery of drugs at the disease site (Liu and Thayumanavan, 2017). Bacterial infections, have been reported by various researchers that the pH level at infection sites is usually lower than the physiological value (7.4). (Gao et al., 2017; Gandhi et al., 2017; Liu et al., 2018; Tate et al., 2002; Gao et al., 2017). Arming nanoparticles with moieties that respond to pH changes has proved successfully in binding them to bacteria and increasing the drug release at sites of infection and bacteria (Radovic-Moreno et al., 2012). However, literature shows that most of the pH responsive systems reported so far are for cancer therapy whilst very few papers report pH-based acid cleavable lipid nanoparticles for antibiotic delivery (Kalhapure et al., 2017a; Kalhapure et al., 2017b; Pichavant et al., 2011; Radovic-Moreno et al., 2012). There is therefore a need to identify novel materials and nanodelivery systems of antibiotics with intrinsic pH responsiveness to maximize their delivery to infection sites (Radovic-Moreno et al., 2012).

Various nano-based delivery systems, such as nanoemulsions (Kumar et al., 2008; Rapoport et al., 2009), liposomes, polymeric nanoparticles (PNs) (Chawla and Amiji, 2002; Dhar et al., 2008; Shenoy and Amiji, 2005), and solid lipid nanoparticles (SLNs) (Gupta et al., 2007; Spada et al., 2012) have been reported for targeted delivery. The fabrication of nanoemulsions needs liquid oils while SLNs use solid lipids, which make them more stable (Geszke-Moritz and Moritz, 2016). In addition, both SLNs and liposomes are made using physiological lipids, but unlike liposomes and PNs, SLNs avoids the use of organic solvents (Briones et al., 2008). These features, their ability to encapsulate both hydrophobic and hydrophilic drugs, and their ease of scaling up and sterilization has led to a growing interest by researchers in SLNs (Gastaldi et al., 2014). SLNs are usually fabricated using solid lipids such as fatty acids, glycerides and waxes which lack pH responsiveness, and results in researchers including pH sensitive materials such as phospholipids in the lipid matrix to achieve pH-responsive delivery (Kashanian et al., 2011; Rostami et al., 2014). Our group recently reported a pH responsive SLN formulation for antibiotic delivery using a stearic acid based acid cleavable lipid for targeted delivery of vancomycin, this being the only study to do so (Kalhapure et al., 2017b). There is therefore a need to widen the pool of available responsive lipids for targeting antibiotics to infection sites. In this project, a novel pH responsive solid lipid, N-(2-morpholinoethyl) oleamide (NMEO), was synthesized using oleic acid and 4-(2-Aminoethyl) morpholine (4-AEM). This material was first synthesized by our group as an intermediate for synthesizing heterocyclic quaternary ammonium surfactants (Jadhav et al., 2016). To the best of our knowledge, it has not been reported as a formulation component for a nanodelivery system of any drug class and disease condition. Oleic acid is a biocompatible, unsaturated fatty acid that finds wide application in drug delivery (Srisuk et al., 2012). It has been used as a penetration enhancer in transdermal delivery systems (Touitou et al., 2002), a stabilizer in liposomes (Bergstrand et al., 2003; Drummond et al., 2000) and magnetic nanoparticles (Darwish, 2017; Soares et al., 2016) and a liquid lipid in nanostructured lipid carriers (Zhao et al., 2016). It also has antibacterial activity, which may enable the fabrication of nanocarriers that can synergize antimicrobial activity of the encapsulated drugs (Huang et al., 2011). 4-AEM is a ligand commonly used to synthesize Schiff bases for application in biological systems. Based on its ability to protonate at low pH, this moiety is used to target acidic micro-environments, such as lysosomes (Wang et al., 2015; Yang et al., 2014; Yu et al., 2012). Hence, we hypothesize that a lipid formed from these two compounds would be biocompatible and display pH responsiveness that could be helpful in targeting bacterial infection sites. Specifically, this study aimed at synthesizing an oleic acid based lipid and subsequently exploring it to formulate pH responsive SLNs for the targeted delivery of vancomycin to manage MRSA infections. *In vitro*, *in silico* and *in vivo* results obtained by loading vancomycin in NMEO based

SLNs are presented in this paper.

2. Materials and methods

2.1. Materials

Analytical grade 4-(2-Aminoethyl) morpholine (4-AEM) was procured from Sigma-Aldrich Co. Ltd., (UK). *p*-Dimethylamino pyridine (DMAP) and oleic acid (OA) were purchased from Sigma-Aldrich Co. Ltd. (USA), and *N,N*-dicyclohexyl carbodiimide (DCC) and 3-(4,5-dimethylthiazol-2-yl)-2,5-diphenyltetrazolium bromide (MTT) were purchased from Merck Co. Ltd., (Germany). Mueller-Hinton Broth (MHB) was obtained from Sigma-Aldrich (USA), while Mueller Hinton Agar (MHA) and Nutrient Broth were bought from Biolab Inc., (South Africa). The water used was purified by an Elix® system from Millipore Corp., (USA), and the bacterial strain used was *S. aureus* Rosenbach ATCC®BAA-1683 (MRSA).

2.2. Methods

2.2.1. Synthesis and characterization of NMEO (Fig. 1)

NMEO was synthesized via steglich esterification (Ha et al., 2008, 2009; Xu et al., 2009), based on a previously reported procedure (Jadhav et al., 2016). In brief, 4.25 g (35.3 mmol) of 4-AEM was slowly added into 250 ml of dry dichloromethane (DCM) containing a mixture of oleic acid 10 g (35.4 mmol), DMAP 0.5 g (4 mmol) and DCC 7.125 g (34.5 mmol) under stirring at room temperature (RT). This mixture was kept under stirring at the same temperature for 24 h, after which the precipitated dicyclohexylurea was removed by filtration. The filtrate was evaporated under reduced pressure to obtain the compound of interest, which was purified by column chromatography. The structure of the synthesized lipid (NMEO) was confirmed by Fourier transform infra-red (FT-IR) spectroscopy, Nuclear magnetic resonance (NMR) imaging (¹H and ¹³C) and mass analysis. Bruker Alpha spectrophotometer (German) and Waters Micromass LCT Premier/TOF-MS instrument (United Kingdom) were used to record the FT-IR and Electrospray ionization mass spectra respectively. ¹H NMR and ¹³C NMR spectra were obtained using Bruker 400/600 Ultrashield™ NMR spectrometer (United Kingdom) at 25 °C.

2.2.2. *In vitro* cytotoxicity

The biosafety of the synthesized NMEO was assessed using an MTT assay following a literature reported procedure (Omolo et al., 2016). The study used human lung epithelial (A549), human embryonic kidney (HEK-293) and human liver (HEP G2) cell lines. The cells (2.2×10^3 /cell) were seeded into 96-well plates, incubated for 24 h and treated with NMEO concentrations of 20, 40, 60, 80 and 100 µg/ml for 48 h. At the end of the 48 h incubation period, the culture medium containing the test material was removed from the wells into which fresh culture medium and MTT solution (100 µl each) were added. These two solutions (MTT solution and culture medium) were removed after 4 h of incubation at 37 °C, and the formed MTT formazan was dissolved by adding dimethylsulfoxide. The absorbance corresponding to each well was measured using a microplate spectrophotometer (Spectrostar nano, Germany) at 540 nm. The culture medium with cells

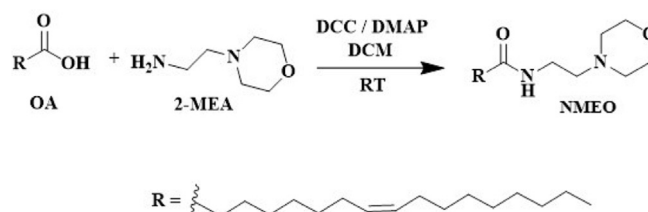


Fig. 1. Synthesis scheme for NMEO.

was used as the positive and those without cells as a negative control, with all experiments being run in six replicates. The following equation was used to determine percentage cell viability:

$$\% \text{ Cell viability} = (A_{540\text{nm}} \text{ treated cells} / A_{540\text{nm}} \text{ untreated cells}) \times 100$$

2.2.3. Surfactant screening and preparation of SLNs

SLNs were formulated using a hot homogenization and ultra-sonification method (Kalhapure et al., 2014), with the oily phase consisting of NMEO (500 mg) as a solid lipid and vancomycin free base (50 mg) and the aqueous phase of surfactant solution in milli-Q water. Four surfactants (Cremophor RH 40, Lutrol F-68, Solutol HS 15 and Tween 80) were screened at a fixed concentration (250 mg) to identify the surfactant with the most desirable physicochemical properties for the formulation of the SLNs. Both phases were heated separately to 80 °C, this being followed by the addition of the aqueous to oily phase once the lipid had melted. The resultant mixture was homogenized at 10,000 rpm for 15 min and sonicated (30% amplitude) for 15 min using an Ultra Turrax T-25 homogenizer (IKA Labor Technik, Germany) and the Omni sonic ruptor 400 Ultrasonic Homogenizer (Kennesaw, GA 30144, USA) respectively. The obtained nanoemulsion was immediately cooled to 20 °C for the lipid to crystallize and form VCM NMEO_SLNs (Souto and Müller, 2006), with the final volume being adjusted to 125 ml using milli Q-water. The same procedure was used for blank (drug-free) NMEO SLNs, while stearic acid SLNs (SA SLNs), as a non-pH responsive nanosystem, were also prepared using the same procedure for comparison to the pH responsive VCM NMEO_SLNs in antibacterial studies.

2.2.4. Particle size (PS), polydispersity index (PDI), zeta potential (ZP) and Morphology

The average PS, PDI and ZP of formulated SLNs were determined by a dynamic light scattering technique. Dilutions were made using milli-Q water or appropriate phosphate buffer solutions, and the parameters were measured at room temperature (25 °C) using a Zetasizer Nano ZS90 (Malvern Instruments, UK), with all parameters being analyzed in triplicate to ensure reliability. The morphological features of the nanoparticles were investigated by transmission electron microscopy (TEM) analysis (Gonçalves et al., 2016). The samples were appropriately diluted, stained with phosphotungstic acid and fixed on a copper grid for drying. The dried samples were analyzed on a JEOL Microscopy (JEM 1010, Japan) with images being acquired at 100 kV.

2.2.5. Entrapment efficiency (EE) and loading capacity (LC)

The amount of drug encapsulated in the SLNs was determined by an ultrafiltration method using Amicon® Ultra-4 centrifugal filter tubes (10 kDa molecular weight cut-off). Samples were placed in the centrifugal filter tube and centrifuged at 3000 rpm at 25 °C for 30 min. After separating the supernatant, the amount of drug in it was analyzed by a UV-Visible spectrophotometer (Shimadzu UV-1650 PC) at 280 nm (Kalhapure et al., 2014). The determination of % EE and % LC was based on Eqs. (1) and (2) respectively (Ma et al., 2014b).

$$\%EE = (\text{Mass of drug in nanoparticles} / \text{Mass of drug added}) \times 100\% \quad (1)$$

$$LC = (\text{Mass of drug in nanoparticles} / \text{Mass of nanoparticles}) \times 100\% \quad (2)$$

2.2.6. Differential scanning calorimetry (DSC)

The DSC measurements of formulation components (individually), physical mixture and the drug were performed by DSC (Shimadzu DSC-60, Japan), and the weighed samples (2 mg) were placed in aluminum pans that were then sealed and scanned from 30 °C to 300 °C under a nitrogen stream at 10 °C/min.

2.2.7. In-vitro drug release study and drug release kinetics

A dialysis tube diffusion technique was used to investigate the *in*

vitro release behavior of drug loaded formulations (pH responsive and non-pH responsive SLNs) that were prepared in triplicate. Briefly, 2 ml of the drug loaded SLNs and their respective blanks were loaded into dialysis tubes (MWCO 14 kDa), sealed, and dialysed against 40 ml phosphate buffer solutions (PBS) (7.4, and 6.0) at 37 °C in an incubator maintained at 100 rpm. At predetermined time intervals, 3 ml samples were withdrawn from the receiver and the amount of vancomycin was determined by a spectrophotometric method (UV-1650PC, Shimadzu, Japan) at 280 nm. To keep the volume of release medium constant and maintain sink conditions, an equal amount of fresh PBS was added after each sampling.

Drug release kinetics were evaluated using a DDSolver Add-In program (Zhang et al., 2010). Six mathematical models were used whereby the correlation coefficient (R^2) and root mean square error (RMSE) were calculated and compared, the models being zero order, first order, Weibull, Korsmeyer-Peppas, Higuchi and Hixson-Crowell.

2.2.8. Physical stability

The short-term physical stability of the VCM_NMEO SLNs was evaluated at 4 °C and at room temperature (RT) for 90 days. The evaluation of the physical appearance of the formulations, as well as their particle size, PDI and ZP, was performed at the end of 30, 60 and 90 days, with the study being performed in triplicate.

2.2.9. Molecular modelling

Molecular modelling was performed to understand the type of interactions that occurred between VCM and NMEO based on a previously reported method with modifications. All molecular modeling techniques were performed using Bovia Materials Studio (MS) 2016 that was installed on the remote server at the Center for High Performance Computing (CHPC) (Cape Town, South Africa). The structure of VCM (PDB:1SHO) was obtained from the RCSB website, while NMEO was drawn using ChemBioDraw Ultra 14. All the structures were cleaned and hydrogen atoms were added, while the smart minimizer algorithm in geometry optimization option available in force module of MS software was used to optimize all the structures to their lowest energy conformations. A universal energy force field was applied and the convergence tolerance criteria set to 0.001 kcal/mol during the geometrical optimization study. The molecular dynamics (MD) study was performed in vacuum to obtain a stable complex of VCM and NMEO, both being initially placed inside the cubic cell (10x10x10 nm), with the crystal builder and amorphous cell module of MS 2016 being used to construct this model. Geometry optimization of the whole system was performed prior to MD simulation using the same protocol, as mentioned above, and optimization of the cell parameters was allowed during energy minimization. The stabilized system was then subjected to MD simulation under periodic boundary conditions, which was performed at room temperature and 4 °C over 50 ps. The final complex structure was then studied for the intermolecular interactions to understand the various non-covalent forces that were responsible for the complex formation, with the Biovia Discovery Studio Visualizer being used to depict the interactions in the drug-lipid complex.

2.2.10. In vitro antibacterial activity

The minimum inhibitory concentration (MIC) of vancomycin loaded SLNs were determined using a broth dilution method (Mohammed Fayaz et al., 2011). After an overnight growth in Nutrient Broth at 37 °C in a shaking incubator (Labcon, USA), the MRSA cultures were diluted with sterile de-ionised water using a densitometer (DEN-1B McFarland, Latvia) to achieve a turbidity of 0.5 McFarland. The bacterial cultures were further diluted 1:150 with sterile de-ionised water to obtain a concentration of 2×10^5 colony forming units (CFUs)/ml. The minimum inhibitory concentration (MIC) of bare VCM, drug-free (blank) NMEO SLNs, VCM loaded SA SLNs (VCM_SA SLNs) and VCM loaded NMEO SLNs (VCM_NMEO SLNs) were determined using the

broth dilution method. The test compounds were serially diluted with Mueller-Hinton Broth 2 in 96-well plates at pH 6.0 and pH 7.4. The plates were incubated in a shaking incubator at 37 °C for 18 h, after which, 10 µl of each dilution was spotted onto Mueller-Hinton Agar (MHA) plates after 24 h of further incubation. The MHA plates were incubated at 37 °C for 18 h, with the studies being performed in triplicate. The blank formulation of NMEO SLNs was used as a negative control, while vancomycin loaded SA SLNs and bare VCM were used as positive controls.

2.2.11. In vivo antibacterial activity

The in vivo antibacterial activity of bare VCM and VCM_NMEO SLNS against MRSA was investigated using a procedure approved by the Animal Research Committee of the University of KwaZulu-Natal (UKZN) (Approval no. AREC/104/015PD). BALB/c mice (18–20 g in weight) were purchased from the University's Biomedical Research Unit and divided into three groups (n = 4) categorized as treatment, positive and negative control groups. 50 µl of MRSA saline suspension (1.5×10^8 CFU/ml) was injected intradermally to the three groups of with their back hair removed and disinfected with 70% ethanol one day before. Half an hour after infection, bare VCM and VCM_NMEO SLNS were injected at the infection sites of the mice categorized as the positive control and treatment groups respectively, while nothing was given to the third group that was used as a negative control. After 48 h, the infected skin was harvested from the sacrificed mice and homogenized in 5 ml of phosphate buffer solution (pH 7.4). The serial dilutions of tissue homogenates were plated on nutrient agar plates (Biolab, South Africa) and incubated at 37 °C, with the number of CFUs being counted after 24 h of incubation (Huang et al., 2011). The histological investigation was performed according to a previously reported procedure (Omolo et al., 2016). Briefly, skin samples were fixed in formaldehyde at 25 °C for seven days, dehydrated using ethanol, implanted in paraffin wax. The tissue wax blocks were sectioned using a microtome (Leica RM2235, Leica Biosystems, Germany) and sections were collected on slides, dried and stained with hematoxylin and eosin (H&E). Sections were examined and captured with a Leica Microscope DM 500, fitted with a Leica ICC50 HD camera (Leica Biosystems, Germany).

2.2.12. Statistical analysis

Statistical analysis of data was performed using one-way analysis of variance (ANOVA), followed by Bonferroni's multiple comparison test using GraphPad Prism® 6 (GraphPad Software Inc., USA). Statistical significance was based on a p-value < 0.05, with the data being expressed as mean ± standard deviation (SD).

3. Results and discussion

3.1. Characterization of NMEO

M.p. 42–44 °C; FT-IR: 3285.91, 2918.5, 2848.71, 1646.85, 1559.86, 1462.07, 1117.96, 777.97, 715.29 cm^{-1} . ^1H NMR (CDCl_3) δ (ppm): 0.836–0.869 (t; 3H; $-\text{CH}_3$), 1.241–1.276 (m; 20H; $-\text{CH}_2$), 1.581–1.616 (q; 2H; $-\text{CH}_2\text{CH}_2\text{COO}-$), 1.958–1.972 (m; 4H; $-\text{CH}_2-\text{CH}=\text{CH}-\text{CH}_2$), 2.00–2.163 (t; 2H; $\text{CH}_2\text{COO}-$), 2.521–2.550 (m; 6H; $-\text{CH}_2-\text{N}(\text{CH}_2)_2$), 3.351–3.379 (t; 2H; $-\text{NHCH}_2\text{CH}_2$), 3.718–3.740 (t; 4H; $-\text{CH}_2\text{OCH}_2$), 5.290–5.328 (m; 72H; $-\text{CH}=\text{CH}-$), 6.25 (s; 1H; $-\text{NH}-$). ^{13}C NMR (CDCl_3) δ (ppm): 14.09, 22.86, 25.72, 27.16, 29.15, 29.27, 29.48, 29.70, 31.88, 35.24, 36.68, 53.23, 57.23, 66.45, 129.70, 129.98, 173.31; ESI-TOF MS m/z : $[\text{M} + \text{H}]^+$ – calculated 395.3638 ($\text{C}_{24}\text{H}_{46}\text{N}_2\text{O} + \text{H}^+$), actual mass 395.3633.

3.2. In vitro cytotoxicity

Exposure of NMEO to the cell lines for a period of 48 h displayed that the novel lipid exhibited a high percentage cell viability across the

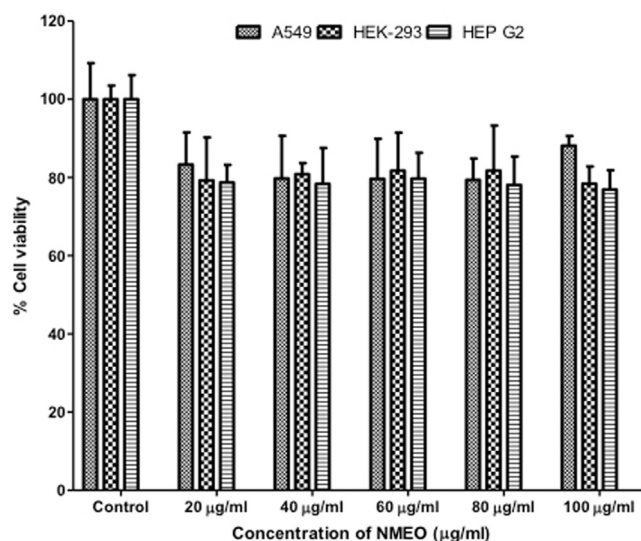


Fig. 2. Cytotoxicity evaluation of various concentrations of NMEO against A549, HEK-293 and Hep G2 cells.

concentration range studied (Fig. 2). NMEO displayed a cell viability between 79.42 and 88.12%, 78.42 to 81.75% and 76.96 to 79.70% for A549, HEK-293 and HEP G2 cells respectively (Fig. 2). The results displayed no dose dependent trends and is consistent with previous studies that report on materials that exhibit cell viability that is independent of the concentration (Romic et al., 2016; Di Gioia et al., 2015; Sikwal et al., 2017).

Literature reports that materials with a cell viability of greater than 75% can be considered as low toxicity in the framework of safety use (Cao et al. 2010). The findings of the MTT study therefore suggest that the use of NMEO will be safe for biological/pharmaceutical applications.

3.3. Preparation of drug-free NMEO SLNs

Initially drug-free SLNs were prepared from the newly synthesized NMEO using several surfactants, the one with acceptable characteristics being selected and its quantity optimized.

3.3.1. Screening and selection of surfactant

Surfactants of different types were screened at a fixed concentration to identify the most suitable one for formulating blank NMEO SLNs with desirable physicochemical characteristics. The surfactants used were Cremophor RH 40, Lutrol F-68, Solutol HS 15 and Tween 80. Of these, Tween 80 displayed the best results in terms of size and PDI (Fig. 3). Similar results were obtained by Ebrahimi and coworkers who studied the effect of different stabilizers (polyvinyl alcohol, Pluronic F 127,

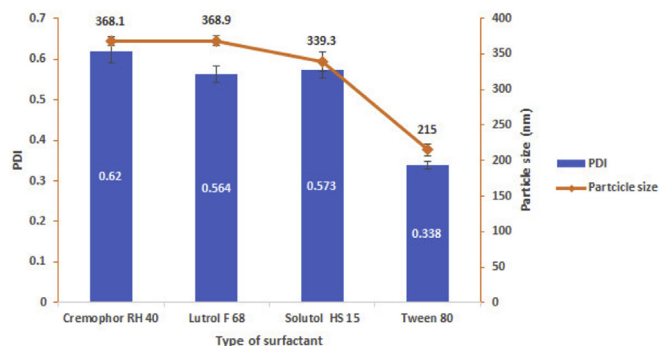


Fig. 3. Effect of surfactant type on size and PDI of SLNs.

Table 1
Effect of surfactant concentration on physicochemical characteristics of drug free NMEO SLNs. The values given are expressed as mean \pm SD, n = 3.

pH	PS (nm)	PDI	ZP (mV)
0.1%			
7.4	215.0 \pm 8.3	0.34 \pm 0.031	-6.03 \pm 0.49
6.0	227.6 \pm 1.5	0.340 \pm 0.025	5.1 \pm 0.250
5.5	211 \pm 1.51	0.369 \pm 0.07	10.4 \pm 1.60
0.12%			
7.4	162.8 \pm 1.6	0.209 \pm 0.03	-5.04 \pm 0.471
6.0	162.0 \pm 5.21	0.171 \pm 0.013	4.4 \pm 1.16
5.5	145.5 \pm 2.4	0.179 \pm 0.01	9.7 \pm 1.9
0.16%			
7.4	146.2 \pm 3.0	0.174 \pm 0.04	-4.7 \pm 0.1
6.0	167.7 \pm 1.8	0.259 \pm 0.022	4.01 \pm 0.82
5.5	168.0 \pm 7.4	0.26 \pm 0.07	9.06 \pm 1.0
0.2%			
7.4	122.2 \pm 5.54	0.129 \pm 0.02	-4.41 \pm 0.88
6.0	124.3 \pm 7.4	0.137 \pm 0.012	3.46 \pm 0.48
5.5	122.6 \pm 3.1	0.152 \pm 0.023	10.4 \pm 0.21
0.24%			
7.4	130.2 \pm 0.74	0.119 \pm 0.026	-4.17 \pm 0.6
6.0	129.1 \pm 1.35	0.095 \pm 0.01	3.28 \pm 0.48
5.5	140.9 \pm 3.24	0.146 \pm 0.037	7.45 \pm 1.77

polyvinyl pyrrolidone, Tween 80 and phosphatidylcholine) on the behavior of SLNs. According to these authors, surfactants of low molecular weight, such as Tween 80, produce small sized particles due to their ability to be quickly adsorb into interfacial surfaces (Ebrahimi et al., 2015), which resulted in it being selected for further studies.

3.3.2. Effect of surfactant concentration

The surfactant (Tween 80) concentration was varied from 0.1% (w/v) to 0.24% (w/v) to determine the optimal concentration. As depicted in Table 1, PS and PDI of the blank formulations decreased with increasing surfactant concentration, with the particle size increasing beyond 0.2%. These results are in line with the findings of other studies related to SLNs (Das et al., 2011) and other types of nanoparticles (Dora et al., 2010; Singh et al., 2010). The ability of a surfactant to produce small particles depends on how fast it gets adsorbed to the particle surfaces before the particles grow through collisions. At higher concentrations, this adsorption process is faster, with the particles being maintained at smaller sizes (Helgason et al., 2009). Therefore, the drug-free formulation composed of 0.2%w/v surfactant was considered suitable to proceed with drug loading.

3.4. Preparation and characterization of drug loaded SLNs

Drug loaded pH responsive SLNs were prepared using VCM, Tween 80 and NMEO as drug, surfactant and pH responsive lipid respectively. Hot homogenization, a method that combines high pressure, thermal and mechanical forces to attain consistent nanosized formulations was used in addition to ultrasonification. The prepared SLNs were characterized for pH responsiveness and other physicochemical characteristics by dispersion in different buffer solutions. PS, PDI and ZP of VCM_NMEO SLNs and VCM_SA SLNs are presented in Table 2 and

Table 2
Effect of pH on VCM loaded formulations. The values given are expressed as mean \pm SD, n = 3.

SLN pH	VCM_NMEO SLNS			VCM_SA SLNs		
	PS (nm)	PDI	ZP (mV)	PS (nm)	PDI	ZP (mV)
7.4	302.8 \pm 0.12	0.292 \pm 0.025	-6.27 \pm 0.017	365.6 \pm 17.8	0.143 \pm 0.021	-7.0 \pm 0.11
6.0	260.7 \pm 9.5	0.261 \pm 0.018	6.05 \pm 0.013	363.8 \pm 15	0.316 \pm 0.022	-4.12 \pm 0.27
5.5	220.5 \pm 1.9	0.380 \pm 0.005	9.39 \pm 0.046	368.1 \pm 12.9	0.209 \pm 0.025	-2.57 \pm 0.09

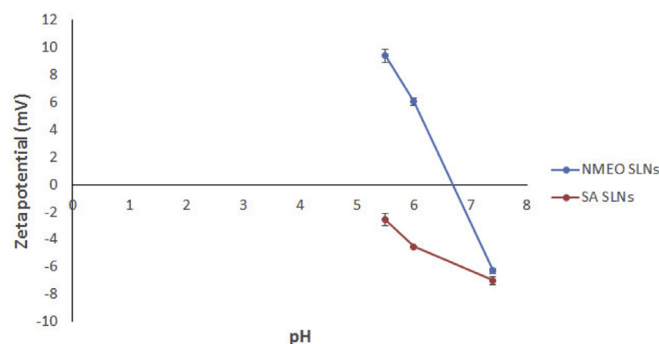


Fig. 4. Effect of pH on zeta potential of VCM_NMEO SLNs.

The zeta potential of VCM_NMEO SLNs changed from -6.27 at pH 7.4 to +9.39 at pH 5.5, and there was a decrease in particle size from 302.8 at pH 7.4 to 220.5 at pH 5.5. The switch from negative to positive zeta potential was not observed for VCM_SA SLNs, which also did not show any major change in size confirmed that the pH-responsiveness of SLNs was due to NMEO. The ability to switch from negative at basic to positive charge at acidic pH is critical for pH-responsive systems for antibiotic delivery as it serves two purposes: i) it helps the system to become more hydrophilic and release higher quantities of the drug in the acidic conditions of infection sites (Mura et al., 2013), and ii) it enables the carrier to bind easily to the negatively charged bacterial cells, enhancing the targeting potential of the system (Chakraborty et al., 2012). Morphological analysis using TEM showed that VCM_NMEO SLNs were discrete and had an almost spherical shape (Fig. 5). The % EE and DL for drug loaded NMEO SLNs were 81.18 \pm 0.57% and 8.1% respectively. While the entrapment efficiency is often a challenge in drug delivery with nano-drug systems, the % EE obtained in this study was higher than several non-pH responsive SLNs reported (Liu et al., 2014; Seedat et al., 2016; Yousry et al., 2016), will be beneficial for reducing drug loss and costs, and will significantly reduce the amount of the drug to be administered. This data therefore confirmed that the NMEO lipid can be used to prepare VCM solid lipid nanoparticles with desirable properties.

3.5. DSC studies

The aim of the DSC studies was to confirm entrapment of VCM in the NMEO SLNs, with the thermograms of SLNs, VCM and NMEO being shown in Fig. 6, the thermal peaks of the latter two being observed at 112.14 °C and 41.22 °C respectively. Analysis of their physical mixture revealed no major shifts in the thermal peaks of the formulation excipients. The lyophilized SLNs exhibited an endothermic peak at 39.71 °C, which can be associated with the NMEO layer. The VCM peak was absent in the SLN's thermogram, indicating that the drug was entrapped in an amorphous form in the lipid matrix (Seedat et al., 2016).

3.6. In vitro drug release profiles and drug release kinetics

The in vitro release profiles of bare VCM, VCM_NMEO SLNs and VCM_SA SLNs are shown in Fig. 7 A and B, with the release of bare VCM at pH 7.4 and pH 6.0 being almost complete within the first 8 h.

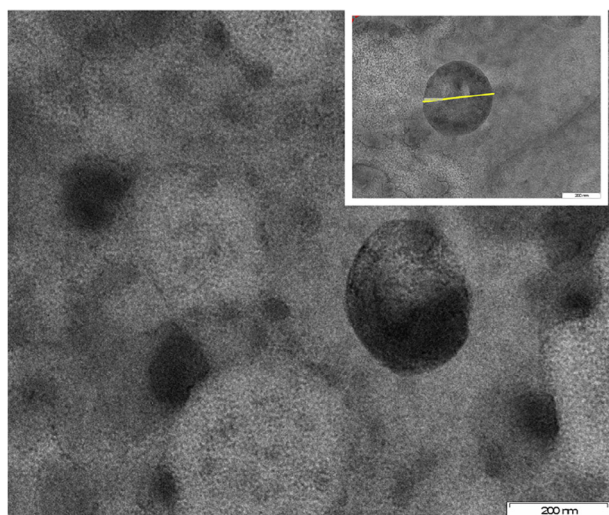


Fig. 5. Morphology of VM_NMEO SLNs.

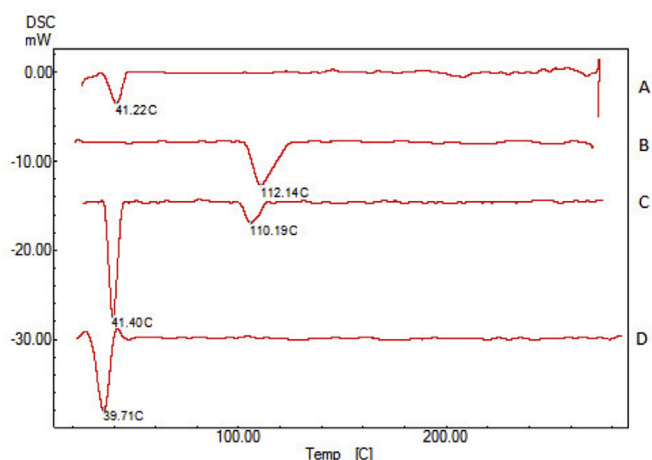


Fig. 6. DSC thermogram of (A) NMEO, (B) VCM (C) physical mixture of VCM and NMEO and (D) lyophilized VCM_NMEO SLNs.

Throughout the study, the amount of VCM released from the VCM_NMEO SLNs was higher at pH 6.0 than pH 7.4. After 8 h, the release of VCM from the VCM_NMEO SLNs was 34.66% at pH 7.4 and 74.89% at pH 6.0. At the end of the study (24 h), drug release was 1.58 times higher at acidic pH than at physiological pH. This increased drug release at pH 6.0 can be due to the pH responsiveness of NMEO, with the protonation of nitrogen atoms of its morpholinoethyl moiety at acidic pH increasing the hydrophilicity of the formulation, promoting faster drug release. Pu et al. (2014) obtained similar results, whereby protonation of the imidazole moiety conjugated to the pendant groups of poly (L-aspartate) triggered release of doxorubicin at acidic conditions from the pH-sensitive poly (L-aspartate)-b-poly (ethylene glycol) micelles.

The release of VCM from the VCM_SA SLNs was sustained at both pH values and did not show any pH dependence, with drug release after 24 h being 87.63% at pH 7.4 and 85.07% at pH 6.0. It can thus be concluded that the pH dependent drug release observed for VCM_NMEO SLNs was linked to NMEO.

The drug release kinetics data of the drug loaded formulations are presented in Table 3. At pH 7.4, both stearic acid and NMEO formulations released vancomycin according to the Weibull model, which is among the kinetic models that have a wide application in describing drug release processes (Koester et al., 2004). The values of R^2 and RMSE were 0.9848 and 2.2925 for the VCM_SA SLNs respective, and 0.9918

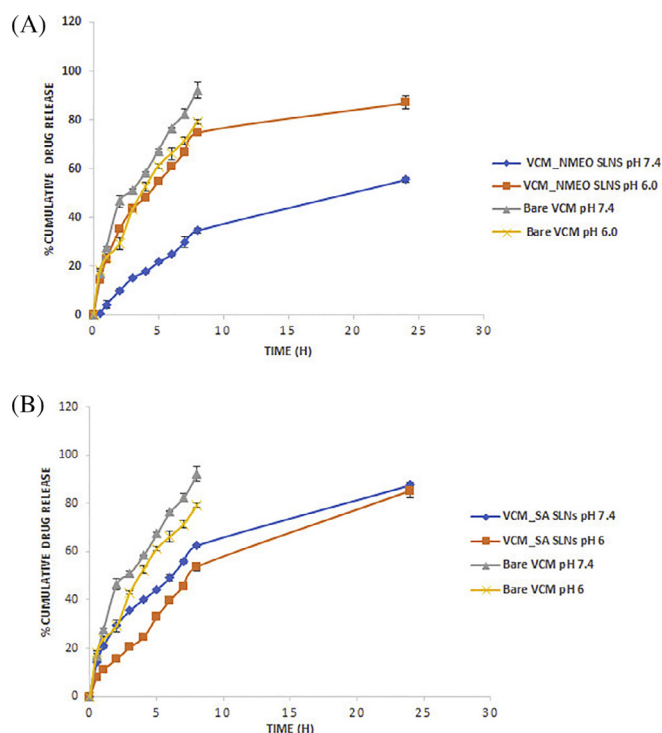


Fig. 7. Effect of pH on drug release profiles of (A) bare VCM and VCM_NMEO SLNs And (B) VCM and VCM_SA SLNs (n = 3).

and 2.1057 for the VCM_NMEO SLNs.

The Weibull release model, as applied to drug release, can best be explained by considering its exponent parameter (β), as it was described by Papadopoulou et al. (Papadopoulou et al., 2006). A value of β between 0.39 and 0.69 suggest that the release mechanism is diffusion in fractal or disordered substrate, but the $0.69 < \beta < 0.75$ suggests that the drug release was by diffusion in normal Euclidian space. The value of exponent parameter (β) for VCM_NMEO SLNs was 0.629, which suggests that the mechanism of VCM release at pH 7.4 was by diffusion in fractal or disordered substrate.

At pH 6.0, Korsmeyer-Peppas was the best fit model, and the R^2 and RMSE values were 0.9922 and 1.8138 respectively for VCM_SA SLN, and 0.9976 and 1.1054 respectively for VCM_NMEO SLN. The value of the release exponent (n) of the Korsmeyer-Peppas model at pH 6.0 was above 0.5, suggesting a non Fickian mechanism of release (Waddad et al., 2013).

3.7. Physical stability

The physical stability of the NMEO SLNs was assessed at 4 °C and at RT for 90 days to understand how the physical stability related parameters were affected by time and storage conditions. The absence of visual signs of instability, and the lack of significant difference in values of particle size, PDI and ZP ($p > 0.05$), proved that the formulation was stable at 4 °C throughout the study period (Table 4). Unlike those at 4 °C, the samples kept at RT were not stable, as revealed by their significant particle growth ($p < 0.05$) and high PDIs. Chemical stability studies on the formulation can be undertaken in the future during formulation optimization studies with the drug of choice.

3.8. Molecular modelling

Molecular modelling was used to investigate and identify the stability of the VCM NMEO SLN system, and the interaction between VCM and NMEO, as this understanding will also explain the release behavior of VCM from the NMEO SLNs. The initial energy of VCM and NMEO

Table 3
Drug release kinetics data for VCM NMEO_SLNs.

Model	Equation	R ²		RMSE		Release exponent (n)	
		7.4	6.0	7.4	6.0	7.4	6.0
Zero order	$Q = k * t + Q_0$	0.6286	0.8626	12.8061	7.8804	–	–
First order	$Q = Q_0 * e^{kt}$	0.9032	0.9608	6.5348	4.2060	–	–
Higuchi	$Q = k * t^{1/2}$	0.9584	0.9924	4.2870	1.8305	–	–
Korsmeyer-Peppas	$Q = k * t^n$	0.9604	0.9976	4.3857	1.1054	0.527	0.566
Hixson-Crowell	$Q^{1/3} = k * t + Q_0^{1/3}$	0.8344	0.9374	8.5487	5.3143	–	–
Weibull	$Q = 1 - \exp[-(t)^{a/b}]$	0.9918	0.9974	2.1057	1.2530	–	–

R² = linear regression coefficient, RMSE = Root mean square error.

were found to be 3894.83 and 274.09 kcal/mol respectively. Geometry optimization using the smart minimizer algorithm in forcite module resulted in producing more stable molecules with final energy of 289.54 kcal/mol for VCM and 41.59 kcal/mol for NMEO (Supplementary materials S1). The MD study revealed the formation of VCM-NMEO complex, with the potential energy, the mass of the complex, increasing from 546.585 kcal/mol to 854.939 kcal/mol by the end of MD study (Fig. 8 A). This confirms the successful formation of the VCM NMEO SLN system ((Florence and Attwood, 2015), while the rise in potential energy also explains the increase in particle size from 122.2 nm for blank to 302.8 nm when VCM was loaded into NMEO SLNs. The stability of the VCM_NMEO SLNs was also studied using MD simulation by monitoring the kinetic energy at room temperature and 4 °C. The kinetic energy, which reflects the entropy of the molecules during the simulation, was reduced by the end of the MD study at both temperatures. At room temperature, the kinetic energy was reduced from 685.88 kcal/mol to 386.34 kcal/mol, while at 4 °C it was reduced from 633.64 kcal/mol to 370.61 kcal/mol. The kinetic energy is known to be reduced at lower temperatures, resulting in reduced free energy and hence a more stable complex. The presence of hydrogen bonds and hydrophobic interaction were visualized using Discovery studio, and contributed to the stability of the VCM_NMEO SLNs (Fig. 8 B). The hydrogen bonds would have a major role in the stability of the VCM_NMEO SLNs, as these bonds are more stable at lower temperatures (Teo et al., 1997). The drug release profiles at pH 7.4 and pH 6 (Fig. 7A and B) may also be explained by these MD studies. The slower release of VCM from the NMEO SLNs at pH 7.4 can be attributed to not only hindrance by the hydrophobic SLNs, but also to the presence of hydrogen bond interactions between VCM and NMEO (Hao and Li, 2011; Ho et al., 2010). Conversely, at pH 6, due to protonation of the nitrogen atom of NMEO, hydrogen bonding may no longer occur, leading to the faster release profile displayed (Fig. 8).

Supplementary data associated with this article can be found, in the online version, at <https://doi.org/10.1016/j.ijpharm.2018.08.025>.

3.9. In vitro antibacterial activity

Table 5 summarizes the results of the in vitro antibacterial activity of bare VCM, drug free and drug loaded pH responsive NMEO SLNs and VCM SA_SLNs against MRSA. The MIC value for bare VCM was 7.8 µg/ml at physiological pH (7.4), and increased to 15.65 µg/ml at acidic pH

Table 4
Effect of storage on physicochemical characteristics of vancomycin loaded NMEO SLNs. The values are expressed as mean ± SD, n = 3.

Storage condition	PS (nm)		PI		ZP (mV)	
	4 °C	RT	4 °C	RT	4 °C	RT
Time (days)						
0	302.8 ± 0.12	302.8 ± 0.12	0.23 ± 0.03	0.23 ± 0.03	–6.27 ± 0.01	–6.27 ± 0.01
30	303.4 ± 5.2	585 ± 1.70	0.253 ± 0.07	0.395 ± 0.02	–6.4 ± 0.4	–6.0 ± 0.6
60	303.7 ± 1.03	588.9 ± 12.3	0.251 ± 0.01	0.422 ± 0.09	–6.50 ± 1.0	–6.2 ± 1.2
90	305.3 ± 3.8	596 ± 22.01	0.343 ± 0.04	0.455 ± 0.01	–6.30 ± 0.7	–6.21 ± 2.2

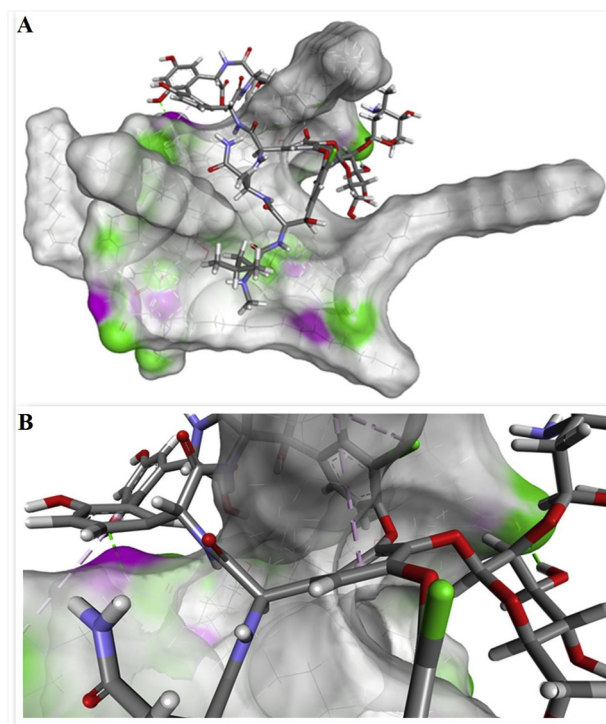


Fig. 8. 3D illustration of vancomycin (stick model) (A) entrapped inside the lipid network (hydrogen bond surface model) by means of hydrogen bond (green lines) and hydrophobic interaction (purple line) (B). (For interpretation of the references to colour in this figure legend, the reader is referred to the web version of this article.)

(6.0). The observed 2-fold loss of activity of bare VCM at acidic pH is consistent with what has been reported by other researchers (Mercier et al., 2002; Radovic-Moreno et al., 2012), and might be due to decreased solubility of vancomycin (Faustino, 2008). Bare VCM had a lower MIC (7.8 µg/ml) than VCM NMEO_SLNs (15.65), an observation consistent with other nanoantibiotic studies of VCM (Kadry et al., 2004; Kalhapure et al., 2014). It should be noted that under in vivo conditions, higher concentrations of VCM would still reach the infection site in the SLN compared to a conventional VCM formulation for better

Table 5

In vitro antibacterial activity of the formulations against MRSA at pH 7.4 and 6.0. The values are expressed as mean \pm SD, n = 3.

Formulation	(MIC μ g/ml)	
	7.4	6.0
Bare VCM	7.8	15.65
NMEO SLNs (drug free)	NA	NA
VCM_NMEO SLNs	15.65	0.244
VCM_SA_SLNs	31.5	31.5

NA = No activity.

activity. In addition, considering the toxicity of VCM, its encapsulation in NMEO SLNs could be useful in mitigating the drugs toxic effects, which includes nephrotoxicity (Dong et al., 2015). At pH 6, VCM NMEO SLNs had a MIC value (0.244 μ g/ml) that was lower than that of bare VCM (15.65 μ g/ml), which indicated that the NMEO SLNs were capable of protecting VCM against loss of its efficacy, which occurs at low pH (Radovic-Moreno et al., 2012).

The MIC value of the VCM_NMEO SLNs decreased from 15.6 μ g/ml at pH 7.4 to 0.244 μ g/ml at pH 6.0, which is equivalent to an almost 64-fold increase in their activity at acidic compared to neutral pH. These results were comparable to those from a study previously reported by our group, whereby VCM-encapsulated pH responsive SLNs (VCM-FB_SA-3M_SLNs) also had an activity against MRSA that was better at acidic than at physiological pH (Kalhapure et al., 2017b). Interestingly, the previous study reported a 4-fold improvement of activity against MRSA at acidic pH, which is lower than the 64-fold increase in activity reported in this study.

In our previous study, pH responsive VCM SLNs (VCM-FB_SA-3M_SLNs) were prepared from a novel acid-cleavable lipid that was meant to facilitate higher drug release only by cleavage of an acid labile link (acetal bond) at the acidic sites. VCM_NMEO SLNs in this study, on the other hand, were made from a lipid that protonates and acquires a positive charge at acidic medium. Superiority of the VCM_NMEO SLNs over the VCM-FB_SA-3M_SLNs can be because the latter influences only VCM release, while the former influences both release of drug from formulation and its interaction with bacteria. Therefore, apart from facilitating the release of the drug by making the system hydrophilic, the positive charge also helps to adhere VCM_NMEO SLNs to bacterial cells, thereby enhancing their activity (Forier et al., 2014).

Conversely, the MIC value of VCM_SA_SLNs against MRSA was 31.5 μ g/ml at pH 7.4, and remained the same at pH 6. This indicated their lack of pH dependent antibacterial activity and confirmed that enhanced antibacterial activity of the formulation (VCM_NMEO SLNs) might be due to the pH responsive NMEO lipid.

3.10. *In vivo* antibacterial activity

For proof of concept, *in vivo* studies in mice using a skin infection model was thereafter performed to confirm the antibacterial activity of VCM_NMEO SLNS, whereby MRSA were delivered intradermally to localize temporarily at the dermal layer, without gaining a deeper entry into the systemic circulation. For each treatment group, the number of colony-forming units (CFUs) were determined and presented as \log_{10} , as shown in Fig. 9. When compared to untreated skin samples, both the VCM_NMEO SLNs and bare VCM significantly reduced the MRSA load in the skin samples treated by them. The mean MRSA load (\log_{10} CFU) recovered from untreated skin samples was 6.58 ± 0.01 , while the values for the VCM_NMEO SLNS and bare VCM treated samples were 4.36 ± 0.10 and 4.97 ± 0.12 respectively. The \log_{10} CFU values for the formulation was statistically lower than both the untreated and VCM only treated ($p < 0.05$). In terms of CFU/ml, the results showed that the bacterial load in mice treated with the VCM_NMEO SLNS was 162.4 times lower than the one in the untreated mice ($p < 0.05$).

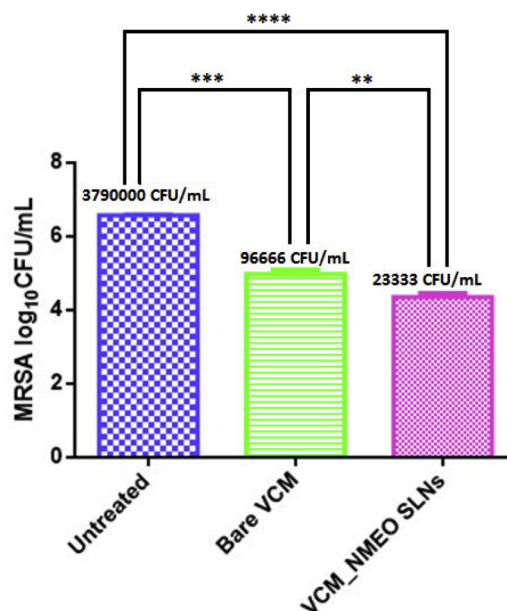


Fig. 9. MRSA burden after 48 h treatment period. Data is presented as mean \pm SD (n = 3). ** denotes significant difference between VCM NMEO SLNs and bare VCM. *** denotes significant difference when bare VCM is compared to untreated samples and **** denotes significant difference between VCM NMEO SLNs and untreated samples.

Bacterial load reduction by VCM_NMEO SLNS was also significantly greater (4.14 times) than that of bare VCM ($p < 0.05$). This clearly suggests that encapsulation of VCM in the NMEO SLNs improved its antibacterial activity.

Vancomycin exerts its antibacterial activity by inhibiting bacterial cell wall synthesis, which it does by diffusing through the cell wall and reaching its target site (terminal D-Ala-d-Ala residues) located on the cell membrane (Meng et al., 2017; Pereira et al., 2007). The thickened cell wall displayed by the MRSA helps the bacteria to resist vancomycin action by trapping the drug and reducing the number of drug molecules that reach the cytoplasmic membrane (Van Bambeke and Struelens, 2008). In our study, the enhanced activity of VCM in NMEO SLNs was probably be due to several factors, such as: i) a faster drug release (Subedi et al., 2009) and improved binding to bacterial cells due to the ability of the NMEO SLNs to acquire positive charge at pathological acidic conditions; ii) improved permeation of VCM through the MRSA cell wall to its target site due to the ability of oleamide portion of the NMEO to act as a permeation enhancer (Lane, 2013), and iii) synergism between VCM and its oleic acid based carrier, which is thought to have inherent anti-MRSA activity also due to its membrane disruption ability (Engelbrecht et al., 2011; Huang et al., 2011). By displaying the possibility of having multiple mechanisms of actions against MRSA, the VCM_NMEO SLNs developed in this study have the potential to be effective in combating the growing threat of bacterial resistance against vancomycin. Data regarding *in vivo* antibacterial studies of antibiotic loaded pH responsive SLNs is limited, and this study could therefore provide a foundation for future studies related to delivering antibiotics using surface switching pH responsive SLNs.

The histomorphological evaluations were performed on excised skin from the untreated, bare VCM and VCM_NMEO SLN group to assess the morphological changes and skin integrity after MRSA infection. The H&E stained slides revealed that the untreated skin samples displayed evidence of tissue inflammation and abscess formation (Fig. 10A). The bare VCM group also showed evidence of swelling and abscess formation, however to a lesser extent than the untreated group (Fig. 10B). The VCM_NMEO SLN group displayed minimal signs of inflammation and no evidence of abscess formation (Fig. 10C). Both the untreated and

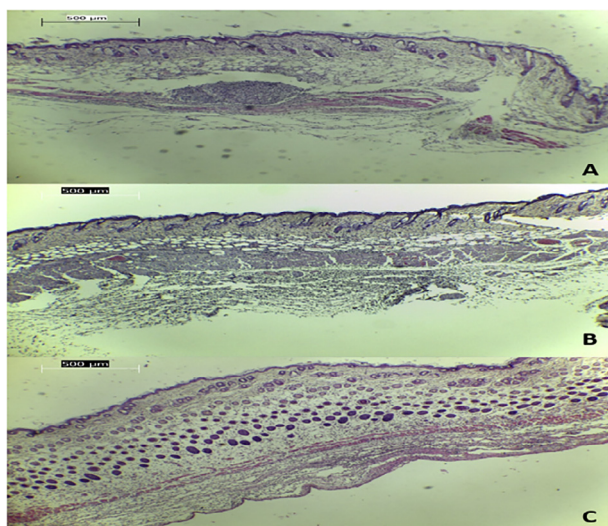


Fig. 10. Photomicrographs of the control and the treated skin samples H&E stained (4X): (A) untreated (B) bare VCM treated and (C) VCM_NMEO SLN treated.

bare VCM group presented with large quantities of white blood cells at the infection site, however this was evidently lower in the VCM_NMEO SLN group (Fig. 10C). The findings of the histomorphological analysis correlate with the CFUs calculated in the in vivo antibacterial study as the skin sample with the most number of recovered bacteria also presents with the highest degree of inflammation, abscess formation and presence of white blood cells. This is due to the greater immune response to the larger number of bacteria present at the infection site of the untreated group. The VCM_NMEO SLN group which displayed the lowest number of isolated bacteria presented with minimal signs of inflammation and no abscess formation, this could be due to a reduced immune response to a statistically lower number of isolated bacteria at the infection site. These findings further exhibit the antimicrobial superiority of the VCM_NMEO SLNs.

4. Conclusion

Nanobased antibiotic carriers are increasingly being recognized as a potential approach to improve the activity of existing drugs in an era when bacterial resistance is rising while the discovery of new antibiotic drugs is declining. In this project, a biosafe oleic acid based pH-responsive-lipid, NMEO, was synthesized, characterized and successfully formulated into pH responsive SLNs. The in vitro release showed that the release of vancomycin from the NMEO SLNs was faster at pH 6 than at pH 7.4, with the MIC value of the formulation against MRSA decreasing by 64-fold at acidic pH. The potential of the NMEO SLNs was also confirmed by their in vivo antibacterial activity. Mean bacterial load of samples treated by NMEO SLNs were 4-fold lower than those treated by bare VCM, and 162-fold lower than untreated samples. Thus, the developed pH responsive NMEO SLNs could be an effective delivery system to improve the performance of vancomycin and other antibiotics against resistant bacteria infections.

Conflict of interest

Authors declare that they have no conflict of interest.

Acknowledgements

We acknowledge the University of KwaZulu-Natal (UKZN), UKZN Nanotechnology Platform and the National Research Foundation (NRF) of South Africa for financing this study. We also thank Biomedical

Resource Unit (BMRU) (UKZN) and the Microscopy and Microanalysis Unit (MMU) (UKZN) for technical assistance and Carrin Martin for proof reading.

References

- Andrade, F., Rafael, D., Videira, M., Ferreira, D., Sosnik, A., Sarmiento, B., 2013. Nanotechnology and pulmonary delivery to overcome resistance in infectious diseases. *Adv. Drug Deliv. Rev.* 65, 1816–1827.
- Bergstrand, N., Arfvidsson, M.C., Kim, J.M., Thompson, D.H., Edwards, K., 2003. Interactions between pH-sensitive liposomes and model membranes. *Biophys. Chem.* 104, 361–379.
- Boucher, H.W., Corey, G.R., 2008. Epidemiology of methicillin-resistant staphylococcus aureus infections. *Clin. Infect. Dis.* 2111, 344–349.
- Briones, E., Isabel Colino, C., Lanao, J.M., 2008. Delivery systems to increase the selectivity of antibiotics in phagocytic cells. *J. Control. Release* 125, 210–227.
- Cao, X.L., Cheng, C., Ma, Y.L., Zhao, C.S., 2010. Preparation of silver nanoparticles with antimicrobial activities and the researches of their biocompatibilities. *J. Mater. Sci. Mater. Med.* 21, 2861–2868.
- Chakraborty, S.P., Sahu, S.K., Pramanik, P., Roy, S., 2012. In vitro antimicrobial activity of nanoconjugated vancomycin against drug resistant *Staphylococcus aureus*. *Int. J. Pharm.* 436, 659–676.
- Chawla, J.S., Amiji, M.M., 2002. Biodegradable poly (o-caprolactone) nanoparticles for tumor-targeted delivery of tamoxifen. *Int. J. Pharm.* 249, 127–138.
- Darwish, M.S.A., 2017. Effect of carriers on heating efficiency of oleic acid-stabilized magnetite nanoparticles. *J. Mol. Liq.* 231, 80–85.
- Das, S., Kiong, W., Kanaujia, P., Kim, S., Tan, R.B.H., 2011. Formulation design, preparation and physicochemical characterizations of solid lipid nanoparticles containing a hydrophobic drug: effects of process variables. *Colloids Surf. B Biointerfaces* 88, 483–489.
- Dhar, S., Gu, F.X., Langer, R., Farokhzad, O.C., Lippard, S.J., 2008. Targeted delivery of cisplatin to prostate cancer cells by aptamer functionalized Pt (IV) prodrug-PLGA-PEG nanoparticles. *PNAS* 105, 17356–17361.
- Di Gioia, S., Sardo, C., Belgiovine, G., Triolo, D., d'Apolito, M., Castellani, S., Carbone, A., Giardino, I., Giammona, G., Cavallaro, G., Conese, M., 2015. Cationic poly-aspartamide-based nanocomplexes mediate siRNA entry and down-regulation of the pro-inflammatory mediator high mobility group box 1 in airway epithelial cells. *Int. J. Pharm.* 2015 (491), 359–366.
- Dong, M., Wang, J., Wu, Y., Chen, B., Yu, M., Wen, A., 2015. International Journal of Infectious Diseases Evaluation of body weight-based vancomycin therapy and the incidence of nephrotoxicity: a retrospective study in the northwest of China. *Int. J. Infect. Dis.* 37, 125–128.
- Dora, C.P., Singh, S.K., Kumar, S., Datusalia, A.K., Deep, A., 2010. Development and characterization of nanoparticles of glibenclamide by solvent displacement method. *Acta Pol. Pharm. Res.* 67, 283–290.
- Drummond, D.C., Zignani, M., Leroux, J.C., 2000. Current status of pH-sensitive liposomes in drug delivery. *Prog. Lipid Res.* 39, 409–460.
- Ebrahimi, H.A., Javadzadeh, Y., Hamidi, M., Jalali, M.B., 2015. Repaglinide-loaded solid lipid nanoparticles: effect of using different surfactants/stabilizers on physicochemical properties of nanoparticles. *Daru* 23, 46.
- Engelbrecht, T.N., Schroeter, A., Hauß, T., Neubert, R.H.H., 2011. Lipophilic penetration enhancers and their impact to the bilayer structure of stratum corneum lipid model membranes: neutron diffraction studies based on the example Oleic Acid. *BBA – Biomembr.* 1808, 2798–2806.
- Vancomycin solubility study. Report to office of generic drugs: <http://www.fda.gov/downloads/Drugs/GuidanceComplianceRegulatoryInformation/Guidances/ucm082291.pdf>.
- Florence, A.T., Attwood, D., 2015. Physicochemical principles of pharmacy. Manufacture, Formulation and Clinical Use. Pharmaceutical Press.
- Forier, K., Raemdonck, K., De Smedt, S.C., Demeester, J., Coenye, T., Braeckmans, K., 2014. Lipid and polymer nanoparticles for drug delivery to bacterial biofilms. *J. Control. Release* 190, 607–623.
- Gandhi, K., Maganti, R.S., Kaur, H., Vinod, K.S., Verma, P., 2017. Formulation and evaluation of sol-gel drug delivery system for intracanal pH sensitive controlled delivery of chlorhexidine. *J. Clin. Diagn. Res.* 11, ZC68-ZC72.
- Gao, P., Nie, X., Zou, M., Shi, Y., Cheng, G., 2011. Recent advances in materials for extended-release antibiotic delivery system. *J. Antibiot. (Tokyo)* 64, 625–634.
- Gao, W., Chen, Y., Zhang, Y., Zhang, Q., Zhang, L., 2017. Nanoparticle-based local antimicrobial drug delivery. *Adv. Drug. Deliv. Rev.*
- Gao, W., Thamphiwatana, S., Angsantikul, P., Zhang, L., 2014. Nanoparticle approaches against bacterial infections. *Wiley Interdiscip. Rev. Nanomed. Nanobiotechnol.* 6, 532–547.
- Gastaldi, L., Battaglia, L., Peira, E., Chirio, D., Muntoni, E., Solazzi, I., Gallarate, M., Dosio, F., 2014. Solid lipid nanoparticles as vehicles of drugs to the brain: Current state of the art. *Eur. J. Pharm. Biopharm.* 87, 433–444.
- Geszke-Moritz, M., Moritz, M., 2016. Solid lipid nanoparticles as attractive drug vehicles: composition, properties and therapeutic strategies. *Mater. Sci. Eng. C* 68, 982–994.
- Gonçalves, L.M.D., Maestrelli, F., Mannelli, L.C., Ghelardini, C., Almeida, A.J., Mura, P., 2016. Development of solid lipid nanoparticles as carriers for improving oral bioavailability of glibenclamide. *Eur. J. Pharm. Biopharm.* 102, 41–50.
- Gupta, Y., Jain, A., Jain, S.K., 2007. Transferrin-conjugated solid lipid nanoparticles for enhanced delivery of quinine dihydrochloride to the brain. *J. Pharm. Pharmacol.* 59, 935–940.
- Ha, S., Ong, L., Win, Y., Koh, T., Yeap, G., 2008. Synthesis of New Schiff Base: 4-[(Pyridin-

- 3-ylmethylene)-amino] phenyldodecanoate. Molbank 3, M582.
- Ha, S.T., Ong, L.K., Ong, S.T., Yeap, G.Y., Wong, J.P.W., Koh, T.M., Lin, H.C., 2009. Synthesis and mesomorphic properties of new Schiff base esters with different alkyl chains. *Chin. Chem. Lett.* 20, 767–770.
- Hao, Y.M., Li, K.A., 2011. Entrapment and release difference resulting from hydrogen bonding interactions in niosome. *Int. J. Pharm.* 403, 245–253.
- Helgason, T., Awad, T.S., Kristbergsson, K., McClements, D.J., Weiss, J., 2009. Effect of surfactant surface coverage on formation of solid lipid nanoparticles (SLN). *J. Colloid Interface Sci.* 334, 75–81.
- Ho, S., Tan, J.P.K., Nederberg, F., Fukushima, K., Colson, J., Yang, C., Nelson, A., Yang, Y., Hedrick, J.L., 2010. Hydrogen bonding-enhanced micelle assemblies for drug delivery. *Biomaterials* 31, 8063–8071.
- Huang, C., Chen, C., Pornpattananankul, D., Zhang, L., Chan, M., Hsieh, M., Zhang, L., 2011. Eradication of drug resistant *Staphylococcus aureus* by liposomal oleic acids. *Biomaterials* 32, 214–221.
- Huh, A.J., Kwon, Y.J., 2011. “Nanoantibiotics”: a new paradigm for treating infectious diseases using nanomaterials in the antibiotics resistant era. *J. Control. Release* 156, 128–145.
- Jadhav, M., Kalhapure, R.S., Rambharose, S., Mocktar, C., Govender, T., 2016. Synthesis, characterization and antibacterial activity of novel heterocyclic quaternary ammonium surfactants. *J. Ind. Eng. Chem.* <https://doi.org/10.1016/j.jiec.2016.12.013>.
- Kadry, A.A., Al-swayeh, S.A., Abd-allah, A.R.A., Bayomi, M.A., 2004. Treatment of experimental osteomyelitis by liposomal antibiotics. *J. Antimicrob. Chemother.* 54, 1103–1108.
- Kalhapure, R.S., Jadhav, M., Rambharose, S., Mocktar, C., Singh, S., Renukuntla, J., Govender, T., 2017a. pH-responsive chitosan nanoparticles from a novel twin-chain anionic amphiphile for controlled and targeted delivery of vancomycin. *Colloids Surf. B Biointerfaces.* <https://doi.org/10.1016/j.colsurfb.2017.07.049>.
- Kalhapure, R.S., Mocktar, C., Sikwal, D.R., Sonawane, S.J., Kathiravan, M.K., Skelton, A., Govender, T., 2014. Ion pairing with linoleic acid simultaneously enhances encapsulation efficiency and antibacterial activity of vancomycin in solid lipid nanoparticles. *Colloids Surf. B Biointerfaces* 117, 303–311.
- Kalhapure, R.S., Sikwal, D.R., Rambharose, S., Mocktar, C., Singh, S., Bester, L., Oh, J.K., Renukuntla, J., Govender, T., 2017b. Enhancing targeted antibiotic therapy via pH responsive solid lipid nanoparticles from an acid cleavable lipid. *Nanomed. Nanotechnol. Biol. Med.* <https://doi.org/10.1016/j.nano.2017.04.010>.
- Kali, A., Stephen, S., Umadevi, S., Kumar, S., Joseph, N.M., Srirangaraj, S., 2013. Changing trends in resistance pattern of methicillin resistant *Staphylococcus aureus*. *J. Clin. Diagnostic Res.* 7, 1979–1982.
- Kashanian, S., Azandaryani, A.H., Derakhshandeh, K., 2011. New surface-modified solid lipid nanoparticles using N-glutaryl phosphatidylethanolamine as the outer shell. *Int. J. Nanomed.* 6, 2393–2401.
- Koester, L.S., Ortega, G.G., Mayorga, P., Bassani, V.L., 2004. Mathematical evaluation of in vitro release profiles of hydroxypropylmethylcellulose matrix tablets containing carbamazepine associated to β -cyclodextrin. *Eur. J. Pharm. Biopharm.* 58, 177–179.
- Kullberg, M.A.X., Mann, K., Owens, J.L.E.E., 2009. A two-component drug delivery system using Her-2-targeting thermosensitive liposomes. *J. Drug Target.* 17, 98–107.
- Kumar, M., Misra, A., Babbar, A.K., Mishra, A.K., Mishra, P., Pathak, K., 2008. Intranasal nanoemulsion based brain targeting drug delivery system of risperidone. *Int. J. Pharm.* 358, 285–291.
- Lane, M.E., 2013. Skin penetration enhancers. *Int. J. Pharm.* 447, 12–21.
- Liu, B., Thayumanavan, S., 2017. Substituent effects on the pH sensitivity of acetals and ketals and their correlation with encapsulation stability in polymeric nanogels. *J. Am. Chem. Soc.* 139, 2306–2317.
- Liu, J., Wang, Z., Li, F., Gao, J., Wang, L., Huang, G., 2014. Liposomes for systematic delivery of vancomycin hydrochloride to decrease nephrotoxicity: characterization and evaluation. *Asian J. Pharm. Sci.* 10, 212–222.
- Liu, P., Xu, G., Pranantyo, D., Xu, L.Q., Neoh, K.-G., Kang, E.-T., 2018. pH-sensitive zwitterionic polymer as an antimicrobial agent with effective bacterial targeting. *ACS Biomater. Sci. Eng.* 4, 40–46.
- Lu, Y., Aimetti, A.A., Langer, R., Gu, Z., 2016. Bioresponsive materials. *Nat. Rev. Mater.* 2, 16075.
- Ma, R.A., Lucia, A., Esperanza, B., Antonio, J., Pe, E., Rocio, E., Celina, S., 2014a. USA300-related methicillin-resistant *Staphylococcus aureus* clone is the predominant cause of community and hospital MRSA infections in Colombian children. *Int. J. Infect. Dis.* 25, 88–93.
- Ma, T., Wang, L., Yang, T., Ma, G., Wang, S., 2014b. Homogeneous PLGA-lipid nanoparticles as a promising oral vaccine delivery system for ovalbumin. *Asian J. Pharm. Sci.* 9, 129–136.
- Mandal, S.M., Pegu, R., Porto, W.F., Franco, O.L., Pratihari, S., 2017. Novel boronic acid derivatives of Bis(indolyl) methane as anti-MRSA agents. *Bioorg. Med. Chem. Lett.* <https://doi.org/10.1016/j.bmcl.2017.03.070>.
- Meng, X., Li, F., Li, F., Xiong, Y., Xu, H., 2017. Vancomycin modified PEGylated-magnetic nanoparticles combined with PCR for efficient enrichment and detection of *Listeria monocytogenes*. *Sensors Actuators B Chem.* 247, 546–555.
- Mercier, R.-C., Stumpo, C., Rybak, M.J., 2002. Effect of growth phase and pH on the in vitro activity of a new glycopeptide, oritavancin (LY333328), against *Staphylococcus aureus* and *Enterococcus faecium*. *J. Antimicrob. Chemother.* 50, 19–24.
- Mohammed Fayaz, A., Girilal, M., Mahdy, S.A., Somsundar, S.S., Venkatesan, R., Kalaichelvan, P.T., 2011. Vancomycin bound biogenic gold nanoparticles: a different perspective for development of anti VRSA agents. *Process Biochem.* 46, 636–641.
- Mura, S., Nicolas, J., Couvreur, P., 2013. Stimuli-responsive nanocarriers for drug delivery. *Nat. Mater.* 12, 991–1003.
- Omolo, C.A., Kalhapure, R.S., Jadhav, M., Rambharose, S., Mocktar, C., Ndesendo, V.M.K., Govender, T., 2016. PEGylated oleic acid: A promising amphiphilic polymer for nano-antibiotic delivery. *Eur. J. Pharm. Biopharm.* 112, 1–13.
- Papadopoulou, V., Kosmidis, K., Vlachou, M., Macheras, P., 2006. On the use of the Weibull function for the discernment of drug release mechanisms. *Int. J. Pharm.* 309, 44–50.
- Pereira, P.M., Filipe, R., Tomasz, A., Pinho, M.G., 2007. Fluorescence ratio imaging microscopy shows decreased access of vancomycin to cell wall synthetic sites in vancomycin-resistant *Staphylococcus aureus*. *J. Antimicrob. Chemother.* 51, 3627–3633.
- Pichavant, L., Bourget, C., Durrieu, M.C., Héroguez, V., 2011. Synthesis of pH-sensitive particles for local delivery of an antibiotic via dispersion ROMP. *Macromolecules* 44, 7879–7887.
- Priya, B., et al., 2009. Stimuli-responsive polymers and their applications in drug delivery. *Biomed. Mater.* 4, 22001.
- Pu, Y., Zhang, L., Zheng, H., He, B., Gu, Z., 2014. *Polym. Chem.* 35, 463–470.
- Radovic-Moreno, A.F., Lu, T.K., Puscasu, V.A., Yoon, C.J., Langer, R., Farokhzad, O.C., 2012. Surface charge-switching polymeric nanoparticles for bacterial cell wall-targeted delivery of antibiotics. *ACS Nano* 6, 4279–4287.
- Rapoport, N.Y., Kennedy, A.M., Shea, J.E., Scaife, C.L., Nam, K., 2009. Controlled and targeted tumor chemotherapy by ultrasound-activated nanoemulsions/microbubbles. *J. Control. Release* 138, 268–276.
- Romic, M.D., Klaric, M.S., Lovric, J., Pepic, I., Cetina-Cizmek, B., Filipovic-Grcic, J., Hafner, A., 2016. Melatonin-loaded chitosan/Pluronic® F127 microspheres as in situ forming hydrogel: an innovative antimicrobial wound dressing. *Eur. J. Pharm. Biopharm.* 107, 67–79.
- Rostami, E., Kashanian, S., Azandaryani, A.H., Faramarzi, H., Dolatabadi, J.E.N., Omidfar, K., 2014. Drug targeting using solid lipid nanoparticles. *Chem. Phys. Lipids* 181, 56–61.
- Seedat, N., Kalhapure, R.S., Mocktar, C., Vepuri, S., Jadhav, M., Soliman, M., Govender, T., 2016. Co-encapsulation of multi-lipids and polymers enhances the performance of vancomycin in lipid-polymer hybrid nanoparticles: in vitro and in silico studies. *Mater. Sci. Eng. C* 61, 616–630.
- Sharma, A., Kumar Arya, D., Dua, M., Chhatwal, G.S., Johri, A.K., 2012. Nano-technology for targeted drug delivery to combat antibiotic resistance. *Expert Opin. Drug Deliv.* 9, 1325–1332.
- Shenoy, D.B., Amiji, M.M., 2005. Poly(ethylene oxide)-modified poly(epsilon-caprolactone) nanoparticles for targeted delivery of tamoxifen in breast cancer. *Int. J. Pharm.* 293, 261–270.
- Sikwal, D.R., Kalhapure, R.S., Jadhav, M., Rambharose, S., Mocktar, C., Govender, T., 2017. Non-ionic self-assembling amphiphilic Janus type polyester dendrimers as new drug delivery excipients. *RSC Adv.* 7, 14233–14246.
- Singh, S.K., Verma, P.R.P., Razdan, B., 2010. Glibenclamide-loaded self-nanoemulsifying drug delivery system: development and characterization. *Drug Dev. Ind. Pharm.* 36, 933–945.
- Soares, P.I.P., Laia, C.A.T., Carvalho, A., Pereira, L.C.J., Coutinho, J.T., Ferreira, I.M.M., Novo, C.M.M., Borges, J.P., 2016. Iron oxide nanoparticles stabilized with a bilayer of oleic acid for magnetic hyperthermia and MRI applications. *Appl. Surf. Sci.* 383, 240–247.
- Sonawane, S.J., Kalhapure, R.S., Govender, T., 2017. Hydrazone linkages in pH responsive drug delivery systems. *Eur. J. Pharm. Sci.* 99, 45–65.
- Sonawane, S.J., Kalhapure, R.S., Rambharose, S., Mocktar, C., Vepuri, S.B., Soliman, M., Govender, T., 2016. Ultra-small lipid-dendrimer hybrid nanoparticles as a promising strategy for antibiotic delivery: In vitro and in silico studies. *Int. J. Pharm.* 504, 1–10.
- Song, J., Hsueh, P., Chung, D.R., Ko, K.S., Kang, C., Peck, K.R., Yeom, J., Kim, S., Chang, H., Kim, Y., Jung, S., Son, J.S., 2011. Spread of methicillin-resistant *Staphylococcus aureus* between the community and the hospitals in Asian countries: an ANSORP study. *J. Antimicrob. Chemother.* 1061–1069.
- Souto, E.B., Müller, R.H., 2006. Investigation of the factors influencing the incorporation of clotrimazole in SLN and NLC prepared by hot high-pressure homogenization. *J. Microencapsul.* 23, 377–388.
- Spada, G., Gavini, E., Cossu, M., Rassu, G., Giunchedi, P., 2012. Solid lipid nanoparticles with and without hydroxypropyl- β -cyclodextrin: a comparative study of nanoparticles designed for colonic drug delivery. *Nanotechnology* 23. <https://doi.org/10.1088/0957-4484/23/9/095101>.
- Srisuk, P., Thongnopnua, P., Raktanonchai, U., Kanokpanont, S., 2012. Physico-chemical characteristics of methotrexate-entrapped oleic acid-containing deformable liposomes for in vitro transepidermal delivery targeting psoriasis treatment. *Int. J. Pharm.* 427, 426–434.
- Subedi, R.K., Kang, K.W., Choi, H.K., 2009. Preparation and characterization of solid lipid nanoparticles loaded with doxorubicin. *Eur. J. Pharm. Sci.* 37, 508–513.
- Tate, S., MacGregor, G., Davis, M., Innes, J.A., Greening, A.P., 2002. Airways in cystic fibrosis are acidified: detection by exhaled breath condensate. *Thorax* 57, 926–929.
- Teo, L., Chen, C., Kuo, J., 1997. Fourier transform infrared spectroscopy study on effects of temperature on hydrogen bonding in amine-containing polyurethanes and poly(urethane - urea)s. *Macromolecules* 30, 1793–1799.
- Timko, B.B.P., Dvir, T., Kohane, D.S., 2010. Remotely triggerable drug delivery systems. *Adv. Mater.* 22, 4925–4943.
- Toutou, E., Godin, B., Karl, Y., Bujanover, S., Becker, Y., 2002. Oleic acid, a skin penetration enhancer, affects Langerhans cells and corneocytes. *J. Control. Release* 80, 1–7.
- Van Bambeke, F., Struelens, M.J., 2008. The bacterial envelope as a target for novel anti-MRSA antibiotics. *Trends Pharmacol. Sci.* 29, 124–134.
- Waddad, Ayman, Abbad, Sarra, Yu, Fan, Munyendo, Were, Wang, Jing, Lv, H., Zhou, Jianping, 2013. Formulation, characterization and pharmacokinetics of Morin hydrate niosomes prepared from various non-ionic surfactants. *Int. J. Pharm.* 456, 446–458.
- Wang, A.Z., Gu, F., Zhang, L., Chan, J.M., Radovic-moreno, A., Shaikh, M.R., Farokhzad, O.C., 2008. Biofunctionalized targeted nanoparticles for therapeutic applications. *Expert Opin. Biol. Ther.* 8, 1063–1070.

- Wang, Q., Zhou, L., Qiu, L., Lu, D., Wu, Y., Zhang, X.-B., 2015. An efficient ratiometric fluorescent probe for tracking dynamic changes in lysosomal pH. *Analyst* 140, 5563–5569.
- Yang, S., Qi, Y., Liu, C., Wang, Y., Zhao, Y., Wang, L., Li, J., Tan, W., Yang, R., 2014. Design of a simultaneous target and location-activatable fluorescent probe for visualizing hydrogen sulfide in lysosomes. *Anal. Chem.* 86, 7508–7515.
- Yousry, C., Fahmy, R.H., Essam, T., El-Laithy, H.M., Elkheshen, S.A., 2016. Nanoparticles as tool for enhanced ophthalmic delivery of vancomycin: a multidistrict-based microbiological study, solid lipid nanoparticles formulation and evaluation. *Drug Dev. Ind. Pharm.* 42, 1752–1762.
- Yu, H., Xiao, Y., Jin, L., 2012. A lysosome-targetable and two-photon fluorescent probe for monitoring endogenous and exogenous nitric oxide in living cells. *J. Am. Chem. Soc.* 134, 17486–17489.
- Xiong, M.H., Bao, Y., Yang, X.Z., Zhu, Y.H., Wang, J., 2014. Delivery of antibiotics with polymeric particles. *Adv. Drug Deliv. Rev.* 78, 63–76.
- Zazo, H., Colino, C.I., Lanao, J.M., 2016. Current applications of nanoparticles in infectious diseases. *J. Control. Release* 224, 86–102.
- Zetola, N., Francis, J.S., Nuermberger, E.L., Bishai, W.R., 2005. Community-acquired methicillin-resistant *Staphylococcus aureus*: an emerging threat. *Lancet Infect. Dis.* 5, 275–286.
- Zhang, Y., Huo, M., Zhou, J., Zou, A., Li, W., Yao, C., Xie, S., 2010. DDSolver: an add-in program for modeling and comparison of drug dissolution profiles. *AAPS* 12, 263–271.
- Zhao, S., Minh, L. Van, Li, N., Garamus, V.M., Handge, U.A., Liu, J., Zhang, R., Willumeit-Romer, R., Zou, A., 2016. Doxorubicin hydrochloride-oleic acid conjugate loaded nanostructured lipid carriers for tumor specific drug release. *Colloids Surf. B Biointerfaces* 145, 95–103.
- Xu, S.P., Lv, P.C., Fang, R.Q., et al., 2009. Synthesis and crystal structure of 2,4-diiodo-6-[(2-morpholin-4-yl-ethylimino)-methyl]-phenolato-zinc(II). *J. Chem. Crystallogr.* 39, 931–934.




Antimicrobial cell penetrating peptides with bacterial cell specificity: pharmacophore modelling, quantitative structure activity relationship and molecular dynamics simulation

Mbuso Faya, Rahul S. Kalhapure, Dinesh Dhumal, Nikhil Agrawal, Calvin Omolo, Krishnacharya G. Akamanchi & Thirumala Govender


To cite this article: Mbuso Faya, Rahul S. Kalhapure, Dinesh Dhumal, Nikhil Agrawal, Calvin Omolo, Krishnacharya G. Akamanchi & Thirumala Govender (2018): Antimicrobial cell penetrating peptides with bacterial cell specificity: pharmacophore modelling, quantitative structure activity relationship and molecular dynamics simulation, Journal of Biomolecular Structure and Dynamics, DOI: [10.1080/07391102.2018.1484814](https://doi.org/10.1080/07391102.2018.1484814)

To link to this article: <https://doi.org/10.1080/07391102.2018.1484814>

 View supplementary material 

 Accepted author version posted online: 26 Jul 2018.
Published online: 13 Nov 2018.

 Submit your article to this journal 

 Article views: 36

 View Crossmark data 



Antimicrobial cell penetrating peptides with bacterial cell specificity: pharmacophore modelling, quantitative structure activity relationship and molecular dynamics simulation

Mbuso Faya^a, Rahul S. Kalhapure^{a*}, Dinesh Dhumal^b, Nikhil Agrawal^a, Calvin Omolo^a, Krishnacharya G. Akamanchi^b and Thirumala Govender^a

^aDepartment of Pharmaceutical Sciences, University of KwaZulu-Natal, Private Bag, Durban, South Africa; ^bDepartment of Pharmaceutical Sciences and Technology, Institute of Chemical Technology, Mumbai, India

Communicated by Ramaswamy H. Sarma

ABSTRACT

Current research has shown cell-penetrating peptides and antimicrobial peptides (AMPs) as probable vectors for use in drug delivery and as novel antibiotics. It has been reported that the higher the therapeutic index (TI) the higher would be the bacterial cell penetrating ability. To the best of our knowledge, no in-silico study has been performed to determine bacterial cell specificity of the antimicrobial cell penetrating peptides (aCPP's) based on their TI. The aim of this study was to develop a quantitative structure activity relationship (QSAR) model, which can estimate antimicrobial potential and cell-penetrating ability of aCPPs against *S. aureus*, to confirm the relationship between the TI and aCPPs and to identify specific descriptors responsible for aCPPs penetrating ability. Molecular dynamics (MD) simulation was also performed to confirm the membrane insertion of the most active aCPPs obtained from the QSAR study. The most appropriate pharmacophore was identified to predict the aCPP's activity. The statistical results confirmed the validity of the model. The QSAR model was successful in identifying the optimal aCPP with high activity prediction and provided insights into the structural requirements to correlate their TI to cell penetrating ability. MD simulation of the best aCPP with 1-palmitoyl-2-oleoyl-sn-glycero-3-phosphocholine (POPC) bilayer confirmed its interaction with the membrane and the C-terminal residues of the aCPP played a key role in membrane penetration. The strategy of combining QSAR and molecular dynamics, allowed for optimal estimation of ligand-target interaction and confirmed the importance of Trp and Lys in interacting with the POPC bilayer.

ARTICLE HISTORY

Received 28 February 2018
Accepted 20 May 2018

KEYWORDS

3D QSAR; pharmacophore modelling; therapeutic index (TI); molecular dynamics simulation; antimicrobial peptide

Abbreviations: A: hydrogen bond acceptor; aCPPs: antimicrobial cell penetrating peptides; AMPs: antimicrobial peptides; ANN: artificial neural network; AntiBP2: antibacterial peptide prediction; APD2: antimicrobial peptide database; COM: centre of mass; CPPs: cell penetrating peptides; F value: Fisher test; H: hydrophobic group; IC₅₀: half maximal inhibitory concentration; LA: lipid A; LINCS: linear constraint solver; LPS: lipopolysaccharides; Lys: lysine; MD: molecular dynamics; MIC: minimum inhibitory concentration; NPT: isothermal-isobaric ensemble; NVT: canonical ensemble; PLS: partial least squares; PME: particle mesh Ewald; PO₄: phosphate group; POPC: 1-palmitoyl-2-oleoyl-sn-glycero-3-phosphocholine; Q²: cross-validation coefficient; QSAR: quantitative structure activity relationship; R: aromatic ring; R²: correlation coefficient; RMSE: root-mean squared error; SD: standard deviation; TI: therapeutic index; Tis: therapeutic indices; Trp: tryptophan; vdW: van der Waals


1. Introduction

The resistance to antibiotics by bacteria poses a considerable threat to global health (Davies & Davies, 2010; Sengupta, Chattopadhyay, & Grossart, 2013), highlighting the need to urgently develop novel antibacterial agents. Bacterial resistance has prompted a search of natural inhibitors, leading to the use of antimicrobial peptides (AMPs) (Wang, Zeng, Yang, & Qiao, 2016), which form an integral part of innate immunity (Branco, Viana, Albergaria, & Arneborg, 2015; Bolintineanu, Hazrati, Davis, Lehrer, & Kaznessis, 2010; Wiesner & Vilcinskis, 2010). AMPs are small, cationic and amphiphilic molecules that are found in

several classes of both prokaryotes and eukaryotes. They have structures such as linear α -helical peptides, β -sheet globular arrangements, and peptides with uncommon sequences including tryptophan and proline (Carnicelli et al., 2013; Michael Henderson & Lee, 2013; Vale, Aguiar, & Gomes, 2014; Wang et al., 2012). They have been seen to be structurally similar to cationic cell penetrating peptides (CPPs), and while their mechanism of action has not been elucidated, it is thought that they primarily target the bacterial cell membrane (Bhonsle, Venugopal, Huddler, Magill, & Hicks, 2007; Lee, Hall, & Aguilar, 2016; Schmidt & Wong, 2013). Cationic AMPs can bind to

CONTACT Thirumala Govendera  govenderth@ukzn.ac.za; Rahul S. Kalhapure  kalhapure@ukzn.ac.za; rahul.kalhapure@rediffmail.com

*Present address: School of Pharmacy, University of Texas at El Paso, 500 W University Ave, El Paso, TX 79968, USA.

 Supplemental data for this article is available online at <http://dx.doi.org/10.1080/07391102.2018.1484814>.

© 2018 Informa UK Limited, trading as Taylor & Francis Group

lipopolysaccharides (LPS) or lipid A (LA) of Gram-negative bacteria. This action leads to membrane permeation through self-promoted uptake and trans-membrane channel formation via a "barrel-stave" or toroidal pore mechanism, or through membrane destruction via a carpet-like mechanism (Mishra et al., 2013; Wang et al., 2012). Several studies have suggested that the success of AMP activity is mediated by its ability to aggregate on the surface of the membrane of bacteria, or to traverse the bacterial cell membrane and interrupt intracellular targets (Carmona-Ribeiro & de Melo Carrasco, 2014; Da Costa, Cova, Ferreira, & Vitorino, 2015; Guilhelmelli et al., 2013; Lv et al., 2014; Malanovic & Lohner, 2015; Tang, Shi, Zhao, Hao, & Le, 2008). However, membrane penetration/disintegration has been reported to be the primary mechanism of action of these cationic AMPs (Huerta-Cantillo & Navarro-García, 2016; Ong, Wiradharma, & Yang, 2014; Porto, Silva, & Franco, 2012; Tsai et al., 2009).

AMPs function with a great deal of similarity to CPPs and share important features that include short sequence lengths (~10–40 residues), net positive charge, and an arrangement of amino acids with a substantial content of non-polar residues. All of these are considered to promote aCPP interaction and insertion with the hydrophobic core of the bacterial membrane bilayer. Small sequence modifications of CPPs can alter their biological effect from cell-penetrating to antimicrobial or vice versa, leading to the formation of antimicrobial cell penetrating peptides (aCPP), which are cell penetrating peptides with antimicrobial properties (Bahnsen, Franzyk, Sandberg-Schaal, & Nielsen, 2013). These peptides have a dual effect which offers bacterial membrane penetration together with antimicrobial activity, as seen with the aCPP penetration (Bahnsen, Franzyk, Sayers, Jones, & Nielsen, 2015; Henriques, Melo, & Castanho, 2006; Pushpanathan, Gunasekaran, & Rajendhran, 2016; Splith & Neundorff, 2011). Other examples of aCPPs include Bac7, which binds to bacterial ribosomal proteins and inhibits protein synthesis, and pep-1-K, which has a high membrane perturbing activity (Bobone et al., 2011; Mardirosian et al., 2014). The aCPPs have been widely reported as antibacterial agents, and as part of conjugates, such as drugs and polymers, and are utilised for the sole purpose of enhancing biological activity (Arnusch et al., 2012; Eckhard et al., 2014; Maekawa et al., 2015; Souto et al., 2013). There have also been reports of aCPPs being used as delivery systems to carry cargo across bacterial membranes (Carmona-Ribeiro & de Melo Carrasco, 2014; Eriksen, Skovsen, & Fojan, 2013; Kingsbury, Boehm, Mehta, Grappel, & Gilvarg, 1984). This is important, as it allows for the dual approach of cell penetration and the release of conjugates to their respective intracellular targets, as well as the biological activity of the aCPPs themselves. The aCPPs offer promising prospects to be utilised as alternative agents to known antibiotics. This is due to their ability to permeate the bacterial cell membrane and its cationic charge, which allows them not only to form pores on the bacterial cell membrane but also to traverse this layer to interfere with intracellular targets (Delcour, 2009; Schmidt & Wong, 2013). Another feature that makes them attractive is their ability to carry cargo

across the bacterial cell membrane (Aparoy, Reddy, & Reddanna, 2012; Burns, McCleerey, & Thévenin, 2016), this strategy being useful to deliver conjugates, such as drugs and polymers. Continued research in these areas is required to identify the optimal aCPPs with high therapeutic indices (TIs). Tools to facilitate the design of potent and selective aCPPs, either as antibiotic entities themselves, or as components of pharmaceutical materials such as polymers, or as ligands for drug delivery carriers are essential to optimise their applications.

Quantitative structure–activity relationships (QSAR) is a useful tool in the rational design of potent and selective aCPPs (Mollica et al., 2018). Frequently used predictive tools, such as AntiBP2 and APD2 databases, are based on sequence analysis and physicochemical features, whereas other predictive models outline more structural-descriptor insight required for the designing of novel AMPs by outlining specific descriptors such as polarity of amino acids, free energy, hydration, and isoelectric point which are all properties responsible for biological activity (Vora et al., 2018; Wang et al., 2012). One such model based on inductive descriptors was developed by Cherkasov (2005), where the prediction was based on artificial neural network (ANN) for a series of newly synthesized polypeptides (Cherkasov, 2005; Torrent, Andreu, Nogués, & Boix, 2011). Taboureau et al. (2006) used GRID to generate 3D descriptors and built a high-performance QSAR model for novispirin AMPs (Taboureau et al., 2006). Fjell et al. (2009) also carried out an ANN virtual screening using physicochemical descriptors to screen for potential AMPs (Fjell et al., 2009). QSAR is an important tool, as it allows for the accurate design and structural elucidation of the descriptors responsible for peptide activity (Porto et al., 2012). This computational tool uses specific physicochemical descriptors that are directly responsible for the mechanism of action of aCPPs (Torrent et al., 2011; Vishnepolsky & Pirtskhalava, 2014). This quantitative method of predicting activity is used to design or modify aCPPs to elucidate their antibacterial activity.

Moreover, pharmacophore models can be generated based either on the ligand or the target, which identifies the groups in the former that are responsible for the potency or the binding targets with respect to the target site (Xie, Qiu, & Xie, 2014). QSAR models developed for antimicrobial peptides correlate their structural features with antimicrobial activity (Toropova, Veselinović, Veselinović, Stojanović, & Toropov, 2015). It has been reported that the higher the TI, the higher the bacterial cell penetrating ability (Aoki & Ueda, 2013; Matsuzaki, 2009; Tripathi, Kathuria, Kumar, Mitra, & Ghosh, 2015). To the best of our knowledge, till date no QSAR models have been used to predict the bacterial cell specificity of a CPP based on its TI. The use of QSAR as a chemo-informatic tool to predict the TI of potential aCPPs by analysing available experimental data will therefore hasten the design and synthesis of novel aCPPs specific for bacterial cell, leading to development of efficient antibacterials. The TI compares the amount of a therapeutic agent to the amount that causes toxicity (Muller & Milton, 2012; Tamargo, Le Heuzey, & Mabo, 2015), with a high TI being preferable for a drug to

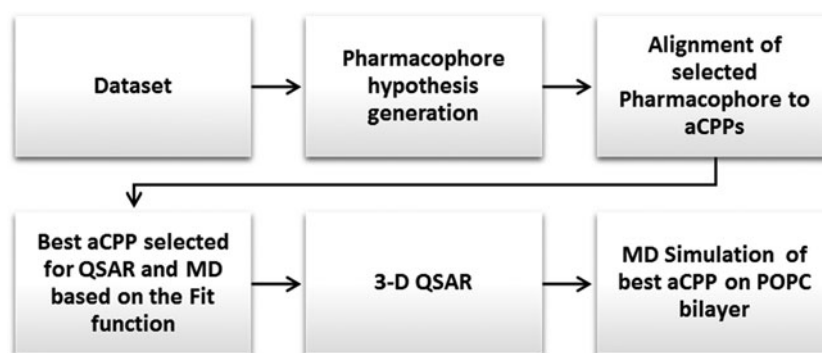


Figure 1. Workflow for identification of best aCPP for membrane penetration.

have a favourable safety profile. It is important in pharmacotherapy as an essential tool for therapeutic drug monitoring to ensure a greater therapeutic benefit without resulting in undesired toxicity (Tamargo, Le Heuzey, & Mabo, 2015). This study aimed to develop a QSAR model to validate the cell penetrating ability of aCPPs based on their TI. The TI was calculated by correlating the minimum inhibitory concentration (MIC) of the aCPPs to their effect on eukaryotic cells, with an indicative TI being calculated by relating the cell viability EC_{50} value to the MIC value. Pharmacophore hypothesis generation and 3D-QSAR were used to understand the cell penetrating ability of the aCPPs utilised based on their TIs. Finally, the validated pharmacophore model was used to identify the best aCPP and from the dataset obtained. The obtained hits were further examined based on the fit function, and the best fit was further tested using molecular dynamics to study its membrane penetrating ability. Molecular dynamic (MD) simulations are widely applied to understand the atomic-level information peptides structures (Agrawal & Skelton, 2016, 2018) and aCPP's interactions with the membranes (Arasteh & Bagheri, 2017; Mizuguchi & Matubayasi, 2018; Velasco-Bolom, Corzo, & Garduño-Juárez, 2017). Thus, an integrated approach comprising of pharmacophore modelling and MD simulation were employed to identify the best aCPPs with optimal membrane penetrating ability across a POPC bilayer membrane. POPC which is a phospholipid that is ubiquitous in cell membranes, contains a phosphatidylcholine (PC) component which provides a structural framework and functions as a permeability barrier (Koymans et al., 2015). POPC has also been found in numerous lipid mixtures used to mimic bacterial cell membranes (Raymonda, Almeida, & Pokorny, 2017). Therefore, in the context of molecular dynamics, this phospholipid serves as a good template for simulations studies to predict ligand–membrane interactions.

2. Materials and methods

2.1. Dataset

The data set was obtained from Park et al. (2009) and Bahnsen et al. (2013), with the TI being calculated and the synthesized peptides showcasing the potent MIC values against *S. aureus* (Bahnsen et al., 2013; Park et al., 2009). The obtained data was randomly divided into 21 training set

compounds, with seven being reserved for a test set. The biological activities ($-\log IC_{50}$) of both datasets were similar, suggesting that the dataset was reasonable. The peptides' 3D structures which served as ligands were generated in Maestro 9.8 molecular modelling package from Schrodinger. Figure 1 describes the computational workflow conducted in this study.

2.2. PHASE methodology

PHASE 3.0 was used for pharmacophore-based alignment and utilized for the QSAR model development (Dixon et al., 2006). Default pharmacophoric features used to develop the pharmacophore model included a hydrogen bond acceptor (A), hydrogen bond donor (D), hydrophobic (H), negative (N), positive (P) and aromatic ring (R). Five steps were used in the process of developing a pharmacophore model, which include ligand preparation, creating pharmacophore sites from a set of features, discovering common pharmacophore, scoring the hypotheses, and building of the QSAR model. The maximum and minimum number of sites was set to five to discover a common pharmacophore. The size of the box of the pharmacophore was set to 2 Å, with the top-ranking hypotheses selected for 3D QSAR analysis, for which grid spacing was 1 Å and the maximum partial least squares (PLS) was set to 3.

2.3. Pharmacophore hypothesis generation

PHASE is an important tool in the identification of 3D structural arrangements of the ligand functional groups, which are common and responsible for inducing biological activity (Kaur, Sharma, & Kumar, 2012). For site generation, the default pharmacophoric features were utilised. The variant AAHRR, for which all the compounds were matched, was searched to generate the best common pharmacophore hypothesis (AAHRR.114). The hypothesis AAHRR.114 was selected as most appropriate as it has the highest survival score (3.984) for common pharmacophore hypothesis, which gives the best alignment of the active ligands. This alignment also gives the fitness to all the inhibitors, while the best aligned ligand gives the maximum fitness. The evaluation of the newly formed common pharmacophore was achieved by comparing the experimental and the calculated activities for the training set molecules. Common

pharmacophore of significant statistical values was selected for molecular alignments.

2.4. Pharmacophore model validation

The aim of the pharmacophore generation was to develop a QSAR model that was statistically significant both internally and externally (Kaur et al., 2012), where the evaluation and predictability of the model being achieved by external validation. A scatter plot of experimental versus predicted activity for the training set showed a substantial linear correlation and a slight difference between the experimental and predicted activity. External validation was used to determine the efficacy of the model. The dataset obtained was separated into training and test set where validation of the model (AAHRR) for the test set was judged by the cross-validation coefficient (Q^2). R^2 was determined for the training set which depicted relevance of the model. The F value (which assesses the statistical significance) and Pearson- R (which measures the strength of the linear relationship between two variables) indicated greater confidence of the model, where a higher F value implies a more significant correlation and a Pearson- R value closer to 1 indicates a strong positive linear correlation. Standard deviation (SD) and Root-mean squared error (RMSE) were calculated which reflected good stability of the model. Model validation is an important step during pharmacophore design, as it determines the success, accuracy and reliability of the developed model (Meraj et al., 2013).

2.5. Molecular dynamic simulations

2.5.1. Peptide structure prediction

The 3D structure of "KLWKLWKKWLK" aCPP was predicted using PEP-FOLD server, which uses a de-novo approach for predicting peptide structure from amino acid sequences (Figure 2(B)). PEP-FOLD server uses a greedy algorithm driven by a coarse-grained force field for predicting the 3D model of a peptide (Shen & Maupetit, 2012).

2.5.2. Molecular dynamics simulations

POPC bilayer was constructed using the CHARMM-GUI membrane builder and contains a total of 128 lipid molecules

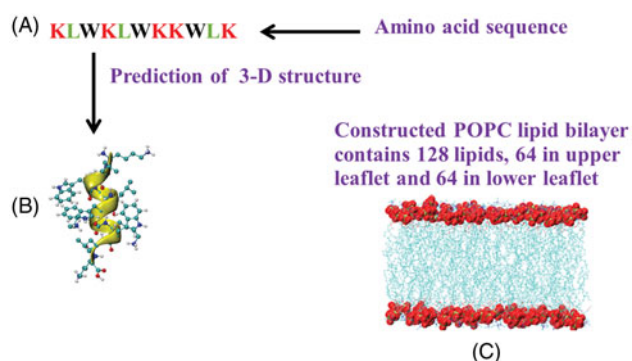


Figure 2. (A) Representation of the single amino acid code of the aCPP peptide. (B) Representation of the predicted 3-D structure of aCPP and (C) shows the constructed POPC lipid bilayer, P atoms have been shown in VdW sphere.

(Wu et al., 2014) (Figure 2(C)). The peptide was placed more than 5 Å away from any lipid molecules of the upper leaflet of the bilayer. The Charmm36 force field was used for peptide and POPC bilayer system, which was solvated using TIP3P water model (Huang & MacKerell, 2013). The system contains a total of 7572 water molecules, and 5Cl⁻ ions were added to neutralize the system. The system was energy minimized using the steepest descent algorithm, and 500 ps simulated annealing under the isobaric–isothermic (NPT) conditions was performed to equilibrate the water molecules around the lipid head group atoms (Bixon & Limn, 1966). The system was further equilibrated for 100 ps with canonical (NVT) ensemble, followed by 1000 ps with NPT ensemble and a 50 ns production run was performed in the NPT ensemble. The hydrogen bond lengths of peptide and lipid molecules were constrained using the LINCS algorithm (Hess & Fraaije, 1997). Particle mesh Ewald (PME) method was used for calculation of long-range electrostatic interactions (Darden et al., 2007). The van der Waals (vdW) and electrostatic interactions were calculated using a cut-off of 1.2 nm. The Parrinello–Rahman method was used for pressure coupling and the Nose–Hoover thermostat was used for temperature coupling (Braga & Travis, 2014; Parrinello & Rahman, 1995). The simulation was performed at a pressure of 1 bar and a temperature of 323 K using the GROMACS package (Hess & Fraaije, 1997).

3. Results

Upon completion of the pharmacophore identification process, 65 variant hypotheses were generated. In this study, 28 aCPPs were used to predict activity using PHASE and fitness score determined (Table 1), with molecules 9, 10, 19, 20, 23 and 28 not being picked up by the system. The most appropriate pharmacophore model (AAHRR.114) to predict aCPP activity had a five-point hypothesis that consisted of two hydrogen bond acceptor (A), one hydrophobic group (H) and two aromatic ring features (R), as shown in Figure 3. Pharmacophore hypothesis scoring values are shown in Table 2. Compound 25 had the best alignment on the pharmacophore AAHRR as shown in Figure 4, and the distance between the sites in the pharmacophore is shown in Figure 5. Alignment of both active and inactive molecules to the hypothesis AAHRR.114 is shown in Figures 6 and 7, respectively. A depiction of the cubes produced for the highest active molecule (compound 25) in the present 3D-QSAR is shown in Figure 8(A–E), where the blue cubes indicate favourable effect on activity and red cubes indicate unfavourable effect. For the 3D-QSAR model generation, the PHASE descriptors were considered as independent variables and the activity values as dependent variables in deriving the 3D-QSAR models by the PLS regression method. The 3D-QSAR was evaluated by the Fisher test (F), correlation coefficient (R^2) and Pearson- R . Table 2 outlines the summary of the 3D-QSAR results. The statistical results of the model exhibited an R^2 value of .9016, RMSE = 0.5911, Q^2 = 0.5311, SD = 0.2072, variance ratio (F) = 36 and Pearson- R = .847. The validation of the above model was achieved by predicting

Table 1. aCPPs for training and test set (Bahnsen et al., 2013; Park et al., 2009)

Entry	Peptide	Set	Therapeutic index (TI)	Biological activity		PHASE predicted activity ($-\log IC_{50}$)	Fitness score
				MIC (μM) against <i>S. aureus</i>	($-\log IC_{50}$)		
1	Penetratin	Training set	4.4†	64	1.806	1.44	0.32
2	penArg	Training set	2.3†	16	1.204	1.30	0.31
3	pen13	Training set	>3.3†	256	2.408	2.07	0.22
4	Pen13Arg	Training set	1.1†	32	1.505	1.86	0.23
5	Penshuf	Training set	0.3†	64	1.806	1.89	0.68
6	PenshufLeu	Training set	0.6†	16	1.204	1.37	0.76
7	PenshufLysLeu	Training set	1.0†	32	1.505	1.48	0.76
8	PenshufArgLeu	Training set	0.3†	16	1.204	1.33	0.76
9	WR8	Training set	10.1†	44	ND	ND	ND
10	Tat13	Training set	<3.3†	>256	ND	ND	ND
11	K8W3	Training set	200*	4	0.602	0.59	2.51
12	KL7W3	Training set	200*	4	0.602	0.53	2.97
13	K6L2W3	Training set	400*	2	0.301	0.51	2.98
14	K3L5W3	Training set	0.8*	4	0.602	0.54	2.99
15	K2L6W3	Training set	0.05*	32	1.505	0.58	2.97
16	R8W3	Training set	100*	8	0.903	0.81	2.46
17	R6L2W3	Training set	100*	4	0.602	0.66	2.50
18	O6L2W3	Training set	200*	4	0.602	0.56	0.72
19	O6X2W3	Training set	100*	4	ND	ND	ND
20	R6L2W3-D	Training set	200*	2	ND	ND	ND
21	Indolicidin	Training set	12.5*	4	0.602	0.53	0.35
22	PenLys	Test set	>3.9†	256	2.408	1.45	0.32
23	PenLeu	Test set	>15.6†	64	ND	ND	ND
24	pen13Lys	Training set	>3.9†	256	2.408	2.02	0.23
25	K5L3W3	Test set	50*	2	0.602	0.52	3
26	K4L4W3	Test set	3.1*	2	0.602	0.53	2.99
27	R7LW3	Test set	200*	4	0.301	0.70	2.48
28	K6L2W3-D	Test set	100*	4	ND	ND	ND

ND, not determined.

†Values taken as such from the literature.

*Values calculated by dividing %cell viability by MIC against *S. aureus*.

ªRepresents peptide sequences: I, Isoleucine; R, Arginine; K, Lysine; M, Methionine; L, Leucine; Q, Glutamine; W, Tryptophan; F, Phenylalanine; O, Pyrrolysine; N, Asparagine; P, Proline; X, Any amino acid.



Figure 3. Pharmacophore hypothesis (AAHRR). Purple sphere—A, green sphere—H and brown ring—R.

Table 2. Summary of 3D-QSAR results

PLS statistical parameters	Results	PLS statistical parameters	Results
Number of molecule in training set	18	R^2	.9016
Number of molecule in test set	6	Q^2	0.5311
Number of PLS factors	3	Standard deviation (SD)	0.2072
Root-mean squared error (RMSE)	0.5911	Variance ratio (F)	36
		Pearson-R	.847

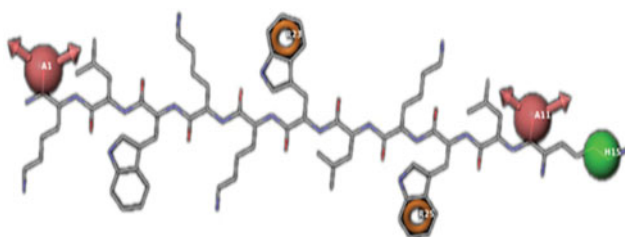


Figure 4. The best common pharmacophore hypotheses for compound 25.

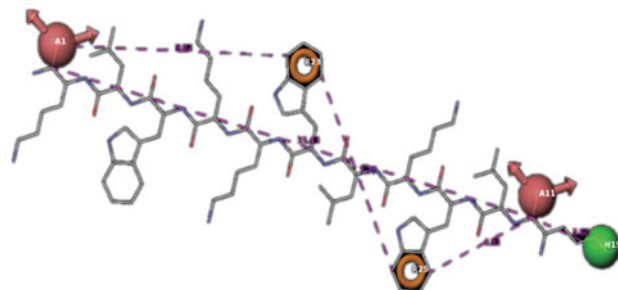


Figure 5. The pharmacophore hypothesis showing distance between the pharmacophoric sites of compound 25.

the biological activities of the training set molecules, as indicated in Table 1. To further confirm the 3-D QSAR results, compound 25 which was considered as the best aCPP based on the fit function was further analysed for its membrane penetrating ability by MD simulation. Figure 9 shows the representative images from the simulation at different time points. The time evolution of the distance of each residue of the aCPP from the POPC bilayer showed that the peptide formed strong interactions with the POPC bilayer at two different time points, one at approximately 28 ns and remained bound until 50 ns (Figure 10). The next time period we observed the peptide to be bound at approximately 109 ns and remained bound until 200 ns. During this time, we observed Lys-1 inserted into the PO4 groups of the membrane (Figure 11). To further observe the closest residues during the binding, average distances for each residues for

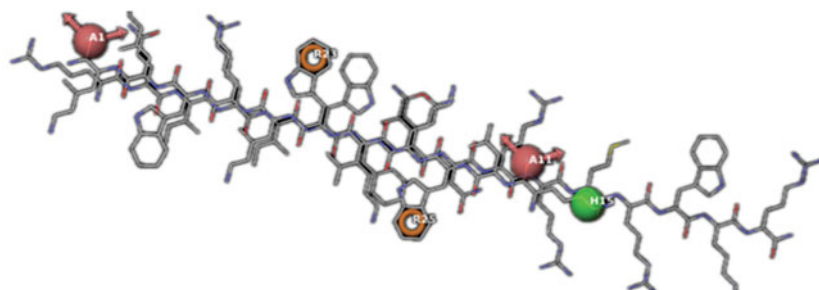


Figure 6. Alignments of active molecules.

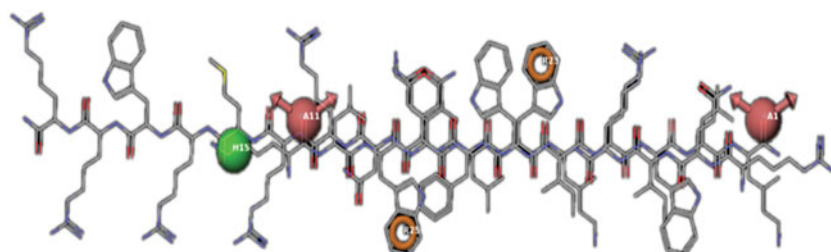


Figure 7. Alignments of inactive molecules.

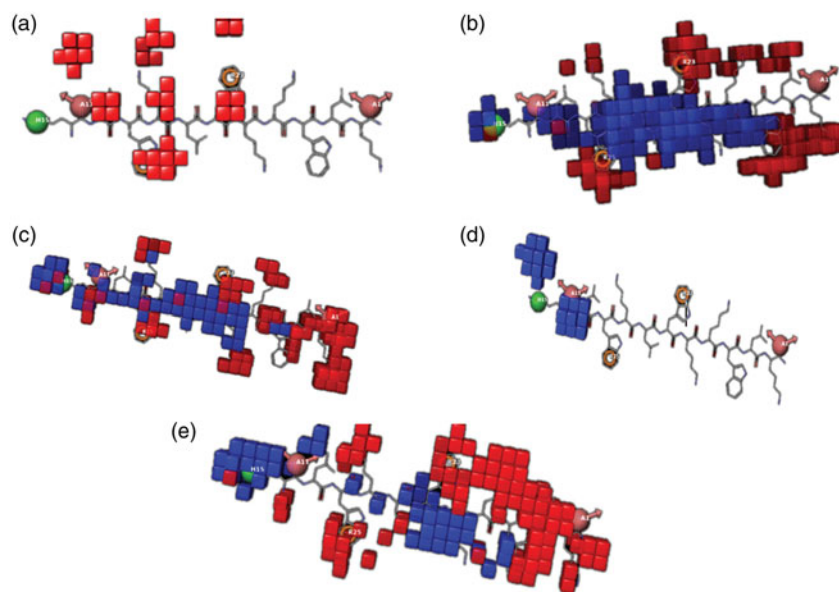


Figure 8. The 3D QSAR model based on compound 25 illustrating (A) hydrogen bond donor groups, (B) hydrophobic groups, (C) Electron withdrawing groups, (D) other effects and (E) combined effects.

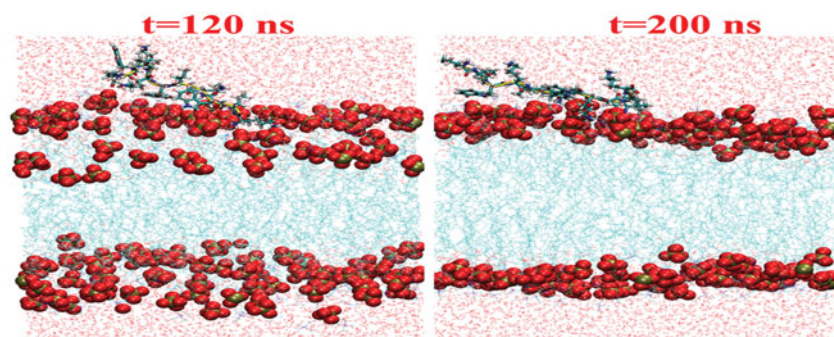


Figure 9. Two representative images of aCPP-POPC lipid bilayer interaction showing interaction, one at 120 ns and at 200 ns. PO₄ atoms of bilayer have been shown in VDW representation and aCPP peptide has been shown in cartoon representation.

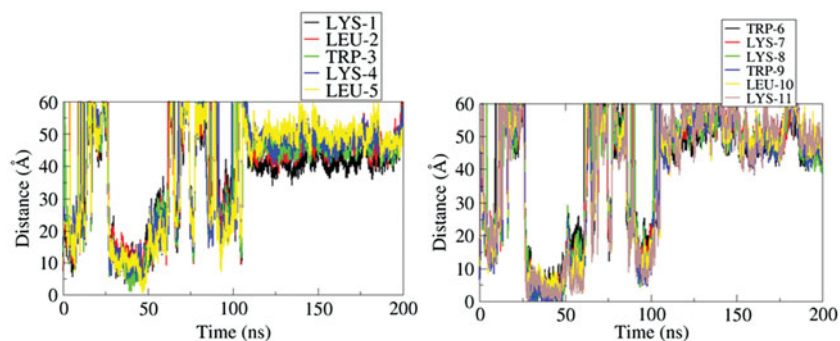


Figure 10. Time evolution of centre of mass (COM) distance between each residue of peptide with the phosphate (PO_4) group of upper leaflet.

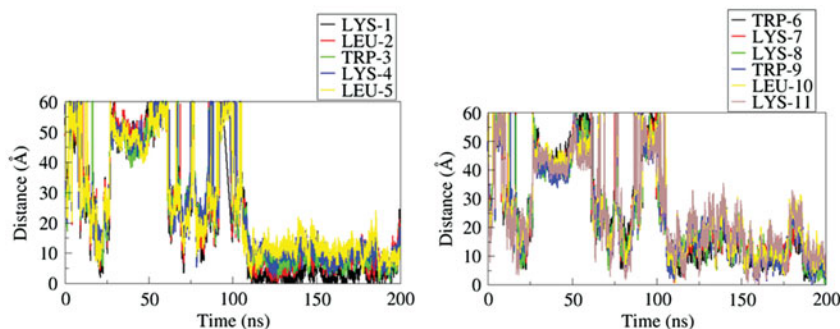


Figure 11. Time evolution of centre of mass (COM) distance between each residue of peptide with the phosphate (PO_4) group of lower leaflet.

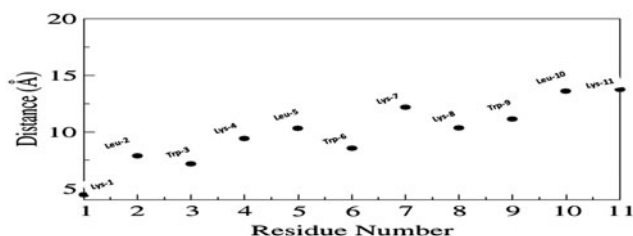


Figure 12. Average distance for the last 20 ns for each residue.

the last 20 ns (180–200 ns) were calculated (Figure 12). As in our simulation we have used periodic boundary conditions (PBC), we observed the peptide to interact with both the lower and upper leaflet of the membrane. Therefore, we have calculated the COM between both leaflets and peptide separately. The last 20 ns (180–200 ns) average distances of each residues (Figure 12) reveal that the Lys-1, Leu-2, Trp-3 and Trp-6 were the closest to the membrane during the binding. The MD simulations therefore confirmed the interaction of compound 25 with the POPC bilayer.

4. Discussion

In this study, pharmacophore and QSAR model development was performed by PHASE. Several hypotheses were generated, with the top-ranking ones being subjected to 3D-QSAR analysis, where the grid spacing was set to 1 Å and the maximum PLS factors set to 3. Partial least squares (PLS) is a statistical method which is used to find the relationship between two matrices and/or finds a linear regression model between variables. The first hypothesis, AAHRR.114, was found to be the best, being characterized by a high survival

score (3.984) and an R^2 of .9016. AAHRR 114 featured two hydrogen bond acceptor (A), one hydrophobic group (H) and two aromatic ring features (R). A R^2 value greater than .5 and close to 1 confirmed the models predictive ability for the compounds (Frimayanti, Yam, Lee, & Othman, 2011). Q^2 measures the robustness and predictive power of the QSAR model and must be ≥ 0.5 but lower than the R^2 value (Veeramany et al., 2011). Compound 25 was the best and comprised of the amino acids, lysine (K-5), leucine (L-3) and tryptophan (W-3), with a positive net charge of +5 and a total hydrophobic ratio of 57%. There are several reports on peptides which are rich in the amino acids lysine, leucine and tryptophan being specific for bacterial membrane penetration that support our findings (Jin et al., 2016; Kim et al., 2013; Nguyen et al., 2010; Su, Doherty, Waring, Ruchala, & Hong, 2009). The positive charge allows the aCPP to interact with the negatively charged bacterial cell membrane whereas the hydrophobicity allows the aCPP to penetrate deeper into the hydrophobic core of the bacterial cell membrane causing membrane lysis and pore formation (Chen et al., 2007). Figure 8(A–E) represents features responsible for activity (blue cubes) and those which attenuate activity (red cubes). Features responsible for activity are specifically represented in Figure 8(B and C) whereas Figure 8(A and D) show features that attenuate activity. Substitutions at the domains represented by the red cubes with amino acids which will increase the aCPP's cationicity will confer favourable activity (Faraz, Verma, & Akhtar, 2016; Mehta, Khokra, Arora, & Kaushik, 2012).

The MD simulation which ran for 200 ns showed spontaneous insertion of the aqueous phase aCPP into the upper and lower leaflet region of the lipid bilayer. The last 20 ns of

the simulation revealed that the Lys-1, Leu-2, Trp-3 and Trp-6 were the closest to the membrane during the binding, revealing the importance of these amino acids in membrane penetration based on their net charge. The importance of charged residues in membrane penetration is well known (Futaki, 2005; Herce & Garcia, 2008; Nakase, Takeuchi, Tanaka, & Futaki, 2008; Persson, Esbjö, Gokso, Lincoln, & Norde, 2004). It could be significant since we observed in our study that the C terminal region (residue 6–11) has more positive charge compared with the N terminal region (residue 1–5), which assisted the C terminal region to insert into the bilayer. Charged Lys side chains have been seen to possess high pKa values and this allows them to form strong electrostatic interactions with membranes, which leads to membrane penetration (Li, Vorobyov, & Allen, 2013). Trp is particularly prevalent among naturally occurring antimicrobial peptides and can strongly interact with hydrophobic membrane components, thus leading to increased antimicrobial activity (Bi, Wang, Dong, Zhu, & Shang, 2014; Li et al., 2013). The MD studies confirmed the importance of Trp and Lys residues in interacting with the POPC lipid bilayer, which allows the peptide to penetrate the model membrane.

5. Conclusion

This study presented the ligand-based pharmacophore and 3-D QSAR model which gave important structural-binding features of aCPPs acting as *S. aureus* antagonists based on their TI. Pharmacophore modelling compares activities with the 3-D arrangement of various physicochemical features. The hypothesis AAHRR.114 was found to be the most appropriate pharmacophore model to determine the best compound with potent activity. AAHRR.114 contains two hydrogen bond acceptors, one hydrogen bond donor, two hydrophobic regions, and one aromatic ring features. The AAHRR.114 model was able to predict the activity of the aCPPs, and the validation results provide additional confidence. The best aCPP was found to be compound 25, with a fitness score of 3 and the PHASE predicted activity of 0.52 being better than the experimental activity (0.602). The proposed 3D-QSAR model AAHRR.114 was useful in estimating the antimicrobial potential and cell penetrating ability of aCPPs, confirm the relationship between the TI and aCPPs, where aCPPs with a higher TI showed good activity and PHASE was also able to predict the possible descriptors responsible for activity. This QSAR approach in analysing aCPP cell penetration, by observation of its TI, can be used for future studies to explore specific descriptors responsible for biological activity that also accounts for cell penetration. Membrane penetration study using MD simulation also revealed the aCPP-POPC bilayer interaction, resulting in the aCPP insertion across the bilayer. The combination of these two computational studies will also lead to the rational design of optimal and novel aCPPs for therapeutic activity and for peptide-conjugate delivery.

Disclosure statement

No potential conflict of interest was reported by the author.

Funding

This work was supported by the College of Health Sciences (CHS), University of KwaZulu-Natal (UKZN), UKZN Nanotechnology Platform and the National Research Foundation (NRF) of South Africa [grant number NRF Grant No. 87790].

References

- Agrawal, N., & Skelton, A. A. (2016). 12-crown-4 ether disrupts the patient brain-derived amyloid-beta-fibril trimer: Insight from all-atom molecular dynamics simulations. *ACS Chemical Neuroscience*, 7(10), 1433–1441. doi:10.1021/acschemneuro.6b00185c
- Agrawal, N., & Skelton, A. A. (2018). Binding of 12-crown-4 with alzheimer's abeta40 and abeta42 monomers and its effect on their conformation: Insight from molecular dynamics simulations. *Molecular Pharmaceutics*, 15(1), 289–299. doi:10.1021/acs.molpharmaceut.7b00966
- Aoki, W., & Ueda, M. (2013). Characterization of antimicrobial peptides toward the development of novel antibiotics. *Pharmaceutics*, 6(8), 1055–1081. doi:10.3390/ph6081055
- Aparoy, P., Reddy, K. K., & Reddanna, P. (2012). Structure and ligand based drug design strategies in the development of novel 5-LOX inhibitors. *Current Medicinal Chemistry*, 19(22), 3763–3778. doi:10.2174/092986712801661112
- Arasteh, S., & Bagheri, M. (2017). Molecular dynamics simulation and analysis of the antimicrobial peptide-lipid bilayer interactions. *Methods in Molecular Biology*, 1548, 103–118. doi:10.1007/978-1-4939-6737-7_8
- Arnusch, C. J., Ulm, H., Josten, M., Shadkchan, Y., Oshero, N., Sahl, H. G., & Shai, Y. (2012). Ultrashort peptide bioconjugates are exclusively antifungal agents and synergize with cyclodextrin and amphotericin B. *Antimicrobial Agents and Chemotherapy*, 56(1), 1–9. doi:10.1128/AAC.00468-11
- Bahnsen, J. S., Franzyk, H., Sandberg-Schaal, A., & Nielsen, H. M. (2013). Antimicrobial and cell-penetrating properties of penetratin analogs: Effect of sequence and secondary structure. *Biochimica et Biophysica Acta - Biomembranes*, 1828(2), 223–232. doi:10.1016/j.bbmem.2012.10.010
- Bahnsen, J. S., Franzyk, H., Sayers, E. J., Jones, A. T., & Nielsen, H. M. (2015). Cell-penetrating antimicrobial peptides-prospectives for targeting intracellular infections. *Pharmaceutical Research*, 32(5), 1546–1556. doi:10.1007/s11095-014-1550-9
- Bhonsle, J. B., Venugopal, D., Huddler, D. P., Magill, A. J., & Hicks, R. P. (2007). Application of 3D-QSAR for identification of descriptors defining bioactivity of antimicrobial peptides. *Journal of Medicinal Chemistry*, 50(26), 6545–6553. doi:10.1021/jm070884y
- Bi, X., Wang, C., Dong, W., Zhu, W., & Shang, D. (2014). Antimicrobial properties and interaction of two Trp-substituted cationic antimicrobial peptides with a lipid bilayer. *Journal of Antibiotics (Tokyo)*, 67(5), 361–368. doi:10.1038/ja.2014.4
- Bixon, M., & Limn, S. (1966). Potential functions and conformations in cycloalkanes. *Tetrahedron*, 23 (2), 769–784. doi:10.1016/0040-4020(67)85023-3
- Bobone, S., Piazzon, A., Orioni, B., Pedersen, J. Z., Nan, Y. H., Hahn, K. S., & Stella, L. (2011). The thin line between cell-penetrating and antimicrobial peptides: The case of Pep-1 and Pep-1-K. *Journal of Peptide Science*, 17(5), 335–341. doi:10.1002/psc.1340
- Bolinteanu, D., Hazrati, E., Davis, H. T., Lehrer, R. I., & Kaznessis, Y. N. (2010). Antimicrobial mechanism of pore-forming protegrin peptides: 100 pores to kill *E. coli*. *Peptides*, 31(1), 1–8. doi:10.1016/j.peptides.2009.11.010

- Braga, C., & Travis, K. P. (2014). A configurational temperature Nosé-Hoover thermostat. *The Journal of Chemical Physics*, 123, 134101. doi:10.1063/1.2013227
- Branco, P., Viana, T., Albergaria, H., & Arneborg, N. (2015). Antimicrobial peptides (AMPs) produced by *Saccharomyces cerevisiae* induce alterations in the intracellular pH, membrane permeability and culturability of *Hanseniaspora guilliermondii* cells. *International Journal of Food Microbiology*, 205, 112–118. doi:10.1016/j.ijfoodmicro.2015.04.015
- Burns, K. E., McCleerey, T. P., & Thévenin, D. (2016). pH-selective cytotoxicity of pHLP-antimicrobial peptide conjugates. *Scientific Reports*, 6(2), 28465. doi:10.1038/srep28465
- Carmona-Ribeiro, A., & de Melo Carrasco, L. (2014). Novel formulations for antimicrobial peptides. *International Journal of Molecular Sciences*, 15(10), 18040–18083. doi:10.3390/ijms151018040
- Carnicelli, V., Lizzi, A. R., Ponzi, A., Amicosante, G., Bozzi, A., & Di Giulio, A. (2013). Interaction between antimicrobial peptides (AMPs) and their primary target, the biomembranes. *Microbial Pathogens and Strategies for Combating Them: Science, Technology and Education*, 2, 1123–1134.
- Chen, Y., Guarnieri, M. T., Vasil, A. I., Vasil, M. L., Mant, C. T., & Hodges, R. S. (2007). Role of peptide hydrophobicity in the mechanism of action of α -helical antimicrobial peptides. *Antimicrobial Agents and Chemotherapy*, 51(4), 1398–1406. doi:10.1128/AAC.00925-06
- Cherkasov, A. (2005). Inductive QSAR descriptors. Distinguishing compounds with antibacterial activity by artificial neural networks. *International Journal of Molecular Sciences*, 6(1–2), 63–86. doi:10.3390/ijms610063
- Da Costa, J. P., Cova, M., Ferreira, R., & Vitorino, R. (2015). Antimicrobial peptides: An alternative for innovative medicines? *Applied Microbiology and Biotechnology*, 99(5), 2023–2040. doi:10.1007/s00253-015-6375-x
- Darden, T., York, D., Pedersen, L., Darden, T., York, D., & Pedersen, L. (2007). Particle mesh Ewald: An N.log(N) method for Ewald sums in large systems. *The Journal of Chemical Physics*, 98, 1–5. doi:10.1063/1.464397
- Davies, J., & Davies, D. (2010). Origins and evolution of antibiotic resistance. *Microbiology and Molecular Biology Reviews*, 74(3), 417–433. doi:10.1128/MMBR.00016-10
- Delcour, A. H. (2009). Outer membrane permeability and antibiotic resistance. *Biochimica et Biophysica Acta*, 1794(5), 808–816. doi:10.1016/j.bbapap.2008.11.005.Outer
- Dixon, S. L., Smondyrev, A. M., Knoll, E. H., Rao, S. N., Shaw, D. E., & Friesner, R. A. (2006). PHASE: A new engine for pharmacophore perception, 3D QSAR model development, and 3D database screening: 1. Methodology and preliminary results. *Journal of Computer-Aided Molecular Design*, 20(10–11), 647–671.
- Eckhard, L. H., Sol, A., Abtew, E., Shai, Y., Domb, A. J., Bachrach, G., & Beyth, N. (2014). Biohybrid polymer-antimicrobial peptide medium against *Enterococcus faecalis*. *PLoS One*, 9(10), e109413. doi:10.1371/journal.pone.0109413
- Eriksen, T. H. B., Skovsen, E., & Fojan, P. (2013). Release of antimicrobial peptides from electrospun nanofibers as a drug delivery system. *Journal of Biomedical Nanotechnology*, 9(3), 492–498. doi:10.1166/jbn.2013.1553
- Faraz, M., Verma, G., & Akhtar, W. (2016). Docking study and ADME prediction of acyl 1, 3, 4-thiadiazole amides and sulfonamides as antitubulin agents. *Arabian Journal of Chemistry*. doi:10.1016/j.arabjc.2016.11.004
- Fjell, C. D., Jenssen, H., Hilpert, K., Cheung, W. A., Panté, N., Hancock, R. E. W., & Cherkasov, A. (2009). Identification of novel antibacterial peptides by chemoinformatics and machine learning. *Journal of Medicinal Chemistry*, 52(7), 2006–2015. doi:10.1021/jm8015365
- Frimayanti, N., Yam, M. L., Lee, H. B., & Othman, R. (2011). Validation of quantitative structure-activity relationship (QSAR) model for photosensitizer activity prediction. *International Journal of Molecular Science*, 12(12), 8626–8644. doi:10.3390/ijms12128626
- Futaki, S. (2005). Membrane-permeable arginine-rich peptides and the translocation mechanisms. *Advanced Drug Delivery Reviews*, 57(2), 547–558. doi:10.1016/j.addr.2004.10.009
- Guilhelmelli, F., Vilela, N., Albuquerque, P., Derengowski, L. da S., Silva-Pereira, I., & Kyaw, C. M. (2013). Antibiotic development challenges: The various mechanisms of action of antimicrobial peptides and of bacterial resistance. *Frontiers in Microbiology*, 4(12), 1–12. doi:10.3389/fmicb.2013.00353
- Henriques, S. T., Melo, M. N., & Castanho, M. A. R. B. (2006). Cell-penetrating peptides and antimicrobial peptides: How different are they? *The Biochemical Journal*, 399(1), 1–7. doi:10.1042/BJ20061100
- Herce, H. D., & Garcia, A. E. (2008). Cell penetrating peptides: How do they do it? *Journal of Biological Physics*, 33, 345–356. doi:10.1007/s10867-008-9074-3
- Hess, B., & Fraaije, J. G. E. M. (1997). LINC: A linear constraint solver for molecular simulations. *Journal of Computational Chemistry*, 18(12), 1463–1472
- Huang, J., & MacKerell, A. D. (2013). CHARMM36 all-atom additive protein force field: Validation based on comparison to NMR data. *Journal of Computational Chemistry*, 34(25), 2135–2145. doi:10.1002/jcc.23354
- Huerta-Cantillo, J., & Navarro-García, F. (2016). Properties and design of antimicrobial peptides as potential tools against pathogens and malignant cells. *Molecules*, 9(10), 12.
- Jin, L., Bai, X., Luan, N., Yao, H., Zhang, Z., Liu, W., & Lu, Q. (2016). A designed tryptophan- and lysine/arginine-rich antimicrobial peptide with therapeutic potential for clinical antibiotic-resistant candida albicans vaginitis. *Journal of Medicinal Chemistry*, 59(5), 1791–1799. doi:10.1021/acs.jmedchem.5b01264
- Kaur, P., Sharma, V., & Kumar, V. (2012). Pharmacophore modelling and 3D-QSAR studies on n(3)-phenylpyrazinones as corticotropin-releasing factor 1 receptor antagonists. *International Journal of Medicinal Chemistry*, 2012, 452325. doi:10.1155/2012/452325
- Kim, S. J., Kim, J. S., Lee, Y. S., Sim, D. W., Lee, S. H., Bahk, Y. Y., & Won, H. S. (2013). Structural characterization of de novo designed L5K5W model peptide isomers with potent antimicrobial and varied hemolytic activities. *Molecules*, 18(1), 859–876. doi:10.3390/molecules18010859
- Kingsbury, W. D., Boehm, J. C., Mehta, R. J., Grappel, S. F., & Gilvarg, C. (1984). A novel peptide delivery system involving peptidase activated prodrugs as antimicrobial agents. Synthesis and biological activity of peptidyl derivatives of 5-fluorouracil. *Journal of Medicinal Chemistry*, 27(11), 1447–1451.
- Koymans, K. J., Feitsma, L. J., Brondijk, T. H. C., Aerts, P. C., Lukkien, E., Lössl, P., ... & Huizinga, E. G. (2015). Structural basis for inhibition of TLR2 by staphylococcal superantigen-like protein 3 (SSL3). *Proceedings of the National Academy of Sciences*, 112(35), 11018–11023.
- Lee, T., Hall, K. N., & Aguilar, M. (2016). Antimicrobial peptide structure and mechanism of action: A focus on the role of membrane structure. *Current Topics in Medicinal Chemistry*, 16(1), 25–39.
- Li, L., Vorobyov, I., & Allen, T. W. (2013). The different interactions of lysine and arginine side chains with lipid membranes. *The Journal of Physical Chemistry*, 117(40), 11906–11920. doi:10.1021/jp405418y
- Lv, Y., Wang, J., Gao, H., Wang, Z., Dong, N., Ma, Q., & Shan, A. (2014). Antimicrobial properties and membrane-active mechanism of a potential α -helical antimicrobial derived from cathelicidin PMAP-36. *PLoS One*, 9(1), e86364. doi:10.1371/journal.pone.0086364
- Maekawa, K., Azuma, M., Okuno, Y., Tsukamoto, T., Nishiguchi, K., Setsukinai, K., & Rokushima, M. (2015). Antisense peptide nucleic acid-peptide conjugates for functional analyses of genes in *Pseudomonas aeruginosa*. *Bioorganic & Medicinal Chemistry*, 23(22), 7234–7239. doi:10.1016/j.bmc.2015.10.020
- Malanovic, N., & Lohner, K. (2015). Gram-positive bacterial cell envelopes: The impact on the activity of antimicrobial peptides. *Biochimica et Biophysica Acta - Biomembranes*, 1858(5), 936–946. doi:10.1016/j.bbamem.2015.11.004
- Mardirossian, M., Grzela, R., Giglione, C., Meinel, T., Gennaro, R., Mergaert, P., & Scocchi, M. (2014). The host antimicrobial peptide Bac71-35 binds to bacterial ribosomal proteins and inhibits protein synthesis. *Chemistry and Biology*, 21(12), 1639–1647. doi:10.1016/j.chembiol.2014.10.009
- Matsuzaki, K. (2009). Control of cell selectivity of antimicrobial peptides. *Biochimica et Biophysica Acta - Biomembranes*, 1788(8), 1687–1692. doi:10.1016/j.bbamem.2008.09.013

- Mehta, H., Khokra, S. L., Arora, K., & Kaushik, P. (2012). Pharmacophore mapping and 3D-QSAR analysis of *Staphylococcus aureus* Sortase A inhibitors. *Der Pharma Chemica*, 4(5), 1776–1784.
- Meraj, K., Kumar, K. K., Shaikheldin, M. S., Azam, S. N., Anugnya, P. R., Kumar, M., & Match, B. (2013). Pharmacophore modelling, 3D-QSAR study and docking of naphthol derivatives as b-raf(v600e) receptor antagonists. *Vedic Research International Bioinformatics & Proteomics*, 1(1), 18–29. doi:10.14259/bp.v1i1.44
- Michael Henderson, J., & Lee, K. Y. C. (2013). Promising antimicrobial agents designed from natural peptide templates. *Current Opinion in Solid State and Materials Science*, 17(4), 175–192. doi:10.1016/j.cossms.2013.08.003
- Mishra, B., Leishangthem, G. D., Gill, K., Singh, A. K., Das, S., Singh, K., & Dey, S. (2013). A novel antimicrobial peptide derived from modified N-terminal domain of bovine lactoferrin: Design, synthesis, activity against multidrug-resistant bacteria and *Candida*. *Biochimica et Biophysica Acta - Biomembranes*, 1828(2), 677–686. doi:10.1016/j.bbame.2012.09.021
- Mizuguchi, T., & Matubayasi, N. (2018). Free-energy analysis of peptide binding in lipid membrane using all-atom molecular dynamics simulation combined with theory of solutions. *The Journal of Physical Chemistry B*, 122, 3219–3229. doi:10.1021/acs.jpcc.7b08241
- Mollica, A., Zengin, G., Durdagi, S., Ekhteiari Salmas, R., Macedonio, G., Stefanucci, A., ... Novellino, E. (2018). Combinatorial peptide library screening for discovery of diverse α -glucosidase inhibitors using molecular dynamics simulations and binary QSAR models. *Journal of Biomolecular Structure and Dynamics*, 22, 1–15.
- Muller, P. Y., & Milton, M. N. (2012). The determination and interpretation of the therapeutic index in drug development. *Nature Reviews Drug Discovery*, 11(10), 751–761. doi:10.1038/nrd3801
- Nakase, I., Takeuchi, T., Tanaka, G., & Futaki, S. (2008). Methodological and cellular aspects that govern the internalization mechanisms of arginine-rich cell-penetrating peptides. *Advanced Drug Delivery Reviews*, 60(4-5), 598–607. doi:10.1016/j.addr.2007.10.006
- Nguyen, L. T., Chau, J. K., Perry, N. A., de Boer, L., Zaat, S. A. J., & Vogel, H. J. (2010). Serum stabilities of short tryptophan- and arginine-rich antimicrobial peptide analogs. *PLoS One*, 5(9), 1–8. doi:10.1371/journal.pone.0012684
- Ong, Z. Y., Wiradharma, N., & Yang, Y. Y. (2014). Strategies employed in the design and optimization of synthetic antimicrobial peptide amphiphiles with enhanced therapeutic potentials. *Advanced Drug Delivery Reviews*, 78, 28–45. doi:10.1016/j.addr.2014.10.013
- Park, K. H., Nan, Y. H., Park, Y., Kim, J. I., Park, I. S., Hahm, K. S., & Shin, S. Y. (2009). Cell specificity, anti-inflammatory activity, and plausible bactericidal mechanism of designed Trp-rich model antimicrobial peptides. *Biochimica et Biophysica Acta - Biomembranes*, 1788(5), 1193–1203. doi:10.1016/j.bbame.2009.02.020
- Parrinello, M., & Rahman, A. (1995). Polymorphic transitions in single crystals: A new molecular dynamics method Polymorphic transitions in single crystals: A new molecular dynamics method, *Journal of Applied Physics*, 52(12), 7182–7190.
- Persson, D., Esbjö, E. K., Gokso, M., Lincoln, P., & Norde, B. (2004). Membrane binding and translocation of cell-penetrating peptides. *Biochemistry*, 43(12), 3471–3489.
- Porto, S., Silva, O. N., & Franco, O. (2012). Prediction and rational design of antimicrobial peptides. In E. Faraggi (Ed.), *Protein structure*. Croatia: InTech.
- Pushpanathan, M., Gunasekaran, P., & Rajendhran, J. (2016). Antimicrobial peptides: Versatile biological properties, *International Journal of Peptides*, 2013(2013), 1–23. doi:10.1155/2013/675391
- Raymonda, M. H., Almeida, P., & Pokorny, A. (2017). Investigation of domains in mixtures of high-melting phospholipids, POPC, and cholesterol. *Biophysical Journal*, 112(3), 224a.
- Schmidt, N. W., & Wong, G. C. L. (2013). Antimicrobial peptides and induced membrane curvature: Geometry, coordination chemistry, and molecular engineering. *Current Opinion in Solid State & Materials Science*, 17(4), 151–163. doi:10.1016/j.cossms.2013.09.004
- Sengupta, S., Chattopadhyay, M. K., & Grossart, H. P. (2013). The multifaceted roles of antibiotics and antibiotic resistance in nature. *Frontiers in Microbiology*, 4(3), 1–13. doi:10.3389/fmicb.2013.00047
- Shen, Y., & Maupetit, J. (2012). PEP-FOLD: An updated de novo structure prediction server for both linear and disulfide bonded cyclic peptides. *Nucleic Acids Research*, 40(5), 288–293. doi:10.1093/nar/gks419
- Souto, A., Montaos, M. A., Balado, M., Osorio, C. R., Rodríguez, J., Lemos, M. L., & Jiménez, C. (2013). Synthesis and antibacterial activity of conjugates between norfloxacin and analogues of the siderophore vancomycin. *Bioorganic & Medicinal Chemistry*, 21(1), 295–302. doi:10.1016/j.bmc.2012.10.028
- Splith, K., & Neundorff, I. (2011). Antimicrobial peptides with cell-penetrating peptide properties and vice versa. *European Biophysics Journal*, 40(4), 387–397. doi:10.1007/s00249-011-0682-7
- Su, Y., Doherty, T., Waring, A. J., Ruchala, P., & Hong, M. (2009). Roles of arginine and lysine residues in the translocation of a cell-penetrating peptide from 13C, 31P, and 19F Solid-State NMR. *Biochemistry*, 48(21), 4587–4595. doi:10.1021/bi900080d
- Taboureau, O., Olsen, O. H., Nielsen, J. D., Raventos, D., Mygind, P. H., & Kristensen, H. H. (2006). Design of novispirin antimicrobial peptides by quantitative structure-activity relationship. *Chemical Biology and Drug Design*, 68(1), 48–57. doi:10.1111/j.1747-0285.2006.00405.x
- Tamargo, J., Le Heuzey, J. Y., & Mabo, P. (2015). Narrow therapeutic index drugs: A clinical pharmacological consideration to flecainide. *European Journal of Clinical Pharmacology*, 71(5), 549–567. doi:10.1007/s00228-015-1832-0
- Tang, Y. L., Shi, Y. H., Zhao, W., Hao, G., & Le, G. W. (2008). Insertion mode of a novel anionic antimicrobial peptide MDpep5 (Val-Glu-Ser-Trp-Val) from Chinese traditional edible larvae of housefly and its effect on surface potential of bacterial membrane. *Journal of Pharmaceutical and Biomedical Analysis*, 48(4), 1187–1194. doi:10.1016/j.jpba.2008.09.006
- Toropova, M. A., Veselinović, A. M., Veselinović, J. B., Stojanović, D. B., & Toropov, A. A. (2015). QSAR modeling of the antimicrobial activity of peptides as a mathematical function of a sequence of amino acids. *Computational Biology and Chemistry*, 59, 126–130. doi:10.1016/j.compbiolchem.2015.09.009
- Torrent, M., Andreu, D., Nogués, V. M., & Boix, E. (2011). Connecting peptide physicochemical and antimicrobial properties by a rational prediction model. *PLoS One*, 6(2), 1–8. doi:10.1371/journal.pone.0016968
- Tripathi, J. K., Kathuria, M., Kumar, A., Mitra, K., & Ghosh, J. K. (2015). An Unprecedented alteration in mode of action of IsCT resulting its translocation into bacterial cytoplasm and inhibition of macromolecular syntheses. *Scientific Reports*, 5, 9127. doi:10.1038/srep09127
- Tsai, C.-W., Hsu, N.-Y., Wang, C.-H., Lu, C.-Y., Chang, Y., Tsai, H.-H. G., & Ruaan, R.-C. (2009). Coupling molecular dynamics simulations with experiments for the rational design of indolicidin-analogous antimicrobial peptides. *Journal of Molecular Biology*, 392(3), 837–854. doi:10.1016/j.jmb.2009.06.071
- Vale, N., Aguiar, L., & Gomes, P. (2014). Antimicrobial peptides: A new class of antimalarial drugs? *Frontiers in Pharmacology*, 5(12), 275. doi:10.3389/fphar.2014.00275
- Veerasingh, R., Rajak, H., Jain, A., Sivadasan, S., Varghese, C. P., & Agrawal, R. K. (2011). Validation of QSAR models - Strategies and importance. *International Journal of Drug Design & Discovery*, 2(3), 511–519.
- Velasco-Bolom, J. L., Corzo, G., & Garduño-Juárez, R. (2017). Molecular dynamics simulation of the membrane binding and disruption mechanisms by antimicrobial scorpion venom-derived peptides. *Journal of Biomolecular Structure and Dynamics*, 36, 2070–2084.
- Vishnepolsky, B., & Pirtskhalava, M. (2014). Prediction of linear cationic antimicrobial peptides based on characteristics responsible for their interaction with the membranes. *Journal of Chemical Information and Modeling*, 54(5), 1512–1523. doi:10.1021/ci4007003
- Vora, J., Patel, S., Sinha, S., Sharma, S., Srivastava, A., Chhabria, M., & Shrivastava, N. (2018). Molecular docking, QSAR and ADMET based mining of natural compounds against prime targets of HIV. *Journal of Biomolecular Structure and Dynamics*, 2018, 1–16.
- Wang, S., Zeng, X., Yang, Q., & Qiao, S. (2016). Antimicrobial peptides as potential alternatives to antibiotics in food animal industry. *International Journal of Molecular Sciences*, 17(5), 603. doi:10.3390/ijms17050603

- Wang, Y., Ding, Y., Wen, H., Lin, Y., Hu, Y., Zhang, Y., & Lin, Z. (2012). QSAR modeling and design of cationic antimicrobial peptides based on structural properties of amino acids. *Combinatorial Chemistry & High Throughput Screening*, 15(4), 347–353. doi:[10.2174/138620712799361807](https://doi.org/10.2174/138620712799361807)
- Wiesner, J., & Vilcinskas, A. (2010). Antimicrobial peptides: The ancient arm of the human immune system. *Virulence*, 1(5), 440–464. doi:[10.4161/viru.1.5.12983](https://doi.org/10.4161/viru.1.5.12983)
- Wu, E. L., Cheng, X., Jo, S., Rui, H., Song, K. C., Dávila-Contreras, E. M., & Klauda, J. B. (2014). CHARMM-GUI membrane builder toward realistic biological membrane simulations. *Journal of Computational Chemistry*, 35(27), 1997–2004. doi:[10.1002/jcc.23702](https://doi.org/10.1002/jcc.23702)
- Xie, H., Qiu, K., & Xie, X. (2014). 3D QSAR studies, pharmacophore modeling and virtual screening on a series of steroidal aromatase inhibitors. *International Journal of Molecular Sciences*, 15(11), 20927–20947. doi:[10.3390/ijms151120927](https://doi.org/10.3390/ijms151120927)



Contents lists available at ScienceDirect

Journal of Drug Delivery Science and Technology

journal homepage: www.elsevier.com/locate/jddst

Conjugates and nano-delivery of antimicrobial peptides for enhancing therapeutic activity



Mbuso Faya^a, Rahul S. Kalhapure^a, Hezekiel M. Kumalo^b, Ayman Y. Waddad^a, Calvin Omolo^a, Thirumala Govender^{a,*}

^a Department of Pharmaceutical Sciences, University of KwaZulu-Natal, Private Bag X54001, Durban 4000, South Africa

^b School of Laboratory Medicine and Medical Sciences, University of KwaZulu-Natal, Medical School, Durban 4000, South Africa

ARTICLE INFO

Keywords:

Antimicrobial peptides (AMPs)
Nano-delivery
AMP-Antibiotic conjugation
Nano-carriers

ABSTRACT

The current global crisis of antibiotic drug resistance is driving the search for novel treatment approaches. Antimicrobial peptides (AMPs) are small molecular weight proteins with varying number of amino acids found in both eukaryotes and prokaryotes. They have recently been targeted as novel antimicrobial agents with the potential to treat multiple-drug resistant infections. Their conjugation with various classes of materials such as antibiotics, polymers, DNA, salts, phenolic derivatives and their delivery via nano carrier systems are strategies being used to enhance their therapeutic efficacy. An update and understanding of their applicability as conjugates and nano delivery are essential to optimise their development and activity. This review focuses on computational studies depicting their permeation through model membranes and identification of physico-chemical descriptors for activity. It also highlights the potential of AMPs and their conjugates and encapsulation into nano delivery systems for improving activity. Further, research to realise their potential as conjugates and delivery via nano carrier systems are also identified. To our knowledge, this current review presents the first account that comprehensively highlights AMPs targeting various microorganisms, and their conjugation to different compounds to showcase the potential for nano delivery alone or in their respective conjugates for enhanced activity.

1. Introduction

Infectious diseases are one of the leading cause of mortality globally, despite modern technological advances of the 21st century on new drugs and diagnostic equipment used to improve healthcare [1,2]. Over the past 10 years in particular, re-emerging infectious diseases have challenged researchers and the public health systems in their efforts to curb the rise of pathogenicity [3–12]. Bacteria possess numerous drug target sites, with the number of exploited sites being relatively small [13]. This gap in the exploitation of bacterial intracellular targets allows for the synthesis and design of newer antimicrobial agents. Antimicrobial drugs have various modes of action, and depend on factors such as their structural conformation and affinity to certain target sites [14]. The most effective antibiotics act as inhibitors of cell wall synthesis (e.g. penicillins, cephalosporins, bacitracin and vancomycin) [15], cell membrane function (e.g. polymixin B and colistin) [16], protein synthesis (e.g. aminoglycosides, macrolides, lincosamides, streptogramins, chloramphenicol, tetracyclines), nucleic acid synthesis (e.g. quinolones, metronidazole, and rifampin) and other metabolic

processes (e.g. sulfonamides and trimethoprim) [17]. Despite the development of numerous potent antibiotics, infections continue to be a challenge to treat, with the bacteria developing strategies to circumvent their action [18–21].

While antibiotics have revolutionised the therapy of infections, several disadvantages with current dosage forms have been observed. These include inadequate concentration at target infection sites, poor penetration of the antibiotics, side effects and poor adherence [22–24]. These limitations have contributed to antibiotic resistance by microorganisms, causing infections on a global scale [25]. The World health organization (WHO) also identified other causes of drug resistance that include the inappropriate use of antibiotics, lack of quality medicines, animal husbandry practices, poor infection control, weak surveillance systems and a lack of progress in developing new vaccines to combat drug resistance [26]. The reduction in effectiveness of a drug [27] is mainly used in the context of pathogenesis, and occurs through a number of mechanisms, such as: (a) drug modifications by enzymes, such as β -lactamases, (b) target site alterations, (c) metabolic pathways alterations, and (d) reduced drug accumulation due to efflux pump

* Corresponding author.

E-mail address: govenderth@ukzn.ac.za (T. Govender).

Table 1
Examples of bacteria resistant to antibiotics.

Bacteria	Type	Drugs resistant to	Ref
Methicillin-resistant <i>Staphylococcus aureus</i> (MRSA)	Gram (+) cocci	Vancomycin, Linezolid, Daptomycin, Eicoplanin	[214]
Vancomycin resistant <i>Staphylococcus aureus</i> (VRSA)	Gram (+) cocci	Erythromycin, Vancomycin	[215]
<i>S. pneumoniae</i>	Gram (+) diplo-coccus	Doxycycline, Erythromycin, Penicillin G	[216]
<i>E. faecium</i> , VRE	Gram (+) cocci	Vancomycin, Streptomycin, Gentamicin, Penicillin, Ampicillin	[217]
<i>E. coli</i>	Gram (–) rods	Ciprofloxacin, Levofloxacin	[218]
<i>P. aeruginosa</i>	Gram (–) rod	Imipenem, Meropenem, non-antipseudomonas Penicillins	[219]
<i>K.pneumoniae</i>	Gram (–) rods	Colistin,	[220]
<i>A. baumannii</i>	Gram (–) rod	Imipenem, Meropenem	[221]

activity [28,29]. Drug resistance has led to the inadequacy of current dosage forms and has significantly hindered the efficacy of antibiotics [30]. This includes resistance to bacteria, such as Methicillin-resistant *Staphylococcus aureus* (MRSA) (resistant to beta-lactams), *E. faecium* (resistant to streptomycin), *K. pneumoniae* (resistant to 2nd and 3rd generation cephalosporins) and *A. baumannii* (Table 1) [31]. The proliferation of multidrug-resistant strains has led to the search for effective therapeutic agents, and has ignited research into the design and synthesis of novel antimicrobial molecules [32,33]. The development of alternative therapeutic agents remains one of the major challenges to circumventing the problem of drug resistance [34]. Antimicrobial peptides (AMPs) represent a new class of potential drug candidate and are proteins of smaller molecular weight (2–8-kDa) that are broad spectrum in their activity against pathogenic bacteria, viruses and fungi [35,36]. They are also known as host defence proteins (HDPs), and are part of the innate immune system found in all classes of life [37]. The discovery of AMPs dates back to 1939, with gramicidins being discovered first and isolated from *B. brevis* [38]. Gramicidins have been used to treat infected wounds on the skin of guinea-pigs [39], which led to their consideration for clinical use, after which they were commercially synthesized as antibiotics. The number of AMPs discovered and/or synthesized to date is above 5000 [40].

AMPs are either natural based obtained from prokaryotes and eukaryotes [41], or synthetic based. They are divided into four structural groups viz. (a) β -sheet; (b) α -helical; (c) loop and (d) extended peptides with broad spectrum activity [42], with α -helix and β -sheets specifically being more common [43]. As AMPs are constructed by coupling amino acids, it is easy to modify their structure [44], which is an advantage in designing various combinations. This ability also allows for the possibility to change the AMP targets and improve their stability against the degradative effects of proteases [45]. AMP activity occurs mainly by disrupting the integrity of the membrane protein, inhibiting DNA and RNA synthesis, or disrupting intracellular targets [46]. AMP action is dependent on their cationic charge, which allows them to be attracted to the anionic membrane of its targets and leads to the destruction of the cell membrane [47,48]. Fig. 1 shows the different mechanisms AMPs used to traverse the bacterial membrane [49]. The AMPs membrane penetrating ability is a major advantage over conventional antibiotics, which may find it difficult to cross bacterial cell membrane and make their way into intracellular targets [50]. Several review papers have highlighted the applicability of AMPs as antibacterial agents for enhancing activity against various organisms, such

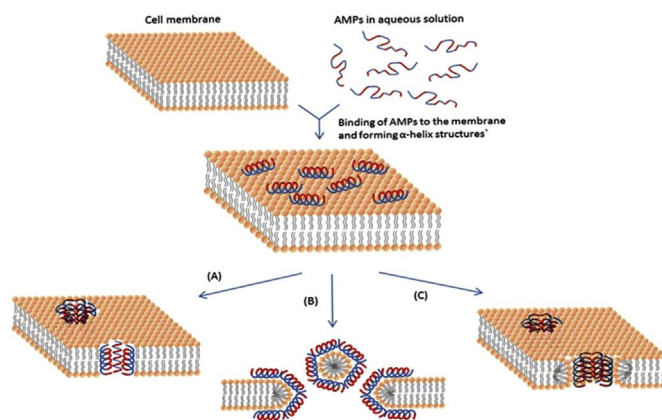


Fig. 1. The various AMPs mechanisms. A represents the Barrel-Stave model (AMPs penetrate the membrane in a perpendicular fashion). B represents the carpet Model (sections of the membrane are coated with AMPs). C represents the Toroidal-pore model (AMPs are in a constant interaction with the membrane phospholipid head groups). AMP Hydrophobic and hydrophilic parts are represented by the colour blue and red respectively. Permission granted [69]. (For interpretation of the references to colour in this figure legend, the reader is referred to the Web version of this article.)

as LL-37, melittin and magainin-II, which are active against *P. aeruginosa*, *L. monocytogenes*, and MRSA respectively [51–53]. A number of AMPs, such as pexiganan acetate, Omiganan, IMX924, Arenicin, Semaglutide and Dulaglutide, were found to be active against Gram positive and negative bacteria, and are now in clinical trials (Table 2). Their intended use was for diabetic ulcers, catheter infection prevention and Type 2 diabetes mellitus [54,55]. Despite their beneficial potent antibiotic activity, their inherent drawbacks, including poor physico-chemical stability, a short circulating plasma half-life and a high haemolytic effect [56] have the potential to render AMPs unusable [57–59]. Various strategies are therefore being used to overcome these limitations. To potentiate their activity, AMPs are also being increasingly explored for conjugation to several classes of materials. The conjugation strategy of AMPs to other compounds amplifies their potential to overcome the current drug resistance crisis [60] as it offers in combination multiple benefits as opposed to the AMP alone. These AMP conjugates can lead to multiple mechanisms of action against bacteria, facilitate self-assembly of AMPs into nanostructures for delivery, achieve intracellular targeting and prolong circulation life [61–64]. Administration of AMPs or its conjugates will eventually require its incorporation into a dosage form for patient administration. The use of current conventional dosage forms will limit the potential of AMPs as they lead to inadequate delivery to the infection site, may not offer protection against degradation by proteases and other degradative enzymes [23,65]. Although it has been noted that the mechanisms of bacterial resistance to AMPs are still not well understood, and their occurrence very unlikely, physico-chemical modifications in the bacterial cell membrane seems to be the first step to developing resistance [66]. Once the bacteria changes the AMP target to make it less susceptible to the action of AMPs, fluidity and bacterial cell permeability decrease due to alterations in the architecture of the outer and inner membranes. Bacterial membrane surface modifications, which can lead to reduced levels of specific membrane proteins and ions, as well as changes in the membrane lipid composition, can promote resistance, which alters the activity of the AMP at its site of action [67,68]. To circumvent this occurrence, the encapsulation or association of these AMPs into nanosized carriers as delivery systems is being explored to achieve targeted delivery to the infection site and reduce resistance [69]. This would provide an added advantage since these nano carriers provide adequate delivery with selective targeting to the infection site as well protection from enzymatic degradation. Also the nano carriers will provide high stability, high carrier capacity, feasibility of incorporation of both hydrophilic and hydrophobic substances, and

Table 2
AMPs under clinical trials and development.

Product	Description	Indication	Phase	Company (location)
Magainin peptide/ pexiganan acetate	22-amino-acid linear antimicrobial peptide, isolated from the skin of the African clawed frog (<i>Xenopus laevis</i>)	Diabetic foot ulcers	3	Dipexium Pharma (White Plains, New York)/Macro Chem/Genaera
Omiganan	Synthetic cationic peptide derived from Indolicidin	Rosacea	2	BioWest Therapeutics/Maruho (Vancouver)
OP-145	Synthetic 24-mer peptide derived from LL-37 for binding to lipopolysaccharides or lipoteichoic acid	Chronic bacterial middle-ear infection	2	OctoPlus (Leiden, The Netherlands)
Novexatin	Cyclic cationic peptide, 1093 daltons	Fungal infections of the toenail	1/2	NovaBiotics (Aberdeen, UK)
Lytixar (LTX-109)	Synthetic, membrane-degrading peptide	Nasally colonized MRSA	1/2	Lytix Biopharma (Oslo)
NVB302	Class B lantibiotic	<i>C. difficile</i>	1	Novacta (Welwyn Garden City, UK)
MU1140	Lantibiotic	Gram-positive bacteria (MRSA, <i>C. difficile</i>)	Preclinical	Oragenics (Tampa, Florida)
Arenicin	21 amino acids; rich in arginine and hydrophobic amino acids	Multiresistant Gram-positive bacteria	Preclinical	Adenium Biotech Copenhagen
Avidocin and purocin	Modified R-type bacteriocins from <i>Pseudomonas aeruginosa</i>	Narrow spectrum antibiotic for human health and food safety	Preclinical	AvidBiotics (S. San Francisco, California)
IMX924	Synthetic 5-amino-acid peptide innate defense regulator	Gram-negative and positive bacteria (improves survival and reduces tissue damage)	Preclinical	Iminex (Coquitlam, British Columbia, Canada)

Adapted from Fox et al., 2013 [222].

feasibility of variable routes of administration and allows controlled drug release from the matrix [70]. Several types of nanoparticles, which are described in this review, such as liposomes, micelles, nanofibers, metallic nanoparticles (silver and gold nanoparticles) and hydrogel nanoparticles, also possess various mechanisms to bypass resistance. Once the AMP is incorporated into these nano systems, it would promote the formation of reactive oxygen species, improve the delivery of the bioactive AMPs by functioning as circulating micro-reservoirs for sustained release at the infection site, and provide resistance to corrosion and oxidation in the case of metallic nano particles [71]. These nano-based drug delivery systems have distinguished themselves as the best approach to mitigate the development of drug resistance by decreased uptake and increased efflux of drug from the microbial cell, biofilm formation and intracellular bacteria. Finally, nanoparticles can target antimicrobial agents to the infection site, which leads to higher drug doses accumulating at the infected site while keeping the total dose of drug administered low. The strategy of having a high local dose at the infection site promotes bacterial killing before resistance could develop, while the lower total dose decreases the possibility that bacteria outside of the nanoparticle site of action will develop drug resistance [72].

Molecular modelling of AMPs is being increasingly reported to understand their mechanisms of action and how they traverse the bacterial cell membrane [73–75]. Studies to identify structural and physicochemical descriptors for AMP activity are also being undertaken. An understanding of such studies is critical to facilitate the design and optimisation of future new conjugates and delivery systems of AMPs.

Reviews thus far on AMPs have focussed on their sources, applications, structural make-up, activity against various classes of bacteria and design [38,76–80]. To date, there is no review paper focusing on AMP-conjugates in combination with the nano delivery of AMPs and molecular modelling approaches as strategies to potentiate the applicability and activity of AMPs. An overview of molecular modelling and quantitative structure activity relationship (QSAR) investigations of AMP activity on the bacterial cell membrane specifically is also lacking. This review paper provides an overview of available computational studies depicting AMP-membrane penetration, as well as their quantitative structure activity relationships (QSAR) that identify the characteristic descriptors responsible for their cell membrane permeation. It focuses mainly on the diversity and broad spectrum antimicrobial activity of AMPs and their conjugates, as well as on the formulation and evaluation of AMPs into various nano delivery systems. Future research

to realise the potential of AMP-conjugates and AMP delivery via nano drug delivery are also identified. This review paper therefore highlights the AMPs ability to target various microorganisms, their conjugation to different antibiotics, polymers and other conjugates, such as phenolic compounds, DNA and salts, which have the potential to enhance AMP activity. This review also highlights the molecular modelling approaches that could structurally elucidate the mechanism of membrane penetration, and showcases the potential for nano delivery AMPs alone and in their respective conjugates for enhanced activity.

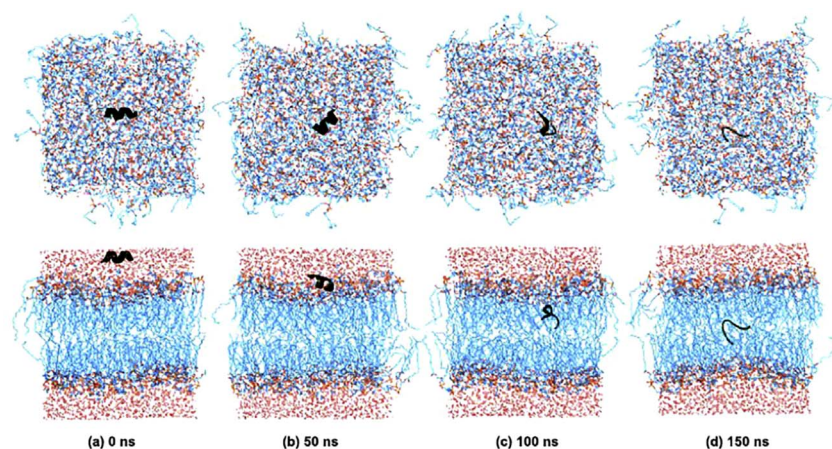
2. *In silico* studies of AMPs in membranes

Since the advancement of computational drug designing and machine learning, *In silico* simulations have become a complementary counterpart to experiments to understand the molecular mechanism of macromolecules and develop novel drug candidates [81]. Molecular modelling approaches, including molecular dynamics and QSAR, have become an integral part of modern drug discovery [82]. An understanding of bacterial membrane penetration by AMPs is key to its utilisation to circumvent drug resistance [83]. The mechanism of membrane penetration by AMPs is not well understood [84], however, *In silico* studies have emerged that utilised complex computational tools to study receptor-ligand interactions and their binding affinities [85]. In the literature, molecular studies, such as molecular dynamics (MD) and quantitative structure-activity relationship (QSAR), have been utilised to understand the mechanical behavior of biomolecules e.g. AMP_s [86–88]. As this review focuses on AMP-conjugates and AMP nano delivery, a mechanistic understanding of the actions of AMPs is important to elucidate their membrane penetration ability. This section will focus on a brief overview of molecular dynamic (MD) simulations of AMPs through model membranes. Quantitative structure-activity relationship (QSAR) is also discussed, which provides a deeper understanding of the structural descriptors that could be attributed to membrane penetration.

2.1. Molecular dynamics (MD) simulations of AMPs in model membranes

Molecular dynamics is an *In silico* method that provides structural insights, binding affinities and stabilities of proteins by complex calculations of time dependent behavior of a molecular system [89]. Its main aim is to provide a simulation that studies the conformational rearrangements of molecules, the interaction and motion of atoms and

Fig. 2. MD simulation depicting the interaction of the amphipathic helical AMP F[Nle]W[Hag]RWWV[Orn]L with an artificial lipid bilayer. Permission granted [78].



molecules according to Newton's equation of motion [90]. MD utilizes force fields (e.g. CHARMM) to estimate the forces between interacting atoms and to calculate the overall energy of system [91]. MD simulations, the integration of Newton's laws of motions generates successive configurations of the evolving system, providing trajectories that specify positions and velocities of the particles over time. From these MD trajectories, a variety of properties can be calculated, including free energy, kinetics measures, and other macroscopic quantities, which can be compared with experimental observables [90]. Khandelia et al. (2008) reviewed the impact of peptides in lipid membranes, and observed that such MD simulations on model membranes are essential for understanding the structural factors that account for membrane permeation, such as peptide amphiphilic character, conformation and electrostatic effects [92]. MD simulations of AMPs in model membranes allow for the behavioral and structural insights of how they are inserted into the lipid bilayers, as well as the outlining factors that influence lipid-peptide interactions, such as membrane thickness, lipid acyl-chain order and dynamics, membrane elasticity, lipid-domain and annulus formation to be described [93,94]. In this review, we focused on the different MD simulation studies as examples to elucidate the AMP-membrane interaction, with the hope that this will give an indication of AMP factors that could attenuate or enhance their membrane penetration potential. Sengupta et al. (2008) conducted a series of simulations with the AMP, Melittin (GIGAVLKVLTTGLPALISWIKRKRQQ) interacting with dipalmitoylphosphatidylcholine (DPPC) bilayers using the GROMACS software package for MD simulations. The GROMOS force field 43a2 was used to interpret the peptide-bilayer interactions. The simulation revealed that two AMPs were inserted into the DPPC bilayer pore, while the remainder were found to line the mouth of the pore [95]. The authors indicated that the AMPs lining the mouth of the pore are expected to give an initial burst effect and then a controlled release behavior will be followed. We believe that this study not only explains the interaction of AMPs with the membrane, but can also indicate the AMPs' release behavior from future liposomal formulations due to the similarity of the components between the liposomes and the membrane bilayer. In another study, Dittmer et al., (2009) conducted a study on incorporating AMPs (alamethicin) into membranes employing liquid-State NMR and MD, with the C monomer from the X-ray crystal structure of alamethicin being used for the system set up. The MD simulations revealed the fluidity of the membrane environment, where the AMP was dissolved rather than incorporated [96]. Dan et al. (2011) reviewed the interaction of the AMP protegrin on lipid bilayer membranes. An interesting observation from this review was that these AMPs interact with the components of the outer membrane, and have an increased bilayer disruption with increased AMP concentration [97].

Using another model lipid bilayer membrane of phosphatidylglycerol (POPG) and phosphatidylcholine (POPC), Wang et al. (2012) conducted a MD simulation of the AMP CM15 at 100 ns. The AMP was

reported to penetrate the model membranes with no hemolytic activity. The study concluded that the initial conformation of the peptide played an important role in inserting the peptide into the model membranes [70]. From this study, we expect that the hydrophobicity of the AMPs could determine their distribution between the lipid bilayer of the membrane and the aqueous core, which is essential in formulating similar structured nanocarriers. In a study conducted by Li et al. (2012), molecular simulations were conducted to propose how a branched AMP disrupts a bacterial membrane, with MD simulations being performed for each model membrane using the CHARMM36 force field. The concentration dependent effects of the branched AMP were studied by performing simulations with varying peptide-lipid ratios: 1:128, 2:128 and 3:128. These ratios corresponded to different concentrations of the AMP, and all the simulations were run for 200 ns using the GROMACS package 4.5. The results indicated that the activity of the branched AMP (B2088) is concentration dependent, and that at higher concentrations (using 3 B2088 molecules with 128 lipid molecules), significant membrane perturbation may occur [87]. This study can be considered significant because it can be used to predict the conjugation of the AMPs with different ratios of polymers, and to interpret the interaction behavior based on an analysis of the entropic energy values, which could affirm the continuity or discontinuity of the interaction. Wang et al. (2016) analyzed the susceptibility of AMPs that incorporated unnatural amino acids against microbial infections. The MD simulation revealed the amphipathic-helix conformation of the designed peptides, as depicted in Fig. 2, which were also seen to unfold when they traversed the simulated lipid bilayer that mimics the bacterial membrane. *In vitro* susceptibility was conducted against *P aeruginosa*, *S. aureus*, and *E. coli*, with one AMP (F[Nle]W[Hag]RWWV[Orn]L) showing very potent antimicrobial activity, having MIC's of 5.6, 18.9 and 11.2 $\mu\text{g/ml}$ for *S. aureus*, *P. aeruginosa* and *E. coli* respectively [98]. We conclude that the importance of the Wang et al. (2016) study is that a correlation between amino acid sequences and bacterial phospholipids could be established to create the foundation for further experimental studies using techniques that investigate the interaction between the AMPs. Balatti et al. (2017) conducted a study on the differential interaction of amphiphilic AMPs (aurein 1.2 and maculatin) with POPC lipid structures using coarse-grained MD simulations. The AMP-lipid simulation was conducted in three initial configurations: (a) peptides in water in the presence of a pre-equilibrated lipid bilayer; (b) peptides inside the hydrophobic core of the membrane; and (c) random configurations that allow self-assembled molecular structures. The results showed that both AMPs were capable of forming membrane aggregation, however, the aurein 1.2 were seen to form pore-like structures, whereas the maculatin formed clusters and induced curvature at low peptide-lipid ratios [99].

The above reports have been useful in demonstrating that the nature of the AMP dictates how it will interact with the bacterial membrane,

and whether it will be incorporated or disintegrate as it interacts with it. These molecular dynamic studies of AMP-membrane interaction allowed for the concise evaluation of the AMPs mechanism of action as they traverse the lipid bilayer. This is important for guiding future research that incorporates peptide conjugates and their delivery in nano systems. It should be noted though that a challenging factor is the experimental validation of computer modelled simulated results, as most MD studies having not been evaluated experimentally [100]. This suggests the need to combine both computational and experimental approaches in AMP design and application. In contrast to the above research, where the authors focused on a single AMP (Protegrin), this review focuses on various AMPs interacting with model membranes, and further postulates that these AMP activities could be enhanced by conjugation strategies.

The remainder of the above studies focused on molecular modelling with AMPs on model membranes. The review of the current literature therefore indicates that there is a considerable gap in molecular dynamic simulations of AMP-antibiotic conjugates and their delivery in nano systems. Research on simulations of AMP-conjugates with model membranes have potentially great prospects, specifically as some target intracellular organelles. An MD study of these conjugates as they penetrate the bacterial membrane, as well as when they interact with intracellular targets, would offer a better understanding of their mechanism and how they could be improved. Only one study so far has reported the modelling on AMP-nanoparticles. This study by Liu, Xu et al. (2009) showed the self-assembly of cationic peptide nanoparticles as an efficient antimicrobial agent. Those nanoparticles showed efficient penetration through the blood brain barrier (BBB) in *S. aureus*-infected meningitis rabbits for the treatment of brain infections [101]. Molecular dynamic studies on the various nano carrier systems that can be used for AMP delivery is therefore highly warranted.

2.2. Quantitative structure activity relationship (QSAR)

QSAR is another well-known computational method used for studying AMPs, and relies on identifying a set of structural or physicochemical descriptors to describe their activity [102,103]. This computational tool provides the added advantage of AMP structure-membrane activity. While most studies employing QSAR modelling to study peptides use this tool to predict structural descriptors attributed to peptide activity, haemolysis and cytotoxicity [104], there are no QSAR model studies that have related the structure of AMPs to their ability to penetrate bacterial membranes. This review provides insights into AMP structural descriptors in relation to their ability to penetrate bacterial membranes. Frecer et al. (2006) developed a QSAR model to analyse the haemolytic effects and antimicrobial activity of cyclic cationic AMPs obtained from protegrin-1. The study utilised the genetic function approximation algorithm to relate antibacterial activity to the AMPs net charge and amphipathicity and the haemolytic activity paralleled with the lipophilicity of the residues from the nonpolar surface of the β -hairpin. However, the results reflected that the protegrins, together with their analogs containing a single or double disulfide bridge, demonstrated greater antimicrobial potency compared to their counterparts, with no disulfide bridges [105]. Jianbo Tong et al. (2008) reported on a novel descriptor of amino acids and its use in designing peptides with the principal component analysis (PCA) method, where 99 molecular indexes of amino acids were examined. For each amino acid, nine principal component scores were selected and applied as new vectors of descriptors. Vector of principal component scores (VSW) were derived from the principal component analysis of the invariant molecular indices of the amino acids. The observed and calculated activities of the AMP sequences were compared, and were found to be very similar [106].

Wang et al. (2012) built a QSAR model of cationic AMPs, basing it on the structural properties of amino acids. The amino acid index database was used to select 89 indices that depicted three classes of AMPs

in the model (Surface-tethered cationic peptides, 101 synthetic cationic polypeptides and novispirin AMPs) in order to calculate the contribution of the amino acids to the activity of the AMPs. The high performance STR-MLR model enabled the prediction of antimicrobial activity and identified the most suitable amino acids in the sequence to be used for designing novel AMPs [107]. The importance of amino acid sequence was highlighted later in another study by Mariya et al. (2015). They built a QSAR model, for which the Monte Carlo method was used, of the activity of AMPs (mastoparan analogs) as a mathematical function of a sequence of amino acids. The results obtained were reasonably good, with the pMIC values being better than those of the experimental pMIC values.

From the above reports, it is clear that the use of QSAR studies is important to establish the most potent descriptors that will allow for optimal AMP activity and will subsequently facilitate the design of optimal AMPs with good antimicrobial activity and less haemolytic effects [108]. Importantly, we believe that these descriptors identified could also be crucial in elucidating the most probable candidates that are important in bacterial cell membrane penetration and nanoparticle formation. As most AMPs main target is the cell membrane, we contend that the descriptors outlined in the above studies not only account for antimicrobial activity but membrane penetration as well. In conjunction with QSAR modelling, more in-depth computational approaches are needed to further describe the mechanism of action of these descriptors on the cell membrane components leading to membrane disruption. Zelezetsky et al. (2006) equates the activity of AMPs to their structural conformation, where α -helical structuring permits optimal spatial arrangement of aliphatic side chains for membrane insertion, and their hydrophobicity allows for deeper insertion into the whole lipid bilayer [109]. We also contend that since the formulation of nano delivery systems requires certain physicochemical conditions, such as pH, hydrophobicity, charge, solubility, entrapment and release profiles [101], QSAR studies could assist in elucidating those descriptors required for nanoparticle formulation, and how these AMPs would behave in those nano systems.

A possible limitation of current QSAR reports on AMPs is that they have mainly focused on the elucidation of possible physicochemical descriptors responsible for activity and those that attenuate activity [103,110]. Studies on membrane destabilization, AMP activity within the bacterial cell wall and how it disrupts intracellular pathways are lacking. Future reports on QSAR studies with AMPs can be strengthened by the inclusion of experimental studies such as DNA based testing for determining lysis of the microbial cell wall and microscale thermophoresis (MST) for determining the intracellular interactions causing the disruption of the intracellular pathways to provide a greater in-depth understanding of how specific descriptors enhance membrane permeation and intracellular interactions [111].

3. AMP-antibiotic conjugates

One approach to enhance the performance of AMPs is the application of conjugation strategies [112]. AMPs can be conjugated to various classes of materials forming AMP-conjugates, and are designed solely for the purpose of combining the antimicrobial power of AMPs with the desired conjugates to effectively kill microorganisms [45,60]. The AMP-antibiotic conjugates offer better biological activities than AMPs alone, this being confirmed by studies focused on using them as vectors to deliver their respective conjugates [113–115].

Conjugation requires knowledge of both the type of conjugates to be used and a thorough understanding of the microorganism being targeted to ensure optimum conjugate activity without attenuating the antibacterial action of the agent intended to be conjugated to the AMP. Novel synthetic routes and various conjugation approaches using antibiotics, polymers, salts, DNA and phenolic derivatives have been reported thus far and are reviewed here under.

Table 3
AMP-Antibiotic conjugates synthesized for activity against microorganisms.

Peptide	Peptide sequence	Antibiotic	Microorganism	Main findings	Ref
UBI ₂₉₋₄₁	GRAKRRMQYNRR	Chloramphenicol (CAP)	<i>S. aureus</i> , <i>E. coli</i> , <i>P. aeruginosa</i>	MIC for CAP-UBI ₂₉₋₄₁ was found to be $3.8 \pm 0.9 \mu\text{g/mL}$ for <i>E. coli</i> and $15.0 \pm 2.6 \mu\text{g/mL}$ for <i>S. aureus</i>	[113]
Tridecaplin (H-TriA1)	WDGSTSDDXGVYS	Rifampicin, Vancomycin, Erythromycin, Levofloxacin	<i>K. pneumoniae</i>	H-TriA1-Rifampicin did not increase the <i>in vitro</i> activity of Rifampicin. Moderate activity was observed with H-TriA1-VMC and H-TriA1-Ery.	[128]
Indolicidin	ILPWKWPWPWRR	Levofloxacin	<i>S. aureus</i> , <i>E. coli</i> , <i>P. aeruginosa</i> , <i>B. subtilis</i>	The conjugate showed moderate activity against the tested strains.	[223]
Magainin 2 Nisin	GIGKFLHSAKKFGKAFVGEIMNS ITSISLCTPGCKTGALMGCNMTATCHCSHVS	Vancomycin Vancomycin	<i>enterococci</i> VSE, VRE, <i>Moraxella</i> <i>catarrhalis</i>	The MIC of Magainin 2-VMC conjugate was 2 and 4 $\mu\text{g/mL}$ against MRSA and VSE respectively. Derivative 5 of the conjugate was found to have good activity with an MIC value of 0.6 $\mu\text{g/mL}$ against VSE (15A797)	[127] [224]
Anoplin temporin L Peptide-resin conjugate CRAMP	GLLKRKTL FVQWFSKFLGRIL FVVKKKKVF KIGEKIKIGQKIKNFFQKLVPOPEQ	Vancomycin Vancomycin Vancomycin Vancomycin	<i>S. aureus</i> <i>S. aureus</i>	DOPC/DOPG vesicles were used for leakage assay where conjugation of temporin L to VMC enhanced its activity. Anoplin-VMC had lower membrane disruption activity. The MIC of the peptide-resin conjugate was 0.0156 $\mu\text{g/mL}$ in the presence of VMC. CRAMP-VMC conjugate did not inhibit bacterial growth better than its separate compounds.	[225] [123] [226]

3.1. AMP-antibiotic conjugates targeting gram positive bacteria

AMP-antibiotic conjugation offers a promising new class of therapeutic agents and great prospects in reviving drugs that were rendered ineffective by microorganisms' resistance strategies. Table 3 reflects some of the AMP and their respective conjugates together with their biological activity towards specific Gram positive and negative bacterial strains. AMPs have the ability to traverse the bacterial cell membrane and disrupt intracellular targets [116], which makes them ideal for conjugation with antibiotics that have difficulty crossing the membrane barrier [117]. In this regard, they would have a dual activity: i) transporting antibiotics across bacterial membranes, and ii) providing their own potent antibacterial activity. This dual role has led researchers to explore conjugation strategies to enhance the activity of antibiotics, as well as to take advantage of the activity of AMPs on bacterial membranes.

Levofloxacin, is a broad spectrum drug that belongs to the fluoroquinolone antibiotic class [118]. Recently, microorganism's resistant against levofloxacin have been discovered in bacteria such as *E. coli*, *P. aeruginosa* and *S. aureus* [119], which has attenuated the activity of this drug. In an early study, to restore the potency of levofloxacin and obtain synergistic activity, this antibiotic was conjugated to indolicidin (ILPWKWPWPWRR), a linear cationic AMP rich in tryptophan (Trp) and proline (Pro), reported to be active against both Gram positive and negative bacteria, fungi, and protozoa. The MIC values ranged from 0.03 to 0.1 $\mu\text{g/mL}$ against *P. aeruginosa* and *S. aureus* and *E. coli*. The conjugate activity was better than the activity of levofloxacin and Indolicidin alone indicating the success of the conjugation in restoring the potency of Levofloxacin. It was hypothesized that the combination of levofloxacin with indolicidin, a highly hydrophobic peptide, may improve delivery of the antibiotic through the outer membrane of the bacteria. In addition, the cationic antimicrobial peptide, Indolicidin is known to further enhance antibiotic delivery by altering the membrane integrity [47]. In the same study, the authors conjugated Tat (GRKKRRQRRRPQ) to Levofloxacin via an amide bond or ester linkage, and evaluated it against a number of strains, including *E. coli*, *P. aeruginosa* and *S. aureus*. The MIC values of the conjugates against the tested strains ranged between 0.08 and 0.12 $\mu\text{g/mL}$ [120]. The conjugate had better activity than TAT alone against all the tested strains and the conjugate also showed better potency compared to Levofloxacin alone against *S. aureus*.

Vancomycin is an antibiotic which interrupts cell wall synthesis by complexation with peptidoglycan precursors and this makes it an ideal antibiotic for conjugation with AMPs for membrane perturbation [121]. It has also been used as a last resort drug to treat serious infections caused by penicillin resistant bacteria [122]. Instead of directly conjugating the antibiotic to the AMP as in the studies above, Cho et al. (2007) investigated another strategy which involved firstly the synthesis of antibacterial peptide-resin conjugates and then its subsequent conjugation to vancomycin. The cationic antimicrobial peptide (CAP)-vancomycin conjugate displayed potent activity against *S. aureus* and *M. luteus*, with MICs of 1.56 $\mu\text{g/mL}$ and 3.12 $\mu\text{g/mL}$ respectively, which revealed that the activity of vancomycin was amplified by the peptide-resin conjugate [123]. Another study by Nigam et al. (2015) evaluating the synthesis of cathelicidin-related antimicrobial peptides (CRAMP)-vancomycin conjugates using different linkers, the results indicating that the conjugate with the short and hydrophobic linkers bearing an aromatic group had better activity compared to those with longer chain linkers without an aromatic group [124]. Other AMPs that have been conjugated to vancomycin include Nisin, Anoplin and temporin L [115]. All these AMPs were seen to have good to moderate antimicrobial activity against Gram-positive bacteria. Using another antibiotic, Schmidt et al. (2014) synthesized a peptide-tobramycin conjugate and tested it against *S. aureus*. The results reflected that the conjugate (Pentobra) was able to destabilize the bacterial membrane and inhibit protein synthesis and also had significant bactericidal

activity towards the Gram positive bacteria [125].

Contrary to the above-mentioned studies where activity was amplified, there is indeed the possibility that activity is decreased. This was shown in a study by Arnusch et al. (2012), where ultra-short peptide bioconjugates were synthesized and evaluated for antimicrobial activity. The conjugates had no activity on all Gram positive strains and were seen to be selective towards fungi [126]. Arnusch et al. (2012) also synthesized vancomycin-Magainin II peptide derivatives via click chemistry and tested them against MRSA, vancomycin susceptible enterococci (VSE) and vancomycin resistant enterococci (VRE). The MIC values of the most promising conjugate was found to be 2–16 µg/mL against MRSA, VSE and VRE respectively [127]. The conjugate had no higher activity on the microorganisms than vancomycin alone where the MIC values were 0.4 µg/mL, 0.5 µg/mL and 128 µg/mL against MRSA, VSE and VRE respectively. Although it would have been useful, these authors did not provide possible reasons for this unexpected finding. We think that factors in the conjugate that could have resulted in the undesirable effect were the choice of the linker, steric hindrance mediated by the vancomycin on the AMP, amino acid sequence and/or electron withdrawing effects in the peptide-linker-vancomycin sequence. With the above knowledge concerning AMP-antibiotic conjugation, the design of these conjugates requires further studies on their activity, such as suitable linkers, how they confer such potent activity with regards to their surface charge and stability to optimise their activity. Using another antibiotic, Schmidt et al. (2014) synthesized a peptide-tobramycin conjugate and tested it against Gram Positive *S. aureus*. The results reflected that the conjugate (Pentobra) was able to destabilize the bacterial membrane and inhibit protein synthesis and also had significant bactericidal activity towards *S. aureus*.

3.2. AMP-antibiotic conjugates targeting gram negative bacteria

In addition to Gram positive bacteria, studies have also focused on targeting Gram negative bacteria. Cochrane et al. (2015) investigated the synthesis of Tridecaptin – antibiotic conjugates, which have activity against Gram-negative bacteria. Tridecaptin was conjugated to rifampicin, vancomycin and erythromycin, the latter combination providing better activity against *K. pneumoniae* infections, with an MIC value of 0.4 µg/mL [128]. The conjugation however did not increase the *in vitro* activity of rifampicin, the lowest MIC being 25 µg/ml against *E. coli* and *A. baumannii*. The authors explained this occurrence as the possibility of the peptide and antibiotic not arriving at the target site together due to possible cleavage by proteolytic enzymes. However, linking the AMP derivative H-TriA₁ to vancomycin resulted in a 16-fold increase in activity against *E. coli*, and an 8-fold increase against multi-drug resistant *K. pneumoniae* and *A. baumannii*. Targeting *E. coli* was the focus also of a study reported by Chen et al. (2015) who synthesized and conjugated chloramphenicol (CAP) to the antimicrobial peptide UBI₂₉₋₄₁, with the *in vitro* studies revealing an enhanced antibacterial activity against *E. coli*. The activity of CAP alone on *E. coli* was 6.2 ± 1.7 µmol/L, whereas that of CAP-UBI₂₉₋₄₁ conjugate on *E. coli* was 3.8 ± 0.9 µmol/L. The toxicity of the conjugate on normal cells decreased significantly compared to CAP and most importantly CAP-UBI₂₉₋₄₁ conjugate exhibited more favourable antibacterial efficacy than CAP alone. In addition, the toxicity of CAP-UBI₂₉₋₄₁ on ordinary cells was reduced noticeably in contrast with CAP alone. Schmidt et al. (2014) also synthesized a peptide-tobramycin conjugate and tested it against *E. coli*. The conjugate (Pentobra) was able to destabilize the bacterial membrane and inhibit protein synthesis and also had significant bactericidal activity towards *E. coli*. These results confirm the importance of AMP-antibiotic conjugation as a synergistic approach in targeting pathogenic microorganisms. The difference in the activity of AMP conjugates against both Gram positive and negative bacteria as shown in these studies indicate the existence of various possibilities causing either increased potency or reduced potency of the AMP-antibiotic conjugates. These could include surface charge of the AMP-

antibiotic conjugate, aggregation before the AMP-antibiotic conjugate enters the cell membrane, site of conjugation as well as the choice of linker used which will effectively decrease or increase the accessibility of the antibiotics. The conjugation of AMPs to antibiotics offers a promising approach in enhancing the therapeutic ability of antibiotics and their targeted delivery to specific intracellular organelles. This approach allows AMPs to be used as delivery vectors as well as antimicrobial agents themselves.

4. Cell culture and *in vivo* models evaluating AMP efficacy

The concept of AMP cell selectivity creates the necessities for evaluation tools to determine the biosafety and efficacy on both *in vitro* and *in vivo* levels. One of the major advantage of the AMPs and AMP conjugates over the conventional antibiotics is their selectivity towards the bacterial cells rather than the host cells. In addition, as the lipid composition of the cell surface determines the selectivity of the AMPs and AMPs conjugates, cell culture studies could consider a good source of information to understand such selectivity, biosafety and efficacy [129]. The antimicrobial peptide Magainin II was tested for its cytotoxicity on tumour cells MCF-7 and normal cells HSF. The cells were stained with FITC-Annexin V and propidium iodide and then observed under fluorescence microscope for their apoptotic or necrotic state, respectively. Quantitatively, FACS analysis was used to determine the number of apoptotic and necrotic cells. The cell viability was also measured using CCK-8 (cell counting kit-8), XTT and MTT [130–132]. The MICs (minimum inhibitory concentration) of cationic helical peptide was investigated using broth microdilution method in which the AMPs or AMPs conjugate were dissolved in broth medium with different range of dilution using 96-well plates and then the absorbance measured spectrophotometrically. Field emission-scanning electron microscopy and confocal microscopy could also be used to determine the antibacterial mechanisms by direct monitoring of bacterial membrane structure as well as pore formation of the bacterial membrane respectively [133]. Bacterial Killing assay to determine MBC (minimum bactericidal concentration) was used by Salomone et al. (2016) when they tested the bactericidal activity of a novel cell penetrating peptide [134]. An alternative technique to MIC and MBC could be flow cytometry which is could have been useful in displaying the penetration potential of these peptides. The effect of Megainin II and Megainin II conjugate on MCF-7 and HSF cell lines were studied using flow cytometry method [131]. The effect of chimeric peptide with disruptive membrane properties when incubated with Hela cell line and the activity of AMPs in conjugation with silver nanoparticles on *E. coli* were studied using FACS (fluorescence activated cell sorting) a synonym for flow cytometry [132,134,135].

Ron-Doitch et al. (2016) determined the antiviral effect of liposomal indolicidin on Herpes Simplex Virus-infected 3D epidermis model, the formation of the tissues was validated and stained with hematoxylin and eosin B stain for further evaluation [135]. Tridecaptin-Antibiotic conjugates was evaluated on C57BL/6L mice infected with *K. pneumoniae* then survival rate was determined using Kaplan-Meier plot. Although the activity of the peptide-antibiotic conjugates retained *in vivo*, variation in the effect depended on the type of AMP-antibiotic conjugates (Rifampicin, Erythromycin and Vancomycin) used. Particularly, Tridecaptin-Erythromycin conjugate exerted better activity than the antibiotic alone [128]. The UBI₂₉₋₄₁ AMP fragment was attached to chloramphenicol antibiotic and ICG02 (near infra-red dye) for targeting *E. coli* and *S. aureus* in ICR mice. The targeting capability was proved by detecting the presence of the ICG02 dye at the site of infection using *in vivo* imaging system [113].

From all of the above studies, it was observed that the AMPs or AMP-conjugates had a higher selectivity toward a wide range of microorganisms with enhanced antibacterial effects. Plausible cytotoxicity and binding affinity towards the cancer cell lines evaluated were also observed, suggesting that these AMPs could be considered for cancer

therapy. *In vivo* murine toxicity was not observed, indicating their biocompatibility and potential for further exploration.

5. AMP polymer conjugates

Polymers such as hyperbranched polyglycerol (HPG), polyethylene glycol (PEG), poly- ϵ -lysine (PLL), Chitosan, and poly Lactic-co-glycolic acid (PLGA) are generally used extensively in drug delivery, where they function as drug carriers across bacterial membrane, and when inside the cell membrane, they disintegrate and release the drug to its specific target site [136]. These polymers have also been used for AMP delivery, and function by protecting them from degradation and allowing them to be released effectively to the target site [63]. The main role of polymeric carriers in antibiotic or peptide delivery is to deliver the cargo to the disease site, to function as protector groups of the cargo being delivered, and to protect the cargo or peptide from degradation by proteases and efflux channels [59]. The following section describes conjugation approaches involving AMPs and polymers.

5.1. AMP- hyperbranched polyglycerol (HPG) conjugates

HPGs are dendritic macromolecules with random branch-on-branch topology, which has numerous advantages [137]. Firstly, HPGs are more hydrophilic than PEG, and secondly, the hyper-branched assembly allows the HPG to efficiently cover the surface more than PEG. Thirdly, HPGs have a number of hydroxyl groups that allow for the attachment of several ligands on the HPG [138]. In a study conducted by Kumar et al. (2015), Aurein 2.2 was conjugated to a hyperbranched polyglycerol (HPG), with the MIC values for the conjugate being determined, and *S. aureus* and *S. epidermidis* being used as test strains. The MICs of the peptide against *S. aureus* and *S. epidermidis* were 16 and 32 $\mu\text{g}/\text{mL}$ respectively, whereas the MICs for the conjugates were 110 $\mu\text{g}/\text{mL}$ and 120 $\mu\text{g}/\text{mL}$ respectively [139]. The authors postulated that the possible reasons for the decreased activity could be due to peptide substitution where a higher peptide density within the conjugate would result in a higher antimicrobial activity. Despite the decrease in activity, the HPGylated peptides were also non-toxic to human umbilical vein endothelial cells (HUVECs) and fibroblasts indicating biocompatibility.

5.2. AMP- polyethylene glycol (PEG) conjugates

PEG is a non-toxic, non-immunogenic and FDA approved polymer used to enhance the biocompatibility of many compounds [140]. PEGylation of peptide drugs has been shown to enhance biocompatibility of the peptide in question [139,141,142]. Conjugation of AMPs with PEG have been undertaken with the aim of prevention of recognition and degradation by proteolytic enzymes and increases the size of the AMP, thus reducing the renal filtration and altering bio-distribution [143]. Guiotto et al. (2003) Pegylated the AMP nisin, and determined their MIC values for a number of bacterial strains. The results showed the nisin-PEG conjugate to be less effective than the original AMP alone, with MIC values of the conjugate ranging from 250 μM for *S. aureus* and > 500 μM for *P. aeruginosa* [144]. In a study by Morris et al. (2012), the AMP CaLL was Pegylated, forming a PEG-CaLL conjugate, with the *in vitro* activity revealing that the CaLL was more active than the conjugate [145]. Benincasa et al. (2015) also studied the PEGylation of the peptide Bac7 and tested the conjugate against *S. typhimurium*, with the MIC values of the BacE-PEG ranging between 4 and 8 μM when assayed in MH broth. The MIC values were also determined in the presence of human serum and plasma, and were 1 μM and 0.25 μM in plasma for the BacE-PEG conjugate in the presence of human serum [146]. The above studies which all showed a decreased activity of the Pegylated AMP as compared to AMP alone, indicate that even with prospects of PEG protecting the AMPs from degradative enzymes and increasing their biocompatibility, there is also a possibility

of activity being compromised. As PEG coats both the hydrophobic and hydrophilic parts of the AMP, this could result in the AMP not being freely available for interaction with the bacterial membrane, thus decreasing its cell penetrative activity. PEG also has a high molecular weight, which confers steric hindrance [147], which could be the reason for the attenuated activity of the AMPs. This phenomenon is well described by Lee et al. (2014), who conducted a molecular simulation of PEGylated peptides. It was seen that the PEG chains wrap around the AMPs and weaken their binding interactions with the lipid bilayers. From the reviewed PEGylated AMPs, it was observed that decreased activity was higher in β -sheets than in α -helical AMPs, indicating a structural influence on PEGylation [148]. The AMPs reported so far for Pegylation were all hydrophilic. Pegylation could be advantageous for highly hydrophobic AMPs as PEG is thought to play a crucial role in increasing their solubility and reducing their antigenicity [55], and as such, can play a crucial role in enhancing the AMP activity.

5.3. AMP-chitosan conjugates

Chitosan is a non-toxic cationic polysaccharide natural polymer with a wide range of biomedical applications [149]. It is also easily absorbable at low pH, and has antacid and antiulcer activities that prevent and weaken drug irritation in the gastrointestinal tract [149,150]. These properties make it an ideal candidate for controlled drug release formulations that would provide an added advantage in AMP-chitosan conjugate formulations. Batista et al. (2009) reported on the novel synthesis of chitosan-pexiganan conjugate through the Sulfo-EMCS Cross-Linker for treating infected skin lesions Fig. 3 [151]. In this study, only the successful conjugation was reported, and no antibacterial studies were performed. But based on the known activities of both chitosan and the antimicrobial peptide pexiganan, the authors indicated that this conjugate is very likely to undergo clinical trials for topical uses [152,153]. Their assertion is supported by the following two studies on chitosan and pexiganan. Flamm et al. (2015) tested a non-conjugated pexiganan against a selected number of resistant strains which included MRSA, *S. aureus*, *E. faecium*, *E. coli*, *K. pneumoniae*, *P. aeruginosa* and *A. baumannii*. The MIC values from these pathogens derived from diabetic foot infections ranged between 16 and 32 $\mu\text{g}/\text{mL}$ [154]. In Costa et al. (2014) described the antibacterial activity of chitosan derivatives on *C. albicans* and the MIC values as being 1 $\mu\text{g}/\text{mL}$ for high molecular weight (HMW) chitosan and 3 $\mu\text{g}/\text{mL}$ for low molecular weight (LMW) chitosan [155]. Therefore, based on the antibacterial activity of these materials individually against the Gram-positive microorganisms, a conjugate would be expected to show enhanced activity towards biofilm disruption. It has been reported that *C. albicans* mycofilms actively enhance *S. aureus* colonization and their interaction in a biofilm mode promotes staphylococcal infections [156]. To date, that is the only study involving the conjugation of pexiganan to chitosan or other polymers and additional experimental research involving pexiganan and chitosan conjugates is required. The above studies involving pexiganan and chitosan activities indicate the potential of this polymer and peptide conjugation strategy to yield good results that can lead to clinical trials. Sahariah et al. (2015) reported on the antimicrobial activity of Anoplin-chitosan conjugates, which were synthesized using Copper-Catalyzed Azide-Alkyne Cycloaddition (CuAAC) chemistry. The conjugates showed promising activity compared to their parent peptide, with the lowest MIC observed against *E. coli* (4 $\mu\text{g}/\text{mL}$) [157]. Future research and reviews should explore the chemical composition of chitosan using computational approaches and how it can be used to enhance biocompatibility of AMPs, this component making it ideal for conjugation studies with AMPs and to enhance the delivery of AMPs.

Polymers have been used broadly as drug delivery vectors, and in the formulation of polymeric nanoparticles due to their improved bioavailability, enhanced encapsulation, controlled drug release and attenuated toxicity demonstrated [158,159]. Their utilisation, in

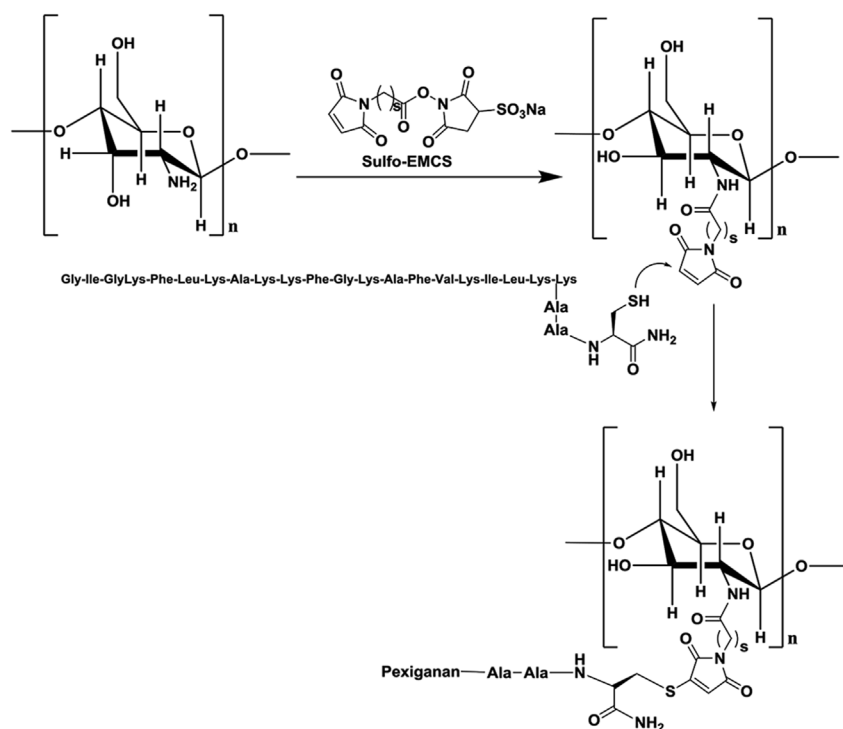


Fig. 3. Pexiganan-chitosan conjugate. Permission granted [125].

conjunction with AMPs, would also offer an enhanced nanoparticle system that contains cell penetrating power due to the cationic properties of AMPs [63]. These types of nano systems would allow AMPs to have a bi-directional approach of enhancing the cell penetrating ability of the nanoparticle as well as interacting with the intracellular organelles.

6. Miscellaneous AMP conjugates

The following section discusses other various AMP conjugates that have been reported.

6.1. AMP-phenolic conjugates

Phenolic groups are found in most drug molecules and have been used in pro-drug modifications to overcome pharmacological barriers that would attenuate drug action [160]. One of the strategies used by phenols is to cover polar groups, and this allows a molecule to be more lipophilic thus promoting membrane permeability [161]. This strategy would be ideal in AMP-phenolic conjugates to effectively deliver the AMP to its target sites through bacterial membrane penetration. Findlay et al. (2012) reported on neomycin-phenolic conjugates with broad-spectrum antibacterial activity. The conjugates had good activity against neomycin sulfate resistant bacteria with low activity towards neomycin susceptible strains. Several conjugates had activity towards MRSA that was also similar to *S. aureus*, while activity against *P. aeruginosa* was slightly increased (64 $\mu\text{m}/\text{mL}$). Therefore, these conjugates displayed improved activity towards Gram positive and negative bacteria. These conjugates had triclosan and clofoctol linkers, which could be responsible for their activity [162]. The phenolic group in antibacterial agents can be used in structural modifications to overcome various properties that could be barriers in the application of the compounds [160]. With the above promising data, future research should explore conjugating phenolic groups to already known AMPs to enhance their bioavailability [163]. There is considerable scope in nano encapsulation of AMP-phenolic conjugates, with an absence of experimental or review studies to elucidate the activity of AMP-phenols in nano systems. As phenols show improved bioavailability and stability,

it is thought that their conjugation with AMPs would provide stability to the formulation and protect them from degradation.

6.2. AMP-DNA conjugates

The strategy of AMP conjugation has been extended to DNA as this offers the potential of to deliver AMPs to nucleic acids.

Ghosal et al. (2012) conducted research on the conjugation of Peptide–Peptide Nucleic Acid (PNA) against *P. aeruginosa*, these being nucleobase oligomers that are regarded as DNA, with a neutral peptide backbone that is stable and resistant to hydrolytic cleavage [164]. These conjugates were synthesized by continuous solid phase synthesis using Boc-chemistry and purified by HPLC. The conjugates had MIC values ranging from 1 to 20 μM , indicating their potential to be used as antibacterial agents and their activity was significantly higher than that of the non-conjugated peptide [165]. Williams et al. (2012) synthesized peptide-oligonucleotide conjugates via solid phase synthesis and its formation was confirmed by reverse phase HPLC, and Maldi-Tof. Antimicrobial activity was not carried out as the authors focussed only on demonstrating the viability of this conjugation strategy, as this is an emerging field. It is envisaged that this field of peptide-DNA nanotechnology will be very useful to direct individual peptides to specific locations on the surface of a DNA nanostructures [166]. Conjugation of AMPs to these nucleic acids would allow AMPs to be utilised as delivery vehicle to pass through the membrane to deliver the nucleic acids into the bacterial nucleus. This would allow the conjugate to inhibit bacterial replication, and to possibly attenuate genetic material that bring about resistance. There is still a considerable gap in research focusing on the nano delivery of AMPs with peptide nucleic acids and the encapsulation of these conjugates would allow effective targeted delivery and a reduction in the dosing frequency.

6.3. AMP-salt conjugates

The strategy of conjugating AMPs to Imidazolium salt is that these salts exhibit biological activity when part of ionic liquids and can form hydrogen bonds with drugs and proteins.

Reinhardt et al. (2014) synthesized Imidazolium salt–peptide

conjugates and screened them for their biological activity. Recent observations suggest that imidazolium cations, when part of ionic liquids, exhibit biological activity. In this study, two AMPs were used: sC18, which is a short C-terminal fragment of the cationic antimicrobial peptide cathelicidin (CAP18) that binds lipopolysaccharide (LPS), and the LL-37 peptide, which also belongs to the group of cathelicidins and shows activity against a wide spectrum of Gram negative and positive bacteria. Conjugation of these peptide-salt conjugates occurred by coupling reactions, and antimicrobial activity was conducted against a wide range of bacteria where the best MIC value was found to be 0.2–0.5 µM against all tested strains [167]. Imidazolium cations in their liquid ionic state function as modifying agents, and in conjugation with AMPs, they can confer their charge for effective membrane penetration. These properties of Imidazolium cations would make them ideal candidates in the formulation of hydrophobic AMPs. Future studies should explore using these cations to improve the conductivity of peptides for effective membrane penetration, and encapsulating AMP-Imidazolium conjugates for improved delivery.

The conjugation of various classes of materials to AMPs using different conjugation strategies all have the same goal of providing a plausible vehicle capable of permeating the bacterial cellular membrane, delivering the desired compound or AMP to the intracellular targets, protecting the AMP from the action of degradative enzymes, enhancing biocompatibility and overcoming pharmacological barriers. Conjugations make use of intrinsic chemical routes that require an understanding of both the AMP and conjugate materials involved in terms of whether or not they would synergistically produce the desired biological outcome as well as knowledge of the biological target with its inherent pathogenicity and intracellular biochemical pathways, which can displace foreign substances, leading to resistance.

As a result of the enhanced biological activity of several conjugates compared to their parent compounds, it is anticipated that their encapsulation into nano systems would provide improved antimicrobial agents that have the ability to permeate the bacterial membrane and interrupt intracellular targets. The formulation of these conjugates in nano systems would also allow for a controlled and sustained release to their specific target sites, reduced toxicity, protection against degradative enzymes, increased bioavailability and high loading capacity, as seen with their parent AMP [168,169].

7. Nano-carriers employed in the delivery of AMPs

Despite their considerable antimicrobial activity, the application of AMPs in clinical settings has been limited by their potential toxicity and vulnerability to chemical degradation by proteases [47]. The encapsulation of AMPs, including their conjugates in suitable nano-carriers, has the potential to target the infection site of bacteria, overcome side effects and protect them from enzymatic degradation [170]. Encapsulating AMPs for effective delivery has been successful in several nanostructures such as liposomes, micelles, nanofibers, metallic nanoparticles (MNPs) and hydrogel nanoparticles [171,172]. Table 4 summarizes the different nano drug delivery systems that have been used thus far for encapsulating AMPs. The main experimental findings, with each of the nano carrier systems reported thus far for AMPs are summarised below.

7.1. Liposomes

Liposomes are spherical vesicles with at least one lipid bilayer and have been used extensively in drug delivery research. They have been found to reduce toxicity, prolong drug half-life, as well as biocompatible and biodegradable properties which makes them very attractive for biomedical investigation [173,174]. They have also been seen to improve the delivery of bioactive molecules by functioning as circulating micro-reservoirs for sustained release [175]. Liposomes can encapsulate both hydrophilic and hydrophobic materials by nature,

Table 4
Nano-carriers used for the delivery of AMPs.

Nano-carrier	AMPs	Spectrum of activity	Main findings & applications	Ref
Liposomes	Nisin	Activity against <i>S. mutans</i>	nisin encapsulated in two lipid molar formations: DPPC/DPPG, DPPC/DPPE, DPPC/SPS had greater in vitro activity against the tested strain.	[227]
Micelles	Nisin	Activity against <i>L. lactis</i>	nisin-loaded liposomes were successful in controlling food spoilage and pathogenic organisms.	[228]
Nanofibers	KSLW-SSM AMP motif (Cys-KR12)	Activity against <i>S. epidermidis</i> Activity against <i>P. aeruginosa</i> , <i>S. aureus</i> , <i>E. coli</i> and <i>S. epidermidis</i>	KSLW loaded in the SSM carrier had no effect on bacterial load in stressed mice. Nanofibers containing Cys-KR12 displayed potent antimicrobial activity against the tested strains & activities on keratinocytes, fibroblasts, & monocytes, which play important roles in the wound healing process.	[187] [229]
Metallic NPs	Bacteriocin NK-2 and LLKKK-18 AMPs coupled to a silver Nanoparticle	Activity against <i>L. sakei</i> , <i>E. faecium</i> Activity against <i>M. smegmatis</i>	The activity of plantaricin 423 in nanofibers was more potent than its activity in the cell free supernatant AMP NK-2 displayed improved killing effect with the AgNPs; NP-1 and NP-2 at a 0.5-ppm concentration.	[230] [195]
Hydrogels	Geoplin-melittin (GM) conjugated to gold nanoparticles Novel AMP immobilized on a soft hydrogel network PEP8R	Activity against <i>S. aureus</i> ; <i>E. coli</i> ; <i>K. pneumoniae</i> ; <i>P. aeruginosa</i> , multidrug-resistant <i>E. coli</i> ; <i>S. haemolyticus</i> Activity against <i>S. aureus</i> and <i>S. epidermidis</i> Activity against <i>E. coli</i> , <i>P. aeruginosa</i> and <i>S. aureus</i>	Peptide LLKKK-18 exhibited activity with NP-2 at 0.5-ppm against <i>M. smegmatis</i> . GM conjugated to AuNPs were found to be more effective in bacterial membrane penetration than the unbound GM and were not toxic to human cells Hydrogel with higher AMP concentration led to a greater antimicrobial activity with cidal effects identified for 6, 8, & 10 wt % hydrogels. The AMP was more active against the Gram-positive bacteria	[199] [231] [232]

making them ideal nano structures for the delivery of amphiphilic compounds [176]. One of the challenges that hinders the activity of the liposomal formulation includes the premature release of the payload before the target site is reached [177,178]. In addition, higher liposomal volumes are necessary when the efficiency of the encapsulation is low for clinical dosage [179]. In separate studies Benech et al. (2002) and Were et al. (2004) studied the activity of nisin encapsulated in liposomes, and found that the encapsulation conferred a higher entrapment efficiency with lower susceptibility to destabilization by nisin. The formulation also had an enhanced efficacy against *L. monocytogenes* compared to the free nisin [180,181]. Using another AMP, Alipour et al. (2008) and Alipour et al. (2009) encapsulated polymyxin B which is a cationic AMP with liposomes targeting resistant Gram-negative bacterial infections. The MICs of the liposomal polymyxin B against Gram-negative strains was significantly lower than the free polymyxin B [182,183]. In the above studies, the activity of the liposomal formulations of polymyxin B was higher than the activity of the un-encapsulated. These four studies only reported antimicrobial activity, encapsulation of AMPs into liposomes and entrapment. No other characterisation data such as release kinetics, essential for formulation optimisation was reported. However, in a more recent study by Ron-Doitch et al. (2016) formulation characterisation was more extensive. They encapsulated the AMP LL-37 in liposomes, and studied its cellular uptake, *in vitro* cytotoxicity and physicochemical properties. The cytotoxicity results showed minimal cytotoxicity in HaCaT cells. From the cellular uptake results (Fig. 4), LL-37 liposomal formulation was taken up more rapidly than the free AMP in all the time periods. The time-dependant uptake of the encapsulated LL-37 was observed as being higher than that of the unbound LL-37 [135]. These studies show the importance of AMP-liposomal formulations in delivering AMPs and the effectiveness of liposomes as delivery vehicles.

7.2. Micelles

Since their discovery in 1984, micelles have gained much attention as nano-based drug delivery systems, especially for poorly water-soluble drugs [184]. Owing to their size, ability to solubilize hydrophobic drugs and achieve target or site-based drug delivery, micelles continue to show great potential as vectors for drug delivery [185]. Micelles possess distinctive structural properties that comprise of two or more hydrophilic and hydrophobic blocks with different solubility ratios in aqueous environment, which makes them effective for drug delivery [186]. Liu et al. (2009) studied cationic AMPs which are capable of self-assembly as potential antimicrobial agents. TEM imaging confirmed the formation of micelles, and the *in vitro* results showed that these micelles had broad spectrum activity with low MIC values [101]. Using another micelle formation strategy, Williams et al. (2012) performed a study on sterically stabilized phospholipid micelles of an antimicrobial wound healing adjunct. The study aimed to examine whether the association of a cationic decapeptide with sterically stabilized nano-micelles (SSMs), would improve stability and *in vivo* antimicrobial effect. *In vitro* assays against *S. epidermidis* reflected reduced activity of the cationic decapeptide in SSM solution, however the *in vivo* studies in animal model

with decapeptide-nano micelles preparations presented no differences in microbial load at post-operative time points. We believe that the loss of activity could be due to electrostatic interactions of the decapeptide with the anionic surface of SSM [187]. The above studies employed micelles to improve activity. To explore another application for micelles Black et al. (2012) reported the self-assembly of peptide amphiphile micelles with the aim of promoting a protective immune response *in vivo*. The formation of the micelles was confirmed by TEM imaging. These peptide amphiphile micelles were found to offer *in vivo* protection from tumours by stimulating T_c cells This study confirmed the use of the peptide amphiphiles in self assembled micelles as a new class of growing nanoparticles that have the ability to induce an immune response [188]. Clearly this study showed that, although these micelles are effective in the entrapment and delivery of AMPs, the choice of the micelle system should be chosen very carefully so that the surface charge of micelles don't interfere with the AMP activity.

7.3. Nanofibers

Nanofibers (fibers with diameters less than 100 nm), which are a product of polymers treated specifically to form filaments, possess great prospective to be used for delivering AMPs and/or AMP-conjugates [189]. These fibers are produced by electro-spinning, which uses electric force to draw charged threads of polymer solution [190], and are developed from both natural and synthetic polymers, such as chitin, chitosan, polyurethane, poly(L-lactic acid) and poly-vinyl alcohol. Nanofibers have large surface to volume ratio and surface-modification possibilities, which make them ideal for AMP-loading and delivery [191]. Heunis et al. (2010) described a novel approach in AMP delivery, where they were incorporated into nanofibers for wound dressings. The AMP plantaricin 423 was encapsulated in nanofibers that were produced by the electro-spinning of polyethylene oxide (PEO). The PEO mobilised AMP showed high activity against *E. faecium* and *L. sakei*. Nanofibers are therefore thought to be the ideal matrix for the immobilization of AMPs, and/or their encapsulation for effective delivery to skin infection [191].

7.4. Metallic nanoparticles

Metallic nanoparticles (MNPs), such as those derived from noble metals, including gold and silver, may serve as potential nano carriers for AMPs and their conjugates. Owing to their large surface area and surface charge, most MNPs easily attach to the surface of bacterial membranes by electrostatic interactions, and thereby interrupt the integrity of the membrane [149,192]. Noble metals are resistant to oxidation and corrosion, which this makes them ideal for nanoparticle formation and reduced toxicity, as most nanoparticles accumulate in the liver, spleen and lymph nodes [193]. Functionalized nanoparticles can be formed by processes such as coupling or adsorption of specific molecules (e.g. AMPs onto MNPs surfaces), with the aim of producing a synergistic approach for the antimicrobial activity of both the NPs and the selected AMP [194]. Silver nanoparticles (AgNPs) have been extensively studied and found to possess potent antimicrobial activities, having been used for decades, especially as antibacterial agent [195]. The mechanism of action has been thought to be directed towards the bacterial cell wall and membrane perturbation, as well as acting on intracellular targets [196]. MNPs have a higher positive zeta potential, promote membrane lysis and penetration when they interact with the negatively charged bacterial membrane [197]. Liu et al. (2013) used a cell penetrating peptide (G3R6YGRKKRRQRRR) which was then used to form silver nanoparticles (AgNPs). The nanoparticles were found to be active against the Gram-positive *B. subtilis* and the Gram-negative *E. coli* [198]. In contrast to the previous studies where the AMPs were used to form the silver nanoparticles, Pal et al. (2016) conducted a study on the activity of an AMP conjugated to a silver nanoparticle against *E. coli*, and the nano-conjugate was reported to enhance

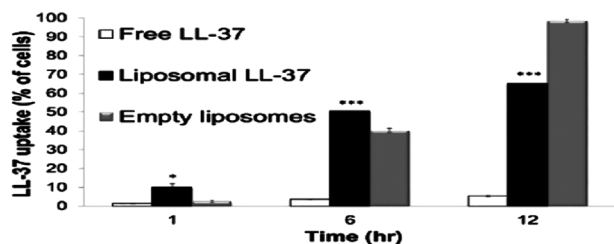


Fig. 4. LL-37 uptake by HaCaT cells (shown as % of cells engulfing treatment) following empty liposomes, free LL-37, or liposomal LL-37. Permission granted [151].

Table 5

List of FDA-Approved Nanomedicines Stratified by Material Category (adapted from D Bobo et al., 2016) [212].

Name	Material description	Nanoparticle advantage	Indication(s)	Year(s) approved
Polymer Nanoparticles – synthetic polymer particles combined with drugs or biologics				
Adagen [®] /pegademase bovine (Sigma-Tau Pharmaceuticals)	PEGylated adenosine deaminase enzyme	Improve circulation time and decreased immunogenicity	Severe combined immunodeficiency disease (SCID)	1990
Cimzia [®] /certolizumab pegol (UCB)	PEGylated antibody fragment (Certolizumab)	Improved circulation time and greater stability <i>in vivo</i> .	Crohn's disease Rheumatoid arthritis Psoriatic Arthritis Ankylosing Spondylitis Multiple Sclerosis (MS)	2008 2009 2013 2013 1996
Copaxone [®] /Glatopa (Teva)	Random copolymer of L-glutamate, L-alanine, L-lysine and L-tyrosine	Large amino-acid based polymer with controlled molecular weight and clearance characteristics		
Eligard [®] (Tolmar)	Leuprolide acetate and polymer (PLGH (poly (DL-Lactide-co-glycolide)))	Controlled delivery of payload with longer circulation time	Prostate Cancer	2002
Macugen [®] /Pegaptanib (Bausch & Lomb)	PEGylated anti-VEGF aptamer (vascular endothelial growth factor) aptamer	Improved stability of aptamer as a result of PEGylation	Macular degeneration, neovascular age-related	2004
Mircera [®] /Methoxy polyethylene glycol-epoetin beta (Hoffman-La Roche)	Chemically synthesized ESA (erythropoiesis-stimulating agent)	Improved stability of aptamer as a result of PEGylation	Anemia associated with chronic kidney disease	2007
Neulasta [®] /pegfilgrastim (Amgen)	PEGylated GCSF protein	Improved stability of protein through PEGylation	Neutropenia, Chemotherapy induced	2002
Pegasys [®] (Genentech)	PEGylated IFN alpha-2a protein	Improved stability of protein through PEGylation	Hepatitis B; Hepatitis C	2002
PegIntron [®] (Merck)	PEGylated IFN alpha-2b protein	Improved stability of protein through PEGylation	Hepatitis C	2001
Renagel [®] [sevelamer hydrochloride]/Renagel [®] [sevelamer carbonate] (Sanofi)	Poly(allylamine hydrochloride)	Increase circulation and therapeutic delivery	Chronic kidney disease	2000
Somavert [®] /pegvisomant (Pfizer)	PEGylated HGH receptor antagonist	Improved stability of protein through PEGylation	Acromegaly	2003
Oncaspar [®] /pegaspargase (Enzon Pharmaceuticals)	Polymer-protein conjugate (PEGylated L-asparaginase)	Improved stability of protein through PEGylation	Acute lymphoblastic leukemia	1994
Krystexxa [®] /pegloticase (Horizon)	Polymer-protein conjugate (PEGylated porcine-like uricase)	Improved stability of protein through PEGylation; introduction of unique mammalian protein	Chronic gout	2010
Plegridy [®] (Biogen)	Polymer-protein conjugate (PEGylated IFN beta-1a)	Improved stability of protein through PEGylation	Multiple Sclerosis	2014
ADYNOVATE (Baxalta)	Polymer-protein conjugate (PEGylated factor VIII)	Improved stability of protein through PEGylation	Hemophilia	2015
Liposome formulations combined with drugs or biologics				
DaunoXome [®] (Galen)	Liposomal Daunorubicin	Increased delivery to tumour site; lower systemic toxicity arising from side-effects	Karposi's Sarcoma	1996
DepoCyt [®] (Sigma-Tau)	Liposomal Cytarabine	Increased delivery to tumour site; lower systemic toxicity arising from side-effects	Lymphomatous meningitis	1996
Marqibo [®] (Onco TCS)	Liposomal Vincristine	Increased delivery to tumour site; lower systemic toxicity arising from side-effects	Acute Lymphoblastic Leukemia	2012
Onivyde [®] (Merrimack)	Liposomal Irinotecan	Increased delivery to tumour site; lower systemic toxicity arising from side-effects	Pancreatic Cancer	2015
AmBisome [®] (Gilead Sciences)	Liposomal Amphotericin B	Reduced nephrotoxicity	Fungal/protozoal infections	1997
Visudyne [®] (Bausch and Lomb)	Liposomal Morphine sulfate Liposomal Verteporfin	Extended release Increased delivery to site of diseased vessels; photosensitive release	Analgesia (post-operative) Macular degeneration, wet age-related; myopia; ocular histoplasmosis	2004 2000
Doxil [®] /Caelyx [™] (Janssen)	Liposomal doxorubicin	Improved delivery to site of disease; decrease in systemic toxicity of free drug.	Karposi's Sarcoma; Ovarian cancer; multiple myeloma	1995 2005 2008
Abelcet [®] (Sigma-tau)	Liposomal Amphotericin B lipid complex	Reduced toxicity	Fungal infections	1995
Curosurf [®] /Poractant alpha (Chiesi farmaceutici)	Liposome-proteins SP-B and SP-C	Increased delivery for smaller volume; reduced doxicity	pulmonary surfactant for Respiratory Distress Syndrome	1999
Micellar nanoparticles combined with drugs or biologics				
Estrasorb [™] (Novavax)	Micellar Estradiol	Controlled delivery of	Menopausal therapy	2003

(continued on next page)

Table 5 (continued)

Name	Material description	Nanoparticle advantage	Indication(s)	Year(s) approved
therapeutic				
Protein nanoparticles combined with drugs or biologics				
Abraxane [®] /ABI-007 (Celgene)	Albumin-bound paclitaxel nanoparticles	Improved solubility; improved delivery to tumour	Breast cancer NSCLC Pancreatic cancer	2005 2012 2013
Ontak [®] (Eisai Inc)	Engineered Protein combining IL-2 and diphtheria toxin	Targeted T-cell specificity; lysosomal escape	Cutaneous T-Cell Lymphoma	1999
Nanocrystals				
Emend [®] (Merck)	Aprepitant	Surface area allows faster absorption and increases bioavailability	Antiemetic	2003
Tricor [®] (Lupin Atlantis)	Fenofibrate	Increases bioavailability simplifies administration	Hyperlipidemia	2004
Rapamune [®] (Wyeth Pharmaceuticals)	Sirolimus	Increased bioavailability	Immunosuppressant	2000
Megace ES [®] (Par Pharmaceuticals)	Megestrol acetate	Reduced dosing	Anti-anorexic	2001
Avinza [®] (Pfizer)	Morphine sulfate	Increased drug loading and bioavailability; extended release	Psychostimulant	2002 (2015)
Focalin XR [®] (Novartis)	Dexamethyl-phenidate HCl	Increased drug loading and bioavailability	Psychostimulant	2005
Ritalin LA [®] (Novartis)	Methylphenidate HCl	Increased drug loading and bioavailability	Psychostimulant	2002
Zanaflex [®] (Acorda)	Tizanidine HCl	Increased drug loading and bioavailability	Muscle relaxant	2002
Vitoss [®] (Stryker)	Calcium phosphate	Mimics bone structure allowing cell adhesion and growth	Bone substitute	2003
Ostim [®] (Heraeus Kulzer)	Hydroxyapatite	Mimics bone structure allowing cell adhesion and growth	Bone substitute	2004
OsSatura [®] (IsoTis Orthobiologics)	Hydroxyapatite	Mimics bone structure allowing cell adhesion and growth	Bone substitute	2003
NanOss [®] (Rti Surgical)	Hydroxyapatite	Mimics bone structure allowing cell adhesion and growth	Bone substitute	2005
EquivaBone [®] (Zimmer Biomet)	Hydroxyapatite	Mimics bone structure	Bone substitute	2009
Invega [®] Sustenna [®] (Janssen Pharms)	Paliperidone Palmitate	Allows slow release of injectable low solubility drug	Schizophrenia Schizoaffective Disorder	2009 2014
Ryanodex [®] (Eagle Pharmaceuticals)	Dantrolene sodium	Faster administration at higher doses	Malignant hyperthermia	2014
Inorganic and metallic nanoparticles				
Nanotherm [®] (MagForce)	Iron oxide	Allows cell uptake and introduces superparamagnetism	Glioblastoma	2010
Feraheme™/ferumoxytol (AMAG pharmaceuticals)	Ferumoxytol SPION with polyglucose sorbitol carboxymethylether Iron sucrose	Magnetite suspension allows for prolonged steady release, decreasing number of doses Allows increased dose	Deficiency anemia iron deficiency in chronic kidney disease (CKD)	2009 2000
Venofer [®] (Luitpold Pharmaceuticals)	Sodium ferric gluconate	Allows increased dose	iron deficiency in chronic kidney disease (CKD)	1999
INFeD [®] (Sanofi Avertis)	Iron dextran (low MW)	Allows increased dose	iron deficiency in chronic kidney disease (CKD)	1957
DexIron [®] /Dexferrum [®] (Sanofi Avertis)	Iron dextran (high MW)	Allows increased dose	iron deficiency in chronic kidney disease (CKD)	1957
Feridex [®] /Endorem [®] (AMAG pharmaceuticals)	SPION coated with dextran	Superparamagnetic character	Imaging agent	1996 (2008)
GastroMARK™; umirem [®] (AMAG Pharmaceuticals)	SPION coated with silicone	Superparamagnetic character	Imaging agent	2001 (2009)

biological activity [132]. This study showed another approach of conjugation which utilises the potency of the AgNP together with the AMP and this provides new insights of AgNP-AMP interactions and how this strategy could be used to enhance biological activity. Gold nanoparticles (AuNPs), which are synthesized by the reduction of HAuCl₄, have lower toxicity than other nanoparticles due to their noble characteristics [199]. AuNPs-AMP conjugates also possess several advantages, such as protecting the AMP from enzymatic degradation, and do not prevent the AMP from folding into its biologically active conformation [200]. In a study by Casciaro et al. (2016), the AMP Esculentin-1a(1–21)NH₂, which was derived from a frog skin, was coated with

gold nanoparticles and evaluated against *P. aeruginosa*. The anti-bacterial results showed that the AMP coated nanoparticles were more potent than the free peptide [201]. In contrast to the studies above, Rai et al. (2016) used a one-step synthesis approach to conjugate the AMP, cecropin-melittin, to gold nanoparticles. The MIC values were also found to be higher than the free AMP [90]. Pradeepa et al. (2017) conducted a study on the application of Nisin gold nanoparticles as a potent antimicrobial agent against *E. faecalis* and *S. aureus*. The synthesized nanoparticles were found to be non-toxic with less hemolytic activity and lower MIC values than Nisin alone [202].

These strategies of utilising AMPs to reduce silver nitrate to form

AgNPs, or conjugating AMPs to AgNPs or AuNPs, combines the high surface charge of these metallic nanoparticles together with the high positive charge of AMPs, which will form a molecule well capable of bacterial membrane lysis [203].

7.5. Hydrogel nanoparticles

Hydrogels are 3-dimensional, cross-linked networks of water-soluble polymers that can be formulated by various approaches, including microparticles, slabs, coatings, films and more specifically, nanoparticles [204]. Hydrogels are used in a wide array of applications, such as in cellular immobilization, tissue engineering and regenerative medicine [205]. The physicochemical makeup of hydrogels has generated much interest for their use as drug delivery systems. They have a highly porous structural makeup, this feature being important, as it allows drug loading into the matrix of the gel and consequent drug release [204,206]. Hydrogel nanoparticle in drug delivery offer mostly pharmacokinetic benefits, as their formulations allow drugs to be slowly eluted, thus retaining a high concentration of the drug in the nearby tissues over a prolonged period of time [207]. Hydrogels are also thought to possess high biocompatible properties due to their high-water content, and their physicochemical resemblance to the native extracellular matrix [208]. Various materials have been exploited so far for the preparation of hydrogels with AMPs to target different organisms. Rajan et al. (2014) designed a study for the controlled release of the AMP subtilisin from polyethylene glycol-based hydrogels, and showed that it was able to inhibit the growth of *G. vaginalis*, with a reduction of 8 log₁₀ CFU/ml [209]. Håkansson et al. (2014) reported on the formulation of the AMP PLX150 in hydroxypropyl cellulose gel (HPC) to target surgical site infections. The PLX150-HPC combination killed more than 95% of *S. aureus*, and presented a dose-dependent activity with a slow release of the AMP from the HPC hydrogel on the wound site [210]. In a study by Babavalian et al. (2015), the AMP CM11 was incorporated into alginate sulfate hydrogels to target MRSA. The MIC and MBC activity of the CM11 peptide were 2–32 mg/L and 16–64 mg/L respectively, and 50% of the CM11 peptide was released from the hydrogel in the first week [211]. Since hydrogel formulations allow sustained release of drugs, incorporation of AMPs into these systems would offer prolonged AMP release at target sites and retain high AMP concentration in the nearby tissues.

Nanocarriers have shown to increase the biocompatibility of AMPs, shield them from degradative enzymes as well as allowing enhancing their release into specific target sites. These nano drug delivery systems should be exploited further for AMP conjugates, with the aim of improving targeted conjugate delivery into intracellular targets and developing plausible nanomedicines. Table 5 reveals a list of FDA approved nano products derived from various materials [212].

8. Conclusions and future perspectives

The continuous evolution of pathogenic bacteria has led to an ongoing search for novel ways to combat antimicrobial drug resistance. The development of resistance to new antibiotic derivatives, and the inability of antibiotics to reach infection sites at effective concentration, pose a major threat to infection control and prevention. However, new approaches, such as the design and application of AMPs, individually or as conjugates and their delivery in nano-carriers, offer promising alternatives to main-stream antibiotics.

Molecular dynamics of AMPs with model membranes and QSAR approaches to identify or understand descriptors in AMPs for activity is important for the eventual design of novel AMPs including their conjugates and nano delivery systems to achieve optimal efficacy and safety. Molecular dynamic studies have been useful in confirming the successful penetration of AMPs across different types of cell membranes. It has also identified key interactions of AMPs with membrane components for penetration. Molecular dynamic studies have been

further successfully exploited for understanding the stability of AMPs with conjugates as well as their stability and encapsulation into nano-carriers. QSAR approaches on AMPs to date have identified the possible structural or physicochemical descriptors integral in influencing activity against bacteria. However, a considerable gap remains in utilising molecular modelling approaches to study the AMP interaction with model membranes. Structure activity relationship of AMPs with respect to membrane penetration is also lacking. Although limited, the findings so far can guide scientists to: 1) design new AMPs with optimal activity 2) select specific sites for conjugation to various compounds without losing their activity and 3) design and select suitable nanocarriers based on the physicochemical descriptors of the AMPs identified. Whilst understanding penetration of the AMPs through membranes is important, the interaction of AMPs as well as AMP-conjugates with intracellular organelles is also critical because it can elucidate the effectiveness of the AMP and AMP-conjugate strategy in being delivered across the membrane for action on intracellular targets to maximise activity. Since much of the MD and QSAR studies so far have focused on the interaction of AMPs with biological membranes, future studies should therefore explore the mechanism of action of the AMPs and their conjugates with intracellular targets such as the nucleus and mitochondria. Whilst computational modelling of nano carriers with AMPs are beginning to emerge, it needs to be extended further to AMP-conjugates in nano-carriers. Molecular modelling studies should be used to identify formulations that can maximise encapsulation and stability of the nano-carriers and also mechanistically explain their formation and release kinetics. MD simulations should be further explored in order to investigate the binding affinities of AMPs with their conjugates. We believe that these MD mechanistic studies will also elucidate the extent of encapsulation with respect to AMP-conjugates in nano systems to further tell us the best nano carrier which can be used to deliver these conjugates.

In this review the potential of AMP as conjugates with antibiotics, polymers and other classes such as DNA, salts and phenolic based compounds to potentiate antibacterial activity have been successfully demonstrated. Of the 4 groups of AMPs i.e. β -sheet, α -helical, loop and extended peptides the α -helical classes have been the most widely studied structural groups of AMPs used for conjugation to various classes of materials. The widely used AMPs used for conjugation are the indolicidin and they were found to have potency across both gram positive and negative bacteria. It is suggested that other classes of materials such as natural compounds from plant extracts and metal complexes could also be potential conjugate components and should be explored. With the conjugation strategy only preliminary characterisation studies such as structural confirmation, *in vitro* antimicrobial activity, cytotoxicity and haemolytic studies, cellular uptake have been reported. Further characterisation studies such as *in vivo* assays and skin lesion studies is required to confirm the efficacy and safety of these conjugates. Further, patient administration of the AMP-conjugates will require its incorporation into a suitable delivery system. Therefore, extensive physicochemical and *in vitro/in vivo* characterisation of drug delivery systems for AMP-conjugates need to be undertaken. Degradation studies of AMP-conjugates as they enter the bacterial membrane should also be conducted, as this will allow for structural manipulation in the design process, and the application of additive factors directed at degradative enzymes. This would greatly enhance the applications of AMPs and broaden their scope in finding therapeutic agents.

Encapsulation of AMPs into five different classes of nano carriers i.e. liposomes, micelles, nanofibers, metallic nanoparticles and hydrogels so far have been successfully achieved with enhanced activity and sustained release. The α -helical group of AMPs only have so far been explored for delivery via nano carriers. However, again these studies are limited in their characterisation which is essential to ensure safety, quality and efficacy for regulatory approval. Future studies should clearly focus on experimental designs to rationally optimise

formulations. Also, in depth characterisation studies to determine the solid phase transformation properties, release kinetics, physicochemical stability, cell uptake mechanisms and *in vivo* efficacy and toxicity testing in animal models should be performed. In addition to encapsulation of the free AMPs into conventional lipid or polymer nanocarriers, the strategy of incorporating the AMP as a structural component of a lipid or polymer which then self assembles to form a nano-system can also be a novel alternative.

The interest in AMPs as therapeutic agents has gained much interest recently, with studies having shown that more than 60 AMPs have reached the market, with some undergoing clinical trials [213], and many having distinguished themselves to be the new front runners in antimicrobial drug development. The current emerging data on AMP-conjugates and nano-delivery of AMPs further demonstrate their potential to be highly effective and advantageous in treating patients suffering with bacterial infections of both susceptible and resistant nature. Collaborations amongst a highly multidisciplinary team of researchers is therefore highly warranted to realise the future commercialisation of AMP-conjugates and AMP nano delivery systems.

Based on the approaches stated in this review, which utilises various strategies in AMP development, it is envisaged that in the next decade we can expect a rise in AMP based antibiotics that will have the ability to circumvent drug resistance. Owing to the emergence of AMP conjugation to various compounds, we believe that AMP development will go beyond the scope of targeting pathogenic bacteria. As natural AMPs possess immunomodulatory functions, we believe that future studies will focus on molecular mimicry by AMPs for T-cell activation, as well as the nano delivery of AMP conjugates to release them to specific immune cells for enhanced immunity.

Collaborations amongst a highly multidisciplinary team of researchers is therefore highly warranted to realise the future commercialisation of AMP-conjugates and AMP nano delivery systems.

Declaration of interest sections

The author reports that there is no conflict of interest on this paper.

Acknowledgement

The authors acknowledge the National Research Foundation (NRF, Grant No. 87790) of South Africa, UKZN College of Health Sciences and UKZN Nanotechnology Platform (Grant No. 88453) for their financial support.

References

- [1] D. Weatherall, B. Greenwood, H.L. Chee, Science and technology for disease control: past, present, and future, in: D.T. Jamison, J.G. Breman (Eds.), *Disease Control Priorities in Developing Countries*, second ed., World Bank, Washington (DC), 2006 (Chapter 5).
- [2] S.S. Morse, Emerging Infections: Condemned to Repeat? Institute of Medicine of the National Academies, 2009, pp. 195–208, <http://dx.doi.org/10.1073/pnas.0703993104>.
- [3] A.S. Fauci, N.A. Touchette, G.K. Folkers, Emerging infectious diseases: a 10-year perspective from the national institute of allergy and infectious diseases, *Emerg. Infect. Dis.* 11 (2005) 519–525, <http://dx.doi.org/10.3201/eid1104.041167>.
- [4] D.M. Morens, G.K. Folkers, A.S. Fauci, The challenge of emerging and re-emerging infectious diseases, *Nature* 430 (2004) 242–249, <http://dx.doi.org/10.1038/nature02759>.
- [5] K.E. Jones, N.G. Patel, M.A. Levy, A. Storeygard, D. Balk, J.L. Gittleman, P. Daszak, Global trends in emerging infectious diseases, *Nat. Lett.* 451 (2008) 990–994, <http://dx.doi.org/10.1038/nature06536>.
- [6] R.J. Coker, B.M. Hunter, J.W. Rudge, M. Liverani, P. Hanvoravongchai, Emerging infectious diseases in southeast Asia: regional challenges to control, *Lancet* 377 (2011) 599–609, [http://dx.doi.org/10.1016/S0140-6736\(10\)62004-1](http://dx.doi.org/10.1016/S0140-6736(10)62004-1).
- [7] A.A. Aguirre, G.M. Tabor, Global factors driving emerging infectious diseases: impact on wildlife populations, *Ann. N. Y. Acad. Sci.* 1149 (2008) 1–3, <http://dx.doi.org/10.1196/annals.1428.052>.
- [8] F.J. Burt, M.S. Rolph, N.E. Rulli, S. Mahalingam, M.T. Heise, Chikungunya: a re-emerging virus, *Lancet* 379 (2012) 662–671, [http://dx.doi.org/10.1016/S0140-6736\(11\)60281-X](http://dx.doi.org/10.1016/S0140-6736(11)60281-X).
- [9] S.L. Stramer, Current perspectives in transfusion-transmitted infectious diseases: emerging and re-emerging infections, *ISBT Sci. Ser.* 9 (2013) 30–36, <http://dx.doi.org/10.1111/voxs.12070>.
- [10] R. Rosenberg, Threat from emerging vectorborne viruses, *Emerg. Infect. Dis.* 22 (2016) 910–911, <http://dx.doi.org/10.3201/eid2205.160284>.
- [11] K.H. Jacobsen, A. Alonso Aguirre, C.L. Bailey, A.V. Baranova, A.T. Crooks, A. Croitoru, P.L. Delamater, J. Gupta, K. Kehn-Hall, A. Narayanan, M. Pierobon, K.E. Rowan, J. Reid Schwebach, P. Seshaiyer, D.M. Sklarew, A. Stefanidis, P. Agouris, Lessons from the ebola outbreak: action items for emerging infectious disease preparedness and response, *EcoHealth* 13 (2016) 200–212, <http://dx.doi.org/10.1007/s10393-016-1100-5>.
- [12] D.J. Weber, W.A. Rutala, W.A. Fischer, H. Kanamori, E.E. Sickbert-Bennett, Emerging infectious diseases: focus on infection control issues for novel coronaviruses (Severe Acute Respiratory Syndrome-CoV and Middle East Respiratory Syndrome-CoV), hemorrhagic fever viruses (Lassa and Ebola), and highly pathogenic avian influenza vi, *Am. J. Infect. Contr.* 44 (2016) 91–100, <http://dx.doi.org/10.1016/j.ajic.2015.11.018>.
- [13] J. Davies, D. Davies, Origins and evolution of antibiotic resistance, *Microbiol. Mol. Biol. Rev.* 74 (2010) 417–433, <http://dx.doi.org/10.1128/MMBR.00016-10>.
- [14] F.C. Tenover, Mechanisms of antimicrobial resistance in bacteria, *Am. J. Infect. Contr.* 34 (2006) 3–10, <http://dx.doi.org/10.1016/j.ajic.2006.05.219>.
- [15] M.A. Kohanski, D.J. Dwyer, J.J. Collins, How antibiotics kill bacteria: from targets to networks, *Nat. Rev. Microbiol.* 8 (2010) 423–435, <http://dx.doi.org/10.1038/nrmicro2333>.
- [16] S. Gupta, D. Govil, P.N. Kakar, O. Prakash, D. Arora, S. Das, P. Govil, A. Malhotra, Colistin and polymyxin B: a re-emergence, *Indian J. Crit. Care Med.* 13 (2014) 49–53, <http://dx.doi.org/10.4103/0972-5229.56048>.
- [17] H.C. Neu, T.D. Gootz, Antimicrobial chemotherapy biochemical basis of antimicrobial action inhibition of bacterial cell wall synthesis, in: S. Baron (Ed.), *Medical Microbiology*, fourth ed., University of Texas Medical Branch at Galveston, Galveston (TX), 1996.
- [18] R.J. Fair, Y. Tor, Perspectives in Medicinal Chemistry Antibiotics and Bacterial Resistance in the 21st Century, (2014), pp. 25–64, <http://dx.doi.org/10.4137/PMC.S14459>.
- [19] T. Burroughs, M. Najafi, S.M. Lemon, S.L. Knobler, The Resistance Phenomenon in Microbes and Infectious Disease Vectors: Implications for Human Health and Strategies for Containment: Workshop Summary, National Academies Press (US), Washington (DC), 2003, <http://dx.doi.org/10.17226/10651>.
- [20] Henry F. Chambers, Frank R. DeLeo, Waves of resistance: *Staphylococcus aureus* in the antibiotic era, *Nat. Rev. Microbiol.* 9 (2009) 629–641, <http://dx.doi.org/10.1038/nrmicro2200>.
- [21] S. Sengupta, M.K. Chattopadhyay, H.P. Grossart, The multifaceted roles of antibiotics and antibiotic resistance in nature, *Front. Microbiol.* 4 (2013) 1–13, <http://dx.doi.org/10.3389/fmicb.2013.00047>.
- [22] J.H. Levison, M.E. Levison, Pharmacokinetics and pharmacodynamics of antibacterial agents, *Infect Dis Clin North Am.* 23 (2009) 791–819, <http://dx.doi.org/10.1016/j.idc.2009.06.008>.Pharmacokinetics.
- [23] P. Gao, X. Nie, M. Zou, Y. Shi, G. Cheng, Recent advances in materials for extended-release antibiotic delivery system, *J. Antibiot.* 64 (2011) 625–634, <http://dx.doi.org/10.1038/ja.2011.58>.
- [24] G. Cheng, H. Hao, S. Xie, X. Wang, M. Dai, L. Huang, Z. Yuan, Antibiotic alternatives: the substitution of antibiotics in animal husbandry, *Front. Microbiol.* 5 (2014) 1–15, <http://dx.doi.org/10.3389/fmicb.2014.00217>.
- [25] A.Y. Hwang, J.G. Gums, The emergence and evolution of antimicrobial resistance: impact on a global scale, *Bioorg. Med. Chem.* 24 (2016) 1–6, <http://dx.doi.org/10.1016/j.bmc.2016.04.027>.
- [26] WHO, Antibiotic Resistance, WHO, 2017 2017 (accessed October 2017) <http://www.who.int/mediacentre/factsheets/antibiotic-resistance/en/>.
- [27] S. Shaikh, J. Fatima, S. Shakil, S.M.D. Rizvi, M.A. Kamal, Antibiotic resistance and extended spectrum beta-lactamases: types, epidemiology and treatment, *Saudi J. Biol. Sci.* 22 (2015) 90–101, <http://dx.doi.org/10.1016/j.sjbs.2014.08.002>.
- [28] R. Laxminarayan, Z. A. Bhutta, A. Duse, T.O. Brien, I.N. Okeke, A. Pablo-mendez, K.P. Klugman, Drug resistance, in: D.T. Jamison, J.G. Breman, A.R. Measham, et al. (Eds.), *Disease Control Priorities in Developing Countries*, second ed., Oxford University Press, Washington (DC), 2006The International Bank for Reconstruction and Development/The World Bank; New York. (Chapter 55).
- [29] M.A. Webber, L.J.V. Piddock, The importance of efflux pumps in bacterial antibiotic resistance, *J. Antimicrob. Chemother.* 51 (2003) 9–11, <http://dx.doi.org/10.1093/jac/dkg050>.
- [30] A. Tatem, D. Rogers, Global transport networks and infectious disease spread, *Adv. Parasitol.* 62 (2006) 293–343, [http://dx.doi.org/10.1016/S0065-308X\(05\)62009-X](http://dx.doi.org/10.1016/S0065-308X(05)62009-X).Global.
- [31] Charles J. Sih, *Pharmaceutical Microbiology*, M. Harris. Bailliere, Tindall & Cox Ltd., 7-8 Henrietta St, London, WC 2, England, 1964 US Agent: The Williams & Wilkins Co., Baltimore 2, Md. 269 pp. *Journal of Pharmaceutical Sciences* 54.1 (1965): 167–168.
- [32] P. Mendez-Samperio, Peptidomimetics as a new generation of antimicrobial agents: current progress, *Infect. Drug Resist.* 7 (2014) 229–237, <http://dx.doi.org/10.2147/IDR.S49229>.
- [33] B. Mishra, G.D. Leishangthem, K. Gill, A.K. Singh, S. Das, K. Singh, I. Kess, A. Dinda, A. Kapil, I.K. Patro, S. Dey, A novel antimicrobial peptide derived from modified N-terminal domain of bovine lactoferrin: design, synthesis, activity against multidrug-resistant bacteria and *Candida*, *Biochim. Biophys. Acta Biomembr.* 1828 (2013) 677–686, <http://dx.doi.org/10.1016/j.bbmem.2012.09.021>.
- [34] G.D. Wright, Q&A: antibiotic resistance: where does it come from and what can we

- do about it? *BMC Biol.* 8 (2010) 123, <http://dx.doi.org/10.1186/1741-7007-8-123>.
- [35] Y.J. Gordon, E.G. Romanowski, A.M. McDermott, A review of antimicrobial peptides and their therapeutic potential as anti-infective drugs, *Curr. Eye Res.* 30 (2005) 505–515, <http://dx.doi.org/10.1080/02713680590968637>.
- [36] S.H. Marshall, G. Arenas, Antimicrobial peptides: a natural alternative to chemical antibiotics and potential for applied biotechnology, *Electron. J. Biotechnol.* 6 (2003) 96–109, <http://dx.doi.org/10.2225/vol6-issue3-fulltext-1>.
- [37] J.M. Ageitos, A. Sánchez-Pérez, P. Calo-Mata, T.G. Villa, Antimicrobial peptides (AMPs): ancient compounds that represent novel weapons in the fight against bacteria, *Biochem. Pharmacol.* (2016), <http://dx.doi.org/10.1016/j.bcp.2016.09.018>.
- [38] T. Nakatsuji, R.L. Gallo, Antimicrobial peptides: old molecules with new ideas, *J. Invest. Dermatol.* 132 (2012) 887–895, <http://dx.doi.org/10.1038/jid.2011.387>.
- [39] D.A. Phoenix, S.R. Dennison, F. Harris, Antimicrobial peptides: their history, evolution, and functional promiscuity, *Antimicrob. Pept.* (2013) 1–37, <http://dx.doi.org/10.1002/9783527652853.ch1>.
- [40] F. Hu, Q. Wu, S. Song, R. She, Y. Zhao, Y. Yang, M. Zhang, F. Du, Antimicrobial activity and safety evaluation of peptides isolated from the hemoglobin of chickens, *BMC Microbiol.* (2016) 1–10, <http://dx.doi.org/10.1186/s12866-016-0904-3>.
- [41] H. Sato, J.B. Feix, Peptide-membrane interactions and mechanisms of membrane destruction by amphipathic alpha-helical antimicrobial peptides, *Biochim. Biophys. Acta Biomembr.* 1758 (2006) 1245–1256, <http://dx.doi.org/10.1016/j.bbame.2006.02.021>.
- [42] P. Perumal, V.P. Pandey, Antimicrobial peptides: the role of hydrophobicity in the alpha helical structure, *J. Pharm. Pharmacogn. Res.* 1 (2013) 39–53.
- [43] D. Eisenberg, The discovery of the alpha-helix and beta-sheet, the principal structural features of proteins, *Proc. Natl. Acad. Sci. U.S.A.* 100 (2003) 11207–11210, <http://dx.doi.org/10.1073/pnas.2034522100>.
- [44] T.I. Al-Warhi, H.M.A. Al-Hazimi, A. El-Faham, Recent development in peptide coupling reagents, *J. Saudi Chem. Soc.* 16 (2012) 97–116, <http://dx.doi.org/10.1016/j.jscs.2010.12.006>.
- [45] A. Reinhardt, I. Neundorff, Design and application of antimicrobial peptide conjugates, *Int. J. Mol. Sci.* 17 (2016) 701, <http://dx.doi.org/10.3390/ijms17050701>.
- [46] F. Guilhaumeli, N. Vilela, P. Albuquerque, L. da S. Derengowski, I. Silva-Pereira, C.M. Kyaw, Antibiotic development challenges: the various mechanisms of action of antimicrobial peptides and of bacterial resistance, *Front. Microbiol.* 4 (2013) 1–12, <http://dx.doi.org/10.3389/fmicb.2013.00353>.
- [47] W. Aoki, M. Ueda, Characterization of antimicrobial peptides toward the development of novel antibiotics, *Pharmaceuticals* 6 (2013) 1055–1081, <http://dx.doi.org/10.3390/ph6081055>.
- [48] M. Bagheri, Cationic antimicrobial peptides (AMPs): thermodynamic characterization of peptide-lipid interactions and biological efficacy of surface-tethered peptides, *ChemistryOpen* (2015) 389–393, <http://dx.doi.org/10.1002/open.201402149>.
- [49] Y. Shai, Mode of action of membrane active antimicrobial peptides, *Biopolym. Pept. Sci. Sect* 66 (2002) 236–248, <http://dx.doi.org/10.1002/bip.10260>.
- [50] S.T. Henriques, M.N. Melo, M.A.R.B. Castanho, Cell-penetrating peptides and antimicrobial peptides: how different are they? *Biochem. J.* 399 (2006) 1–7, <http://dx.doi.org/10.1042/BJ20061100>.
- [51] G.N. Tew, D. Clements, H. Tang, L. Arnt, R.W. Scott, Antimicrobial activity of an abiotic host defense peptide mimic, *Biochim. Biophys. Acta Biomembr.* 1758 (2006) 1387–1392, <http://dx.doi.org/10.1016/j.bbame.2006.03.001>.
- [52] U. Wnorowska, K. Niemirowicz, M. Myint, S.L. Diamond, M. Wroblewska, P.B. Savage, P.A. Janmey, R. Bucki, Bactericidal activity of cathelicidin LL-37 and select cationic lipids against the hypervirulent *P. aeruginosa* strain LESB58, *Antimicrob. Agents Chemother.* 59 (2015) 3808–3815, <http://dx.doi.org/10.1128/AAC.00421-15>.
- [53] X. Wu, A.K. Singh, X. Wu, Y. Lyu, A.K. Bhunia, G. Narsimhan, Characterization of antimicrobial activity against *Listeria* and cytotoxicity of native melittin and its mutant variants, *Coll. Surf. B Biointerf.* 143 (2016) 194–205, <http://dx.doi.org/10.1016/j.colsurfb.2016.03.037>.
- [54] K. Midura-Nowaczek, A. Markowska, A. Peptides, Antimicrobial peptides and their analogs: searching for new potential therapeutics, *Perspect. Medicin. Chem.* 6 (2014) 73–80, <http://dx.doi.org/10.4137/PMC.S13215>.
- [55] K. Fosgerau, T. Hoffmann, Peptide therapeutics: current status and future directions, *Drug Discov. Today* 20 (2015) 122–128, <http://dx.doi.org/10.1016/j.drudis.2014.10.003>.
- [56] J.X. Huang, S.L. Bishop-Hurley, M.A. Cooper, Development of anti-infectives using phage display: biological agents against bacteria, viruses, and parasites, *Antimicrob. Agents Chemother.* 56 (2012) 4569–4582, <http://dx.doi.org/10.1128/AAC.00567-12>.
- [57] K. Fosgerau, T. Hoffmann, Peptide therapeutics: current status and future directions, *Drug Discov. Today* 20 (2015) 122–128.
- [58] L. Otvos, J.D. Wade, Current challenges in peptide-based drug discovery, *Front. Chem.* 2 (2014) 8–11, <http://dx.doi.org/10.3389/fchem.2014.00062>.
- [59] X. Ding, J. Boney-montoya, B.M. Owen, A.L. Bookout, C. Coate, D.J. Mangelsdorf, S.A. Kliewer, β Klotho is required for fibroblast growth factor 21 effects on growth and metabolism, *Cell Metab.* 16 (2013) 387–393, <http://dx.doi.org/10.1016/j.cmet.2012.08.002>.
- [60] J.C. Lainson, M.F. Fuenmayor, S.A. Johnston, C.W. Diehnelt, Conjugation approach to produce a *Staphylococcus aureus* synbody with activity in serum, *Bioconj. Chem.* 26 (2015) 2125–2132, <http://dx.doi.org/10.1021/acs.bioconjchem.5b00420>.
- [61] P. Nicolas, Multifunctional host defense peptides: intracellular-targeting antimicrobial peptides, *FEBS J.* 276 (2009) 6483–6496, <http://dx.doi.org/10.1111/j.1742-4658.2009.07359.x>.
- [62] V. Castelletto, G.E.N.Z. Zhu, I.W. Hamley, Self-assembly of pegylated peptide conjugates containing a modified amyloid β -peptide fragment, 26 (2010) 9986–9996, <http://dx.doi.org/10.1021/la100110f>.
- [63] M. Sobczak, C. Debek, E. Oledzka, R. Kozłowski, Polymeric systems of antimicrobial peptides-strategies and potential applications, *Molecules* 18 (2013) 14122–14137, <http://dx.doi.org/10.3390/molecules181114122>.
- [64] A. Patel, A.K. Mitra, Recent developments in protein and peptide parenteral delivery approaches, *Ther. Deliv.* 3 (2014) 337–365, <http://dx.doi.org/10.4155/tde.14.5>.
- [65] J. Renukuntla, A.D. Vadlapudi, A. Patel, S.H. Boddu, A.K. Mitra, Approaches for enhancing oral bioavailability of peptides and proteins, *Int. J. Pharm.* 447 (2013) 75–93, <http://dx.doi.org/10.1016/j.ijpharm.2013.02.030>.
- [66] D.I. Andersson, D. Hughes, Mechanisms and consequences of bacterial resistance to antimicrobial peptides, *Drug Resist. Updates* 26 (2016) 43–57, <http://dx.doi.org/10.1016/j.drug.2016.04.002>.
- [67] S. Maria-Neto, K.C. de Almeida, M.L.R. Macedo, O.L. Franco, Understanding bacterial resistance to antimicrobial peptides: from the surface to deep inside, *Biochim. Biophys. Acta* 1848 (2015) 3078–3088, <http://dx.doi.org/10.1016/j.bbame.2015.02.017>.
- [68] G. Yu, D. Baeder, R. Regoes, J. Rolff, Predicting drug resistance evolution: antimicrobial peptides Vs. Antibiotics, *bioRxiv* (2017) 138107, <https://doi.org/10.1101/138107>.
- [69] M. Kovalainen, J. Mönkäre, J. Riikonen, U. Pesonen, M. Vlasova, J. Salonen, Novel delivery systems for improving the clinical use of peptides, *Pharmacol. Rev.* (2015) 541–561.
- [70] S. Gelperina, K. Kisich, M.D. Iseman, L. Heifets, The potential advantages of nanoparticle drug delivery systems in chemotherapy of tuberculosis, *Am. J. Respir. Crit. Care Med.* 172 (2005) 1487–1490, <http://dx.doi.org/10.1164/rccm.200504-613PP>.
- [71] R.Y. Pelgrift, A.J. Friedman, Nanotechnology as a therapeutic tool to combat microbial resistance, *Adv. Drug Deliv. Rev.* 65 (2013) 1803–1815, <http://dx.doi.org/10.1016/j.addr.2013.07.011>.
- [72] B.D. Brooks, A.E. Brooks, Therapeutic strategies to combat antibiotic resistance, *Adv. Drug Deliv. Rev.* 78 (2014) 14–27, <http://dx.doi.org/10.1016/j.addr.2014.10.027>.
- [73] D.A. Phoenix, S.R. Dennison, F. Harris, Anionic antimicrobial peptides, *Antimicrobial Peptides*, Wiley-VCH Verlag GmbH & Co. KGaA, Weinheim, Germany, 2013, pp. 83–113, <http://dx.doi.org/10.1002/9783527652853>.
- [74] Y. Wang, D.E. Schlamadinger, J.E. Kim, J.A. McCammon, Comparative molecular dynamics simulations of the antimicrobial peptide CM15 in model lipid bilayers, *Biochim. Biophys. Acta* 1818 (2012) 1402–1409, <http://dx.doi.org/10.1016/j.bbame.2012.02.017>.
- [75] R.M. Epanand, C. Walker, R.F. Epanand, N.A. Magarvey, K. Hilpert, *Biochimica et Biophysica Acta Molecular mechanisms of membrane targeting antibiotics*, *BBA - Biomembr* 1858 (2016) 980–987, <http://dx.doi.org/10.1016/j.bbame.2015.10.018>.
- [76] N.K. Brogden, K.A. Brogden, Will new generations of modified antimicrobial peptides improve their potential as pharmaceuticals? *Int. J. Antimicrob. Agents* 38 (2011) 217–225, <http://dx.doi.org/10.1016/j.ijantimicag.2011.05.004>.
- [77] W. Aoki, K. Kuroda, M. Ueda, Next generation of antimicrobial peptides as molecular targeted medicines, *J. Biosci. Bioeng.* 114 (2012) 365–370, <http://dx.doi.org/10.1016/j.jbiosc.2012.05.001>.
- [78] J.B. Peravali, S.R. Kotra, K. Sobha, R. Nelson, K.V. Rajesh, K.K. Pulicherla, Antimicrobial peptides: an effective alternative for antibiotic therapy, *MJPM* (2013) 1–7.
- [79] C.D. Fjell, J.A. Hiss, R.E.W. Hancock, G. Schneider, Designing antimicrobial peptides: form follows function, *Nat. Rev. Drug Discov.* 11 (2011), <http://dx.doi.org/10.1038/nrd3591>.
- [80] C. Bayl-jones, D. Bubeck, M.A. Dunstone, The mystery behind membrane insertion: a review of the complement membrane attack complex, *Philos. Trans. R Soc. Lond B Biol. Sci.* 472 (2017) 1726, <http://dx.doi.org/10.1098/rstb.2016.0221>.
- [81] M. De Vivo, M. Masetti, G. Bottegoni, A. Cavalli, Role of molecular dynamics and related methods in drug discovery, *J. Med. Chem.* 59.9 (2016) 4035–4061, <http://dx.doi.org/10.1021/acs.jmedchem.5b01684>.
- [82] A.V. Potemkin, M.A. Grishina, V.A. Potemkin, Grid-based continual analysis of molecular interior for drug discovery, *QSAR and QSPR, Curr. Drug Discov. Technol.* 14 (2017) 181–205, <http://dx.doi.org/10.2174/1570163814666170207144018>.
- [83] P. Klahn, Natural Product Reports Bifunctional antimicrobial conjugates and hybrid antimicrobials, *Nat. Prod. Rep.* 34 (2017) 832–885, <http://dx.doi.org/10.1039/C7NP00006E>.
- [84] S. Futaki, A. Gr, F. Madani, S. Lindberg, Mechanisms of cellular uptake of cell-penetrating peptides, *J. Biophys.* 2011 (2011), <http://dx.doi.org/10.1155/2011/414729>.
- [85] D. Bartuzi, A.A. Kaczor, K.M. Targowska-duda, Recent advances and applications of molecular Docking to G Protein-coupled receptors, *Molecules* 22.2 (2017) 340, <http://dx.doi.org/10.3390/molecules22020340>.
- [86] A.A. Langham, H. Khandelia, B. Schuster, A.J. Waring, R.I. Lehrer, Y.N. Kaznessis, Correlation between simulated physicochemical properties and hemolytic activity of proteoglycan-like antimicrobial peptides: predicting experimental toxicity, *Peptides* 29 (2008) 1085–1093, <http://dx.doi.org/10.1016/j.peptides.2008.03.018>.
- [87] J. Li, S. Liu, R. Lakshminarayanan, Y. Bai, K. Pervushin, C. Verma, R.W. Buerman, Molecular simulations suggest how a branched antimicrobial peptide perturbs a bacterial membrane and enhances permeability, *Biochim. Biophys. Acta* 1828

- (2013) 1112–1121, <http://dx.doi.org/10.1016/j.bbame.2012.12.015>.
- [88] B. Orioni, G. Bocchini, J.Y. Kim, A. Pallechi, G. Grande, S. Bobone, Y. Park, J. Il Kim, K. soo Hahn, L. Stella, Membrane perturbation by the antimicrobial peptide PMP-23: a fluorescence and molecular dynamics study, *Biochim. Biophys. Acta Biomembr.* 1788 (2009) 1523–1533, <http://dx.doi.org/10.1016/j.bbame.2009.04.013>.
- [89] J. Li, J. Koh, S. Liu, R. Lakshminarayanan, J.M. Conlon, Membrane active antimicrobial peptides: translating mechanistic insights to design, *Front. Neurosci.* 11 (2017) 1–18, <http://dx.doi.org/10.3389/fnins.2017.00073>.
- [90] A. Rai, S. Pinto, T. Velho, A.F. Ferreira, C. Moita, U. Trivedi, M. Evangelista, M. Comune, K.P. Rumbaugh, P.N. Simões, L. Moita, L. Ferreira, One-step synthesis of high-density peptide-conjugated gold nanoparticles with antimicrobial efficacy in a systemic infection model, *Biomaterials* 85 (2016), <http://dx.doi.org/10.1016/j.biomaterials.2016.01.051>.
- [91] K. Vanommeslaeghe, O. Guvench, A.D. MacKerell, *Molecular mechanics*, *Curr. Pharm. Des.* 20 (2014) 3281–3292.
- [92] H. Khandelia, J.H. Ipsen, O.G. Mouritsen, The impact of peptides on lipid membranes, *Biochim. Biophys. Acta* 1778 (2008) 1528–1536, <http://dx.doi.org/10.1016/j.bbame.2008.02.009>.
- [93] J.L. Velasco-Bolom, G. Corzo, R. Garduño-Juárez, Molecular dynamics simulation of the membrane binding and disruption mechanisms by antimicrobial scorpion venom-derived peptides, *J. Biomol. Struct. Dyn.* (2017) 1–15, <http://dx.doi.org/10.1080/07391102.2017.1341340>.
- [94] D. Balleza, Mechanical properties of lipid bilayers and regulation of mechanosensitive function: from biological to biomimetic channels, *Channels* 6 (2012) 220–233, <http://dx.doi.org/10.4161/chan.21085>.
- [95] D. Sengupta, H. Leontiadou, A.E. Mark, S.J. Marrink, Toroidal pores formed by antimicrobial peptides show significant disorder, *Biochim. Biophys. Acta Biomembr.* 1778 (2008) 2308–2317, <http://dx.doi.org/10.1016/j.bbame.2008.06.007>.
- [96] J. Dittmer, L. Thøgersen, J. Underhaug, K. Bertelsen, T. Vosegaard, J.M. Pedersen, B. Schiøtt, E. Tajkhorshid, T. Skrydstrup, N.C. Nielsen, Incorporation of antimicrobial peptides into membranes: a combined liquid-state NMR and molecular dynamics study of Alamethicin in DMPC/DHPC bilayers, *J. Phys. Chem. B* 113 (2009) 6928–6937, <http://dx.doi.org/10.1021/jp811494p>.
- [97] D.S. Bolintineanu, Y.N. Kaznessis, Computational studies of proteoglycan antimicrobial peptides: a review, *Peptides* 32 (2011) 188–201, <http://dx.doi.org/10.1016/j.peptides.2010.10.006>.
- [98] Y. Wang, Y.J. yang, Y.N. Chen, H.Y. Zhao, S. Zhang, Computer-aided design, structural dynamics analysis, and in vitro susceptibility test of antibacterial peptides incorporating unnatural amino acids against microbial infections, *Comput. Meth. Progr. Biomed.* 134 (2016) 215–223, <http://dx.doi.org/10.1016/j.cmpb.2016.06.005>.
- [99] M. Pickholz, Differential interaction of antimicrobial peptides with lipid structures studied by coarse-grained molecular dynamics simulations, *Molecules* 22.10 (2017) 1775, <http://dx.doi.org/10.3390/molecules22101775>.
- [100] Y. Wang, J.P. Ulmschneider, S. Zhao, How reliable are molecular dynamics simulations of membrane active antimicrobial peptides, *Biophys. J.* 108 (2015), <http://dx.doi.org/10.1016/j.bpj.2014.11.461> 78a.
- [101] L. Liu, K. Xu, H. Wang, P.K.J. Tan, W. Fan, S.S. Venkatraman, L. Li, Y.-Y. Yang, Self-assembled cationic peptide nanoparticles as an efficient antimicrobial agent, *Nat. Nanotechnol.* 4 (2009) 457–463, <http://dx.doi.org/10.1038/nnano.2009.153>.
- [102] K. Roy, S. Kar, R.N. Das, A Primer on QSAR/QSPR Modelling: Fundamental Concepts, Springer, 2015, <http://dx.doi.org/10.1007/978-3-319-17281-1>.
- [103] B.F. Begam, J.S. Kumar, Computer assisted QSAR/QSPR approaches – a review, *Indian J. Sci. Technol.* 9 (2016), <http://dx.doi.org/10.17485/ijst/2016/v9i8/87901>.
- [104] A.P. Toropova, A.A. Toropov, M. Beeg, M. Gobbi, M. Salmona, Utilization of the Monte Carlo method to build up QSAR models for hemolysis and cytotoxicity of antimicrobial peptides, *Curr. Drug Discov. Technol.* 14 (2017) 229–243, <http://dx.doi.org/10.2174/1570163814666170525114128>.
- [105] V. Frecer, QSAR analysis of antimicrobial and haemolytic effects of cyclic cationic antimicrobial peptides derived from proteoglycan-1, *14* (2006) 6065–6074, <http://dx.doi.org/10.1016/j.bmc.2006.05.005>.
- [106] J. Tong, S. Liu, P. Zhou, B. Wu, Z. Li, A novel descriptor of amino acids and its application in peptide QSAR, *J. Theor. Biol.* 253 (2008) 90–97, <http://dx.doi.org/10.1016/j.jtbi.2008.02.030>.
- [107] Y. Wang, Y. Ding, H. Wen, Y. Lin, Y. Hu, Y. Zhang, Q. Xia, Z. Lin, QSAR modeling and design of cationic antimicrobial peptides based on structural properties of amino acids, *Comb. Chem. High Throughput Screen.* 15 (2012) 347–353.
- [108] G. Kasetty, P. Papareddy, M. Kalle, V. Rydengård, M. Mörgelin, B. Albigier, M. Malmsten, A. Schmidtchen, Structure-activity studies and therapeutic potential of host defense peptides of human thrombin, *Antimicrob. Agents Chemother.* 55 (2011) 2880–2890, <http://dx.doi.org/10.1128/AAC.01515-10>.
- [109] I. Zelezetsky, A. Tossi, Alpha-helical antimicrobial peptides—Using a sequence template to guide structure-activity relationship studies, *Biochim. Biophys. Acta Biomembr.* 1758 (2006) 1436–1449, <http://dx.doi.org/10.1016/j.bbame.2006.03.021>.
- [110] D. Juretić, D. Vukičević, D. Petrov, M. Novković, V. Bojović, B. Lučić, N. Ilić, A. Tossi, Knowledge-based computational methods for identifying or designing novel, non-homologous antimicrobial peptides, *Eur. Biophys. J.* 40 (2011) 371–385, <http://dx.doi.org/10.1007/s00249-011-0674-7>.
- [111] O.M. De Bruin, H.C. Birnboim, A method for assessing efficiency of bacterial cell disruption and DNA release, *BMC Microbiol.* (2016) 1–10, <http://dx.doi.org/10.1186/s12866-016-0815-3>.
- [112] S.C. Park, Y. Park, K.S. Hahn, The role of antimicrobial peptides in preventing multidrug-resistant bacterial infections and biofilm formation, *Int. J. Mol. Sci.* 12 (2011) 5971–5992, <http://dx.doi.org/10.3390/ijms12095971>.
- [113] H. Chen, C. Liu, D. Chen, K. Madrid, S. Peng, X. Dong, M. Zhang, Y. Gu, Bacteria-targeting conjugates based on antimicrobial peptide for bacteria diagnosis and therapy, *Mol. Pharm.* 12 (2015) 2505–2516, <http://dx.doi.org/10.1021/acs.molpharmaceut.5b00053>.
- [114] S.Z. Ferreira, H.C. Carneiro, H.A. Lara, R.B. Alves, J.M. Resende, H.M. Oliveira, L.M. Silva, D.A. Santos, R.P. Freitas, Synthesis of a new peptide-coumarin conjugate: a potential agent against cryptococcosis, *ACS Med. Chem. Lett.* 6 (2015) 271–275, <http://dx.doi.org/10.1021/ml500393q>.
- [115] P.M.S.D. Cal, M.J. Matos, G.J.L. Bernardes, Trends in therapeutic drug conjugates for bacterial diseases: a patent review, *Expert Opin. Ther. Pat.* 27 (2017) 179–189 <https://doi.org/10.1080/13543776.2017.1259411>.
- [116] N. Malanovic, K. Lohner, Antimicrobial peptides targeting gram-positive bacteria, *Pharmaceuticals* (2016), <http://dx.doi.org/10.3390/ph9030059>.
- [117] A.O. Rodriguez, E.A. Papanastasiou, M. Juba, B. Bishop, Covalent modification of a ten-residue cationic antimicrobial peptide with levofloxacin, *Front. Chem.* 2 (2014) 71, <http://dx.doi.org/10.3389/fchem.2014.00071>.
- [118] K.F. Croom, K.L. Goa, Levofloxacin: a review of its use in the treatment of bacterial infections in the United States, *Drugs* 63 (2003) 2769–2802, <http://dx.doi.org/10.2165/00003495-200363240-00008>.
- [119] P.D. Lister, D.J. Wolter, N.D. Hanson, Antibacterial-resistant *Pseudomonas aeruginosa*: clinical impact and complex regulation of chromosomally encoded resistance mechanisms, *Clin. Microbiol. Rev.* 22 (2009) 582–610, <http://dx.doi.org/10.1128/CMR.00040-09>.
- [120] K. Ösapay, D. Tran, A.S. Ladokhin, S.H. White, A.H. Henschen, M.E. Selsted, Formation and characterization of a single Trp-Trp cross-link in indolicidin that confers protease stability without altering antimicrobial activity, *J. Biol. Chem.* 275 (2000) 12017–12022, <http://dx.doi.org/10.1074/jbc.275.16.12017>.
- [121] H. Matsumoto, T. Kimura, T. Hamawaki, A. Kumagai, T. Goto, K. Sano, Y. Hayashi, Y. Kiso, Design, synthesis, and biological evaluation of anti-HIV double-drugs: conjugates of HIV protease inhibitors with a reverse transcriptase inhibitor through spontaneously cleavable linkers, *Bioorg. Med. Chem.* 9 (2001) 1589–1600, [http://dx.doi.org/10.1016/s0968-0896\(01\)00045-1](http://dx.doi.org/10.1016/s0968-0896(01)00045-1).
- [122] C.L. Ventola, The antibiotic resistance crisis: part 1: causes and threats, *P&T* 40 (2015) 277–283.
- [123] W.M. Cho, B.P. Joshi, H. Cho, K.-H. Lee, Design and synthesis of novel anti-bacterial peptide-resin conjugates, *Bioorg. Med. Chem. Lett.* 17 (2007) 5772–5776, <http://dx.doi.org/10.1016/j.bmlc.2007.08.056>.
- [124] N.M. Mishra, Y. Briers, C. Lamberigts, H. Steenackers, S. Robijns, B. Landuyt, J. Vanderleyden, L. Schoofs, R. Lavigne, W. Luyten, E.V. Van der Eycken, Evaluation of the antibacterial and antibiofilm activities of novel CRAMP-vancomycin conjugates with diverse linkers, *Org. Biomol. Chem.* 13 (2015) 7477–7486.
- [125] N.W. Schmidt, S. Deshayes, S. Hawker, A. Blacker, A.M. Kasko, G.C.L. Wong, Engineering persister-specific antibiotics with synergistic antimicrobial functions, *ACS Nano* 8 (2014) 8786–8793, <http://dx.doi.org/10.1021/nn502201a>.
- [126] C.J. Arnusch, H. Ulm, M. Josten, Y. Shadkhan, N. Osherov, H.-G. Sahl, Y. Shai, Ultrashort peptide bioconjugates are exclusively antifungal agents and synergize with cyclodextrin and amphotericin B, *Antimicrob. Agents Chemother.* 56 (2012) 1–9, <http://dx.doi.org/10.1128/AAC.00468-11>.
- [127] C.J. Arnusch, R.J. Pieters, E. Breukink, Enhanced membrane pore formation through high-affinity targeted antimicrobial peptides, *PLoS One* 7 (2012), <http://dx.doi.org/10.1371/journal.pone.0039768>.
- [128] S.A. Cochrane, X. Li, S. He, M. Yu, M. Wu, J.C. Vederas, Synthesis of tridecaptin-antibiotic conjugates with in vivo activity against gram-negative bacteria, *J. Med. Chem.* 58 (2015) 9779–9785, <http://dx.doi.org/10.1021/acs.jmedchem.5b01578>.
- [129] K. Matsuzaki, Control of cell selectivity of antimicrobial peptides, *Biochim. Biophys. Acta Biomembr.* 1788 (2009) 1687–1692, <http://dx.doi.org/10.1016/j.bbame.2008.09.013>.
- [130] R. Anghel, D. Jitaru, L. Bădescu, M. Bădescu, M. Ciocoiu, The cytotoxic effect of magainin ii on the MDA-MB-231 and M14K tumour cell lines, *BioMed. Res. Int.* 2013 (2013), <http://dx.doi.org/10.1155/2013/831709>.
- [131] S. Liu, H. Yang, L. Wan, H. Cai, S. Li, Y. Li, J. Cheng, X. Lu, Enhancement of cytotoxicity of antimicrobial peptide magainin II in tumor cells by bombesin-targeted delivery, *Acta Pharmacol. Sin.* 32 (2011) 79–88, <http://dx.doi.org/10.1038/aps.2010.162>.
- [132] I. Pal, V.P. Brahmakhatr, S. Bera, D. Bhattacharyya, Y. Quirishi, A. Bhunia, H.S. Atreya, Enhanced stability and activity of an antimicrobial peptide in conjugation with silver nanoparticle, *J. Coll. Interf. Sci.* 483 (2016) 385–393, <http://dx.doi.org/10.1016/j.jcis.2016.08.043>.
- [133] N. Wiradharma, M. Khan, L. Yong, C.A.E. Hauser, S. Voon, S. Zhang, Y. Yang, Biomaterials the effect of thiol functional group incorporation into cationic helical peptides on antimicrobial activities and spectra, *Biomaterials* 32 (2011) 9100–9108, <http://dx.doi.org/10.1016/j.biomaterials.2011.08.020>.
- [134] F. Salomone, F. Cardarelli, M. Di Luca, C. Boccardi, R. Nifosi, G. Bardi, L. Di Bari, M. Serresi, F. Beltram, A novel chimeric cell-penetrating peptide with membrane-disruptive properties for efficient endosomal escape, *J. Control. Release* 163 (2012) 293–303, <http://dx.doi.org/10.1016/j.jconrel.2012.09.019>.
- [135] S. Ron-Doitch, B. Sawodny, A. Kühbacher, M.M.N. David, A. Samanta, J. Phopase, A. Burger-Kentscher, M. Griffith, G. Golomb, S. Rupp, Reduced cytotoxicity and enhanced bioactivity of cationic antimicrobial peptides liposomes in cell cultures and 3D epidermis model against HSV, *J. Control. Release* 229 (2016) 163–171, <http://dx.doi.org/10.1016/j.jconrel.2016.03.025>.
- [136] A.W. Du, M.H. Stenzel, Drug carriers for the delivery of therapeutic peptides, *Biomacromolecules* 15 (2014) 1097–1114, <http://dx.doi.org/10.1021/>

- bm500169p.
- [137] Y. Zheng, S. Li, Z. Weng, C. Gao, Hyperbranched polymers: advances from synthesis to applications, *Chem. Soc. Rev.* 44 (2015) 4091–4130, <http://dx.doi.org/10.1039/C4CS00528G>.
- [138] Y. Deng, J.K. Saucier-Sawyer, C.J. Hoimes, J. Zhang, Y.E. Seo, J.W. Andreyecsk, W.M. Saltzman, The effect of hyperbranched polyglycerol coatings on drug delivery using degradable polymer nanoparticles, *Biomaterials* 35 (2014) 6595–6602, <http://dx.doi.org/10.1016/j.biomaterials.2014.04.038>.
- [139] P. Kumar, R.A. Shenoi, B.F.L. Lai, M. Nguyen, J.N. Kizhakkedathu, S.K. Straus, Conjugation of aurein 2.2 to HPG yields an antimicrobial with better properties, *Biomacromolecules* 16 (2015) 913–923, <http://dx.doi.org/10.1021/bm5018244>.
- [140] X.Y. Liu, J.M. Nothias, A. Scavone, M. Garfinkel, J.M. Millis, Biocompatibility investigation of polyethylene glycol and alginate-poly-L-lysine for islet encapsulation, *ASAIO J.* 56 (2010) 241–245, <http://dx.doi.org/10.1097/MAT.0b013e3181d7b8e3>.
- [141] J. Khandare, T. Minko, Polymer-drug conjugates: progress in polymeric prodrugs, *Prog. Polym. Sci.* 31 (2006) 359–397, <http://dx.doi.org/10.1016/j.progpolymsci.2005.09.004>.
- [142] G. Pasut, Polymers for protein conjugation, *Polymers* 6 (2014) 160–178, <http://dx.doi.org/10.3390/polym6010160>.
- [143] M.J. Roberts, M.D. Bentley, J.M. Harris, Chemistry for peptide and protein PEGylation, *Adv. Drug Deliv. Rev.* 64 (2012) 116–127, <http://dx.doi.org/10.1016/j.addr.2012.09.025>.
- [144] A. Guiotto, M. Pozzobon, M. Canevari, R. Manganello, M. Scarin, F.M. Veronese, PEGylation of the antimicrobial peptide nisin A: problems and perspectives, *Farmacol.* 58 (2003) 45–50, [http://dx.doi.org/10.1016/S0014-827X\(02\)01301-0](http://dx.doi.org/10.1016/S0014-827X(02)01301-0).
- [145] C.J. Morris, K. Beck, M.A. Fox, D. Ulaeto, G.C. Clark, M. Gumbleton, Pegylation of antimicrobial peptides maintains the active peptide conformation, model membrane interactions, and antimicrobial activity while improving lung tissue biocompatibility following airway delivery, *Antimicrob. Agents Chemother.* 56 (2012) 3298–3308, <http://dx.doi.org/10.1128/AAC.06335-11>.
- [146] M. Benincasa, S. Zahariev, C. Pelillo, A. Milan, R. Gennaro, M. Scocchi, PEGylation of the peptide Bac7(1-35) reduces renal clearance while retaining antibacterial activity and bacterial cell penetration capacity, *Eur. J. Med. Chem.* 95 (2015) 210–219, <http://dx.doi.org/10.1016/j.ejmech.2015.03.028>.
- [147] M. Zhang, J. Lei, Y. Shi, L. Zhang, Y. Ye, D. Li, C. Mu, Molecular weight effects of PEG on the crystal structure and photocatalytic activities of PEG, *RSC Adv.* 6 (2016) 83366–83372, <http://dx.doi.org/10.1039/C6RA12988A>.
- [148] H. Lee, Molecular modeling of PEGylated peptides, dendrimers, and single-walled carbon nanotubes for biomedical applications, *Polymers* 6 (2014) 776–798, <http://dx.doi.org/10.3390/polym6030776>.
- [149] M. Santos, A. Fonseca, P. Mendonça, R. Branco, A. Serra, P. Morais, J. Coelho, Recent developments in antimicrobial polymers: a review, *Materials* 9 (2016) 599, <http://dx.doi.org/10.3390/ma9070599>.
- [150] S. Hong, S. Yoo, H. Kim, J. Lee, Chitosan-based multifunctional platforms for local delivery of therapeutics, *Mar. Drugs* 15.3 (2017) 60, <http://dx.doi.org/10.3390/md15030060>.
- [151] M.K.S. Batista, M. Galleli, A. Adeva, C.A.R. Gomes, P. Gomes, Facile regioselective synthesis of a novel chitosan-pexiganan conjugate with potential interest for the treatment of infected skin lesions, *Synth. Commun.* 39 (2009) 1228–1240, <http://dx.doi.org/10.1080/00397910802517855>.
- [152] R.C. Goy, S.T.B. Morais, O.B.G. Assis, Evaluation of the antimicrobial activity of chitosan and its quaternized derivative on *E. Coli* and *S. aureus* growth, *Brazilian J. Pharmacogn.* 26 (2016) 122–127, <http://dx.doi.org/10.1016/j.bjp.2015.09.010>.
- [153] E.J.C. Goldstein, D.M. Citron, K.L. Tyrrell, E.S. Leocio, In vitro activity of Pexiganan and 10 comparator antimicrobials against 234 isolates including 93 *Pasteurella* spp. and 50 anaerobic bacteria recovered from animal bite wounds, *Antimicrob. Agents Chemother.* 61.6 (2017), <http://dx.doi.org/10.1128/AAC.00246-17>.
- [154] R.K. Flamm, P.R. Rhomberg, K.M. Simpson, D.J. Farrell, H.S. Sader, R.N. Jones, In vitro spectrum of pexiganan activity when tested against pathogens from diabetic foot infections and with selected resistance mechanisms, *Antimicrob. Agents Chemother.* 59 (2015) 1751–1754, <http://dx.doi.org/10.1128/AAC.04773-14>.
- [155] E. Costa, S. Silva, F. Tavora, M. Pintado, Antimicrobial and antibiofilm activity of chitosan on the oral pathogen *Candida albicans*, *Pathog* 3 (2014) 908–919, <http://dx.doi.org/10.3390/pathogens3040908>.
- [156] R. Kean, R. Rajendran, J. Haggarty, E.M. Townsend, B. Short, K.E. Burgess, S. Lang, O. Millington, W.G. Mackay, C. Williams, G. Ramage, *Candida albicans* mycofilms support *Staphylococcus aureus* colonization and enhances miconazole resistance in dual-species interactions, *Front. Microbiol.* 8 (2017) 1–11, <http://dx.doi.org/10.3389/fmicb.2017.00258>.
- [157] P. Sahariah, K.K. Sørensen, M.Á. Hjálmsdóttir, Ó.E. Sigurjónsson, K.J. Jensen, M. Másson, M.B. Thygesen, Antimicrobial peptide shows enhanced activity and reduced toxicity upon grafting to chitosan polymers, *Chem. Commun.* 51 (2015) 11611–11614, <http://dx.doi.org/10.1039/c5cc04010h>.
- [158] S. Sakuma, M. Suita, Y. Masaoka, M. Kataoka, N. Nakajima, N. Shinkai, H. Yamauchi, K. Hiwatari, H. Tachikawa, R. Kimura, S. Yamashita, Oligoarginine-linked polymers as a new class of penetration enhancers, *J. Control. Release* 148 (2010) 187–196, <http://dx.doi.org/10.1016/j.jconrel.2010.08.022>.
- [159] M.S.H. Akash, K. Rehman, S. Chen, Natural and synthetic polymers as drug carriers for delivery of therapeutic proteins, *Polym. Rev.* 55 (2015) 371–406, <http://dx.doi.org/10.1080/15583724.2014.995806>.
- [160] J.M. Ferriz, J. Vin, Prodrug design of phenolic drugs, *Curr. Pharm. Des.* 16.18 (2010) 2033–2052.
- [161] J. Rautio, K. Laine, M. Gynther, J. Savolainen, Prodrug approaches for CNS delivery, *AAPS J.* 10 (2008) 92–102, <http://dx.doi.org/10.1208/s12248-008-9009-8>.
- [162] B. Findlay, G.G. Zhanel, F. Schweizer, Neomycin-phenolic conjugates: polycationic amphiphiles with broad-spectrum antibacterial activity, low hemolytic activity and weak serum protein binding, *Bioorg. Med. Chem. Lett.* 22 (2012) 1499–1503, <http://dx.doi.org/10.1016/j.bmcl.2012.01.025>.
- [163] N. Yin, M.A. Brimble, P.W.R. Harris, J. Wen, Medicinal chemistry enhancing the oral bioavailability of peptide drugs by using chemical modification and other approaches, *Med. Chem.* 4 (2014) 763–769, <http://dx.doi.org/10.4172/2161-0444.1000227>.
- [164] A. Ghosal, P.E. Nielsen, Potent antibacterial antisense peptide-peptide nucleic acid conjugates against *Pseudomonas aeruginosa*, *Nucl. Acid Ther.* 22 (2012) 323–334, <http://dx.doi.org/10.1089/nat.2012.0370>.
- [165] G. Montagner, V. Bezzerri, G. Cabrini, E. Fabbri, M. Borgatti, I. Lampronti, A. Finotti, P.E. Nielsen, R. Gambari, An antisense peptide nucleic acid against *Pseudomonas aeruginosa* inhibiting bacterial-induced inflammatory responses in the cystic fibrosis IB3-1 cellular model system, *Int. J. Biol. Macromol.* 99 (2017) 492–498, <https://doi.org/10.1016/j.ijbiomac.2017.02.011>.
- [166] B.A.R. Williams, J.C. Chaput, Synthesis of peptide-oligonucleotide conjugates using a heterobifunctional crosslinker, *Curr. Protoc. Nucl. Acid Chem.* (2010) 4–41, <http://dx.doi.org/10.1002/0471142700.nc0441s42>.
- [167] A. Reinhardt, M. Horn, J.P.G. Schmauck, A. Bröhl, R. Giernoth, C. Oelkrug, A. Schubert, I. Neundorff, Novel imidazolium salt-peptide conjugates and their antimicrobial activity, *Bioconj. Chem.* 25 (2014) 2166–2174, <http://dx.doi.org/10.1021/bc500510c>.
- [168] A. Carmona-Ribeiro, L. de Melo Carrasco, Novel formulations for antimicrobial peptides, *Int. J. Mol. Sci.* 15 (2014) 18040–18083, <http://dx.doi.org/10.3390/ijms151018040>.
- [169] Y.A. Pérez, C.M. Urista, J.I. Martinez, M.D.C.D. Nava, F.A.R. Rodriguez, Functionalized polymers for enhance oral bioavailability of sensitive molecules, *Polymers* 8 (2016) 1–22, <http://dx.doi.org/10.3390/polym8060214>.
- [170] A.M. Carmona-Ribeiro, L.D. de M. Carrasco, Novel formulations for antimicrobial peptides, *Int. J. Mol. Sci.* 15 (2014) 18040–18083, <http://dx.doi.org/10.3390/ijms151018040>.
- [171] A. Brandelli, Nanostructures as promising tools for delivery of antimicrobial peptides, *Mini Rev. Med. Chem.* 12 (2012) 731–741, <http://dx.doi.org/10.2174/138955712801264774>.
- [172] S. Sandreschi, A.M. Piras, G. Batoni, F. Chiellini, Perspectives on polymeric nanostructures for the therapeutic application of antimicrobial peptides, *Nanomedicine* 11 (2016) 1729–1744, <http://dx.doi.org/10.2217/nmm-2016-0057>.
- [173] M.L. Immordino, F. Dosio, L. Cattel, Stealth liposomes: review of the basic science, rationale, and clinical applications, existing and potential, *Int. J. Nanomed.* 1 (2006) 297–315, <http://dx.doi.org/10.1023/A:1020134521778>.
- [174] M. Çağdaş, A.D. Sezer, S. Bucak, Liposomes as potential drug carrier systems for drug delivery, *Nanotechnol. Nanometer. Appl. Nanotechnol. Drug Deliv.* (2014) 1–50, <http://dx.doi.org/10.5772/57028>.
- [175] P. Urban, J. Jose Valle-Delgado, E. Moles, J. Marques, C. Diez, X. Fernandez-Busquets, Nanotools for the delivery of antimicrobial peptides, *Curr. Drug Targets* 13 (2012) 1158–1172, <http://dx.doi.org/10.2174/138945012802002302>.
- [176] M. Alavi, N. Karimi, M. Safaei, Application of various types of liposomes in drug delivery systems, *Adv. Pharm. Bull.* 7.1 (2017) 3–9, <http://dx.doi.org/10.15171/apb.2017.002>.
- [177] G. Tiwari, R. Tiwari, B. Sriwastawa, L. Bhati, S. Pandey, P. Pandey, S.K. Bannerjee, Drug delivery systems: an updated review, *Int. J. Pharm. Investig.* 2 (2012) 2–11, <http://dx.doi.org/10.4103/2230-973X.96920>.
- [178] P. da Silva Malheiros, D.J. Daroit, A. Brandelli, Food applications of liposome-encapsulated antimicrobial peptides, *Trends Food Sci. Technol.* 21 (2010) 284–292, <http://dx.doi.org/10.1016/j.tifs.2010.03.003>.
- [179] A. Akbarzadeh, R. Rezaei-Sadabady, S. Davaran, S.W. Joo, N. Zarghami, Y. Hanifepour, M. Samiei, M. Kouhi, K. Nejati-Koshki, Liposome: classification, preparation, and applications, *Nanoscale Res. Lett.* 8 (2013) 102, <http://dx.doi.org/10.1186/1556-276X-8-102>.
- [180] R.O. Benech, E.E. Kheadr, C. Lacroix, I. Fliss, Antibacterial activities of nisin Z encapsulated in liposomes or produced in situ by mixed culture during Cheddar cheese ripening, *Appl. Environ. Microbiol.* 68 (2002) 5607–5619, <http://dx.doi.org/10.1128/AEM.68.11.5607-5619.2002>.
- [181] L.M. Were, B. Bruce, P.M. Davidson, J. Weiss, Encapsulation of nisin and lysozyme in liposomes enhances efficacy against *Listeria monocytogenes*, *J. Food Prot.* 67 (2004) 922–927.
- [182] M. Alipour, M. Halwani, A. Omri, Z.E. Suntres, Antimicrobial effectiveness of liposomal polymyxin B against resistant Gram-negative bacterial strains, *Int. J. Pharm.* 355 (2008) 293–298, <http://dx.doi.org/10.1016/j.ijpharm.2007.11.035>.
- [183] M. Alipour, Z.E. Suntres, M. Halwani, A.O. Azghani, A. Omri, Activity and interactions of liposomal antibiotics in presence of polyanions and sputum of patients with cystic fibrosis, *PLoS One* 4 (2009) 1–9, <http://dx.doi.org/10.1371/journal.pone.0005724>.
- [184] W. Xu, P. Ling, T. Zhang, Polymeric micelles, a promising drug delivery system to enhance bioavailability of poorly water-soluble drugs, *J. Drug Deliv.* 2013 (2013), <http://dx.doi.org/10.1155/2013/340315>.
- [185] P. Zhang, X. Qian, Z. Zhang, C. Li, C. Xie, W. Wu, X. Jiang, Supramolecular amphiphilic polymer-based micelles with seven-armed polyoxazoline coating for drug delivery, *ACS Appl. Mater. Interfac.* 9.7 (2017) 5768–5777, <http://dx.doi.org/10.1021/acami.6b14464>.
- [186] A. Harada, K. Kazunori, Polyion complex micelle formation from double-hydrophilic block copolymers composed of charged and non-charged segments in aqueous media, *Polym. J.* (2017), <http://dx.doi.org/10.1038/pj.2017.67>.

- [187] R.L. Williams, S.B. Lim, H. Onyuksel, P.T. Marucha, Sterically stabilized phospholipid micelles reduce activity of a candidate antimicrobial wound healing adjunct, *Int. J. Pept. Res. Ther.* 18 (2012) 195–203, <http://dx.doi.org/10.1007/s10989-012-9292-1>.
- [188] M. Black, A. Trent, Y. Kostenko, J.S. Lee, C. Olive, M. Tirrell, Self-assembled peptide amphiphile micelles containing a cytotoxic t-cell epitope promote a protective immune response in vivo, *Adv. Mater.* 24.28 (2012) 3845–3849, <http://dx.doi.org/10.1002/adma.201200209>.
- [189] J. Wang, W. Vermerris, Antimicrobial nanomaterials derived from natural products—a review, *Materials* 9 (2016) 255, <http://dx.doi.org/10.3390/ma9040255>.
- [190] H.J. Lee, Y.H. Park, W.G. Koh, Fabrication of nanofiber microarchitectures localized within hydrogel microparticles and their application to protein delivery and cell encapsulation, *Adv. Funct. Mater.* 23 (2013) 591–597, <http://dx.doi.org/10.1002/adfm.201201501>.
- [191] L.M.T. Dicks, T.D.J. Heunis, Nanofibers offer alternative ways to the treatment of skin infections, *J. Biomed. Biotechnol.* 2010 (2010), <http://dx.doi.org/10.1155/2010/510682>.
- [192] N. Beyth, Y. Hour-Haddad, A. Domb, W. Khan, R. Hazan, N. Beyth, Y. Hour-Haddad, A. Domb, W. Khan, R. Hazan, Alternative antimicrobial approach: nano-antimicrobial materials, evidence-based complement, *Altern. Med.* 2015 (2015) 1–16, <http://dx.doi.org/10.1155/2015/246012>.
- [193] H. Zazo, C.G. Millán, C.I. Colino, J.M. Lanao, Chapter 15-applications of metallic nanoparticles in antimicrobial therapy, in: Alexandru Mihai BT. Grumezescu (Ed.), *Antimicrobial Nanoarchitectonics*, Elsevier, 2017, pp. 411–444 <https://doi.org/10.1016/B978-0-323-52733-0.00015-X>.
- [194] M. Veerapandian, K. Yun, Functionalization of biomolecules on nanoparticles: specialized for antibacterial applications, *Appl. Microbiol. Biotechnol.* 90 (2011) 1655–1667, <http://dx.doi.org/10.1007/s00253-011-3291-6>.
- [195] S. Mohanty, P. Jena, R. Mehta, R. Pati, B. Banerjee, S. Patil, A. Sonawane, Cationic antimicrobial peptides and biogenic silver nanoparticles kill mycobacteria without eliciting dna damage and cytotoxicity in mouse macrophages, *Antimicrob. Agents Chemother.* 57 (2013) 3688–3698, <http://dx.doi.org/10.1128/AAC.02475-12>.
- [196] S. Prabhu, E.K. Poulouse, Silver nanoparticles: mechanism of antimicrobial action, synthesis, medical applications, and toxicity effects, *Int. Nano Lett.* 2 (2012) 32, <http://dx.doi.org/10.1186/2228-5326-2-32>.
- [197] G. Franci, A. Falanga, S. Galdiero, L. Palomba, M. Rai, G. Morelli, M. Galdiero, Silver nanoparticles as potential antibacterial agents, *Molecules* 20 (2015) 8856–8874, <http://dx.doi.org/10.3390/molecules20058856>.
- [198] L. Liu, J. Yang, J. Xie, Z. Luo, J. Jiang, Y.Y. Yang, S. Liu, The potent antimicrobial properties of cell penetrating peptide-conjugated silver nanoparticles with excellent selectivity for gram-positive bacteria over erythrocytes, *Nanoscale* 5 (2013) 3834–3840, <http://dx.doi.org/10.1039/c3nr34254a>.
- [199] A. Rai, S. Pinto, M.B. Evangelista, H. Gil, S. Kallip, M.G.S. Ferreira, L. Ferreira, High-density antimicrobial peptide coating with broad activity and low cytotoxicity against human cells, *Acta Biomater.* 33 (2016) 64–74, <http://dx.doi.org/10.1016/j.actbio.2016.01.035>.
- [200] P. Wadhvani, N. Heidenreich, B. Podyeyn, J. Bürck, A.S. Ulrich, Biomaterials Science Antibiotic gold: tethering of antimicrobial peptides to gold nanoparticles maintains conformational flexibility of peptides and improves trypsin, *J. Biomater. Sci.* 5.4 (2017) 817–827, <http://dx.doi.org/10.1039/c7bm00069c>.
- [201] B. Casciaro, M. Moros, S. Rivera-fernandez, A. Bellelli, M. De Fuente, M.L. Mangoni, Gold-Nanoparticles coated with the antimicrobial peptide Esculentin-1a(1-21)NH₂ as a reliable strategy for antipseudomonal drugs, *Acta Biomater.* 47 (2016) 170–181, <http://dx.doi.org/10.1016/j.actbio.2016.09.041>.
- [202] K.U. Bhat, S.M. Vidya, Journal of Drug Delivery Science and Technology Nisin gold nanoparticles assemble as potent antimicrobial agent against *Enterococcus faecalis* and *Staphylococcus aureus* clinical isolates, *J. Drug Deliv. Sci. Technol.* 37 (2017) 20–27, <http://dx.doi.org/10.1016/j.jddst.2016.11.002>.
- [203] V.V. Mody, R. Siwale, A. Singh, H.R. Mody, Introduction to metallic nanoparticles, *J. Pharm. Bioallied. Sci.* 2 (2017) 282–289, <http://dx.doi.org/10.4103/0975-7406.72127>.
- [204] J. Zhu, R.E. Marchant, Design properties of hydrogel tissue-engineering scaffolds, *Expert Rev. Med. Devices* 8 (2011) 607–626, <http://dx.doi.org/10.1586/erd.11.27>.
- [205] T.R. Hoare, D.S. Kohane, Hydrogels in drug delivery: progress and challenges, *Polymer* 49 (2008) 1993–2007, <http://dx.doi.org/10.1016/j.polymer.2008.01.027>.
- [206] M. Hamidi, A. Azadi, P. Ra, Hydrogel nanoparticles in drug delivery, *Adv. Drug Deliv. Rev.* 60 (2008) 1638–1649, <http://dx.doi.org/10.1016/j.addr.2008.08.002>.
- [207] L.J. del Valle, A. Diaz, J. Puigalfi, Hydrogels for biomedical applications: cellulose, chitosan, and protein/peptide derivatives, *Gels* 3.3 (2017) 27.
- [208] W.B. Liechty, et al., Polymers for drug delivery systems, *Annu. Rev. Chem. Biomol. Eng.* 1 (2010) 149–173 <https://http://dx.doi.org/10.1146/annurev-chembioeng-073009-100847>.
- [209] S.S. Rajan, V.L. Cavera, X. Zhang, Y. Singh, M.L. Chikindas, P.J. Sinko, Polyethylene glycol-based hydrogels for controlled release of the antimicrobial subtilisin for prophylaxis of bacterial vaginosis, *Antimicrob. Agents Chemother.* 58 (2014) 2747–2753, <http://dx.doi.org/10.1128/AAC.02446-14>.
- [210] J. Håkansson, C. Björn, K. Lindgren, E. Sjöström, V. Sjöstrand, M. Mahlapuu, Efficacy of the novel topical antimicrobial agent pxl150 in a mouse model of surgical site infections, *Antimicrob. Agents Chemother.* 58 (2014) 2982–2984, <http://dx.doi.org/10.1128/AAC.00143-14>.
- [211] H. Babavalian, A.M. Latifi, M.A. Shokrgozar, S. Bonakdar, S. Mohammadi, M.M. Moghaddam, Analysis of healing effect of alginate sulfate hydrogel dressing containing antimicrobial peptide on wound infection caused by methicillin-resistant *Staphylococcus aureus*, *Jundishapur J. Microbiol.* 8 (2015) 0–6, <http://dx.doi.org/10.5812/jjm.28320>.
- [212] D. Bobo, K.J. Robinson, J. Islam, K.J. Thurecht, S.R. Corrie, S.R. Corrie, Nanoparticle-based medicines: a review of FDA-approved materials and clinical trials to date, *Pharm. Res.* 33.10 (2016) 2373–2387, <http://dx.doi.org/10.1007/s11095-016-1958-5>.
- [213] L. Zhang, T.J. Falla, Antimicrobial peptides: therapeutic potential, *Expert Opin. Pharmacother.* 7 (2006) 653–663, <http://dx.doi.org/10.1517/14656566.7.6.653>.
- [214] D.C. Kaur, S.S. Chate, Study of antibiotic resistance pattern in methicillin resistant *Staphylococcus Aureus* with special reference to newer antibiotic, *J. Glob. Infect. Dis.* 7 (2015) 78–84, <http://dx.doi.org/10.4103/0974-777X.157245>.
- [215] P.S. Loomba, J. Taneja, B. Mishra, Methicillin and vancomycin resistant *S. Aureus* in hospitalized patients, *J. Glob. Infect. Dis.* 2 (2010) 275–283, <http://dx.doi.org/10.4103/0974-777X.68535>.
- [216] G.M.S. Soares, L.C. Figueiredo, M. Faveri, S.C. Cortelli, P.M. Duarte, M. Feres, Mechanisms of action of systemic antibiotics used in periodontal treatment and mechanisms of bacterial resistance to these drugs, *J. Appl. Oral. Sci.* 20 (2012) 295–309, <http://dx.doi.org/10.1590/S1678-77572012000300002>.
- [217] H.S. Gold, Vancomycin-resistant enterococci: mechanisms and clinical observations, *Clin. Infect. Dis.* 33.2 (2001) 210–219.
- [218] S. Rath, R.N. Padhy, Prevalence of Fluoroquinolone Resistance in *Escherichia coli* in an Indian Teaching Hospital and Adjoining Communities, vol. 10, *J. Taibah Univ. Med. Sci.*, 2015, pp. 504–508 <https://doi.org/10.1016/j.jtumed.2015.02.009>.
- [219] K. Streeter, M. Katouli, *Pseudomonas aeruginosa*: a review of their pathogenesis and prevalence in clinical settings and the environment, 2 (2016) 25–32, <http://dx.doi.org/10.7508/iem.2016.01.008>.
- [220] N. Woodford, P.M. Tierno, K. Young, L. Tysall, M.I. Palepou, E. Ward, R.E. Painter, D.F. Suber, D. Shungu, L.L. Silver, K. Inglima, J. Kornblum, D.M. Livermore, Outbreak of *Klebsiella pneumoniae* producing a new carbapenem-hydrolyzing class A beta-lactamase, KPC-3, in a New York Medical Center, *Antimicrob. Agents Chemother.* 48 (2004) 4793–4799, <http://dx.doi.org/10.1128/AAC.48.12.4793>.
- [221] J. Fishbain, A.Y. Peleg, Treatment of acinetobacter infections, *Clin. Infect. Dis.* 51 (2010) 79–84, <http://dx.doi.org/10.1086/653120>.
- [222] J.L. Fox, Antimicrobial peptides stage a comeback, *Nat. Publ. Gr* 31 (2013) 379–382, <http://dx.doi.org/10.1038/nbt.2572>.
- [223] K.A. Ghaffar, W.M. Hussein, Z.G. Khalil, R.J. Capon, M. Skwarczynski, I. Toth, Levofloxacin and indolicidin for combination antimicrobial therapy, *Curr. Drug Deliv. 12* (2015) 108–114.
- [224] C.J. Arnsch, A.M.J.J. Bonvin, A.M. Verel, T.M. Wouter, R.M.J. Liskamp, B. De Kruijff, R.J. Pieters, E. Breukink, R. Enterococci, The vancomycin – nisin (1 – 12) hybrid restores activity against vancomycin resistant Enterococci, *Biochem* 47.48 (2008) 12661–12663, <http://dx.doi.org/10.1021/bi801597b>.
- [225] C. Chamorro, M.A. Boerman, C.J. Arnsch, E. Breukink, R.J. Pieters, Enhancing membrane disruption by targeting and multivalent presentation of antimicrobial peptides, *Biochim. Biophys. Acta-Biomembranes* 1818 (2012) 2171–2174, <http://dx.doi.org/10.1016/j.bbmem.2012.04.004>.
- [226] N.M. Mishra, Y. Briers, C. Lamberigts, H. Steenackers, S. Robijns, B. Landuyt, J. Vanderleyden, L. Schoofs, R. Lavigne, W. Luyten, E. V Van der Eycken, Evaluation of the antibacterial and antibiofilm activities of novel CRAMP-vancomycin conjugates with diverse linkers, *Org. Biomol. Chem.* 13 (2015) 7477–7486, <http://dx.doi.org/10.1039/c5ob00830a>.
- [227] K. Yamakami, H. Tsumori, Y. Shimizu, Y. Sakurai, K. Nagatoshi, Cationic lipid content in liposome-encapsulated nisin improves sustainable bactericidal activity against *Streptococcus mutans*, *Open Dent. J.* 4 (2016) 360–366, <http://dx.doi.org/10.2174/1874210616021001360>.
- [228] R. Laridi, E.E. Kheadr, R.O. Benez, J.C. Vuilleumard, C. Lacroix, I. Fliss, Liposome encapsulated nisin Z: optimization, stability and release during milk fermentation, *Int. Dairy J.* 13 (2003) 325–336, [http://dx.doi.org/10.1016/S0958-6946\(02\)00194-2](http://dx.doi.org/10.1016/S0958-6946(02)00194-2).
- [229] D.W. Song, S.H. Kim, H.H. Kim, K.H. Lee, C.S. Ki, Y.H. Park, Multi-biofunction of antimicrobial peptide-immobilized silk fibroin nanofiber membrane: implications for wound healing, *Acta Biomater.* 39 (2016) 146–155, <http://dx.doi.org/10.1016/j.actbio.2016.05.008>.
- [230] T.D.J. Heunis, M. Botes, L.M.T. Dicks, Encapsulation of *Lactobacillus plantarum* 423 and its bacteriocin in nanofibers, *Probiotics Antimicrob. Proteins* 2 (2010) 46–51, <http://dx.doi.org/10.1007/s12602-009-9024-9>.
- [231] R.T.C. Cleophas, J. Sjöllema, H.J. Busscher, J.A.W. Kruijtzter, R.M.J. Liskamp, Characterization and activity of an immobilized antimicrobial peptide containing bactericidal PEG-hydrogel, *Biomacromolecules* 15 (2014) 3390–3395, <http://dx.doi.org/10.1021/bm500899r>.
- [232] A. McCloskey, B. Gilmore, G. Laverty, Evolution of antimicrobial peptides to self-assembled Peptides for Biomaterial applications, *Pathogens* 3 (2014) 791–821, <http://dx.doi.org/10.3390/pathogens3040791>.